Synthesis and Characterization of Novel Silicate Prodrugs and Block Copolymers for Use into Nanoparticle Drug Delivery

A DISSERTATION
SUBMITTED TO THE FACULTY OF THE GRADUATE SCHOOL
OF THE UNIVERSITY OF MINNESOTA BY

Andrew Robert Michel

IN PARTIAL FULFILLMENT OF THE REQUIREMENTS
FOR THE DEGREE OF
Doctor of Philosophy

Thomas R. Hoye, Advisor

October 2015

Acknowledgements

Without the love and support of my family, friends, teachers, and colleagues my further education in chemistry would not be a reality. I am forever thankful for the encouragement, prospective, and reassurance throughout my academic career.

First and foremost, I would like to thank my advisor Professor Tom Hoye; over five years he has been ever patient, wise, kind, and a true leader by example. Tom posses an uncanny way with words and has inspired me during the toughest of times. Early in my graduate school career, my grandmother passed away, and through his condolence and reassurance I was able to bounce back and persevere. He has taught me the ins and outs of being a detailed oriented chemist when analyzing complex problems. Also the teaching of numerous chemical strategies and the philosophy of the science are concepts he has bestowed upon me. We have had many discussions about the experimental design, interpreting results, presenting effectively, and writing concisely. Whether it was late at night writing manuscripts, grants, or during group meetings, Tom has constantly taught me to have fun while working hard. Tom, I am eternally grateful for the time you have spent to help cultivate my scientific career and outlook on life.

I would also like to thank my informal advisors: Professor Chris Macosko and Professor Jayanth Panyam. Chris has provided polymer and nanoparticle expertise. He has expanded my scientific reasoning and instilled an end goal/bigger picture mentality when working on a collaborative project. Jayanth has advised and taught me countless pharmaceutical concepts. His guidance in the biological aspect of the project has greatly extended my graduate education. I am very grateful for both of their advice and motivation. I would also like to thank Macosko group students Dr. Zhengxi Zhu, Jing Han, Kevin Pustulka, and

Ge Qu for their efforts on this project. Professor Alon McCormick and Han Seung Lee have provided lots of theoretical discussions and microscopy experiments to visualize the nanoparticles.

I am in debt for the tremendous effort Stephen Kalscheuer has put forth with the cell and animal studies. Not only was Steve a great collaborator he quickly became a friend. I owe him a lot for his assistance any of the biology experiments I executed.

I have had the privilege of working with many talented chemists, both past members as well as current members of the Hoye Group. Adam Wohl bestowed my thesis project and established the foundation of the chemistry in which I built and expanded upon. I thank him for his relentless work on the project and bringing lots of fun to the lab environment! The former group members that have guided me through my initial studies (classwork, written exam) and were astounding role models were Dr. Amanda Schmidt, Dr. Matthew Jansma, Dr. Susana Emond, Dr. Cagri Izgu, and Dr. Susan Brown. More recently helping with their technical expertise and providing helpful discussions were Dr. Patrick Willoughby, Dr. Brian Woods, and Sean Ross.

My family has given me the love and support I need to be successful and have kept me grounded throughout. My wife Maggie has supported me though my entire graduate school and has inspired me by her drive and work ethic. Without their love, understanding, and encouragement I would not be where I am today.

I dedicate this thesis to
my family and my wife.

Abstract

Silicate ester prodrugs are a novel family of labile prodrugs by which both physical (i.e., solubility) and chemical (i.e., rates of hydrolysis back to the parent drug) characteristics may be easily tuned. Block co-polymers of well-defined composition, namely poly(ethylene glycol)-*b*-poly(lactic-*co*-glycolic acid) (PEG-*b*-PLGA), were synthesized to serve as the drug carrier. These innovative drugs and FDA approved polymers have been effectively coupled with a formulation technique known as flash nanoprecipitation (FNP). FNP of a selected silicate ester prodrug of paclitaxel and PEG-*b*-PLGA yields nanoparticles of ca. 120 nm diameter and consisting of ca. 50 wt% of the paclitaxel silicate prodrug. An MDA-MB-231 (breast cancer) cell culture assay was used to demonstrate *in vitro* efficacy of both taxane silicate prodrugs themselves as well as the loaded nanoparticles from FNP. Upon administration to tumor-bearing mice the silicate prodrugs hydrolyze in the tumor microenvironment, thereby releasing the cytotoxic parent drug. Tumor size was monitored via bioluminescence, and the silicate prodrug-containing nanoparticles showed statistically equivalent efficacy (and minimal associated side effects) when compared to equivalent dosings of the commercially used Taxol® and Abraxane®.

The silicate chemistry is not specific to the taxane family of drugs. In the second part of thesis I will present recent findings on this front. The scope of the functional groups selected was based upon the availability of the drugs and the novelty of the subsequent silicate functionalization. The general background of each drug and utility will also be discussed. Finally, in the last section of this thesis, efforts towards the utilization of silicates in the hexadehydro-Diels-Alder (HDDA) reaction are presented.

Table of Contents

List of Tables

List of Figures

List of Schemes

List of Abbreviations

Appendix II: List of Abbreviations

°C	degree Celsius
Ac	acetyl
Ac_2O	acetic anhydride
AcOH	acetic acid
APCI	atmospheric-pressure chemical ionization
app	apparent, in NMR spectroscopy
ATRP	atom transfer radical polymerization
AUC	area under the curve
BCP	block copolymer
BMS	Bristol-Myers Squibb
Bn	benzyl
boc	butoxycarbonyl
br	broad, in NMR spectroscopy
brsm	based on recovered starting material
Bz	benzoyl
Calc'd	calculated
CIJ	confined impingement jet
CIJ-D	confined impingement jet with dilution
clog P	calculated log partition coefficient
CrEL®	Cremophor EL® (i.e., polyoxyethyleneglycerol triricinoleate 35)
CTF	confined tangential flow
d	doublet, in NMR spectroscopy

DAD	diode array detector
DBU	1,8-diazabicyclo[5.4.0]-undec-7-ene
DCC	dicyclohexylcarbodiimide
DCM	dichloromethane
DEAD	diethyl azodicarboxylate
DHA	docosahexaenoic acid
DIAD	diisopropyl azodicarboxylate
DIPC	diisopropylcarboiimide
DLS	dynamic light scattering
DMAP	4-dimethylaminopyridine
DMEM	Dulbecco's Modified Eagle Medium
DMF	*N,N*-dimethylformamide
DMSO	dimethyl sulfoxide
dn/dc	specific refractive index
DSC	differential scanning calorimetry
DTX	docetaxel
EDCI	*N*-(3-dimethylaminopropyl)-*N'*-ethylcarbodiimide hydrochloride
epi	epimer
EPR	enhanced permeation and retention
equiv	equivalent
ESI	electrospray ionization
Et_2O	diethyl ether
Et_3N	triethylamine
EtOAc	ethyl acetate
EtOH	ethanol
FDA	Food and Drug Administration
FNP	flash nanoprecipitation

g	gram(s)
GC	gas chromatography
GC-MS	gas chromatography-mass spectrometry
GPC	gel permeation chromatography
h	hour(s)
HIV	human immunodeficiency virus
HPLC	High Performance Liquid Chromatography
HR ESI-MS	High resolution electrospray ionization-mass spectrometry
HRMS	high resolution mass spectrometry
HSA	Human Serum Albumin
Hz	Hertz
i-Pr (or iPr)	iso-propyl
I.S.	Internal Standard
IC_{50}	half maximal inhibitory concentration
IR	infrared
I.V.	intravenous
J	coupling constant, in NMR spectroscopy
k	rate constant
k_{app}	apparent rate constant
KHMDS	Potassium bis(trimethylsilyl)amide
k_{obs}	observed rate constant
k_{rel}	relative rate constant
LC	Liquid Chromatography
LC-MS	Liquid chromatography-mass spectrometry
LC-MS-MS	Liquid chromatography-(tandem)mass spectrometry
LLE	liquid-liquid Extraction
LOD	limit of detection
log P	log partition coefficient

LOQ	limit of quantification
M	molar
M#	mouse number
m	multiplet, in NMR spectroscopy
MALS	multiangle light scattering
Me	methyl
ACN	acetonitrile
MeOH	methanol
MHz	megahertz
min	minute(s)
MIV	multi-inlet vortex
mmol	millimole(s)
Mn	number average molecular weight
mp	melting point
MPLC	medium pressure liquid chromatography
MS	mass spectrometry
Ms	methanesulfonyl
MS	molecular sieve
MTBD	7-methyl-1,5,7-triazabicyclo[4.4.0]dec-5-ene
MTBE	methyl tert-butyl ether
MTD	maximum tolerated dose
MTS	3-(4,5-dimethylthiazol-2-yl)-5-(3-carboxymethoxyphyenyl)-2-(4-sulfophenyl)-2H-tetrazolium
MTT	3-(4,5-dimethylthiazol-2-yl)-2,5-diphenyltetrazolium bromide
MW	weight average molecular weight
n-Bu (or ^{n}Bu)	normal-butyl
n-Hex (or ^{n}hex)	normal-hexyl
n-Oct (or ^{n}Oct)	normal-octyl

n.d.	not determined
ND	none detected
NHS	*N*-hydroxy-succinimide
nm	nanometer(s)
nM	nano Molar
NMR	nuclear magnetic resonance
PBS	phosphate buffer saline
PCF	plant cell fermentation
PCL	polycaprolactone
PDI	polydispersity index
PEG	poly(ethylene glycol)
PEG-*b*-PLGA	poly(ethylene glycol)-block-poly(lactic-co-glycolic acid)
PEO	poly(ethylene oxide)
PGA	poly(glycolic acid)
Ph	phenyl
PLA	poly(lactic acid)
PLGA	poly(lactic-co-glycolic acid)
PMMA	poly(methyl methacrylate)
PPh_3	triphenylphosphine
ppm	parts per million
PS	Poly(styrene)
PTX	paclitaxel
py	pyridine
q	quartet, in NMR spectroscopy
R	rectus, configuration
Rf	ratio to front
ROTEP	ring opening trans-esterification polymerization
r.t.	room temperature

R.t.	retention time
s	singlet, in NMR spectroscopy
S	sinister, configuration
SAR	structure activity relationship
SDEV	standard deviation
sec	second(s)
SEC	size-exclusion chromatography
SEM	scanning electron microscopy
sept	septet, in NMR spectroscopy
SPE	solid-phase extraction
t	triplet, in NMR spectroscopy
t-Bu (or ^{t}Bu)	tertiary-butyl
$t_{1/2}$	half life time
TBD	1,5,7-triazabicyclo[4.4.0]dec-1-ene
TBS	tertiary-butyldimethyl
TEA (or NEt_3)	triethylamine
TEM	transmission electron microscopy
TEOS	tetraethyl orthosilicate (i.e., tetraethoxysilane)
TES	triethylsilyl
Tf	trifluoromethanesulfonyl
TFA	trifluoroacetic acid
T_g	glass transition
THF	tetrahydrofuran
TIPOS	tetraisopropyl orthosilicate (i.e., triisopropoxysilane)
TIPS	triisopropylsilyl
TLC	thin layer chromatography
T_m	melting transition
TMEDA	tetramethylethylenediamine

TMOS	tetramethyl orthosilicate (i.e., tetramethoxysilane)
TMS	trimethylsilyl
Tol	4-methylphenyl
Ts	p-toluenesulfonyl
Tween® 80	Polysorbate 80
vol%	volume percent
wt%	weight percent

♣ Part I ♣

Anticancer Drug Delivery: Silicon Conjugation, Nanoparticle Formulation, Biological Evaluation

Chapter 1. Paclitaxel Delivery: Background and Motivation

1.1. Cancer Patient Outlook and Statistics

Cancer is the second most frequent cause of death in the United States, trailing heart disease by only 4%.[1] Without belaboring the prevalence of the disease in a variety of tissues, an excerpt of a lengthy table from the American Cancer Society is shown in Table 1.1 below. The estimated number of new cancer cases and the number of deaths for 2014 is broken down by sex and cancer type. In the column next to the total number of cases and deaths, the percentage of the particular type of cancer is calculated in comparison to all sites. From this data, one can quickly see that breast cancer in women is the most prominent of all cancer types. Fortunately, breast cancer is not the leading cause of deaths for patients with any form of cancer. Also highlighted in Table 1.1, lung cancer is the second most common cancer in both men and woman, and also the leading cause for cancer deaths.

Table 1.1 | Cancer statistics [new cases and estimated deaths, US, 2014].[1]

	Estimated New Cases						Estimated Deaths					
	Male		Female		Total		Male		Female		Total	
All Sites	855,220		810,320		1,665,540		310,010		275,710		585,720	
Breast	2,360	0.3%	232,670	29%	235,030	14%	430	0.1%	40,000	15%	40,430	7%
Prostate	233,000	27%	–	–	233,000	14%	29,480	10%	–	–	29,480	5%
Lung & bronchus	116,000	14%	108,210	13%	224,210	13%	86,930	28%	72,330	26%	159,260	27%
Colon & rectum	71,830	8%	65,000	8%	136,830	8%	26,270	8%	24,040	9%	50,310	9%
Urinary bladder	56,390	7%	18,300	2%	74,690	4%	11,170	4%	4,410	2%	15,580	3%
Melanoma of the skin	43,890	5%	32,210	4%	76,100	5%	6,470	2%	3,240	1%	9,710	2%
Kidney & renal pelvis	39,140	5%	24,780	3%	63,920	4%	8,900	3%	4,960	2%	13,860	2%
Non-Hodgkin lymphoma	38,270	4%	32,530	4%	70,800	4%	10,470	3%	8,520	3%	18,990	3%
Oral cavity & pharynx	30,220	4%	12,220	2%	42,440	3%	5,730	2%	2,660	1%	8,390	1%
Thyroid	15,190	2%	47,790	6%	62,980	4%	830	0%	1,060	0.4%	1,890	0%
Leukemia	30,100	4%	22,280	3%	52,380	3%	14,040	5%	10,050	4%	24,090	4%
Pancreas	23,530	3%	22,890	3%	46,420	3%	20,170	7%	19,420	7%	39,590	7%
Liver & intrahepatic bile duct	24,600	3%	8,590	1%	33,190	2%	15,870	5%	7,130	3%	23,000	4%
Esophagus	14,660	2%	3,510	0%	18,170	1%	12,450	4%	3,000	1%	15,450	3%
Ovary	–	–	21,980	3%	21,980	1%	–	–	14,270	5%	14,270	2%
Uterine corpus	–	–	52,630	6%	52,630	3%	–	–	8,590	3%	8,590	1%
Brain & other nervous system	12,820	1%	10,560	1%	23,380	1%	8,090	3%	6,230	2%	14,320	2%

[1] Siegel, R.; Naishadham, D. Cancer Statistics, 2014. *CA Cancer J. Clin.* **2014,** *64,* 9-29.

For the purpose of this thesis, we have chosen to focus our studies toward breast cancer unless otherwise noted. It is of interest to us to determine the frequency an oncologist turns to chemotherapy when treating a breast cancer patient compared to other forms of treatment such as surgery or radiation therapy. The main factor an oncologist is influenced by when prescribing treatment is the progression of the disease.

There are different systems used to diagnose a stage of breast cancer, the most elaborate assesses cancers in three ways: *i.*) the size of the tumor and its growth or incorporation into nearby areas (T), *ii.*) the occurrence of the tumor to regional lymph node (N), and *iii.*) the metastases (M) of the tumor to distant areas. These three criteria make up the TNM staging system, the most commonly used system clinically. Once each value is determined, collectively a stage is diagnosed as I-IV, where stage I is invasive breast cancer and IV is the most advanced of the disease.

Table 1.2 I Female breast cancer treatment patterns by stage, 2008.[2]

	Early Stage (I and II)	Late Stage (III and IV)
BCS alone	10 %	2 %
BCS + RT	30 %	1 %
BCS + RT + chemo	17 %	10 %
Mastectomy alone	17 %	7 %
Mastectomy + chemo	14 %	20 %
Mastectomy + RT	1 %	2 %
Mastectomy + RT + chemo	4 %	31 %
Nonsurgical treatement	6 %	18 %
No treatment	1 %	7 %
Total surgical	93 %	73 %
Total RT	52 %	44 %
Total chemo	35 %	61 %

BCS = breast-conserving surgery, RT = radiation therapy, Chemo = chemotherapy and may include common targeted therapies. Totals may not sum to 100 % due to rounding

Table 1.2, shown below, describes the cases in which an oncologist turns to surgery, radiation therapy, and/or chemotherapy. Interestingly, the first

treatment prescribed is surgery but as the disease progresses the oncologist turns to chemotherapy in hopes to remedy any metastases.[2]

Due to the necessity of chemotherapy to treat breast cancer, it is of great interest to develop brand new anticancer agents, to improve upon the outcome of chemotherapy. Also, the development of sophisticated drug delivery vehicles of current chemotherapeutics has the potential to both mitigate side effects and enhance the therapeutic outcome.

1.2. Challenges of Chemotherapeutic Drug Delivery

Chemistry allows for the creation of "custom" small molecule drugs, which can be tuned at will to alter the physiochemical properties to achieve the desired biological effect. The synthesis of a family of related drugs gives the chemist a clear picture of what can be altered on the pharmacophore of the drug while maintaining activity and gives an understanding of the structure activity relationship of the drug. Through enough iterations of small changes on the drug an optimum candidate is developed, but some side effects can still linger. It is worth mentioning that through an infinite number of small changes a discrete small molecule could be developed to achieve the desired biological effect without any undesirable side effects. To mitigate some of the side effects associated, as well as bypassing a poor physical property with these drugs (water solubility), the notion of packing these toxic molecules in a well-defined delivery vehicle has come to the forefront of anti-cancer research.

Developments in polymer chemistry allows for the synthesis of well-defined macromolecules, which can be used as the drug delivery vehicle. More specifically the polymerization of biocompatible polyesters from a water-soluble

[2] Siegel, R.; Naishadham, D. Cancer Statistics, 2012. *CA Cancer J. Clin.* **2012,** *62,* 10-29. [National Cancer Database, American College of Surgeons Commission on Cancer, **2008** Data Submission.]

polymer initiator is an excellent drug delivery system for many anti-cancer agents. If the carrier macromolecule does not aid in the biological performance of the drug it is referred to as an excipient. Recent advances in placing a tumor-targeting agent on the delivery system has shown to enhance the effectiveness of the excipient performance, much a kin to the use of a zip code in our own mail delivery system. Due to the arsenal of tools available to a chemist namely: *i.*) Synthesis of tailored small drug molecules, *ii.*) Polymerization of well defined macromolecular drug delivery vehicles, and *iii.*) Ability to analytically discern the effectiveness of combining the two materials, the chemistry is the key to create a novel general strategy for the delivery of drugs. However the creation of the system is only one part to the process to birth a new drug formation.

The creation a new formulation for the delivery of chemotherapeutics requires a broad range of expertise due to the monumental tasks of: *i.*) controlling the physical properties of the drug while maintaining the biochemical activitiy *ii.*) creating and optimizing the excipient used to allow for the delivery of the agent *iii.*) determining the efficacy and the overall safety of the formulation. These three tasks require the interdisciplinary approach to make headway in the field of drug delivery. The collaborative effort between chemistry, chemical engineering, and pharmaceutics allows for the design and evaluation of the new formulations discussed in this thesis.

1.3. The Development of Paclitaxel as the Gold Standard

1.3.1 Paclitaxel Discovery

The United States Department of Agriculture screened extracts of parts of the pacific yew tree, *Taxus brevifolia,* for anticancer activity against KB cancer cells in 1962. Cytotoxicity was confirmed and expanded upon via *in vivo* studies of mouse leukemia by Wall in 1966.[3] Pure paclitaxel (**PTX**) extracts were later isolated in 0.01% yield from the bark and found to be the cytotoxic agent. McPhail and co-workers elucidated the structure through degradation strategies to reveal the side chain and the 10-deacetylbaccatin III core, also found in a similar yew tree species.[4] Interest dulled when poor *in vivo* studies came forth, but was revived with the discovery of the unprecedented binding properties of **PTX** by Horwitz in 1979.[5] The agent binds to tubulin monomers to promote the assembly of microtubules, and this stabilization depletes the necessary tubulin concentration required for mitosis. Eventually the restriction of mitosis leads to cell death.[6]

Due to the discovery of microtubule stabilization, poor yields of paclitaxel obtained from the pacific yew, and promising phase I clinical trials the supply of paclitaxel dwindled and new methodology was required to meet the demand for paclitaxel.[4] Both total and semi synthetic strategies were explored, below some notable synthesis are briefly mentioned.

---

[3] Kingston, D. G. I. Taxol, a Molecule for All Seasons. *Chem. Commun.* **2001**, *10*, 867–880.

[4] Kingston, D. G. I. The Shape of Things to Come: Structural and Synthetic Studies of Taxol and Related Compounds. *Phytochemistry* **2007**, *68*, 1844–1854.

[5] Rao, S.; Orr, G. A.; Chaudhary, A. G.; Kingston, D. G.; Horwitz, S. B. Characterization of the Taxol Binding Site on the Microtubule. 2-(M-Azidobenzoyl)Taxol Photolabels a Peptide (Amino Acids 217-231) of Beta-Tubulin. *J. Biol. Chem.* **1995**, *270*, 20235–20238.

[6] Schiff, P. B.; Fant, J.; Horwitz, S. B. Promotion of Microtubule Assembly *in vitro* by Taxol. *Nature* **1979**, *277*, 1–3.

1.3.2 Notable Synthesis of Paclitaxel

Potier and coworkers successfully isolated 10-deacetyl-baccatin III from the needles of the European yew, *T. baccata* which does not require harvesting the bark of the pacific yew tree. Holton's semisynthesis from this renewable resource helped to create a commercially viable supply, but more research was required, to increase the efficiency of the synthesis.[7,8] The final step of this synthesis protected the 7-hydroxyl of **102a** as a triethylsilyl (TES) ether (**102b**), which was then coupled as the lithium alkoxide to the *β*-lactam **101** as shown in Scheme 1.1.[7]

Scheme 1.1 I Holton's semisynthesis from 10-deacetyl-baccatin III.[3]

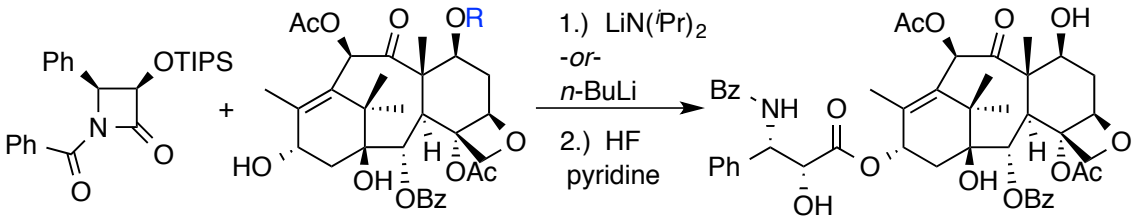

	R
101	
102a	H
102b	TES = $SiEt_3$
	PTX

Holton also developed the first total synthesis of **PTX** from the natural product ß-patchoulene oxide. His synthesis is relatively short (~37 steps) due to the wise choice of this complex starting material.[9]

[7] Holton, R. Semi-synthesis of Taxane Derivatives using Metal Alkoxides and Oxazinones. U.S. Patent 5, 254, 703, October 19, **1993.**

[8] Patel, R. Tour De Paclitaxel: Biocatalysis for Semisynthesis. *Annu. Rev. Microbiol.* **1998**, *98*, 361-395.

[9] Holton, R. A.; Kim, H. B.; Somoza, C.; Liang, F.; Biediger, R. J.; Boatman, P. D.; Shindo, M.; Smith, C. C.; Kim, S. First Total Synthesis of Taxol. 2. Completion of the C and D Rings. *J. Am. Chem. Soc.* **1994**, *116*, 1599–1600.

Nearly simultaneously, Nicolaou published an elegant total syntheis in 1994 (highlights are shown in Scheme 1.2).[10] This convergent synthesis utilizes the two advanced intermediates **104** and **107**, both made via Diels-Alder transformations from starting materials **103** and **105**/**106** respecivielty. These compounds underwent a Shapiro coupling to yield **108,** followed by a McMurry coupling (**108** to **109**) to achieve the baccatin core **109,** which was further derivitized to yield the baccatin III analogue. From the baccatin III bioprecursor **110**, an allylic oxidation and sodium borohydride reduction gave compound **102**. Holton's semisynthetic approach (cf. Scheme 1.1) was then used to synthesize paclitaxel.

Though both of these studies expanded the scope of synthetic methodology, neither was industrially useful to meet the current demand. A plant cell fermentation (PCF) process developed by Bristol-Myers Squibb (BMS) along with the late stage semisynthetic methodology of Holton are utilized to create a large supply of the chemotherapeutic agent.[11]

[10] Nicolaou, K. C.; Yang, Z.; Liu, J. J.; Ueno, H.; Nantermet, P. G.; Guy, R. K.; Claiborne, C. F.; Renaud, J.; Couladouros, E. A.; Paulvannan, K. Total Synthesis of Taxol. *Nature* **1994**, *367*, 630–634.

[11] Venkat, K. In *Pure Appl. Chem.,* Proceedings of the International Conference on Biodiversity and Bioresources, (Phuket), Thialand, November 23-27, **1997**.

Scheme 1.2 | Nicolaou's key intermediates en route of the total synthesis of paclitaxel.[3,10]

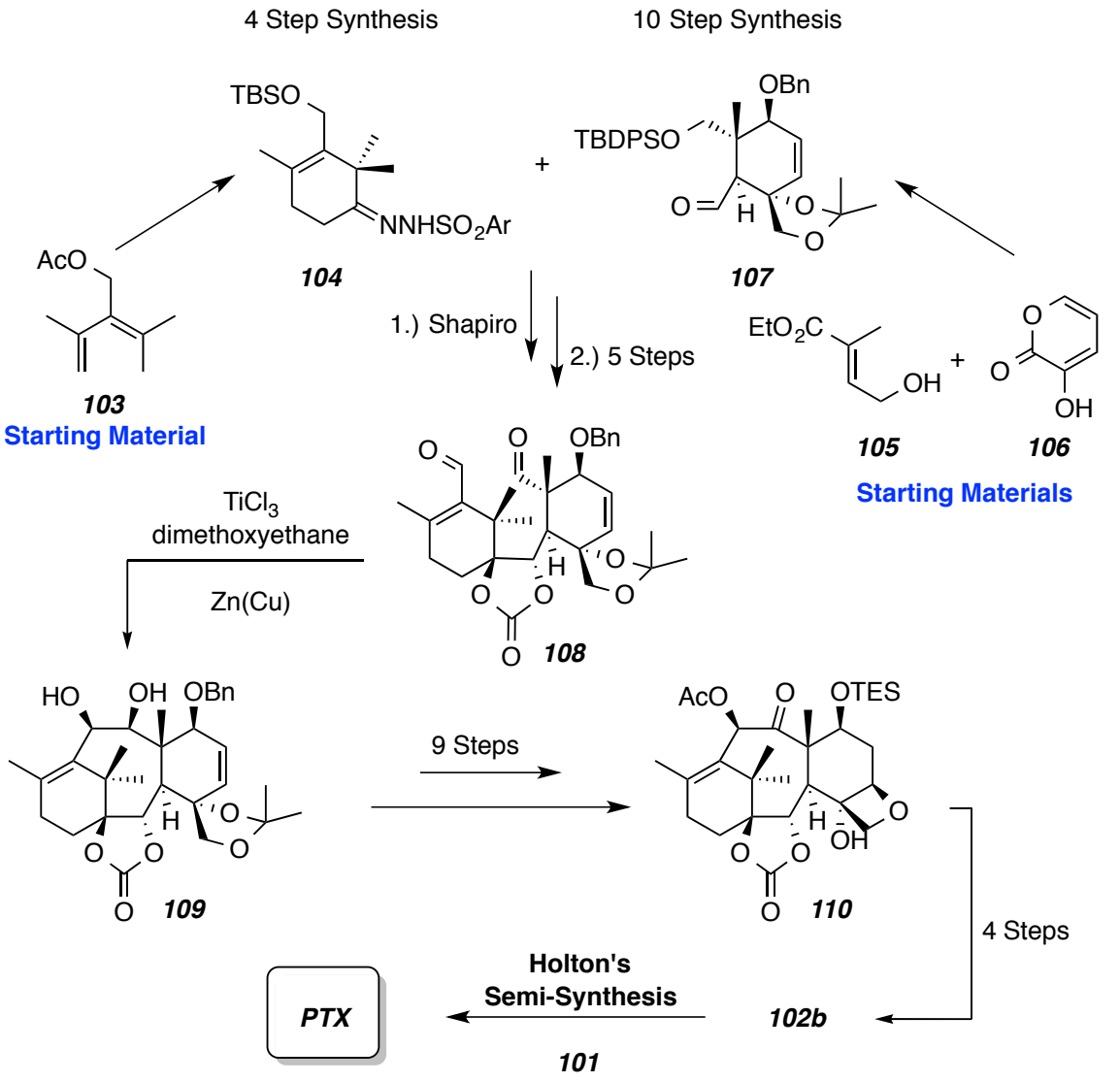

1.3.3 Chemical Derivatization of Paclitaxel

To generate analogues or prodrugs of **PTX**, a full understanding of the chemical reactivity of the molecules needs to be defined. Kingston was the initial investigator to examine the reactivity of PTX to a variety of conditions, which is presented in a clockwise fashion in Scheme 1.3. Kingston fist looked at the oxidation of the three alcohols present in PTX.[12] Initial attempts to oxidize the C-7 hydroxyl to the ketone, involved protecting the C-2' hydroxyl as an ester, followed by deprotection. However, when the C-2' hydroxyl was successfully protected as the acetate ester, they had difficulty removing it following the oxidation at C-7.[12] Instead of protecting the C-2' hydroxyl; when **PTX** alone is reacted with Jones reagent, the C-7 hydroxyl oxidizes cleanly to the C-7 oxo-derivative **111** shown in Scheme 1.3. The Kingston group could also oxidize the C-2' position, however an excess of the Jones reagent and prolonged reaction times were required. They ultimately conclude that the C-2' secondary-alcohol is less reactive due to its alpha position to carbonyl (C-1').

Lastly, from the C-7 oxo-PTX 111 they were able to open up the oxetane ring by treatment with 1,8-diazabicyclo[5.4.0]-undec-7-ene (DBU) to form **112**. Attempts were made with mild aqueous bases, however without the basicity of DBU the reactions lead to a mixture of products.[12] The seco-PTX derivative **112** was of great interest to probe the importance of the conformationally-rigid oxetane ring on the biological activity. All attempts to reduce the C-7 ketone of **112**, provided complex mixtures due to the reactivity of the other functional groups present in **112**.

Derivatives at C-13 are desirable to probe the side chain bioactivity of **PTX**. Researchers could capitalize on the semi-synthesis of Holton by reacting baccatin III with a variety of *β*-lactams (c.f. Scheme 1.1) to install different C-13 side chains, however the baccatin III precursor is isolated in a low yield from the

[12] Magri, N. F.; Kingston, D. G. I. Modified Taxols. 2. Oxidation Products of Taxol. *J. Org. Chem.* **1986**, *51*, 797–802.

pacific yew tree needles.[13] The Kingston group experimented with **PTX** to determine the lability of the C-13 ester linkage to obtain baccatin III (116, Scheme 1.3). Initial attempts at solvolysis of PTX with sodium isopropoxide in isopropanol yielded a mixture of the desired baccatin III (**116**) and the epimer baccatin V (**115**) as well as the cleaved side chain to give carboxylic acid **113**. If the reaction was allowed to react for an extended time, more of the baccatin V (**115**) was obtained, so they abandoned this route.[14]

Interestingly, the Kingston group showed that the C-13 side chain could be reductively cleaved when **PTX** is reacted with a borohydride reagent. Upon further optimization of the reducing agent, they found that tetrabutylammonium borohydride produced a 97% yield of baccatin III (**116**), a minor amount of 115, and the diol **114**. Isolation of the diol **114** proved that the cleavage occurs reductively and not through hydrolysis of the ester. They conclude that the C-2' hydroxyl at the α position is required for the reductive cleavage, which also shows the enhanced lability compared to the C-2, C-4, and C-10 esters. To further prove this assistance of the C-2' hydroxyl, the reductive cleavage at C-13 did not occur when the C-2' was acetylated. Lastly, baccatin III (**116**) was acetylated with excess acetic anhydride (AcO_2), pyridine (py), and 4-(dimethylamino)pyridine (DMAP) to give the C-7 mono-acetylated product **117** first, followed by the C-13 and C-7 bis-acetylated product **118** when heat was applied to the reaction. Not only did this experiment settle the contradictory reactivity differences that two different groups reported, it showed that the C-7 hydroxyl is more nucleophilic than the C-13 hydroxyl and must be protected to install a different side chain at C-13.[14]

Attempts at epimerization of the C-2' methine of PTX proved challenging.[13] They first protected both of the reactive hydroxyls with 2,2,2-trichloroethyl

[13] Magri, N. F.; Kingston, D. G. Modified Taxols, 4. Synthesis and Biological Activity of Taxols Modified in the Side Chain. *J. Nat. Prod.* **1988**, *51*, 298–306.

[14] Magri, N. F.; Kingston, D. G. I.; Jitrangsri, C.; Piccariello, T. Modified Taxols. 3. Preparation and Acylation of Baccatin III. *J. Org. Chem.* **1986**, *51*, 3239–3242.

chloroformate (**119**) to give them the bis-trichloroethylcarbonates of **PTX**, namely PTX-2',7-[$COOCH_2CCl_3$]$_2$ (**120**). Unfortunately, treatment of **120** with DBU did not epimerize the more reactive methine at C-2', instead deprotonation of the amide at C-3' occurred. The resulting amide anion at C-3' cyclized onto the carbonate and elimination of 2,2,2-trichloroethan-1-ol gave the oxazolidinone derivative of PTX. Removal of the protecting group at C-7 with zinc dust and acetic acid afforded analogue **121**. Although interesting in structure, the compound was inactive in the KB cancer cells showing a cytotoxicity that was 20,000 fold less potent when compared with **PTX**.[13]

The Kingston lab also looked at the nuceophilic character of PTX by reacting it with four electrophilic reagents.[15] When reacted with acetyl chloride, surprisingly they obtained drastically rearranged product. To probe the structure, systematic studies were conducted.

The bis-protection of **PTX** was achieved by reacting with excess triethylsilyl chloride (TES–Cl) and imidazole (imid.) to obtain the PTX-2',7-[$Si(Et)_3$]$_2$ compound (not shown). After isolation, the C-1 hydroxyl was converted to the mesylate by the reaction with methanesulfonyl chloride (Ms–Cl) and triethylamine (TEA) at -15 ˚C. Upon warming to 0 ˚C, an elimination occurred through a rearrangement of the A-ring of **PTX** which gave **122a**. Deprotection of the silylethers using pyridinium floride gave the skeleton **122b**. The ^{1}H-NMR of this rearranged product matched with the A-ring protons when **PTX** was reacted with acetylchloride, however there was significant difference in the spectrum at the oxetane ring. Interestingly, the tubulin depolymerization protein assay of **122** showed only a 3-fold decrease in potency compared to **PTX**. However like **121**, when the compound was exposed to the entire cell (KB cell culture assay) it showed that rearranged product **122** was not cytotoxic.[15]

[15] Samaranayake, G.; Magri, N. F.; Jitrangsri, C.; Kingston, D. G. I. Modified Taxols. 5. Reaction of Taxol with Electrophilic Reagents and Preparation of a Rearranged Taxol Derivative with Tubulin Assembly Activity. *J. Org. Chem.* **1991**, *56*, 5114–5119.

Scheme 1.3 I Synthetic transformations of **PTX** from "modified taxols by David G. I. Kingston."[12,13,14,15]

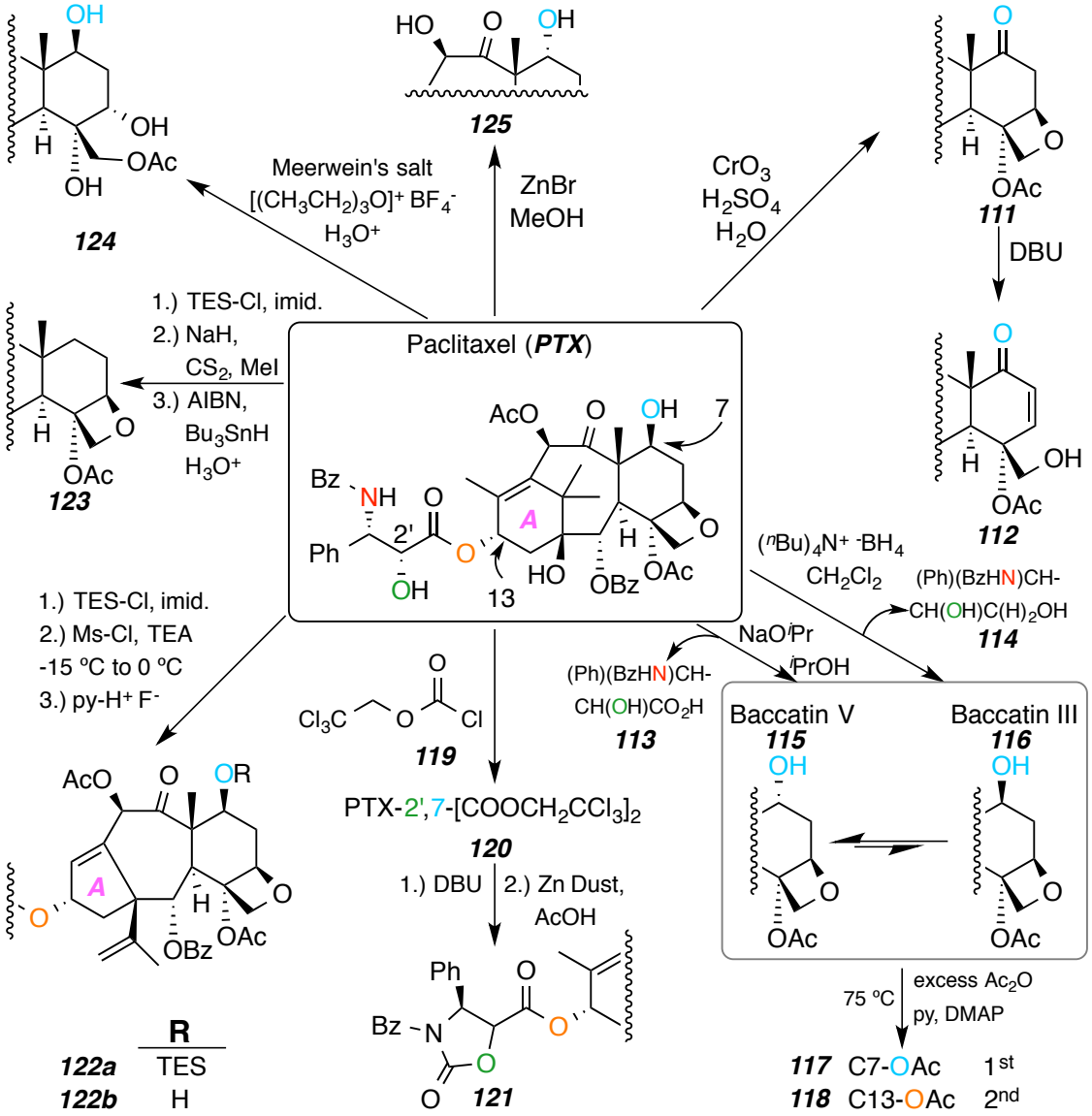

To explore the fate of the oxetane ring under the acetyl chloride conditions, **PTX** was reacted with Meerwein's salt (triethyloxonium tetrafluoroborate) to afford the ring opened and rearranged product **124**. They hypothesize the product arises through the alkylation of the oxetane ring to the oxonium ion, participation of the neighboring acetoxy group to form the ortho-ester that upon hydrolysis in acidic media cleanly gives **124**. The ^{1}H-NMR shifts matched closely with their acetyl chloride conditions. This ring opened derivative

124 showed essentially no activity in either the tubulin depolymerization or the *in vitro* assay.[15] The mildest set of conditions for the reaction of PTX with an electrophilic reagent (zinc bromide in methanol) epimerized the C-7 hydroxyl and also deacetylated the C-10 position to gave **125** as the major compound (likely through solvolysis with methanol). The epimer retained cytotoxicity when compared to **PTX**.[15]

To understand the role of the C-7 hydroxyl for the biological activity of **PTX**, the Kingston group removed it. A mono-protection at the C-2' hydroxyl of **PTX** was quantitatively accomplished with TES-Cl and imidazole. Treatment of the mono-silyl protected **PTX** with sodium hydride (NaH) followed by an excess of the carbon disulfide (CS_2) and methyliodide (MeI) yielded a S-methyl xanthate which could be removed through radical chemistry pioneered by Barton. The S-methyl xanthate of **PTX** was removed by tributyltin initiated by azobis-isobutyronitrile (AIBN) at 75 ˚C. Deprotection of the C-2' silyl ether with dilute acid yieled the C-7 deoxypaclitaxel **123**. The deoxy-PTX **123** was found to be more cytotoxic than that of the **PTX** by 40 fold in the P-388 leukemia cell assay. This suggests that the C-7 hydroxyl is not required to retain biological activity.[16]

Kingston also explored the use of water soluble prodrugs,[17] a method for seperating **PTX** from other Taxane analogues,[18] the Deacylation and Reacylation of Baccatin III,[19] and the use of 7-substituted photoaffinity analogues of **PTX**.[20],[21]

---

[16] Chaudhary, A. G.; Rimoldi, J. M.; Kingston, D. G. I. Modified Taxols. 10. Preparation of 7-Deoxytaxol, a Highly Bioactive Taxol Derivative, and Interconversion of Taxol and 7-Epi-Taxol. *J. Org. Chem.* **1993**, *58*, 3798–3799.

[17] Zhao, Z.; Kingston, D. G. I.; Crosswell, A. R. Modified Taxols, 6. Preparation of Water-Soluble Prodrugs of Taxol. *J. Nat. Prod.* **1991**, *54*, 1607–1611.

[18] Kingston, D. G.; Gunatilaka, A. A.; Ivey, C. A. Modified Taxols, 7. a Method for the Separation of Taxol and Cephalomannine. *J. Nat. Prod.* **1992**, *55*, 259–261.

[19] Samaranayake, G.; Neidigh, K. A.; Kingston, D. G. Modified Taxols, 8. Deacylation and Reacylation of Baccatin III. *J. Nat. Prod.* **1993**, *56*, 884–898.

[20] Rimoldi, J. M.; Kingston, D. G.; Chaudhary, A. G.; Samaranayake, G.; Grover, S.; Hamel, E. Modified Taxols, 9. Synthesis and Biological Evaluation of 7-Substituted Photoaffinity Analogues of Taxol. *J. Nat. Prod.* **1993**, *56*, 1313–1330.

All of which lead to a firm understanding of the structure activity relationship of **PTX** summarized below.

1.3.4 Structure Activity Relationship

The total synthesis of paclitaxel showed the power of synthetic organic chemistry and also provided intermediate compounds, which were evaluated for activity against cancer cells. All of the insight gained from the total syntheses of **PTX**, derivatization studies, and activity studies of the intermediates led to an understanding of the drug's structure activity relationship (SAR).[3] The most relevant observations from the SAR studies are described in (Figure 1.1).

The structure consists of a complex fused ring system and an amide tail, both of which are important for cytotoxicity. The oxetane ring creates rigidity in the rest of the **PTX** structure and causes the C-4 position acetate to be in the proper orientation to serve as a hydrogen bond acceptor to the tubulin protein. The C-7 oxygen is not critical for activity, but swapping it for a larger atom greatly reduces the potency.[3,16] A tight non-covalent binding of **PTX** to the protein is essential for any activity, the two accessible hydroxyl groups located at the 2' and 7 positions on the molecule have a varying tolerance for modification, due steric space available (C-7 hydroxyl) or for hydrogen bonding (C-2' hydroxyl). Alteration of the 7-position hydroxyl has shown that the activity remains when esterified with a small group, epimerized, or even removed. The 2'-hydroxyl, the most reactive of the three hydroxyls, shows very little tolerance to retain activity once modified. Interestingly, acetylation of the 2'-hydroxyl shows similar activity to the parent suggesting that the small analogues at the 2' position can be made as long as there is steric space and the electronics allow for hydrogen binding to the

[21] Kingston, D. G. I.; Jagtap, P. G.; Yuan, H.; Samala, L. The Chemistry of Taxol and Related Taxoids. Progress in the Chemistry of Organic Natural Products; Springer Vienna: Vienna, **2002**, *84*, 53–225.

protein.[22] The functionalities highlighted in green can be altered without a significant loss in activity, and in many cases improves the potency. By utilizing the SAR, derivatives have been created in attempts to boost or alter activity, stability, solubility, absorption, distribution, metabolism, and excretion.

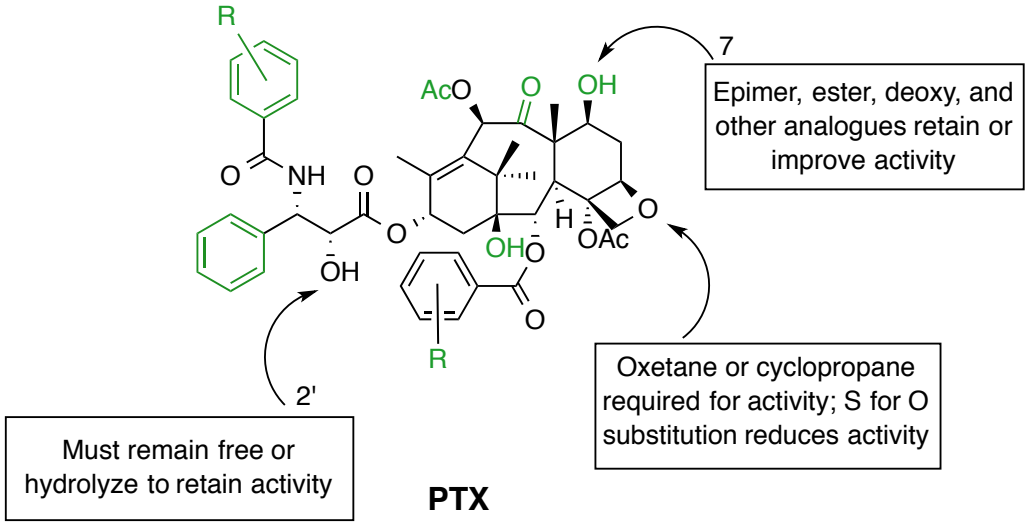

Figure 1.1 | The structure activity relationship of paclitaxel (adapted from ref. 3,4)

1.3.5 Paclitaxel Analogues

Many researches have developed analogues of paclitaxel by utilizing the information gained during the detailed the SAR experiments. The most successful analogue is the closely related compound docetaxel (**DTX**). Building off of Holton's semisynthesis (cf., Scheme 1.1), **102** is protected and esterified with a highly functionalized side chain. After the selective deprotection of both benzyl groups and subsequent Boc protection of the resulting free amine, **DTX** is synthesized in good yield (Figure 1.2).[23] This synthetic analogue improves upon the poor hydrophilicity found in **PTX** by swapping the benzoyl group for the

[22] Snyder, J. P.; Nettles, J. H.; Cornett, B.; Downing, K. H.; Nogales, E. The Binding Conformation of Taxol in Beta-Tubulin: a Model Based on Electron Crystallographic Density. *Proc. Natl. Acad. Sci. U.S.A.* **2001**, *98*, 5312–5316.

[23] Sisti, N. Method for Docetaxel Synthesis. U.S. Patent 5,688,977, November 18, **1997**.

butoxycarbonyl at the C-3' nitrogen and removing the acetyl at C-10.[24] This compound is currently formulated and given clinically as Taxotere® which will be discussed in Chapter 1.4.

A less developed analogue of **PTX**, (BMS-184476) **126**, utilizes a thio-methyl ether at the C-7 hydroxyl position which has been shown to improve cytotoxicity and overcomes drug resistance in multiple cell lines.[25] The derivative **126** can be synthesized in three steps from **PTX**. First a TES protection of the C-2' hydroxyl is required; then treatment with methylthiomethyl ether and deprotection of the TES ether provides **BMS-184476** (**126**) in good yield.[26]

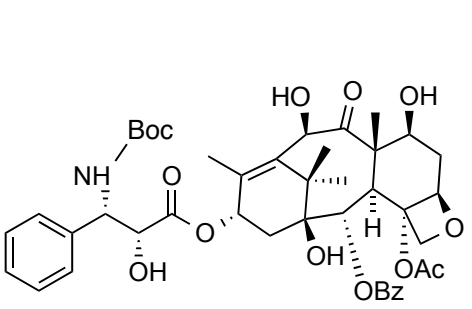

Docetaxel (DTX)

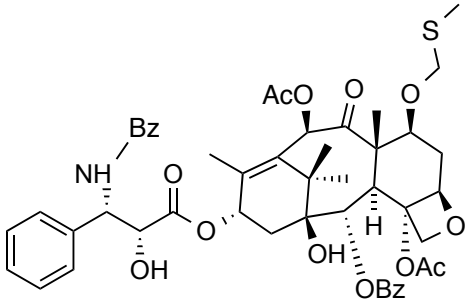

BMS-184476

126

Figure 1.2 l Synthetic taxane analogues that are in the clinic or in clinical trials.

1.3.6 Second Generation and Beyond: Derivatives of Paclitaxel

The brief set of paclitaxel analogues shown in chapter 1.3.4 contain minor variations to the paclitaxel pharmacophore and are currently used in the clinic or are in clinical trials. Later generations of **PTX** derivatives have been developed

[24] Sparreboom, A.; van Tellingen, O.; Nooijen, W. J.; Beijnen, J. H. Preclinical Pharmacokinetics of Paclitaxel and Docetaxel. *Anti-cancer Drugs* **1998**, *9*, 1-17.

[25] Rose, W.; Fairchild, C.; Lee, F. Y. F. Preclinical Antitumor Activity of Two Novel Taxanes. *Cancer Chemoth. and Pharm.* **2001**, *47*, 97-105.

[26] Altstadt, T. J.; Fairchild, C. R.; Golik, J.; Johnston, K. A.; Kadow, J. F.; Lee, F. Y.; Long, B. H.; Rose, W. C.; Vyas, D. M.; Wong, H.; Wu, M.-J.; Wittman, M. D. Synthesis and Antitumor Activity of Novel C-7 Paclitaxel Ethers: Discovery of BMS-184476. *J. Med. Chem.* **2001**, *44*, 4577–4583.

for the potential of a drastic increase in potency accompanied with better biophysical properties.[27] Most notably, the work of both Ojima[28] and Georg[29] capitalizes on the SAR studies to synthesize molecules that have cytotoxicity against cancer lines that have a resistance to **PTX**.

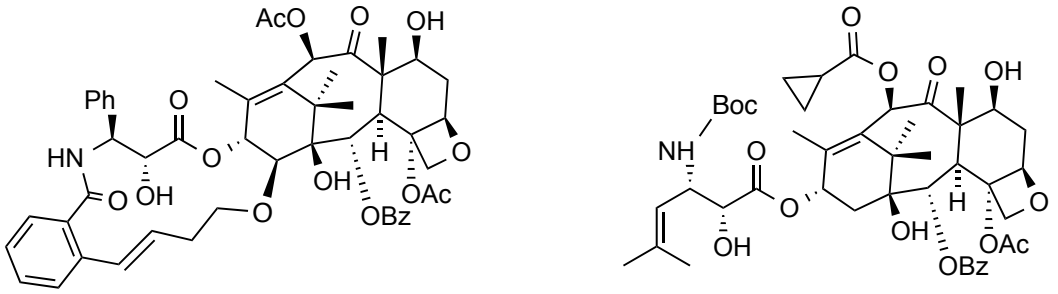

SB-T-2054 ***SB-T-1214***

127 ***128***

Figure 1.3 l Second and third generation **PTX** analogues.

Although these compounds have significantly improved the shortcomings of **PTX** in some aspects, the biophysical properties are not ideal and further the need for excipients to effectively solubilize the drug for *in vivo* studies. More importantly the lack of specificity for tumor cells as opposed to healthy cells, requires further modification. Creating prodrugs from **PTX** is a *different* approach for the safe delivery of **PTX** to cancer cells. Instead of optimizing analogues to give the ideal biophysical properties, one makes a temporary modification to the drug.

[27] Kingston, D. G. I. A Natural Love of Natural Products. *J. Org. Chem.* **2008**, *73*, 3975–3984.

[28] Ojima, I.; Das, M. Recent Advances in the Chemistry and Biology of New Generation Taxoids *J. Nat. Prod.* **2009**, *72*, 554–565.

[29] Rice, A.; Liu, Y.; Michaelis, M. L.; Himes, R. H.; Georg, G. I.; Audus, K. L. Chemical Modification of Paclitaxel (Taxol) Reduces P-Glycoprotein Interactions and Increases Permeation Across the Blood-Brain Barrier in Vitro and in Situ. *J. Med. Chem* **2005**, *48*, 832–838.

1.4. Common strategies used to make PTX prodrugs

Prodrugs are derivatives of a compound that temporarily change the physical and biological properties of the parent drug. Upon exposure to an external stimulus such as enzymatic degradation, metabolism, near infrared light (NIR), or simple water hydrolysis, the bioactive parent drug is released.[30] Specifically, **PTX** is typically modified at either the 2'- or the 7- hydroxyl due to synthetic accessibility. The prodrugs most commonly created from the derivatization of **PTX** aim to improve upon the poor water solubility of the parent drug; thus the major focus in this area of research has been to attach hydrophilic groups to **PTX**.

A less common prodrug approach is to improve the specificity of **PTX** towards cancer cells. To meet this broad goal, researchers have made prodrugs of **PTX** by functionalization with tumor targeting agents[31] or antibodies.[32] The targeting agents used serve the purpose to either *i.*) guide the therapeutic agent (**PTX**) to the cancer sight, thereby localizing a large concentration of the drug, or *ii.*) to provide a transport mechanism across the cancer cell wall, for the selective uptake to tumor tissues.

Figure 1.4 below summarizes strategies used to temporarily alter the chemical and biological properties of **PTX** until chemical cleavage occurs.[33] The general Figure is read in a clockwise fashion as the molecular increases from small molecule prodrugs, isomer conjugates, small molecule tumor targeting

[30] Sinkula, A. A.; Yalkowsky, S. H. Rationale for Design of Biologically Reversible Drug Derivatives: Prodrugs. *J. Pharm. Sci.* **1975**, *64*, 181–210.

[31] Majumdar, S.; Duvvuri, S.; Mitra, A. K. Membrane transporter/ receptor-targeted prodrug design: strategies for human and veterinary drug development. *Adv. Drug Delivery Rev.* **2004**, *56*, 1437-1452.

[32] Schmidt, F.; Ungureanu, I.; Duval, R.; Pompon, A.; Monneret, C. Cancer Chemotherapy: a Paclitaxel Prodrug for ADEPT (Antibody-Directed Enzyme Prodrug Therapy). *Eur. J. Org. Chem.* **2001**, *2001*, 2129–2134.

[33] Skwarczynski, M.; Hayashi, Y.; Kiso, Y. Paclitaxel Prodrugs: Toward Smarter Delivery of Anticancer Agents. *J. Med. Chem.* **2006**, *49*, 7253–7269.

agents, macromolecule (peptide, polymer, and protein) conjugates, and lastly the up and coming field of antibody-drug conjugates.[34]

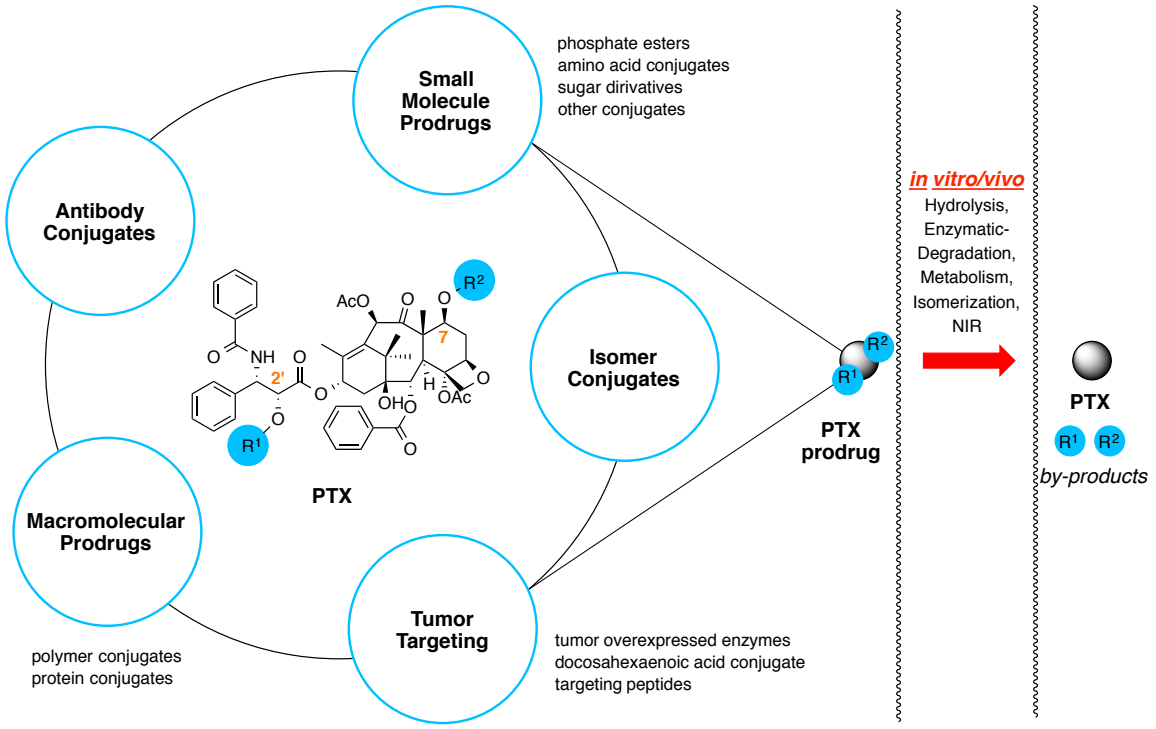

Figure 1.4 I Prodrug chart shows 5 prodrug strategies of paclitaxel (modified from ref. 33).

Many different prodrugs have capitalized on the reactivity of the 2' and 7 hydroxyls of **PTX** with the common goal to deliver the drug exclusively to tumor cells thereby reducing problematic side effects. Keeping the SAR (cf., Figure 1.1) in mind, it has been observed that R^1 (Figure 1.1) must be cleaved under physiological conditions to return the free hydroxyl and to maintain biological activity. This 2'-OH is critical for the potency of the drug due to hydrogen bonding with the amino acid residues of the α- and β-tubulin.[35] The R^2 group can

[34] Yewale, C.; Baradia, D.; Vhora, I.; Misra, A. Proteins: Emerging Carrier for Delivery of Cancer Therapeutics. *Expert. Opin. Drug Deliv.* **2013**, *10*, 1429–1448.

[35] Xiao, H.; Verdier-Pinard, P.; Fernandez-Fuentes, N.; Burd, B.; Angeletti, R.; Fiser, A.; Horwitz, S. B.; Orr, G. A. Insights Into the Mechanism of Microtubule Stabilization by Taxol. *Proc. Natl. Acad. Sci. U.S.A.* **2006**, *103*, 10166–10173.

be varied and does not necessarily need to be cleaved.[3] Examples of derivatives at these positions include phosphate esters,[36] amino acids,[37] sugars,[38] bioactive precursors,[39] tumor tissue targeting agents,[40, 41] antibodies,[42] and polymer conjugates.[43]

To render hydrophobic drugs water soluble, phosphate salts serve as exceptional prodrugs. Specifically, synthesis of the prodrug is achieved through the treatment of **PTX** with LDA at -30 °C to form the dianion followed by addition of dibenzyl pyrophosphate. Hydrogenolysis of the benzyl group to afford the corresponding acids and conversion into the sodium salts gave compounds **129** or **129'** (Figure 1.5). This approach was taken to acquire the phosphate at the 2' or 7 hydroxyl group, after initial attempts using standard phosphorylation conditions such as using $POCl_3$ failed.[45] The phosphate esters are thought to be cleaved enzymatically by endogenous phosphatases that revert the prodrug to the parent compound and the corresponding benign byproducts. Although the water solubility increased for **129**, phosphatases could not cleave the phosphate esters, presumably due to the steric hindrance of **PTX**, resulting in decreased

[36] Vyas, D. M.; Wong, H.; Crosswell, A. R.; Casazza, A. M.; Knipe, J. O.; Mamber, S. W.; Doyle, T. W. Synthesis and Antitumor Evaluation of Water Soluble Taxol Phosphates. *Bioorg. Med. Chem. Lett.* **1993**, *3*, 1357–1360.

[37] Paradis, R.; Pagé, M. New Active Paclitaxel Amino Acids Derivatives with Improved Water Solubility. *Anticancer Res.* **1998**, *18*, 2711–2716.

[38] de Bont, D. B. A.; Leenders, R. G. G.; Haisma, H. J.; van der Meulen-Muileman, I.; Scheeren, H. W. Synthesis and Biological Activity of β-glucuronyl Carbamate-based Prodrugs of Paclitaxel as Potential Candidates for ADEPT. *Bioorg. Med. Chem. Lett.* **1997**, *5*, 405–414.

[39] Hayashi, Y.; Skwarczynski, M.; Hamada, Y.; Sohma, Y.; Kimura, T.; Kiso, Y. A Novel Approach of Water-soluble Paclitaxel Prodrug with No Auxiliary and No Byproduct: Design and Synthesis of Isotaxel. *J. Med. Chem.* **2003**, *46*, 3782–3784.

[40] Hemamalini, S.; Chander, M.; Baker, S.; He, L. Tumor Targeting by Covalent Conjugation of a Natural Fatty Acid to Paclitaxel. *Clin. Cancer Res.* **2001**, *7,* 3229–3238.

[41] Bradley, M.; Swindell, C.; Anthony, F. Tumor targeting by Conjugation of DHA to Paclitaxel. *J. Control. Release* **2001**, *74*, 233-236.

[42] Dubowchik, G.; Mosure, K.; Knipe, J. Cathepsin B-sensitive Dipeptide Prodrugs. 2. Models of Anticancer Drugs Paclitaxel (Taxol®), Mitomycin C and Doxorubicin. *Bioorg. Med. Chem. Lett.* **1998**, *8*, 3347-3352.

[43] Greenwald, R.; Choe, Y.; McGuire, J. Effective Drug Delivery by PEGylated Drug Conjugates. *Adv. Drug Deliver. Rev.* **2003**, *55*, 217-250.

efficacy.[36] To combat these issues Bristol-Myers Squibb (BMS) is researching conjugation of phosphate esters to paclitaxel via long hydrocarbon linkers, in hopes that greater steric accessibility will allow the enzymes to cleave the prodrug.[44]

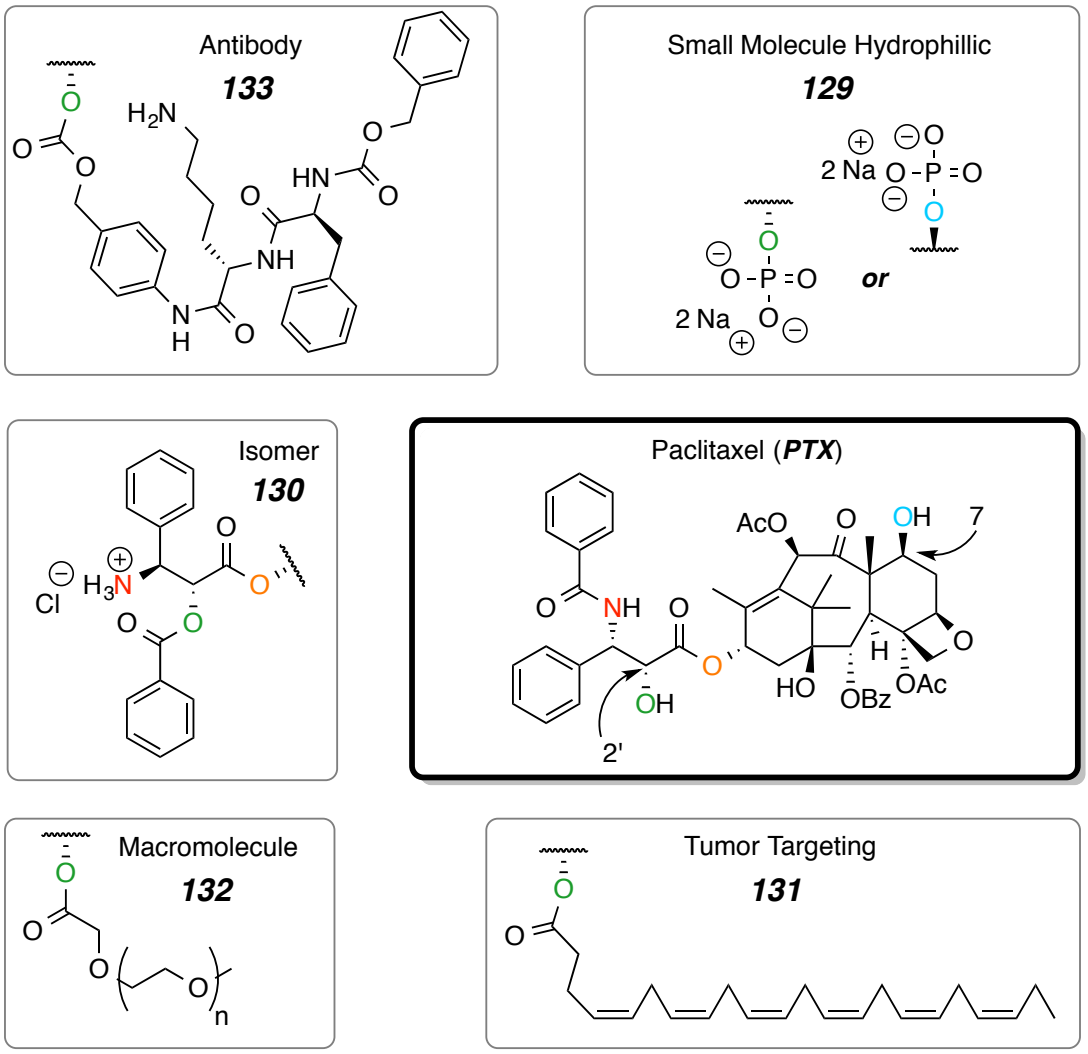

Figure 1.5 I Prodrug conjugates of paclitaxel corresponding to the 5 different categories (small molecule, isomers, tumor targeting, macromolecules, antibody).

[44] Vyas, D. M.; Ueda, Y.; Wong, H.; Matiskella, J. D.; Hauck, S.; Mikkilineni, A. B.; Farina, V.; Rose, W. C.; Casazza, A. M. *ACS Symposium Series*; Georg, G. I.; Chen, T. T.; Ojima, I.; Vyas, D. M., Eds. ACS Symposium Series, 1947 American Chemical Society: Washington, DC, 2009; Vol. 583, pp. 124–137.

Isotaxel (**130**, Figure 1.5) uses a very clever approach to prodrug strategy, in that it avoids additional functionalization of the parent drug all-together. To accomplish the temporary change in physical properties without adding in additional moieties on the drug, Isotaxel **130** utilizes isomerization chemistry. The taxane is an isomer of paclitaxel with the benzoyl group linked to the 2'-hydroxyl instead of the amine at the 3' position. The free amine is then converted to the hydrochloride salt so that it is much more water-soluble. Upon *in vivo* administration, the Isotaxel is isomerized back to **PTX** through an O-N intramolecular acyl migration.[45] The efficacy of **130** is dependent on the rate of re-isomerization, which is pH dependent.[39]

To capitalize on the temporary functionalization of the prodrugs, research has focused on biasing **PTX** to accumulate in tumor tissue preferentially over healthy tissue. For example, the covalent binding of **PTX** to a tumor-targeting agents such as biotin **429** or folic acid has been developed.[46] These targeting agents exploit the minor yet real differences between healthy cells and cancer cells. It has been shown that cancer cells over-express many different enzymes and receptors, and passively uptake macromolecules more easily than healthy cells.[47] Also cancer cells have lower concentrations of oxygen and a lower pH.[48,49] These differences can be taken advantage of to allow for selective delivery of the prodrug. Since tumor tissues require a large energy supply to

[45] Skwarczynski, M.; Sohma, Y.; Kimura, M.; Hayashi, Y.; Kimura, T.; Kiso, Y. O–N Intramolecular Acyl Migration Strategy in Water-soluble Prodrugs of Taxoids. *Bioorg. Med. Chem. Lett.* **2003**, *13*, 4441–4444.

[46] Yashveer Singh, M. P. P. J. S. Recent Trends in Targeted Anticancer Prodrug and Conjugate Design. *Curr. Med. Chem.* **2008**, *15*, 1802.

[47] Carvalho, I.; Milanezi, F.; Martins, A.; Reis, R. M.; Schmitt, F. Overexpression of Platelet-Derived Growth Factor Receptor Alpha in Breast Cancer Is Associated with Tumour Progression. *Breast Cancer Res.* **2005**, *7*, R788–R795.

[48] Jin, S.; Wan, J.; Meng, L.; Huang, X.; Guo, J.; Liu, L.; Wang, C. Biodegradation and Toxicity of Protease/Redox/pH Stimuli-Responsive PEGlated PMAA Nanohydrogels for Targeting Drug Delivery. *ACS Appl. Mater. Interfaces* **2015**, ASAP.

[49] Xiong, M.-H.; Bao, Y.; Du, X.-J.; Tan, Z.-B.; Jiang, Q.; Wang, H.-X.; Zhu, Y.-H.; Wang, J. Differential Anticancer Drug Delivery with a Nanogel Sensitive to Bacteria-Accumulated Tumor Artificial Environment. *ACS Nano* **2013**, *7*, 10636–10645.

keep up with rapidly growing vasculature and size,[50] conjugating **PTX** with a fatty acid side chain has proved very useful. The prodrug **131** (Figure 1.5) shows the lengthy hydrophobic docosahexaenoic acid appended to the 2'-hydroxyl position of **PTX**, which is hydrolytically cleaved during the metabolism of the fatty acid.[40] Interestingly, this prodrug has an improved solubility in plasma; therefore, less surfactant is needed to administer the drug, which will be discussed further in Chapter 1.4.

The prodrug that has shown the most significant improvement in water solubility of **PTX** is the covalent linkage to a hydrophilic macromolecule, a poly(ethyleneglycol) (PEG), which yields prodrug **132** (Figure 1.5). When the 2' hydroxyl is bonded to a 5 kDa PEG-polymer, the solubility increases significantly. An impressive 660 mg of the conjugate can dissolve in 1 mL of water, which is ca. 95 mg/mL **PTX**.[43] This clearly shows the utility of conjugation of **PTX** to a PEG polymer, since the typical water solubility of **PTX** is merely 0.25 - 0.56 mg/mL.[44,51] *In vitro* studies also showed great promise, with an IC50 of 15 nM and 17 nM in the P388/O and L1210/O cancer cell lines respectively, compared with free PTX (6 nM, 6 nM).[52] However, *in vivo* testing showed less efficacy than the commercial paclitaxel formulation.

Currently being explored is the linkage of prodrug **133** (Figure 5) with mono clonal antibodies (mAbs).[42] To develop these large antibody complexes, the benzyl protected short amino acid linker **133** has been conjugated to **PTX**. After deprotection and reductive amination of **133** with a mono-clonal antibody, the complex targeting agent is formed. When the antibody cytotoxic agent binds to the antigen, the drug is actively transported into the cell where, upon

[50] Garber, K. Energy Deregulation: Licensing Tumors to Grow. *Science* **2006**, *312*, 1158–1159.

[51] Damen, E. W. P.; Wigerinck, P. H. G.; Braamer, L.; Sperling, D.; de Vos, D.; Scheeren, H. W. Paclitaxel Esters of Malic Acid as Prodrugs with Improved Water Solubility. *Bioorg. Med. Chem. Lett.* **2000**, *8*, 427–432.

[52] Greenwald, R. B.; Pendri, A.; Bolikal, D. Highly Water Soluble Taxol Derivatives: 2′-Polyethyleneglycol Esters as Potential Prodrugs. *Bioorg. Med. Chem. Lett.* **1994**, *4,* 2465–2470.

hydrolysis, the parent drug is released.[53] This strategy gives good insight into the development of polypeptide/antibody polymer conjugates that we plan to explore for delivery of our formulation (Chapter 4, Future Outlook).

Although these prodrugs serve as a guide for developing hydrophilic prodrugs of **PTX**, it should be noted that the main topic of this thesis is to create prodrugs that are more hydrophobic than the parent compound (Chapter 2) for formulation into nanoparticles. The development of small molecule hydrophobic and hydrolytically labile silicate prodrugs of **PTX** will be discussed in Chapter 3 of this thesis. Extrapolating from the traditional prodrug research suggests that the modification may occur on either or both the 2' and/or 7 positions can be functionalized to yield a hydrophobic prodrug. Although creating a prodrug that is less water-soluble may seem counter productive, it is advantageous in the context of nanoparticle drug delivery. Current clinical formulations discussed below, show the need for better formulations of PTX.

1.4 Clinically Relevant Taxane Formulations

Taxane chemotherapeutics are formulated using a variety of techniques with the common goal of delivering the chemotherapeutic drug to the tumor tissue without causing side effects to the patient. The current, commercially available formulations are summarized in Table 1.3.[54] From this comparison, it is possible to envision an advanced formulation that maximizes the amount of taxane in the formulation with minimal adverse effects on a patient.

The administration technique of **PTX** or its analogues most relevant to this thesis is intravenous delivery. This technique can be quite time consuming, painful, and cause life threating reactions at the injection site, mainly due to the excipient used to solubilize the taxane. The method of administration also has

[53] Smith, T. A. D.; Cheyne, R. W. Predicting Tumour Response to Anti-HER1 Therapy using Medical Imaging: a Literature Review and in vitro Study of [18F]-FDG Incorporation by Breast Cancer Cells Responding to Cetuximab. *J. Biomed. Sci.* **2011**, *68*, 158–166.

[54] Hennenfent, K. L. Novel Formulations of Taxanes: a Review. Old Wine in a New Bottle? *Ann. Oncol.* **2006**, *17*, 735–749.

significant benefits in contrast to oral delivery. If adverse side effects begin to develop in a patient, the dosage of the pharmaceutical can be reduced or the treatment can be aborted instantly. I.V. injection has benefits resulting from bypassing the gastrointestinal tract: a lower toxicity in the stomach and intestines is observed, the drug is not forced to pass through a barrier into the blood stream, and first-pass liver metabolism is avoided.[55]

Paclitaxel chemotherapy is routinely and most commonly prescribed as the Taxol® formulation. Specifically, the medication consists of 6 mg of paclitaxel per mL of CrEL®. A single dose is around 156 mg of paclitaxel. CrEL® consists of a 50:50 mixture of poly-oxyethyleneglycerol triricinoleate castor oil (ca. 3 kDa) and dehydrated ethanol. This ion-free solution is not unique to paclitaxel; it is a well-studied solubilizer developed for the delivery of hydrophobic drugs via the self-assembly of micellular structures in which the hydrophobic components are contained in the center. Unfortunately the poor water solubility of paclitaxel requires oncologists to use an exorbitant amount of CrEL® to administer the drug. This formulation (Taxol®) is very problematic due to the inherent bioactivity of CrEL®. The most notable side effect due to high levels of CrEL is acute hypersensitivity (rash) at the injection site.[56] Although this effect can be reduced with pretreatment of corticosteroids and antihistamines, 40% of patients still experience this effect and 1.5%-3% have life threatening reactions.[57,58] Additional attempts to remedy this side effect include longer infusion times. However, neurotoxicity has been seen in peripheral neurons due to the solubilizer and the

[55] Sparreboom, A.; Van Asperen, J.; Mayer, U.; Schinkel, A. H.; Smit, J. W.; Meijer, D. K. F.; Borst, P.; Nooijen, W. J.; Beijnen, J. H.; Van Tellingen, O. Limited Oral Bioavailability and Active Epithelial Excretion of Paclitaxel (Taxol) caused by P-glycoprotein in the Intestine *P. Natl. Acad. Sci. USA* **1997**, *94*, 2031-2035.

[56] Gelderblom, H.; Verweij, J.; Nooter, K.; Sparreboom, A. Cremophor EL: the Drawbacks and Advantages of Vehicle Selection for Drug Formulation. *Eur. J. Cancer.* **2001**, *37*, 1590–1598.

[57] Weiss, R.; Donehower, R.; Wiernik, P. Hypersensitivity Reactions from Taxol. *J. Clin. Oncol.* **1990**, *8*, 1263-1268.

[58] Friedland, D.; Gorman, G.; Treat, J. Hypersensitivity Reactions From Taxol and Etoposide. *J. Natl. Cancer I.* **1993**, *85*, 2036.i

longer infusion times. Another disappointing result associated with the administration of Taxol® is a distorted pharmacokinetic profile.[59] Specifically, paclitaxel binds to serum lipoproteins and leads to poor biodistribution and clearance.[60] All these downfalls in Taxol® have led researchers to study better formulations.

Docetaxel (**DTX**) is inherently less hydrophobic than **PTX**, which results in a formulation containing a different solubilizer known as polysorbate 80 (Tween® 80). [61 , 62] Although this formulation (Taxotere®) overcomes some of the shortcomings of Taxol® by alleviating the frequency of hypersensitivity and decreasing neurotoxicity slightly, problems still persist with drug disposition.[63] Poor clearance and distribution of the drug is still observed.[64,65]Since Taxotere® only moderately improved upon the Taxol® formulation and the therapeutic outcome of patients was the same, other delivery agents were explored.

Tumor targeting agents are very useful tools to selectively deliver **PTX**. The Taxoprexin® formulation contains 8 milligrams of **131** (cf., Figure 1.5) per milliliter of CrEL® and 5% dextrose.[54] Having the targeting agent allows for 80% less CrEL® to be used, but, again, hypersensitivity and neurotoxicity is still

---

[59] van Tellingen, O.; Huizing, M. Cremophor EL Causes (Pseudo-) Non-linear Pharmacokinetics of Paclitaxel in Patients. *Brit. J. Cancer* **1999**, *81*, 330-335.

[60] Schwartz, E.; Einzig, A.; Strauman, J. Phase I trial of taxol Given as a 24-hour Infusion every 21 Days: Responses Observed in Metastatic Melanoma. *J. Clin. Oncol.* **1987**, *5*, 1232-1239.

[61] Crown, J. Docetaxel and Paclitaxel in the Treatment of Breast Cancer: A Review of Clinical Experience. *Oncologist* **2004**, *9*, 24–32.

[62] Bernstein, B. Docetaxel as an Alternative to Paclitaxel After Acute Hypersensitivity Reactions. *Ann. Pharmacother.* **2000***, 34*, 1332-1335.

[63] Norris, L. B.; Qureshi, Z. P.; Bookstaver, P. B.; Raisch, D. W.; Sartor, O.; Chen, H.; Bennet C.L. Polysorbate 80 Hypersensitivity Reactions: a Renewed Call to Action. *J. Community Support. Oncol.* **2010**, *7*, 425–428.

[64] Eckhoff, L.; Nielsen, M.; Moeller, S.; Knoop, A. TAXTOX - a Retrospective Study Regarding the Side Effects of Docetaxel Given as Part of the Adjuvant Treatment to Patients with Primary Breast Cancer in Denmark from 2007 to 2009. *Acta Oncologica.* **2011**, *50*, 1075–1082.

[65] Sparreboom, A.; van Tellingen, O.; Nooijen, W. J.; Beijnen, J. H. Tissue Distribution, Metabolism and Excretion of Paclitaxel in Mice. *Anti-cancer Drugs* **1996**, *7*, 78–86.

observed in patients.[66] Even though the lipophilic group of **131** has a higher affinity for plasma proteins than **PTX**, it has been shown that Taxoprexin® delivers more paclitaxel to tumor tissue than the Taxol® formulation.[40,41] Due to the persisting acute toxicity associated with the use of emulsification agents, research has been focused on formulating **PTX** into a biocompatible excipient.

To completely avoid the use of a surfactant to deliver paclitaxel to tumor tissues, the Abraxis company has developed a bio-based formulation dubbed Abraxane®. Abraxane® consists of 900 mg of human serum albumin (HSA, a natural plasma protein) and 100 mg of **PTX**. When the lyophilized powder of HSA/**PTX** is resuspended into 20 mL of 0.9% NaCl, stable nanoparticles are formed.[67,68,69] The nanoparticles have a size range of 130-150 nm. The HSA is believed to protect the drug and deliver it by the gp60 receptor. The gp60 receptor is albumin specific and abundantly expressed on tumor cells.[70] Abraxane® delivers more active drug than the Taxol® formulation due to active transport across endothelial cells and the use of dosages containing 5-10 times greater amounts of paclitaxel.[4] However, in terms of patients receiving taxane-based chemotherapy for the first time, Abraxane® did not significantly improve upon the survival time when compared against Taxol®. Second-line administration (patients who have received treatment before) of this formulation improves the survival time by approximately 10 weeks. “Abraxane's wholesale cost is $5,100 a dose every 3 weeks, which is 16 times as much as generic

[66] Harries, M.; O'Donnell, A.; Scurr, M.; Reade, S. Phase I/II Study of DHA–paclitaxel in Combination with Carboplatin in Patients with Advanced Malignant Solid Tumours. *Brit. J. Cancer* **2004**, *91*, 1651-1655.

[67] Desai, N. Methods for *in vivo* delivery of Substantially Water Insoluble Pharmacologically Active Agents and Compositions Useful Therefor. U.S. Patent 5,439,686, August 8, **1995**.

[68] U.S. FDA approved leaflet Abraxane Package Insert Version 12. **2005**, 1–26.

[69] Dosio, F.; Arpicco, S.; Brusa, P.; Stella, B.; Cattel, L. Poly(ethylene glycol)–human serum albumin–paclitaxel Conjugates: Preparation, Characterization and Pharmacokinetics. *J. Control. Release* **2001**, 1–11.

[70] Nyman, D. W. Phase I and Pharmacokinetics Trial of ABI-007, a Novel Nanoparticle Formulation of Paclitaxel in Patients With Advanced Nonhematologic Malignancies. *J. Clin. Oncol.* **2005**, *23*, 7785–7793.

paclitaxel."[71] The significant difference seen in second-line administration, led to the FDA approval of Abraxane® for treatment of metastatic breast cancer after relapse or chemotherapy failure. Abraxane® still does not show a great benefit in first-line patients and the sheer cost of the drug makes other formulations more appealing.[69, 72]

Genexol-PM is a micellular formulation consisting of many low molecular weight block-copolymers. The amphiphilic block copolymer monomethoxy-poly(ethylene glycol)-poly(D,L-lactide) (mPEG-D,L-PLA) solubilizes the paclitaxel into micelles of 20-50 nm.[73] The ca. 75% polymer particles are redispersed in a 5% dextrose solution and administered to patients. Genexol-PM is currently in clinical trials, despite a slight hypersensitivity in patients like the other formulations based on **PTX**.[74,75] Unfortunately, all of the formulations based on the **PTX** and **DTX** are poly-glycoprotein (P-gp) substrates. The P-gp transporter removes the drug out of the tumor cells by way of an efflux pump. This removal of the drug creates a resistance to the taxane class in many cancers.

[71] Herper, M. Cancer Man. *Forbes* **2009**, 1–2.

[72] Sparreboom, A. Comparative Preclinical and Clinical Pharmacokinetics of a Cremophor-Free, Nanoparticle Albumin-Bound Paclitaxel (ABI-007) and Paclitaxel Formulated in Cremophor (Taxol). *Clin. Cancer Res.* **2005**, *11*, 4136–4143.

[73] Joshi-Hangal, R. Paclitaxel Formulation. U.S. Patent, 6,538,020, March 25, **2011**.

[74] Kim, T. Y. Phase I and Pharmacokinetic Study of Genexol-PM, a Cremophor-Free, Polymeric Micelle-Formulated Paclitaxel, in Patients with Advanced Malignancies. *Clin. Cancer Res.* **2004**, *10*, 3708–3716.

[75] Lee, K. S.; Chung, H. C.; Im, S. A.; Park, Y. H.; Kim, C. S.; Kim, S.-B.; Rha, S. Y.; Lee, M. Y.; Ro, J. Multicenter Phase II trial of Genexol-PM, a Cremophor-free, Polymeric Micelle Formulation of Paclitaxel, in Patients with Metastatic Breast Cancer. *Breast Cancer Res. Tr.* **2007**, *108*, 241–250.

Table 1.3 | Comparison of paclitaxel formulations (adapted from Ref. 54).

Pharmaceutical	**Taxol®**	**Taxotere®**	**Taxoprexin®**	**Abraxane®**	**Genexol®**
Active Agent	**PTX**	**DTX**	**10**	**PTX**	**PTX**
% Active Agent	1.1%	3.6%	73%	10%	16.7%
Delivery Agent	CrEL	Tween® 80	CrEL	Albumin	PEG-PLA
I.V. inj. Time	1, 3, or 24 h	1 h	2 h	30 min	3 h
Pre-Medication	Required	Required	Required	Not Needed	Not Needed
P-gp substrate	Yes	Yes	Yes	Yes	Yes
Dose (mg/m^2)[a]	200-390	70-275	200–1100	135–375	135–390
MTD 3 weeks[b]	250 mg/m^2	275 mg/m^2	1100 mg/m^2	300 mg/m^2	390 mg/m^2

[a]Dosage varied based upon cancer type and severity.
[b]Maximum tolerated dose (MTD), beneficial dose with minimal side effects patient varies with patients

One should note that, although these formulations are used clinically, serious limitations are present due to the amount of drug present in comparison to the excipient used. It would be beneficial to have a formulation with a large loading of the drug that will release in a controlled fashion. To achieve this large dose formulation, one can envision a nanoparticle formulation consisting of an amphiphilic block copolymer (BCP) and a hydrophobic drug. The larger sized nanoparticle would resemble the self-assembled micelles, Genexol®.4 The drug and the hydrophobic portion of the BCP resides in the core of the particle and the hydrophilic portion of the BCP is displayed on the corona. More of the particle design and will be discussed in Chapter 2.

Chapter 2. Nanoparticle Drug Delivery

2.1 Flash Nanoprecipitation

2.1.1 Confined Impingement Jet Mixer with Dilution

To effectively formulate **PTX** or **DTX** with minimal excipient, which we refer to as high loading of the drug, the technique of flash nanoprecipitation (FNP), pioneered by Prud'homme showed that stable nanoparticles can be formed even at drug loadings past 50 wt%.[76] FNP can produce kinetically trapped nanoparticles of ca. 100 nm in size and not the thermodynamic micelles typically produced through self-assembly of a drug and amphiphilic block copolymers. Self-assembled micelles made through an oil/water emulsion have a much lower loading level of the organic solute ca. 1-10 wt% (uncommon up to 25 wt%) and a diameter of 50-80 nm.[77] Although the sizes are dependant on the MW of the two blocks in the block copolymer used in their formulations. Due to the low loading of micelles, we turned to the FNP process to achieve our nanoparticle formulations.

The FNP process overcomes low aqueous solubility via encapsulation of hydrophobic organic molecules (e.g., drugs) in the core of a particle comprising of amphiphilic block copolymers.[78] In this technique, rapid impingement mixing of water and a miscible organic solvent (in which the hydrophobic drug and block copolymer are co-dissolved) results in encapsulation of the hydrophobic portion

[76] Prud'homme, R.; Saad, W. Paclitaxel Conjugate Block Copolymer Nanoparticle Formation by Flash Nanoprecipitation. *Nanotech.* **2006**, *2*, 824-826.

[77] Kataoka, K.; Matsumoto, T.; Yokoyama, M.; Okano, T. Doxorubicin-Loaded Poly (Ethylene Glycol)–Poly (B-Benzyl-L-Aspartate) Copolymer Micelles: Their Pharmaceutical Characteristics and Biological Significance. *J. Control. Release* **2000**, *64*, 143–153.

[78] Ansell, S. M.; Johnstone, S. A.; Tardi, P. G.; Lo, L.; Xie, S.; Shu, Y.; Harasym, T. O.; Harasym, N. L.; Williams, L.; Bermudes, D.; Liboiron, B. D.; Saad, W.; Prud'homme, R. K.; Mayer, L. D. Modulating the Therapeutic Activity of Nanoparticle Delivered Paclitaxel by Manipulating the Hydrophobicity of Prodrug Conjugates. *J. Med. Chem.* **2008**, *51*, 3288–3296.

of the polymer and the hydrophobic solute.[79,80] The hydrophilic block of the copolymer ensures that the particles are soluble in the water as shown in Figure 2.1.

2.1.2 FNP Mixer Designs

Different mixers have been developed to maximize the utility of the FNP process. The confined impingement jet (CIJ) mixer uses equal volumes of organic and aqueous solvents at equal speeds (Figure 2.1, panel a). This is the most straightforward process, but it is restricted by the need for equal amounts of solvent to work properly.[79] The ease of use of the CIJ mixer is realized with the use of hand-operated syringes to press the two streams in < 1 second. Without access to different solvent ratios, supersaturated concentrations cannot be achieved in all cases, and only highly hydrophobic solutes can be efficiently captured and retained in the nanoparticle core.

The confined tangential flow (CTF) mixer offsets the two solvent streams instead of meeting orthogonally like the CIJ mixer. This offset allows the user to prepare a sample in which different volumes of solvent and anti-solvent are used, and ultimately sufficient entrapment of moderately hydrophobic drugs (Figure 2.1, panel b).[81,82] By introducing more inlet streams, the process can be customized for different organic solutes, co-encapsulation of two different drugs, and independent control of each stream. The multi-inlet vortex (MIV) mixer (Figure 2.1, panel c) allows for the greatest control in achieving uniform

[79] Zhu, Z.; Anacker, J. L.; Ji, S.; Hoye, T. R.; Macosko, C. W.; Prud'homme, R. K. Formation of Block Copolymer-Protected Nanoparticles via Reactive Impingement Mixing. *Langmuir* **2007**, *23*, 10499–10504.

[80] Zhu, Z. Polymer Stabilized Nanosuspensions Formed via Flash Nanoprecipitation: Nanoparticle Formulation, Formulation, and Stability. Ph.D. Dissertation, University of MN, Minneapolis, MN, **2010**. 1-240.

[81] Johnson, B. K. Flash NanoPrecipitation of Organic Actives via Confined Micromixing and Block Copolymer Stabilization. Ph.D. Dissertation, Princeton University, Princeton, NJ, **2003**. 1-337.

[82] Saad, W. S. Drug Nanoparticle Formation via Flash Nanoprecipitation: Conjugation to Encapsulate and Control the Release of Paclitaxel. Ph.D. Dissertation, Princeton University, Princeton, NJ, **2007**. 1-198.

nanoparticles.[83,84] Both of these the latter, more sophisticated mixers are typically run with syringe pumps for consistent flow rates of each stream and optimum mixing of each component.

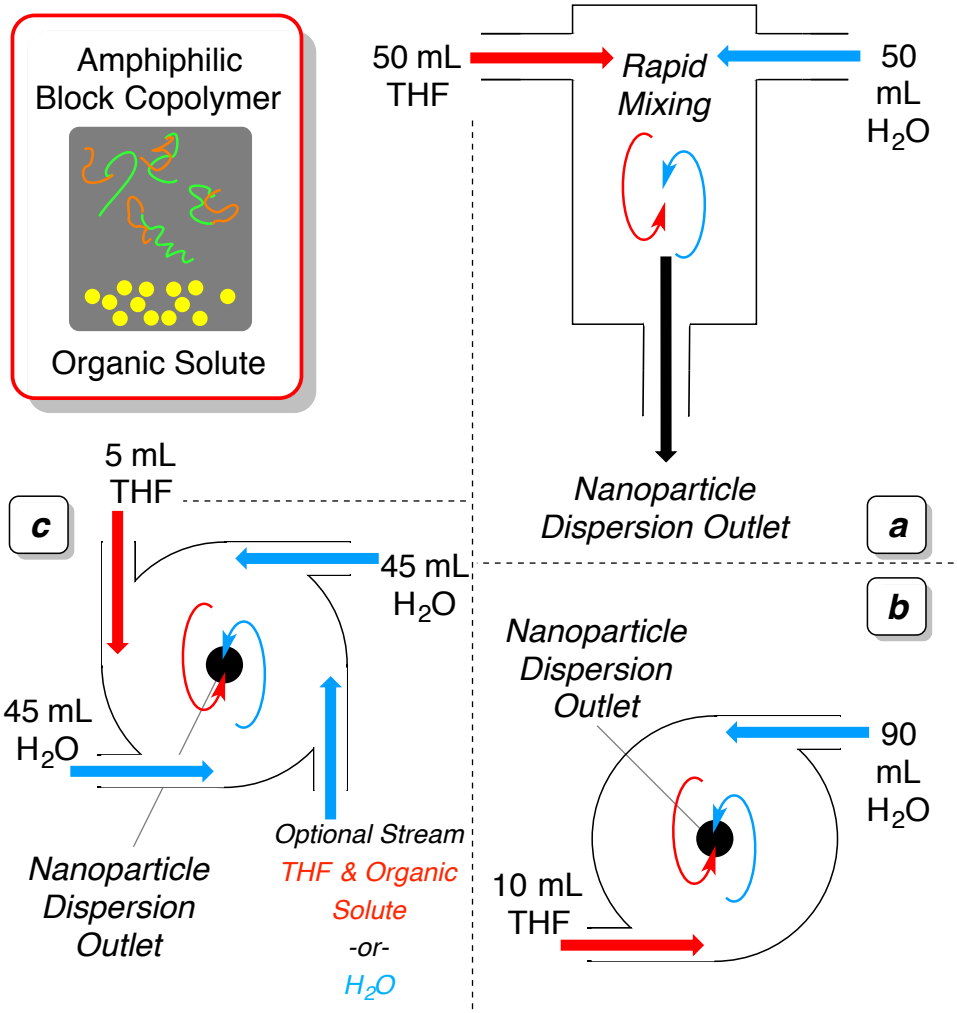

Figure 2.1 I Mixers used for flash nanoprecipitation (FNP) **a.)** confined impingement jet (CIJ) **b.)** confined tangential flow (CTF) **c.)** multi-inlet vortex (MIV) [adapted from ref 81,83,84].

[83] Shen, H.; Hong, S.; Prud'homme, R. K.; Liu, Y. Self-assembling Process of Flash Nanoprecipitation in a Multi-inlet Vortex mixer to Produce Drug-loaded Polymeric Nanoparticles. *J. Nanopart. Res.* **2011**, *13*, 4109–4120.

[84] Liu, Y.; Prudhomme, R. Optimized Descriptive Model for Micromixing in a Vortex Mixer. *Chem. Eng. Commun.* **2010**, *197*, 1068-1075.

The confined impingement jet mixer with a dilution (CIJ-D) stage is presented in Figure 2.2. For this design two solvent streams enter the mixing chambers at right angles and at the same rate. This is commonly done with two hand-operated syringes at the top of the mixer. Since the total volume in each syringe must be the same, the final nanoparticle formulation contains a large amount of the organic solvent. A dilution tank containing water was utilized to reduce the vol% of the organic medium, which leads to nanoparticles that are kinetically trapped and have a better stability profile.[85,86] Due to the ease of operation, the CIJ-D mixer was used for all of our experiments unless otherwise noted. Unfortunately the flow rates of the two mixing solvents are fixed due to the backpressure of each stream on the other, so other mixers would need to be used to optimize the loading and to reduce the amount of organic solvent used (cf. 2.1).

[85] Han, J.; Zhu, Z.; Qian, H.; Wohl, A. R.; Beaman, C. J.; Hoye, T. R.; Macosko, C. W. A Simple confined impingement jets mixer for flash nanoprecipitation. *J. Pharm. Sci.* **2012**, *101*, 4018–4023.

[86] Pustulka, K. M.; Wohl, A. R.; Lee, H. S.; Michel, A. R.; Han, J.; Hoye, T. R.; McCormick, A. V.; Panyam, J.; Macosko, C. W. Flash nanoprecipitation: Particle structure and stability. *Mol. Pharmaceut.* **2013**, *10*, 4367–4377.

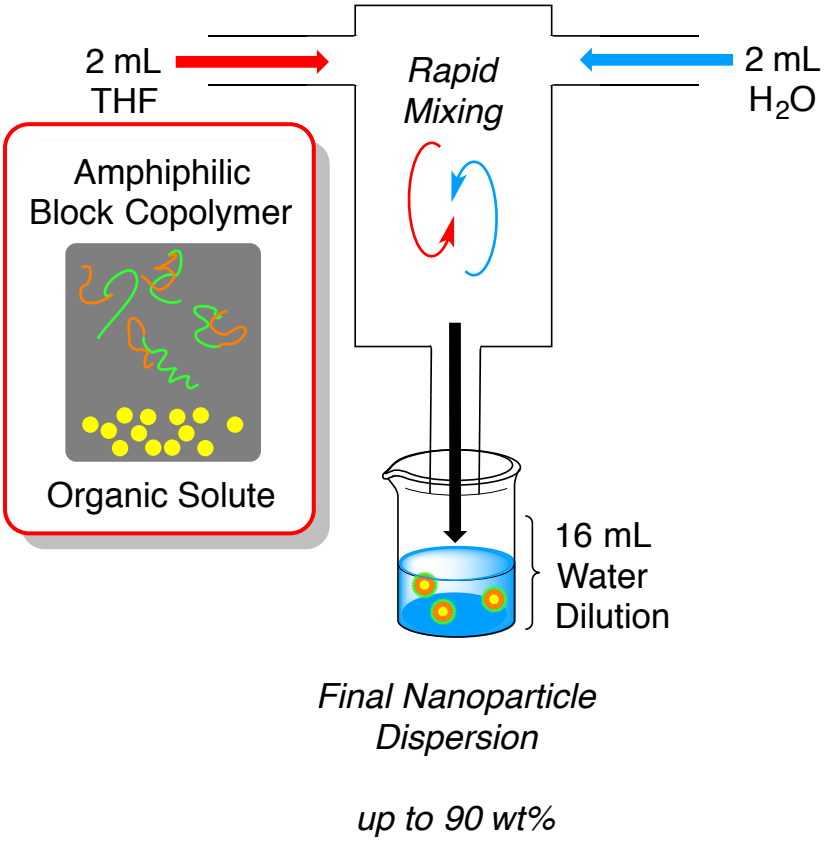

Figure 2.2 I Flash nanoprecipitation (adapted from ref. 85,86).

2.2 Flash Nanoprecipitation Experiments

2.2.1 Initial Model Drug Experiments

Due to the hydrophobic nature of β-carotene and its bright color, it was chosen as a model for a hydrophobic drug for the CIJ mixer experimentation.[78] The solute, β-carotene, and block polymer, poly(ethylene oxide)-*b*-poly(styrene) (PEO-*b*-PS), were impingement mixed in the CIJ mixer to achieve an impressive 87% β-carotene wt/wt formulation that was fully encapsulated by the polymer. The size regime associated with this formulation varied between ~80-400 nm in diameter. These sizes are typical values from multiple runs. Although the variation was not ideal, all particles were considered as an acceptable size for

passive uptake of cancer cells by the enhanced permiation and retention (EPR) effect (Chapter 2.4).[79]

Although this model study showed the proof of concept, the choice of the solute and block polymer has some downsides. β-Carotene has no chemotherapeutic properties and its hydrophobicity is much higher than typical drugs we envisioned using. Also the block polymer used (PEO-*b*-PS) is not biodegradable and not FDA approved, which forbids its use in formulations for use in humans. From these restrictions on the formulation, the solute or drug was changed to a chemotherapeutic and the polymer was changed to a biodegradable block polymer.

2.2.2 FNP of Paclitaxel

Paclitaxel was chosen for its hydrophobicity and track record of chemotherapeutic properties. The first experiment with the desired substrate, paclitaxel, and block polymer, poly(ethylene glycol)-block-poly(lactic-co-glycolic acid) [(PEG-*b*-PLGA), 2k-10k] was attempted using the CIJ mixer.[79] The particles formed displayed sizes ranging from 90-285 nm, and were 34 wt% **PTX**. This loading level is a great improvement when compared to the clinically relevent formulations described in Chapter 1. Unforunately, after 15 minutes, **PTX** crystallized out of the particle core through a phenomenon known as Ostwald ripening.[87] Zhu confirmed the formation of crystal growth after 90 mins by spraying the suspension on a silicon wafer for scanning electron microscopy (SEM) shown in Figure 2.3, panel a.[80] I repeated the experiment with the CIJ-D mixer and a different block polymer (mPEG-*b*-PLGA, 5k-10k) and observed crystal growth within an hour visible to the naked eye (Figure 2.3, b). This showed that although the PEG-*b*-PLGA polymer is biocompatable, when used in conjunction with **PTX** the FNP process was troublesome. Other polymers need

[87] Voorhees, P. W. The Theory of Ostwald Ripening. *J. Stat. Phys.* **1985**, *38*, 231–252.

to be explored in hopes to improve the stability of **PTX** nanoparticles formed by FNP.[88]

Despite the ease and reliability of FNP to form stable nanoparticles in the case of model studies, attempts to formulate **PTX** in nanoparticles via this methodology were unsuccessful.[89] In this case, paclitaxel was not hydrophobic enough to stay in the core; instead "leaking out" and crystallizing within minutes after FNP of **PTX** with a PEG-*b*-PLGA polymer.[86,89]

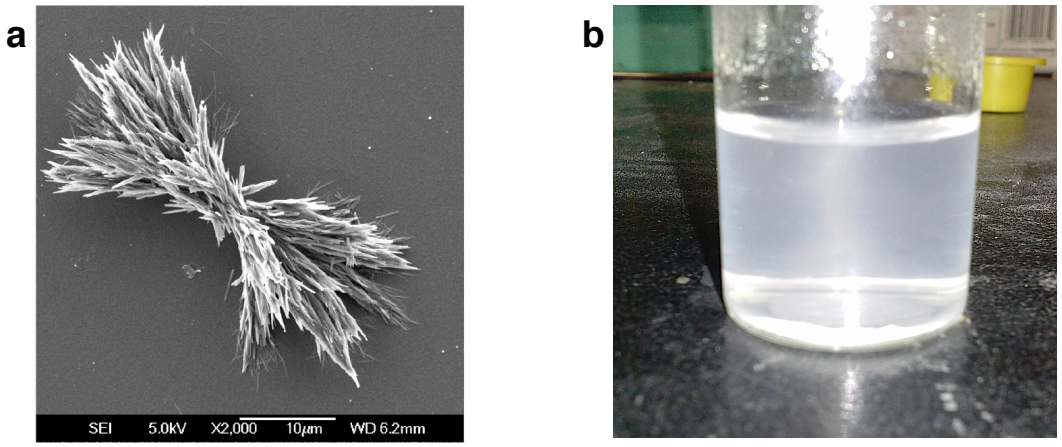

Figure 2.3 I Experiments showing the Ostwald ripening of **PTX** from nanoparticles **a.)** SEM image taken by Zhu et al. **b.)** Photo of nanoparticle suspension with **PTX**

To remedy this shortcoming, a prodrug that is more hydrophobic than that of the parent was envisioned to stay in the core of the particle and release out **PTX** in a controlled fashion. As mentioned before, prodrugs are typically created to temporally increase the hydrophilicity of a drug. The following chapter gives a detailed overview on the strategies used to make hydrophobic prodrugs of **PTX** for the possible use as nanoparticle formulations by way of the FNP process.

[88] Zhu, Z. Effects of amphiphilic diblock copolymer on drug nanoparticle formulation and stability. *Biomaterials* **2013**, *34*, 10238–10248.

[89] Zhu, Z. Flash Nanoprecipitation: Prediction and Enhancement of Particle Stability via Drug Structure. *Mol. Pharm.* **2014**, *11*, 776–786.

2.3 Hydrophobic Esters of PTX and DTX

Ironically, **PTX** is too hydrophobic to be administered to patients in a saline solution without complication, but not hydrophobic enough to stay in nanoparticles. While most research has focused on increasing the water solubility of **PTX**, hydrophobic modification has been minimally studied.

Prud'homme and co-workers prepared a suite of hydrophobic ester prodrugs of **PTX** shown in Scheme 2.1. Appended to the 2'-position of **PTX,** the linkers **206-208** provided conjugation of **PTX** to the very lipophilic alcohols **201a-203a**. To form these linkers cyclic anhydrides **204** and **205** were opened under basic conditions by alcohols **201a-203a**. The lipophilic linkers **206-208** were then conjugated with **PTX** using diisopropylcarboiimide (DIPC) and dimethylaminopyridine (DMAP) to yield the hydrophobic **PTX** conjugates **209-211**.

Unfortunately, when the prodrugs are tested for *in vitro* efficacy, 3 to 60 times the concentration of **PTX** was required to achieve the same therapeutic outcome.[78] This suggests that the prodrugs are not hydrolyzing back to **PTX** in an adequate time frame. In addition, precipitation of these hydrophobic prodrugs in aqueous media can occur, which can compromise the cytotoxicity study. Interestingly, those derived from cyclic anhydride **205** have an increased potency due to a proposed inclination for the 3-oxa group to hydrolyze quicker than the **204** derivatives. Thus, to make effective hydrophobic prodrugs, the ease of hydrolysis is a critical issue. In the case of **211b** it was noted that, although a decent IC_{50} value was found, the prodrug-loaded nanoparticle was not stable after 1–2 weeks when stored as a solution.

Scheme 2.1 I Conjugation of **PTX** to form hydrophobic prodrugs: summary of structure and *in vitro* activity (altered from ref. 78).

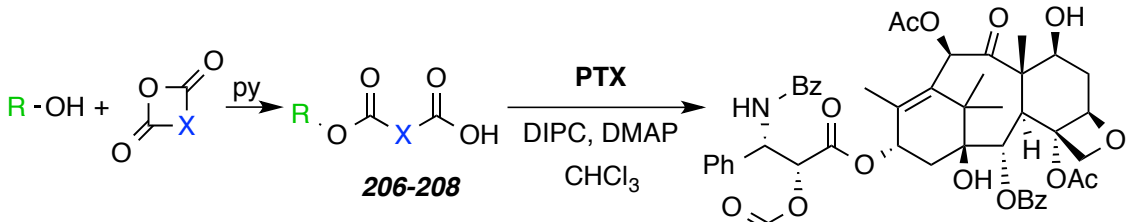

ROH	X		R	X
201a	***204***	***206a***	*201*	*204*
202a	$-CH_2CH_2-$	***206b***	*201*	*205*
203a	***or***	***207a***	*202*	*204*
	205	***207b***	*202*	*205*
	$-CH_2OCH_2-$	***208b***	*203*	*205*

209-211	R	X
209a	*201*	*204*
209b	*201*	*205*
210a	*202*	*204*
210b	*202*	*205*
211b	*203*	*205*

R	[a] *In vitro* IC_{50} ± SD (nM)
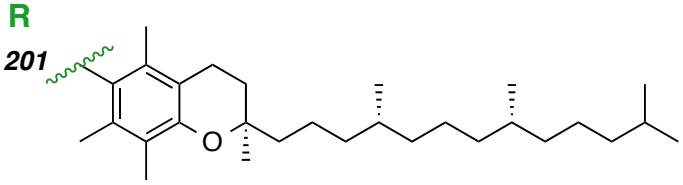 ***201***	***209a*** 158 ± 72
	209b 13.4 ± 2.4
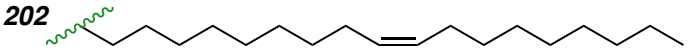 ***202***	***210a*** 67.0 ± 5.9
	210b 15.9 ± 0.7
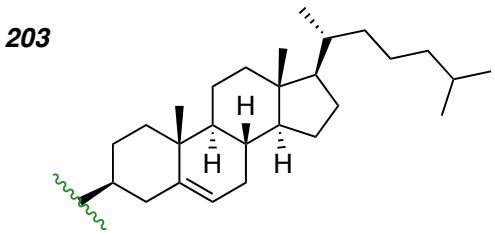 ***203***	***211b*** 24.1 ± 0.6 [b]

[a] IC_{50} values in triplicate of MCF-7 breast cancer cell line. IC_{50} of **PTX** is 3.8 ± 0.6.
[b] Value not applicable to *in vivo* studies due to particle stability over time.

The nanoparticle formulations were examined by different pharmaceutics experiments such as: circulation and plasma elimination, partitioning kinetics, and efficacy. Ansell and coworkers strongly encourage the necessity of *in vivo* testing early on in the formulation process to distinguish the subtle differences in

each formulation. Although they obtained varied results for the *in vitro* and *in vivo* studies, they concluded that the chemical properties of each prodrug dictated its performance and not the delivery vehicle itself. More specifically, the rate at which the parent compound is released is governed by the nature of the covalent bond between the hydroxyl of **PTX** and the hydrophobic functionality. This research provided the insight that a delicate balance is needed when creating hydrophobic prodrugs of **PTX** for particle formulation**.** To be formulated into nanoparticles or micelles the conjugating bond needs to be *stable* enough to keep the prodrug in the core of the particle for storage and administration and yet needs to be *labile* for efficient hydrolysis and release to return the cytotoxicity of the parent drug.

A few other research groups have developed hydrophobic ester prodrugs of **PTX**.[90,91,92] Instead of utilizing FNP to make nanoparticles, they chose to allow the hydrophobic constructs of **PTX** to self-assemble into either micelles or nanoparticles when mixed with an amphiphilic block polymer. A select set of prodrugs is shown in Figure 2.4 below, with examples chosen from reports in which the particles created with these prodrugs were tested *in vivo.*

Forrest and co-workers synthesized a suite of hydrophobic esters following a previous protocol developed by Ali.[91] They could functionalize the 2'-hydroxyl with a fatty acid (**217**) by performing a DCC and DMAP esterification. Alternatively, they accessed the less reactive 7-hydroxyl by first protecting the 2'-hydroxyl with a TBS ether (**214**), then esterifying to yield compounds like **215**. Following the deprotection of the silylether with TBAF, the desired R^2-derivatives

[90] Mura, S.; Zouhiri, F.; Lerondel, S.; Maksimenko, A.; Mougin, J.; Gueutin, C.; Brambilla, D.; Caron, J.; Sliwinski, E.; LePape, A.; *et al.* Novel Isoprenoyl Nanoassembled Prodrug for Paclitaxel Delivery. *Bioconjugate Chem.* **2013**, *24*, 1840–1849.

[91] Ali, S.; Ahmad, I.; Peters, A.; Masters, G.; Minchey, S.; Janoff, A.; Mayhew, E. Hydrolyzable Hydrophobic Taxanes: Synthesis and Anti-Cancer Activities. *Anti-cancer Drugs* **2001**, *12*, 117–128.

[92] Ma, P.; Rahima Benhabbour, S.; Feng, L.; Mumper, R. J. 2′-Behenoyl-Paclitaxel Conjugate Containing Lipid Nanoparticles for the Treatment of Metastatic Breast Cancer. *Cancer Lett.* **2013**, *334*, 253–262.

(**216**) were synthesized. The six (**216a-217c**) prodrugs, shown in Figure 2.4, were then formulated into micelles.[93]

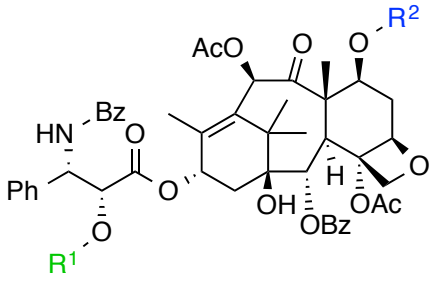

214-218	**R¹**	**R²**
PTX	H	H
214	TBS	H
215	TBS	212c
216a	H	212a
216b	H	212b
216c	H	212c
217a	212a	H
217b	212b	H
217c	212c	H
[a]218	212d	H

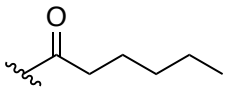

212a

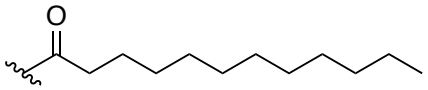

212b

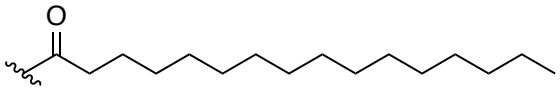

212c

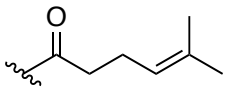

212d

Figure 2.4 I Hydrophobic prodrug esters developed by Forrest et al. Figure adapted from reference (93). [a] Compound synthesized and tested by Mura et al.[90]

Each prodrug (**216a-217c**) was dissolved in acetone with a 5k-10k PEG-*b*-PCL polymer, and added with a syringe pump dropwise into vigorously stirred water over 15 minutes. The organic solvent was removed by blowing air over the contents, which also reduced the overall volume of the suspension. Finally, they passed the micelle mixture through a porous filter to remove any unincorporated solid prodrug and polymer. Particle diameters were measured by dynamic light

[93] Forrest, M. L.; Yáñez, J. A.; Remsberg, C. M.; Ohgami, Y.; Kwon, G. S.; Davies, N. M. Paclitaxel Prodrugs with Sustained Release and High Solubility in Poly(Ethylene Glycol)-B-Poly(E-Caprolactone) Micelle Nanocarriers: Pharmacokinetic Disposition, Tolerability, and Cytotoxicity. *Pharm. Res.* **2007**, *25*, 194–206.

scattering (DLS) and gave sizes ranging from 27-44 nm. They also determined the loading levels of the micelles, to be approximately 20 wt% of the prodrug to the polymer. Yet, once again, like the ester prodrugs made by Prud'homme, only the **216a** prodrug showed cytotoxicity comparable to free drug. Further investigations into the pharmacokinetic parameters and the biodistribution of the **216a** micelle formulation via a jugular vein injection into a rat model, led these workers to conclude that the formulation had benefits when compared to the clinical Taxol® formulation.[93] They attributed these benefits to the enhanced permeation and retention (EPR) effect, which will be discussed in detail in Chapter 2.4.

The Couvreur group from France has also explored the use of hydrophobic ester prodrugs of **PTX**. Described a recent publication, they used an isoprenoid (**212d**) ester of PTX (**218**) as shown in Figure 2.4.[90] The ester is formed by the use of EDCI and DMAP with the desired acid; this methodology analogues to their previous report of the esterification of a squalene fatty acid.[94,95] The squalene ester of **PTX** showed a poor cytotoxicity profile in comparison to the free **PTX**, which subsquantely changed to a smaller ester chain present in **218** to improve the IC_{50} value.[90]

Nanoparticles were prepared with a PEG-SQ [MePEG-Trisnorsqualene, (2k)] polymer [made by the O-alkylation of the sodium alkoxide of polyethelyeneglycol (PEG-O^-Na^+) with 1,1',2-trisnorsqualene methanesulfonate (SQ-Ms)].[90] To form the particles the isoprenoid prodrug **218** and the polymer were dissolved in ethanol and added dropwise under rapid stirring into water. The organic solvent was removed by rotary evaporation and the resulting suspension stored at 4 ˚C. The nanoparticles formed rapidly with a diameter of

[94] Desmaële, D.; Gref, R.; Couvreur, P. Squalenoylation: a Generic Platform for Nanoparticular Drug Delivery. *J. Control. Release* **2012**, *161*, 609–618.

[95] Reddy, L. H.; Marque, P. E.; Dubernet, C.; Mouelhi, S. L.; Desmaele, D.; Couvreur, P. Preclinical Toxicology (Subacute and Acute) and Efficacy of a New Squalenoyl Gemcitabine Anticancer Nanomedicine. *J. Pharmacol. Exp. Ther.* **2008**, *325*, 484–490.

200 nm measured by DLS, and interestingly showed a very high loading level of 82 wt% of the **PTX** derivative. An *In vitro* assay showed the particles to be less potent than the free drug by 10 fold. *In vivo* bioluminence imaging of the particles showed an improvement in comparison to the Taxol® formulation when given as a tail vein injection to a balb/c mouse model. Also the tail (injection site) showed healthy tissue even after five consecutive injections of their nanoparticle formulation. This was in a stark contrast to the highly necrotic (dead) tails found in the Taxol® treated mice.[90]

Although these formulations did not achieve the desired therapeutic outcome, they serve as precedence for the development of hydrophobic prodrugs of **PTX** that are capable of forming stable particles of various sizes. As noted by the groups, esters of **PTX** containing large hydrophobic esters that do not quickly hydrolyze back to the parent drug limit their utility. It presents the opportunity to create a more liable prodrug with sufficient hydrophobicity.

2.4 The Enhanced Permeation and Retention (EPR) Effect

The enhanced permeation and retention (EPR) effect serves as a primary basis for considering the use of nanotherapeutics in cancer therapy. In contrast to the blood vessels supplying most normal organs, tumor blood vessels lack a continuous endothelial cell coverage and basement membrane. Delivery vehicles in the colloidal size range (including polymeric nanoparticles, liposomes, and micellar systems) are typically excluded from normal organs but are able to passively accumulate in tumors because of this leaky vasculature. Lack of well-developed lymphatic drainage enhances retention of these vehicles once in the tumors. The EPR effect can result in decreased toxicity and increased efficacy of an encapsulated drug.[96]

[96] Swindell, C. S.; Krauss, N. E.; Horwitz, S. B.; Ringel, I. Biologically active taxol analogs with deleted A-ring side chain substituents and variable C-2' configurations. *J. Med. Chem.* **1991**, 34, 1176–1184.

The physiological differences between that of healthy tissue and diseased tissue (cancerous, inflamed, infected) allows for the passive uptake of macromolecules into the diseased tissues. Depicted in Figure 2.5, the enhanced permeation and retention (EPR) effect shows the selectivity for the accumulation of macromolecules into tumor tissue. Small molecules can pass through the tight junctures of the blood capillaries in the endothelial cell layer (green, Figure 2.5).

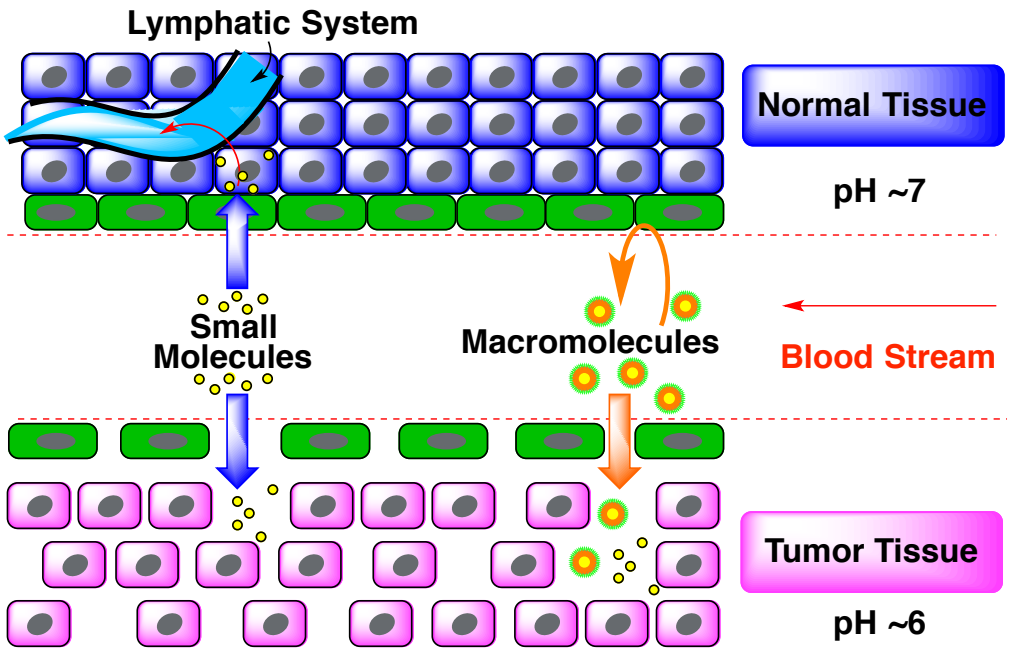

Figure 2.5 I Enhanced permeation and retention (EPR) effect (adapted from Haag et al.).[97]

Macromolecules (large molecules, cells) on the other hand are too large to fit through the narrow passages; they can however enter through the “leaky” endothelial layer present in cancer tissue. The blood capillaries of the cancerous tissue are widened to allow for maximum blood and nutrient flow to the fast growing tissue. Also, this diseased tissue has a poor lymphatic drainage system compared to healthy tissue. Due to the poor waste drainage, once

macromolecules enter the tumor cell matrix they tend to remain inside and are not readily cleared out.[97]

The optimal size of macromolecules or nanoparticles to allow for size selectivity in the passive uptake of macromolecules into the tumor tissue compared to the healthy tissue is still debated.[98,99] Many research groups claim that the smaller the particle size the better for the uptake. However there is a lower limit to allow for the differentiation from small molecules of <1 kDa. Also a longer blood circulation time is required for the accumulation of the macromolecules into the tumor tissue. Most healthy organisms have a renal clearance cutoff of ca. 30-50 kDa to restrict the loss of body proteins into the bladder.[100] This molecular weight converts to a volume of ca. 2-5 nm.[101] Having a hydrodynamic radius larger than 5 nm allows for a prolonged circulation and, therefore, greater accumulation into tumor tissue.

Due to the "person-specific" nature of cancer, possessing a variety of phenotypes, a generic size of particle or macromolecule is not important. The optimal drug delivery system is simply one that works by taking advantage of the weak points like the EPR effect expressed by diseased tissues. In addition to the EPR effect, tumor tissues are also hypoxic, which leads to a lower pH value (shown in Figure 2.5).[102] The lower pH can be advantageous for the development of acid labile prodrugs, which will be discussed more in Chapter 3.

---

[97] Haag, R.; Kratz, F. Polymer Therapeutics: Concepts and Applications. *Angew. Chem. Int. Ed.* **2006**, *45*, 1198–1215.

[98] Fang, J.; Nakamura, H.; Maeda, H. The EPR Effect: Unique Features of Tumor Blood Vessels for Drug Delivery, Factors Involved, and Limitations and Augmentation of the Effect. *Adv. Drug Deliv. Rev.* **2011**, *63*, 136–151.

[99] Tang, L.; Yang, X.; Yin, Q.; Cai, K.; Wang, H.; Chaudhury, I.; Yao, C.; Zhou, Q.; Kwon, M.; Hartman, J. A.; *et al.* Investigating the Optimal Size of Anticancer Nanomedicine. *Proc. Natl. Acad. Sci. U.S.A.* **2014**, *111*, 15344–15349.

[100] P. Caliceti, F. M. Veronese, Pharmacokinetic and biodistribution properties of poly(ethylene glycol)-protein conjugates *Drug Deliv. Rev.* **2003**, *55*, 1261–1277.

[101] Erickson, H. P. Size and Shape of Protein Molecules at the Nanometer Level Determined by Sedimentation, Gel Filtration, and Electron Microscopy. *Biol. Proced. Online* **2009**, *11*, 32–51.

[102] Harris, A. L. Hypoxia—a Key Regulatory Factor in Tumour Growth. *Nat. Rev. Cancer.* **2002**, *2*, 38–47.

2.5 Introduction to Silicon Chemistry

Although the functionality of orthosilicates {$Si(OR^1)_4$, $Si(OR^1)_3(OR^2)$, $Si(OR^1)_2(OR^2)_2$, $Si(OR^1)_2(OR^2)(OR^3)$, $Si(OR^1)(OR^2)(OR^3)(OR^4)$} has been studied before and is an old chemistry,[103] the use in the context of prodrug formulation is quite novel. By varying the nature of the R-groups, great control of the physical and chemical properties of the silicates can be obtained. This strategy is very attractive due to straightforward synthesis to access an array of radically different prodrugs. More specifically the hydrophobicity of the prodrug (cLogP) can be tuned by choosing an alkyl-R of varying carbon chain length or "greasiness". Also the hydrolytic lability can be selected by the steric bulk surrounding the silicon center. Since this approach to prodrugs is unexplored, there is a void in covered chemistries within patent literature, which can be capitalized upon.

To start the discussion of the orthosilicate chemistry described in this thesis, a little nomenclature is needed to clarify the compounds. Historically the names have been derived from the simplest parent compound SiH_4 (silane). As heavier atoms replace the hydrogens the name is adjusted to reflect the new compound as shown in the five examples below. The nomenclature changes when four oxygen atoms are bound to the silicon to reflect the simplest parent compound $Si(OH)_4$ (orthosilicic acid). This naming is shown in the three examples below. When one hydrogen is replaced with a hydroxyl the compound is a silanol. Uniquely when there are four Si-O bonds the compound is denoted as a silicate as shown with tetraethyl orthosilicate or tetraethyl silicate (TEOS).[104]

[103] Ebelmen, M. *Ann. Chim. Phys.* **1845** *15,* 319.

[104] Arkles, B. Silicon Esters. In *Kirk-Othmer Encyclopedia of Chemical Technology, Fourth Edition, Volume 22*; Kroschwitz, J. I.; Howe-Grant, M., ed. John Wiley & Sons, Inc: New York, 1997, 69–81.

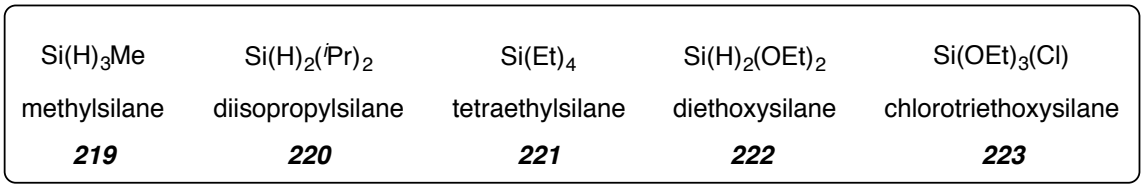

Figure 2.6 I Silane nomenclature used for the distinction between silicate esters and silanes.

The naming of $Si(OEt)_4$ and related compounds (4 Si-O bonds) is further complicated by multiple references citing them as a silicon or silicate esters. In discussion the "ester" is typically dropped and the compounds are referred to as "silicates". This creates confusion with the inorganic chemistry and geology communities because silicate anions (SiO_4^{-4}) are frequently encountered.[105] The use of silicates or silicate esters in this thesis will always describe a compound with the formula of {$Si(OR^1)_4$, $Si(OR^1)_3(OR^2)$, $Si(OR^1)_2(OR^2)_2$, $Si(OR^1)_2(OR^2)(OR^3)$, $Si(OR^1)(OR^2)(OR^3)(OR^4)$} and not the anion common in inorganic chemistry.

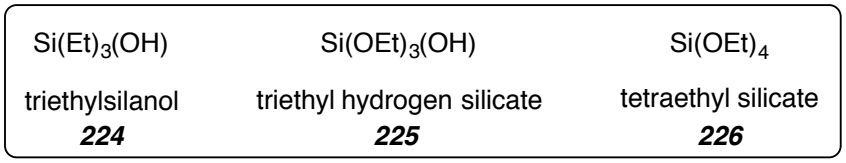

Figure 2.7 I Silanol nomenclature used for the distinction between silicate esters and silanols.

[105] Wright, J. R. Bolt, R. O.; Goldschmidt, A.; Abbott, A. D. Silicate Esters and Related Compounds. I. Synthesis of Certain Tetraalkoxysilanes, Polyalkoxysilanes, Bis-(trialkoxysilyl)-alkanes, and Related Intermediates. *J. Am. Chem. Soc.* **1957**, *80*, 1733–1737.

2.6 Prior Research using Silicon for Biomaterial Nanoparticles

Although the use of hydrophobic silicon-based prodrugs envisioned to form stable nanoparticles was novel and an innovative strategy developed in the Hoye labs, recent published work shows the strategy of silicon functionalization of drugs can be applied to a variety of systems (Chapters 3, 6-7). During the development of this technology, there was a lack of direct precedent for the use of tetraalkoxysilanes as prodrug constructs.

The Cheng group from the University of Illinois at Urbana-Champaign published their work with trialkoxyalkylsilane derivatives of known drugs for the incorporation into silica nanoparticles with well-defined architecture. The basic strategy employed by Cheng is to derivative the drug through a thioether ester linkage to form the trimethoxysilyl camptothecin (Figure 2.8, **227**) or trimethoxysilyl paclitaxel (Figure 2.8, **228**).[106,107] The trialkoxyalkylsilane is used to anchor the prodrug into a nanoparticle composed of bulk silica (TEOS). By using a modified Stöber process they are able to make monodisperse particles that can be adorned with PEG. One should note that this strategy is different from the simple silicate promoiety and precipitation with a block copolymer discussed in this thesis. Nanoparticles prepared by the Cheng and coworkers showed desirable biocompatibility and biodistribution; however due to the *in vivo* stability of the thioether ester linkage a modification to the linker was required.[108]

[106] Tang, L.; Yang, X.; Dobrucki, L. W.; Chaudhury, I.; Yin, Q.; Yao, C.; Lezmi, S.; Helferich, W. G.; Fan, T. M.; Cheng, J. Aptamer-Functionalized, Ultra-Small, Monodisperse Silica Nanoconjugates for Targeted Dual-Modal Imaging of Lymph Nodes with Metastatic Tumors. *Angew. Chem. Int. Ed.* **2012**, *51*, 12721–12726.

[107] Tang, L.; Fan, T. M.; Borst, L. B.; Cheng, J. Synthesis and Biological Response of Size-Specific, Monodisperse Drug–Silica Nanoconjugates. *ACS Nano* **2012**, *6*, 3954–3966.

[108] Tang, L.; Gabrielson, N. P.; Uckun, F. M.; Fan, T. M.; Cheng, J. Size-Dependent Tumor Penetration and in VivoEfficacy of Monodisperse Drug–Silica Nanoconjugates. *Mol. Pharm.* **2013**, *10*, 883–892.

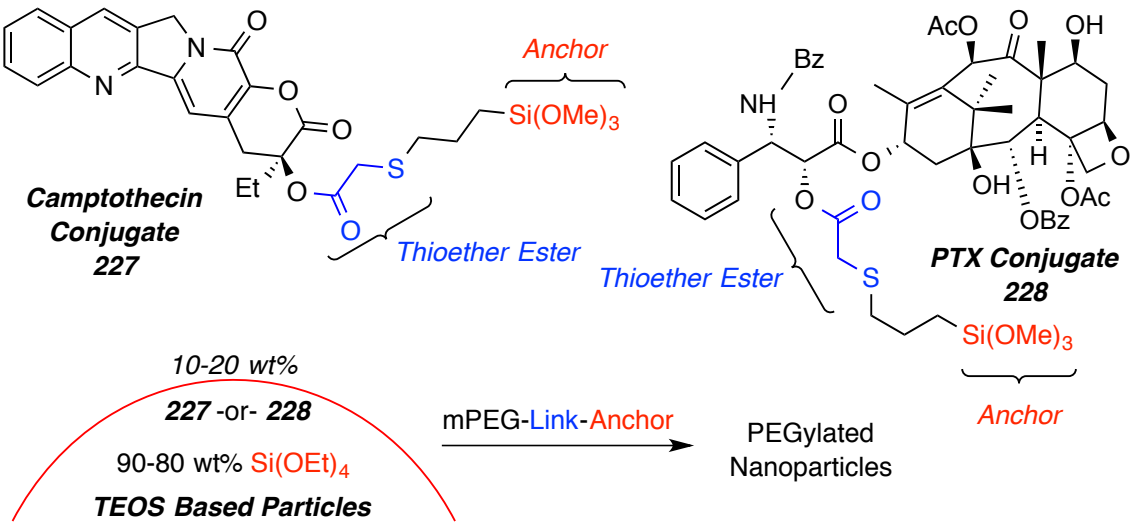

Figure 2.8 I The structures of the thioether ester linked silicon-based prodrugs and nanoparticle strategy reported by Cheng.[106,107,108,109]

Wang took advantage of Cheng's design,[109] the development of two modified linkers, one of which is shown in Figure 2.9, allow for the facile cleavage of the drug from the silicon anchor and the linker. Wang et. al report that the higher levels of glutathione in cancer cells allow for the cleavage of the disulfide bond shown in the camptothecin conjugate **229**. This cleavage allows for the molecule to be released from the silicon particle (made by in the same fashion as Cheng et. al) as the free thiol **230**. Finally, by way of a cyclization onto carbamate, the parent drug **232** is exposed along with the cyclic byproduct **231**. Wang and co-workers also have developed a hydrazine-based linker (not shown) that is responsive toward pH. By utilizing these labile linkers, the *in vitro* anticancer cytotoxicity indicated that the nanoparticle formulations were comparable to the parent drugs after 72 hours of incubation with cancer cells.[110]

[109] Tang, L.; Cheng, J. Nonporous Silica Nanoparticles for Nanomedicine Application. *Nano Today* **2013**, *8*, 290–312.

[110] Xu, Z.; Liu, S.; Kang, Y.; Wang, M. Glutathione- and pH-Responsive Nonporous Silica Prodrug Nanoparticles for Controlled Release and Cancer Therapy. *Nanoscale* **2015**, *7*, 5859–5868.

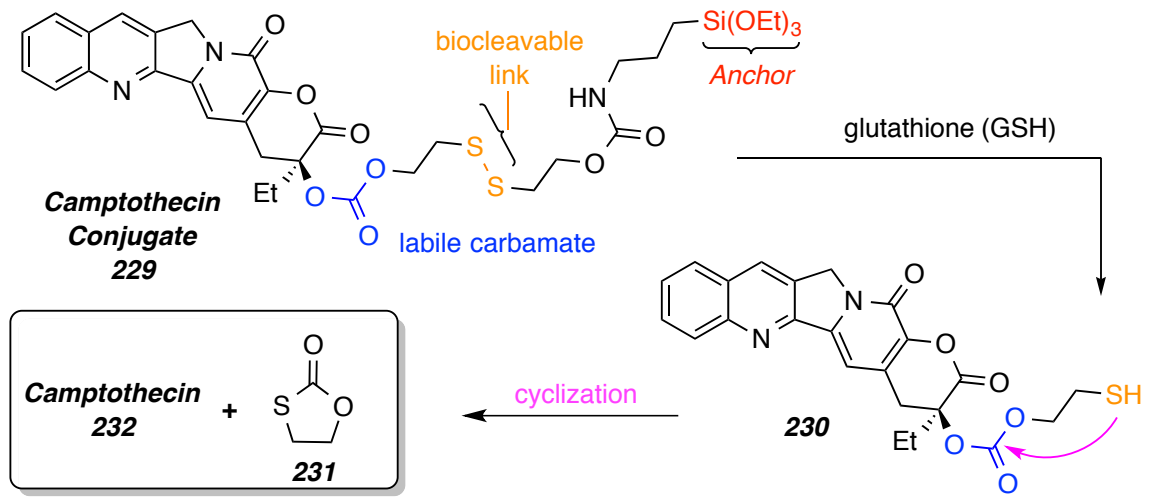

Figure 2.9 I Modified linker structure to increase the bio-lability reported by Wang.[110]

The DeSimone group has also utilized silyl ethers as hydrolytically labile linkers on biomaterials. Instead of using an ester or carbonate as the proximal functional group and the silicon at the distil site on the prodrug, DeSimone reversed the positions for his prodrug system. This is very beneficial due to the inherit lability of the silyl ether compared to an ester, disulfide, or carbonate. Under acidic conditions the dialkyldialkoxysilanes cleaved the drug from the biomaterials. With DeSimone's engineering expertise the group has successfully fashioned a variety of bio-devices (e.g. sutures, stents) and drug delivery systems (e.g. nanoparticles). The silyl ether bond stability towards acidic conditions can be modified by the choice of alkyl group as shown in Figure 2.10. More specifically, they modified the steric bulk around the silicon using diethyl, diisopropyl, and di-tert-butyl groups. When a model non-toxic drug was attached to the dialkyldialkoxysilane linker, they observed nontoxic biological properties of the compound as a whole or from byproducts resulting from the hydrolysis.[111,112]

[111] Parrott, M. C.; Luft, J. C.; Byrne, J. D.; Fain, J. H.; Napier, M. E.; DeSimone, J. M. Tunable Bifunctional Silyl Ether Cross-Linkers for the Design of Acid-Sensitive Biomaterials. *J. Am. Chem. Soc.* **2010**, *132*, 17928–17932.

Moving from the model systems that demonstrated the proof of principle and *in vitro* benign behavior of the silyl ether link, DeSimone and coworkers reported the use of dialkoxydialkysilanes as prodrugs of camptothecin (**233**), gemcitabine (**234**), and dasatinib (**235**) shown in Figure 2.10. A suite of three different dialkyl groups was examined to determine the effect of steric bulk on the release rates of their prodrugs. Namely the [(ethyl, **233a, 234a, 235a**), (isopropyl, **233b, 234b, 235b**), and (tert-buyl, **233c, 234c, 235c**)] versions of the prodrugs along with hydroxyethyl acrylate were cross-linked with PEG-diacrylate **236** through the acrylate moiety to form a polymer network.

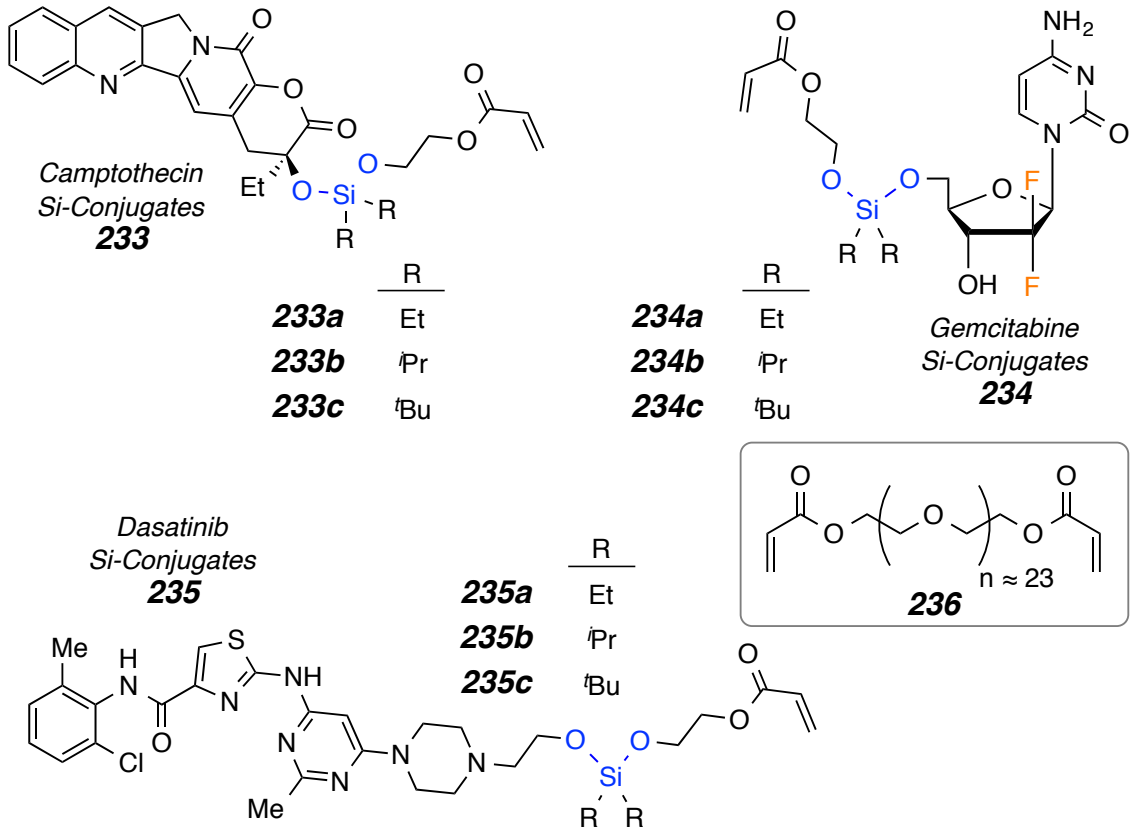

Figure 2.10 I Structures of all dialkoxydialkyl silane drug derivatives **233-235** reported by DeSimone.[112]

[112] Parrott, M. C.; Finniss, M.; Luft, J. C.; Pandya, A.; Gullapalli, A.; Napier, M. E.; DeSimone, J. M. Incorporation and Controlled Release of Silyl Ether Prodrugs From PRINT Nanoparticles. *J. Am. Chem. Soc.* **2012**, *134*, 7978–7982.

The PEG-diacrylate (MW=1000) served as the hydrophilic portion, so that the macromolecule could be formulated into nanoparticles. Interestingly, they determined that the hydrolysis and subsequent release of the parent drug was influenced by the steric bulk of the two alkyl units around the silicon. This report gives encouraging results and precedent for the use of silicon as a prodrug construct that we will discuss in Chapter 3.

Instead of incorporating dual functionality into the prodrug, we envisioned utilizing the silicon atom as both the labile moiety and anchoring into the nanoparticle through FNP.[113] More specifically, Cheng used an ester as the labile link to release the drug and the silane as the anchor into nanoparticles, Wang utilized a disulfide and carbonate as the labile linker and silane as the anchor, and lastly DeSimone used the silane as the labile link and a cross linked polymer ester as the anchor. We hypothesize that a silane of an appropriate hydrophobicity can serve as both the labile linker and the anchor to release the drug from nanoparticle. This can be accomplished by the encapsulation of a drug-silicon-conjugate into a block copolymer through FNP.

Before embarking on the design and synthesis of silanes or silicates for use as prodrug constructs, I performed a series of Reaxys® searches to determine the prevalence of functionalization at each hydroxyl in **PTX**.[114] Reaxys allows for wild cards to serve as any group (G*). Initial substance searches using G* at C-1,C-2', or C-7 quickly show that functionalization at the C-2' position is the most common (721 vs 370 vs 2) and of those the silanes/silicates of **PTX** are shown in grey. The 2',7-functionalized **PTX** is also quite prevalent. The number of reactions that generated a generic G* functionalized product **237-243** from PTX is shown in the fourth column from the right. Again the 2'-monofunctionalized **PTX** (**238**) is dominate. However the 2',7-bis functionalized (**242**) has 113 hits

[113] Hoye, T. R.; Wohl, A. W.; Macosko, C. W.; Panyam, J. Silicate prodrugs and nanoparticles. U.S. Patent Application PCT/US2012/040247, May 31, 2012.

[114] Reaxys, version 2.19790.2; Elsevier; 2015; RRN 969209 (accessed July 13, 2015).

compared with the 90 hits of the 7-monofunctionalized **PTX** compound (**239**). This suggests that the bis-derivative is typically made first followed by cleavage of the 2'-group. This is further confirmed in the second column from the right. The bis-functionalized **242** is made from **238** considerably more than from **239**. Also **239** arises from the bis-functionalized **242** more frequently than from **PTX** itself (184 hits vs. 91 hits). There is little to no reactivity at the C-1 hydroxyl (**237**, **240**, **241**, **243**). These searches match well with the literature reactivity differences of the hydroxyls of PTX, namely C-2' > C-7 >> C-1.

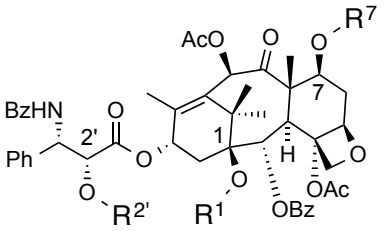

							Substances		*Reactions From:*			
									PTX		**Compounds**[a-d]	
	R1		**R2'**		**R7**		**Hits**		**Hits**		**Hits**	
237	G*	$Si(G^*)_3$	H	H	H	H	2	0	0	0	1[a]	0[a]
238	H	H	G*	$Si(G^*)_3$	H	H	721	60	256	16	19[b]	2[b]
239	H	H	H	H	G*	$Si(G^*)_3$	370	80	91	5	184[b]	6[b]
240	G*	$Si(G^*)_3$	G*	$Si(G^*)_3$	H	H	0	0	0	0	0	0
241	G*	$Si(G^*)_3$	H	H	G*	$Si(G^*)_3$	6	0	0	0	0	0
242	H	H	G*	$Si(G^*)_3$	G*	$Si(G^*)_3$	289	16	113	9	156[c]/16[d]	4[c]/0[d]
243	G*	$Si(G^*)_3$	G*	$Si(G^*)_3$	G*	$Si(G^*)_3$	1	0	0	0	1[b]	0[b]

G* = any group except hydrogen [a] from **240**, [b] from **242**, [c] from **238**, [d] from **239**

Figure 2.11 I Reaxys® searches showing the prevalence of hydroxyl functionalization of **PTX**. Reaction searches were run from every compound to the others and contained 0 hits unless otherwise noted in columns 12 and 13.

Chapter 3. Silicate Ester Prodrugs of PTX & DTX

3.1 Silicate Ester Prodrug Hypothesis

Below is a summary of the lengthy background information found in chapters 1 and 2, used to refresh and orient the reader to our hypothesis. Paclitaxel (**PTX**) is a potent antimitotic antitumor compound. It is the active agent in front-line chemotherapeutic drugs used for treatment of a variety of cancers.[115,, 54] Because it is only minimally water-soluble, **PTX** is administered to humans as a drug formulation that is formed by its solubilization with an emulsifier (a 1:1 (v/v) mixture of polyethoxylated castor oil and absolute ethanol), with human serum albumin, or with PEG-PLA. These formulations comprise a significant advance in chemotherapeutics, but the drug loading is relatively low (1.1, 10, and 16.7 wt% **PTX**, respectively), and in the case of the first significant undesirable side effects of the emulsifier are experienced by some patients. Similarly, the closely related taxane docetaxel (**DTX**) is administered as an ethanolic suspension of 4 wt/vol% **DTX** in polysorbate 80.

Because these taxanes are such effective cytotoxins, new conceptual and practical strategies for improving the administration of PTX and DTX remain desirable. In particular, drug delivery vehicles containing higher drug loading levels than currently in the front-line drug formulations mentioned above have the potential to be quite advantageous. Accordingly, we envision that proper matching of the physicochemical properties of a taxane derivative with a suitable polymer-based drug carrier might allow for formulation of an effective nanoparticle drug delivery entity. One potentially attractive strategy is the incorporation of drugs into block-copolymer(BCP)-based nanoparticles (NPs) by rapid co-precipitation of the drug and the BCP in a process known as flash

[115] Ismael, G. F. V.; Rosa, D. D.; Mano; M. S., Awada, A. Novel cytotoxic drugs: Old challenges, new solutions. *Cancer Treat. Rev.* **2008**, *34*, 81–91.

nanoprecipitation (FNP).[116,117] This can provide NPs with dimensions attractive from a drug delivery perspective and that are highly loaded (to ≥50 wt%) with the small molecule drug agent. FNP has been used to prepare NPs comprising PTX and various BCPs–in particular, the biocompatible poly(ethylene glycol)-*b*-poly(ester) amphiphilic block polymers PEG-PCL, PEG-PLA, or PEG-PLGA [where the poly(ester) is poly(caprolactone), poly(lactic acid), or poly(lactic/glycolic acid), respectively].[85,86] However, the resulting aqueous dispersions of these PTX-loaded NPs were kinetically unstable; the **PTX** exited the hydrophobic core of the particle and crystallized in the exterior in a matter of minutes, presumably via the mechanism of Ostwald ripening.[82,80] We envision that this undesirable process could be arrested by use of a modified taxane derivative that is *more* hydrophobic than the parent drug molecule. Moreover, if that derivative is susceptible to reversion back to the parent taxane, say by simple hydrolysis, then it could serve as a taxane prodrug.[118]

We hypothesize that silicate esters, tetra-alkoxy silanes [$(RO)_4Si$], comprise a class of prodrugs that are well suited for the encapsulation into nanoparticles. The general concept is portrayed in Figure 3.1. A parent drug molecule containing a reactive hydroxyl group is converted to its tetraalkoxysilane (the silicate derivative) by reaction with a trialkoxychlorosilane[119] derivatizing agent.[120] Eventual hydrolytic cleavage returns

[116] Johnson, B. K.; Prud'homme, R. K. Chemical processing and micromixing in confined impinging jets. *AIChE.* **2003**, *49*, 2264–2282.

[117] Johnson, B. K.; Prud'homme, R. K. Flash nanoprecipitation of organic actives and block copolymers using a confined impinging jets mixer. *Aust. J. Chem.* **2003**, *56*, 1021–1024.

[118] Wohl, A. R.; Michel, A. R.; Kalscheuer, S.; Macosko, C. W.; Panyam, J.; Hoye, T. R. Silicate esters of paclitaxel and docetaxel: synthesis, hydrophobicity, hydrolytic stability, cytotoxicity, and prodrug potential. *J. Med. Chem.* **2014**, *57*, 2368–2379.

[119] Corriu, R. J. P.; Granier, M.; Lanneau, G. F. Synthesis and reactivity of bis(triethoxysilyl)methane, tris(triethoxysilyl)methane and some derivatives. *J. Organomet. Chem.* **1998**, *562*, 79–88.

[120] Wohl, A. R. Synthesis and characterization of silicate esters prodrugs and poly(ethylene glycol)-b-poly(lactic-co-glycolic acid) block copolymers for formulation into prodrug-loaded nanoparticles. Ph.D. Dissertation, University of Minnesota, Minneapolis, 2012.

the parent drug. Note that a number of studies imply that orthosilicic acid [$Si(OH)_4$], the ultimate stoichiometric byproduct of silicate ester cleavage, does not pose any significant toxicity issues.[121, 122, 123] The nature of the three auxiliary R groups in the silicate prodrug (Figure 3.1) would provide considerable flexibility in allowing for adjustment of the degree of hydrophobicity as well as the hydrolytic stability of the derivative.[118]

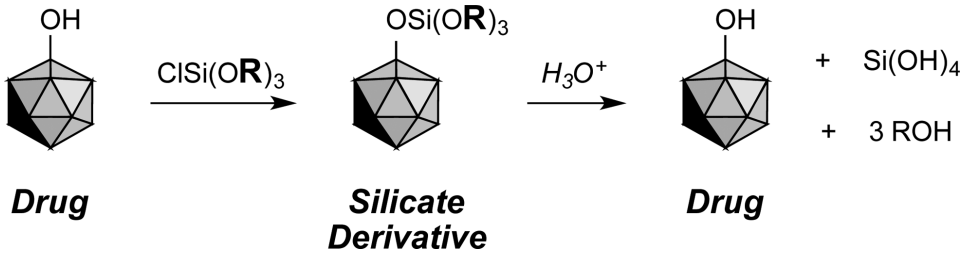

Figure 3.1 I Potential silicate prodrug strategy. Modification of a hydroxyl group in the drug with a trialkoxychlorosilane generates the (labile) silicate derivative, which following administration under- goes hydrolysis to return the free drug along with benign alcohol and orthosilicic acid byproducts.

After the appropriate model studies using simple alcohols were established some of which are presented in Part II: Chapter VI of this thesis, attention was devoted to **PTX** and **DTX**. In this chapter the synthesis and selected properties of the desired taxane based silicates are reported. Also the inherit lability: *i.*) rates of hydrolysis of the silicates back to the parent drugs, *ii.*) stability in biologically relevant media, and iii.) prodrug form after cell uptake are shown.

[121] Gitelman, H. J.; Alderman, F.; Perry, S. J. Renal handling of silicon in normals and patients with renal insufficiency. *Kidney Int.* **1992**, *42*, 957–959.

[122] Marco-Franco, J. E.; Torres, V. E.; Nixon, D. E.; Wilson, D. M.; James, E. M.; Bergstrahl, E. J.; McCarthy, J. T. Oxalate, silicon, and vanadium in acquired cystic kidney disease. *Clin. Nephrol.* **1991**, *35*, 52–58.

[123] Anglin, E. J.; Cheng, L.; Freeman, W. R.; Sailor, M. J. Porous silicon in drug delivery devices and materials. *Adv. Drug Deliv. Rev.* **2008**, *60*, 1266–1277.

3.2 Silicate Ester Prodrugs of PTX and DTX

From the extensive reactivity studies of **PTX** presented in Chapters 1 and 2, we were confident that the reactions of chlorosilanes with **PTX** or **DTX** would occur smoothly. We were however worried about the inherit lability associated with the silicate esters and whether purification on silica gel would cleave the functionality and return it back to the parent drug. A suite of chlorotrialkoxysilanes was synthesized from silicon tetrachloride and aliphatic alcohols with a varying degree of steric hindrance at the silicon center, which will be described in detail in Chapter 3.3. Gratifyingly, the initial model studies showed that silicates survived column chromatography and likewise the taxane-based silicates could also be purified.[120]

When describing the silicate esters of either **PTX** or **DTX**, we chose to name them according to the extent of functionalization. When the C-2' hydroxyl was modified the 2'-mono description shown in Figure 3.2 was used, namely mono PTX-2'-$Si(OR)_3$. Likewise the C-7 position was named as a 7-mono silicate, PTX-7-$Si(OR)_3$. Lastly the 2',7-bis descriptor is used when both positions are modified with a silicate. Although functionalization at the C-10 hydroxyl of **DTX** is achievable, we opted to simply test the reaction, but refrained from taking these compounds on for sake of reducing the complexity. Nevertheless, when referring to a near exhaustive derivatization of **DTX** the 2',7,10-tris designation refers to DTX-2',7,10-$[Si(OR)_3]_3$.

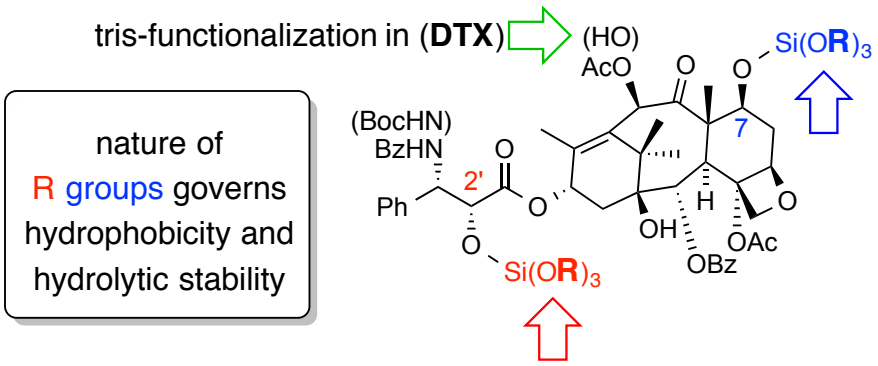

Figure 3.2 I Paclitaxel silicate conjugation at either the 2'-hydroxyl or the 7-hydroxyl renders the drug highly hydrophobic.

3.3 Synthesis of Silicate Ester Prodrugs of PTX and DTX

To functionalize each taxane with a silicate ester, we took advantage of the known reactivity difference of the free hydroxyl groups in either **PTX** or **DTX** (Scheme 4). The reactivity rates are gleaned from the total synthesis and analogue synthesis presented in Chapter 1. In **PTX** the three hydroxyl groups are derivativized in a relative rate of C2' > C7 > C1,[124, 3] which reflects, principally, the relative steric hindrance among the three. In **DTX** the order of reactivity is C-2' > C-7 > C-10 > C-1. Selective mono-silylation at C2' in PTX to give the silicates **301a-c** was best achieved when a trialkylamine (e.g. triethylamine) was used as the base to promote reaction with the appropriate chlorosilane reagent (**305a-c**).

The preparation of the requisite chlorosilanes **305b**,[125] **305c**,[126] **305d**,[127] and **306**[128, 129] is indicated in Scheme 3.1 (panel c); **305a** and **305e** are

[124] Skwarczynski, M.; Hayashi, Y.; Kiso, Y. Paclitaxel prodrugs: Toward smarter delivery of anticancer agents. *J. Med. Chem.* **2006**, *49*, 7253–7269.

[125] Gerrard, W.; Howe, B. K. The behaviour of 1,1,1,3,3,3-hexachloropropan-2-ol with inorganic non-metal halides. *J. Chem. Soc.* **1955**, 505–510.

[126] Chappelow, C. C.; Elliot, R. L.; Goodwin, J. T. The phenylation and methylation of alkoxychlorosilanes. *J. Org. Chem.* **1960**, *25*, 435–439.

commercially available. Use of the hindered tertiary alkylamine rather than pyridine showed greater selectivity for C2'-mono-silicate ester production with minimal formation of the C2',C7-bis-silicate esters.

In the case of the hindered trimenthyloxychlorosilane reagent (**301d**), the second silylation at C7 was very slow. Accordingly, we experienced little difficulty in using the less selective catalyst, pyridine for the preparation of trimenthyl silicate derivatives. The mixed, *tert*-butoxy-containing silicates **301f-h** were prepared using an excess of the bulky electrophile $(t\text{BuO})_2\text{SiCl}_2$ (**306**) and pyridine as the base. As with the menthyl-containing reagent **301d**, we again did not observe competitive reaction at C7. Addition of an excess of ethanol (for **301f**) or acetic acid (for **301g**) to substitute the second chloride (as well as consume the excess of **306** still present) allowed isolation of the mixed silicates **301f-h**, respectively, albeit in overall modest to low yields. On one occasion a small amount of the tri(*tert*)butyl silicate **301e** was isolated from an experiment using an *in situ*-generated (and less pristine) lot of the chlorosilane reagent **306**. Attempts to prepare **301e** using a commercial sample of $(t\text{-BuO})_3\text{SiCl}$ (**305e**) and pyridine, even at elevated temperatures, gave no evidence of reaction. We presume that **301e** was produced by way of the intermediate PTX-Si(O-*t*Bu)$_2$Cl followed by subsequent reaction with *t*-BuOH.

The PTX C2',C7-bis-silicate esters **302a-d** were best prepared using the less hindered pyridine as the base and a larger excess (3-4 equiv) of the $(\text{RO})_3\text{SiCl}$ **305a-c**. The C7-mono-silicate **303a-c** derivative of PTX was accessed by selective hydrolytic cleavage [trifluoroacetic acid (TFA), H_2O, acetone] of the more labile C2'-silicate ester present in the bis-derivative **302a-c**, respectively.

---

[127] Beckman, J.; Daketernieks, D.; Tiekink, E. R. T. Chiral trialkoxysilanols derived from terpene alcohols. Molecular structures of tris([(1S)-endo]-(–)-bornoxy)silanol and tetrakis((–)-menthoxy)silane. *J. Organomet. Chem.* **2002,** *648*, 188-192.

[128] Gerrard, W.; Woodhead, A. H. Interaction of alcohols with silicon tetrachloride. *J. Chem. Soc.* **1951**, 519–522.

[129] Miner, C. S., Jr.; Bryan, L. A.; Holysz, R. P., Jr.; Pedlow, G. W., Jr. *tert*-Alkoxyaminosilanes. *Indust. Engin. Chem.* **1947**, *39*, 1368–1371

Similarly, the DTX 2'-monosilicate esters **304a-e** (Scheme 3.1, panel b) were prepared. In these experiments we chose to use a different tertiary amine, *n*-butyl(dimethyl)amine, and, as we conjectured, it showed comparably good C2' vs. C7 selectivity as triethylamine but a faster reaction rate under otherwise identical conditions.[118]

Scheme 3.1 I [a] Synthesis of silicate ester derivatives of PTX (**301a-h**, **302a-d**, and **303a-b**, panel **a**) and DTX (**304a-e**, panel **b**) and of the necessary chlorosilane derivatizing agents (**305** and **306**, panel **c**).

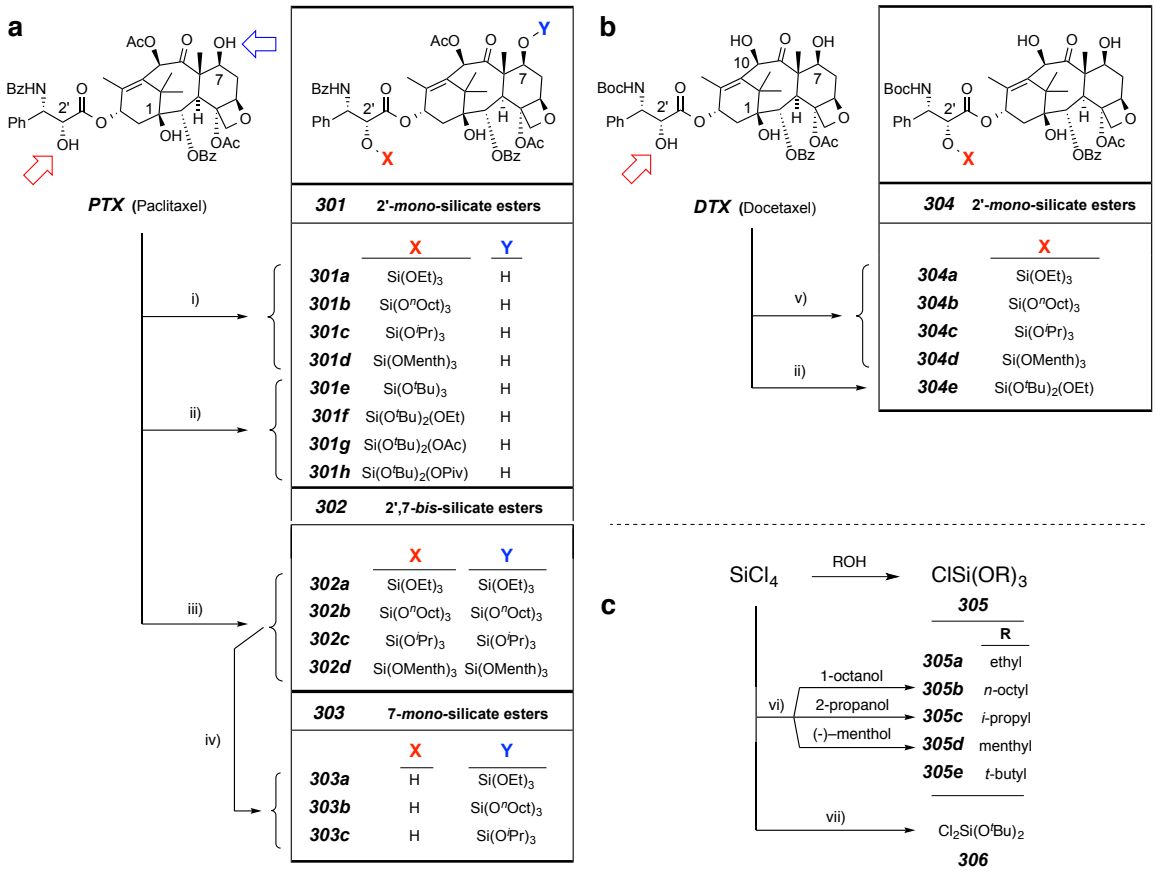

[a] Conditions: (i) $SiCl(OR)_3$ (**305a-d**), NEt_3 (for **301a-c**) or py (for **301d**), THF. (ii) $SiCl_2(O^tBu)_2$ (**306**), py, THF; then EtOH (for **301f** or **301e**) or AcOH (for **301g**) or PivOH (for **301h**). (iii) $SiCl(OR)_3$ (**305a-c**), py, THF. (iv) acetone, water, TFA (90/9/1, v/v/v). (v) $SiCl(OR)_3$ (**305a-d**), *n*-$BuNMe_2$ (for **304a-c**) or py (for **304d**), THF. (vi) alcohol, rt, pentane. (vii) *t*-BuOH (2.1 equiv), py, THF. Yield of chromatographed taxane silicate: **301a** (91%); **301b** (81%); **301c** (65%); **301d** (62%); **301e** (18%); **301f** (93%); **301g** (66%); **301h** (12%); **302a** (85%); **302b** (77%); **302c** (67%); **302d** (35%); **303a** (91%, brsm); **303b** (66%, brsm); **303c** (77% brsm); **304a** (65%); **304b** (64%); **304c** (85%); **304d** (44%); **404e** (60%). brsm = based on recovered starting material.

3.4 Synthesis of "Specialty" Prodrugs of PTX and DTX

Several more-exotic silicate constructs were also synthesized to address new questions. These prodrugs were used to probe different aspects of the silicate prodrug strategy and/or to provide a proof of concept. Triethylsilylether **308a** was used to test the importance of a silicate ester moiety for cytotoxicity. The hydrogen-silane **313** was synthesized to determine the stability of PTX-silanes through hydrolysis. Extreme hydrophobicity present in the phytol derived silicate **319**, was explored to determine the effecton particle size and subsequently release. Lastly, the **DTX** bis-silicate **320a** was used as a control to verify the cytotoxicity of the analogous **PTX** bis-silicates.

Following the functionalization procedure of **PTX** with the requisite chlorosilane as shown in Scheme 3.1, the synthesis of the PTX-2'-TES (**308a**) went smoothly when **PTX** was reacted with triethylsilylchloride (TES-Cl) in the presence of pyridine base (Scheme 3.2). The reaction proceeded more slowly than the analogous reaction with triethoxychlorosilane (**305a**), showing only 50% conversion after 12 hours at room temperature. The heating of the reaction to 45 ˚C for 3 hours resulted in > 90% conversion as determined by LC-MS. Following purification by MPLC, a 45% yield of the product was obtained.

Scheme 3.2 I Synthesis of 2'-triethylsilyl protected paclitaxel PTX (**308a**).

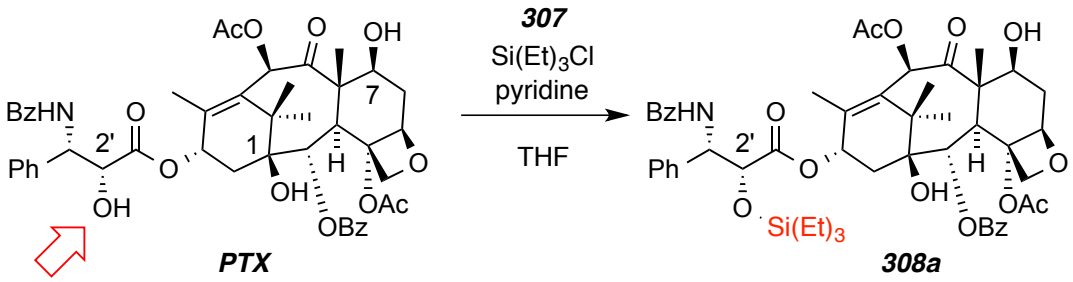

The protection of **PTX** as its TES-ether **308a** allowed us to compare the lability of a PTX-silicate [PTX-2'-$Si(OR)_3$] to that of a silylether of **PTX** [PTX-2'-

SiR_3]. As discussed in detail below the half-life for hydrolysis of the silylether **308a** was observed to be 15 times slower than that of the corresponding silicate **301a** (Table 3.2). The cytotoxicity of **308a** was also compared to that of the silicate **301a**; it showed a 25-fold decrease in potency (Table 3.4). Also upon hydrolysis the trialkylsilyl moiety is converted to the trialkylsilanol which raise a separate set of toxicity issues.[130] These studies show the importance of using a silicate as a prodrug construct over alkyl-silane chemistry.

Since the trialkylsilane based prodrug **308a** showed poor cytotoxicity, a slower rate of hydrolysis, and degrades into the silanol, the hydrogen-based silanes were explored. Trichlorosilane (**310**) was reacted with 2.2 equivalents of *n*-octanol to afford the monochlorosilane **311** (Scheme 3.3). Since a slight excess of the alcohol was used, the corresponding trioctyloxysilane (**312**) was observed by GC-MS. The reaction mixture containing 80% of the monochlorosilane was used without purification and reacted with **PTX** in the presence of *N,N*-dimethylbutylamine base. The hydrogen-based silane, PTX-2'-$Si(H)(O^nOCt)_2$ **313**, was obtained in a 59 % yield as shown in scheme 3.3.

[130] Showell, G. A.; Mills, J. S. Chemistry Challenges in Lead Optimization: Silicon Isosteres in Drug Discovery. *Drug Discov. Today* **2003**, *8*, 551–556.

Scheme 3.3 I Synthesis of PTX-2'-dioctyloxysilane (**313**).

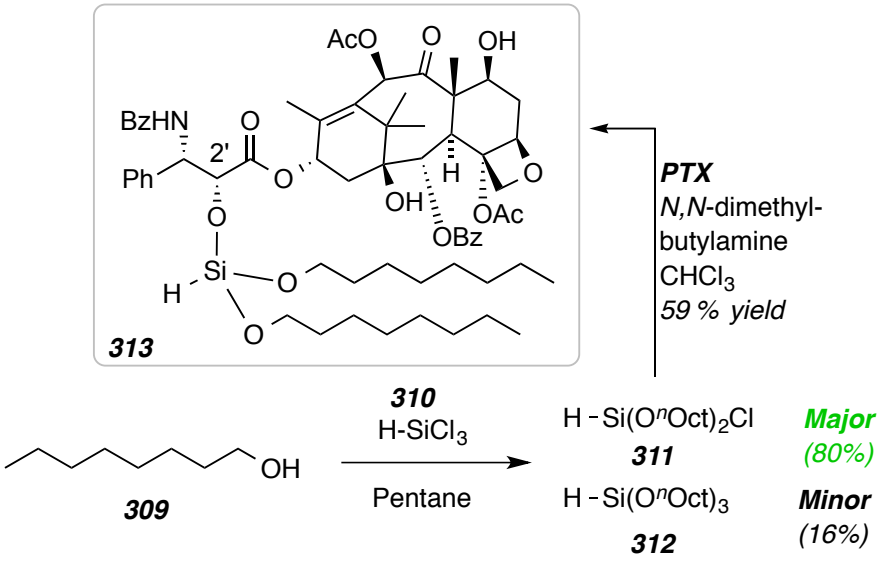

The hydrolysis rate of (**313**) was compared to the relative rate of the analogous silicate PTX-2'-Si(O^nOct)$_3$ (**301b**) (Table 3.2). Silane **313** is 1.5 times slower than **301b**. This indicates that the use of hydrogen for the replacement of a primary alkoxy group does not increase lability. Although the hydrolysis data is encouraging, no biological experiments were performed on the compound. Interestingly, the use of the silane allows for the reduction in the molecular weight of the prodrug while maintaining the hydrolytic stability.

Instead of exploring more of the hydrogen based silanes rate of hydrolysis, we turned our attention to drastically alter the hydrophobicity of silicate based prodrugs. We envisioned creating a hydrophobic prodrug that was so lipophilic that the release from a nanoparticle would not occur unless the silicate hydrolyzed. To meet this goal, we turned to dihydrophytol (DHP) as the lipophilic side chain.

Phytol (**314**) was hydrogenated by hydrogen at 40 psi in the presence of water and sodiumbicarbonate over a powdered bed of platinum(II)oxide (scheme

3.4).[131] Dihydrophytol **315** was purified by flash chromatography, to provide the primary alcohol. The removal of the alkene was done to mitigate any problems that may arise from silylation of an allyl alcohol. The addition of DHP to silicon tetrachloride required the use of pyridine and THF to facilitate the formation of the tridihydrophytolchlorosilane (**316**) as well as the fully substituted silicate (**317**). Attempts were made without the presence of base, however only the mono- and di- adduct were observed. The mixture containing the monochlorosilane was added to **PTX** dissolved in THF and allowed to react for > 96 hours. Periodically, an aliquot of the reaction was removed and analyzed by NMR spectroscopy. Once downfield shifts were observed on the C2' and C7 methine protons the reaction was purified by MPLC. We were pleased when the crude 1H-NMR indicated functionalization to the product, because previous attempts to generate the product with varied sources of the chlorosilane **316** and the different bases in THF had failed.

[131] Burns, C. J.; Field, L. D.; Hashimoto, K.; Petteys, B. J.; Ridley, D. D.; Rose, M. Synthesis of Stereoisomerically Pure Monoether Lipids. *Aust. J. Chem.* **1999**, *52*, 387–394.

Scheme 3.4 I Synthesis of PTX-7-Si(DHP)$_3$ (**303p**) from phytol (**314**).

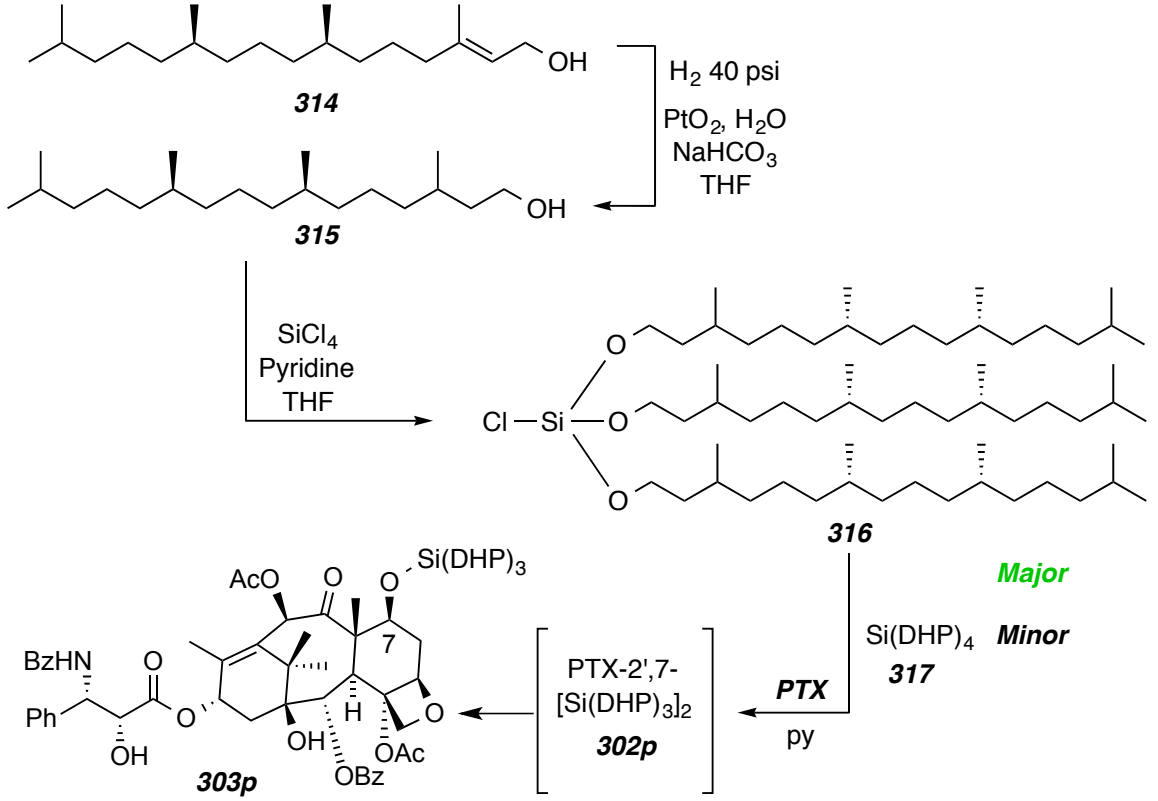

After three sequential purifications by MPLC, the C7 functionalized prodrug (**303p**) was isolated and characterized by NMR. We hypothesize that the bis-adduct (**302p**) was formed, but during all of the handling the C2' silicate cleaved. Although the C2' prodrug was not isolated, the C7 prodrug (**303p**) analogous to **303b** provided a stable sample that was used to probe the effect of hydrophobicity. Due to the recovery of a small amount of a material the reaction was optimized in hopes to obtain the C2'-silicate **301p**.

Initial attempts at optimizing the reaction included: *i.*) heating the reaction mixture (**PTX**, py, **316**, and THF) up to 45 ˚C, *ii.*) changing the source of chlorosilane to a more pure starting material **316**, *iii.*) changing the base to *N,N*-dimethylbutylamine, and *iv.*) changing the solvent to $CDCl_3$ or CH_2Cl_2. Gratifyingly, when the solvent was changed to a chlorinated system in which

everything was homogenous throughout the reaction (pyridinium chloride salt was fully soluble in $CDCl_3$) the reaction proceeded smoothly. The $CDCl_3$ solvent system was chosen to easily monitor the reaction by ^{1}H-NMR. The C2'-silicate was isolated by MPLC along with a minor amount of bis-functionalized material. The stability of **301p** was probed through hydrolysis and is compared in chapter 3.5. I was thrilled to synthesize this compound as it has the highest hydrophobicity to date with a clogP of 8.50, and yet a reasonable rate of hydrolysis ($t_{1/2}$ = 130 mins).

Scheme 3.5 I Synthesis of PTX-2'-Si(DHP)$_3$ (**301p**)

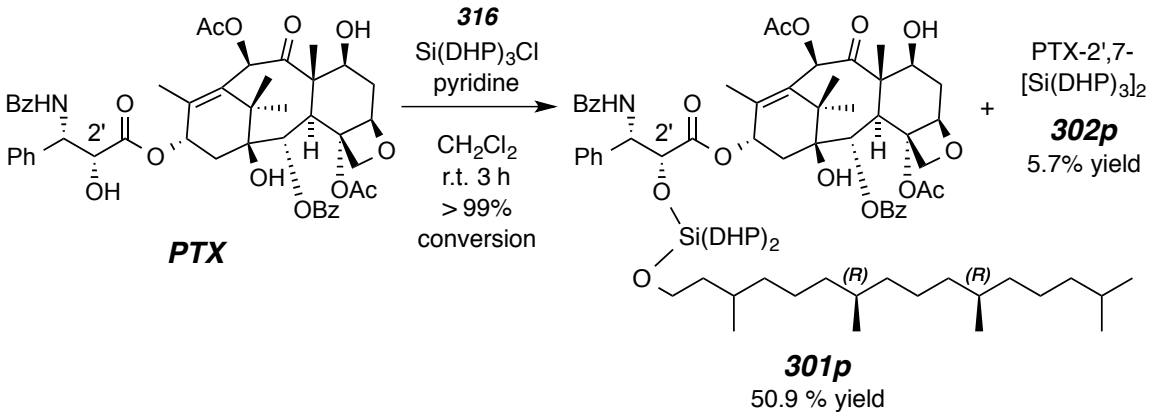

We were very interested in determining the size of the particles generated with the highly hydrophobic silicate **301p**, as particle size tended to decrease with an increasing hydrophobicity. Nanoparticles were fabricated by the FNP process (details of which are presented in Chapter 4) and showed an intensity average diameter of 101 ± 2 nm and a pdi of 0.22 ± 0.02. The particle diameter of 100 nm falls with in the EPR range (Chapter 2) and the pdi indicates that range of particle sizes is modestly uniform. All of these values: hydrophobicity, hydrolytic lability, and particle size are very encouraging for our silicate prodrug and nanoparticle strategy.

Lastly, the bis-functionalized prodrug of DTX was synthesized to compare with the IC_{50} values of the analogous PTX-2,7-[Si(OEt)$_3$]$_2$. The synthesis

followed the bis-functionalization procedure shown in Scheme 3.6, however the functionalization had to be monitored due to the use an excess of the silyating agent (**305a**) and the ability to derivatize the C10 hydroxyl in DTX (scheme 3.6). Upon full conversion of the reaction the bis-silicate ester (**318a**) was isolated after column chromatography. As expected the derivatization increased the IC_{50} compared to the mono-functionalized **304a** and the parent DTX (Table 3.4). This trend followed the decrease in potency as seen in the PTX series of silicates.

Although reactions with an excess of **305a** and **305c** showed the formation of tris-adducts in which the C10 hydroxyl is also functionalized by LC-MS, we chose refrain from isolating these compounds. Ultimately, the C10 hydroxyl could serve as another handle to modify hydrophobicity and hydrolytic lability.

Scheme 3.6 I Synthesis of bis-silicate ester of **DTX** (**318a**).

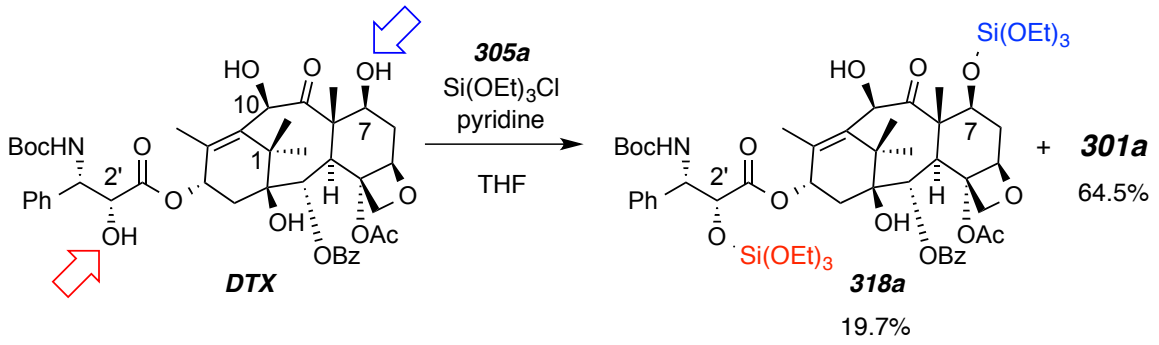

3.5 Hydrophobicities and Hydrolytic Lability of Taxane Prodrugs

3.5.1 Hydrophobicity Indicators for Taxane Prodrugs

The relative hydrophobicities of the silicate esters was assessed in several ways. Qualitatively, we observed the expected trend that the silicates with greasier alkyl groups traveled faster on silica gel during thin layer and preparative chromatographic experiments. A more quantitative measure of this same trend was observed from measurement of the retention times on a reversed-phase HPLC column (Table 3.1, column 4). In addition, two empirical indicators of hydrophobicity show similar trends: *i.*) calculated octanol:water partition coefficients (cLogP values, Table 3.1, column 5)[132] and *ii.*) calculated aqueous solubilities (Table 3.1, column 6).[133] It has been noted that calculated hydrophobicities can vary tremendously depending on the weights assigned for each functional group in the empirical equations.[134]

Additional calculated values of the octanol:water partition coefficients from a variety of programs is shown in the supporting information (SI, Table S3.1). The calculated water solubility gives a sense of the highly hydrophobic nature of these prodrugs (SI, Table S3.2). Lastly, empirical calculations of the structure are shown in SI Table S3.3. The calculated volume, total number of non hydrogen atoms/number of oxygen and nitrogen atoms/number of O-H and N-H bonds [natoms/nON/nOHNH], number of rotable bonds [nrotbonds], and Molecular Polar Surface Area [TPSA], serve as guidelines to determine how "drug like" the prodrugs are. Although none of these calculated values solely

[132] Tetko, I. V.; Gasteiger, J.; Todeschini, R.; Mauri, A.; Livingstone, D.; Ertl, P.; Palyulin, V. A.; Radchenko, E. V.; Zefirov, N. S.; Makarenko, A. S.; Tanchuk, V. Y.; Prokopenko, V. V. Virtual computational chemistry laboratory—design and description. *J. Comput. Aid. Mol. Des.* **2005**, *19*, 453–463.

[133] Tetko, I. V.; Tanchuk, V. Y.; Kasheva, T. N.; Villa, A. E. Estimation of aqueous solubility of chemical compounds using E-state indices. *J. Chem. Inf. Comput. Sci.* **2001**, 41, 1488–1493.

[134] Eros, D.; Kovesdi, I.; Orfi, L.; Takacs-Novak, K.; Acsady, G.; Keri, G. Reliability of logP predictions based on calculated molecular descriptors: a critical review. *Curr. Med. Chem.* **2002**, *9*, 1819–1829.

defines the drugs, collectively they are indicative of molecular structure and show the breath of this silicate prodrug strategy for nanoparticle formulations.

Table 3.1 | Hydrophobicity indicators for the silicate esters **301–313.**

Sub-strate	2' alkyl	7 alkyl	retention time t_R (min)[a] C18 (ODS)	calcd octanol:water partition coefficient (cLogP)[b]	calculated aqueous solubility (cLogS[133] mg/L)
PTX	-	-	10.5	3.20	5.56
301a	Et	-	13.8	4.96	2.66
301b	^{n}Oct	-	22.1	7.74	0.24
301c	^{i}Pr	-	15.4	5.60	1.57
301d	menthyl	-	24.5	7.37	0.25
301f	(^{t}Bu)$_2$/Et	-	16.1	5.81	0.94
301g	(^{t}Bu)$_2$/Ac	-	– [c]	5.32	0.98
301h	(^{t}Bu)$_2$/Piv	-	16.2[d]	5.83	0.66
301p	DHP	-	– [e]	8.50	0.028
302a	Et	Et	16.6	6.31	1.70
302b	^{n}Oct	^{n}Oct	– [e]	8.59	0.13
302c	^{i}Pr	^{i}Pr	18.9	6.84	0.87
302d	menthyl	menthyl	– [e]	8.06	0.090
302p	DHP	DHP	– [c]	7.88	0.021
303a	-	Et	14.6	5.05	2.33
303b	-	^{n}Oct	24.6	7.84	0.22
303c	-	^{i}Pr	16.4	5.64	1.44
303p	-	DHP	– [e]	8.52	0.025
308a (PTX-SiEt$_3$)		-	15.4	5.40	1.06
313	(^{n}Oct)$_2$/H	-	23.2	7.07	0.27
DTX	-	-	10.9	2.83	12.72
304a	Et	-	14.1	4.05	6.84
304b	^{n}Oct	-	22.4	7.34	0.32
304c	^{i}Pr	-	15.9	4.99	3.78
304d	menthyl	-	26.1	7.02	0.29
304e	(^{t}Bu)$_2$/Et	-	16.4	5.29	2.58
318a	Et	Et	13.9[f]	5.81	3.92

[a] Each retention time was determined by gradient elution‡ from LC-MS on an (octadecyl)silyl (ODS, C18) column [5 µm, 4.6 (i.d.) x 150 mm] using a flow rate of 1 mL/min. ‡56/44% methanol/water to 98/2% methanol/water (15 mM NH_4OAc) over 15 min followed by an appropriate final hold time.

[b] aLogP[132] data shown here; see SI (Table S3.1) for the values from these additional empirical predictors of cLogP: AC logP, KOWWIN, miLogP, XLOGP3; the trends among the values from any of these methods are very similar for all of the predictors.

[c] Not determined.

[d] retention time was determined by gradient elution‡ from LC-MS on an (octadecyl)silyl (ODS, C18) column [5 µm, 4.6 (i.d.) x 150 mm] using a flow rate of 1 mL/min. ‡28/72% methanol/water to 98/2% methanol/water (15 mM NH_4OAc) over 30 min followed by an appropriate final hold time. The pivilate hydrolysis product silanol had a R_t of 13.8 min.

[e] Not observed; elution time >60 min.

[f] retention time was determined by gradient elution‡ from LC-MS on an (octadecyl)silyl (ODS, C18) column [5 µm, 4.6 (i.d.) x 150 mm] using a flow rate of 1 mL/min. ‡75/25% methanol/water to 98/2% methanol/water (15 mM NH_4OAc) over 15 min followed by an appropriate final hold time.

As anticipated the “specialty silicates” derived from the 18-carbon isoprenoid phytol gave the greatest hydrophobicities. Interestingly, the aLogP program begins to top off at a value of 8.5, as the **302p** prodrug showed a lower clogP than either of the mono-silicates (**301p**, **303p**). This further validates the need to use multiple clogP values to give a *feel* of hydrophobicity.

3.5.2 Hydrolytic Lability of Taxane Prodrugs

We anticipated that these silicates would also differ in their hydrolytic lability given the differences in steric bulk at the silicon atom of the silicate esters across the series. We explored this question by devising a ^{1}H NMR spectroscopy-based method [135] to establish the relative rates of chemical hydrolysis of the derivatives (Table 3.2). By design, these silicate esters were sufficiently highly hydrophobic to render them only marginally soluble in buffered aqueous solutions. To get meaningful fundamental understanding of the hydrolytic lability under acidic conditions, we deemed it essential to identify a common set of conditions under which each of the silicates would be fully soluble—that is, homogeneity is paramount. We determined that a 10:1 (vol:vol) ratio of acetone:water would solubilize all of these silicates at concentrations suitable for NMR analysis. We then established that use of 1% TFA in this solvent mixture (measured pH = 0.8) at ambient temperature led to rates of silicate ester cleavage that could be conveniently monitored spectroscopically. The change in intensity over time of the chemical shifts of H2', H3', H7, and/or the OC*H* resonances in the R groups as the silicates were cleaved to release PTX and ROH was monitored. For all silicates not containing a menthyloxy or *t*-butoxy moiety (Table 3.2, footnote b), we saw no evidence for partially hydrolyzed silanol intermediates [i.e., $(RO)_nSi(OH)_{4-n}$]. This suggests that the initial hydrolysis event (i.e., cleavage of the first Si–OR bond) is the rate-limiting step and that the initially formed monohydroxysilane then degrades, sequentially but faster, to release all of its alcohol moieties, including the free drug.

The relative rates of hydrolysis (k_{rel}) of **301**-**304**, normalized to the least reactive silicate, the PTX-menthyloxysilicate **301d**, are shown in Table 3.2. As anticipated, increase in steric bulk of the silicate near the silicon center slows its

[135] Turner, C. W.; Franklin, K. J. Studies of the hydrolysis and condensation of tetraethylorthosilicate by multinuclear (^{1}H ^{17}O ^{29}Si) NMR spectroscopy. *J. Non-Cryst. Solids* **1986**, *91*, 402–415.

hydrolysis rate. The k_{rel} values differ by >2000 between the extremes of the triethyl PTX-silicate **301a** vs. the hindered trimenthyl silicate ester **301d**. The hydrolysis rates for the triethyl vs. trioctyl silicates **301a** vs. **301b** (for PTX) or **304a** vs. **304b** were similar (difference in k_{rel} of ca. 3), which shows that the hydrophobicity of the silicate can be significantly altered with only a small accompanying change in the relative hydrolysis rate. PTX-silicates at the more hindered C7-position hydrolyzed ca. 7-15 times more slowly than those at C2'. Moreover, (i) the rate difference for cleavage of silicates at these two sites increased slightly as the bulk of the alkyl groups increased in the series of ethyl to n-octyl to iso-propyl, and (ii) the trends were the same whether comparing the differences at C7 vs. C2' for both the mono-silicates (**301a** vs. **303a**, **301b** vs. **303b**, and **301c** vs. **303c**) as well as those same sites within each of the bis-silicates **302a**-**c**.

Table 3.2 I The relative rates of hydrolysisa of the PTX (**301-303**, **308**, **313**) or DTX (**304**) silicates. The krel values are benchmarked relative to that of the PTX-trimenthyloxy derivative **301d**, the PTX-silicate having the slowest observed rate of hydrolysis.

Sili-cate	at C2'				at C7			
	2'-silicate alkyl	$t_{1/2}$ (min)	k_{obs} (10^{-6} s^{-1})	ca. k_{rel}	7-silicate alkyl	$t_{1/2}$ (min)	k_{obs} (10^{-6} s^{-1})	ca. k_{rel}
301a	**Et**	3.7	3100 ±900	**18,000**	**–**			
301b	**^{n}Oct**	12	960 ±40	**5,600**	**–**			
301c	**^{i}Pr**	120	97 ±6	**570**	**–**			
301d[b]	**menthyl**	69,000	0.17 ±0.002	**1.0**	**–**			
301f[b]	**(^{t}Bu)$_2$/Et**	12,000	0.96 ±0.1	**5.6**	**–**			
301g[b]	**(^{t}Bu)$_2$/Ac**[c]	35	330 ±20	**1,900**	**–**			
301p	**DHP**	130	89 ±2	**530**	**–**			
302a	**Et**	4.6	2500 ±100	**15,000**	**Et**	33	350 ±20	**2100**
302b	**^{n}Oct**	18	640 ±10	**3,800**	**^{n}Oct**	200	58 ±4	**340**
302c	**^{i}Pr**	130	89 ± 5	**520**	**^{i}Pr**	1500	7.8 ±2	**46**
303a	**–**				**Et**	30.	380 ±10	**2200**
303b	**–**				**^{n}Oct**	150	77 ±5	**450**
303c	**–**				**^{i}Pr**	1700	6.7 ±2	**39**
308a	**(*PTX-SiEt$_3$*)**	56	210 ±2	**1,200**	**–**			
313	**(^{n}Oct)$_2$/H**	19	610 ±6	**3,600**	**–**			
304a	**Et**	11	1100 ±100	**6,500**	**–**			
304b	**^{n}Oct**	26	440 ±40	**2,600**	**–**			
304c	**^{i}Pr**	260	45 ±5	**260**	**–**			
304d[b]	**menthyl**	78,900	0.15 ±0.02	**0.88**	**–**			
304e[b]	**(^{t}Bu)$_2$/Et**	13,600	0.85 ±0.09	**5.0**	**–**			

[a] Each silicate in a solution of acetone-d_6/D_2O/CF_3CO_2H (90/9/1) at a concentration of ca. 0.01 M was kept at ca. 22 °C and the reaction progress monitored periodically and continuously by ^1H NMR spectroscopy. [b] NMR analysis suggested the presence of steady-state levels (typically ≤10%) of intermediate, partially cleaved silicates [i.e., $(RO)_{4-n}Si(OH)_n$, where n = 1-3], which underwent further clean conversion of the fully hydrolyzed alcohols, including the taxane. [c] Acetyl (CH_3CO), which is part of an acetoxy substituent on the silicate oxygen atom.

Control over the hydrolysis is required to give a slow release over time and to avoid a burst of drug and by-products. The rate and the mechanism of hydrolysis of the prodrugs resemble that of model studies of tetramethyl orthosilicate (TMOS) and tetraethylorthosilicate (TEOS). The rate of hydrolysis is pseudo-first order by way of an S_N2 mechanism (assuming the hydrolysis mechanism is similar to the TMOS and TEOS silicates). This kinetic data requires an excess of water and is solvent-dependant. Systematic studies to further understand the hydrolysis of mixed orthosilicate prodrugs based upon their steric and electronic features have been performed and a manuscript describing these results is in preparation.

The rate can be easily tuned by the use of different alcohols used to create the silicate. Both steric and electronic effects can be tuned to give optimal hydrolysis and release from nanoparticles. Even though the longer aliphatic alcohol **315** yielded an extremely more hydrophobic silicate **301p** compared to **301d**, the rate of hydrolysis was 530 times faster than **301d** and similar to the less hydrophobic isopropyl derived silicate **301c**.

We were interested in the difference in hydrolysis rate as a function of pH. A 1:100 D_3PO_4:D_2O stock solution was made. The pD was adjusted by adding in an appropriate volume of a K_3PO_4 : D_2O stock solution. Five values of pD were made using the procedure above as well as a control in which the only D_2O was used for the ^1H-NMR analysis. The pD was calculated by measuring the pH and

adding 0.4 and the values are presented in Table 3.3 below.[136,137,138] From the five ranges of pH, two were taken on to determine the hydrolysis rate as a comparison to the TFA standard conditions.

Table 3.3 I The relative rate of hydrolysis as a function of pH for **301b**.

Acid/ D_2O	pD	D_2O (vol%)[a]	Stock Volume (μL)	Organic Volume (μL)	Calculated Half-life (min)	K_{rel}[c]
d-TFA	1.2	90%	100	900[b]	12	720
D_3PO_4	2.4	99%	700	300[c]	6,900	1.3
CD_3CO_2D	2.8	90%	50	450[b]	210	42.0
CD_3CO_2D	2.8	90%	50	450[c]	2100	4.1
D_3PO_4	4.5	99%	–	–	–	–
D_3PO_4	5.4	99%	700	300[c]	8,600	1.0
D_3PO_4	6.4	99%	–	–	–	–
D_2O	7.5	100%	700	300[c]	8,600	1.0
D_3PO_4	8.0	99%	–	–	–	–

[a] Volume % (vol%) of D_2O present in the Acid/D_2O stock solution [b] The PTX-Si(O^nOct)$_3$ **301b** (~2.0 mg) was dissolved in d_6-Acetone and the aqueous solution was kept at ca. 22 °C and the reaction progress monitored periodically and continuously by ^{1}H NMR spectroscopy. [c] The PTX-Si(O^nOct)$_3$ **301b** (~2.0 mg) was dissolved in d_4-Methanol and the aqueous solution was kept at ca. 22 °C and the reaction progress monitored periodically and continuously by ^{1}H NMR spectroscopy. [c] K_{rel} is the relative rate of hydrolysis when compared to the D2O control solution set at K_{rel} = 1.0.

As the acidity of the solution decreased a much slower hydrolysis rate was determined by integrating the conversion of the prodrug back to parent PTX and

[136] Glasoe, P. K.; Long, F. A.; Use of glass electrodes to measure acidities in deuterium oxide. *J. Phys. Chem.* **1960,** *64,* 188—189.

[137] Gary, R.; Bates, R. B.; Robinson, R. A. Second dissociation" constant of deuteriophosphoric acidin deuterium oxide from 5-50°. Standardization of a pD scale. *J. Phys. Chem*. **1964**, *68*, 6–9.

[138] Long, F. A.; Dahlgren, G. Relative hydrogen bonding of deuterium. I. Ionization constants of maleic and fumaric acids of their nonethyl esters in H_2O and D_2O. *J. Am. Chem. Soc.* **1960,** *82,* 1303—1308.

the evolution of octanol during the course of the experiment. We were surprised that the rate decreased dramatically. As expected, once the solution was around typical biological pH the rate of hydrolysis was ca. the same as the no acid control sample (D_2O only). This study shows that the silicate ester prodrugs are actually quite stable in aqueous environments. Further analysis of the stability of the prodrugs in presented later in this chapter.

3.6 In Vitro Cytotoxicity of PTX and DTX Prodrugs

Cytotoxicity of the PTX-silicates (**301-303, 308a**) and DTX-silicates (**304a-304e, 318a**) was examined against MDA-MB-231 cells (Table 3.4). We used this as a model cell line representing triple negative breast cancer, a malignancy for which taxanes are used as front-line agents. Silicates having faster rates of hydrolysis (Table 3.2) tend to show cytotoxicities similar to those of the parent taxane. This suggests that the silicate esters are hydrolyzed back to **PTX** or **DTX** either in the culture medium or inside the cell during the course of the assay. Experiments to determine the form of **302a** inside and outside the cell are presented in Chapter 3.7. The details of the experimental design to determine the IC_{50} values are shown in the supporting information for Chapter 3.

Table 3.4 I Cytotoxicity (IC_{50}) of **PTX**, PTX-silicates (**301-303**), PTX-silane (**308a**) **DTX**, and DTX-silicates (**304,318a**) in MDA-MB-231 cells.[a]

PTX Compounds		IC_{50} (nM)[b]	DTX Compounds	IC_{50} (nM)[b]
	PTX	5.6	***DTX***	1.0
	301a	8.3	***304a***	2.5
	301b	7.0	***304b***	9.7
	301c	4.2	***304c***	0.2
	301d	590	***304d***	720
	301f	260	***304e***	430
	302a	12	***318a***	6.5
	302b	280		
	302c	1600		
	302d	240		
	303a	18		
	303b	290		
	303c	260		
PTX-2'-$SiEt_3$	***308a***	220		

[a] Cell viability was measured after 72 h. [b] The reported data are the median values for the distribution of IC_{50} values falling within the 95% confidence interval.

We were interested in a possible increase in the *in vitro* cytotoxicity of the silicate prodrugs with the use of acidic medium for the cell assay. It was envisioned that the increased acidity of the medium would more closely mimic the microenvironment of tumor tissue. To accomplish this, stock solutions of acidic cell culture media (pH ~ 2.5) were further diluted in each well by adding 100 μL of the acidic media to cells with 100 μL of regular growth media [(Minimum Essential Medium (MEM) with 10% Fetal Bovine Serum (FBS)] to obtain a pH = 5.75. The prodrugs were then added as a DMSO stock solution at different concentrations. The plate was then placed in a cell culture incubator at 37 ˚C for 72 h. An MTT assay was performed to determine the IC_{50} as done before (Supporting Information) and tabulated below. The IC_{50} values of the regular growth media (RGM) are reproduced below (left side of columns 2 and 4

Table 3.5) to serve as a comparison with the acidic media treated cells. The cells treated with media at pH = 5.75 show a slight increase in the potency. However, they did not show an equal potency in the IC_{50} when compared with the parent drug, **PTX** or **DTX**. The **303b** prodrug did show an overall increase in potency, likely due to hydrolysis in the media. The slow hydrolyzing prodrug **304d** showed little to no cytotoxicity in RGM, but gave a more potent IC_{50} value when treated in acidic media. Although improved cytotoxicities were shown by this experiment, we chose not to probe other compounds further *in vitro*. We instead turned our attention toward *in vivo* experiments for the nanoparticle formulations (Chapter 6).

Table 3.5 l Cytotoxicity (IC_{50}) of PTX, PTX-silicates (**301-303**), DTX, and DTX-silicates (**304**) in MDA-MB-231 cells in: *i.*) regular growth media (RGM) Values in grey have been reproduced from Table 3.4 and included for reference, and *ii.*) acid growth media.

PTX Compounds	IC_{50} (nM)[a]	DTX Compounds	IC_{50} (nM)[a]
PTX	5.6 l 3.3	***DTX***	1.0 l 0.40
301b	7.0 l 4.6	***304a***	2.5 l 1.8
302b	280 l 230	***304d***	720 l 130
302d	240 l 220		
303b	290 l 130		

[a] Cell viability was measured after 72 h in acidic media at pH = 5.75. The reported data are the median values for the distribution of IC_{50} values falling within the 95% confidence interval.

3.7 Prodrug Stability in Biologically Relevant Media

Although the hydrolytic lability determined *in situ* by ^{1}H-NMR is useful in determining trends of silicate prodrug stability, it did not provide conditions that the prodrugs would likely be subjected to during typical experiments. We first examined the stability of the prodrugs to wet acetonitrile (ACN). These conditions were explored to determine apparent stability for a long queue of samples for HPLC analysis after tissue extraction.

To probe the stability and storage of **302a**, a stock solution of 302a was made in ACN. An aliquot containing 20 μg of **302a** was diluted to in 1 mL of HPLC grade ACN that contained 5 μL of water in a septa capped HPLC vial and placed on the auto-sampler of an LC-MS. Over the course of 22 days a 5 μL injection was analyzed for the amount of the bis-silicate **302a**, mono-silicate **303a**, and **PTX** species present by calculating the integration values at 227 nm from a calibration curve (all samples were run in triplicate). The percentage of each species was plotted as a function of time as shown in Figure 3.3 below. The raw integral value at 227 nm for each species and the calibration curve is shown in the supporting information (SI, Figures S3.5–S3.7).

The bis-functionalized **302a** is reasonably stabile in ACN for ca. a week, at which point there is 50% of the mono-silicate **303a**. After another week sitting in the HPLC vial at room temperature, essentially all of the **302a** prodrug has cleaved at the 2'-position to give **303a** and yet no free **PTX** can be quantified. This stability study offers the suggestion that prodrug stock solutions in ACN are not entirely stable, the apparent half-life ($t_{1/2}$) of **302a** in wet acetonitrile is one week, and that the **303a** prodrug is very stable in ACN.

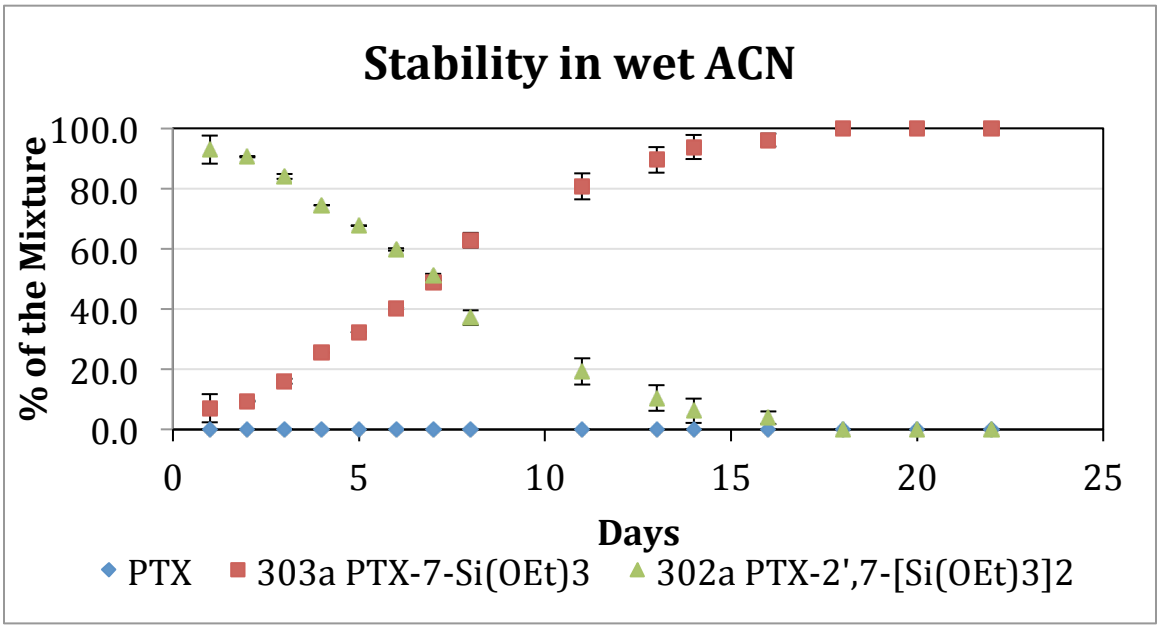

Figure 3.3 I The **302a** prodrug stability in wet acetonitrile over the course of 22 days plotted as a percentage of the total mixture vs. time.

We were interested in the fate of the silicate prodrugs when subjected to phosphate buffered saline (PBS). By performing the same procedure described above in an aqueous system, we could compare the rate of degradation iwith other aqueous conditions such as: the NMR hydrolysis, cell uptake, and later release data collected by Jing Han.[139] In this experiment 20 μg of **302a** was dissolved in 0.5 mL of ACN, and 0.5 mL PBS, pH 7.4. The ACN was used to ensure homogeneity of the very hydrophobic prodrug. The samples were then allowed to sit capped at room temperature in the LC-MS auto-samper. Over the course of 22 days, the amount of compounds **302a**, **303a**, and **PTX** were calculated by the integration values at 227 nm, as described before.

In an aqueous buffer system, **302a** is completely converted to the mono-silicate **303a** in only three days, and further hydrolysis of the mono silicate prodrug to free **PTX** ensues (Figure 3.4). The apparent half-life of **302a** was on

[139] Han, J. Diblock copolymer stabilized nanoparticles for drug delivery via flash nanoprecipitation. Ph.D. Dissertation, University of Minnesota, Minneapolis, 2014.

the order of hours, which implies that the unprotected silicate prodrug is extremely labile in aqueous buffers. Not shown, are the results of an acid study in which a formic acid buffer (pH 4.5) system was used as the co-solvent with ACN. The experiment with an acidic solvent system showed very fast hydrolysis of **302a** completely to give **PTX** in less than 1 day and **303a** was not observed. These studies demonstrate the importance of the polymer to protect the labile prodrug.

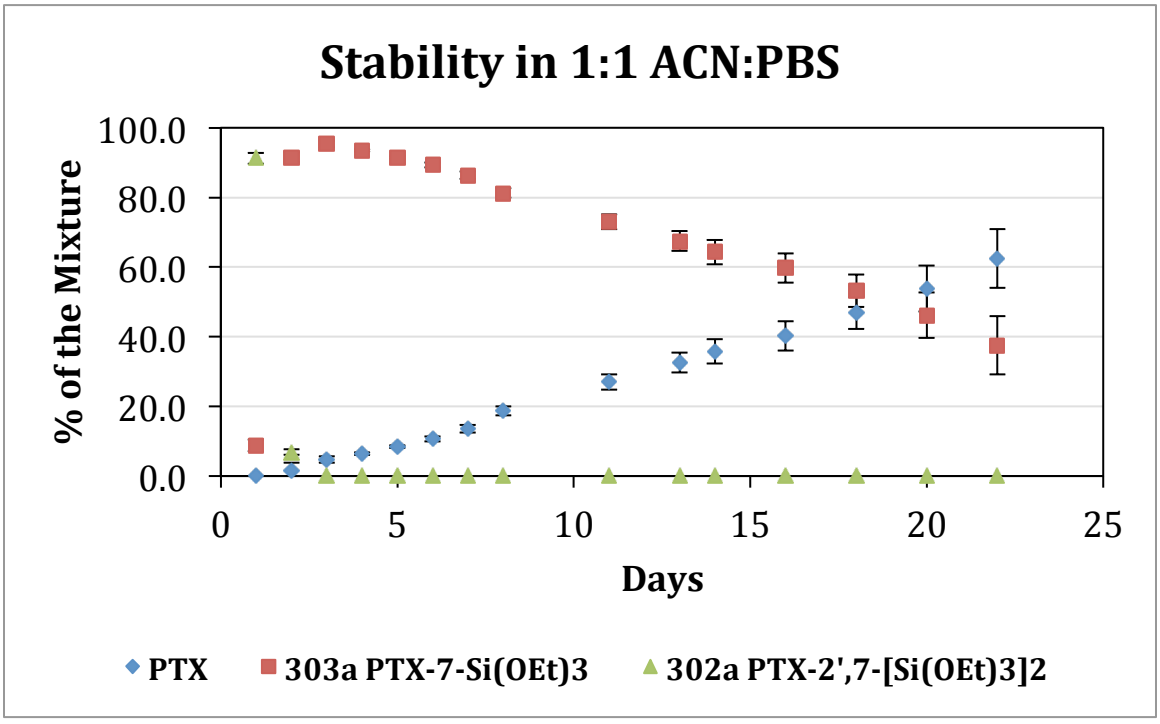

Figure 3.4 I The **302a** prodrug stability in a 1:1 mixture of acetonitrile to PBS (pH =7.4) over the course of 22 days plotted as a percentage of the total mixture vs. time.

To probe the stability in a more biologically relevant system, Gibco® Minimum Essential Medium (MEM) with 10 % fetal bovine serum (FBS) was used as the matrix. Stock solutions of PTX-2'-Si(O^{n}Oct)$_3$ (**301b**), PTX-7-Si(O^{n}Oct)$_3$ (**303b**), PTX-2'-Si(O^{i}Pr)$_3$ (**301c**), were prepared at 1 mg/mL in ACN. A 40 μL aliquot of each was placed into six separate HPLC vials which corresponded to 20 μg of each prodrug. To each sample 10 μL of a 1 mg/mL **DTX** stock solution

was added to serve as an internal standard (I.S.). The resulting 50 μL of ACN containing the prodrugs and **DTX** was diluted with 950 μL of MEM 10% FBS media. The samples were then placed on the auto-sampler and held at room temperature over the course of 150 hours. At predetermined time points 5 μL injections were analyzed by LC-MS. We were pleased to find that the media did not interfere with the chromatography or the mass spectrometry, which showed small amount of matrix components eluting well before the compounds on a C-18 Ace® column. The integral values at 227 nm were analyzed against a calibration curve of the ratio of **PTX/DTX** or (**301b/DTX**, **303b/DTX**, **301c/DTX**) respectively. From the raw integral values the percentage of **PTX** to prodrug was plotted as a function of time to determine the stability of each toward media hydrolysis.

The most labile of the prodrugs **301b** ($t_{1/2}$ = 12 mins NMR) analyzed by this method showed immediate hydrolysis in the media, only 4% of the prodrug remained after 4 hours (Figure 3.5). This suggests that for the *in vitro* cytotoxicity assay the cells are treated predominately with the parent drug and accounts for the equal potency of **301b**.

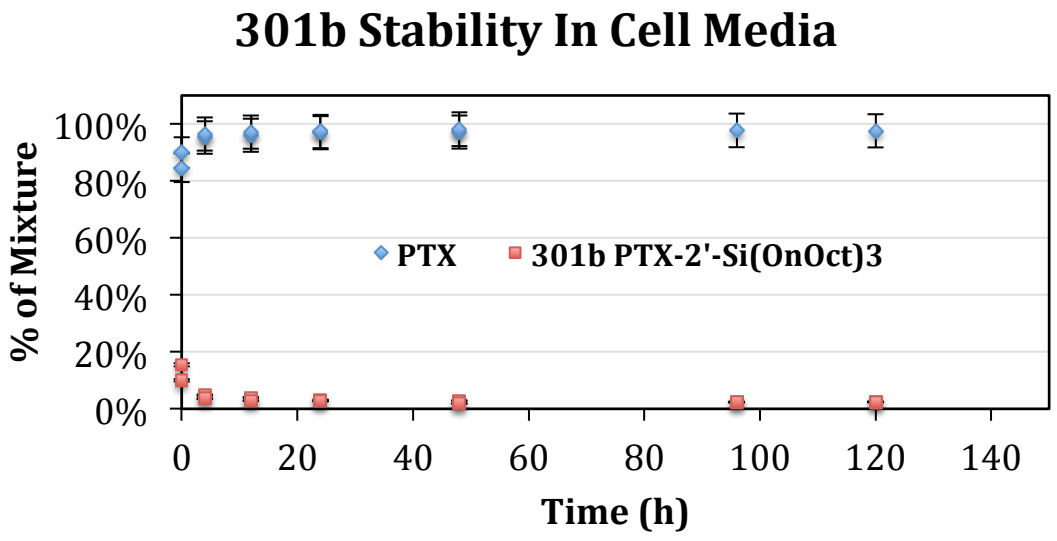

Figure 3.5 I The **301b** prodrug stability in MEM with 10% FBS PBS (pH =7.4) over the course of 150 hours plotted as a percentage of the total mixture vs. time.

The slower hydrolyzing prodrug **303b** ($t_{1/2}$ = 150 mins, NMR) that has a similar hydrophobicity was analyzed in a similar fashion. This compound showed complete stability toward the media catalyzed hydrolysis even up to 288 hours; only ca. 2% of **PTX** was observed (Figure 3.6). We speculate that this increase in media stability is due the formation of micelles in aqueous environment (when compared to 301c). The lack of reversion back to the parent drug correlates with the 50-fold decrease in potency in the *in vitro* cytotoxicity of **303b**.

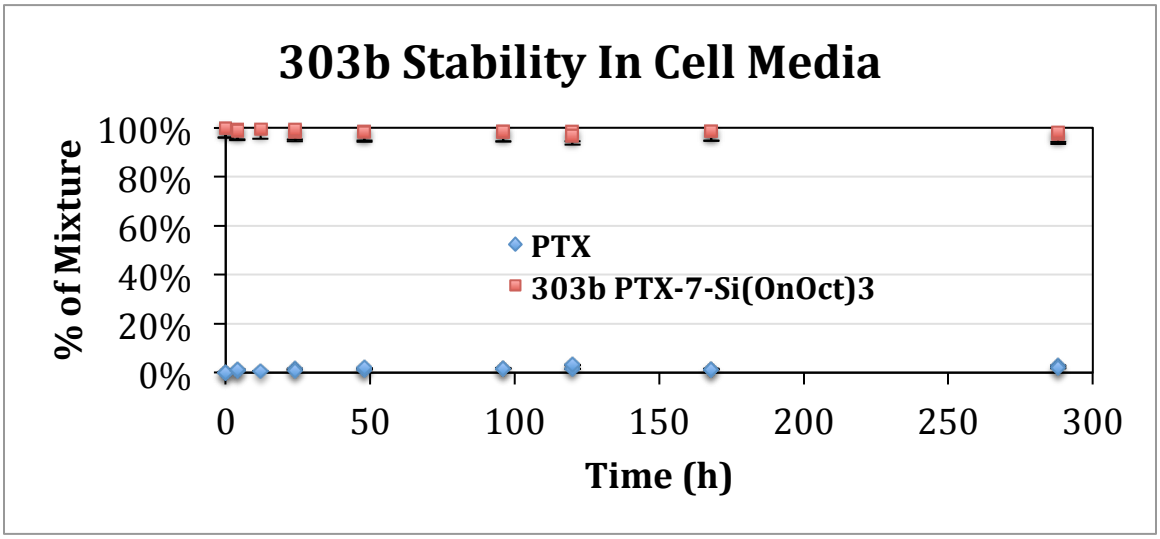

Figure 3.6 I The **303b** prodrug stability in MEM with 10% FBS PBS (pH =7.4) over the course of 300 hours plotted as a percentage of the total mixture vs. time.

Guided by the apparent enhanced cytotoxicity of **301c** with an IC_{50} of 4.2 nM compared to 5.6 nM of **PTX**, we wished to determine the form of the prodrug in the MEM media. Interestingly, we found that only 20% of **301c** reverts back to **PTX** over the course of 72 hours (Figure 3.7). Although the hydrolysis rate ($t_{1/2}$ = 120 mins, NMR), is close to that of **303b**, the lower hydrophobicity diminishes the propensity for micelle formation. We hypothesize that **301c** can serve as both a prodrug to reveal **PTX** overtime and that it is perhaps a new bioactive compound that binds to microtubules as well. A quick examination of a crystal structure of **PTX** bound to a microtubule suggests there is room in the hydrophobic pocket for

the silicate.[140,,141] I modified the 7-position of **DTX** to estimate the silicate **304c**, and is included in the appendices (Figure S3.4) to provide a very crude idea of the possible binding. Further docking experiments and ultimately a crystal structure are needed to confirm this hypothesis.

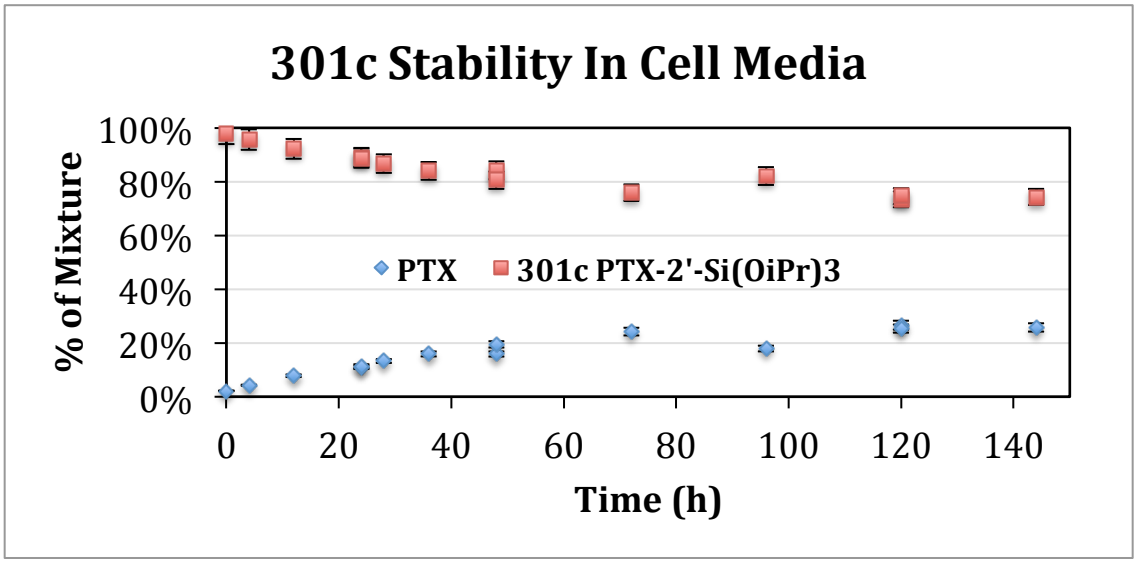

Figure 3.7 I The **301c** prodrug stability in MEM with 10% FBS PBS (pH =7.4) over the course of 150 hours plotted as a percentage of the total mixture vs. time.

Encouraged by the LC-MS quantification results of the prodrugs treated with media, we wanted to determine the fate of **302a** during an MDA-MB-231 breast cancer cell assay. The form of the prodrug both inside and outside of the cells was examined, as well as the total amount taken up into the cells, and the amount remaining in the media. Due to the presence of cellular debris, an extraction procedure was developed which gave reliable quantitation during LC-MS analysis.

[140] Li, H.; DeRosier, D. J.; Nicholson, W. V.; Nogales, E.; Downing, K. H. Microtubule Structure at 8 Å Resolution. *Structure* **2002**, *10*, 1317–1328.

[141] Amos, L. A.; Löwe, J. How Taxol Stabilises Microtubule Structure. *Chem. Biol.* **1999**, *6*, R65–R69.

50,000 MDA-MB-231 cells were seated in each well of a 24 well plate and allowed to grow for one day in the presence of growth media at 37 ˚C provided by a cell incubator. To begin the experiment, we removed the media and replaced it with 0.5 mL of media containing the drug at a concentration of 10 μM or 100 μM and 1% FBS or 10% FBS, the experimental design is shown in Figure 3.8 below. At 24 h and 48 h the media was removed, extracted, and analyzed by extracting the ions in the mass spectrum of an LC-MS run. The remaining cells were also removed from the plate with trypsin, lysed with acetonitrile, extracted and analyzed by LC-MS. The amount of **302a**, **303a**, and **PTX** were quantified from a calibration curve in which **DTX** was used as the I.S. and found in the supplementary information (S3.5). Media samples that did not contain cells served as controls to obtain an extraction efficiency of 81% recovery.

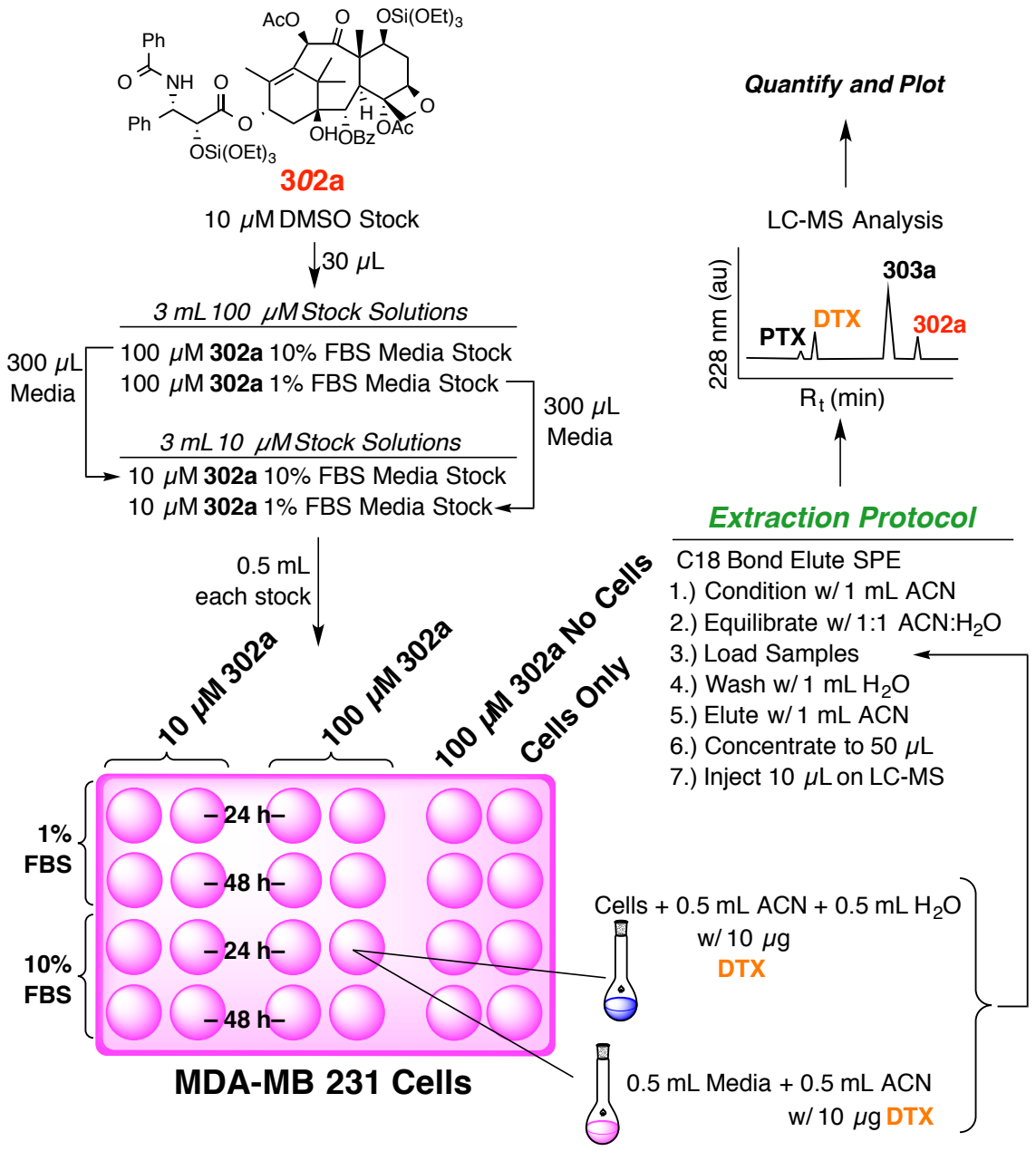

Figure 3.8 I The cell uptake experimental design, extraction procedure, and depiction of LC-MS chromatogram.

The form of the prodrug **302a**, **303a**, and **PTX** in the media was plotted as a percentage of the total taxane present in the mixture shown in Figure 3.9. The prodrug hydrolyzed to the mono-functionalized silicate after the first 24 hours which shows an enhancement when compared to the 1:1 ACN:PBS summary

from above. The results from both 1% and 10% FBS were combined as we assumed the amount of protein present would not effect the rate of hydrolysis of the prodrug. Interestingly, after 48 hours the bis-silicate **302a** could not be detected in the cell media. The analysis of the prodrug form was not performed on the 10 μM treated media.

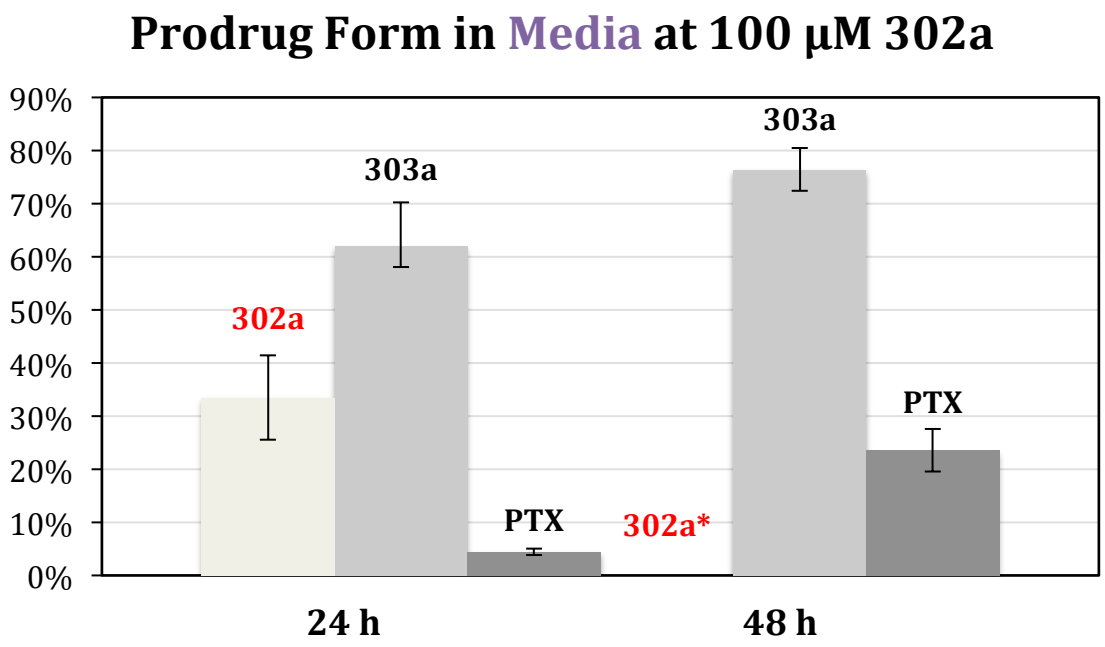

Figure 3.9 I The form of the prodrug in the 1% and 10% FBS media from the MDA-MB-231 cell uptake assay observed at 24 h and 48 h. *not detected.

We then analyzed the form of the prodrug contained inside the cells after 24 h and 48 h for all cells treated at 10 μM and 100 μM **302a**. Unfortunately like the media study, the results from the 10 μM concentration could not be quantified. Unlike the in the bulk media, **302a** was present as the dominate form even after 48 hours. Also both time points show similar ratios (**302a**:**303a**:**PTX**) in the form of the prodrug with **302a** being the dominate form. This indicated that the hydrolysis is generally slower in the cell compared to the bulk media. The increase in hydrophobicity of **302a** compared with that of **303a** and free **PTX**

suggests a second benefit of enhanced lipophilicity for the prodrug strategy. The molecules an improved lipophilicity and leads to a more facile uptake into the cells determined from the cell uptake study. This is very encouraging for our future nanoparticle formulations as it suggests more of the prodrug accumulation into tumor cells.

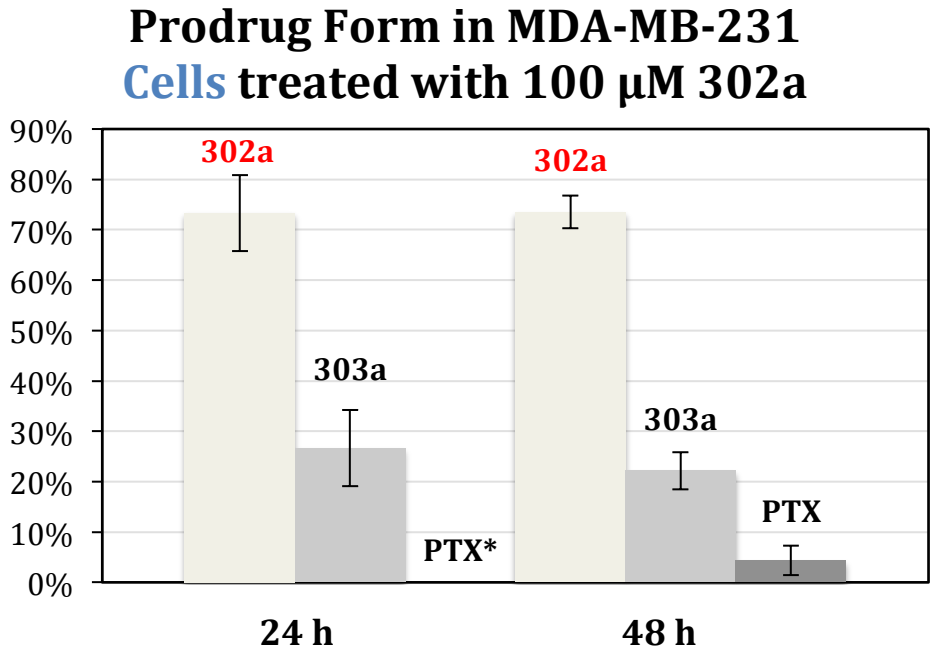

Figure 3.10 I The form of the prodrug up-taken into the MDA-MB-231 cells observed at 24 h and 48 h after being treated at 100 μM **302a** in both 1% and 10% FBS media. *not detected.

The difference in the total amount of **PTX** present in the cells at 24 h and 48 h was determined based on the percentage of FBS in the media. We hypothesized that the media containing a higher amount of protein would restrict the uptake of the prodrug into the cells. By quantifying the total amount taxane (**302a**, **303a**, and **PTX**), we quickly saw a validation of the hypothesis. Cells treated at 100 μM of the prodrug in 10% FBS media showed significantly less drug present in the cells. Due to the small volume of the cells in comparison to

the 0.5 mL of media, far less of the drug was present in the cells. The plot comparing the two is shown in Figure 3.12.

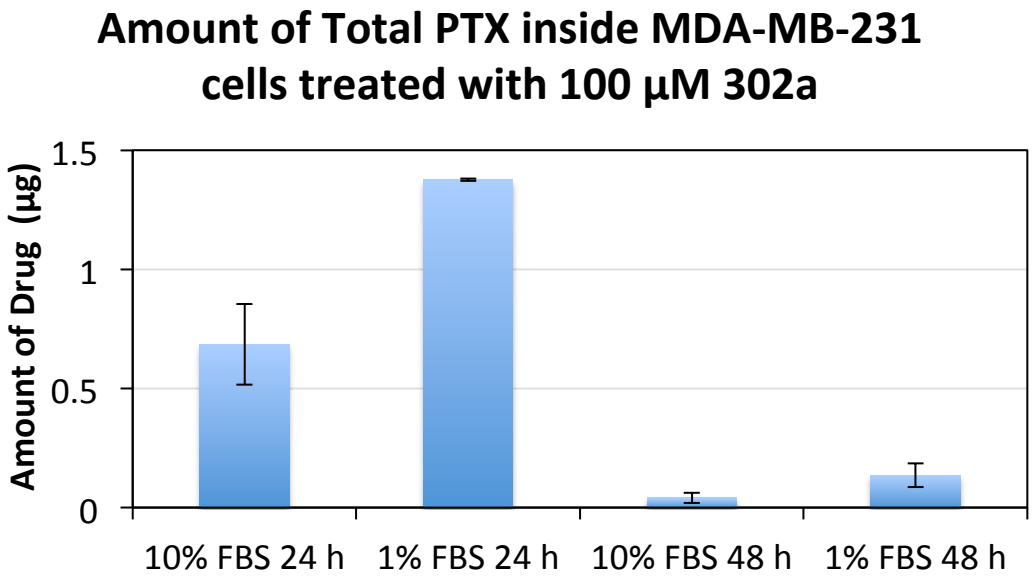

Figure 3.11 I The total amount of taxane (**302a**, **303a**, and **PTX**) present inside the MDA-MB-231 cells after 24 h and 48 h.

The total amount of drug quantified both inside and outside the cells is presented in Figure 3.12. From these values the mass balance and validation of the extraction procedure is determined. Each well was treated at 100 μM of **302a** using 0.5 mL of the media corresponds to 58.9 μg of **302a**. Taking in account the molecular weight of the prodrug (1178 μg/μmol) to that of PTX (854 μg/μmol), the available taxane to quantify was 42.7 μg. Overall, 75% of the PTX components were retained in the media and 1% was up-taken into the cells. This mass balance of 76% is slightly lower than the extraction efficiency for the protocol described in the Figure 3.11 above, which was 81% for media controls (without cell treatment). Similar efficiency (64%) was quantified from the 10 μM treated media and is lower due to the 10-fold decrease in concentration of the prodrug. The lower mass balance present seen in the 48 h incubation time is likely due to

tight binding to proteins present in the media and lost during the extraction procedure.

The total amount of protein present in the cell assay was determined by a Bradford assay. The total amount of drug was normalized as a ratio to the total protein and plotting in the SI Figure S3.8. This further confirms that the higher 10% FBS content reduces the quantifiable amount of drug by the protocol shown in Figure 3.12.

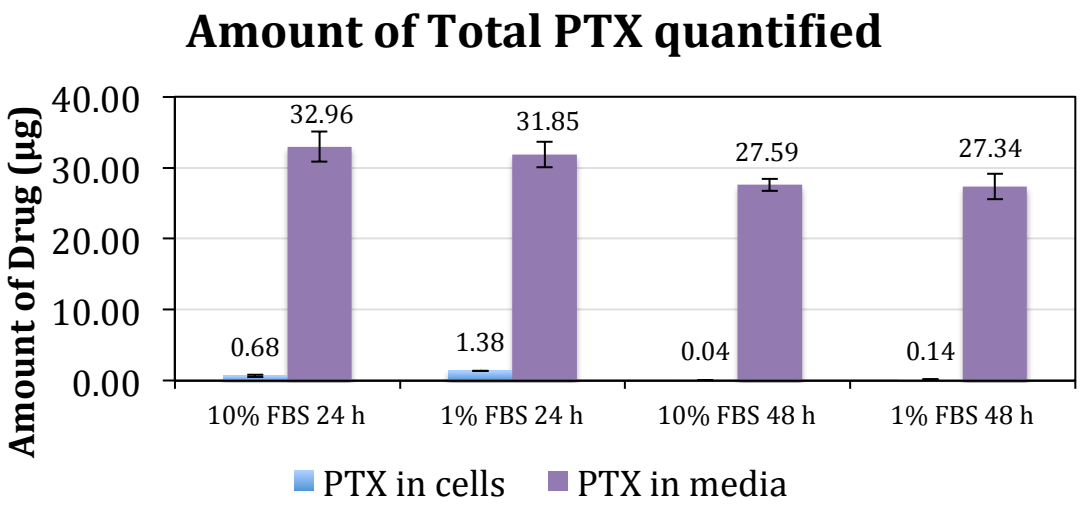

Figure 3.12 I The total amount of taxane (**302a**, **303a**, and **PTX**) quantified both inside the MDA-MB-231 cells and retained in the media after 24 h and 48 h.

To further understand the stability of the prodrug over time and probe the beneficial qualities of the polymer (to protect and deliver the prodrug) future stability studies will focus on more biologically relevant media with the nanoparticle preparations. Mouse plasma can easily be obtained from control mice and split into a series of aliquots *i.*) prodrugs free in solution *ii.*) prodrugs free in solution solubilized via Cremophor EL® and *iii.*) prodrugs in a 5k-10k mPEG-PLGA nanoparticle formulation. The samples will be placed in an incubator at 37 ˚C and two samples will be removed every 30 minutes and

extracted through the solid phase extraction (SPE) technique presented above to determine the ratios of free drug to prodrug. Standards will be run to verify good recovery and ensure that the prodrug hydrolysis does not occur by way of the SPE protocol. This experiment will give insight to the stability of the prodrug when circulating *in vivo*. Further studies of stability and total drug amounts in tissue homogenates are presented in Chapter 5.

3.8 Chapter 3 Conclusions

A new class of prodrug–silicate esters has been shown in this thesis chapter. The strategy provides the ability to control both the hydrophobicity and the hydrolysis rate of these drug derivatives. Each of these features provides a mechanism through which *i.*) drug encapsulation into nanoparticles and *ii.*) release properties from nanoparticles can be tuned. We have determined relative rates of hydrolysis of these silicates via ^{1}H NMR spectroscopic analysis. Cytotoxicity studies were performed against the MDA-MB-231 cell line. Silicates **301a-c**, **302a**, **303a**, and **304a-c** all showed IC_{50} values similar to that of their parent taxane, suggesting hydrolysis in the culture medium and/or inside the cell. The IC_{50} values spanned a range of ca. 10^3 for each of the **PTX** and **DTX** family of taxanes. Certain of these silicates are further evaluated in subsequent chapters for their ability to form small, stable, block copolymer-based nanoparticles as potential drug-delivery constructs.

Chapter 4. Block Polymer & Nanoparticle Formulation Studies

4.1 Biocompatible Polymers

4.1.1 Synthesis of PEG-*b*-PLGA

In tandem with the development of FNP techniques, biocompatible block copolymers have been developed to effectively solubilize and protect prodrugs without being biologically active or toxic. This section will discuss previous techniques to synthesize a variety of block co-polymers and the techniques employed to create functionalized polymers for coupling with tumor-targeting ligands for medical applications.[142] Specifically, polyesters synthesized from lactide or glycolide (among many monomers) are of great interest due to the controllable rate of degradation *in vivo* via the citric acid cycle.[143] The hydrolysis of ester bonds releases lactic acid and glycolic acid, both of which are naturally found in the body. PLGA has FDA approval in drug delivery polymers, sutures, and implants.

To create polymers from lactide (Scheme 4.1, **401**) and glycolide (Scheme 4.1, **402**), Ring-Opening Transesterification Polymerization (ROTEP) techniques have been utilized.[73] It should be noted that this field contains a wealth of knowledge and innovation yet is only briefly discussed in this thesis and is specifically for drug delivery applications. For ROTEP of **401** and **402** to occur, a variety of catalysts have been explored to give sufficient polymerization of the two monomers. The two common organometallic catalysts used to convert the dilactones to the long, linear, aliphatic ester backbone of linear polyesters are

[142] Kim, S.; Cho, S.; Chu, L. Biotin-Conjugated Block Copolymeric Nanoparticles as Tumor-Targeted Drug Delivery Systems. *Macromol. Res.* **2007**, *15*, 646-655.

[143] Dechy-Cabaret, O.; Martin-Vaca, B. Controlled Ring-opening Polymerization of Lactide and Glycolide. *Chem. Rev.* **2004**, *104*, 6147-76.

tin(II) octoate $Sn(Oct)_2$, or aluminum(III) isopropoxide $Al(O\textit{i}\text{-}Pr)_3$.[144,145] Since these catalyst leave heavy metal contaminates in the product, they are not suited for the biological purposes and do not meet FDA guidelines unless stringent purification is performed.

Scheme 4.1 I Co-Polymerization of *rac*-lactide [**(±)-401**] and glycolide (**402**) (adapted from ref 146)[146]

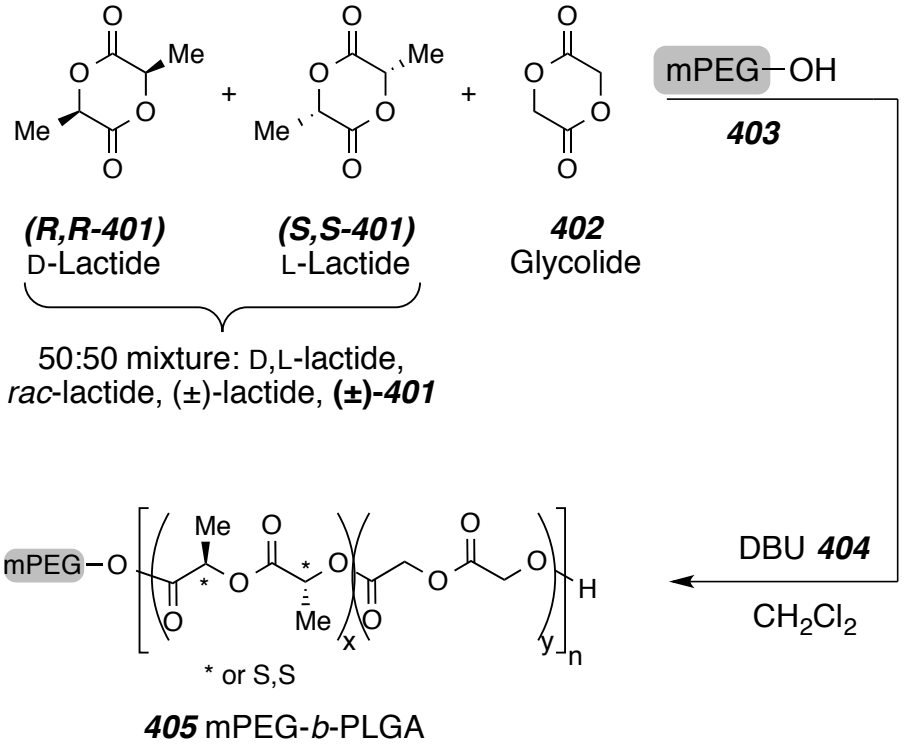

Alternatively, organocatalysts have been developed to catalyze the polymerization without the need of the heavy metals. These catalysts perform these polymerizations efficiently and produce polymers with narrow polydispersity indices (PDIs), which indicate that all growing polymer chains are of similar

[144] Liggins, R. Polyether-polyester Diblock Copolymers for the Preparation of Paclitaxel Loaded Polymeric Micelle Formulations. *Adv. Drug Deliver. Rev.* **2002**, *54*, 191-202.

[145] Kowalski, A.; Duda, A.; Penczek, S. Kinetics and Mechanism of Cyclic Esters Polymerization Initiated with Tin(II) Octoate. 3. †Polymerization of l, l-Dilactide. *Macromolecules* **2000**, *33*, 7359–7370.

[146] Qian, H.; Wohl, A. R.; Crow, J. T.; Macosko, C. W.; Hoye, T. R. A Strategy for Control of "Random" Copolymerization of Lactide and Glycolide: Application to Synthesis of PEG- b-PLGA Block Polymers Having Narrow Dispersity. *Macromolecules* **2011**, *44*, 7132—7140.

length or uniform. The organocatalysts used in ROTEP of most relevance to this thesis include the amidines and guanidines such as those shown in Figure 4.1 and compared in Table 4.1 with L-lactide as the monomer.[147,148]

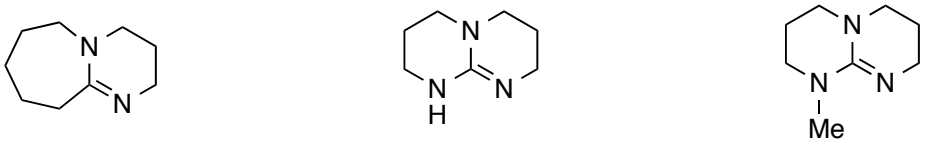

404 DBU ***406*** TBD ***407*** MTBD

Figure 4.1 I Guanidine and amidine organocatalysts used for ROTEP.

Table 4.1 I Comparison of the organocatalysts used for ROTEP of L-lactide (adapted from Ref. 148).

Catalyst	cat. (%)[a] - {$[M]_0/[I]_0$}	Time (h)	conv. (%)[b] - solvent	M_n[c] (g mol^{-1})	PDI[c]
TBD	0.1 – {100}	20 s	99 – CH_2Cl_2	24 200	1.19
	0.1 – {500}	1 min	95 – CH_2Cl_2	62 600	1.11
MTBD	1 – {100}	0.5	92 – $CDCl_3$	17 900	1.05
	0.5 – {500}	0.5	99 – $CDCl_3$	55 300	1.10
DBU	1 – {100}	1	99 – $CDCl_3$	21 000	1.05
	1 – {500}	2	98 – $CDCl_3$	85 000	1.08

[a] Percentage relative to monomer.
[b] Measured by ^1H NMR.
[c] Measured by GPC in THF relative to PS standard.

[147] Kamber, N. E.; Jeong, W.; Waymouth, R. M.; Pratt, R. C.; Lohmeijer, B. G. G.; Hedrick, J. L. Organocatalytic Ring-Opening Polymerization. *Chem. Rev.* **2007**, *107*, 5813–5840.

[148] Lohmeijer, B. G. G.; Pratt, R. C.; Leibfarth, F.; Logan, J. W.; Long, D. A.; Dove, A. P.; Nederberg, F.; Choi, J.; Wade, C.; Waymouth, R. M.; Hedrick, J. L. Guanidine and amidine organocatalysts for ring-opening polymerization of cyclic esters. *Macromolecules* **2006**, *39*, 8574–8583.

The organocatalysts 1,5,7-triazabicyclo[4.4.0]dec-5-ene (TBD) **406**, 7-methyl-1,5,7-triazabicyclo[4.4.0]dec-5-ene (MTBD) **407**, and 1,8-diazabicyclo[5.4.0]undec-7-ene (DBU) **404** have different reactivities toward L-lactide. The comparison in Table 4.1 serves as a good starting point for the development of PLGA polymers by systematically checking the reactivity of the catalyst toward lactide. TBD is the most reactive organocatalyst, but produces the most variation of polymer molecular weights (broad PDIs) due to transesterification of growing polymer chains. MTBD reacts quickly with suitable PDI values, however we opted to use the DBU catalyst is this research due to the slower reaction rate and tighter PDI values.[148] Scheme 4.1 shows the polymerization of monomers **401** and **402** are initiated by a methoxy capped polyethylene oxide (MeO-PEO) [which is referred to in this thesis as a methoxy capped polyethylene glycol (mPEG)] to undergo ROTEP to form the random block copolymer mPEG-*b*-PLGA **405**. This is rather difficult since the glycolide **402** reacts significantly faster than the lactide. Since a rate is a rate constant times a concentration, the rate of lactide and glycolide can be matched if the concentration of **402** is reduced by slow infusion over time. This offset in concentration of **402** in the reaction mixture allows for the rate of ROTEP for the two monomers to be equal and thus a random block copolymer can be created.[146] We explored a variety of molecular weights of the random block co-polymer, but ultimately settled on using a 5k-10k mPEG-PLGA for the subsequent FNP studies.

Table 4.2 I A comparison of polymers made by DBU-catalyzed ROTEP.

Polymer (targeted)	$M_{n(PEG)}$	$M_{n(PLGA)}$ [a]	Ratio [a,b] LA : GA	PDI [c]
PEG_5-PL_1G_1A	5K	1.88K	75 : 25	1.03
PEG_5- $PL_{1.5}G_{1.5}A$	5K	2.52K	63 : 37	1.05
PEG_5- PL_4G_1A	5K	4.12K	70 : 30	–
PEG_5-PL_4G_1A	5K	4.44K	90 : 10	–
PEG_5- PL_3G_3A	5K	7.11K	53 : 47	1.05
PEG_5-$PL_{10}A$	5K	9.65K	100 : 0	–
PEG_5-PL_5G_5A	5K	9.22K	59 : 41	1.05
PEG_5-PL_5G_5A	5K	9.26K	69 : 31	1.15
PEG_5-PL_5G_5A	5K	10.59K	55 : 45	–
PEG_5-PL_5G_5A	5K	11.34K	52 : 48	–
PEG_5-PL_5G_5A [d]	5K	12.77K	59 : 41	–
PEG_5-PL_5G_5A	5K	13.86K	64 : 36	1.02
PEG_5-PL_5G_5A	5K	15.38K	70 : 30	–
PEG_5-$PL_{20}A$	5K	17.85K	100 : 0	–
$PL_5G_{2.5}A$-PEG_5-$PL_5G_{2.5}A$	5K	17.60K	74 : 26	1.05

[a] Results based on NMR spectroscopy
[b] Mass ratio of the repeat units
[c] Results based on GPC (THF, 1 mL/min) measurements against a polystyrene standard
[d] d_n/d_c = 0.1850 (mL/g) from size exclusion chromatography multi-angle light scattering (SEC-MALS).

4.2 Nanoparticle Formulations of Model Compounds

4.2.1 Drug Encapsulation and Model Compound Synthesis

Flash nanoprecipitation (FNP) experiments were performed to create nanoparticles of uniform size, high drug loading by weight, and easy processing. An organic solvent of either THF or acetone was used to dissolve an amphiphilic block copolymer (mPEG-*b*-PLGA) and hydrophobic organic solute. This solvent is impinged against an equal amount of a miscible anti-solvent, usually water as discussed in Chapter 2.[80] In the small mixing chamber, the polymer organizes as the hydrophobic block and hydrophobic organic solute in the core, while the hydrophilic block spans and solubilizes the particles on the outside. The mixing is extremely fast, ca. 15 milliseconds, and requires very little organic solvent, making this process easily scalable. The rapid mixing of the polymer and hydrophobic solute create kinetically trapped nanoparticles. If the mixing occurs too slowly, the particles form thermodynamic micelles. Due to this rapid encapsulation of FNP, the particles can contain a much higher weight percentage (wt%) of the organic solute.[82]

In order to effectively study this methodology, model compounds were chosen that contained sufficient hydrophobicity, as well as being cost efficient by not containing expensive taxanes. β-Carotene is a reddish-orange hydrocarbon with a measured logP of 14.76 and is a precursor to vitamin A.[149] We chose to conduct many of the nanoparticles with this compound due to its availability and lack of synthetic preparation. To ensure that the FNP process is fully compatible with the silicate methodology the tetra-menthoxy silicate [short hand, $(MenO)_4Si$ (**411**)] was synthesized. These compounds allowed for the exploration of loading levels, morphology, and stability of resulting nanoparticle formulations. Lastly, a series of iodine containing compounds (**413**) were made to explore the final

[149] Mojaat, M.; Foucault, A.; Pruvost, J.; Legrand, J. Optimal Selection of Organic Solvents for Biocompatible Extraction of Beta-Carotene From Dunaliella Salina. *J. Biotechnol.* **2008**, *133*, 433–441.

morphology of the nanoparticles by cryogenic-transmission electron microscopy (Cryo-TEM). The heavy iodine was chosen to improve the contrast of the images.

The initial attempts to synthesize **411** with an excess of (-)-menthol (**409**) in pentane showed the monochlorosilane **410** and starting material by GC-MS. Even allowing the reaction to continue overnight, did not push the reaction to completion. Addition of pyridine smoothly facilitated full conversion of **411**, and a 95 % yield was obtained following MPLC purification.

An aliquot of **410** was reacted with triiodophenol (**412**) in pyridine and THF. Following 2 hours of reaction, two sequential rounds of MPLC purified the crude mixture containing trimenthoxy-triiodophenol silicate (**413)** and **411**. The appearance of **411** was attributed to excess **409** in the pentane solution used for the reaction.

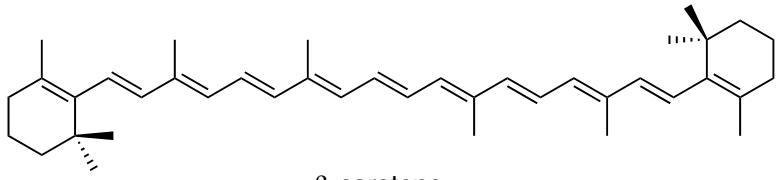

β-carotene

408

Figure 4.2 I Highly hydrophobic model compound (**408**) used for FNP studies.

Scheme 4.2 I Highly hydrophobic model compounds (**411**, **413**) used for FNP studies.

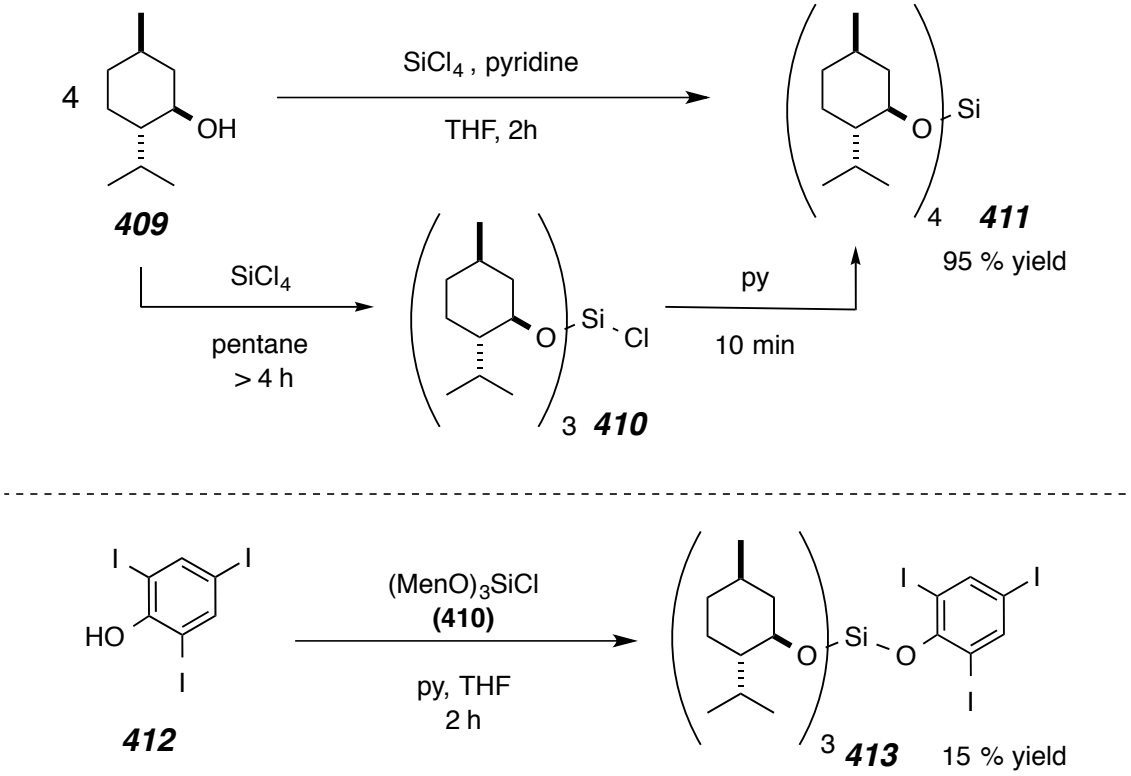

4.2.2 Effect of Loading on Nanoparticle Size and Stability

One advantage of the FNP process to make BCP protected nanoparticles is the ability to make particles with a high loading of the cargo of interest. The theoretical loading level is the ratio (w/w) of the mass of the drug to that of the drug plus the BCP that was introduced in the THF stream during FNP. To better understand how loading affects nanoparticle stability, particles were made with varying loadings of $(MenO)_4Si$ (**411**), while the total concentration of dissolved solute was kept constant. The particle size was measured by DLS and the measurement repeated multiple times. There was a tight distribution within the replicate measurements but considerable variability when different batches of particles were prepared. Typically, particle size increased from about 75 nm with

no $(MenO)_4Si$ (**411**), to ca. 100 nm at 50% $(MenO)_4Si$ (**411**) loading, to ca. 200 nm at 90% $(MenO)_4Si$ loading, as shown in Figure 4.3. These results also show that varying the loading levels provides a means to control particle size.

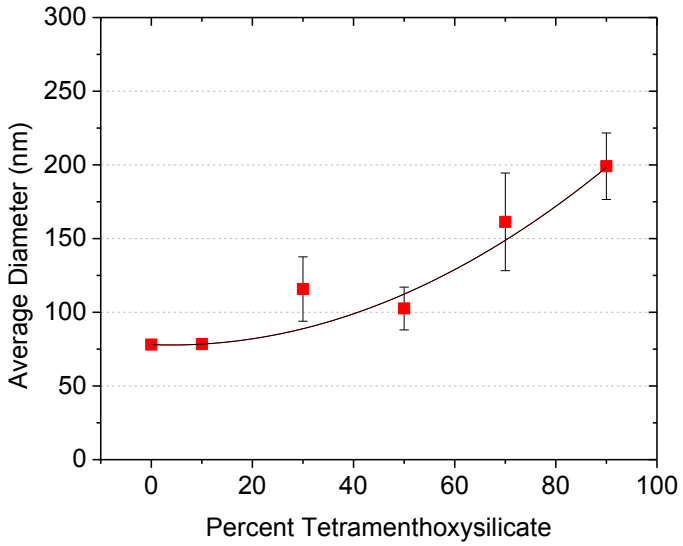

Figure 4.3 I Effect of loading level on nanoparticle size in FNP. All particles were made using 5k-10k PEG-b-PLGA and $(MenO)_4Si$. The ratio of polymer to $(MenO)_4Si$ was varied while the total solute concentration was kept constant.

We next compared the nanoparticle stability of the $(MenO)_4Si$ (**411**) solute with the nanoparticles filled with β-carotene (**408**) at the same two loading levels shown in Figure 4.4. The intensity average diameter or z-average size and polydispersity (pdi) of the particles are shown in the bar graph in Figure 4.4. The $(MenO)_4Si$ particles at either 50% or 90% loading were stable for a week and even up to a month in suspension! A 0.9 wt% NaCl was added to mimic the salt concentration in blood, to which the particles did not aggregate and remained below 200 nm in size.

Particles made using β-carotene (**408**) at either 50% or 90% loading were stable for up to a week in suspension. However, they were unstable when either standing in solution for a month or by treatment with NaCl. The large increase in

particle size to ca. 250 nm in the 90% loading is suggestive of nanoparticle aggregation. While both molecules have similar calculated logP (clogP) values [9.72 for β-carotene (**408**), 9.19 for $(MenO)_4Si$ (**411**)] we hypothesized that they may differ in morphology inside the core of the nanoparticle, or the difference in stability could be due to the difference in zeta potential.[150]

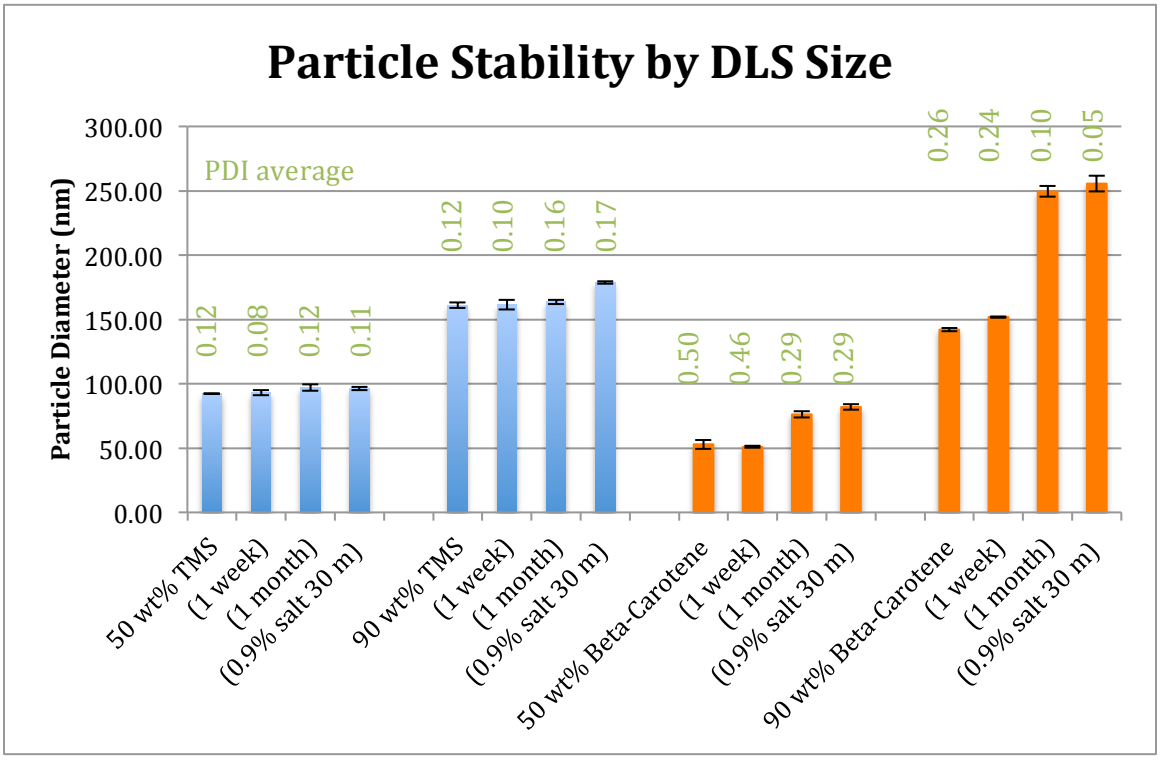

Figure 4.4 I Effect of loading level on nanoparticle size and stability for $(MenO)_4Si$ [blue] and β-carotene [orange]. DLS measurements were made *i.)* immediately following FNP, *ii.)* after 1 week in suspension, *iii.)* after 1 month in suspension, and *iv.)* after addition of salt and standing for 30 min. All particles were made using 5k-10k PEG-*b*-PLGA and $(MenO)_4Si$ or β-carotene.

Also we were interested in determining if the instability of the 90 wt% β-carotene nanoparticles was a result of residual THF. Particles were made using the same methods as before. Acetone was chosen as an alternating solvent to

[150] Abdelwahed, W.; Degobert, G.; Stainmesse, S.; Fessi, H. Freeze-Drying of Nanoparticles: Formulation, Process and Storage Considerations. *Adv. Drug Deliv. Rev.* **2006**, *58*, 1688–1713.

probe the effect of the choice of water-miscible solvent may have on the FNP process and stability of the resulting nanoparticles. Four batches of particles were made and adding in 0.9 wt% NaCl tested the nanoparticle stability. The images of the suspensions themselves are shown in Figure 4.5 and the DLS measurements are shown in Figure 4.6.

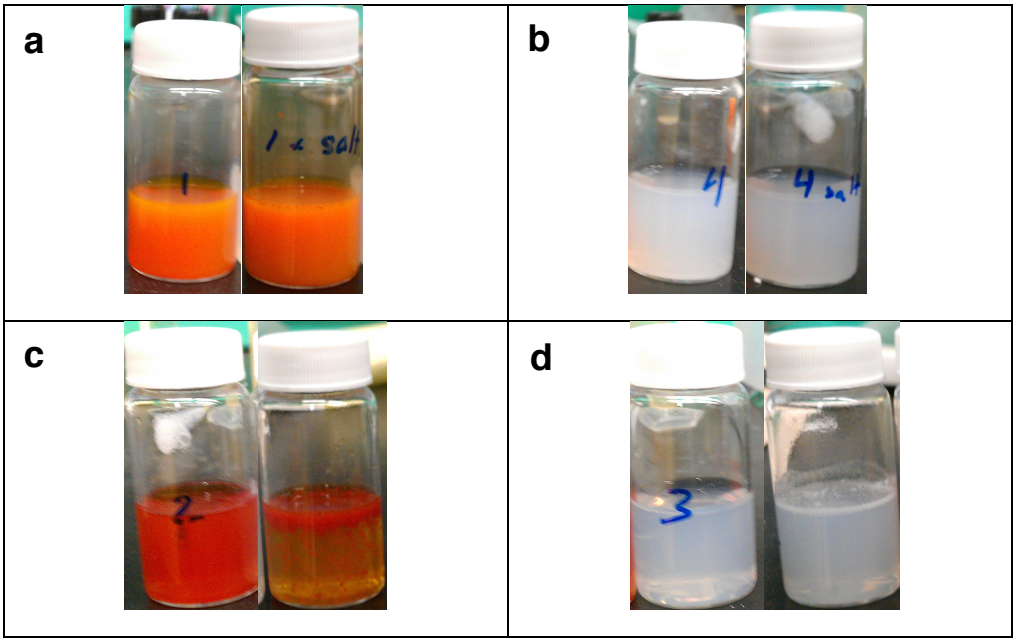

Figure 4.5 I Photos of 90 wt% solute nanoparticle suspensions prepared by FNP with **a.)** β-carotene in 10% v/v THF without salt (left) with salt (right), **b.)** $(MenO)_4Si$ in 10% v/v THF without salt (left) with salt (right), **c.)** β-carotene in 10% v/v acetone without salt (left) with salt (right), **d.)** $(MenO)_4Si$ in 10% v/v acetone without salt (left) with salt (right).

The images show major differences between THF and acetone for use in FNP to make β-carotene nanoparticles at 90% loading. The nanoparticles have a diameter of ca. 150 nm in size (Figure 4.6) but begin to aggregate upon the addition of salt as shown in the image (Figure 4.5, panel a, right) and the increase in size to ca. 280 nm, bar graph Figure 4.6. The $(MenO)_4Si$ loaded nanoparticles are stable in the THF suspension even with the addition of salt as

shown in the image (Figure 4.5, panel b, right) and do not increase in size (Figure 4.6).

We performed the FNP using acetone as the water-miscible organic solvent and observed a drastic difference in particle size between the β-carotene and the $(MenO)_4Si$ loaded at 90 wt% particles. The β-carotene particles gave a dark red appearance (Figure 4.5, panel c, left), had a large particle diameter of 2,500 nm and broad PDI of 1.0 shown in Figure 4.6. Treating these particles with salt at a 0.9 wt% concentration lead to rapid flocculation of β-carotene (Figure 4.5, panel c, right). Due to the large crystals of the solute out of solution, a DLS measurement could not be obtained. These observations indicate that acetone is not a good solvent for FNP of β-carotene. The $(MenO)_4Si$ particles gave a more transparent appearance when acetone was used instead of THF [compare (Figure 4.5, panel d, left) to (Figure 4.5, panel b, left)]. This more transparent hue is due to the smaller particle diameter of ca. 150 nm and narrow pdi of 0.15 as shown in Figure 4.6. Unfortunately, treating these particles salt at a 0.9 wt% concentration lead to precipitation of $(MenO)_4Si$ on the walls of the vial (Figure 4.5, panel d, right). Due to the $(MenO)_4Si$ dropping out of solution, a DLS measurement could not be obtained. These observations indicate that acetone is not a good solvent for FNP of $(MenO)_4Si$ when salt is added, but removal of acetone would be beneficial.

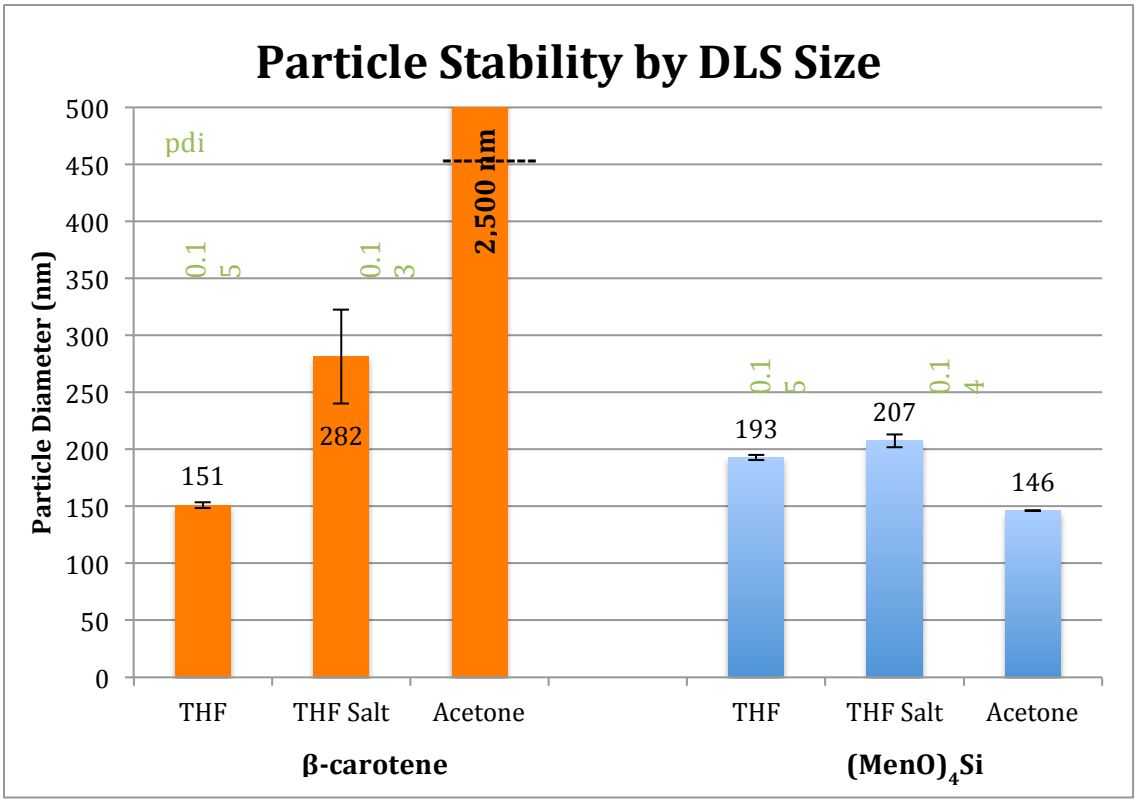

Figure 4.6 I Particle stability of nanoparticles loaded at 90% with and β-carotene [orange] or $(MenO)_4Si$ [blue] and mPEG-*b*-PLGA (5k-10k). DLS measurements were made *i.)* immediately following FNP with THF, *ii.)* after 30 min incubation at 0.9 wt% NaCl, *iii.)* immediately following FNP with acetone.

4.2.3 Effect of Nanoparticle Zeta-Potential and Morphology on Stability

We were very interested in the drastic difference in stability of nanoparticles loaded with either β-carotene and $(MenO)_4Si$. We measured the zeta-potential of the particles presented in Figures 4.4 and 4.5, because the zeta-potential is an important indicator of stability. Below in Table 4.3 shows the values for the nanoparticles prepared using THF as the water-miscible organic solvent, the particles prepared with acetone were not measured due to the lack of stability.

Table 4.3 | The electrokinetic parameters of nanoparticles loaded at 90 wt% with either β-carotene or $(MenO)_4Si$ and mPEG-*b*-PLGA (5k-10k) block copolymer.

Conditions	Zeta-Potential (mV)	Mobility (μmcm/Vs)	Conductivity (mS/cm)
β-carotene NPs (THF)	-10.50 ± 0.14	-0.83 ± 0.01	0.06 ± 0.00
β-carotene NPs (0.9 wt% NaCl)	-0.84 ± 0.32	-0.07 ± 0.03	16.15 ± 0.92
$(MenO)_4Si$ NPs (THF)	-29.05 ± 0.07	-2.28 ± 0.01	0.01 ± 0.00
$(MenO)_4Si$ NPs (0.9 wt% NaCl)	-0.73 ± 0.02	-0.06 ± 0.00	13.90 ± 0.99

The zeta-potential for the nanoparticles made with $(MenO)_4Si$ (-29 mV) is three times that of the analogues β-carotene NPs (-10 mV). This difference is enough to be classified differently in colloidal literature shown in Table 4.4.[151] The electrophoretic mobility of the particles correlates with the zeta-potential of each particle (Table 4.3 column 2). As expected when salt is added to the particle suspensions the zeta-potential drops to essentially zero (Table 4.3 column 1) for both sets of particles, but the $(MenO)_4Si$ particles do not aggregate. Also the conductivity of the solution is increased when the salt is added (Table 4.3 column 3).

Table 4.4 | The stability behavior of colloids as a function of zeta-potential.[151]

Zeta-Potential (mV)	Stability Behavior of the Colloid
0 ± 5	Rapid coagulation or flocculation
± 10 to ± 30	Incipient instability
± 30 to ± 40	Moderate stability
± 40 to ± 60	Good stability
Greater than ± 60	Excellent stability

Since the zeta-potentials both dropped with the addition of salt for the β-carotene NPs as well as the $(MenO)_4Si$ NPs, we anticipated both to aggregate in solution. To further probe this stark contrast in stability between particles loaded

[151] Greenwood, R. Review of the Measurement of Zeta Potentials in Concentrated Aqueous Suspensions Using Electroacoustics. *Adv. Colloid Interfac.* **2003**, *106*, 55–81.

with β-carotene or $(MenO)_4Si$, we studied the solute morphology within the core of the nanoparticles. X-ray diffraction shown in Figure 4.7, was used to determine the crystallinity of the small molecule encapsulated in nanoparticles.

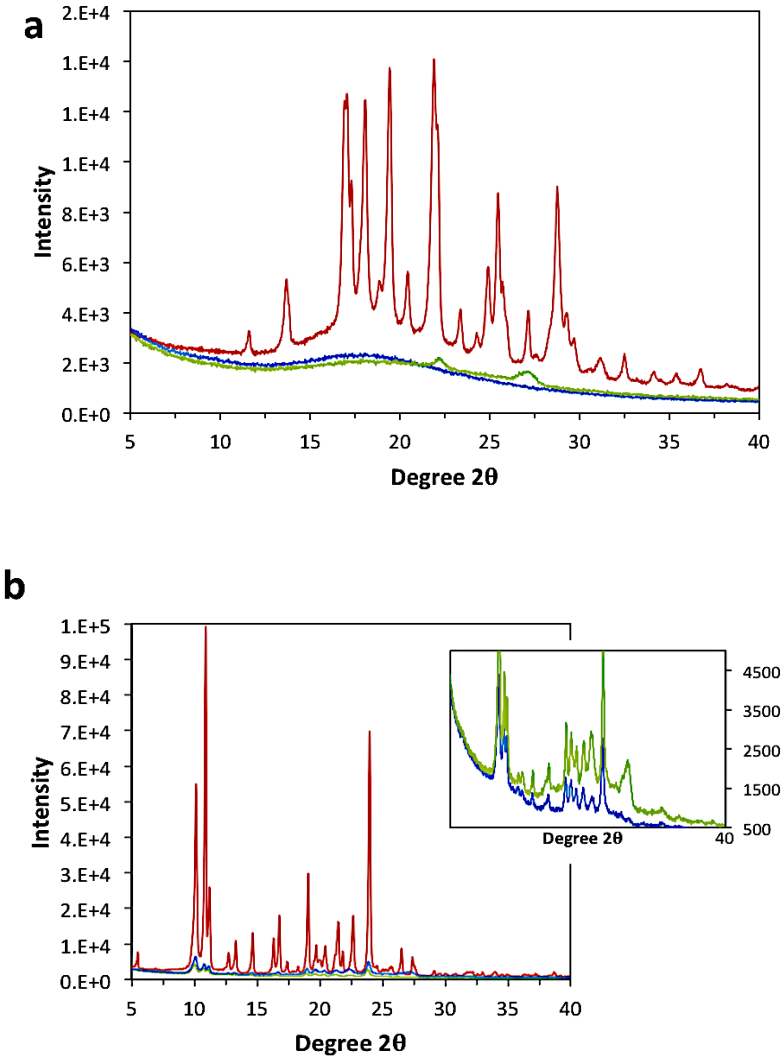

Figure 4.7 I X-ray powder diffraction (XRD) of **a.)** β-carotene and **b.)** tetramenthoxysilicate ($(MenO)_4Si$) as the pure compound (red) vs. nanoparticles (5k-10k mPEG-*b*-PLGA BCP) loaded with 90 wt% (blue) and 50 wt% (green) $(MenO)_4Si$. The inset with expanded scale clearly shows the $(MenO)_4Si$ remains crystalline in the 90 wt% and 50 wt% nanoparticles.

The XRD pattern was collected on a PANalytical X'Pert Pro MPD diffractometer equipped with a cobalt anode (45 kV, 40 mA, λ = 1.790 Å) and an X-Celerator detector with the help of Yuqiang Qian.

Interestingly, the particles made with β-carotene are amorphous in the core at both 50 and 90 wt%, while those made with $(MenO)_4Si$ remain crystalline throughout the two loading levels. This difference in morphology leads to the differences in stability of the two different compounds with nominally the same hydrophobicity. While we have shown that FNP can be used to make nanoparticles from a variety of compounds provided they are of sufficiently high hydrophobicity,[86] the internal structure of the particles is critical for understanding stability. Although the cLogP values of compounds provides an initial guide for selecting organic solutes or drugs for the FNP process, the morphology inside the core and zeta-potential are crucial indicators for long term stability.

Improved understanding of the nanoparticle structure is vital, because it affects the release of the organic solute or, more critical, drug release in terms of this project. For example, a loaded drug may release from the particles more quickly if the particle has a loosely packed structure with some hydrophilic blocks incorporated into the core vs. a tightly packed core shell structure.

Nanoparticles were made using hydrophobic compounds containing the heavy atom iodine. Iodine was chosen in hopes to provide an improved contrast of images taken cryogenic transmission electron microscopy (cryo-TEM) taken by Han Seung Lee compared to particles loaded with β-carotene.[86] Particles were initially formed by FNP of the commercially available iodohexadecane (**414**) with mPEG-*b*-PLGA (5k-10k) at 10 wt%. Unfortunately these particles did not show a well-defined spherical particle and did not show a distinct core shell structure (Figure 4.8, panel b).

We next attempted to fashion particles from triiodophenol (**412**) itself due to the presence of three heavy iodine atoms per molecule, however the hydrophobicity of the compound was insufficient and the particles were not stable.[86] The utility of silicate ester chemistry was proven again, as particles made with the hydrophobic trimenthoxy-triiodophenol silicate (**413)** gave excellent particle shape (Figure 4.8, panel a) and an imoproved contrast in the

core shell nature of the particles. The particles for this study were fashioned at 50 wt% **413** and with a mPEG-*b*-PLGA (5k-10k) polymer.

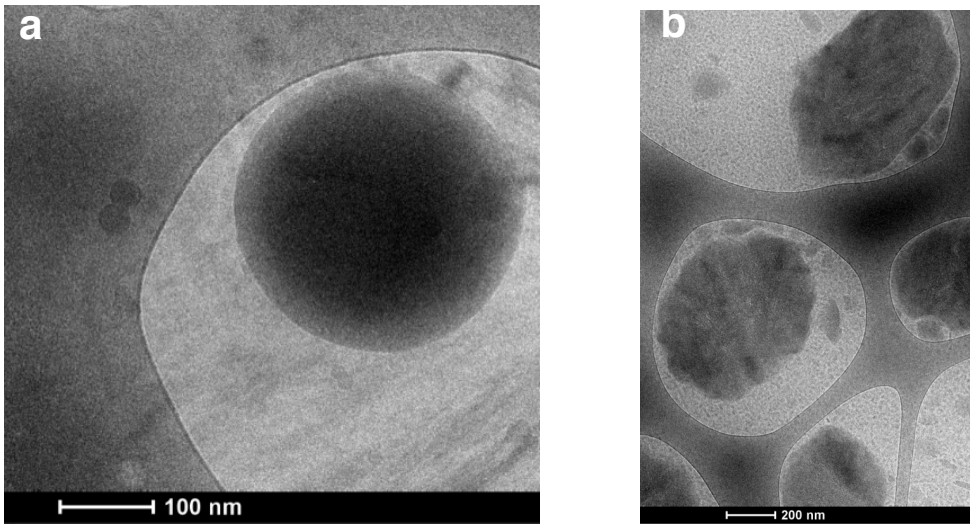

Figure 4.8 I a) FNP prepared, Trimenthoxy(triiodophenol)Silicate (**413**) nanoparticles loaded at ca. 50 wt% with mPEG-PLGA (5k-10k) **b**) FNP prepared, iodohexadecane ($C_{16}H_{33}I$**, 414**) nanoparticles loaded at ca. 10 wt% with mPEG-PLGA (5k-10k)

These model drugs proved that high loading of hydrophobic compounds into nanoparticles is attainable with the FNP process. The marriage of silicate chemistry with the FNP concept was shown with the use of the tetramenthoxy silicate (**411**) and (**413**). We next turned our attention to the hydrophobic prodrugs of **PTX** shown in Chapter 3.

4.3 Nanoparticle Formulations of PTX Silicates

4.3.1 Introduction

A number of barriers diminish the translational success of nanomedicine.[152] A key challenge is the limited intra-tumoral distribution of drug delivery carriers, since their transport within the tumor is highly inefficient. Distal regions receiving lower drug exposure often harbor the more aggressive tumor cells. Thus, achieving therapeutic drug concentrations in these under-supplied regions would represent a significant advance. Many recent studies have shown that particles that are in the sub-100 nm size range demonstrate improved tumor accumulation and, more importantly, improved tumor penetration.[153,154,155] While many techniques are available to fabricate nanocarriers in the ≤100 nm size range, it is extremely difficult to achieve reasonable drug loading in such small particles. Most colloidal carriers can be loaded to a mere ≤10 wt%.

Flash nanoprecipitation (FNP), a technique pioneered by Prud'homme (Chapter 2),[117] enables the synthesis of sub-100 nm nanoparticles with very high drug loading (Chapter 4.2).[78,86,117,156] FNP requires rapid turbulent mixing of organic solutes dissolved in a water-miscible organic solvent (e.g., tetrahydrofuran, acetone, acetonitrile) with the antisolvent, water, in a confined

[152] Tarr, B. D.; Yalkowsky, S. H. A new parenteral vehicle for the administration of some poorly water soluble anti-cancer drugs. *J. Parenter. Sci. Technol.* **1987**, *41*, 31–3.

[153] ABRAXANE™ for Injectable Suspension (paclitaxel protein-bound particles for injectable suspension) (albumin-bound). http://www.accessdata.fda.gov/drugsatfda_docs/label/2005/021660lbl.pdf (accessed April 26, 2015).

[154] Gradishar, W. J.; Tjulandin, S.; Davidson, N.; Shaw, H.; Desai, N.; Bhar, P.; Hawkins, M.; O'Shaughnessy, J. Phase III trial of nanoparticle albumin-bound paclitaxel compared with polyethylated castor oil-based paclitaxel in women with breast cancer. *J. Clin. Oncol.* **2005**, *23*, 7794–803.

[155] Smith, J. Overview of breast cancer drug therapy. *US PHARMACIST.* **2005**, *30*, 9.

[156] Pustulka, K. M. Polymer stabilized nanosuspension via flash nanoprecipitation: particle formulation, structure and freeze drying. M.S. Dissertation, University of Minnesota, Minneapolis, 2012.

space. When the solvent and antisolvent streams meet and mix, the solutes rapidly precipitate into nanoparticles due to supersaturation. The encapsulating agent used in FNP is typically an amphiphilic block copolymer (BCP), such as poly(ethylene glycol)-*b*-poly(lactic-co-glycolic acid) (PEG-*b*-PLGA). The hydrophobic block of BCP co-precipitates with the drug, while the hydrophilic block provides steric stabilization on the nanoparticle surface.

In this chapter, we evaluated the use of FNP to fabricate nanoparticles of paclitaxel (**PTX**), a widely used anticancer agent. Studies have shown that FNP-loaded, PEG-*b*-PLGA-based nanoparticles loaded with **PTX** alone are not stable;[78,80,82,89] rapid Ostwald ripening of the freshly prepared nanoparticles leads to precipitation of **PTX** from the 90-95% aqueous dispersion in which the initial FNP formulations are produced (Chapter 2.2.2).[80,86,89,156] This phenomenon is likely due to a sufficient water solubility and inherent crystallinity of **PTX**. It is paradoxical that although **PTX** is too hydrophobic a drug to be dissolved in aqueous medium and therapeutically administered, it is still too hydrophilic to be efficiently encapsulated and stabilized as a nanoparticle by FNP.

To render **PTX** more hydrophobic, we have developed a series of PTX-prodrugs containing silicate esters [i.e., PTX-O-Si$(OR)_3$] (Chapter 3).[118,120] The silicate moiety is hydrolytically labile and serves as a prodrug to release the parent compound in biological media. We have shown that both the hydrophobicity as well as the rate of hydrolysis of the prodrug can be tailored. The goal of the current study was to evaluate the use of the FNP technique coupled with the silicate ester prodrug technology to fabricate nanoparticles suitable for **PTX** delivery. Using *in vitro* and *in vivo* models, we have identified factors affecting the regeneration of **PTX** from PTX-silicate prodrug-loaded nanoparticles.

4.3.2 PTX-silicate prodrugs

The paclitaxel silicate prodrugs studied (i.e., **301-303**) are shown at the top of Table 4.5. Their molecular weight, calculated octanol/water partition coefficients (cLogP), and relative rates of chemical hydrolysis (in aqueous acetone containing trifluoroacetic acid) are given in Table 4.5.[118] Collectively, these show that the hydrophobicity can be tuned based upon the nature of the alkyl group present in the silicate ester(s) moiety. Greater hydrophobicity of the prodrug allows for the formation of stable nanoparticle suspensions, a property not attainable with FNP-produced PEG-*b*-PLGA nanoparticles loaded with PTX alone.[80,78,82,86,89,156] The size of the alkyl groups in the silicate also affects the relative hydrolysis rates of silicate cleavage. The hydrolytic stability of each prodrug plays a significant role in the overall rate of drug release, as discussed below.

Table 4.5 I Structures and properties (hydrophobicity and hydrolytic lability) of the PTX-containing silicate prodrugs used in this study.[118]

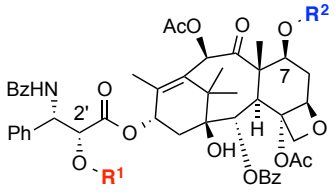

	R1	R2	shorthand descriptor	MW	hydrophobicity: cLogP[a]	hydrolytic lability: k_{rel}[b]	hydrolytic lability: $t_{1/2}$ (min)
PTX	H	H	paclitaxel	854	3.2	N/A	N/A
301a	$Si(OEt)_3$	H	PTX-2'-$Si(OEt)_3$	1016	5.0	18,000	3.7
301b	$Si(O^nOct)_3$	H	PTX-2'-$Si(O^nOct)_3$	1269	7.7	5,600	12
301c	$Si(O^iPr)_3$	H	PTX-2'-$Si(O^iPr)_3$	1058	5.6	570	120
301f	$Si(O^tBu)_2(OEt)$	H	PTX-2'-$Si(O^tBu)_2(OEt)$	1072	5.8	5.6	12,000
301d	$Si(Omenthyl)_3$	H	PTX-2'-$Si(Omenthyl)_3$	1347	7.4	1.0	69,000
303a	H	$Si(OEt)_3$	PTX-7-$Si(OEt)_3$	1016	5.1	2,200	30
303b	H	$Si(O^nOct)_3$	PTX-7-$Si(O^nOct)_3$	1269	7.8	450	150
302a	$Si(OEt)_3$	$Si(OEt)_3$	PTX-2',7-$[Si(OEt)_3]_2$	1178	6.3	15,000 (R^1) 2,100 (R^2)	4.6 (R^1) 33 (R^2)

[a] aLogP values from ALOPS 2.1.[132] [b] hydrolysis was performed in homogenous solutions of 90:9:1 volume ratio of acetone-d_6:D_2O:CF_3CO_2H and the k_{rel} values are benchmarked against the silicate **301d**, which showed the slowest rate of silicate cleavage[118]

4.3.2 Nanoparticle Preparation

The nanoparticles were fabricated by flash nanoprecipitation (FNP)[116] using a CIJ-D mixer (Chapter 2.1).[85] In brief, to achieve a ca. 50 equiv wt% of **PTX**, the molecular weight of the prodrug was factored into consideration by use of the following equation.

$$\text{mass of prodrug to obtain 50 wt\% PTX} = \text{mass polymer (mg)} \times \left(\frac{\text{MW Prodrug}}{\text{MW PTX}} \right)$$

Specifically, an amount of PTX-prodrug containing the equivalent of 25 mg of free **PTX** and 25 mg of PEG-*b*-PLGA were dissolved in 2.5 mL of THF and impinged against 2.5 mL of deionized water in a CIJ-D mixer and further diluted into 45 mL of water. Blank polymer nanoparticles (i.e., containing no PTX-silicate) were also prepared and used as a control group for *in vitro* and *in vivo* cytotoxicity studies. PEG-*b*-PLGA (25 mg) was dissolved in 2.5 mL of THF and impinged against 2.5 mL of deionized water and further diluted into 45 mL of water.

The size of the freshly prepared nanoparticles was measured by dynamic light scattering (DLS) on a Delsa™ Nano C (Beckmann Coulter) instrument. Samples for DLS were prepared by diluting the nanoparticle suspension with water immediately after CIJ-D mixing. The intensity average size, d_I, and polydispersity index PDI calculated (via the cumulants method) by the instrument were recorded. Measurements were taken in triplicate.

To remove unencapsulated prodrug and free polymer from the nanoparticle suspension, ultracentrifugation was performed on the initial FNP

suspension at 50,000 rpm and 4 ºC for 30 min. After each round of centrifugation, the supernatant, which contained a considerably higher wt% of polymer than that used in the initial preparation (^{1}H NMR, Figures S4.9-S4.10), was removed using a transfer pipet. The pellet was resuspended in 25 mL of water and the process repeated twice. After the third ultracentrifugation, the pellet was collected and lyophilized using a Freeze Dryer System (Labconco) at -45 ºC for 24 h to remove residual water. The overall mass recovery varied following the rounds of three centrifugations for different formulations; it typically ranged from 30–80%.

The prodrug loading level of the lyophilized nanoparticles was further assessed by high performance liquid chromatography (HPLC, Model 508, Beckmann Coulter, CA) or ^{1}H-NMR analysis. To determine loading by HPLC, 1 mg of lyophilized nanoparticles was suspended in 1 mL of acetonitrile (ACN) and agitated for 24 h, during which time the organic materials (block copolymer and PTX-silicate derived components) were solubilized. An aliquot (30 μL) of the resulting suspension was injected onto a C-18 HPLC column (4.6 × 250 mm with 5 μm packing). The mobile phase consisted of a mixture of acetonitrile and water (75:25) and was delivered at a flow rate of 1 mL/min. The amounts of **PTX** and the PTX-silicate prodrug were quantified by UV detection at 228 nm against a series of calibration curves for **PTX** and the appropriate PTX-silicate, created over a range of concentrations from 3.125 to 100 μg/mL. Alternatively the loading level and efficiency of prodrug incorporation was assessed from ^{1}H-NMR integrations of various resonances in a solution of the final lyophilized, drug-loaded nanoparticle pellet. A portion (ca. 3 mg) was dissolved in $CDCl_3$, a solvent in which all components of the loaded nanoparticles are readily soluble. Equations describing these quantification methods are given in the Supporting Information for Chapter 4 (SI, Figure S4.8).

4.3.4 Nanoparticle Characterization

An initial set of loaded nanoparticles was prepared using the most easily synthesized silicates **301** and **302**. The intensity average size (d_I) and size distribution (PDI) for each preparation was measured in triplicate by dynamic light scattering (DLS); the results are given in Table 4.6. The suspensions of nanoparticles (as initially formulated in 5% THF/water) remained homogeneous and stable for 1 (for **301a**) to several (for **301b**) to >14 (for **301c, 301d, 301f**) days before showing significant aggregation, as determined both by visual inspection and DLS measurements. As the hydrophobicity of the PTX-silicate prodrug increased (higher cLogP), the resulting loaded nanoparticles sizes tended to decrease.

Preliminary release studies with some of these preparations showed "burst-release" behavior[139] that is characteristic of samples containing both loaded nanoparticles as well as a portion of free (pro)drug that is not protected by the block copolymer. [157] We therefore implemented a protocol using ultracentrifugation to pelletize the loaded nanoparticles (3x) followed by final lyophilization to produce dry-powdered preparations of the loaded nanoparticles. This means of preparation largely removed the initial burst phase of the release profiles. Redispersion of the lyophilized powder in water, aided by probe tip sonication, gave nanoparticles that showed evidence of aggregation as judged from the larger sizes revealed by DLS analysis (Table 4.6). Freeze-drying induced aggregation and resulted in an increase in particle size, as has been reported for other nanoparticle structures.[86,156,158,159]

---

[157] Huang, X.; Brazel, C.S. On the importance and mechanisms of burst release in matrix-controlled drug delivery systems. *J. Control. Release*. **2001**, *73*, 121–136.

[158] Lee, M. K.; Kim, M. Y.; Kim, S.; Lee, J. Cryoprotectants for freeze drying of drug nano-suspensions: effect of freezing rate. *J. Pharm. Sci.* **2009**, *98*, 4808–4817.

[159] Schuch, H.; Klingler, J.; Rossmanith, P.; Frechen, T.; Gerst, M.; Feldthusen, J.; Müller, A. H. E. Characterization of Micelles of Polyisobutylene- Block-Poly(Methacrylic Acid) in Aqueous Medium. *Macromolecules* **2000**, *33*, 1734–1740.

The levels of prodrug loaded into these final lyophilized nanoparticles are listed in Table 4.6. The nanoparticles contained ca. 50-75 wt% of PTX-silicate. Because the supernatant from the centrifugation contained a greater portion of polymer than PTX-derived material (NMR analysis), the final PTX-silicate loading levels of the nanoparticle formulations were typically greater than the wt% of silicate charged in the initial FNP procedure. The very high load level that can be achieved using FNP formulation in combination with hydrophobic prodrugs of **PTX** is one of the main advantages of this nanoparticle formulation and approach.

Evidence for high encapsulation was also demonstrated for a silicate derivative loaded particle. PTX-2',7-$[Si(OEt)_3]_2$ (**302a**) particles were flash precipitated with an equal mass of PEG-b-PLGA (5k-10k). Control particles were made without using any stabilizing PEG-b-PLGA. The particles were freeze-dried following FNP and then redispersed in water. Diethyl ether, a good solvent for the silicate but not for PEG or the BCP, was then used to extract each of these two aqueous dispersions. The content of the ether extract was analyzed by 1H NMR spectroscopy. Without block copolymer protection >85% of the silicate derivative was recovered, while with PEG-b-PLGA protection the particles only lost 7% of their silicate content even after multiple extractive washings with ether. This result also demonstrates that > 90% of the silicate was encapsulated in the nanoparticle core.

Table 4.6 I Size, prodrug loading levels, and cytotoxicities of nanoparticles loaded with PTX-silicates.

	Before centrifugation		After centrifugation, lyophilization, and resuspension				
Pro-drug	d_l (nm)	PDI	d_l (nm)	PDI	PTX-silicate loading (wt%)[a]	PTX loading (wt%)[b]	IC_{50} (nM)
PTX	-	-	-	-	-	-	77
301a	140	0.10	420	0.25	63.0	53.0	71
301b	83	0.16	210	0.23	65.0	43.7	220
301c	140	0.17	200	0.34	58.0	46.8	14
301f	86	0.09	240	0.36	73.5	58.6	1000
301d	95	0.08	200	0.31	73.5	46.6	650
302a	120	0.13	310	0.65	60.4	43.8	80

[a] PTX-silicate prodrug loading is the wt% of encapsulated silicate derivative in the loaded nanoparticles following centrifugation; [b] PTX loading is the wt% of PTX that can be regenerated from silicate derivative in the loading nanoparticles following centrifugation. It is calculated using PTX-silicate loading and the MW of PTX and silicate derivatives.

Cryo-transmission electron microscopy was used to examine various features of the loaded nanoparticle preparations. Selected cryo-TEM images are shown in Figure 4.6. The image in panel A shows the spherical nature of the freshly prepared loaded nanoparticles. In addition, a core-shell morphology is clearly evident. The core is rich in PTX-silicate, which is more electron dense than PLGA.

Nanoparticles were examined following centrifugation, lyophilization, and redispersion into PBS. These were loaded with PTX-2'-$Si(OEt)_3$ (**301a**), the most hydrolytically labile silicate. When examined immediately after redispersion, the

core-shell structure was still intact (Figure 4.9, B). However, the particle size had grown due to aggregation as represented by the chain of particles in the right side of Figure 4.9, B and Figure S4.12. This is consistent with the increased d_I measured by DLS (Table 4.6). After 24 h in suspension, another sample of these nanoparticles was imaged. The size had diminished and the cores disappeared (Figure 4.9, C), suggesting that hydrolysis and/or release of **PTX** and/or the PTX-silicate was occurring during that aging period. Similar results were observed for particles made from PTX-2′7,-[Si(OEt)$_3$]$_2$ (**302a**), which hydrolyzed rapidly, lost their cores and appear to shrink while PTX-2'Si(O^{t}Bu)$_2$(OEt) (**301f**), with very slow hydrolysis, did not change with 24 h aging (see Figure S4.11).

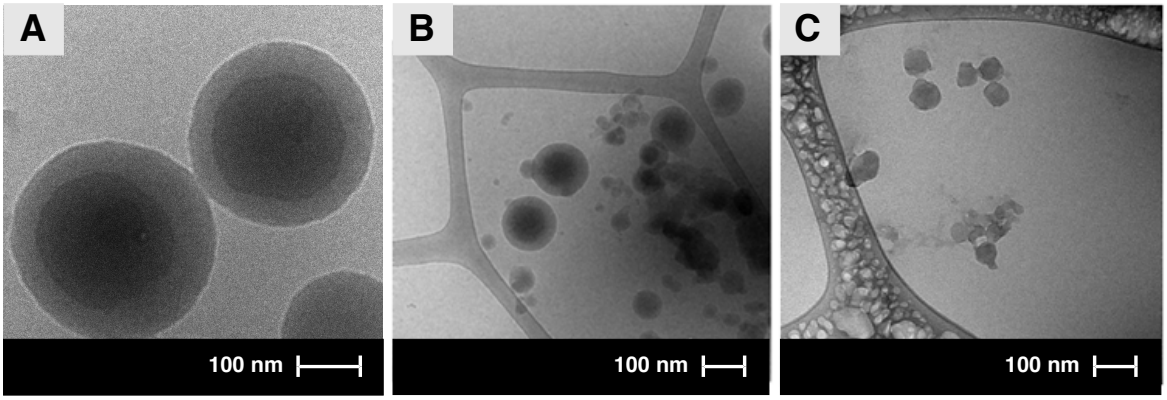

Figure 4.9 I Cryo-TEM images of nanoparticles loaded with PTX-2'-Si(OEt)$_3$ (**301a**). **A)** freshly prepared (i.e., prior to centrifugation), **B)** lyophilized, immediately following redispersion into PBS after centrifugation, and **C)** lyophilized following redispersion into PBS and aging for 24 h in a dialysis cassette suspended in PBS (pH 7.4).

The structure and morphology of nanoparticles (freeze-dried, 5k-10k PEG-*b*-PLGA nanoparticles made using the CIJ-D mixer) was also evaluated using DSC. Typically, DSC studies of polymers utilize the "second run" of the trace so that the measured properties are independent of the polymer's thermal history. In the case of the FNP-produced polymers, however, data from the "first run" are instructive. The "first run" DSC trace of unloaded PEG-*b*-PLGA nanoparticles exhibited a strong T_m of the crystalline PEG block at ca. 50 °C as shown in Figure

4.10. This is a depressed melting transition temperature relative to the pure PEG homopolymer (which exhibited a T_m of ca. 60 °C in a control experiment). This observation is consistent with incomplete phase segregation. The T_g from the PLGA block was not obvious in the trace, but it is conceivable that there is a weak, broad glass transition at ca. 20 °C whereas the T_g of pure PLGA is 39 °C.[86] This observation is consistent with some polyether/polyester mixing.[160]

Recrystallization of the PEG did not occur upon cooling and the "second run" DSC trace exhibited a single T_g. This result was reproduced when the polymer was cooled at an exceedingly slow rate (1 °C•sec^{-1}), consistent with a thermodynamically stable, phase-mixed system. Based on these results, a reasonable conclusion is that the polymer blocks are largely, but not exclusively, phase-segregated following FNP and lyophilization. This further supports the core-shell structure of these nanoparticles.

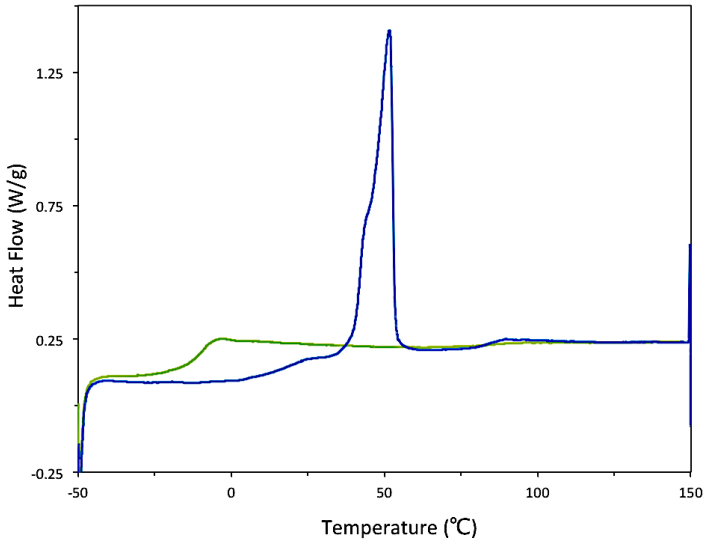

Figure 4.10 I The DSC trace of the FNP-precipitated and freeze dried 5k-10k PEG-*b*-PLGA BCP (**405**) shows a strong PEG T_m on the "first run" (blue) indicative of significant phase segregation of the kinetically trapped nanoparticle. A single T_g on the "second run" (green) is characteristic of a phase mixed state at equilibrium.

[160] Kulinski, Z.; Piorkowska, E.; Gadzinowska, K.; Stasiak, M. Plasticization of poly(L-lactide) with Poly(propylene Glycol). *Biomacromolecules* **2006**, *7*, 2128–35.

With a basic understanding of the DSC behavior of the precipitated polymer, we turned our attention to the analysis of a paclitaxel silicate, PTX-2′7,-$[Si(OEt)_3]_2$ (**302a**), loaded nanoparticle. Particles were made using an equal mass of BCP and the silicate in the CIJ-D mixer and were lyophilized immediately after nanoprecipitation. Again, a strong, depressed PEG T_m at ~50 °C was evident (Figure 4.11). Additionally, there was a broad melting point centered at ~105 °C. This endothermic peak occurs at a lower temperature and is broader than that for the pure PTX silicate (red curve in Figure 4.11) indicating an impure, crystalline melting transition of the PTX silicate. After cooling, a single T_g was again noted during the second heating cycle, a feature consistent with a well-mixed, silicate-loaded polymer film (rather than nanoparticles).

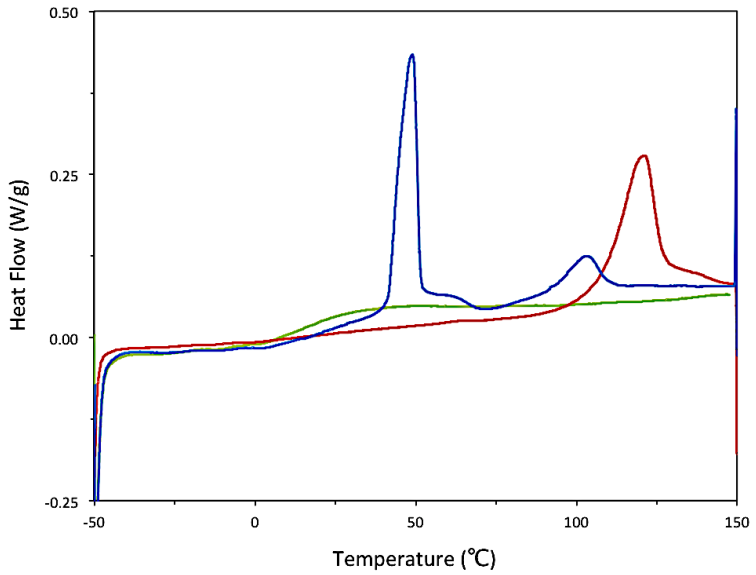

Figure 4.11 I The DSC trace of the FNP-precipitated and freeze-dried nanoparticle composed of equal mass of 2',7-bis(triethoxy)-PTX-Si and 5k-10k PEG-*b*-PLGA BCP shows a strong PEG T_m and a broad melting point attributed to a depressed melting of the PTX silicate on the "first run" (blue) and a single T_g associated with a phase mixed film in the "second run" (green). The pure 2',7-bis(triethoxy)-PTX-Si (red) is overlaid on the DSC trace showing a higher T_m and sharper melting transition.

We also performed powder x-ray diffraction as done with the model systems (c.f. Figure 4.7). The prodrugs were predominately amorphous in the core of the nanoparticles, which is advantageous for the future release profiles. The powder XRD profiles of the nanoparticles made with **301b** and **302a** are shown (SI, Figures S4.1 and S4.2). Nanoparticles made with **301a**, **301c**, **301d**, and **301f** were also made and showed similar results and are not shown in this thesis.

4.3.5 *In Vitro* Drug Release Profiles

PTX and PTX-silicate release studies were performed by Jing Han on selected PTX-silicate-loaded nanoparticles using dialysis mini capsules with a semipermeable membrane. Control experiments showed that diffusion of the drug or prodrug alone through the membrane occurred readily. An aqueous suspension of either **PTX** or PTX-2',7-$[Si(OEt)_3]_2$ (**302a**) was placed in the capsule, which was then immersed in buffer (pH = 7.4). Departure of each compound from the capsule was monitored over time. Both compounds were absent after 3 hours (SI, Figure S4.3). This showed that diffusion of **PTX** or a PTX-silicate could be expected to occur rapidly once each was no longer inside a nanoparticle.

We next studied the release of **PTX** and the PTX-silicate from several of the prodrug-loaded nanoparticle preparations. These studies were conducted at 37 ˚C and representative plots for release of PTX-2'-$Si(O^nOct)_3$ (**301b**) from the loaded nanoparticles are shown in Figure 4.12. The release and retention plots for nanoparticles loaded with **301a** or with **301b** at pH 7.4 and pH 5.0 are provided in the SI (Figures S4.4-S4.7). The amount of total drug/prodrug was measured both inside and outside the dialysis capsules. The amounts released and retained 12, 24, and 48 h are given in Table 4.7 (for **301a** and **301b** at pH = 7.4) and Table 4.8 [for **301**(**a-d,f**)] at pH = 5.0). These measurements indicated good overall mass-balance. In general, the release rates were faster at the lower pH.

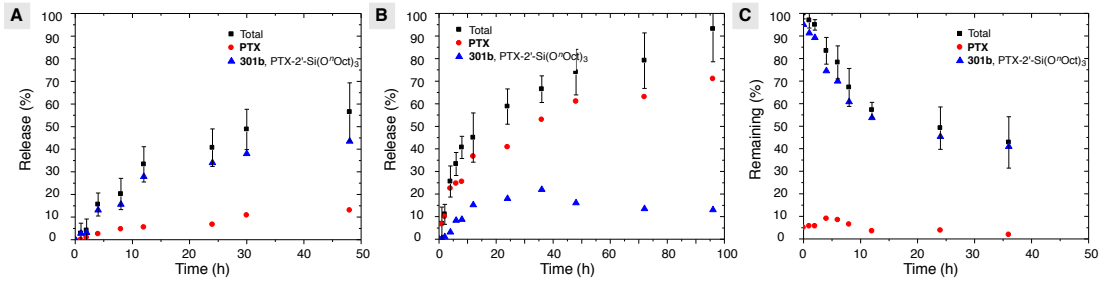

Figure 4.12 I Release profiles for nanoparticles loaded with PTX-2'-Si(O^{n}Oct)$_3$ (**301b**). **A.** Appearance of **301b** and free **PTX** to the exterior of the dialysis cassette at pH = 7.4. **B.** Appearance of **301b** and free **PTX** to the exterior of the dialysis cassette at pH = 5.0. **C.** Amount of **301b** and **PTX** remaining inside the dialysis cassette at pH = 7.4.

Table 4.7 I Release profiles over time of the percent of PTX plus PTX-silicate prodrug released into PBS at pH = 7.4.

Time (h)	301a [PTX-2'-Si(OEt)$_3$]		301b [PTX-2'-Si(O^{n}Oct)$_3$]	
	%Released[a]	%Retained[a]	%Released[a]	%Retained[a]
12	39±6	51±5	33±8	57±3
24	52±6	50±6	41±8	49±9
48	63±8	34±5	56±13	–

[a] Total amount of the PTX-silicate plus free PTX, as measured by HPLC analysis.

Table 4.8 I Release profiles over time of the percent of PTX plus PTX-silicate prodrug released into acetate buffered saline at pH = 5.0.

Time (h)	301a [PTX-2'-Si(OEt)$_3$]		301b [PTX-2'-Si(O^{n}Oct)$_3$]		301c [PTX-2'-Si(O^{i}Pr)$_3$]	
	% Released[a]	% Retained[a]	% Released[a]	% Retained[a]	% Released[a]	% Retained[a]
12	76±11	25±12	45±5	46±6	36±5	65±4
24	99±6	0.4±1.3	58±7	36±17	42±8	55±11
≥48	--	--	74±10	27±20	50±15	37±7

Time (h)	301f [PTX-2'-Si(O^{t}Bu)$_2$(OEt)]		301d [PTX-2'-Si(Omenthyl)$_3$]	
	% Released[a]	% Retained[a]	% Released[a]	% Retained[a]
12	32±4	69±10	35±7	65±8
24	40±5	60±13	49±9	50±14
≥48	53±11[b]	46±13[b]	89±17[c]	10±9[c]

[a] Total amount of the PTX-silicate plus free PTX, as measured by HPLC analysis. [b] 216 hr . [c] 168 hr.

4.3.6 *In vitro* cytotoxicity of PTX-silicate prodrug-loaded PEG-*b*-PLGA nanoparticles (uncentrifuged) against the aggressive 4T1 breast cancer cell line

To probe the efficacy of **302a** and nanoparticles loaded with 50 wt% of **302a**, a cyctotoxicity assay was performed on an aggressive breast cancer cell line (4T1). The 4T1 cells divide rapidly and were chosen as a challenge for our highly loaded nanoparticle formulation.

To perform these studies, the 4T1 cells were incubated at 37 ˚C, and non-viable cells were removed from the cell culture media by vacuum and washing with Dulbecco's modified eagle medium (DMEM). The viable cells remained adhered to the bottom of the culture flask. To free the cells, trypsin (5 mL) was added and the culture was incubated for 5 minutes at which time an equal amount of DMEM neutralized the enzyme. The cells were centrifuged, resuspended in new media (12 mL), counted, diluted to 10,000 cells per 100 µL and recounted, and finally plated. The cells retained in different wells of the plate were treated with one of the following drug formulations dissolved in DEM media: *i.*) **PTX,** *ii.*) **302a,** *iii.*) uncentrifuged nanoparticles consisting of **302a** (ca. 50 wt%) and a 5k-10k mPEG-*b*-PLGA (**405**), and *iv.*) empty unloaded nanoparticles 5k-10k mPEG-*b*-PLGA (**405**) only at concentrations ranging from 100 nM to 1 μM of **PTX** equivalent and incubated for 72 h at 37 ˚C.

The cells were treated with MTS to give a blue color that can be detected by UV-Vis absorption, and the concentration of viable cells compared to untreated cells can be determined. The percentage of viable cells is plotted against the concentration to show the efficacy of the treatments against 4T1 cells. As shown in **Figure 4.13**, the prodrug **302a** is as viable as the parent drug at concentrations of 500 nM or greater. Although the assay shows only 50% cell death, the drugs are considered a success, due to the aggressive nature of the 4T1 cell line. It is likely that the breast cancer cells have some resistance to the

PTX based treatments due to the relatively high concentrations required to inhibit cell growth.

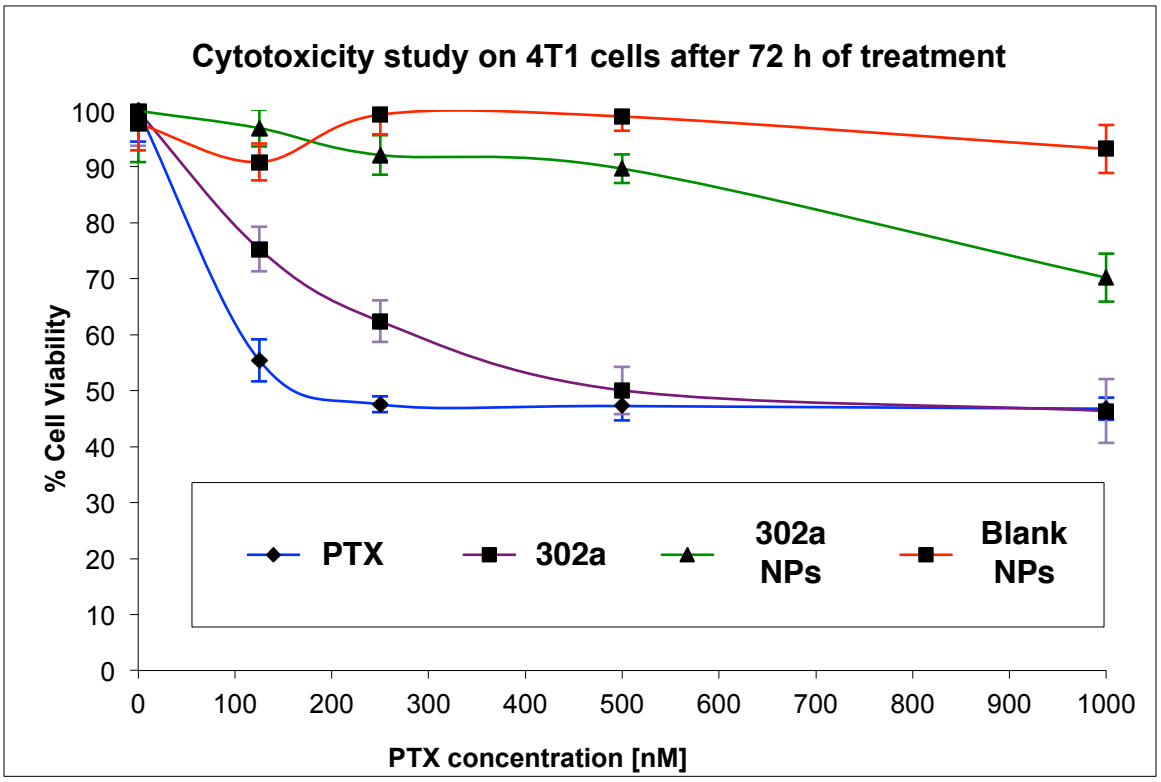

Figure 4.13 I Cytotoxicity Assay against 4T1 Aggressive Breast Cancer Cell Line.

4.3.7 *In vitro* cytotoxicity of PTX-silicate prodrug-loaded PEG-*b*-PLGA nanoparticles (centrifuged)

We have previously reported the cytotoxicity of prodrugs **301**-**303** alone toward the MDA-MB-231 human breast cancer cell line,[118] which has been shown to be less aggressive.[161] As we described there, "silicates having faster rates of hydrolysis [cf. Table 3.4] tend to show cytotoxicities similar to those of the parent taxane. This suggests that the silicate esters are hydrolyzed back to

[161] Larive, R. M.; Moriggi, G.; Menacho-Márquez, M.; Cañamero, M.; de Álava, E.; Alarcón, B.; Dosil, M.; Bustelo, X. R. Contribution of the R-Ras2 GTP-Binding Protein to Primary Breast Tumorigenesis and Late-Stage Metastatic Disease. *Nat. Commun.* **2014**, *5*, 3881.

PTX … either in the culture medium or inside the cell during the course of the assay." We have now examined the cytotoxicities of the prodrug-loaded nanoparticles.

Cytotoxicity of nanoparticle formulations loaded with six different prodrugs [**301**(**a**-**d**,**f**) and **302a**] was evaluated in the MDA-MB-231 cells and the IC_{50} data are shown in Table 4.6. The ethyl-containing silicate prodrugs of PTX **301a** and **302a** show a cytotoxicity profile similar to that of free **PTX**. The cytotoxicity of the PTX-2'-Si(O^nOct)$_3$ (**301b**) nanoparticles was considerably lower, consistent with the fact that only a small portion of **301b** had been observed to hydrolyze to free **PTX** in the PBS release experiments at pH = 7.4. The nanoparticle formulation containing **301c** is more potent than that loaded with **301a**, which, interestingly, mirrors the relative IC_{50} values of **301c** not in nanoparticles and **PTX**.[118] Finally, the formulations containing the hindered and, therefore, hydrolytically stable PTX-silicates **301f** and **301d** showed very low cytotoxicity, which is consistent with our early observations made with these silicates.[118] The *in vitro* cytotoxicities of the PTX-silicate loaded nanoparticle formulations are provided in Figure 4.14.

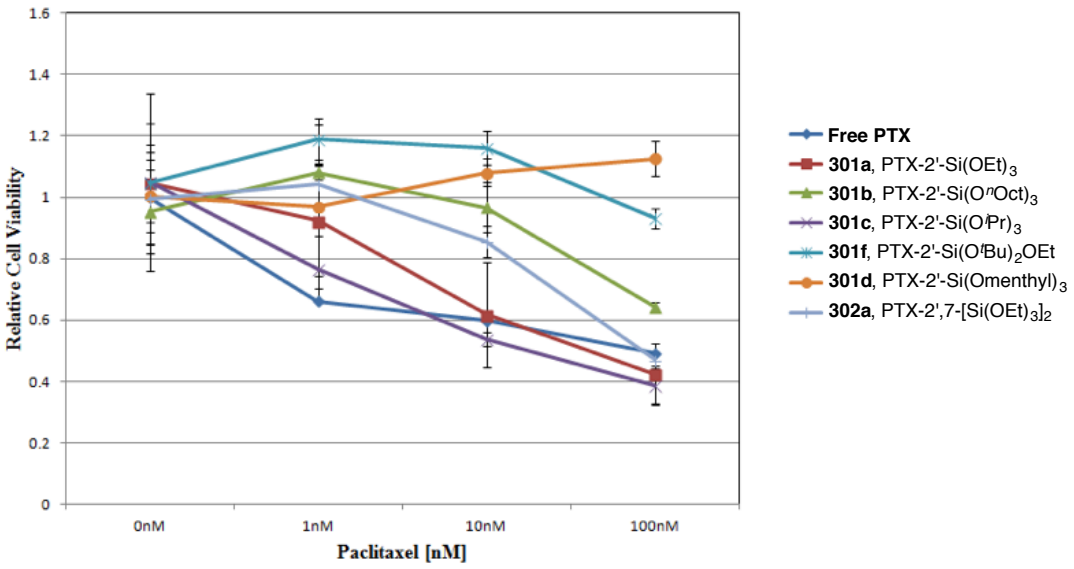

Figure 4.14 I *In vitro* cytotoxicity of nanoparticle formulations of **301**(**a**-**d**,**f**) and **302a**.

4.4 Nanoparticle Design Future Outlook

4.4.1 End Group Functionalization

Alternatively, the copolymerization can be achieved with a benzyl-protected PEG macro-initiator (BnO-PEG-OH), **415** to allow for further modification of the polymer. This is useful for the covalent attachment a targeting ligand to the hydrophilic portion of the polymer. The hydrophilic functionalization allows for the ligand to be exposed and presented to the cell for tumor targeting. The benzyl-protected PEG **415** can be synthesized by benzyloxyethanol **415** initiated anionic polymerization of ethylene oxide shown in Scheme 4.3.[162] Upon ROTEP, the BnO-PEG-b-PLGA is synthesized and subsequently acetylated. Finally, the benzyl group is deprotected through hydrogenolysis to yield the very useful precursor polymer **416**. The exposed alcohol of the PEG in **416** can be oxidized via Swern conditions to the aldehyde[163] **417a** or to carboxylic acid **418a** by Jones conditions.[164] The aldehyde **417a** can also undergo Lindgren oxidation to yield **418a**. The precursor **416** can also undergo a Mitsunobu reaction to create a maleimido derivative **419a**[165,166] or undergo reaction with sodium azide to produce a terminal azide **420a** suitable for click chemistry with an alkyne linked peptide to form 1,2,3-triazoles.[165] The elimination of the Tosyl-PEG can be accomplished with ammonium hydroxide to yield **421a**. Alternatively, the amine

[162] Reed, N. N.; Janda, K. D. A One-step Synthesis of Monoprotected Polyethylene glycol Ethers. *J. Org. Chem.* **2000**, *65*, 5843–5845.

[163] Wirth, P. Chemical Modification of Horseradish Peroxidase with Ethanal-methoxypolyethylene glycol: Solubility in Organic Solvents, Activity, and Properties. *Bioorg. Chem.* **1991**, *19*, 133–142.

[164] Kulkarni, M. Single Step Room Temperature Oxidation of Poly(ethylene glycol) to Poly(oxyethylene)-dicarboxylic acid. *J. Appl. Polym. Sci.* **1998**, *70*, 883-890.

[165] Gill, H. S.; Tinianow, J. N.; Ogasawara, A.; Flores, J. E.; Vanderbilt, A. N.; Raab, H.; Scheer, J. M.; Vandlen, R.; Williams, S.-P.; Marik, J. A Modular Platform for the Rapid Site-specific Radiolabeling of Proteins with 18F Exemplified by Quantitative Positron Emission Tomography of Human Epidermal Growth Factor Receptor 2. *J. Med. Chem.* **2009**, *52*, 5816–5825.

[166] Ji, S.; Zhu, Z.; Hoye, T. R.; Macosko, C. W. Maleimide Functionalized Poly(ε-caprolactone)-b-poly(ethylene glycol) (PCL-PEG-MAL): Synthesis, Nanoparticle Formation, and Thiol Conjugation. *Macromol. Chem. Phys.* **2009**, *210*, 823.

can be synthesized by reduction with hydrogen gas and palladium on carbon [Pd/(C)] or by a Staudinger reduction. To ensure the chemistries work with the precious block copolymer **416** the model commercial MeO-PEG-OH (**403**) can be used to obtain **417b**, **418b**, **419b**, **420b**, and **421b**.

Scheme 4.3. End functionalization of the free hydroxyl of the PEG terminus.

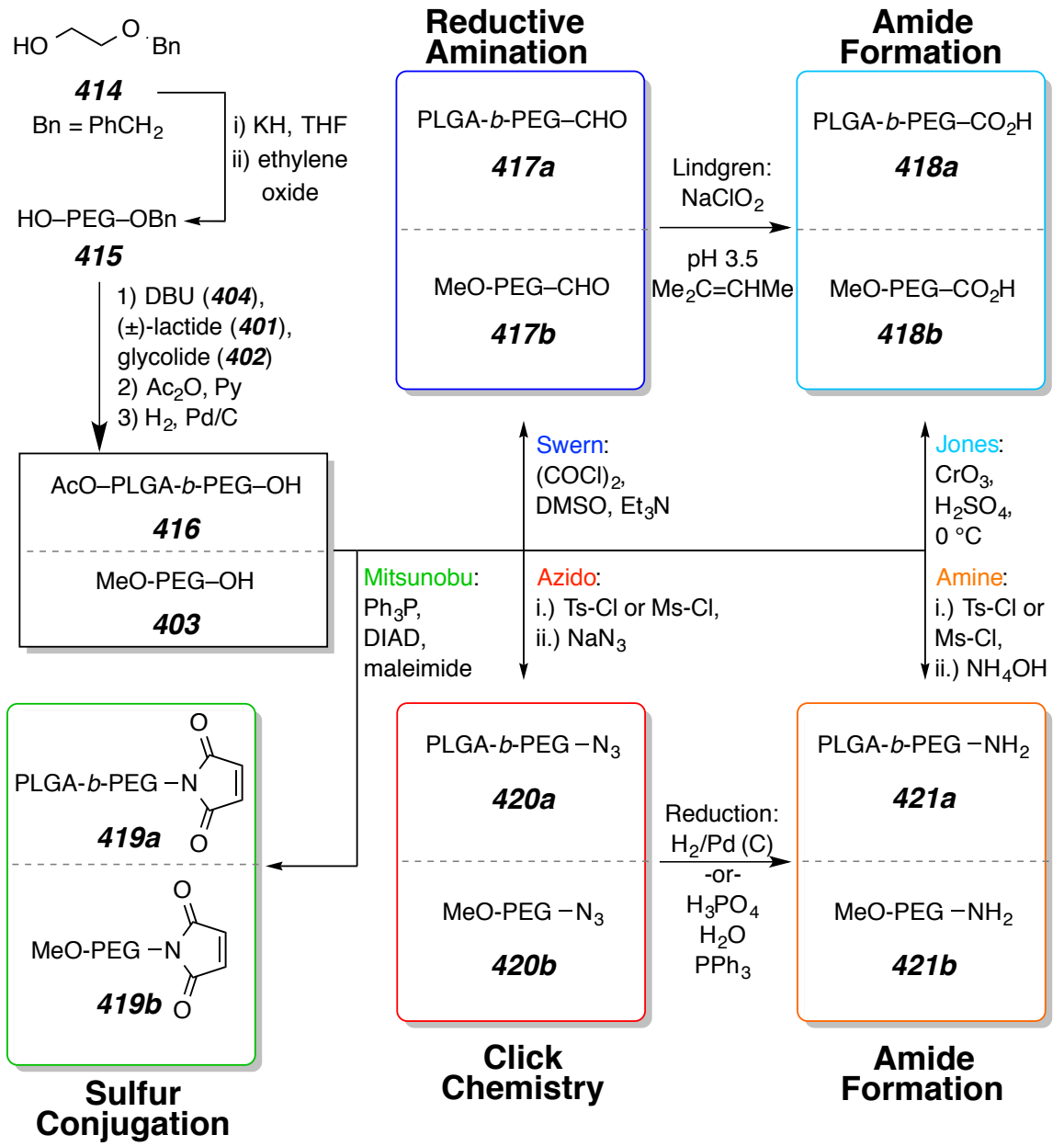

The functionalization at the PEG terminus of the block copolymer serves as an important tool to couple tumor targeting peptides to the surface of the nanoparticles. The two oxidized polymers **417a-b** and **418a-b** can form amide bonds with the terminal amines via reductive amination and amide bond formation respectively.[167] The maleimide **419a-b** can undergo addition with a sulfur containing ligand to achieve the macromolecular coupling.[168] The azido polymers **420a-b** can undergo click chemistry. Lastly, the amino polymers **421a-b** can form amide bonds with targeting molecules that contain carboxylic acids.

Previous research has showed the utility inclusion of tumor targeting peptides on the surface of the nanoparticle to direct the accumulation of nanoparticles to the tumor tissues and away from metabolic pathways.[169] Progress towards the functionalization of PEG is presented here as well as efforts to modify the end groups of block-copolymers.[170]

Model studies with MeO-PEG-OH (**403**) were designed to mimic the chemical reactivity of the HO-PEG terminus in HO-PEG-PLGA-OAc. The methoxy protected 5 kDa polymer (mPEG) **403**, as summarized in Scheme 4.3 was used for the optimization and exploration to install an amine at the terminus. First, tosylation of the terminal alcohol in **403** gave MeO-PEG-OTs (**422b**, not shown). Displacement by sodium azide (NaN_3) gave the azido polymer **420b,** which can undergo click chemistry (Scheme 4.5 and 4.6). Alternatively, the azide **420b** was reduced to the amine through hydrogenation to give the primary amine **421b,** which can be directly coupled to peptides.

---

[167] Chae, S. Y.; Kim, T. H.; Park, K.; Jin, C.-H.; Son, S.; Lee, S.; Youn, Y. S.; Kim, K.; Jo, D.-G.; Kwon, I. C.; Chen, X.; Lee, K. C. Improved Antitumor Activity and Tumor Targeting of NH(2)-terminal-specific PEGylated Tumor Necrosis Factor-Related Apoptosis-inducing Ligand. *Mol. Cancer Ther.* **2010**, *9*, 1719–1729.

[168] Song, S.; Liu, D.; Peng, J.; Sun, Y.; Li, Z.; Gu, J. Peptide Ligand-mediated Liposome Distribution and Targeting to EGFR Expressing Tumor in vivo. *Int. J. Pharm.* **2008**, *363*, 155-161.

[169] Wang, M.; Thanou, M. Targeting Nanoparticles to Cancer. *Pharmacol. Res.* **2010**, *62*, 90–99.

[170] Tong, R.; Tang, L.; Ma, L.; Tu, C.; Baumgartner, R.; Cheng, *J. Chem. Soc. Rev.* **2014**, *43*, 6982–7012.

The azido-PEG is particularly useful due to the orthogonal reactivity with an alkyne to give a triazole via click chemistry. This chemistry is useful when linking functionalizing macromolecules covalently.[171] To achieve this, we first synthesized a small linker molecule to bind to a peptide or tumor targeting agent e.g. biotin, and also to introduce the alkyne functionality. The synthesis of the amino alkyne linker is presented in Scheme 4.4. The 2-[2-(2-chloroethoxy)ethoxy]ethanol **423** was used as the starting material to create the small linker that underwent azide substitution to give compound **424**. This azido alcohol was reacted with propargyl bromide **425** to yield the azide alkyne **426**. A Staudinger reaction successfully reduced the azide to amine **428** in the presence of the alkyne, however the purification by flash chromatography after each step was problematic. Therefore, an alternative route was explored. In this route, the propargylation of **423** to give compound **427** occurred under the previously described reaction conditions.[172,173] Treatment with ammonia in methanol also gave the linker **428** in a shorter synthetic reaction sequence.

[171] Zhang, S.; Chan, K. H.; Prud'homme, R. K.; Link, A. J. Synthesis and Evaluation of Clickable Block Copolymers for Targeted Nanoparticle Drug Delivery. *Mol. Pharm.* **2012**, *9*, 2228–2236.

[172] Polito, L.; Monti, D.; Caneva, E.; Delnevo, E.; Russo, G.; Prosperi, D. One-step Bioengineering of Magnetic Nanoparticles via a Surface Diazo Transfer/Azide-Alkyne Click Reaction Sequence. *Chem. Comm.* **2008**, *5,* 621–623.

[173] Natarajan, A.; Du, W.; Xiong, C.; DeNardo, G. Construction of Di-scFv through a Trivalent Alkyne–azide 1, 3-dipolar Cycloaddition. *Chem. Comm.* **2007**, *7*, 695-697.

Scheme 4.4 I Synthesis of a small linker for macromolecule conjugation.[173]

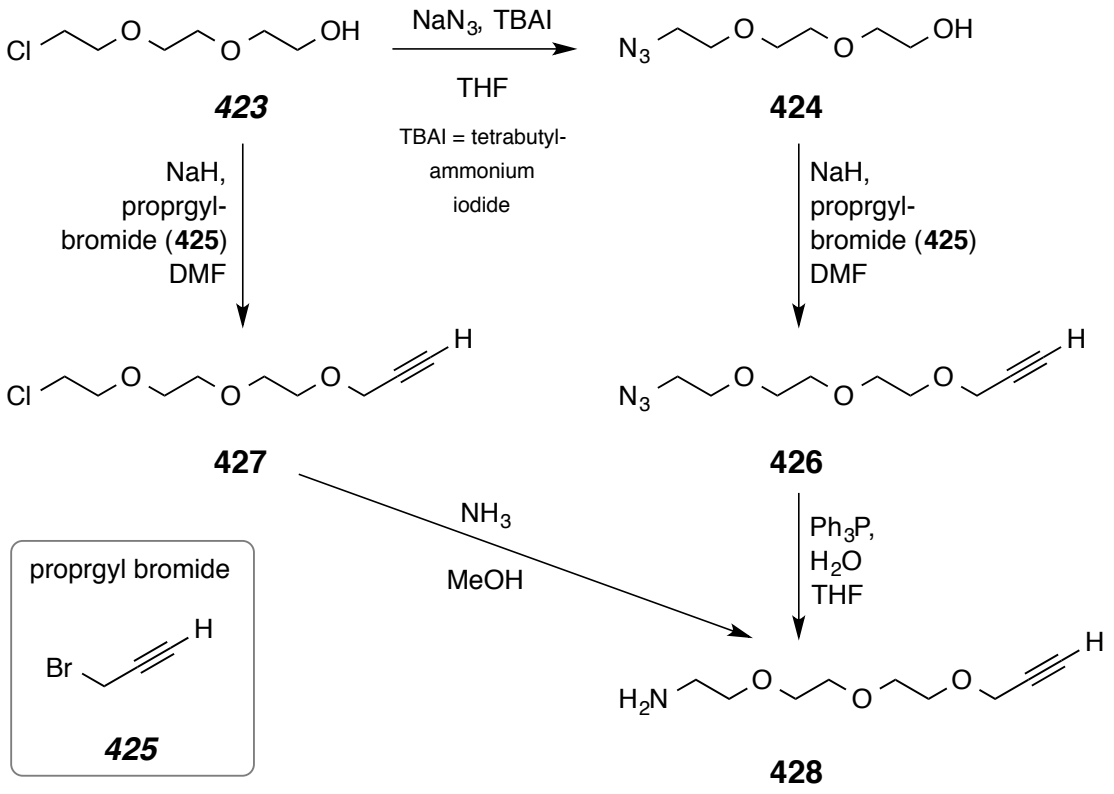

4.2.2 Polymer Conjugation

The amino alkyne linker **428** serves as a dual coupling reagent. It can first couple to a peptide (or another biological molecule such as biotin **429** or folic acid) to form a peptide bond, as shown in Scheme 4.6.[167] Following this coupling, click chemistry of **430** can conjugate the targeting agent to polymer **420a** or **420b** to give the biologically active polymer **431a** and **431b**.[165] The polymer **430a**, when R is PLGA, can then be impingement mixed with mPEG-*b*-PLGA and the silicate prodrug to produce nanoparticles suitable for targeting tumor tissues. Biotin is proposed here since antibody conjugates of biotin have been shown to target tumor tissues.

We first probed the click reaction conditions with a model system to determine if the azido-polymer (**420b**) would be tractable throughout, shown in

Scheme 4.5. The initial set of conditions used a strong base (DBU) to serve as a ligand for the copper and a simple alkyne (ethynyltrimethylsilane) to form the triazole. We were pleased that the reaction occurred (SI, Figure S14) and the resulting polymer was recovered after precipitation. Our attention turned to the click chemistry of the biotin-linker **430** and the PEG-N_3 (**420b**) as well as the block polymer **420a**[120].

Scheme 4.5 I Click coupling chemistry with a model system

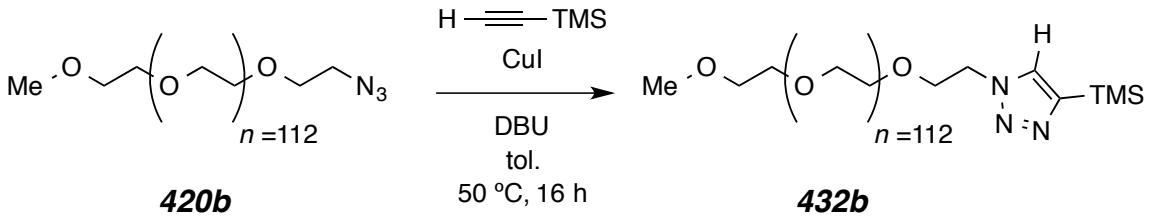

420b ***432b***

Scheme 4.6 I Coupling chemistry with tumor targeting agent biotin.

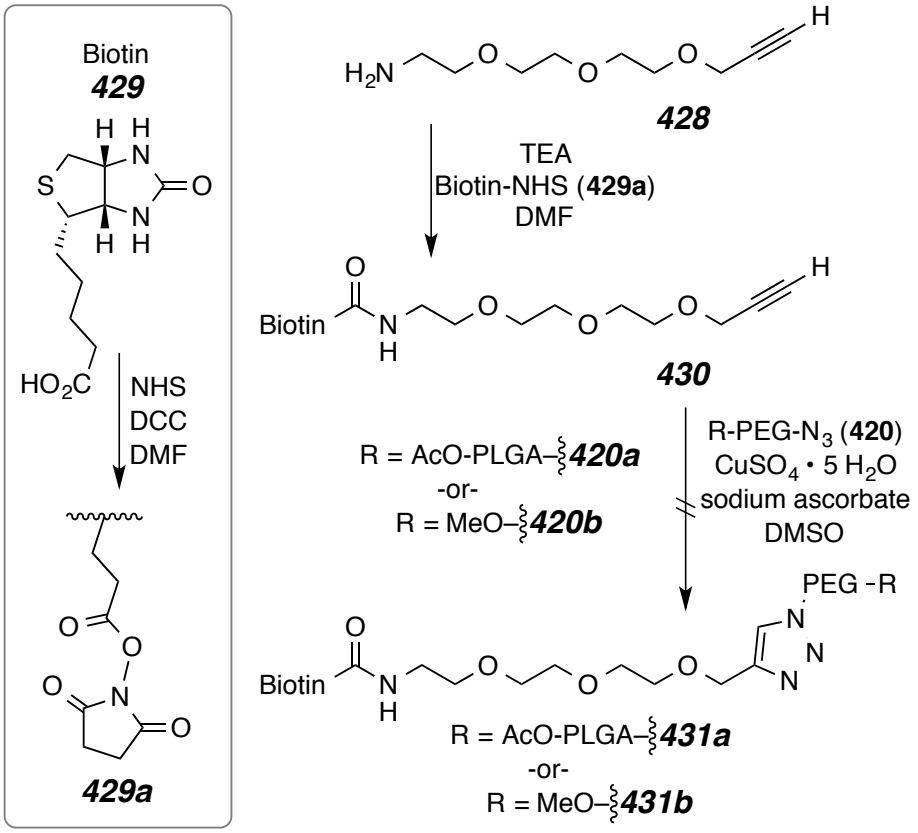

Unfortunately, the click chemistry has proved to be problematic; unfortunately the use of an exotic ligand was required for the simple click chemistry with a different substrate (not shown). Although obtainable, we chose to explore nanoparticle formulations without the use of a targeting agent. There is still a lot of work to be done with the optimization presented in Scheme 4.3. The coupling of different targeting agents (antibodies or polypeptides) to functionalized polymers **417**, **418**, **419**, **420**, and **421** provides many opportunities to develop and synthesize unique functionalized polymers, designed for the targeting of tumor tissues to improve drug distribution *in vivo* while utilizing a variety of chemical transformations. More specifically the conjugation of **417a**, **418a**, **419a**, and **421**, to unique peptides/antibodies through amide or sulfur bonds are of great interest for future studies. These targeting ligands have been shown to target and destroy tumor cells through apoptotic pathways, but will not be discussed further in this thesis.

4.4.2 Polymer Backbone Functionalization

We were also interested in the functionalization of the hydrophobic backbone of our block copolymer mPEG-*b*-PLGA (**405**). A series of monomers were synthesized for this purpose some of which are shown in Scheme 4.7 below.[174,175,176] The (S)-4-((benzyloxy)methyl)-1,3-dioxolan-2-one (**437**) or the benzyl protected lactide (**438**) can undergo polymerization with the macroinitiator mPEG-OH (**403**), as described before, to yield a functionalized block copolymer. After the hydrogenation of the benzyl protecting group a free hydroxyl is revealed. We envisioned that this hydroxyl could be captured with either a fluorescent tag or even a silicate prodrug. Both of these goals to capture the free hydroxyls about the polymer backbone are quite lofty, so we pursued making the polymers first and foremost.

The benzyl (Bn) and *tert*-Butyl carbamate (Boc) protected serine (**434**) is commercially available, so we entered the synthesis with this reagent. The Boc group was easily removed by TFA in methylene chloride to give the free amide (**435**). Sodium nitrite and sulfuric acid converted the amide to the valuable common intermediate (**436**). Following the work of Pasquato,[174] the reaction with triphosgene over activated charcoal afforded the (S)-4-((benzyloxy)methyl)-1,3-dioxolan-2-one (**437**) in reasonable yield. Alternatively, a dimerization reaction with *p*-toluenesulfonic acid to evolve water can be performed, though dilute conditions and a long reaction time is required.[175] With the monomers in hand we

[174] Tang, L.; Deng, L. Dynamic Kinetic Resolution via Dual-Function Catalysis of Modified Cinchona Alkaloids: Asymmetric Synthesis of Alpha-Hydroxy Carboxylic Acids. *J. Am. Chem. Soc.* **2002**, *124*, 2870–2871.

[175] Leemhuis, M.; van Nostrum, C. F.; Kruijtzer, J. A. W.; Zhong, Z. Y.; Breteler, ten, M. R.; Dijkstra, P. J.; Feijen, J.; Hennink, W. E. Functionalized Poly(A-Hydroxy Acid)S via Ring-Opening Polymerization: Toward Hydrophilic Polyesters with Pendant Hydroxyl Groups. *Macromolecules* **2006**, *39*, 3500–3508.

[176] Pounder, R. J.; Dove, A. P. Synthesis and Organocatalytic Ring-Opening Polymerization of Cyclic Esters Derived From L-Malic Acid. *Biomacromolecules* **2010**, *11*, 1930–1939.

next explored the co polymerization with *rac*-lactide (**401**) and the subsequent deprotection.

Scheme 4.7 I Synthesis of benzyl-protected monomers

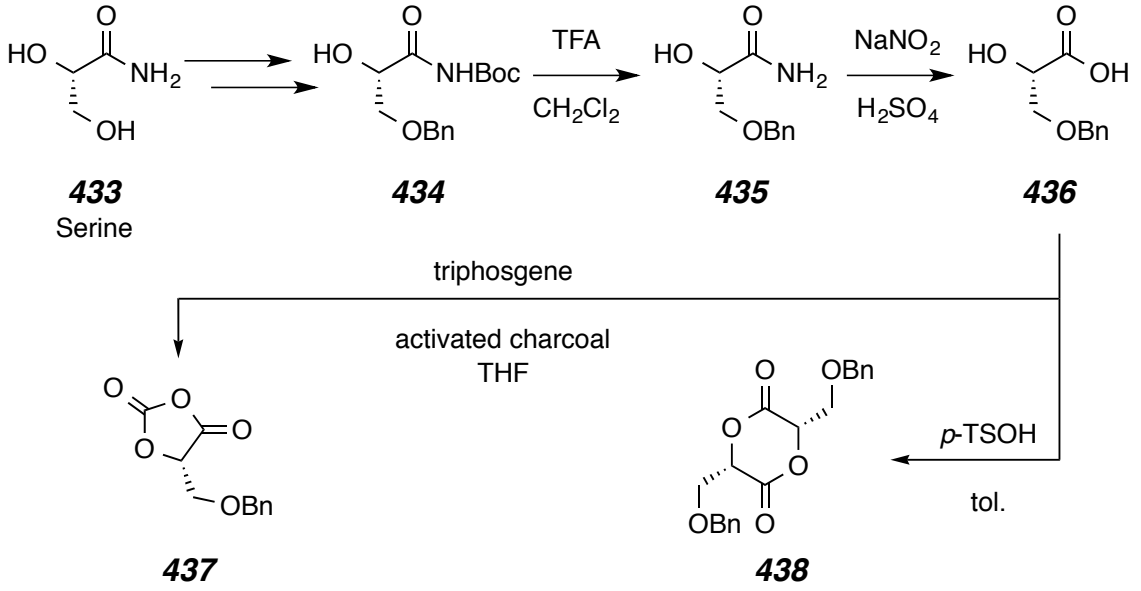

An initial set of three ^{1}H-NMR experiments with the benzyl protected lactide (**438**), *rac*-lactide (**401**), mPEG-OH (**403**) initiator, and DBU (**404**) were performed to observe the different rate of polymerization between the two monomers. Molar ratios of each experiment were: (**438**:**401**:**401**:**404**) *i.*) 1.2:0.9:1:0.24, *ii.*) 1.7:0:1:0.31, and *iii.*) 0.7:3.6:1:0.27. Although, kinetic rates were not determined the benzyl protected lactide (**438**) was observed to undergo polymeriztion much faster than the *rac*-lactide (**401**). We were excited to make polymers with this monomer and determine the feasibility of the deprotection.

The polymerization of the benzyl protected lactide (**438**) was iniated with mPEG-OH (**403**), and DBU (**404**) as the catalyst. The reaction was monitored by removing alloquots ca. every 15 mins over the course of an hour. The polymerization was quenched with benzoic acid and percipitaed into ice cold ether to yield the desired benzyl protected block copolymer **438** shown in Scheme 4.8. The polymer was then dried in a vaccuum oven overnight.

Scheme 4.8 I Synthesis of benzyl-protected block copolymer **438**.

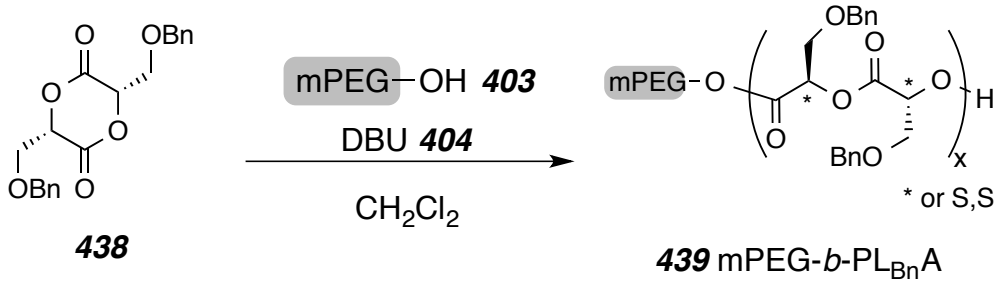

438 **439** mPEG-*b*-$PL_{Bn}A$

A set of random block copolymers from the benzyl protected lactide (**438**) and *rac*-lactide (**401**) were synthesized as shown in Scheme 4.9 below. A short summary of the different molecular weights achieved is also shown in Table 4.9. Unfortunately, the extent of random incorporation was not determined as more detailed ^{13}C-NMR studies and kinetics data are required.

Scheme 4.9 I Synthesis of random poly(ethylene glycol)-b-poly(benzyl-lactide-co-lactide) block copolymers **438**.

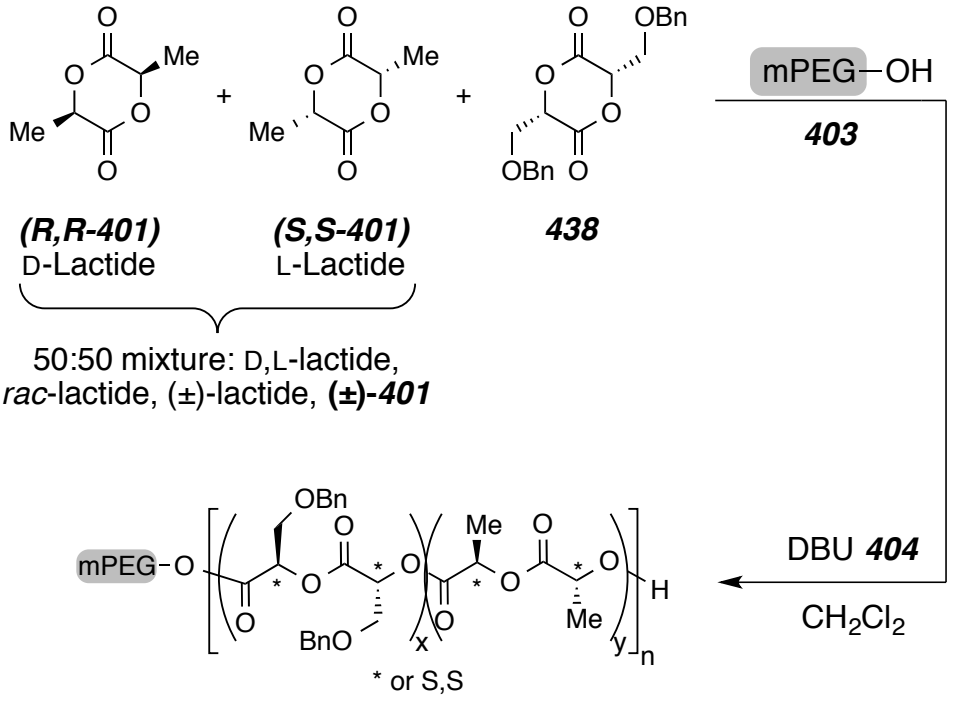

440 mPEG-*b*-$PL_{Bn/Me}A$

Table 4.9 l A comparison of polymers made by DBU-catalyzed ROTEP

Polymer (targeted)	$M_{n(PEG)}$	$M_{n[PL(Bn/Me)A]}$ [a]	Ratio [a,b] $LA_{Bn} : LA_{Me}$	PDI [c]
PEG $_5$-PL(Bn)A	5K	11.2K	100 : 0	–
PEG $_5$-PL(Bn_6/Me_{10})A	5K	16.3K	37 : 63	–
PEG $_5$-PL(Bn_9/Me_8)A	5K	16.6K	53 : 47	1.08
PEG $_5$-PL(Bn_9/Me_9)A	5K	18K	50 : 50	–

[a] Results based on NMR spectroscopy
[b] Mass ratio of the repeat units
[c] Results based on GPC ($CHCl_3$, 1 mL/min) measurements against a polystyrene standard

We conducted a trial reaction for the deprotection of the benzyl group under hydrogen with palladium on carbon. The hydrogenolysis was monitored by the evolution of toluene by ^{1}H-NMR. After two days of reaction the polymer was ca. 14% deprotected. While this result provided a proof of concept, the reaction was not explored further. We instead focuced on new developements of the project toward novel silicate deravatives presented in Chapter 7 of this thesis.

Chapter 5. *In Vivo* Evaulation of Nanoparticles

5.1 *In Vivo* efficiency of Nanoparticle Formulations

5.1.1 Efficacy of PTX-silicate prodrug-loaded PEG-*b*-PLGA nanoparticles (uncentrifuged) against the aggressive 4T1 breast cancer tumors via tail vein injection

With the efficacy of the prodrug established against the 4T1 cells *in vitro*, animal testing was performed to determine the degree of tumor reduction over time, and also the distribution of the drug throughout the mouse. Not only will these studies show the efficiency of the chemotherapy formulations, they will also give insight into the form of the drug over time. By understanding distribution of the nanoparticles in the mice models, the nanoparticle prodrug formulation can be improved upon.

C57/B16 wild type mice were purchased from Charles River Labs and seeded with approximately 1 million 4T1 cells in the fat pad of the mice. The tumor grows quickly and the cells metastasize to the lungs, liver, bone, and brain in 3-6 weeks. The resulting tumors were allowed to grow to a volume of approximately 150 mm^3. Once the tumors grew to the suitable size (1 week) the mice were randomized and treated with one of the following formulations at a single dosage of 40 mg equivalent **PTX** per kg of mouse: *i.*) Taxol® *ii.*) PTX-2',7-$[Si(OEt)_3]_2$ (**302a)** in Cremophor EL® *iii.*) (**302a**) nanoparticles *iv.*) untreated *v.*) saline only vi) Cremophor EL®. Since there were only 30 mice available, the number of mice to receive each treatment was *i.*) n=4 *ii.*) n=8 *iii.*) n=8 *iv.*) n=2 *v.*) n=4 *vi.*) n=4. Since the saline treated mice also served as a control a small number of mice were used for the untreated control group. The tumor size was monitored over the course of 2 weeks via caliper measurements every day. These sizes were compared to the initial tumor volume and plotted against time and presented in Figure 5.1.

Although the control mice did not survive the 2-week period due to cancer tumor growth, the drug formulations could still be compared. Once tumors grow to a size greater than ca. 10 times their original size, the mice must be euthanized. The experimental formulations are as effective as Taxol® *in vivo* during the time course (14 days) of the study. Much like the cytoxicity assay, the tumor cells are so aggressive that they do not fully regress over the course of the experiment, but continue to grow even after treatment. The rate of tumor growth is clearly inhibited by paclitaxel in mice treated with some formulation containing paclitaxel. The study also showed that the nanoparticle formulation is essentially the same as Taxol®, which is very significant. And as expected, the nanoparticle formulation reduced hypersensitivity in the tail vein of the mice.

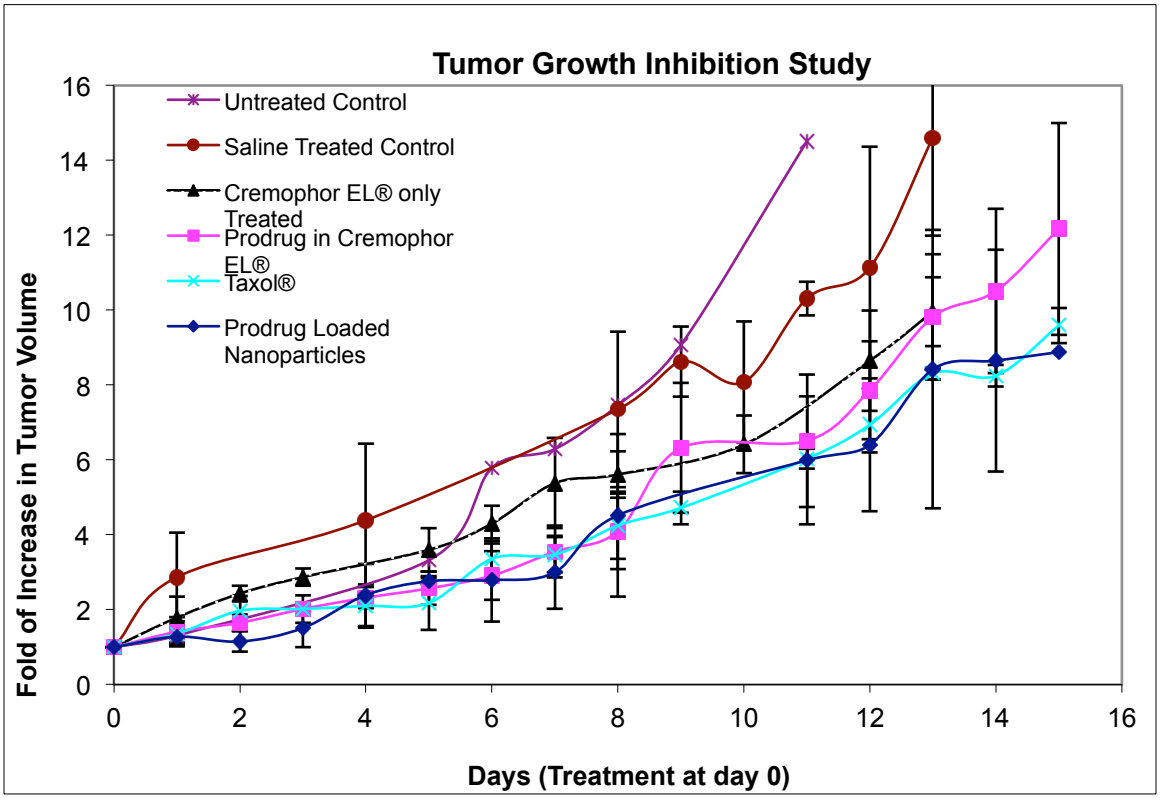

Figure 5.1 I Tumor inhibition study against C57/B16 Wild Type Mice bearing 4T1 Tumors

5.1.2 Efficacy of PTX-silicate prodrug-loaded PEG-*b*-PLGA nanoparticles (uncentrifuged) against the MDA-MB-231 breast cancer tumors via tail vein injection[120]

The samples of NPs prepared from the PTX-2',7-$[Si(OEt)_3]_2$ **(302a)** that we used for *in vivo* studies performed by Stephen Kalscheuer were ***uncentrifuged*** particles prior to being administered. As described in Chapter 4, we now know this to be a suboptimal choice. Despite the significant burst release characteristics of these particles,[139] we observed therapeutic efficacy that was comparable to commercial formulations. We anticipated that formulations prepared using centrifugation (unencapsulated free drug/prodrug removed), which show more sustained drug regeneration behavior will enable significant improvement in efficacy.

The *in vivo* efficacy of **302a** uncentrifuged-nanoparticles (NPs) was evaluated in mice xenografted with orthotopic MDA-MB-231 tumors. This cell line was stably transfected with luciferase to enable quantitative bioluminescence imaging of tumor growth. Three active **PTX**-based drug formulations were administered (≥5 animals for each group): **302a** nanoparticles, Taxol®, and Abraxane® at equimolar quantities of **PTX** (50 μmol kg^{-1}). Non-drug loaded CrEL® and blank PEG-*b*-PLGA NP control groups were also included. The **PTX** treatment showed significant inhibition of tumor growth relative to the controls and that all three formulations (**302a** nanoparticles, Taxol®, and Abraxane®) were statistically comparable in their protective capacity (Figure 5.2). Upon completion of the study, the toxicological profile was determined for each of the three treatment groups. Qualitatively, tail tissue near the injection site in the mice treated with CrEL® alone or Taxol® were necrotic, suggesting significant inflammation from the CrEL® excipient[56] while those treated with the NPs showed no visible necrosis. Notably, in four of five Abraxane®-treated mice, aspartate transaminase (AST) levels were significantly above the “expected” levels for Balb/c nude mice (not shown).[120] Additionally, in three of five mice in the

Abraxane® group, measured alanine transaminase (ALT) levels were significantly higher than expected. Taken together, these results suggest potential liver damage. Lymphocytopenia (low white blood cell level) was noted in all three mice examined in the Taxol® group, in two out of three mice in the Abraxane® group, and in one of three in the **302a**-treated mice. Less pronounced blood and liver toxicity would be consistent with the hypothesis that **302a** provides lower levels of toxic agent over a longer duration by virtue of slow release of **PTX** from NPs.

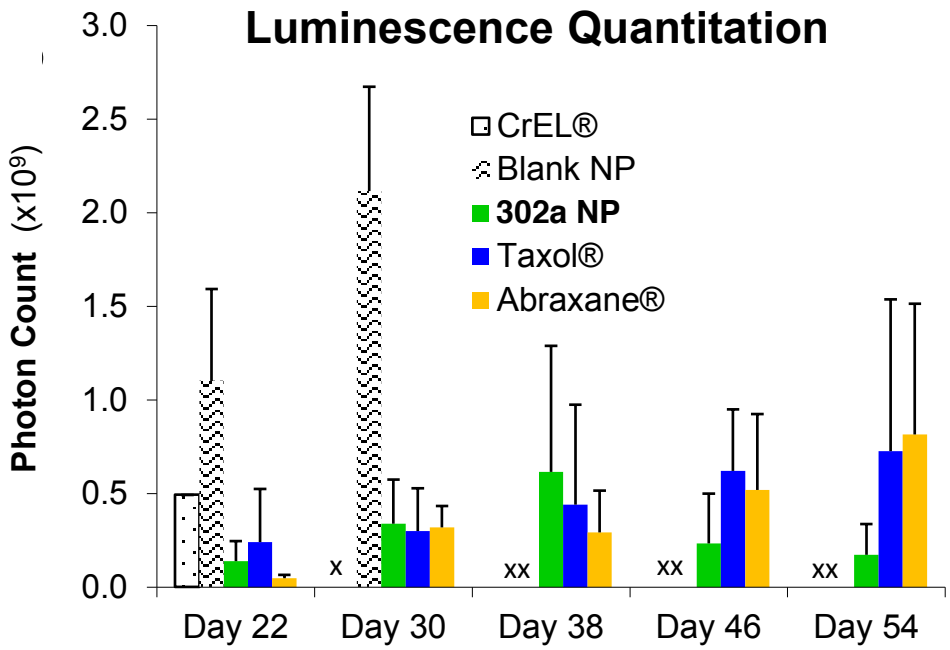

Figure 5.2 I Relative antitumor efficacy of **302a-NP**s, Taxol®, and Abraxane® as determined by photon flux from the primary tumor site via bioluminescence imaging. Luciferin was administered at 150 mg•kg^{-1} by i.p. injection on an every 8 day schedule. Photon intensity from the primary tumor site was determined for ≥4 mice at each time point. CrEL® and blank NP groups are shown up to the time point preceding euthanasia or death, "x", of a majority of the group

5.1.3 Efficacy of PTX-silicate prodrug-loaded PEG-*b*-PLGA nanoparticles (centrifuged) against the MDA-MB-231 breast cancer tumors via intratumoral injection

Labile prodrugs that showed significant stability as well as cytotoxicity, either alone[118] or in the nanoparticle formulation (i.e., **301b**, **301c**, **303a, 303b, 302a**) were chosen for an intratumoral injection study in a xenograft mouse model. The ratio of the prodrug to polymer in the initial FNP feeds, the total mass of loaded nanoparticles recovered following ultracentrifugation (3x) and lyophilization, the DLS-measured size and size distribution, and the load levels of PTX-silicate (expressed as equivalent wt% of **PTX**) are presented in the SI (Table S5.1). This study showed (Figure 5.3) that all nanoparticles slowed tumor growth rates relative to a control using blank nanoparticles. Particles containing PTX-silicates having faster hydrolysis rates [e.g., PTX-2'-Si(O^nOct)$_3$ (**301b**) and PTX-7-Si(OEt)$_3$ (**303a**), see Table 3.2] were the most effective in inhibiting tumor growth. These studies also show that even a single dose of these silicate prodrug nanoparticles is capable of inhibiting tumor growth over a prolonged period, pointing to their ability to sustain PTX levels in the tumor tissue.

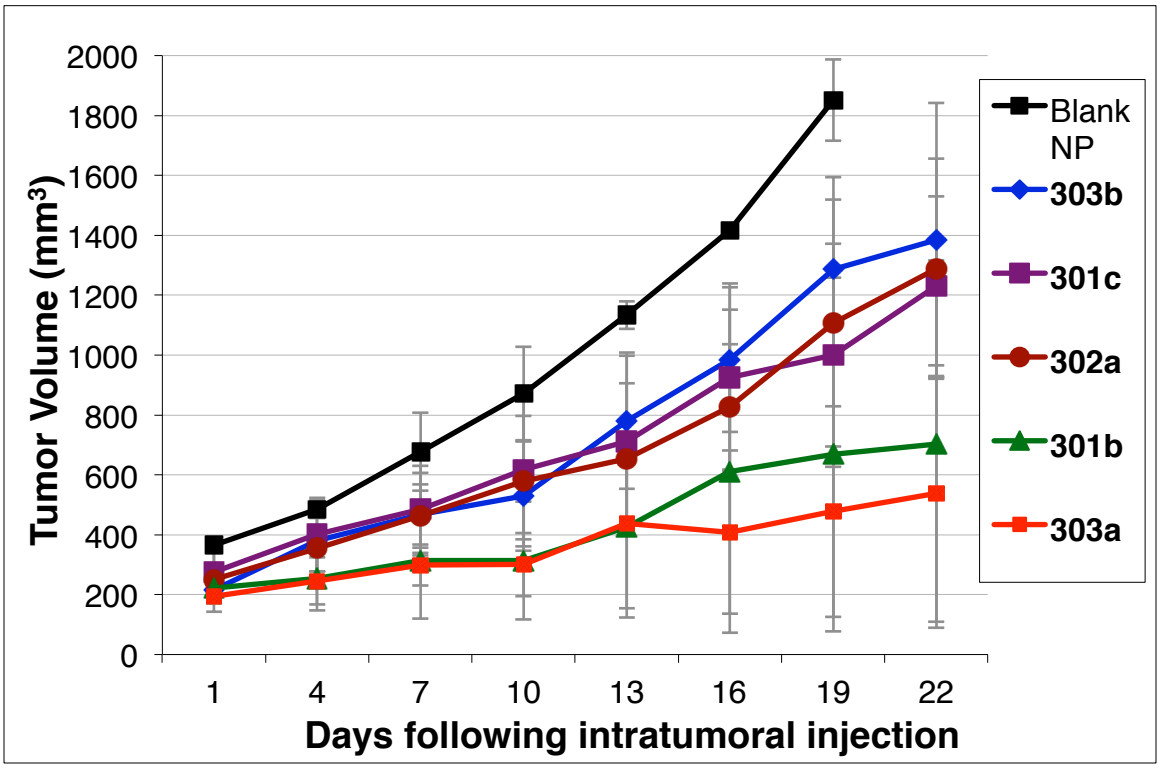

Figure 5.3 I Intratumoral injection of nanoparticles loaded with PTX-2'-Si(O^nOct)$_3$ (**301b**), PTX-2'-Si(O^iPr)$_3$ (**301c**), PTX-7-Si(OEt)$_3$ (**303a**), PTX-7-Si(O^nOct)$_3$ (**303b**), and PTX-2',7-[Si(OEt)$_3$]$_2$ (**302a**) at equivalent dose (i.e., the same amount of **PTX** if all prodrug has reverted back to **PTX** and is no longer in the nanoparticles) in comparison to a control with empty nanoparticles.

5.1.4 *In Vivo* efficacy conclusions

The combination of FNP and silicate prodrug strategy enabled the fabrication of nanoparticles in a size range desirable for tumor drug delivery, with high **PTX** loading levels, and sustained drug-release properties. Particle size, drug loading, and drug release rates were a function of the hydrophobicity of the prodrug. The *in vitro* and *in vivo* anticancer activities correlated with the hydrolysis rates of the prodrug. Future studies will examine the *in vivo* efficacy of these formulations following intravenous administration. Overall, the FNP/silicate prodrug strategy is a promising approach for delivering **PTX** while avoiding the side effects associated with the use of large quantities of nanoparticle excipients.

5.2 Maximum Tolerated Dose (MTD) Studies

5.2.1 *In Vivo* MTD Study via Tail Vein injection

A cohort of C57BL/6 mice were purchased from The Jackson Laboratory for the maximum tolerated dose (MTD) study. The 19 mice (n) were randomly divided into one of five different groups: *i.*) untreated control (n=3), *ii.*) low dose **301b** in CrEL® (n=4), *iii.*) low dose **301b** in centrifuged nanoparticle formulation (n=4), *iv.*) high dose **301b** in CrEL® (n=4), and *v.*) high dose **301b** in centrifuged nanoparticle formulation (n=4). Each group of treated mice received either a low dose of 40 mg/kg or a high dose of 80 mg/kg **PTX** equivalent at the outset via tail vein injection followed by a second dose of the same concentration one week later. All animals were sacrificed on the 3rd week following treatment and the essential tissues and blood were harvested for further analysis. Liver, kidneys, lungs, and spleen were removed and placed into a -80 ºC freezer until analysis. Liver samples were extracted and results are presented in Chapter 5.3. A cardiac puncture of the heart of each sacrificed mouse allowed for the removal of the whole plasma.

The whole mouse blood plasma was sent to IDEXX Bioresearch for analysis. The hematology and liver function biomarkers were determined to see if any adverse side effects from the formulations were present in the mice. The values were compared to the untreated control mice as well as the normal range for the mouse model used. The white blood cell count (WBC) shows that mice given any of the prodrug formulations of **301b** fell within the normal range and was equivalent with the untreated control (Figure 5.4). Generally, this parameter shows that the formulations do not cause neutropenia in the animal models.

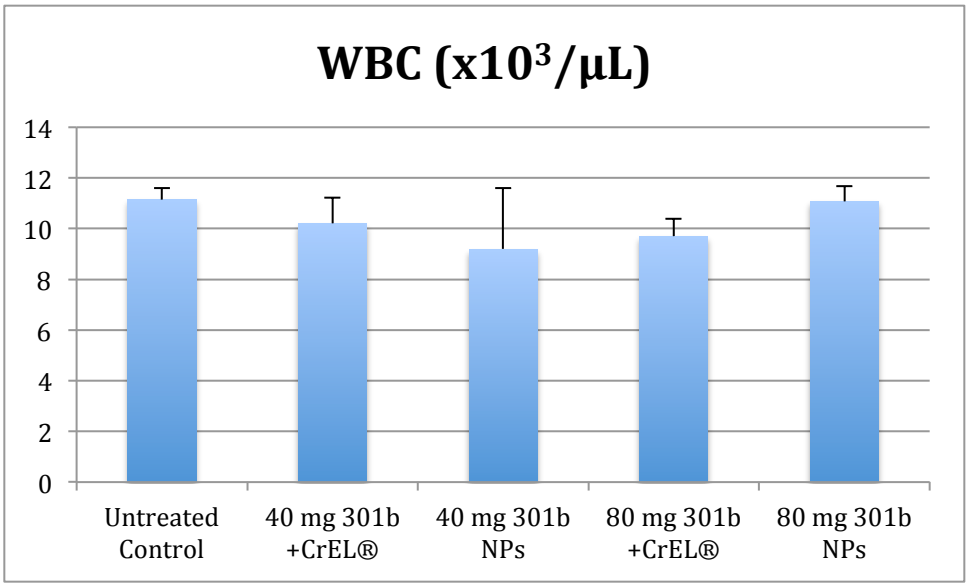

Figure 5.4 I Absolute number of white blood cells (WBC) counted in the whole mouse plasma of mice treated with formulations of PTX-7-Si(O^nOct)$_3$ (**303b**). [normal range 5.0-13.7 x $10^3/\mu$L]

The other hematology results: segmented neutrophils percentage (Figure S5.1), the absolute number of segmented neutrophils (Figure S5.2), lymphocytes percentage (Figure S5.3), the absolute number of lymphocytes (Figure S5.4), monocytes percentage (Figure S5.5), the absolute number of monocytes (Figure S5.6), eosinophils percentage (Figure S5.7), the absolute number of eosinophils (Figure S5.8), basophils percentage (Figure S5.9), the absolute number of basophils (Figure S5.10), red blood cell (RBC) count (Figure S5.11), the amount of hemoglobin (Figure S5.12), the percentage of red blood cells present (HCT) (Figure S5.13), the mean cell volume (MVC) of red blood cells (Figure S5.14), the mean cell hemoglobin (MCH) (Figure S5.15), the mean corpuscular oglobin concentration (MCHC) (Figure S5.16), number of platelets (S5.17), and the number of reticulocytes (Figure S5.18) are presented in the supporting information appendix of Chapter 5 at the end of this thesis.

The whole mouse plasma was also tested from various proteins present in the blood that are biomarkers for liver, kidney, and pancreatic damage. The two most indicative markers (alanine aminotransferase (ALT) and aspartate aminotransferase (AST)) are shown in Figures 5.5 and 5.6 below. High levels of ALT and AST when compared to the untreated control animals indicate liver damage. Interestingly, none of the treated animals showed a statistical significant increase in either ALT or AST levels, which suggests that liver function is normal in treated animals.

The other biomarkers to determine liver, kidney, and pancreatic function are shown in the supporting information of Chapter 5 of the appendix as: the concentration of albumin (ALB) (Figure S5.19), the concentration of globulins (GLOB) (Figure S5.20), the ratio of albumin to globulins (ALB/GLOB) (Figure S5.21), the amount of alkaline phosphatase (ALKP) (Figure S5.22), the amount of gamma glutamyl transpeptidase (GGT) (Figure S5.23), and the total protein (TP) (Figure S5.24).

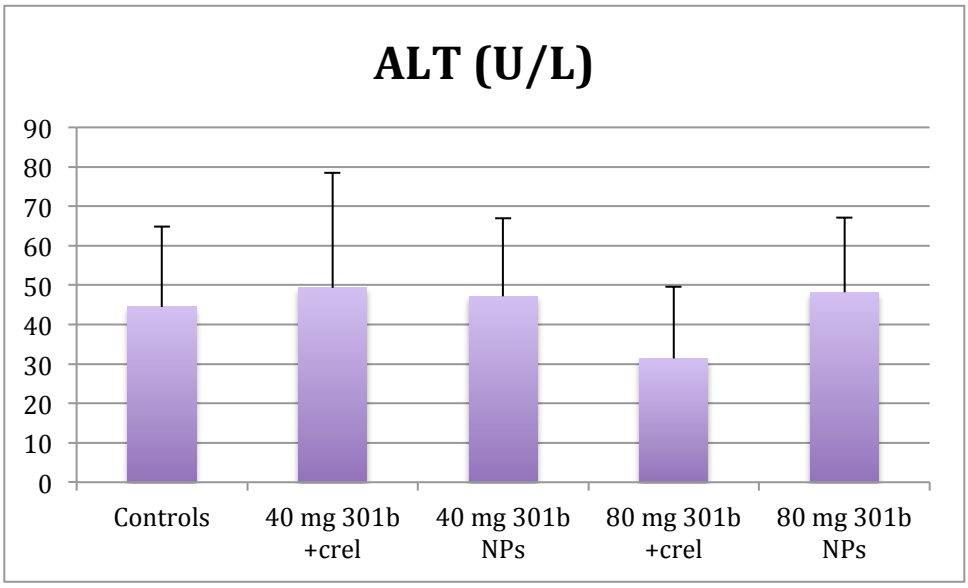

Figure 5.5 I Amount of alanine aminotransferase (ALT) measured in mouse plasma as activity units per liter (U/L).

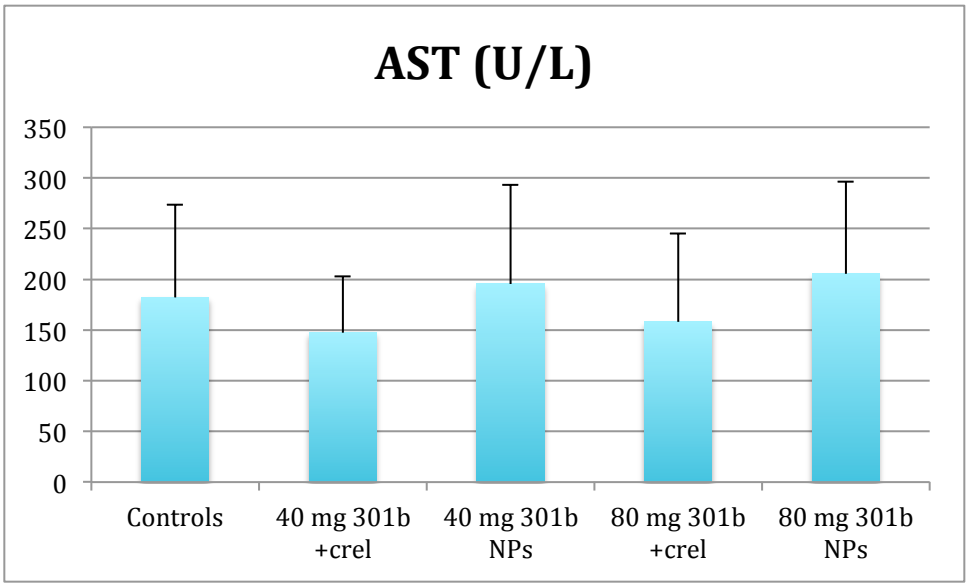

Figure 5.6 I Amount of aspartate aminotransferase (AST) measured in mouse plasma as activity units per liter (U/L).

5.2.2 *In Vivo* MTD Conclusions

We were very pleased with the results of the MTD study, in that all of the treated mice with the prodrug formulation of **301b** in either CrEl® or nanoparticles showed essentially the same toxicity to the animals. Even at the highest concentration of 80 mg/kg **PTX** equivalent with prodrugs did not diminish the total white blood cell count, red blood cell count, or platelets found in the plasma. Also the ALT and AST levels did not rise in comparison to the untreated control, suggesting that no liver damage has occurred. In addition, no substantial dip in animal body weight occurred over the course of the study. All these results show that the MTD for **301b** is much greater than that of Taxol® (20 mg/kg) or Genexol® (60 mg/kg).[177] Further studies are required to determine the MTD of our nanoparticle silicate prodrug formulation.

[177] Kim, S. C.; Kim, D. W.; Shim, Y. H.; Bang, J. S.; Oh, H. S.; Wan Kim, S.; Seo, M. H. In Vivo Evaluation of Polymeric Micellar Paclitaxel Formulation: Toxicity and Efficacy. *J. Control. Release* **2001**, *72*, 191–202.

5.3 Drug Distribution and Extraction

More can be learned from the *in vivio* experiments if the drug and/or prodrug can be isolated from the tissues of the mice. Drug disposition typically occurs in less than 24 hours after administration, and in most cases 8 hours is suitable for the drug to disperse throughout the body. Since the drug distribution is so fast, mice were sacrificed shortly after the administration of the drug for our initial experiments. Also weights of each mouse can be compared to determine toxicity effects of the formulations.

5.3.1 Extraction Techniques for Paclitaxel

To determine the drug distribution *in vivo,* minute concentrations must be recovered, analyzed, and quantified from within various tissues, while removing various impurities from the biological matrix analyzed. Accomplishing the difficult task of recovering small amounts of drugs in complex mixtures requires a variety of complementary extraction techniques and chromatographic parameters, which we have been developing. Pretreatment of tissue samples by solid-phase extraction (SPE) or liquid-liquid extraction (LLE) is required to remove interfering proteins and other bio-molecules. SPE uses preparatory columns packed with hydrocarbon capped silica to hold hydrophobic molecules while impurities are removed through a series of wash steps. LLE achieves this through precipitation of proteins, centrifugation, and removal of the supernate. Many improvements in these two pretreatment techniques can be made to increase the speed, recovery of the analyte (efficiency), and removal of contaminates.

High performance liquid chromatography (HPLC) with UV detection at 227 nm is the most common method for analysis of paclitaxel, but is limited by the detection threshold as shown in Table 5.1. Liquid chromatography in tandem with mass spectrometry (LC-MS) increases sensitivity by detection of the ionizing molecules through electrospray and analyzing their respective masses. This

technique can be expanded upon, to achieve analyte quantification at even lower concentration, by selection of the ions in the first mass spectrometer and further analysis of their masses with a second mass detector. This technique is known as liquid chromatography tandem mass spectrometry (LC-MS-MS). Different approaches used to extract paclitaxel from a variety of matrices and the tools used to analyze them are summarized in Table 5.1. This information serves as a starting place to develop extraction and analysis methods of highly hydrophobic and labile silicate prodrugs of paclitaxel.

Table 5.1 l Extraction techniques to recover paclitaxel from different tissues.

Research Group, Date	Matrix abv.[b]	Technique abv.[c]	Efficie-ncy(%)	Detection[a] Method	LOQ[b] (ng/mL)
Beijen, 1995[178]	Hp & Mt	SPE C_N	89%	C_8 / HPLC	10
Bannister, 2002[179]	Dp	LLE (MTBE 2.5x)[d]	NA	C_{18} / LC-MS	0.1
Beijen, 2004[180]	Hp, Htu, Mb	LLE (MTBE 5x)[d]	72%	C_{18} / LC-MS-MS	0.1
Chi, 2005[181]	Mt	LLE (EA 100x)[d]	>95%	C_{18} / HPLC	10
Peterson, 2006[182]	Hp	SPE C_N	NA	C_{12} / LC-MS-MS	0.5
Matsubara, 2007[183]	Hp	SPE C_{18}	>90%	C_{18} / HPLC	3

[178] Huizing, M. T.; Sparreboom, A.; Rosing, H.; van Tellingen, O.; Pinedo, H. M.; Beijnen, J. H. Quantification of Paclitaxel Metabolites in Human Plasma by High-Performance Liquid Chromatography. *J. Chromatogr. B* **1995**, *674*, 261–268.

[179] McChesney, J.; Zygmunt, J.; Bannister, S. Measurement of paclitaxel in biological matrices: high-throughput liquid chromatographic-tandem mass spectrometric quantification of paclitaxel and metabolites in human and dog plasma *J. Chromatogr. B* **2003**, *785*, 253-261.

[180] Rosing, H.; Beijnen, J. A Simple and Sensitive Assay for the Quantitative Analysis of Paclitaxel in Human and Mouse Plasma and Brain Tumor Tissue using Coupled Liquid Chromatography and Tandem Mass Spetrometry. *J. Mass Spectrom.* **2004**, *39*, 1506-1512.

[181] Kim, S. C.; Yu, J.; Lee, J. W.; Park, E.-S.; Chi, S.-C. Sensitive HPLC Method for Quantitation of Paclitaxel (Genexol in Biological Samples with Application to Preclinical Pharmacokinetics and Biodistribution. *J. Pharmaceut. Biomed.* **2005**, *39*, 170–176.

[182] Gréen, H.; Vretenbrant, K.; Norlander, B.; Peterson, C. Measurement of Paclitaxel and its Metabolites in Human Plasma using Liquid Chromatography/Ion Trap Mass Spectrometry with a Sonic Spray Ionization Interface. *Rapid Commun. Mass Sp.* **2006**, *20*, 2183–2189.

[183] Suno, M.; Ono, T.; Iida, S.; Umetsu, N.; Ohtaki, K.-I.; Yamada, T.; Awaya, T.; Satomi, M.; Tasaki, Y.; Shimizu, K.; Matsubara, K. Improved High-performance Liquid Chromatographic

[a] Column used / Detection Method (HPLC only = UV-vis), C_{18} = octadecyl-silica, C_{12} = dodecyl-silica, C_8 = octyl-silica, C_N = cyano-silica
[b] Limit of Quantification (LOQ) based on less than 20% variation from calibration curve. All calibration curves were formed from ratios to an appropriate internal standard (I.S.).
[c] Abbreviations- Dog Plasma (Dp), Human Plasma (Hp), Human Tumor (Htu), Mouse Brain (Mb), Mouse Tissues (Mt).
[d] Abbreviations- Solid-Phase Extraction (SPE), Liquid-Liquid Extraction (LLE), Methyl *tert*- butyl ether (MTBE), Ethyl acetate (EA).
[e] Example (EA 100x vol) signifies an extraction volume of EA 100 times the volumes of tissue homogenate or blood sample.

5.3.2 Extraction protocol of PTX from various tissues

A group of C57/B16 wild type mice (n=32) was seeded with 1 million 4T1 tumor cells and allowed to grow to a volume of approximately 150 mm^3. Eight mice each were put into four groups and injected in the tail vein with one of the following formulations at a dose of 40 mg equivalent of **PTX** per kg of mouse *i.*) Taxol®, *ii.*) PTX-2',7-[$Si(OEt)_3]_2$ **(302a)** in Cremophor EL®, *iii.*) **302a** loaded nanoparticles (50 wt%, PEG-*b*-PLGA, 5k-10k), *iv.*) untreated (control). After 2 hours of treatment, 4 mice from each group were euthanized. The other 16 mice (4 per group) were euthanized after 8 hours. The euthanized mice were dissected to harvest 7 important tissue samples: brain, lungs, heart, liver, spleen, kidneys, and tumor. Since the drug was administered intravenously, there was little need to collect any part of the gastrointestinal tract or excrement due to a low rate of back adsorption.[184,185] Each tissue was collected, weighed as a wet mass (some residual blood), and stored in a -80 ºC freezer until extraction and analysis.

Detection of Paclitaxel in Patient's Plasma using Solid-Phase Extraction, and Semi-micro-bore C18 Separation and UV detection. *J. Chromatogr. B* **2007**, *860*, 141–144.

[184] Martinez, M. A Mechanistic Approach to Understanding the Factors Affecting Drug Absorption: a Review of Fundamentals. *J. Clin. Pharmacol.* **2002**, *42*, 620-643.

[185] Varma, M.; Sateesh, K. Functional Role of P-glycoprotein in Limiting Intestinal Absorption of Drugs: Contribution of Passive Permeability to P-glycoprotein Mediated Efflux Transport. *Mol. Pharm.* **2005**, *2*, 12-21.

Before the tissues could be analyzed, and the drug/prodrug quantified, a series of controls was needed to validate the extraction methods and ensure that acceptable recovery was possible. By spiking in known concentrations of paclitaxel or prodrug along with docetaxel (as an internal standard) into untreated tissues, it was possible to determine extraction efficiencies. Two different approaches, LLE and SPE, were explored to extract the compounds cleanly and prepare the samples for analysis by both HPLC and LC-MS.

Paclitaxel and **DTX** are very similar in structure (cf. Figure 3.2), while the prodrug is highly hydrophobic, making separation quite difficult. A slow gradient method followed by a 100% organic method was developed. Mobile phase A was a 95:5 H_2O:MeOH mixture buffered with 15 mM ammonium acetate (NH_4OAc) and mobile phase B was 98:2 MeOH:H_2O buffered with 15 mM (NH_4OAc). The tissue matrix from which the analytes are extracted further complicates this task. (Small peptides and phosphates typically survive the preparatory step.) A gradient method was developed on an analytical Agilent XDB-C18 4.6 mm x 50 mm column with particle size of 1.8 μm. A constant flow rate of 0.5 mL was maintained throughout the analysis. The percentage of mobile phase B compared to A (%B) started at 55% and increased to 80% over the course of 10 minutes to separate **PTX** and **DTX**, the %B then ramped to 100% in 5 minutes, and remained there for another 5 minutes to elute the relatively nonpolar analyte **302a**. The %B returned to 55% in 3 minutes to allow the column to re-equilibrate at this mobile phase ratio until the next 10 μL injection. The characteristic mass spectrum of each compound can be clearly seen in the “negative ion” mode, and their corresponding integrals in the UV chromatogram are observed at 227 nm for quantification against a calibration curve.

A LLE method was developed due to the lower cost associated with the procedure and less sample handling during the single extraction on the tissues would reduce losses as well. The seven samples of different tissue types were

homogenized in 4 mL of de-ionized water to create a slurry of the solid tissues. The samples were then frozen at -80° C for 5 hours, after which they were lyophilized for 24-48 hours to remove the water. The dried weights were recorded and known concentrations of **PTX** or **302a** were spiked in along with **DTX** as the internal standard (I.S.). Each sample was extracted with 3 mL of ethyl acetate overnight. The samples were centrifuged at 16,000 rpm and a 2 mL aliquot of the supernate was transferred and concentrated by a stream of nitrogen (N_2). The samples were re-dissolved in 1 mL of acetonitrile (ACN) and analyzed by HPLC. Initial attempts with one extraction showed poor efficiency and recovery of the drugs out of the tissues (Column 2, Table 5.2). Multiple extractions (3 times of 3 mL of ethyl acetate each) were performed on the tissue samples, which increased the extraction efficiency. However, the amount of time for sample preparation also increased. Also, multiple extractions overnight can lead to the hydrolysis of **302a** to give **PTX** as shown in mixed solvent system stability of **302a** (Chapter 3, Figure 3.4). An average of 60% recovery was noted by comparing the concentrations measured to a standard curve.

A series of seven SPE cartridges were screened to determine the recovery from known concentrations of **PTX**, **302a**, and the I.S. **DTX** in methanol and PBS without tissue present. The SPE cartridges were first conditioned with methanol to wet the silica and remove any residual manufacturing impurities. They were then equilibrated with PBS buffer and the sample was loaded. The load eluent was analyzed by HPLC to confirm that the column retained the analytes. A second wash of 50:50 methanol:PBS washed the samples to remove the majority of the impurities that may be present. Again, this eluent was analyzed by HPLC to test retention during this step. Finally the compounds were eluted off of the adsorbant with 2.5 mL of ACN. The eluate was concentrated by drying under a nitrogen stream and reconstituted in the HPLC mobile phase. Excellent recovery was observed in most cartridges. Interestingly, cyano bond material (C_N) did not retain **PTX** well but gave 95% recovery of **302a**. The C_{18} gave optimal recovery of ≥ 90% for all 3 compounds (**PTX**, **302a**, **DTX**).

Table 5.2 I Comparison of extraction efficiencies of each technique.

Technique	LLE[a]	LLE[a]	LLE[b]	SPE[a]	SPE[b]
Tissue	1x3mL EA	3x3mL EA	3x3mL EA	C_{18}	C_{18}
Brain	8 ± 0%	55 ± 10%	64 ± 2%	–	–
Heart	30 ± 26%	59 ± 12%	57 ± 13%	85 ± 3%	98 ± 10%
Lungs	16 ± 0%	56 ± 13%	52 ± 5%	–	–
Liver	69 ± 7%	66 ± 12%	48 ± 1%	41 ± 1%	34 ± 5%
Spleen	54 ± 18%	84 ± 41%	33 ± 16%	–	–
Kidneys	43 ± 3%	60 ± 12%	48 ± 9%	68 ± 3%	90 ± 9%
Tumor	33 ± 4%	83 ± 31%	52 ± 10%	79 ± 16%	–

[a] Extraction efficiency of **PTX**.
[b] Extraction efficiency of prodrug **302a**.

To extract drugs out of the animal tissues, the solid phase extraction method with C_{18} adsorbent was employed due to the high recovery of spiked samples and good extraction efficiencies established in the control experiments. Although there are many stages to prepare the samples for analysis, the extraction can be accomplished in 1 day as opposed to LLE. Also there is no need to lyophilize or extract overnight due to the highly hydrophobic nature of the C_{18} adsorbent.

5.3.3 Bio-distribution study of PTX-silicate prodrug-loaded PEG-*b*-PLGA nanoparticles (uncentrifuged) against the aggressive 4T1 breast cancer tumors via tail vein injection

Liver tissue samples from the prodrug distribution experiment were homogenized in 3 mL of PBS buffer for every gram of wet tissue weight. The homogenate was then split into equal volumes for duplicate or triplicate analysis. To each sample, 5 μg of **DTX** was added along with an aliquot of methanol that was half the volume of the tissue sample. Adding the internal standard at this point allows the ratio of drug to I.S. to be quantified without the errors associated

with quantitative transfer of small volumes. The addition of methanol also precipitates many of the proteins, which are removed upon centrifugation at 16,000 rpm. By precipitating the proteins, the samples are effectively washed once, thereby increasing column lifetime and affinity of the adsorbent for the analytes. After the columns were conditioned with methanol and equilibrated with PBS buffer, the supernate of the ~30% methanol/PBS homogenate containing the analytes and I.S. was loaded onto the cartridge. The sample was then washed with a 50:50 MeOH:PBS solution, which after elution was analyzed to ensure drug retention as done in control experiments. The analytes were finally eluted with 2.5 mL of ACN and concentrated over nitrogen. The samples were re-dissolved in 1 mL of ACN and analyzed by the LC-MS method described above in Section 3.3. The AUC in the UV region of **PTX** and **302a** were calculated and divided with the integral of I.S. **DTX** to produce a ratio. This ratio could be evaluated against a linear calibration curve of integration ratios (**PTX**/**DTX**) or (**302a**/**DTX**) vs. known concentrations of **PTX** or **302a**. Back-calculation of dilutions from the tissue and efficiency of extraction allow the total amount of drug to be calculated as a ratio of the initial wet mass of the tissue. Figure 5.7 shows the concentrations calculated for each formulation performed in triplicates.

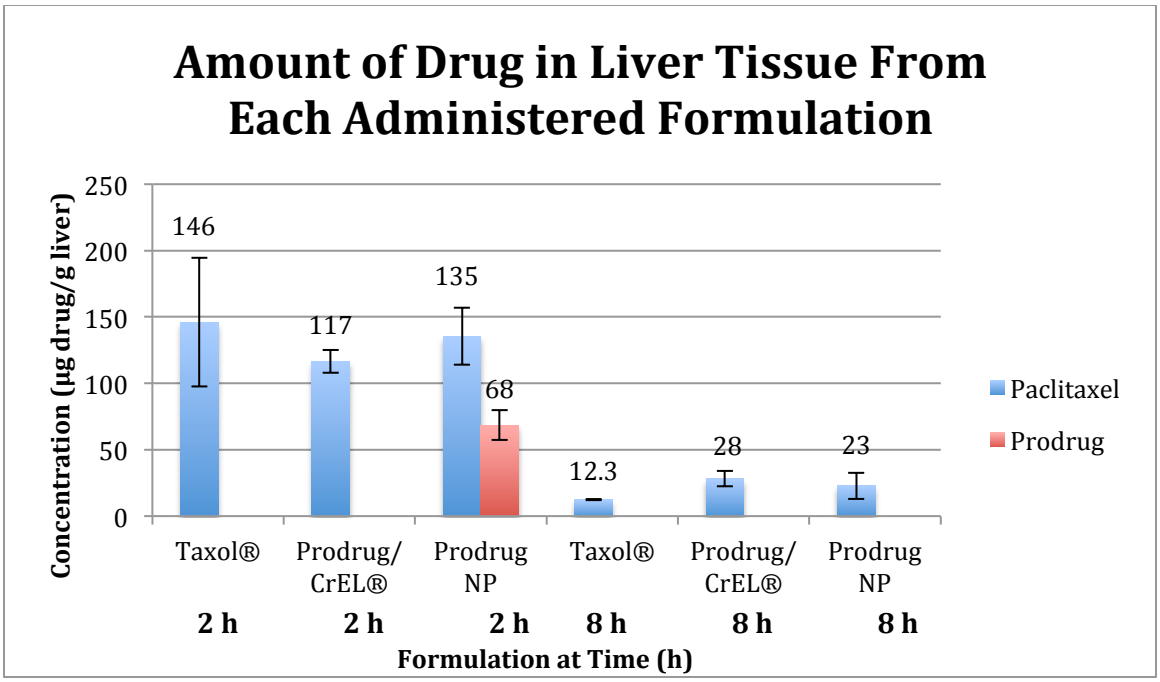

Figure 5.7 I Bar graph depicting the amount of drugs in the liver 8 Hours. Each measurement is from 3 different measurements (sample split in 3 and extracted) of liver homogenates and repeated with another liver from a different mouse. (Prodrug = **302a**)

After 2 hours, there is approximately 120 μg of **PTX** per gram of liver tissue in all 3 treatments. This reveals there is no significant difference between each formulation accumulation in the liver over the course of 2 hours. Interestingly, the prodrug is observed in the case of the silicate prodrug nanoparticle treatment at 2 hours. This shows the ability of the polymer nanoparticle to protect the labile prodrug from immediate hydrolysis. Approximately 0.01% of the liver tissue homogenate is **PTX** at 2 hours. Over the course of 8 hours, the drug concentrations in the liver are significantly lower, as expected. The Taxol® formulation is the lowest. This suggests that the drug is readily cleared from the liver while the prodrug formulations take longer for clearance of the drug.

Another study was conducted on tumor tissue, but concentrations were not detectable except for **302a** administered in CrEL®, which had a concentration of 2.9 ± 0.9 μg of **PTX** per gram of tumor tissue. Finding little or no drug in the tumor tissue is surprising since the extraction efficiency was high for the tumor tissue (Table 5.2). It is possible that the concentrations are below the limit of quantification (LOQ), which is 100 ng/mL due to the presence of soluble proteins that can suppress the signal, or an absolute limit of detection (LOD) of 1.0 ng of **PTX,** and, thus, it is difficult to draw conclusions regarding the drug localization in the tumors.

5.3.3 Bio-distribution study of PTX-silicate prodrug-loaded PEG-*b*-PLGA nanoparticles (centrifuged) in C57BL/6 mice via tail vein injection

Liver samples were removed from the -80 ºC freezer and allowed to thaw to room temperature at which point 10 μg of **DTX** was added from a 1 mg/mL stock solution to the liver to serve as the I.S. Quality controls were made from the untreated control group livers by adding in a known concentration of 1mg/mL stock solution of **PTX** (50.7 μg, 101.5 μg, 203 μg) for mouse liver 1 (M1), M2, M3 respectively. The livers were wetted with 2 mL of saline and homogenized. The samples were loaded onto an equilibrated SPE cartridge by adding 1 mL of ACN and eluting the solvent mixture. LC-MS-MS revealed no PTX, DTX, or **301b** in the load step. The analytes were eluted with 3 mL of methanol, concentrated on the rotary evaporator, dissolved in 1 mL of methanol, filtered through a 0.2 μm syringe filter, and injected (5 μL) as triplicates on the LC-MS-MS. Samples and quality controls were quantified by a calibration curve of the ratio of **PTX**/**DTX** and tabulated in Figure 5.8 below.

Unfortunately the quality controls showed a matrix effect with the liver tissue and gave an observed value greater than that of the known concentration especially at higher concentrations of **PTX**. Nevertheless, the graph provides an estimate for the amount of drug retained after the 3 week MTD study.

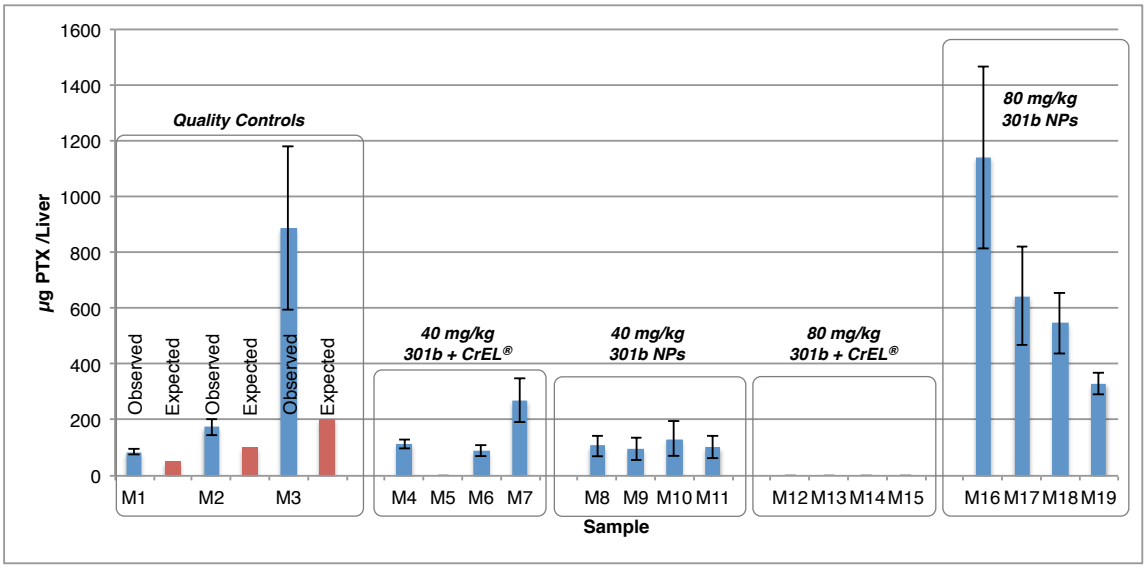

Figure 5.8 I Amount of **PTX** quantified by LC-MS-MS in each mouse model (M1-M19) for each treatment group in the MTD study.

In either low dose treatment group at the (40mg/kg) the liver retained ca. 200 μg of PTX which accounts for ca. 12% of the total dose injected into the animals. The high dose treatment group of 80 mg/kg **PTX** equivalent **301b** in CrEL® dosed twice could not be quantified. However, the high dose treatment with 80 mg/kg **PTX** equivalent **301b** in our nanoparticle formulation dosed twice showed an average of ca. 660 μg of PTX in each liver sample which accounts for ca. 21% of the entire dose injected into the tail vein of the mice. The animals receiving nanoparticle formulations tolerated the 2x 100 μL dosing much better than those treated with CrEL® formulations as expected.

The total amount of PTX quantified was divided by the total wet mass of the liver and tabulated in Figure 5.9 below. From this graph the low dose formulations show significantly less **PTX** per mg of liver. While the mice tolerated the high dose treatments for the MTD studies (Chapter 5.2) the extraction data suggest that multiple doses at 40 mg/kg are beneficial as less drug is retained by the liver. For the current efficacy study underway presented in the future outlook

Chapter 5.4 we opted to dose at 40 mg/kg of two prodrugs namely **301a** and **301b**.

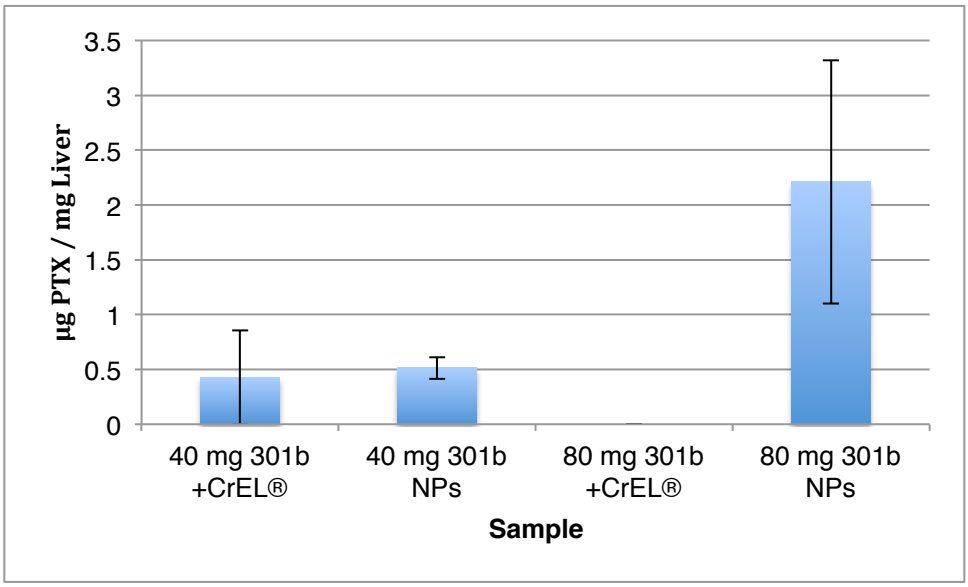

Figure 5.9 I Amount of **PTX** quantified by LC-MS-MS per mg liver sample for each treatment group.

5.4 Future Outlook

Further research is required to finish a complete distribution study of centrifuged nanoparticles. The future outlook of the project is very promising. The nanoparticle formulation will continue to be optimized through the conjugation of polymers to tumor targeting peptides and antibodies. The effectiveness of these modifications can be analyzed through *in vitro* studies, and efficacy and tissue distribution studies *in vivo*.

Lastly a cohort of 40 Balb/c Nu/Nu mice were purchased from Jackson Labs. Mice were transfected with MDA-MB-231-Luc+ cancer cells and tumors allowed to grow to 100 mm^3. The nude mice six each were randomly divided into one of six groups: *i.*) untreated saline control *ii.*) Taxol®, *iii.*) PTX-2'-$Si(OEt)_3$ (**301a**) in CrEL®, *iv.*) **301a** formulated in nanoparticles (centrifuged), *v.*) PTX-2'-

$Si(O^nOct)_3$ (**301b**) in CrEL®, or *vi.*) **301b** formulated in nanoparticles (centrifuged). Tail vein injections at 40 mg/kg dosing will allow for a comparison of the efficacy of the two different prodrugs. This study is currently underway, however we are optimistic in the outcome of our silicate prodrug loaded nanoparticle formulations.

♣ Part II♣

Non-Taxane Silicate Chemisty:

Chapter 6. Model Silicates: Exploring New Functionality

6.1 Introduction

Silicate esters [also known as orthosilicate esters or tetraalkoxysilanes, $Si(OR)_4$][186] comprise a class of organic compounds that has been known for well over 150 years.[103] More generally, silicate esters (and other organosilicon species[187,188]) have been widely studied primarily due to applications in sol-gel forming processes. Recently, we have a growing interest in the potential application of silicate derivatives as prodrugs, a setting in which hydrolytic cleavage of the $(RO)_3Si—XDrug$ (X = O, N) bond is essential for release of the parent drug molecule. [112,118]

Hydrolysis rates have been reported for the two simplest members of the silicate ester family, tetramethyl and tetraethyl orthosilicate (TMOS and TEOS, respectively), driven primarily by their wide use in sol-gel-forming processes.[189] The techniques used to monitor the hydrolysis of these silicate esters include gas chromatography,[190] Raman spectroscopy,[191] and nuclear magnetic resonance (NMR) spectroscopy.[135,192] Acid-catalyzed hydrolysis in mixed aqueous-organic

[186] Most generally, names for compounds containing silicon are named from the simplest silane, SiH_4. However, compounds that consist of four Si-O bonds are commonly named as a derivative of orthosilicic acid rather than as a silane derivative.

[187] Bassindale, A. R.; Taylor, P. G. Reaction Mechanisms of Nucleophilic Attack at Silicon. In *The Chemistry of Organic Silicon Comounds*. Patai, S.; Rappoport, Z., eds. John Wiley & Sons, Inc: New York, 1989, 839-892 and references therein.

[188] Holmes, R. R. The Stereochemistry of Nucleophilic Substitution at Tetracoordinated Silicon. *Chem. Rev.* **1990**, *90*, 17-31 and references therein.

[189] Aelion, R.; Loebel, A.; Eirich, F. Hydrolysis of Ethyl Silicate. *J. Am. Chem. Soc.* **1950**. *69*, 61-75.

[190] Ro, J. C.; Chung, I. J. Sol-Gel Kinetics of Tetraethylorthosilicate (TEOS) in Acid Catalyst. *J. Non-Cryst. Solids* **1989**, *110*, 26-32.

[191] Zerda, T. W.; Hoang, G. Effects of Solvents on the Hydrolysis Reaction of Tetramethyl Orthosilicate. *Chem. Mater.* **1990**, *2*, 372-376.

[192] Assink, R. A.; Kay, B. D.; Study of Sol-Gel Chemical Reaction Kinetics by NMR *Annu. Rev. Mater. Sci.* **1991**, *21*, 491-513.

media has been interpreted to occur via an S_N2 mechanism in a process that is pseudo first-order in water and with a rate that is solvent dependent.[193] TMOS and TEOS are hydrolytically labile under both acidic and basic conditions.

Occasional qualitative inferences have been drawn about the relative hydrolytic lability of silicates. For instance, gelation times, used as a proxy for hydrolysis, of tetramethyl, tetraethyl, and tetra-*n*-butyl orthosilicates were found to be approximately two days, 10 days, and 25 days, respectively, when the compounds were stored without "special precautions."[194] While not entirely satisfying from the perspective of quantified information, observations such as these give a hint of the subtle steric alterations that influence the rate of hydrolysis of silicate esters. In more recent studies, sterically hindered silicate esters have been synthesized and reported to hydrolyze very slowly, but these studies also were not quantitative.[127,195]

We have been able to locate only a single study designed to quantify the hydrolysis rates of several silicate esters.[196] This involved a comparison of four different compounds; all symmetrical tetraalkoxysilanes: ethoxy, *n*-butoxy, *n*-hexyloxy, and 2,3-dimethylbutoxy. These experiments demonstrated an approximately six-fold slower hydrolysis rate with increasing aliphatic chain length (from ethyl to *n*-hexyl) and an approximately 17-fold slower hydrolysis rate with a branched side chain.[196] However, these studies are slightly compromised by the analytical method used to measure the rates. Karl Fisher titration is now

[193] Zerda, T. W.; Hoang, G. Effects of Solvents on the Hydrolysis Reaction of Tetramethyl Orthosilicate. *Chem. Mater.* **1990**, *2*, 372-376.

[194] Arkles, B. Silicon Esters. In *Kirk-Othmer Encyclopedia of Chemical Technology, Fourth Edition, Volume 22*; Kroschwitz, J. I.; Howe-Grant, M., ed. John Wiley & Sons, Inc: New York, 1997, 69-81.

[195] Clausen, R. P.; Bols, M. The First Tri- and Tetraalkoxysilanes with Four Different Substituents. *J. Org. Chem.* **1997**, *62*, 4457-4464.

[196] Brinker, C. J. Hydrolysis and Condensation of Silicates: Effects on Structure. *J .Non-Cryst. Solids* **1988**, *100*, 31-50.

known to consume both water and silanols, so the absolute rate constants measured are considered to be not entirely reliable.[197]

We describe here experiments that establish broader trends in the relative hydrolytic lability of more extensive series of structurally related silicate esters as well as some analogs thereof. These results provide guidance on how to further capitalize on the applications of silicate derivatives[194] in various settings.

6.2 Hydrolytic Lability of Model Silicates

The relative hydrolysis rates of several sets of silicates, as well as a few related silanols and silane derivatives, were studied by ^{1}H NMR spectroscopy. Typically, experiments were performed in a 10:1 volume ratio of acetone-d_6:D_2O containing 1% (by volume) of one of trifluoroacetic acid (TFA), acetic acid (AcOH), or, for the case of TEOS, triethylamine (TEA) as a hydrolysis catalyst.

Principally three types of silicates were studied (**601**-**603**). The synthesis strategies used to prepare each class are summarized in Figure 6.1. Many of the tetra-alkyl (and the tetra-phenyl) silicates **601** are commercially available. Others were prepared by reaction of tetrachlorosilane ($SiCl_4$) with excess alcohol (ROH), sometimes in pentane alone (with evolution of HCl) or, for hindered ROH reactants, in the presence of a non-nucleophilic amine base like pyridine. Likewise, some trialkoxychlorosilanes can be purchased; others were made by reaction of $SiCl_4$ with three equivalents of alcohol. Subsequent reaction with a different alcohol, a phenol, a carboxylic acid provided **602** or with an amine or amide gave **603**.

[197] Brinker, C. J.; Scherer, G. W. Hydrolysis and Condensation II: Silicates. In *Sol-Gel Science: The Physics and Chemistry of Sol-Gel Processing*. Academic Press, Inc: San Diego, CA, **1990**, 97-233.

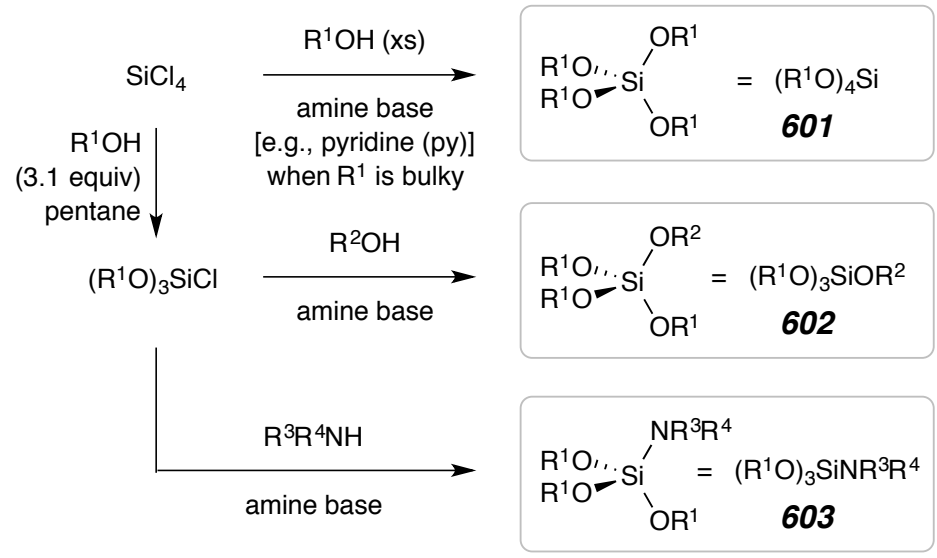

Figure 6.1 I General approaches used for the synthesis of each of the three classes of silicates (601–603) whose hydrolysis rates are compared.

As a representative example that shows the protocol we used for determining hydrolysis half-lives (rates), we show in Figure 6.2 the case of tetraisopropyl orthosilicate (**601e**). Its hydrolysis in acetone-d_6:D_2O:TFA-*d* (90:9:1) was monitored by ^{1}H NMR spectroscopy over time. The integration values corresponding to the resonances for the isopropyl methine protons of silicate **601e** were compared with those of the released *i*-PrOH. This substrate is typical in that no resonances for any intermediate silanols [e.g., (^{i}PrO)$_3$SiOH] (or their anhydro-dimers) were detected during the course of reaction. This suggests that hydrolytic cleavage of the first alkoxy is the slowest compared with all of the remaining three events that lead, ultimately, to silicic acid [Si(OH)$_4$] (and its oligomers[198]) and four equivalents of released *i*-PrOH.

[198] Belton, D. J.; Deschaume, O.; Perry, C. C. An overview of the fundamentals of the chemistry of silica with relevance to biosilicification and technological advances. *FEBS J.* **2012**, *279* 1710–1720.

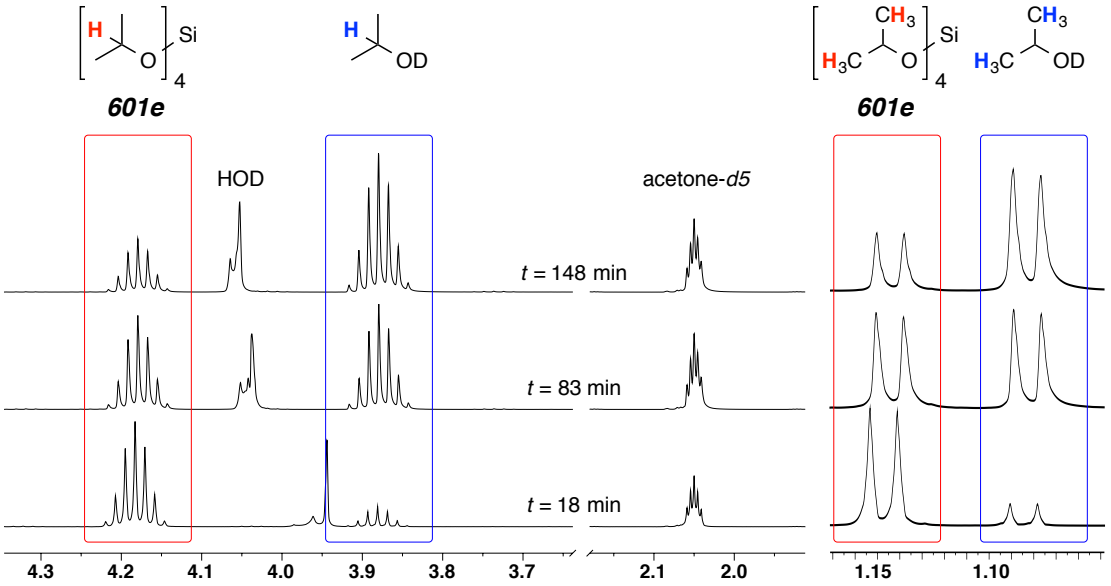

Figure 6.2 I NMR monitoring of the hydrolysis of **601e** in 90:9:1 acetone-d_6:D_2O:TFA-OD at 22 °C.

Using this methodology, we determined the half-lives for hydrolysis of the six tetra-alkoxy (**601a-f**) and two tetra-aryloxy (**601g-h**) silanes shown in Table 6.1. The first four of these all contain four primary alkoxy groups. Their rates of hydrolytic cleavage slowly decrease as the alkyls grow longer, but only over a span of <7 in relative rates. In fact one can discern a plateauing effect; the incremental decrease diminishes for each additional two carbons present in the termini of each chain. The k_{rel} values for the first three entries (ethyl, butyl, and hexyl silcates **601a-c**) are entirely in accord with the relative reactivities reported by Brinker.[196] The (tetra-isopropyl)silicate (**601e**, cf. Figure 6.2), which contains branched secondary alkyl groups, has a yet slower rate [25.9 times slower than TEOS (**601a**) and ca. 4 times slower than the octylsilicate **601d**]. Tetramenthyl silicate (**601f**), also having four secondary alkoxy groups but, of course, of much greater "long-range" (or "outer sphere") steric bulk, has a dramatically increased stability toward hydrolysis.

Table 6.1 I Hydrolytic lability of symmetrical silicates **601a-h**.

601	**$(RO)_4Si$**	**R**	**TFA**		**AcOH**
			$t_{1/2}$ (min)	**k_{rel}**	**$t_{1/2}$ (min)**
601a	$(EtO)_4Si$	ethyl	3.1 ± 0.1	1	2,300
601b	$(n\text{-BuO})_4Si$[a]	*n*-butyl	12.0 ± 1.0	3.8	
601c	$(n\text{-HexO})_4Si$	*n*-hexyl	17.5 ± 0.3	5.6	
601d	$(n\text{-OctO})_4Si$[a]	*n*-octyl	21.0 ± 1.0	6.7	
601e	$(i\text{-PrO})_4Si$	*i*-propyl	81.3 ± 2.6	25.9	>40 days
601f	$(menthylO)_4Si$[b]	menthyl	>16 days		
601g	$(4\text{-MePhO})_4Si$[c]	4-methylphenyl	6	1.9	
601h	$(MesO)_4Si$[a]	2,4,6-trimethylphenyl	64	20.4	1,300

[a] Measured by Dr. Adam Wohl.

[b] This highly hydrophobic silicate was only partially soluble in the 10% aqueous acetone medium used for the other hydrolyses in this table. Its cleavage was studied, instead, under homogenous conditions using a 98:1:1 volume ratio of acetone:D_2O:TFA. For comparison, TEOS (**601a**) measured in this less polar reaction medium showed a reduced rate of hydrolysis ($t_{1/2}$ = 33 ± 1.0 min).

[c] Measured by Dr. Yutaka Miura.

The mechanism for acid catalyzed hydrolysis is shown in Figure 6.3 below, a menthol containing silicate has been chosen to clearly show the effect of steric bulk on the rate of hydrolysis. Starting in the top left of the figure, one of the alcohols becomes protonated by the acidic environment. Subsequently the association of water occurs and a geometry change is induced from tetrahedron (where all of the bulky alkoxy groups are ca. 109.5º from one another) to trigonal bipyamidal. The silicon center becomes five coordinate and adopts a trigonal bipyramidal geometry in which one of the bulky groups is placed 90º from the other three. This steric strain of the close alkoxy groups reduces the propensity to hydrolyze due to the energy requirement to achieve this conformation. Once in this conformation the bulky sterically congested alcohol must leave from the axial position relative to the incoming water (top right).

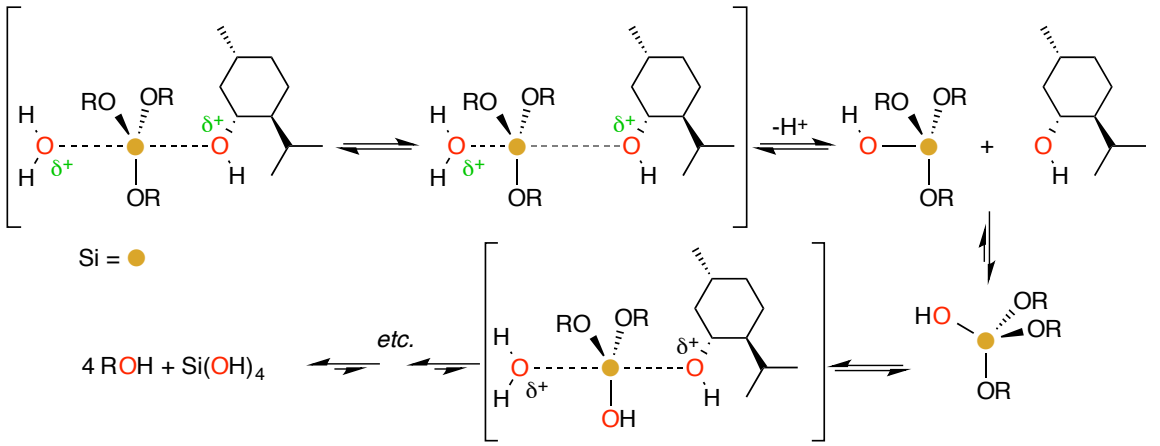

Figure 6.3 I The mechanism for acid catalyzed hydrolysis.

Following the loss of a proton, the conformation reverts back to tetrahedral, forms the stable silanol, and the process repeats. However, in the case of very bulky silanols like **602f** and **602h** placing the bulky alkyl group in the axial position of the trigonal bipyramidal intermediate is disfavored in comparison to the hydroxyl group in the axial position. In essense, since the leaving group must be in the axial position, the silanol in the axial position of the incoming water is degenerate. Only when the bulky group is axial (bottom middle) to the incoming water can the reaction proceed to completion (bottom left). This suggests why bulky silanols are stable and have a considerably slower rate of hydrolysis compared to less bulky silicates.

The rate of hydrolysis was measured as described above for mixed silicates **602a-j** (Table 6.2). A clear trend can be seen with the increase in steric bulk around the silicon center from **602a** to **602d** with k_{rel} values ranging from 1.0 to 12.4. When the steric bulk around the silicon center is great (**602e**, **602f**, **602h**, **602i**), the rate of hydrolysis slows considerably. Having an aryloxy instead of a bulky alkoxy group (compare **602a** to **602g**) increases the rate of hydrolysis.

Table 6.2 I Hydrolytic lability of silicates (**602a-e**, **602g**, **602i**), silanols (**602f**, **602h**), and silane (**602j**).

602	**$(R^1O)_3SiOR^2$**	**R^1**	**R^2**	**TFA**		**AcOH**
				$t_{1/2}$ (min)	**k_{rel}**	**$t_{1/2}$ (min)**
602a	$(EtO)_3Si(O$menthyl$)^a$	ethyl	menthyl	17 ± 1	1.0	–
602b	$(n\text{-}BuO)_3Si(O$menthyl$)^a$	*n*-butyl	menthyl	49 ± 2	2.9	–
602c	$(n\text{-}OctO)_3Si(O$menthyl$)^a$	*n*-octyl	menthyl	79 ± 5	4.6	–
602d	$(i\text{-}PrO)_3Si(O$menthyl$)^a$	*i*-propyl	menthyl	210 ± 10	12.4	–
602e	(menthyl$O)_3$Si(OEt)^{a,b}	menthyl	ethyl	13,000 ± 1,000	764.7	–
602f	(menthyl$O)_3$Si(OH)	menthyl	hydroxyl	7,600 ± 250	445.2	–
602g	$(EtO)_3Si(Op\text{-}Tol)^a$	ethyl	4-methyl phenyl	9.1	0.54	7,100
602h	$(t\text{-}BuO)_3Si(OH)$	*t*-butyl	hydroxyl	602 ± 68	35.4	–
602i	$(t\text{-}BuO)_3Si$ (OCOCH=CHPh)	*t*-butyl	cinnamoyl	7,900 ± 740	462.1	> 14,400 (10 days)
602j	$(t\text{-}Bu)_2(Me)Si$ (OCOCH=CHPh)	TBS	cinnamoyl	2.60 ± 0.18	0.15	30.8 ± 3.2

[a] Measured by Dr. Adam Wohl.

[b] This highly hydrophobic silicate was only partially soluble in the 10% aqueous acetone medium used for the other hydrolyses in this table. Its hydrolysis was studied, instead, in a 98:1:1 volume ratio of acetone:D_2O:TFA.

Lastly, the hydrolytic lability of the cinnamoyl-silicate (**602i**) and cinnamoyl-silane (**602j**) were compared (synthesis can be found in the experimental section for this chapter). We were surprised that the rate of hydrolysis of the silane was much faster ($t_{1/2}$ = 2.60 min) than that of the silicate ($t_{1/2}$ = 7,900 min). This is due

to the drastic difference in steric bulk between the two, as a silicon alkoxy bond is weaker than a silicon alkyl bond.

We then tested the hydrolytic lability of amino- and amido- silicates or silanes **603a-e** (Table 6.3). The synthesis for these compounds can be found in the experimental section of this chapter at the end of this thesis. The hydrolysis was measured in less acidic conditions (AcOH), because a rate could not be obtained in the TFA conditions as before due to the extremely weak nitrogen-silicon bond (N-Si). The rates of hydrolysis of the amido-silanes (**603a** and **603b**) are similar and are only slightly faster than amido-silicate **603c** due to the steric bulk present in **603c**. The same tend is observed for the amino-silane (**603d**) vs. the amino-silicate (**603e**). These silicates hydrolyze approximately twice as slowly as the corresponding silanes.

Table 6.3 I Hydrolytic lability of amino-silicate (**603e**), amido-silicate (**603c**), amino-silane (**603d**), and amido-silanes (**603a**, **603b**)**.**

603	**$(R^1O)_3SiOR^2$**	**R^1**	**R^2**	**AcOH**	
				$t_{1/2}$ (min)	**k_{rel}**
603a	(*t*-Bu)$_2$(Me)Si(benzamido)	*t*-butyl$_2$methyl	benzamido	6.5 ± 0.3	1.4
603b	(*i*-Pr)$_3$Si(benzamido)	*i*-propyl	benzamido	4.5 ± 0.6	1.0
603c	(*t*-BuO)$_3$Si(benzamido)	*t*-butyl	benzamido	8.8 ± 0.5	2.0
603d	(*t*-Bu)$_2$(Me)Si(morpholino)	*t*-butyl$_2$methyl	morpholino	7.5 ± 0.9	1.7
603e	(*t*-BuO)$_3$Si(morpholino)	*t*-butyl	morpholino	15.0 ± 0.9	3.3

6.3 Nanoparticle Formulations of Model Silicate Prodrugs

Nanoparticles were made by FNP as presented before in Chapters 2 and 4. We chose to examine two silicates having new functionality compared to those

we have studied earlier (cinnamic-silicate **602i** and morpholine-silicate **603e**). Either silicate (**602i** or **603e**) and the mPEG-*b*-PLGA block copolymer (5k-10k) were dissolved in 4.0 mL of THF. The THF solution was impingement mixed against 4.0 mL of H_2O in the CIJ-D FNP mixer. The resulting nanoparticles were diluted into 42 mL of water. From this suspension an aliquot of 20 μL was taken and diluted to 1 mL in a DLS cuvette.

The mass of each prodrug model compound and mass of polymer used are presented in Table 6.4 (columns 3 and 4). The intensity average size (d_i) and the PDI of the resulting nanoparticle formulations are also shown in Table 6.4 (columns 5 and 6). The DLS plot for **602i** nanoparticles can be found in the experimental section Figure S6.1.

Table 6.4 I Nanoparticles loaded with ca. 50 wt% of silicate prodrug model compounds **602i** and **603e**.

Compound Number	Short Hand Descriptor	Amounts		DLS	
		Prodrug (mg)	Polymer (mg)	**d_i (nm)**	PDI
602i	Cinn-Si(O^tBu)$_3$	18.0	20.2	118.7	0.150
603e	Morph-Si(O^tBu)$_3$	25.9	28.9	338.9	0.165

We were very pleased with the DLS measurements of the freshly prepared nanoparticle suspensions. However, as expected, when the suspensions containing 10% THF were allowed to stand for 1 week the particles ca. doubled in size and the PDI broadened, likely due to aggregation. In the case of the morpholine-silicate the particle size actually shrunk, likely due to hydrolysis of the N-Si bond. We also froze and lyophilized the solutions after 1 week to determine if the prodrugs were still intact. ^{1}H-NMR analysis in $CDCl_3$ showed that: **602i** had had not degraded at all (no free cinnamic acid resonances were detected) and the **603e** had fully degraded to free morpholine.

These results are very encouraging for future silicate synthesis and nanoparticle formulation of novel drugs with different functionality. We quickly focused our attention on the synthesis of novel silicate prodrugs with differing functionality and nanoparticle formulations thereof.

Chapter 7. Novel Silicate Prodrugs

7.1 Novel Silicate Prodrug Synthesis

We next looked to expand on the prodrug scope to other known drugs. The drugs were chosen for the functionality present and not nessecarily their biological activity. For each drug, monochlorosilanes with varying steric bulk were chosen to determine the feasibility of synthesis and purification. The cLogP and the calculated logS were determined for each silicate as done before.[132] After a sufficient quantity of each silicate prodrug was made, the hydrolytic degradation was measured. Either very acidic (TFA) or slightly acidic (AcOH) *in situ* ^{1}H-NMR hydrolysis conditions mentioned previously were utilized with these novel silicate prodrugs. To probe the biological activity of the silicate prodrugs, we tested five of them *in vivo* against MDA-MB-231 breast cancer cells, even if the drugs chosen were not anti-cancer agents.

7.1.1 Dexamethasone

Dexamethasone (**701**) has a variety of uses due to its anti-inflammitory and immunosuppressant properties.[199] This synthetic glucocorticoid has been used in the treatment of meconium aspiration syndrome, hyperinfection syndrome, retinal disease, and certain types of cancer. Although there is a wide biological interest in the drug, we were interested in the feasibility of the silicate prodrug strategy on the steroid.

The steroid dexamethasone was chosen mainly for its primary hydroxyl alpha to the C-20 ketone. Although there are other hydroxyls present in the

[199] Sauvage, A.; Levy, M. *Dexamethasone: Therapeutic Uses, Mechanism of Action and Potential Side Effects*; Nova Science Pub Incorporated; 2013.

molecule, only the most sterically accessible C-21 alcohol was functionalized with one of the monochlorosilanes (**305**) shown in Scheme 7.1.

Scheme 7.1 I Synthesis of dexamethasone silicates (**702a-c**).

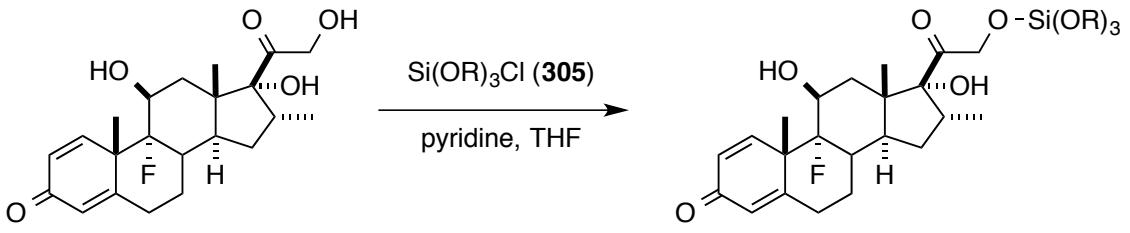

Dexamethasone

701

702	***R***
a	***Et***
b	***^{n}Oct***
c	***^{i}Pr***

For the synthesis of the triethoxydexamethasone silicate (**702a**), the standard pyridine (base) and the commercially available monochlorosilane (**305a)** in THF were utilized. The reaction went smoothly to the product, as determined by crude ^{1}H-NMR and LC-MS analysis. The proper masses were found for the product when an aliquot of the reaction mixture was resolved on the LC-MS: 555 $[m+H]^{+}$ positive mode, and 613 $[m+OAc]^{-}$ negative mode. Unfortunately the product could not be purified by MPLC; a preponderance of starting material was recovered.

We succeeded in the synthesis and isolation of the trioctyloxydexamethasone silicate (**702b**). Again the standard reaction conditions were employed to achieve the synthesis. Experimental details for the reaction and the full characterization can be found in the experimental section for chapter 7 at the end of this thesis.

Lastly, the bulky triisopropoxydexamethasone silicate (**702c**) was made under the same conditions. Proton NMR showed that the product was only 70%

pure after MPLC purification. The cLogP and the cLogS were calculated and tabulated in Table 7.1 (Chapter 7.2). Instead of pursuing these silicates further, we chose to explore the silicate prodrug strategy on different drugs presented later in this chapter.

7.1.2 Ibuprofen

Ibuprofen (**703**) was chosen to show that the starting drug does not need to be entirely pure before functionalization. It also serves as another carboxylic acid example, like the cinnamic acid, shown in Chapter 6. The nonsteroidal anti-inflammatory drug is commonly used for pain relief and fever reduction. Lastly, ibuprofen is an over the counter medication and tablets are very cheap.

Tablets of ibuprofen were crushed and ground into a fine powder in a motor and pestle. The resulting powered was extracted with ethyl acetate and the slurry was passed through a short plug of Celite®. This extraction protocol provided the starting material with > 95% purity and minimal handling only provided a 77% recovery of the ibuprofen. Since the drug is not expensive an optimized extraction procedure was not developed.

The standard set of conditions (pyridine as the base and THF as the solvent) was utilized to synthesize the tri-tertbutoxyibuprofen silicate **704** from the extracted ibuprofen and the commercially available tri-tertbutoxychlorosilane (**305e**). Unfortunately multiple purifications were required to separate the starting **305e** from the final product **704** so a poor yield was obtained. Further optimization of the purification would be required if there was more interest in the prodrug. The cLogP and the cLogS of the parent ibuprofen and the silicate are shown in Table 7.1. Also the hydrolytic lability is shown in Table 7.2 (Chapter 7.2). by using the acid *in situ* NMR conditions presented in Chapters 3 and 6.

Scheme 7.2 I Synthesis of ibuprofen silicate **704** from extracted ibuprofen **703**.

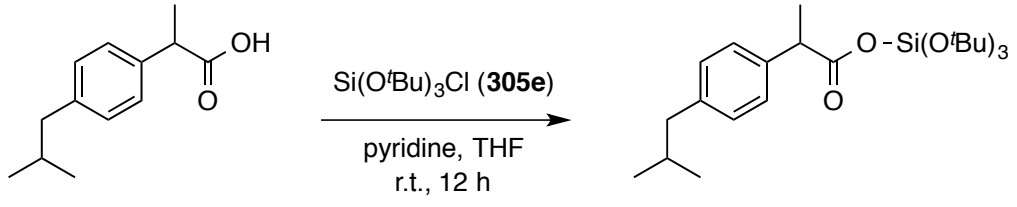

Ibuprofen

703 ***704***

7.1.3 Salinomycin

Salinomycin (**705**) is a polyether ionophore that binds sodium or potassium and restricts the movement across cell membranes. Due to its mechanism of action, salinomycin is an effective antibacterial agent even against problematic bacteria. The drug is produced by the *Streptomyces albus*, strain ATCC 21838 and harvested in an impure form for use as a coccidiostat (anti-parasitic) in the poultry industry as a feed additive.[200] Salinomycin has been shown to selectively target cancer initiating or cancer stem cells, the problematic cells that are responsible for cancer recurrence after remission.[201]

Not only is salinomycin interesting with regards to its biological activity, the chemical structure is also quite intriguing. It contains 18 stereocenters with three hydroxyls at C-9, C-20, and C-28. All of these have the possibility of being functionalized with the silicate methodology. The C-1 carboxylic acid can also be functionalized, [202] and proved to be the most reactive toward the silicate

[200] Paulus, E. F.; Kurz, M.; Matter, H. Solid-State and Solution Structure of the Salinomycin-Sodium Complex: Stabilization of Different Conformers for an Ionophore in Different Environments. *J. Am. Chem. Soc.* **1998**, *120*, 8209-8221.

[201] Borgström, B.; Huang, X.; Pošta, M.; Hegardt, C.; Oredsson, S.; Strand, D. Synthetic Modification of Salinomycin: Selective O-Acylation and Biological Evaluation. *Chem. Comm.* **2013**, *49*, 9944–9946.

[202] Huczyński, A.; Janczak, J.; Stefańska, J.; Antoszczak, M.; Brzezinski, B. Synthesis and Antimicrobial Activity of Amide Derivatives of Polyether Antibiotic-Salinomycin. *Bioorg. Med. Chem. Lett.* **2012**, *22*, 4697–4702.

chemistry. Purification is difficult in part because the polyacetal ring system isomerizes when stored in aqueous media.[203] The mechanism suggests that slightly acidic media (e.g. silica gel) would enhance the rate of isomerization of the polyacetal to a furan.[203]

Chicken fodder that contains ca. 12% salinomycin (**705**) by weight was graciously donated for the subsequent synthesis of silicate prodrugs of the drug. A total of 114 g of the feed additive was suspended into 500 mL of chloroform and allowed to stir overnight. The resulting slurry was filtered through Celite® and washed with CH_2Cl_2. A column of 200 g of silica gel was used to purify the crude salinomycin. It was eluted with 400 mL of ethyl acetate. A yellow solid was obtained (7.29 g, ca. 90% purity). The salinomycin could be further purified by reverse-phase MPLC (95% methanol: 5% H_2O) to obtain white crystalline salinomycin with a purity of > 95%.

For the synthesis of the salinomycin silicates, the yellow solid with ca. 90% purity was used. For the synthesis of the least hindered silicate of salinomycin, **706a**, triethylamine was used as the base and triethoxychlorosilane (**305a**) was used as the silylating agent. With the addition of the monochlorosilane, the reaction turned cloudy right away. However LC-MS showed only a 50% conversion. The reaction mixture was allowed to stir at r.t. over the weekend, which showed full conversion of starting material to the product (ESI-APCI positive scan 930 $[m+NH_4]^+$, 935 $[m+Na]^+$). We attempted to purify the product by reverse phase MPLC (C18, 90:10, MeOH:H_2O), but could not isolate a product with sufficient purity as the bridged dimer $(EtO)_3Si\text{-}O\text{-}Si(OEt)_3$ was present in the fractions.

We next looked to increase the steric hindrance around the carboxylic acid with use of the triisopropoxychlorosilane (**305c**) and pyridine as the base. The

[203] Davis, A. L.; Harris, J. A.; Russell, C.; Wilkins, J. Investigations by HPLC-Electrospray Mass Spectrometry and NMR Spectroscopy Into the Isomerisation of Salinomycin. *Analyst* **1999**, *124*, 251-256.

reaction went smoothly to the product as confirmed by LC-MS product (ESI-APCI positive scan 972 $[m+NH_4]^+$, 977 $[m+Na]^+$). The product **705b** was purified by normal phase MPLC and fully characterized, found in the experimental section for this chapter.

To test the accessibility of the C-1 carboxylic acid, we used the sterically encumbered tri-tertbutoxychlorosilane (**305e**) and *N,N*-dimethylbutyl amine as the base. Unfortunately, the reaction did not go to completion even after heating to 35 ºC and waiting for 1 week. The LC-MS showed only a 5% conversion to the product (ESI-APCI positive scan 1014 $[m+NH_4]^+$, 1019 $[m+Na]^+$). from the starting material.

Scheme 7.3 I Synthesis of salinomycin silicates (**706a-c**).

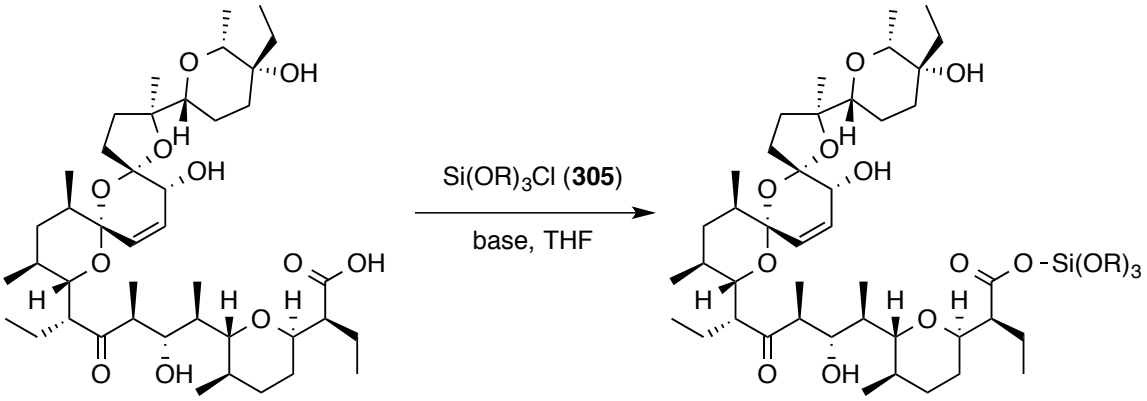

Salinomycin

705

706	***R***
a	***Et***
b	***^{i}Pr***
c	***^{t}Bu***

Lastly, a silane was made of salinomycin to serve as a reference for the complicated NMR spectra of the silicates **706**. Salinomycin and *N,N*-dimethylbutylamine were dissolved in THF and allowed to stir at r.t. for 5 mins. Triisopropylsiyl chloride (TIPS-Cl, **615**) was added by Wiretrol® and the reaction

mixture instantly turned cloudy. The mixture was stirred for 48 h. The THF was removed the solid residue was triturated with a mixture of hexanes:EtOAc (1:1), and the resulting slurry was filtered through a short plug of Celite® to remove the pyridinium salt. The filtrate was concentrated under reduced pressure, and the residue was purified by MPLC to yield the SAL-TIPS (**715**, not shown) as a white, crystalline solid. The full characterization can be found in the experimental section of this chapter.

With all the different silicates and silanes, we calculated the cLogP and cLogS shown in Table 7.1 (Chapter 7.2). We performed a cell viability assay with **706b** and the parent salinomycin. However, the concentrations tested were not sufficient to induce cell death (IC50 > 10 μM). Also the **706b** silicate was formulated into nanoparticles, which is presented in Chapter 7.3, Table 7.3.

7.1.4 5-Fluorouracil

5-Fluorouracil (5-FU**, 707**) is a pyrimidine analog that is a suicide inhibitor of thymidylate synthase. The irreversible binding makes 5-FU an important antimetabolite class drug for the treatment of a variety of cancers. 5-Fluorouracil is used for the treatment of breast, liver, ovarian, gastrointestinal, colon, head, and neck cancers.[204] The dose is typically given through I.V. like **PTX**, or a topical cream. We sought to apply the silicate prodrug technology to this drug in hopes of making nanoparticle formulations.

The pyrimidine analogue has two reactive nitrogen atoms that have been modified previously.[205,206] We looked to capitalize on this reactivity to make bis-

[204] Chi, G.; Wang, X.; Chen, R. Synthesis of Novel N1-(2-Furanidyl)-5-Fluorouracil Derivatives of A-Hydroxy (Thio) Phosphonates. *Heteroatom Chem.* **2002**, *13,* 211—215.

[205] Pizzirani, D.; Pagliuca, C.; Realini, N.; Branduardi, D.; Bottegoni, G.; Mor, M.; Bertozzi, F.; Scarpelli, R.; Piomelli, D.; Bandiera, T. Discovery of a New Class of Highly Potent Inhibitors of Acid Ceramidase: Synthesis and Structure-Activity Relationship (SAR). *J. Med. Chem.* **2013**, *56*, 3518–3530.

functionalized silicates that diminish the water solubility of the drug for further FNP formulation into nanoparticles. Since the parent compound is water soluble, the typical reaction conditions had to be modified. We simply used the base as the solvent to allow for homogenous conditions throughout the reaction, shown in Scheme 7.4.

Scheme 7.4 I Synthesis of bis-functionalized 5-fluorouracil silicates (**708a-c**).

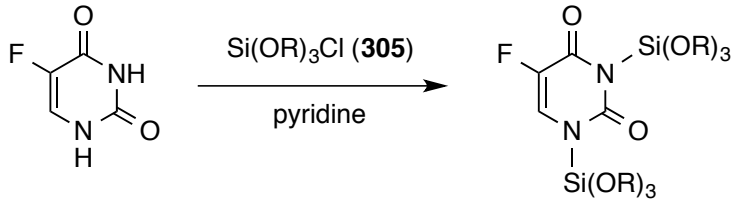

5-Fluorouracil

707

708	***R***
a	***Et***
b	***^{i}Pr***
c	***^{t}Bu***

Since the molecular weight for the 5-fluorouracil (**707**) starting material is low, we were pleased that it could be ionized and detected by GC-MS. Performing the gas phase analysis allowed us to observe the formation of products without the possibility of cleavage of the N-Si bond. The **708a** product was synthesized with pyridine as the base and triethoxychlorosilane (**305a**) as the silylating agent. GC-MS [30 m x 0.25 mm ID, HP-5, 50 °C/1.5 min/10 °C min-1/290 °C, (5029021)] with a retention time (t_R) of 9.03 min showed a mass to charge ratio [m/z] 454 ($M^{+\bullet}$), 439 ($M^{+\bullet}$ -CH_3), and 409 ($M^{+\bullet}$ -C_2H_5O) that matched the product. The **708b** product was synthesized with pyridine as the base and triisopropoxychlorosilane (**305c**) as the silylating agent. GC-MS [30 m x 0.25 mm

[206] Benci, K.; Wittine, K.; Radan, M.; Cetina, M.; Sedić, M.; Kraljević Pavelić, S.; Pavelić, K.; Clercq, E. D.; Mintas, M. The Unsaturated Acyclic Nucleoside Analogues Bearing a Sterically Constrained (Z)-4“-Benzamido-2-”Butenyl Moiety: Synthesis, X-Ray Crystal Structure Study, Cytostatic and Antiviral Activity Evaluations. *Bioorg. Med. Chem.* **2010**, *18*, 6249–6257.

ID, HP-5, 50 °C/1.5 min/10 °C min-1/290 °C, (5029021)] with a retention time (t_R) of 9.09 min showed a mass to charge ratio [m/z] 538 ($M^{+\bullet}$), and 479 ($M^{+\bullet}$ - C_3H_7O). Unfortunately, neither **708a** nor **708b** could be purified or isolated through silica gel chromatography.

We were delighted with the synthesis of **708c**, the tri-tertbutoxychlorosilane (**305e**) and pyridine cleanly converted the starting 5-fluorouracil to the product. The **708c** product was stable to purification and fully characterized in the experimental section of this chapter.

The calculated hydrophobicity and solubility for each silicate (**708a-c**) synthesized is tabulated in Table 7.1 (Chapter 7.2). Further studies were done with **708c**. The hydrolytic lability in the standard acidic conditions and in less acidic conditions was determined. An *in vitro* cytotoxicity assay against MDA-MB-231 was also performed. However, the dosing concentrations were too low to induce cell death. Lastly, the **708c** prodrug was loaded into nanoparticles, using the FNP process. The particle sizes are shown in Table 7.3 (Chapter 7.3). We are encouraged by the change in hydrophobicity demonstrated with this prodrug. The parent drug is completely water-soluble and upon silylation with **305e**, it becomes insoluble.

7.1.5 Dacarbazine

Dacarbazine (DTIC, **709**) is an alkylating agent that destroys cells though the irreversible addition of an alkyl group to the cell's DNA.[207] Dacarbazine is bioactivated by the liver through an oxidation followed by a subsequent demethylation. This intermediate then degrades to diazomethane, which is the

[207] Amirmostofian, M.; Pourahmad Jaktaji, J.; Soleimani, Z.; Tabib, K.; Tanbakosazan, F.; Omrani, M.; Kobarfard, F. Synthesis and Molecular-Cellular Mechanistic Study of Pyridine Derivative of Dacarbazine. *Iran J. Pharm. Res.* **2013**, *12*, 255–265.

true alkylating agent.[208] It is typically administered to cancer patients by I.V. under direct supervision of medical personal, and has been used in the treatment of Hodgkin lymphoma, sarcoma, pancreatic cancer, and malignant melanoma.

Modification of dacarbazine (**709**) has been studied before.[209] However, silylation has not been explored. We were interested in the biological activity and encouraged by the results of the benzamide and the 5-fluorouracil silicates. Due to the water solubility of **709**, we changed the reaction conditions to a stronger base and DMF as solvent.

Dacarbazine (**709**) and DBU were dissolved in DMF. The yellow reaction mixture was stirred for 5 mins and tri-tertbutoxychlorosilane (**305e**) was added by syringe, and the mixture turned completely clear after 30 mins. The DMF was removed by a high vacuum rotary evaporator and the residue was resuspended in a mixture of hexanes:EtOAc (2:1), filtered, and purified by normal phase chromatography to give the two different bis-functionalized silicates **710a** and **710b** as white crystalline solids (Scheme 7.5). The full experimental procedure and characterization is presented in the experimental section.

Scheme 7.5 I Synthesis of dacarbazine silicates **710a** and **710b**.

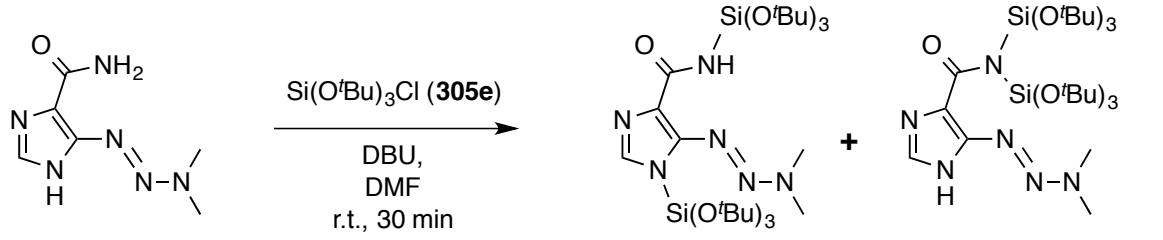

Dacarbazine ***709***

Dacarbazine-silicate ***710a***

Dacarbazine-silicate ***710b***

[208] Horton, J. K.; Stevens, M. F. A New Light on the Photo-Decomposition of the Antitumour Drug DTIC. *J. Pharm. Pharmacol.* **1981**, *33*, 808–811.

[209] Shealy, Y. F.; Krauth, C. A. Imidazoles. I. Coupling Reactions of 5-Diazoimidazole-4-Carboxamide. *J. Org. Chem.* **1962**, *27* (6), 2150-2154.

The calculated hydrophobicity (cLogP) and solubility (cLogS) for each silicate (**710a** and **710b**) is tabulated in Table 7.1. Further studies were done with **710a**. The hydrolytic lability in the less acidic conditions was determined (Table 7.2). An *in vitro* cytotoxicity assay against MDA-MB-231 was also performed however the dosing concentrations were too low to induce cell death. Lastly, the **710a** prodrug was loaded into nanoparticles, using the FNP process. The particle sizes are shown in Table 7.3. Again the drastic change in hydrophobicity demonstrated with this prodrug shows the power of the silicate prodrug strategy.

7.1.6 Imiquimod

Imiquimod (**711**) was discovered at the 3M pharmaceutical division as an immune response modifier. Although they were pursuing the drug and analogues for use as anti-viral for HSV-2 (herpes) and HIV prevention, imiquimod was shown to induce the production of cytokines, which in turn triggers an immune response to eradicate the foreign virus or cell. Due to its mechanism of action, **711** has been approved for the treatment of genital warts, actinic keratosis, and basal cell carcinoma.[210] It is administered as a cream for the skin conditions described above.

We were mainly interested in the free amine present in the molecule and whether it could be functionalized and the resulting derivatives purified. We were also interested in the topical cream, like 5-FU, application and envisioned that the increased hydrophobicity induced by the silicate prodrug methodology would increase the skin penetration when applied. We sought to apply the silicate methodology, to determine the *in vitro* cytotoxicity, and to test the stability of silicates made from **711**.

[210] Gerster, J. F.; Lindstrom, K. J.; Miller, R. L.; Tomai, M. A.; Birmachu, W.; Bomersine, S. N.; Gibson, S. J.; Imbertson, L. M.; Jacobson, J. R.; Knafla, R. T.; *et al.* Synthesis and Structure-Activity-Relationships of 1H-Imidazo[4,5-C]Quinolines That Induce Interferon Production. *J. Med. Chem.* **2005**, *48*, 3481–3491.

Scheme 7.6 I Synthesis of imiquimod silicate **712**.

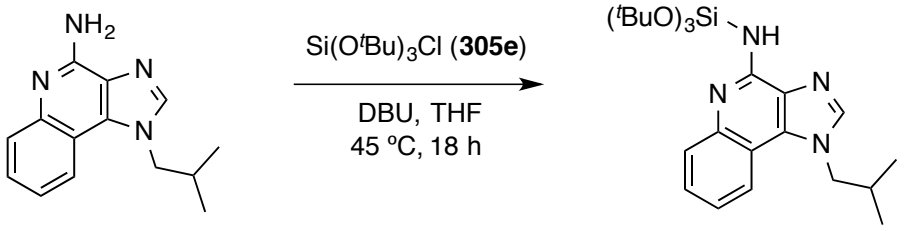

Imiquimod ***Imiquimod-silicate***

711 ***712***

Imiquimod **711** and DBU were dissolved in THF. The reaction mixture was stirred for 5 min and tri-*tert*-butoxychlorosilane (**305e**) was added by syringe and the mixture turned slightly cloudy. The mixture was heated to 45 °C for 18 h and more precipitate formed as the reaction progressed. The THF was removed and the residue was resuspended in a mixture of hexanes:EtOAc (1:1), filtered, and purified by MPLC to yield the imiquimod-silicate (**712**) as a white crystalline solid.

The calculated hydrophobicity (cLogP) and solubility (cLogS) for **711** and **712** are tabulated in Table 7.1 (Chapter 7.2). The hydrolytic lability was not determined, because the product was not very stable. When **712** was dissolved in $CDCl_3$, after two days ca. 50% had degraded back to the parent drug **711**. An *in vitro* cytotoxicity assay against MDA-MB-231 was also performed. However, the dosing concentrations were too low to induce cell death.

7.1.7 Ciprofloxacin

Ciprofloxacin is a fluoroquinolone that is in its second generation of development.[211] The drug inhibits DNA gyrase, which prevents the unraveling of supercoiled DNA, required for cell division and multiplication. By inhibiting this

[211] Ward, T. R.; Turunen, B. J.; Haack, T.; Neuenswander, B.; Shadrick, W.; Georg, G. I. Synthesis of a Quinolone Library From Ynones. *Tetrahedron Lett.* **2009**, *50*, 6494–9497.

enzyme, ciprofloxacin has been used as a broad-spectrum antibiotic. The medication has excelltent skin penetration and can be formulated for oral or I.V. administration.[212] It is the most widely used quinolone antibiotic, and has 12-FDA approvals for human use. It is also used in combination with other antibiotics in empirical treatment of infections where the bacterium hasn't been fully identified. It is however not effective against antibiotic resistant strains of bacteria.

Due to wide spread use, multiple ways of formulation, and structure we looked to employ the silicate prodrug methodology with this drug. Ciprofloxacin contains a piperazine ring, common to many pharmaceuticals. It also contains a carboxylic acid, which could also be functionalized.[213] In Scheme 7.7 the different silicate made of ciprofloxacin are shown.

Scheme 7.7 I Synthesis of ciprofloxacin silicates (**714a-b**).

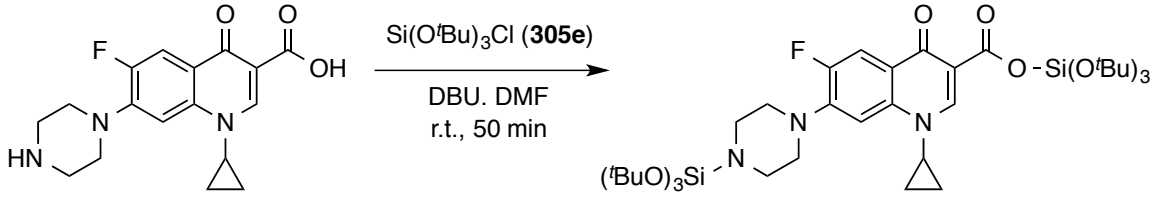

Ciprofloxacin ***Ciprofloxacin-silicate***

713 ***714***

Ciprofloxacin (**713**) and DBU were dissolved in 4 mL of DMF. The green-yellow reaction mixture was stirred for 5 mins and tri-*tert*-butoxychlorosilane (**305e**) was added. The reaction turned clear after 50 mins. The DMF was removed by a high vacuum rotary evaporator and the yellow oil residue was

[212] Varanda, F.; de Melo, M. P.; Caco, A. I. Solubility of Antibiotics in Different Solvents. 1. Hydrochloride Forms of Tetracycline, Moxifloxacin, and Ciprofloxacin. *Ind. Eng. Chem. Res.* **2006**, *45,* 6368−6374.

[213] Zieba, A.; Maślankiewicz, A.; Sitkowski, J. 1H, 13C and 15N NMR Spectra of Ciprofloxacin. *Magn. Reson. Chem.* **2004**, *42*, 903–904.

resuspended in a mixture of hexanes:EtOAc, filtered, and purified by MPLC to yield **714** as a white crystalline solid.

The cLogP and cLogS for the ciprofloxacin-silicate **714** and the parent drug **713** is tabulated in Table 7.1. The hydrolytic lability in both acidic conditions was determined by *in situ* NMR monitoring (Table 7.2). An *in vitro* cytotoxicity assay against MDA-MB-231 was also performed. However, the dosing concentrations were too low to induce cell death. Lastly, the **714** prodrug was loaded into nanoparticles, using the FNP process. The particle sizes are shown in Table 7.3 (Chapter 7.3).

7.1.8 Erlotinib and Gefitinib

Erlotinib (**713**) and gefitinib (not shown) are both epidermal growth factor receptor (EGFR) inhibitors. This inhibition blocks signaling in cancer cells that over express EGFR. Both are used for the treatment of non-small cell lung cancer as well as pancreatic cancer.[214] They both contain a secondary amine positioned between two aromatic rings.[215] We envisioned that the silicate methodology could functionalize this amine.

Unfortunately a stable silicate prodrug could not be made from either erlotinib or gefitinib. We exhaustively altered the reaction conditions to generate the product but all attempts failed. Briefly the monochlorosilanes (**305a-e**) were all tried with a variety of bases [pyridine, *N,N*-dimethylbutylamine, sodium hexamethyldisilazide (NaHMDS), sodium hydride (NaH), butyl lithium (*n*-BuLi), and diisopropylethyl amine (DIPEA)] at different temperatures [-78 ºC, r.t., and 35-45 ºC] and different durations of reaction [4 h – 1 week]. We were successful

[214] Rocha-Lima, C. M.; Soares, H.P.; Raez, L. E.; Singal, R. EGFR Targeting of Solid Tumors. *Cancer Control.* **2007**, *14,* 295-304.

[215] Marzaro, G.; Guiotto, A.; Pastorini, G.; Chilin, A. A Novel Approach to Quinazolin-4(3H)-One via Quinazoline Oxidation: an Improved Synthesis of 4-Anilinoquinazolines. *Tetrahedron* **2010**, *66*, 962–968.

when methyl iodide was used as the electrophile instead of a monochlorosilane, which shows that the secondary amine is moderately reactive. We were pleased when a more reactive silane, triisopropylsilyl trifluoromethanesulfonate (**717**), afforded the erlotinib silane **718**.

Scheme 7.8 I Synthesis of erlotinib silane **718**.

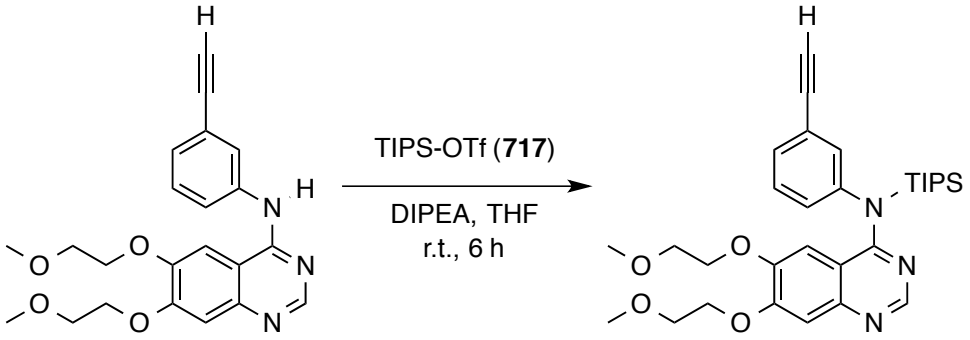

Erlotinib

716 ***718***

Erlotinib (**716**) and diisopropylethylamine (DIPEA) were dissolved in THF. The reaction mixture was stirred for 5 mins and triisopropylsilyl trifluoromethanesulfonate (**717**) was added by syringe and the mixture turned yellow. The mixture was stirred for 6 h and a white precipitate formed as the reaction progressed. The THF was removed and the residue was resuspended in a mixture of hexanes:EtOAc, filtered, and purified by MPLC to yield **718** as a white crystalline solid.

Encouraged by this, we reacted triethoxychlorosilane (**305a**) or triisopropoxychlorosilane (**305c**) with triflic acid followed by a subsequent reaction of crude mixture with erlotinib. Even though color changes (red-green) were observed, only the starting material could be recovered. After many attempts we abandoned the pursuit of silicate prodrugs of erlotinib or gefitinib.

7.2 Hydrophobicity and Hydrolytic Lability of Novel Silicate Prodrugs

7.2.1 Hydrophobicity Indicators for Novel Silicate Prodrugs

The relative hydrophobicities of the silicate esters was assessed in several ways. Qualitatively, we observed the expected trend that the silicates with greasier alkyl groups traveled faster on silica gel during thin layer and preparative chromatographic experiments. In addition, two empirical indicators of hydrophobicity show similar trends: *i.*) calculated octanol:water partition coefficients (cLogP values, Table 7.1, column 3)[132] and *ii.*) calculated aqueous solubilities (Table 3.1, column 4-5).[133] Recall, It has been noted that calculated hydrophobicities can vary tremendously depending on the weights assigned for each functional group in the empirical equations.

The power of the silicate prodrug strategy can be clearly seen in the case of the water soluble drugs (**707**, **709**, **711**, and **713**) which all have calculated aqueous solubility above 50 mg/mL. Once functionalized as a silicate the water solubility drops to below to around 5 mg/mL ca. 10 times less soluble than the original drug. Although this non-traditional approach to prodrug fabrication appears to go in the opposite direction in terms of administration, the silicate prodrug affinity for the polyester core of a nanoparticle is drastically increased.

Table 7.1 I Hydrophobicity indicators for the drugs and silicate prodrugs **701–718.**

Compound Number	Short Hand Descriptor	calcd octanol:water partition coeffient (cLogP)[132]	calcd water solubility coeffient (cLogS)[132]	Calculated aqueous solubility[133] (mg/L)
701	Dexamethasone	1.93	-3.89	20.5
702a	Dex-Si(OEt)$_3$	3.78	-4.72	8.92
702b	Dex-Si(O^{n}Oct)$_3$	8.28	-7.07	0.85
702c	Dex-Si(O^{i}Pr)$_3$	4.52	-5.31	4.94
703	Ibuprofen	3.50	-3.48	30.8
704	Ibu-Si(O^{t}Bu)$_3$	7.46	-6.8	1.11
705	Salinomycin	4.48	-5.4	4.52
706a	Sal-Si(OEt)$_3$	6.05	-5.61	3.66
706b	Sal-Si(O^{i}Pr)$_3$	6.52	-5.81	3.00
706c	Sal-Si(O^{t}Bu)$_3$	7.15	-6.26	1.91
715	Sal-TIPS	7.20	-6.39	1.68
707	5-Fluorouracil	-0.58	-1.35	259
708a	5-FU-[Si(OEt)$_3$]$_2$	3.61	-4.29	13.70
708b	5-FU-[Si(O^{i}Pr)$_3$]$_2$	5.14	-5.33	4.84
708c	5-FU-[Si(O^{t}Bu)$_3$]$_2$	6.92	-6.84	1.07
709	Dacarbazine	-0.32	-2.13	119
710a	Dacarb-[Si(O^{t}Bu)$_3$]$_2$	7.24	-5.32	4.89
710b	Dacarb-N[Si(O^{t}Bu)$_3$]$_2$	6.77	-5.86	2.85
711	Imiquimod	2.83	-2.99	50.3
712	Imiq-Si(O^{t}Bu)$_3$	7.17	-5.24	5.30
713	Ciprofloxacin	-0.57	-2.39	91.6
714	Cipro-[Si(O^{t}Bu)$_3$]$_2$	8.18	-5.39	4.56
716	Erlotinib	3.13	-4.64	9.66
718	Erlot-TIPS	5.99	-5.42	4.43

7.2.2 Hydrolytic Lability of Novel Silicate Prodrugs

We anticipated that these silicates would also differ in their hydrolytic lability based upon the nature of the oxygen-silicon or nitrogen-silicon bond. Each silicate that was tested contained the bulkiest alkoxy moieties (-O^{t}Bu) around the silicon center. As before we explored the acid lability by a ^{1}H NMR spectroscopy-

based method[118] to establish the relative rates of chemical hydrolysis of the derivatives (Table 7.2). By design, these silicate esters were sufficiently highly hydrophobic to render them only marginally soluble in buffered aqueous solutions. To get a meaningful fundamental understanding of the hydrolytic lability under acidic conditions, we deemed it essential to identify a common set of conditions under which each of the silicates would be fully soluble—that is, homogeneity is paramount. We determined that a 10:1 (vol:vol) ratio of acetone:water would solubilize all of these silicates at concentrations suitable for NMR analysis. We then established that use of 1% TFA in this solvent mixture (measured pH = 0.8–1.2) at ambient temperature led to rates of silicate ester cleavage that could be conveniently monitored spectroscopically. Alternatively the use of 1% acetic acid (AcOH) in this solvent mixture (measured pH = 2.8) at ambient temperature led to rates of silicate ester cleavage that could more conveniently be monitored when the use of TFA was too fast.

The change in intensity over time of the chemical shifts of distint resonances of each silicate, and/or the -OC(CH_3)$_3$ resonances in the R groups as the silicates were cleaved to release the drug and *t*-butanol was monitored. The half-life of each silicate is indicated in Table 7.2 as well as the observed rate $K_{obs.}$ Although no trend in steric bulk was tested for the silicates chosen as was done in the taxane case (Chapter 3), the general lability is clearly shown depending on the nature of silicate prodrug.

Table 7.2 I Hydrolytic lability of silicate prodrugs **704, 708c, 710a, and 714.**

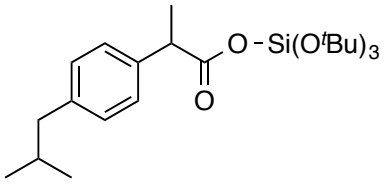

704

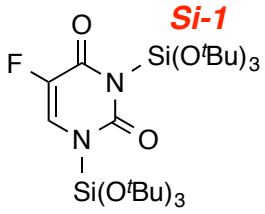

708c

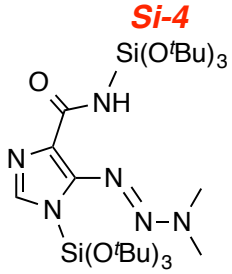

710a

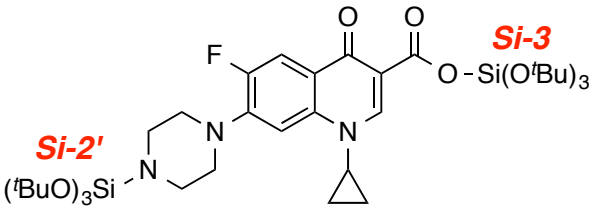

714

Compound Number	Short Hand Descriptor	TFA		AcOH	
		$t_{1/2}$ (min)	Kobs (s^{-1})	**$t_{1/2}$ (min)**	Kobs (s^{-1})
704	Ibu-Si(O^{t}Bu)$_3$	3,100 ± 580	3.8 x 10^{-6}	–	–
708c	5-FU-[Si(OtBu)$_3$]$_2$ (Si-1), (Si-3)	2.6	4.5 x 10^{-3}	45,000 ± 6.900	2.6 x 10^{-7}
710a	Dacarb-[Si(OtBu)$_3$]$_2$ (Si-4)	–	–	7.4 ± 0.9	1.6 x 10^{-3}
710a	Dacarb-[Si(OtBu)$_3$]$_2$ (Si-2)	–	–	510 ± 14	2.3 x 10^{-5}
714	Cipro-[Si(OtBu)$_3$]$_2$ (Si-2')	3.8	3.0 x 10^{-3}	7.2 ± 2.0	1.7 x 10^{-3}
714	Cipro-[Si(OtBu)$_3$]$_2$ (Si-3)	21	5.5 x 10^{-4}	6,900 ± 870	1.7 x 10^{-6}

The nitrogen-silicon bond is the most labile as shown with the amide-silicate at Si-4 of the dacarbazine silicate prodrug **710a** and in **714** at Si-2'. The

half-life for cleavage for either bond is 7 mins in the less acidic conditions. This is a drastic difference for the 5-fluorouracil **708c**, which is 45,000 mins. Also no intermediate mono-functionalized 5-Fluorouracil silicate was found in the ^{1}H-NMR spectrum. Both of the silicates degrade at near the same rate or when the first falls off the other is quickly lost. We presume the much slower rate is due to the steric congestion around the drug by the close proximity of both silicate groups. This can be also seen in the imidazole silicon bond in **710a**, as its half life is 510 mins. Lastly, the two carboxylic acid silicates **704** and **714** show considerable differences in the rate of cleavage due to the nature of the rest of the drug. Although the hydrolysis rates show the inherit stability of the novel silicate prodrugs, we were excited to test them in our FNP process and determine if stable nanoparticles could be made.

7.3 Nanoparticle Formulations of Novel Silicate Prodrugs

Nanoparticles preparations were made as presented in Chapters 2, 4, and 6. We were encouraged by the nanoparticle formulations loaded with the cinnamic-silicate and the morpholine-silicate. The 5-fluorouracil-silicate **708c** (8.9 mg) and a mPEG-*b*-PLGA block copolymer (5k-10k, 6.3 mg) were dissolved in 1.5 mL of THF. The THF solution was impingement mixed against 1.5 mL of H_2O in the FNP device. The resulting nanoparticles were diluted into 17 mL of water. From this suspension an aliquot of 20 μL was taken and diluted to 1 mL in a DLS cuvette.

Following the same procedure to produce 0.1 percent solids nanoparticle suspensions loaded at 50 wt% as above, three other novel silicate prodrugs (**706b**, **710a**, and **714**) were chosen to test the FNP conditions. The mass of each prodrug and mass of polymer used are presented in Table 7.3 (columns 3 and 4). The intensity average size (d_i) and the PDI of the resulting nanoparticle formulations are also shown in Table 7.3 (columns 5 and 6). The DLS plot for

706b nanoparticles can be found in the experimental section (Figure S7.1). Lastly, it was observed that particles above 500 nm were not very stable and tended to aggregate overtime.

Table 7.3 I Nanoparticles loaded with ca. 50 wt% of silicate prodrugs **704, 708c, 710a, and 714** and drug **707**.

Compound Number	Short Hand Descriptor	Amounts		DLS	
		Prodrug (mg)	Polymer (mg)	**d_i (nm)**	PDI
706b	Sal-Si(O^iPr)$_3$	5.8	7.0	132.0	0.081
707	5-Fluorouracil	6.4	5.2	513.7	0.240
708c	5-FU-[Si(OtBu)$_3$]$_2$	8.9	6.3	103.2	0.150
710a	Dacarb-[Si(OtBu)$_3$]$_2$	5.5	8.4	54 μm	–
714	Cipro-[Si(OtBu)$_3$]$_2$	6.4	6.3	159.6	0.227

We were very pleased with the DLS measurements of the freshly prepared nanoparticle suspensions. However as expected, when the suspensions containing 10% THF were allowed to stand for 1 week the particles ca. doubled in size and the PDI broadened, likely due to aggregation. We also froze and lyophilized the solutions after 1 week to determine if the prodrugs were still intact. ^{1}H-NMR analysis in $CDCl_3$ showed that: **706b** had degraded ca. 50%, **710a** had fully degraded (no resonances detected for the drug due to solubility in $CDCl_3$), and **714** had completely lost the silicate at the piperazine ring (Si-2') and 25% of the Si-3 carboxylic acid silicate had cleaved. A proton spectrum was not taken for the **706b** nanoparticles after 1 week in solution. Although the particles grew and degraded in suspension after 1 week, this was expected and enforces the prodrug strategy in that the silicates are cleaved within a week of aqueous treatment.

Only a handful of drugs were studied, we are very thrilled with the novel silicate prodrugs synthesized and formulated and have shown that the utility of

marrying the FNP process with the silicate methodology. We anticipate the use of this technology on new and old drug candidates that need to be packaged appropriately for subsequent administration. Many exciting new drug candidates fall through the pipeline due to undesirable properties that could be mitigated through nanoparticle formulation. Likewise, many old drugs have been discontinued due to side effects. The use of this technology has the potential to mitigate them and effectively deliver the drug to the proper site. We eagerly await the next chapter in the silicate prodrug loaded nanoparticle drug delivery.

Supplementary Information

For Chapters 2–7

General Experimental for Chapters 2–7

^{1}H, ^{13}C, and ^{19}F NMR spectra were taken on Varian Inova 500 (500 MHz), and Bruker Avance 500 (500 MHz, 400 MHz) spectrometers. ^{1}H NMR chemical shifts in $CDCl_3$ are referenced to TMS (0.00 ppm). Intractable multiplets resulting from overlap of one or more peaks are labeled as "m" and denoted with a range of ppm. ^{13}C NMR chemical shifts in $CDCl_3$ are referenced to chloroform (77.23 ppm). The following format is used to report resonances: chemical shift in ppm [multiplicity, coupling constant(s) in Hz, integral, and assignment]. ^{1}H NMR assignments are indicated by structure environment, e.g., CH_aH_b or numbering of the molecule. Some complex structures are numbered in order to simplify proton assignment numbering and naming. Coupling constant analysis was guided by methods we have described by Hoye and coworkers.[216,217]

Infrared spectra were recorded on a Midac Corporation Prospect 4000 FT-IR spectrometer. The most intense peaks are reported, and all spectra were collected in attenuated total reflectance (ATR) mode as thin films on a germanium window. High-resolution mass spectrometry (HRMS) measurements were performed on a Bruker BioTOF II (ESI-TOF) instrument using PEG as an internal standard/calibrant. Samples were introduced as solutions in CH_2Cl_2, methanol, or acetonitrile with sodium formate to assist in the ionization. LC-MS refers to liquid chromatography mass spectrometry, with different methods and columns which are described before diagnostic mass to charges are presented. Differential scanning calorimetry (DSC) was conducted on a TA Instruments

[216] Hoye, T. R.; Hanson, P. R.; Vyvyan, J. R. A practical guide to first-order multiplet analysis in ^{1}H NMR spectroscopy. *J. Org. Chem.* **1994**, *59*, 4096–4103.

[217] Hoye, T. R.; Zhao, H. A method for easily determining coupling constant values: An addendum to "A practical guide to first-order multiplet analysis in ^{1}H NMR spectroscopy." *J. Org. Chem.* **2002**, *67*, 4014–4016.

Discovery DSC (New Castle, DE). The instrument was calibrated using an indium standard. All samples were prepared using T-Zero hermetic pans (ca. 5 mg).

MPLC refers to medium pressure liquid chromatography (25-200 psi) using hand-packed columns of Silasorb silica gel (18-32 μm, 60 Å pore size) or Teledyne RediSep Gold Silica (20-40 μm, 60 Å pore size), a Waters 510 HPLC pump, a Waters R401 differential refractive index detector, and a Gilson 112 UV detector. Flash chromatography was performed using E. Merck silica gel (230-400 mesh). Thin layer chromatography was performed on glass or plastic backed plates of silica gel and visualized by UV detection and/or a solution of ceric ammonium molybdate, anisaldehyde, potassium permanganate, or phosphomolybdic acid.

Reactions requiring anhydrous conditions were performed under an atmosphere of nitrogen or argon in flame or oven dried glassware. Anhydrous THF, Et_2O, toluene, and CH_2Cl_2 were taken immediately prior to use after being passed through a column of activated alumina. Reported (external) reaction temperatures are the temperature of the heating bath. Those reactions carried out in deuterated solvents were performed directly in a capped 5 mm NMR sample tube.

Materials and Methods for Chapter 3

Triethylamine and pyridine were purified by distillation over CaH_2. *N,N*-Dimethyl-*n*-butylamine was stored over 3 Å molecular sieves. The known tri-*n*-octyloxychlorosilane, tri-*i*-propoxychlorosilane, trimenthyloxychlorosilane, and di-*t*-butoxydichlorosilane were synthesized from silicon tetrachloride and *n*-octanol, *i*-propanol, (–)-menthol, and *t*-butanol (the liquids, each dried over activated 3Å molecular sieves overnight), respectively. Tetrahydrofuran was dried by being

passed through an activated alumina column. Ethanol (anhydrous) was further dried by storing overnight over activated 3Å molecular sieves. Ethyl acetate (EtOAc, ACS grade) and hexanes (ACS grade) were used as received. The d_6-acetone and *d*-chloroform were dried over activated 3Å molecular sieves overnight. D_2O was used as received.

General Procedures for Chapter 3

All thin layer chromatography (TLC) data were collected on glass- or plastic-backed plates coated with F-254 indicator. Visualization was done by UV-light and/or staining with phosphomolybdic acid (PMA). Medium pressure liquid chromatography (MPLC) purifications were performed using columns dry-packed with ca. 25-35 μm silica gel. The MPLC apparatus was pressurized with a dual piston HPLC pump. Compound detection was performed by using a UV absorbance detector at 254 nm and a differential refractometer in series. Each silicate ester was purified by MPLC, under conditions that achieved effective separation of starting taxane, monosilicate, and bis-silicate esters, shortly before being used in the cytotoxicity study. Each compound whose cytotoxicity is reported in Table 3.4 was purified in this fashion, at which point it was shown to be of >95% purity by HPLC analysis in a C18- or C8-reversed phase column.

^{1}H NMR spectra were taken on a 500 MHz (^{1}H) instrument. All ^{1}H characterization spectra were taken in $CDCl_3$ and chemical shifts (δ) are referenced to tetramethylsilane at δ = 0.00. All ^{13}C NMR characterization spectra were taken in $CDCl_3$ on either a 125 MHz (^{13}C) or a 75 MHz (^{13}C) instrument and referenced to $CHCl_3$ at δ = 77.23. The following abbreviations are used to describe the NMR signals: s (singlet), d (doublet), t (triplet), q (quartet), sept (septet), m (multiplet), br (broad), and app (apparent). Coupling constants (*J*) are reported in Hz. High resolution mass spectra were collected on an ESI-TOF instrument using poly(ethylene glycol) (PEG) or poly(propylene glycol) (PPG) as

an internal standard. Infrared spectra were recorded using an FT-IR instrument. All samples were collected in attenuated total reflectance (ATR) mode as thin films on a germanium window. Melting point data were collected on a hot stage and are uncorrected.

Silicate Ester Hydrolysis Rate Studies:

The PTX-silicate (ca. 10 mg) was dissolved in 900 μL of d_6-acetone. To this homogenous solution, 100 μL of a 9:1 v/v solution of D_2O:TFA was added, and the solution was vigorously mixed. As instrumentation became more sensitive, the solvents were cut in half for the remainder of the hydrolysis experiments. ^{1}H NMR spectra were taken (16 or 32 transients) at 500 MHz at multiple time points (8-30) over the course of more than three half-lives for all but the slowest reacting silicates. The study was conducted at room temperature (rt = 22 °C ± 1.0 °C). The relative integration values were used to determine the extent of hydrolysis. Typically, resonances for the 2'- and/or 7-methine protons for the starting taxane silicate and the product free taxane (PTX or DTX) vs. that of H5 (a remote proton whose chemical shift was invariant for the two species) were integrated in a baseline-corrected spectrum using MestRe-C® or iNMR© software. Data were plotted as growth or decay curves as ln[species observed] vs. time. The slope of each linear correlation gave the reported k_{obs} value. The indicated errors are the observed standard deviation from three replications of the experiment. The $t_{1/2}$ values were calculated under the assumption that the process was pseudo-first order. The k_{rel} data presented in Table 3.2 are the ratios of k_{obs} for each silicate divided by that for the most slowly hydrolyzed silicate (**301d**).

***In vitro* Studies:**

*Cell Culture Cytotoxicity (IC_{50} Determination) Studies***.** MDA-MB-231 and MDA-MB-231 luciferase positive cells[218] were maintained independently in minimum essential medium (MEM) supplemented with 1% pen/strep and 10% fetal bovine serum (FBS) at 37 °C in a humidified incubator. MDA-MB-231 cells were obtained from the American Type Culture Collection. MDA-MB-231 Luc+ cells were obtained from Caliper Life Sciences. For cytotoxicity studies, MDA-MB-231 cells were seeded at 8,000 cells/well in a 96 well plate in 100μL MEM with 5% FBS. Taxane and taxane silicate stock solutions (10 mM) were prepared in DMSO. Each stock solution was serially diluted in MEM with 5% FBS and 100 μL of the solutions were pipetted into the 96 well plate. Concentration ranges were from 1–10,000 nM for PTX-silicates and 0.1–1000 for DTX-silicates. After 72 hours 30 μL of 3-(4,5-dimethylthiazol-2-yl)-2,5-diphenyltetrazolium (MTT) bromide reagent was added to each well. Absorbance at 490 nm was monitored on a 96 well plate UV/Vis detector at 60 minutes. Viable cells reduce the tetrazolium compound and the absorbance (and the concentration) of the product correlates to the number of viable cells. IC_{50} values were determined by nonlinear regression analysis of log concentration vs. response data obtained from the MTT assay. The IC_{50} was interpolated from the resulting curves using Graphpad Prism v5.1.

[218] Shahani, K.; Swaminathan, S. K.; Freeman, D.; Blum, A.; Ma, L.; Panyam, J. Injectable sustained release microparticles of curcumin: A new concept for cancer chemoprevention. *Cancer Res*. **2010** *70*, 4443–4452.

Materials and Methods for Chapter 4

β-Carotene (≥97%), betulin (≥98%), curcumin (≥80%), triethylamine (TEA; ≥99.5%), octanoic acid (≥98%), silicon tetrachloride (99%), water (H_2O; HPLC grade), methanol (HPLC grade), dichloromethane (anhydrous; ≥99.8%), and tetrahydrofuran (THF; HPLC grade) were purchased from Aldrich. Triethoxychlorosilane (95%) was purchased from Gelest Incorporated. Acetone was purchased as ACS grade from Fischer chemical. Acetone-d_6 (D, 99.9%) and D_2O (D, 99.9%) were purchased from Cambridge Isotope Laboratories Incorporated. Paclitaxel was obtained from Phytogen Life Sciences. 2,4,6-Triiodophenol was obtained from Alfa Aesar (98% purity). Hydrocortisone was obtained from MP Biomedical (99.6% by HPLC, USP). PS(10k)-b-PEG(5k) (M_w/M_n = 1.05) was purchased from Polymer Source. (D,L)-Lactide [or (rac)-lactide] was purchased from Altasorb and purified by recrystallization from toluene; glycolide was purchased from Altasorb and was purified by recrystallization from THF. Monomethoxy PEG (M_n = 2000 and 5000 $g \cdot mol^{-1}$, denoted mPEG(2k or 5k)-OH), PEG-diol (HO-PEG(5k)-OH), monomethoxy diethylene glycol, ε- caprolactone 97%, (1R)-(–)-10-camphorsulfonic acid (98%), and 1,8-diazabicyclo[5.4.0]undec-7-ene were purchased from Aldrich, and mPEG(10k)-OH was purchased from JenKem Technology. Prior to its use in synthesizing mPEG-containing BCPs, mPEG-OH was dried by azeotropic distillation from toluene or by dissolution in dry dichloromethane and storage overnight on oven-dried molecular sieves in an airtight culture tube.

The polymer PEG-b-PLGA (MW: 5k-10kDa) and suite of PTX-silicate prodrugs were synthesized as previously reported (Chapter 3). Paclitaxel was obtained from Phytogen Life Sciences. Water (H_2O, HPLC grade), tetrahydrofuran (THF, HPLC grade), and acetonitrile (ACN, HPLC grade) were

purchased from Sigma-Aldrich and used as received. CDCl3 was purchased from Cambridge Isotope Laboratories, Inc. Ethanol (anhydrous) was purchased from Decon Labs, Inc. Monosodium phosphate and disodium phosphate were purchased from Fisher Scientific. Phosphate buffered saline was prepared by dissolving 3.12 g of monosodium phosphate, 20.74 g of disodium phosphate, and 9 g of sodium chloride in 1 L of water to achieve a pH = 7.4. The 10 mM acetate buffer was prepared by dissolving 0.21 g of glacial acetic acid, 0.52 g of anhydrous sodium acetate, and 9 g of sodium chloride in 1 L of water to achieve a pH of 5.0. Slide-A-Lyzer dialysis mini capsules (MWCO: 10 kDa, 0.5-1 mL) were purchased from Thermo Scientific.

General Procedures for Chapter 4

4.3.3 Nanoparticle Morphology

The morphology of the nanoparticles was observed by cryo-TEM and the procedure was explained in detail previously.[219] Samples were prepared from either the nanoparticle suspension or the dried nanoparticle powder. A lacey carbon Cu grid (01881, 200-mesh, Ted Pella, Ltd., Redding, CA) was glow discharged in a vacuum evaporator at 70 mTorr (DV-502A, Denton Vacuum Moorestown, NJ) for 30 seconds to create a hydrophilic surface on the carbon coated side of the grid. A 2–3 μL volume of the fresh nanoparticle suspension was pipetted onto the carbon side at 22 °C in a Mark III Vitrobot chamber (FEI Company, Hillsboro, OR) with a relative humidity of ~100 %. The excess sample was blotted with grade 595 blotting paper (Ted Pella, Ltd., Redding, CA) once or twice with an ~1.5 mm offset parameter for 5 seconds to form a thin liquid film.

[219] Lee, H. S.; Morrison, E. D.; Frethem, C. D.; Zasadzinski, J. A.; McCormick, A. V.; Cryogenic electron microscopy study of nanoemulsion formation from microemulsions. *Langmuir* **2014,** *30,* 10826-10833.

Three seconds after blotting, the sample was plunged into liquid ethane cooled by liquid nitrogen.

The resulting vitrified sample was transferred to a Gatan 626 cryo-transfer unit (Gatan, Pleasanton, CA) at -194 °C and then characterized at -178 °C in the microscope. A 120 kV FEI Tecnai Spirit BioTWIN was used; images were taken digitally with an Eagle™ 2k CCD camera (FEI Company, Hillsboro, OR) in low-dose mode. The images were processed with the TEM Imaging and Analysis software package (version 4.2 SP1, build 816, FEI Company, Hillsboro, OR). To enhance the phase contrast, the images were deliberately under-focused to 2-4 μm with an objective lens. The degree of under-focus was controlled intentionally both to create Fresnel fringes (white rings on the boundary of nanoparticle structure) and to enhance the contrast between the core and shell regions in nanoparticles. Occasionally, beam damage was used to differentiate the polymer versus drug particles. In these instances, the diblock copolymer PEG-*b*-PLGA was susceptible to selective damage by the electron beam, producing bubbles.

4.3.4 Silicate Release Measurements

Lyophilized nanoparticles (15 mg) were redispersed in 15 mL of PBS buffer using micro-tip (1/8") sonication (Misonix Sonicator 3000, NY) in pulse mode for 5 minutes, with an increasing power of 3 to 9 volt within 1 minute. After every 1 minute of sonication, the tube containing nanoparticles was immersed in an ice/water bath to dissipate the heat generated by sonication. After 5 minutes, 500 µL aliquots of the nanoparticle suspension were placed into mini dialysis capsules (MW cutoff size: 10,000 Da, Pierce Biotech, Rockford, IL, US). A total of 30 capsules were immersed, 3 each, in ten 1L solutions of PBS buffer at pH 7.4 and, separately, pH 5.0. The beakers were held at 37 °C and agitated at 100 rpm

on an incubated orbital shaker. At predetermined time intervals (0, 1, 2, 4, 8, 12, 24, 48, 72, 96 h), three capsules were removed and frozen at -80 ºC. To assay the amount of PTX-silicate and **PTX** *remaining inside* particles at each time point, the contents of each frozen capsule were lyophilized for 24 h. Acetonitrile (1 mL) was added to each capsule of dried particles and buffer salts, and the resulting suspension was transferred to a 2 mL glass vial. The vial was capped, sealed with Parafilm M® to prevent evaporative loss, and allowed to stand overnight. Undissolved buffer salts remained at the bottom of the vials. An aliquot of the supernatant was analyzed by HPLC and the amounts of **PTX** and PTX-silicate were quantified against calibration curves. To assay the amount of *released* PTX-silicate and **PTX**, each 1 L external buffer solution was lyophilized in twenty-one 60 mL centrifuge tubes. The powdered contents of three sets of seven tubes were consolidated into three separate vials. Each was leached overnight with the same volume of acetonitrile and the supernatant assayed by HPLC as above. Release studies in pH 5.0 buffer were conducted using the same protocols.

4.3.6 *In vitro* Cell Growth Inhibition

Cytotoxicity studies were conducted using, MDA-MB-231 Luc+ breast cancer cells (Caliper Life Sciences, Hopkinton, MA). Cells were maintained in minimum essential medium (MEM) supplemented with 10% fetal bovine serum (FBS) and 1% penicillin/streptomycin in a humidified incubator held at 37 °C. For the cytotoxicity studies, MDA-MB-231 cells were seeded at 5,000 cells/well in a 96 well plate containing 100 μL of MEM supplemented with 5% FBS. Following attachment, cells were treated with free **PTX** or PTX-silicate prodrug-loaded nanoparticles. For free **PTX**, a stock solution was prepared in DMSO (10 mM) and then diluted in regular growth media. Cells were incubated with the **PTX** control or each of the loaded nanoparticle formulations for 4 hours, then washed with fresh medium and finally incubated with fresh medium for an additional 72

hours. Cell viability was determined at the end of the study using the MTT assay. Untreated cells and cells treated with empty nanoparticles were used as controls. The IC_{50} was interpolated from the resulting curves using Graphpad Prism (v5.1, Graphpad Software Inc. La Jolla CA, USA).

General Procedures for Chapter 5

In vivo Tumor Injection:

The entire animal studies were performed in accordance to the policies approved by the University of Minnesota's IACUC. Female Balb/c nu/nu immunocompromised mice were purchased from Charles River Labs (Wilmington MA, USA). For xenograft studies, 7.5 x 10^5 MDA-MB-231 Luc^+ cells were suspended in 100 μL of Dulbecco's phosphate buffered saline (DPBS) and mixed with an equal volume of Matrigel®. Subcutaneous injection into mammary pad #9, located near the left flank, was performed with a 26-gauge needle attached to a 0.5 cc syringe.

Based on the prodrug loading levels (Table S5.1), each nanoparticle formulation was weighed and resuspended in buffered saline such that a 10 microliter volume of the resulting nanoparticle suspension contained 40 micrograms of PTX-equivalent dose. Resuspension of the nanoparticles involved initial vortexing (ca. 1 min) followed by five cycles of probe sonication. Each cycle involved sonication for 1 minute at 5W, followed by 30 seconds of off time. Following probe sonication, 10 microliters of nanoparticle suspension was manually injected directly into tumors (average tumor volume ~100 mm). The mice were anaesthetized using isoflurane during nanoparticle administration. Tumor volume measurements were taken with an electronic caliper. Tumor volumes were calculated from the formula: Volume= (L^2 x W)/2. The day when treatments were administered was considered Day 0.

Experimental Section for Chapter 3

2'-*O*-[(Triethoxy)silyl]paclitaxel (301a).

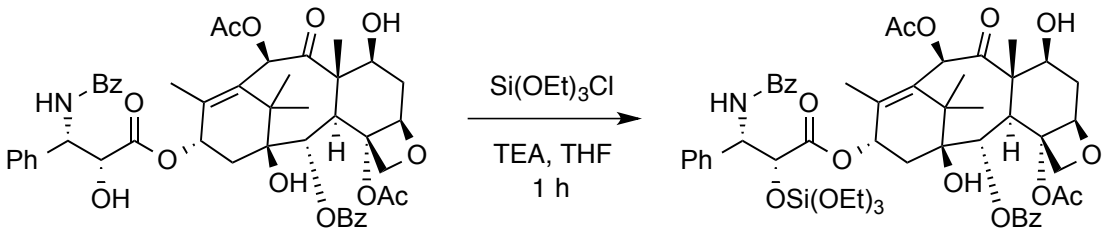

PTX ***301a***

Paclitaxel (55.3 mg, 0.0648 mmol, 1.0 equiv) was dissolved in dry THF (1.0 mL) in an oven-dried culture tube fitted with a Teflon-lined cap and magnetic stir bar. Triethylamine (20 μL, 0.130 mmol, 2.0 equiv) was added by Wiretrol®. Triethoxychlorosilane (**305a**) (25 μL, 0.0127 mmol, 2.0 equiv) was then added, and a white precipitate was immediately observed. The culture tube was sealed and the suspension was allowed to stir for 1 hour at room temperature. The reaction slurry was diluted with a mixture of hexanes:EtOAc (1:1) and filtered through a short plug of Celite® to remove the triethylammonium salt. The filtrate was concentrated under reduced pressure, and the residue was redissolved in a mixture of hexanes:EtOAc (1:1). Chromatography (SiO_2, 1:1 hexanes:EtOAc) via MPLC yielded the title compound as a white, crystalline solid (59.6 mg, 0.0587 mmol, 90.6%).

^{1}H NMR (500 MHz, $CDCl_3$): δ 8.12 (dd, J = 8.5, 1.4 Hz, 2H, C2O_2C-*o*-Ph), 7.78 (dd, J = 8.5, 1.3 Hz, 2H, C3'NHCO-*o*-Ph), 7.62 (tt, J = 7.5, 1.2 Hz, 1H, C2O_2C-

p-Ph), 7.56-7.46 (m, 3H, C2O_2C-*m*-Ph and C3'NHCO-*p*-Ph), 7.43-7.36 (m, 6H, C3'-*o*-Ph, C3'-*m*-Ph and C3'NHCO-*m*-Ph), 7.29 (tt, *J* = 6.5, 2.2 Hz, 1H, C3'-*p*-Ph), 7.19 (d, *J* = 8.6 Hz, 1H, C3'NH), 6.28 (s, 1H, H10), 6.24 (br dd, *J* = 9, 9 Hz, 1H, H13), 5.72 (dd, *J* = 8.5, 3.2 Hz, 1H, H3'), 5.68 (d, *J* = 7.1 Hz, 1H, H2), 4.97 (dd, *J* = 9.4, 2.0 Hz, 1H, H5), 4.96 (d, *J* = 3.3 Hz, 1H, H2'), 4.43 (ddd, *J* = 10.9, 6.4, 4.5 Hz, 1H, H7), 4.32 (d, *J* = 8.5 Hz, 1H, H20α), 4.20 (d, *J* = 8.5 Hz, 1H, H20β), 3.80 (d, *J* = 7.2 Hz, 1H, H3), 3.71 [q, *J* = 7.0 Hz, 6H, C2'OSi(OC*H_2*CH_3)$_3$], 2.56 (ddd, *J* = 14.7, 9.6, 6.5 Hz, 1H, H6α), 2.45 (s, 3H, C4OAc), 2.44 (br s, 1H, C7OH), 2.32 (dd, *J* = 15.4, 9.4, Hz, 1H, H14α), 2.24 (s, 3H, C10OAc), 2.08 (dd, *J* = 15.2, 8.8 Hz, 1H, H14β), 1.90 (d, *J* = 1.2 Hz, 3H, C18H_3), 1.89 (ddd, *J* = 14.5, 11.0, 2.4 Hz, 1H, H6β), 1.68 (s, 3H, C19H_3), 1.64 (br s, 1H, C1OH), 1.24 (s, 3H, C17H_3), 1.15 [t, *J* = 7.0 Hz, 9H, C2'OSi(OCH$_2$C*H_3*)$_3$], and 1.13 (s, 3H, C16H_3).

^{13}C NMR (75 MHz, $CDCl_3$): δ 204.0, 171.6, 171.0, 170.1, 167.3, 167.2, 143.0, 138.2, 134.2, 133.9, 132.9, 132.0, 130.4, 129.3, 128.9 (x2), 128.8, 128.2, 127.3, 126.8, 84.6, 81.2, 79.3, 76.7, 75.8, 75.3, 75.1, 72.3, 71.5, 59.7, 58.7, 55.6, 45.7, 43.4, 35.7, 35.6, 27.0, 23.0, 22.4, 21.1, 18.2, 14.9, and 9.8.

HRMS (ESI) Calc'd for $C_{53}H_{65}NNaO_{17}Si$ $[M + Na]^+$ 1038.3914, found 1038.3942.

IR (thin film) 3500 (br), 2977, 2898, 1744, 1730, 1636, 1580, 1540, 1487, 1452, 1371, 1314, 1268, 1240, 1170, 1145, 1078, 1025, 978, 908, 854, 797, and 710 cm^{-1}.

mp = 131-134 °C. **TLC** R_f (1:1 hexanes:EtOAc) = 0.45.

2-*O*-[(Tri-*n*-octyloxy)silyl]paclitaxel (301b).

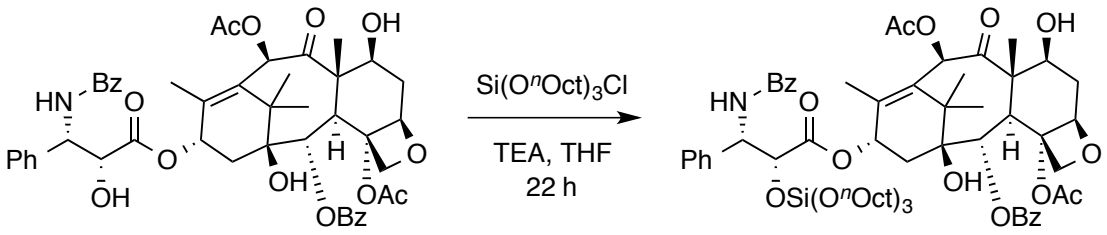

PTX ***301b***

Paclitaxel (76.0 mg, 0.0890 mmol, 1.0 equiv) was dissolved in dry THF (1.5 mL) in an oven-dried culture tube fitted with a Teflon-lined cap and magnetic stir bar. Triethylamine (60 μL, 0.430 mmol, 4.8 equiv) was added by Wiretrol®. A 1.67:1 mixture of tri-*n*-octyloxychlorosilane (**305b**):tetra-*n*-octyloxysilane (0.200 mg, 0.257 mmol, 2.9 equiv of tri-*n*-octyloxychlorosilane) was added and a white precipitate was immediately observed. The culture tube was capped and the suspension was allowed to stir for 22 h at room temperature. The reaction slurry was diluted with a mixture of hexanes:EtOAc (1:1), the slurry filtered through a short plug of Celite® to remove the triethylammonium salt, the filtrate concentrated under reduced pressure, and the residue redissolved in a mixture of hexanes:EtOAc (2:1). Chromatography (SiO_2, 2:1 hexanes:EtOAc) via MPLC yielded the title compound as a white, crystalline solid (91.5 mg, 0.0721 mmol, 81.0%).

^{1}H NMR (500 MHz, $CDCl_3$): δ 8.13 (dd, *J* = 8.5, 1.5 Hz, 2H, C2O_2C-*o*-Ph), 7.77 (dd, *J* = 8.5, 1.4 Hz, 2H, C3'NHCO-*o*-Ph), 7.62 (tt, *J* = 7.4, 1.3 Hz, 1H, C2O_2C-*p*-Ph), 7.55-7.46 (m, 3H, C2O_2C-*m*-Ph and C3'NHCO-*p*-Ph), 7.43-7.35 (m, 6H,

C3'-*o*-Ph, C3'-*m*-Ph and C3'NHCO-*m*-Ph), 7.28 (tt, *J* = 6.9, 1.7 Hz, 1H, C3'-*p*-Ph), 7.19 (d, *J* = 8.6 Hz, 1H, C3'NH), 6.28 (s, 1H, H10), 6.25 (br dd, *J* = 9, 9 Hz, 1H, H13), 5.72 (dd, *J* = 8.6, 3.2 Hz, 1H, H3'), 5.68 (d, *J* = 7.1 Hz, 1H, H2), 4.97 (dd, *J* = 9.8, 2.1 Hz, 1H, H5), 4.96 (d, *J* = 3.2 Hz, 1H, H2'), 4.44 (ddd, *J* = 10.9, 6.7, 4.2 Hz, 1H, H7), 4.31 (d, *J* = 8.4 Hz, 1H, H20α), 4.20 (d, *J* = 8.3 Hz, 1H, H20β), 3.80 (d, *J* = 7.1 Hz, 1H, H3), 3.61 {t, *J* = 6.8 Hz, 6H, C2'OSi[OCH_2(CH_2)$_6$$CH_3$]$_3$}, 2.56 (ddd, *J* = 14.8, 9.6, 6.6 Hz, 1H, H6α), 2.47 (d, *J* = 4.1 Hz, 1H, C7OH), 2.44 (s, 3H, C4OAc), 2.32 (dd, *J* = 15.4, 9.4 Hz, 1H, H14α), 2.24 (s, 3H, C10OAc), 2.07 (dd, *J* = 15.4, 8.8 Hz, 1H, H14β), 1.89 (d, *J* = 1.4 Hz, 3H, C18H_3), 1.89 (m, 1H, H6β), 1.68 (s, 3H, C19H_3), 1.65 (br s, 1H, C1OH), 1.48 [tt, *J* = 6.9, 6.9 Hz, 6H, C2'OSi(OCH_2CH_2(CH_2)$_5$$CH_3$)$_3$], 1.32-1.22 {m, 33H, C2'OSi[OCH_2CH_2(CH_2)$_5$$CH_3$]$_3$ and C17H_3}, 1.13 (s, 3H, C16H_3), and 0.88 {t, *J* = 6.9 Hz, 9H, C2'OSi[OCH_2CH_2(CH_2)$_5$CH_3]$_3$}.

^{13}C NMR (75 MHz, $CDCl_3$): δ 204.0, 171.5, 170.9, 170.1, 167.2, 167.2, 143.0, 138.3, 134.3, 133.9, 132.9, 132.0, 130.4, 129.3, 128.9 (x2), 128.8, 128.1, 127.3, 126.8, 84.7, 81.2, 79.3, 76.6, 75.8, 75.3, 74.9, 72.4, 71.4, 64.1, 58.7, 55.5, 45.7, 43.4, 35.8, 35.7, 32.4, 32.0, 29.54, 29.52, 27.0, 25.8, 23.0, 22.9, 22.4, 21.1, 14.9, 14.3, and 9.8.

HRMS (ESI) Calc'd for $C_{71}H_{101}NNaO_{17}Si$ $[M + Na]^+$ 1290.6731; found 1290.6749.

IR (thin film) 2926, 2855, 1730, 1665, 1643, 1602, 1581, 1518, 1484, 1453, 1371, 1312, 1271, 1240, 1174, 1094, 1025, 985, 926, 907, 851, 801, 777, and 711 cm^{-1}.

mp = 60–63 °C. **TLC** R_f (3:1 hexanes:EtOAc) = 0.15.

2'-*O*-[(Tri-*i*-propoxy)silyl]paclitaxel (301c).

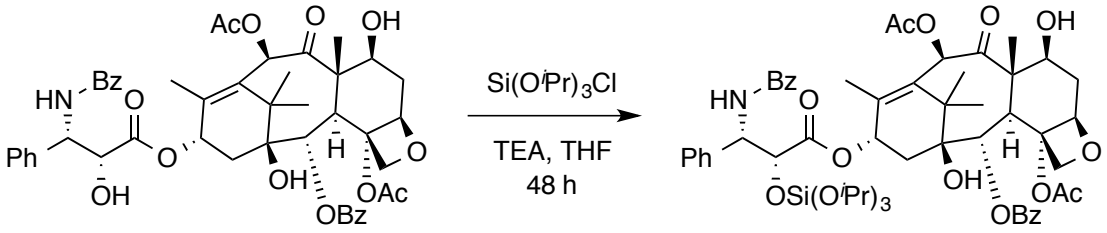

PTX ***301c***

Paclitaxel (38.8 mg, 0.0454 mmol, 1.0 equiv) was dissolved in dry THF (1.0 mL) in an oven-dried culture tube fitted with a Teflon-lined cap and magnetic stir bar. Triethylamine (25 μL, 0.179 mmol, 3.9 equiv) was added by Wiretrol®. A 2.9:1 mixture of tri-*i*-propoxychlorosilane (**305c**) : tetra-*i*-propoxysilane (0.155 mg, 0.132 mmol, 2.9 equiv of tri-*i*-propoxychlorosilane) was added. The culture tube was capped and a white precipitate was observed within minutes. The suspension was stirred at room temperature for 48 hours and the cloudy, heterogeneous reaction mixture was noted to be slightly yellowed. The suspension was diluted with a mixture of hexanes:EtOAc (1:1), the slurry filtered through a short plug of Celite® to remove the triethylammonium salt, the filtrate concentrated under reduced pressure, and the residue redissolved in a mixture of hexanes:EtOAc (1:1). Chromatography (SiO_2, 1:1 hexanes:ethyl acetate) via MPLC yielded the title compound as a white, crystalline solid (31.1 mg, 0.0294 mmol, 64.7%).

^{1}H NMR (500 MHz, $CDCl_3$): δ 8.11 (dd, J = 8.5, 1.4 Hz, 2H, C2O_2C-*o*-Ph), 7.79 (dd, J = 8.4, 1.3 Hz, 2H, C3'NHCO-*o*-Ph), 7.62 (tt, J = 7.6, 1.3 Hz, 1H, C2O_2C-

p-Ph, 1H), 7.55-7.47 (m, 3H, C2O_2C-*m*-Ph and C3'NHCO-*p*-Ph), 7.44-7.35 (m, 6H, C3'-*o*-Ph, C3'-*m*-Ph and C3'NHCO-*m*-Ph), 7.27 (tt, *J* = 7.0, 1.7 Hz, 1H, C3'-*p*-Ph), 7.17 (d, *J* = 8.5 Hz, 1H, C3'NH), 6.28 (s, 1H, H10), 6.19 (br dd, *J* = 9, 9 Hz, 1H, H13), 5.69 (dd, *J* = 8.5, 3.6 Hz, 1H, H3'), 5.68 (d, *J* = 6.7 Hz, 1H, H2), 4.98 (d, *J* = 3.6 Hz, 1H, H2'), 4.96 (dd, *J* = 9.7, 2.4 Hz, 1H, H5), 4.44 (ddd, *J* = 10.9, 6.6, 4.1 Hz, 1H, H7), 4.31 (d, *J* = 8.4 Hz, 1H, H20α), 4.20 (d, *J* = 8.4 Hz, 1H, H20β), 4.13 {sept, *J* = 6.1 Hz, 3H, C2'OSi[OC*H*$(CH_3)_2]_3$}, 3.80 (d, *J* = 7.1 Hz, 1H, H3), 2.56 (ddd, *J* = 14.8, 9.8, 6.6 Hz, 1H, H6α), 2.47 (d, *J* = 4.1 Hz, 1H, C7OH), 2.42 (s, 3H, C4OAc), 2.29 (dd, *J* = 15.4, 9.4 Hz, 1H, H14α), 2.24 (s, 3H, C10OAc), 2.06 (dd, *J* = 15.4, 8.9 Hz, 1H, H14β), 1.91 (d, *J* = 1.4 Hz, 3H, C18H_3), 1.88 (ddd, *J* = 14.3, 11.0, 2.4 Hz, 1H, H6β), 1.76 (br s, 1H, C1OH), 1.68 (s, 3H, C19H_3), 1.23 (s, 3H, C17H_3), 1.15 {d, *J* = 6.1 Hz, 9H, C2'OSi[OCH$(CH_3)_a$(CH_3)$_b]_3$}, 1.12 {d, *J* = 6.1 Hz, 9H, C2'OSi[OCH(CH_3)$_a$(CH_3)$_b]_3$}, and 1.12 (s, 3H, C16H_3).

^{13}C NMR (125 MHz, $CDCl_3$): δ 204.1, 171.5, 171.1, 170.1, 167.3, 167.2, 143.1, 138.3, 134.4, 133.9, 132.9, 131.9, 130.4, 129.4, 128.9 (x2), 128.8, 128.1, 127.3, 127.0, 84.7, 81.2, 79.3, 76.7, 75.9, 75.3, 74.9, 72.3, 71.5, 66.7, 58.7, 55.8, 45.7, 43.4, 35.8, 35.7, 27.0, 25.44, 25.42, 23.0, 22.4, 21.1, 15.2, and 9.8.

HRMS (ESI) Calc'd for $C_{56}H_{71}NNaO_{17}Si$ $[M + Na]^+$ 1080.4383; found 1080.4380.

IR (thin film) 3500 (br), 2974, 2934, 1729, 1666, 1603, 1583, 1515, 1485, 1452, 1371, 1313, 1269, 1241, 1174, 1114, 1052, 985, 897, 850, 800, 773, and 712 cm^{-1}.

mp = 126–129 °C. **TLC** R_f (1:1 hexanes:EtOAc) = 0.45.

2'-[(Trimenthyloxy)silyl]paclitaxel (301d).

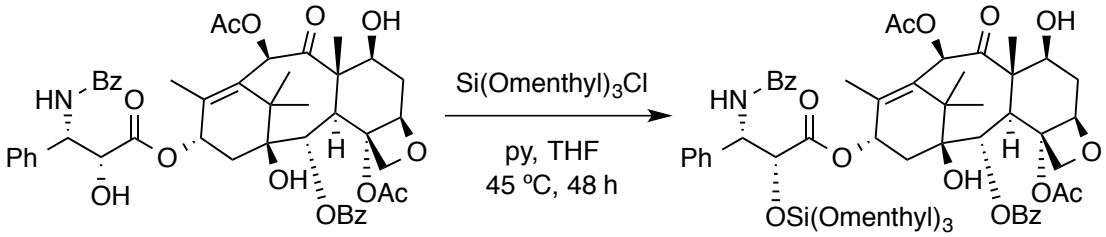

PTX ***301d***

Paclitaxel (95.0 mg, 0.111 mmol, 1.0 equiv) was dissolved in dry THF (8.0 mL) in an oven-dried culture tube fitted with a Teflon-lined cap and magnetic stir bar. Pyridine (100 μL, 1.24 mmol, 11.2 equiv) was added by Wiretrol®. Trimenthyloxychlorosilane (**305d**, judged to contain 90% of the chlorosilane (579.1 mg, 0.986 mmol, 8.9 equiv) by ^{1}H NMR analysis, was added by Wiretrol®. The culture tube was capped and the suspension was allowed to stir for 12 h at 45 ºC. The THF was removed by evaporation under reduced pressure, the solid residue was triturated with a mixture of hexanes:EtOAc (3:1), and the resulting slurry was filtered through a short plug of Celite® to remove the pyridinium salt. The filtrate was concentrated under reduced pressure, and the residue was purified by MPLC (SiO_2, 3:1 hexanes:EtOAc) to yield the title compound as a white, crystalline solid (94.2 mg, 0.069 mmol, 62%).

^{1}H NMR (500 MHz, $CDCl_3$): δ 8.11 (dd, *J* = 8.3, 1.3 Hz 2H, O_2C-*o*-Ph, 7.77 (dd, *J* = 8.1, 1.0 Hz, 2H, C3'NHCO-*o*-Ph), 7.60 (tt, *J* = 7.4, 1.3 Hz, 1H, C2O_2C-*p*-Ph), 7.53-7.47 (m, 3H, C2O_2C-*m*-Ph and C3'NHCO-*p*-Ph), 7.43-7.36 (m, 6H, C3'-*o*-Ph, C3'-*m*-Ph and C3'NHCO-*m*-Ph), 7.30 (tt, *J* = 7.0, 1.6 Hz, 1H, C3'-*p*-Ph), 7.11 (d, *J* = 8.5 Hz, 1H, C3'NH), 6.28 (s, 1H, H10), 6.22 (ddq, *J* = 10.3, 9.3,

1.4 Hz, 1H, H13), 5.72 (dd, *J* = 8.5, 3.5 Hz, 1H, H3'), 5.68 (d, *J* = 7.1 Hz, 1H, H2), 5.10 (d, *J* = 3.5 Hz, 1H, H2'), 4.97 (dd, *J* = 9.6, 2.3 Hz, 1H, H5), 4.45 (ddd, *J* = 10.8, 6.7, 4.1 Hz, 1H, H7), 4.30 (dd, *J* = 8.6, 0.9 Hz, 1H, H20α), 4.20 (d, *J* = 8.5, 1.1 Hz, 1H, H20β), 3.80 (d, *J* = 7.1 Hz, 1H, H3), 3.64 (ddd, *J* = 10.6, 10.6, 4.3 Hz, 3H, $H1_{menth}$), 2.57 (ddd, *J* = 14.8, 9.8, 6.6 Hz, 1H, H6α), 2.48 (d, *J* = 4.1 Hz, 1H, C7OH), 2.39 (s, 3H, C4OAc), 2.30 (dd, *J* = 15.3, 9.5 Hz, 1H, H14α), 2.25 (s, 3H, C10OAc), 2.20 (dsep, *J* = 2.6, 7.0 Hz, 3H, $H7_{menth}$), 2.12 (dd, *J* = 15.9, 9.0 Hz, 1H, H14β), 1.92-1.86 (m, 4H, $H6eq_{menth}$ and H6β), 1.88 (d, *J* = 1.3 Hz, 3H, H18 $=CCH_3$), 1.80 (s, 1H, C1OH), 1.68 (s, 3H, H19 $O=CCCH_3$), 1.61 (m, 3H, $H4eq_{menth}$), 1.58 (dddd, *J* = 13.0, 3.0, 3.0, 3.0 Hz, $H3eq_{menth}$), 1.28-1.24 (m, 6H, $H5_{menth}$), 1.25 (s, 3H, $C(Me)C16H_3$), 1.16-1.10 (dddd, 3H, *J* = 11.2, 11.2, 2.8, 2.8 Hz $H2_{menth}$), 1.14 [s, 3H, $C(Me)C17H_3$], 0.92 (ddd, *J* = 12, 12, 12 Hz, 3H, $H6ax_{menth}$), 0.91-0.85 (m, 3H, $H3ax_{menth}$), 0.87 (d, 9H, *J* = 7.1 Hz, $H8_{menth}$), 0.83 (d, *J* = 6.6 Hz, 9H, $H10_{menth}$), 0.83-0.77 (dddd, *J* = 12.3, 12.3, 12.3, 3.0 Hz, 3H, $H4ax_{menth}$), and 0.74 (d, *J* = 6.9 Hz, 9H, $H9_{menth}$).

^{13}C NMR (125 MHz, $CDCl_3$): δ 204.1, 171.6, 170.7, 170.0, 167.2, 167.1, 143.2, 138.1, 134.2, 133.8, 132.6, 132.0, 130.4, 129.3, 129.0, 128.9, 128.8, 128.1, 127.3, 126.9, 84.7, 81.1, 79.3, 76.7, 75.8, 75.3, 74.5, 74.2, 71.4 ($C1_{menth}$), 71.36, 58.7, 55.5, 49.7 ($C2_{menth}$), 45.6, 45.0 ($C7_{menth}$), 43.4, 35.9, 35.7, 34.5 ($C5_{menth}$), 31.7 ($C6_{menth}$), 27.0, 25.4 ($C3_{menth}$), 22.9 ($C4_{menth}$), 22.7, 22.5 ($C8_{menth}$), 22.4, 21.4 ($C9_{menth}$), 21.1, 15.8 ($C10_{menth}$), 15.1, and 9.8.

HRMS (ESI) Calc'd for $C_{67}H_{103}NNaO_{17}Si$ $[M + Na]^+$ 1368.7206; found 1368.7275.

IR (thin film) 3443, 2953, 2925, 2870, 1762, 1718, 1496, 1452, 1368, 1316, 1274, 1245, 1162, 1108, 1083, 1070, 1052, 1026, 987, 890, 765, and 751 cm^{-1}.

mp = 115–118.5 °C. **TLC** R_f (9:1 hexanes:EtOAc) = 0.20.

2'-*O*-[(Tri-*t*-butoxy)silyl]paclitaxel (301e).[a]

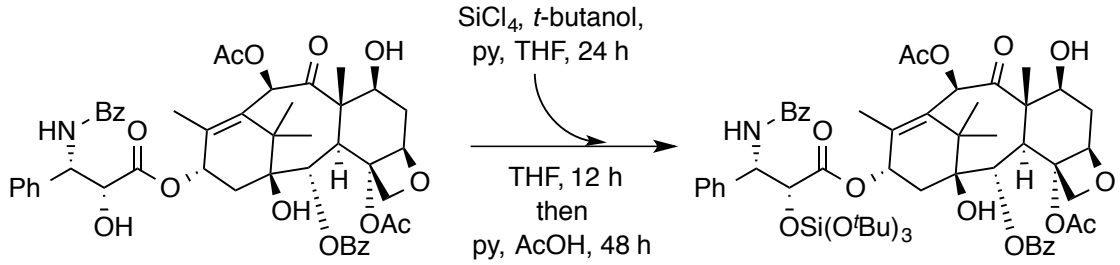

PTX ***301e***

[a]Compound synthesized by Dr. Wohl and included here for reference.

Paclitaxel (PTX, 49.8 mg, 0.0583 mmol, 1.0 equiv) was dissolved in dry THF (1.0 mL) in an oven-dried culture tube with a Teflon-lined cap and magnetic stir bar. In a separate oven-dried culture tube fitted with a Teflon-lined cap, $SiCl_4$ (0.40 mL, 2.6 mmol), pyridine (0.84 mL, 10.4 mmol), *t*-butanol (0.73 mL, 7.6 mmol), and THF (ca. 10 mL) were combined and the mixture was stirred for 24 h. A 1 mL aliquot of this silylating reagent mixture was added to the tube containing PTX. The culture tube was capped and the solution was allowed to stir at room temperature overnight. To the resulting suspension, additional pyridine (50 μL, 0.62 mmol, 13 equiv) and glacial acetic acid (50 μL, 0.87 mmol, 24 equiv) were added. The mixture was allowed to stir for an additional 48 hours at room temperature. The reaction suspension was diluted with EtOAc, the slurry was filtered through a short plug of Celite® to remove the pyridinium salt, the filtrate was concentrated under reduced pressure, and the residue was redissolved in a mixture of hexanes:EtOAc (2:1). Chromatography (SiO_2, 2:1 hexanes:EtOAc) via

MPLC yielded **301e** (11.2 mg, 0.0107 mmol, 18.4%). Material collected from two later eluting fractions gave mass spectral evidence for the chloride PTX-Si(O-*t*Bu)$_2$Cl (23.0 mg, 0.0212 mmol, 36.3%) and the silanol PTX-Si(O-*t*Bu)$_2$OH (8.6 mg, 0.0078 mmol, 13.4%).

^{1}H NMR (500 MHz, $CDCl_3$): δ 8.11 (dd, *J* = 8.8, 1.7 Hz, 2H, C2O$_2$C-*o*-Ph), 7.78 (dd, *J* = 8.8, 1.8 Hz, 2H, C3'NHCO-*o*-Ph), 7.61 (tt, *J* = 7.3, 1.2 Hz, 1H, C2O$_2$C-*p*-Ph, 1H), 7.56-7.34 (m, 9H, C2O$_2$C-*m*-Ph, C3'NHCO-*p*-Ph, C3'-*o*-Ph, C3'-*m*-Ph, and C3'NHCO-*m*-Ph), 7.30-7.24 (m, 1H, C3'-*p*-Ph), 7.05 (d, *J* = 8.5 Hz, 1H, C3'NH), 6.29 (s, 1H, H10), 6.17 (br dd, *J* = 9, 9 Hz, 1H, H13), 5.74-5.66 (m, 2H, H2 and H3'), 5.16 (d, *J* = 2.9 Hz, 1H, H2'), 4.97 (dd, *J* = 9.2, 2.3 Hz, 1H, H5), 4.45 (app br dd, *J* = 11, 6 Hz, 1H, H7), 4.31 (d, *J* = 8.4 Hz, 1H, H20α), 4.20 (d, *J* = 8.6 Hz, 1H, H20β), 3.80 (d, *J* = 7.0 Hz, 1H, H3), 2.57 (ddd, *J* = 15.2, 9.9, 6.7 Hz, 1H, H6α), 2.47 (br d, *J* = 4 Hz, 1H, C7OH), 2.42 (s, 3H, C4OAc), 2.32 (dd, *J* = 15.9, 9.6, Hz, 1H, H14α), 2.25 (s, 3H, C10OAc), 2.17 (br dd, *J* = 14, 5 Hz, 1H, H14β), 1.93 (br d, *J* = 1 Hz, 3H, C18H$_3$), 1.89 (br m, 1H, H6β), 1.78 (br s, 1H, C1OH), 1.68 (s, 3H, C19H$_3$), 1.24 {overlapping s, 27H, C2'OSi[OC(C*H$_3$*)$_3$]$_3$ and s, 3H, C17H$_3$}, and 1.13 (s, 3H, C16H$_3$).

^{13}C NMR (125 MHz, $CDCl_3$): δ 204.1, 171.6, 171.1, 170.1, 167.4, 167.2, 143.2, 138.3, 134.5, 133.9, 132.8, 131.9, 130.4, 129.4, 128.97, 128.95, 128.8, 128.0, 127.3, 126.9, 84.7, 81.2, 79.3, 76.7, 75.9, 75.3, 74.2, 73.9, 72.4, 71.4, 58.7, 55.5, 45.7, 43.4, 36.0, 35.7, 31.4, 27.0, 23.0, 22.4, 21.1, 15.3, and 9.8.

IR (thin film) 3500 (br), 2973, 2929, 1729, 1670, 1511, 1483, 1452, 1389, 1367, 1268, 1242, 1183, 1124, 1069, 1025, 985, 835, 800, 758, and 711 cm^{-1}.

HRMS (ESI) Calc'd for $C_{59}H_{77}NNaO_{17}Si$ $[M + Na]^+$ 1122.4853; found 1122.4901.

mp = 134–138 °C.

2'-*O*-[(Di-*t*-butoxy)(ethoxy)silyl]paclitaxel (301f).

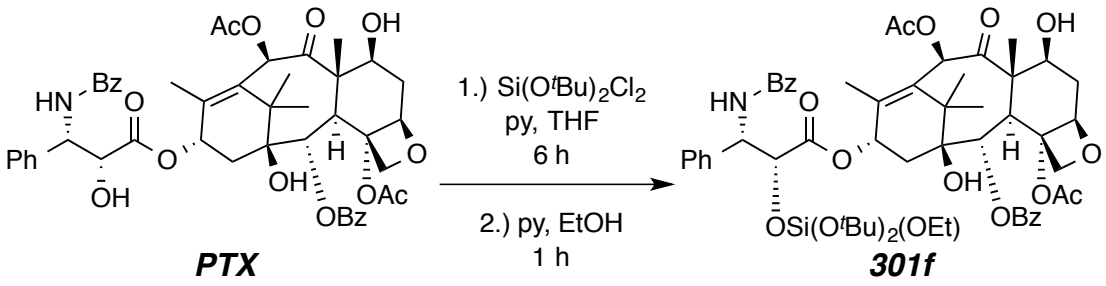

PTX ***301f***

Paclitaxel (111.0 mg, 0.13 mmol, 1.0 equiv) was dissolved in dry THF (3.0 mL) in an oven-dried culture tube fitted with a Teflon-lined cap and magnetic stir bar. Pyridine (100 μL, 1.24 mmol, 9.5 equiv) was added by syringe. A distilled sample of di-*t*-butoxydichlorosilane (**306**) (304.1 mg, 1.24 mmol, 10 equiv) was added by Wiretrol®. The culture tube was sealed and the solution was allowed to stir at room temperature. A small amount of a white precipitate was observed after ca. 30 minutes, and the reaction mixture was noted to be cloudy and heterogeneous after stirring for 6 hours. To this suspension, additional pyridine (100 μL, 1,24 mmol, 10 equiv) and anhydrous ethanol (dried overnight over 3Å molecular sieves, 1.0 mL, 17.2 mmol, 132 equiv) were added. The mixture was allowed to stir for one additional hour at room temperature. The suspension was diluted with a mixture of hexanes:EtOAc (1:1), the slurry was filtered through a short plug of Celite® to remove the pyridinium salt, the filtrate was concentrated under reduced pressure, and the residue was redissolved in a mixture of hexanes:EtOAc (2:1). Chromatography (SiO_2, 2:1 hexanes:EtOAc) via MPLC yielded the title compound as a white, crystalline solid (130.0 mg, 0.12 mmol, 93.3%).

^{1}H NMR (500 MHz, $CDCl_3$): δ 8.11 (dd, *J* = 8.5, 1.4 Hz, 2H, C2O_2C-*o*-Ph), 7.79 (dd, *J* = 8.4, 1.4 Hz, 2H, C3'NHCO-*o*-Ph), 7.62 (tt, *J* = 7.4, 1.3 Hz, 1H, C2O_2C-*p*-Ph, 1H), 7.56-7.46 (m, 3H, C2O_2C-*m*-Ph and C3'NHCO-*p*-Ph), 7.45-7.33 (m, 6H, C3'-*o*-Ph, C3'-*m*-Ph and C3'NHCO-*m*-Ph), 7.30-7.22 (m, 1H, C3'-*p*-Ph), 7.15 (d, *J* = 8.4 Hz, 1H, C3'NH), 6.28 (s, 1H, H10), 6.18 (br dd, *J* = 9, 9 Hz, 1H, H13), 5.68 (d, *J* = 7.2 Hz, 1H, H2), 5.66 (dd, *J* = 8.3, 3.6 Hz, 1H, H3'), 5.01 (d, *J* = 3.6 Hz, 1H, H2'), 4.97 (dd, *J* = 9.7, 2.3 Hz, 1H, H5), 4.44 (ddd, *J* = 10.8, 6.6, 4.1 Hz, 1H, H7), 4.31 (d, *J* = 8.4 Hz, 1H, H20α), 4.19 (d, *J* = 8.4 Hz, 1H, H20β), 3.79 (d, *J* = 7.0 Hz, 1H, H3), 3.64 (q, *J* = 7.0 Hz, 2H, C2'OSiOC*H_2*CH_3), 2.56 (ddd, *J* = 14.8, 9.7, 6.6 Hz, 1H, H6α), 2.45 (d, *J* = 4.1 Hz, 1H, C7OH), 2.41 (s, 3H, C4OAc), 2.28 (dd, *J* = 15.4, 9.4, Hz, 1H, H14α), 2.24 (s, 3H, C10OAc), 2.05 (dd, *J* = 15.3, 9.0 Hz, 1H, H14β), 1.90 (d, *J* = 1.4 Hz, 3H, C18H_3), 1.88 (ddd, *J* = 14.4, 11.1, 2.5 Hz, 1H, H6β), 1.68 (s, 4H, C1OH and C19H_3), 1.26 (s, 9H, C2'OSiOC(C*H_3*)$_2$], 1.25 (s, 9H, C2'OSiOC(C*H_3*)$_2$], 1.23 (s, 3H, C17H_3), and 1.13 (overlapping t, *J* = 7.0 Hz, 3H, C2'OSiCH_2C*H_3* and s, 3H, C16H_3).

^{13}C NMR (125 MHz, $CDCl_3$): δ 204.1, 171.5, 171.0, 170.0, 167.3, 167.2, 143.1, 138.4, 134.4, 133.9, 132.8, 131.9, 130.4, 129.4, 128.90, 128.89, 128.8, 128.1, 127.3, 127.0, 84.7, 81.2, 79.3, 76.6, 75.9, 75.3, 74.9, 73.99, 73.98, 72.3, 71.4, 59.3, 58.7, 55.8, 45.7, 43.4, 35.8, 35.7, 31.41, 31.38, 27.0, 22.9, 22.3, 21.1, 18.2, 15.1, and 9.8. IR (thin film) 3500 (br), 2976, 2936, 1726, 1665, 1603, 1582, 1514, 1485, 1452, 1389, 1368, 1312, 1270, 1242, 1179, 1128, 1069, 1025, 981, 909, 853, 821, 800, 775, 733, and 711 cm^{-1}.

HRMS (ESI) Calc'd for $C_{57}H_{73}NNaO_{17}Si$ $[M + Na]^+$ 1094.4540; found 1094.4579.

mp = 130–134 °C. **TLC** R_f (2:1 hexanes:EtOAc) = 0.2.

2'-*O*-(Di-*t*-butoxyacetoxysilyl)paclitaxel (301g).[a]

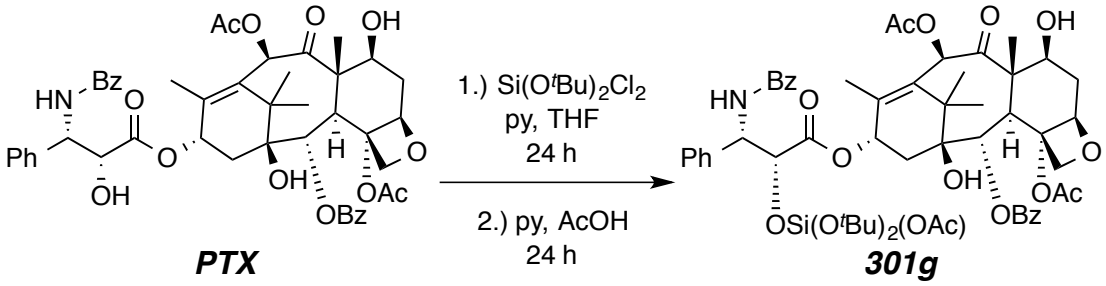

PTX ***301g***

[a]Compound synthesized by Dr. Wohl and included here for reference.

Paclitaxel (33.5 mg, 0.0392 mmol, 1.0 equiv) was dissolved in THF (1.0 mL, dried by distillation from sodium/benzophenone) in an oven-dried culture tube with a Teflon-lined cap and magnetic stir bar. Pyridine (50 μL, 0.618 mmol, 16 equiv) was added by Wiretrol®. A distilled sample of di-*t*-butoxydichlorosilane (**306**) (0.0524 mg, 0.214 mmol, 5.5 equiv) was added by Wiretrol®. The culture tube was sealed and the solution was allowed to stir at room temperature for 24 hours. The reaction mixture was noted to be cloudy and heterogeneous after stirring overnight. To the suspension, pyridine was again added (50 μL, 0.618 mmol, 16 equiv). Immediately afterward, glacial acetic acid (50 μL, 0.873 mmol, 22 equiv) was added. The mixture was allowed to stir for an additional 24 hours at room temperature. The reaction suspension was diluted with EtOAc, the slurry filtered through a short plug of Celite® to remove the pyridinium salt, the filtrate concentrated under reduced pressure, and the residue redissolved in a mixture of hexanes:EtOAc (2:1). Purification (SiO_2, 2:1 hexanes:EtOAc) using MPLC yielded the title compound (28.0 mg, 0.0258 mmol, 65.8%).

^{1}H NMR (500 MHz, $CDCl_3$): δ 8.13 (dd, *J* = 8.5, 1.4 Hz, 2H, C2O_2C-*o*-Ph), 7.81 (dd, *J* = 8.5, 1.4 Hz, 2H, C3'NHCO-*o*-Ph), 7.63 (tt, *J* = 7.4, 1.3 Hz, 1H, C2O_2C-*p*-Ph), 7.54 (t, *J* = 7.9 Hz, 2H, C2O_2C-*m*-Ph), 7.48 (tt, *J* = 7.4, 1.9 Hz, 1H, C3'NHCO-*p*-Ph), 7.43-7.34 (m, 6H, C3'-*o*-Ph, C3'-*m*-Ph, and C3'NHCO-*m*-Ph), 7.30-7.21 (m, 2H, C3'-*p*-Ph and C3'NH), 6.28 (s, 1H, H10), 6.13 (br dd, *J* = 9, 9 Hz, 1H, H13), 5.69 (dd, *J* = 8.5, 3.9 Hz, 1H, H3'), 5.66 (d, *J* = 7.2 Hz, 1H, H2), 5.19 (d, *J* = 4.0 Hz, 1H, H2'), 4.96 (dd, *J* = 9.6, 2.1 Hz, 1H, H5), 4.44 (ddd, *J* = 10.8, 6.4, 4.3 Hz, 1H, H7), 4.31 (d, *J* = 8.4 Hz, 1H, H20α), 4.20 (d, *J* = 8.3 Hz, 1H, H20β), 3.79 (d, *J* = 7.0 Hz, 1H, H3), 2.56 (ddd, *J* = 14.9, 9.9, 6.6 Hz, 1H, H6α), 2.45 (overlapping m, 1H, C7OH and s, 3H, C4OAc), 2.30-2.18 (overlapping m, 1H, H14α and s, 3H, C10OAc), 1.97-1.84 (m, 8H, H14β, C18H_3, SiOAc, and H6β), 1.67 (s, 3H, C19H_3), 1.61 (s, 1H, C1OH), 1.30 (s, 9H, C2'OSiOC(CH_3)$_2$], 1.26 (s, 9H, C2'OSiOC(CH_3)$_2$], 1.22 (s, 3H, C17H_3), and 1.12 (s, 3H, C16H_3).

^{13}C NMR (75 MHz, $CDCl_3$): δ 204.1, 171.6, 170.9, 170.3, 170.2, 167.2, 167.1, 143.2, 138.2, 134.4, 133.9, 132.7, 131.8, 130.4, 129.4, 128.92, 128.85, 128.7, 128.1, 127.4, 127.1, 84.7, 81.1, 79.3, 76.6, 75.9, 75.4, 75.31, 75.27 (x2), 72.3, 71.6, 58.7, 56.1, 45.7, 43.3, 35.70, 35.68, 31.34, 31.32, 26.9, 23.1, 22.9, 22.4, 21.1, 15.2, and 9.8.

HRMS (ESI) Calc'd for $C_{57}H_{71}NNaO_{18}Si$ $[M + Na]^+$ 1108.4333; found 1108.4360.

2'-*O*-(Di-*t*-butoxypivaloxysilyl)paclitaxel (301g).

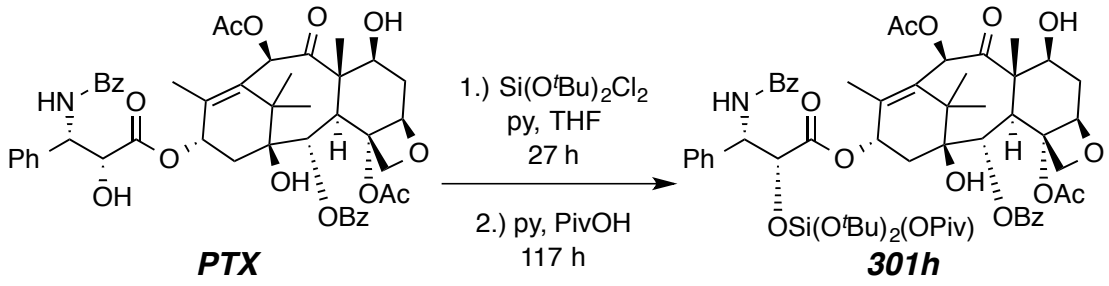

PTX ***301h***

Paclitaxel (81.0 mg, 0.0949 mmol, 1.0 equiv) was dissolved in THF (2.0 mL) in an oven-dried culture tube with a Teflon-lined cap and magnetic stir bar. Pyridine (10 µL, 0.124 mmol, 1.3 equiv) was added by Wiretrol®. A distilled sample of di-t-butoxydichlorosilane (0.46 mg, 0.189 mmol, 2 equiv) was added by Wiretrol®. The culture tube was sealed and the solution was allowed to stir at room temperature for 27 hours. Pyridine (50 µL, 0.62 mmol, 4.5 equiv) and pivalic acid (75.5 mg, 0.749 mmol, 7.8 equiv) were co-dissolved in dry THF (1 mL), and the solution was added in a single portion to the reaction vesicle., The mixture was allowed to stir for an additional 113 hours at room temperature. An aliquot of the reaction mixture was removed, concentrated to dryness under reduced pressure, and analyzed by crude LC-MS ($[M+H]^+$, m/z = 1129). Analysis showed that ca. 25% conversion to **301h**. The remainder of the reaction slurry stirred for an additional 4 hours. A second aliquot of the reaction mixture was removed, concentrated to dryness under reduced pressure, and analyzed by crude ^{1}H NMR spectroscopy. The remainder of the reaction suspension was diluted with EtOAc, the slurry filtered through a short plug of Celite® to remove the pyridinium

salt, the filtrate concentrated under reduced pressure, and the residue redissolved in a mixture of hexanes:EtOAc (2:1). Chromatography (SiO_2, 2:1 hexanes:EtOAc) via MPLC yielded the title compound as a mixture of ca. (30 mg, 0.026 mmol, 28%). The mixture of products was further purified on a reversed-phase an ACE 121-1520 C18 150 x 21.2 mm 5μM particle size semi-prep HPLC column with an isocratic elution solvent of MeOH:H_2O (98%:2%) at 10.5 mL/min to yield PTX, PTX-2'-Si(O^tBu)$_2$OH, and a minor amount of **301h** (12 mg, 0.011 mmol, 1%). The methanol:water was removed by rotary evaporation and the residual removed by storage under high vacuum for ≥ 24h.

^{1}H NMR (500 MHz, $CDCl_3$)160: δ 8.12 (dd, J = 8.6, 1.4 Hz, 2H, C2O_2C-o-Ph), 7.80 (dd, J = 8.2, 1.1 Hz, 2H, C3'NHCO-o-Ph), 7.60 (br tt, J = 7, 1 Hz, 1H, C2O_2C-p- Ph), 7.54-7.35 (m, 9H, C2O_2C-m-Ph, C3'NHCO-p-Ph, C3'-o-Ph, C3'-m-Ph, and C3'NHCO-m-Ph), 7.31 (t, J = 7.0 Hz, 1H, C3'-p-Ph), 7.07 (d, J = 9.3 Hz, 1H, C3'NH), 6.28 (s, 1H, H10), 6.22 (br dd, J = 9, 8 Hz, 1H, H13), 5.82 (dd, J = 9.0, 2.5 Hz, 1H, H3'), 5.68 (d, J = 7.5 Hz, 1H, H2), 5.20 (d, J = 2.4 Hz, 1H, H2'), 4.96 (dd, J = 9.3, 2.2 Hz, 1H, H5), 4.44 (br m, 1H, H7), 4.30 (d, J = 8.8 Hz, 1H, H20α), 4.20 (d, J = 8.6 Hz, 1H, H20β), 3.80 (d, J = 6.9 Hz, 1H, H3), 2.56 (ddd, J = 14.4, 9.7, 6.3 Hz, 1H, H6α), 2.45 (overlapping m, 1H, C7OH and s, 3H, C4OAc), 2.37 (dd, J = 14.8, 8.5 Hz, 1H, H14α), 2.25 (s, 3H, C10OAc), 1.97-1.84 (overlapping m, 1H, H14β and s, 3H, C18H_3), 1.68 (overlapping m, 1H, H6β and s, 3H, C19H_3), 1.59 (br s, 1H, C1OH), 1.33 [s, 9H, C2'OSiOC(CH_3)$_2$], 1.32 [s, 9H, C2'OSiOC(O)C(CH_3)$_3$], 1.31 [s, 9H, C2'OSiOC(CH_3)$_2$],, 1.22 (s, 3H, C17H_3), and 1.13 (s, 3H, C16H_3).

^{13}C NMR (125 MHz, $CDCl_3$): δ 202.5, 180.5 [C2'OSiO*C*(O)C(CH_3)$_3$],172.7, 170.3, 169.0, 167.2, 167.1, 140.3, 138.2, 133.9, 133.8, 132.1, 130.4, 129.4, 129.3,

129.2, 128.9 (2x), 128.5, 127.3, 127.2, 84.5, 81.5, 78.8, 77.4, 76.8, 76.0, 74.9, 73.3, 72.6, 66.3 (2x) [C2'OSiO*C*$(CH_3)_2$], 58.5, 55.0, 47.0, 43.4, 36.8 [C2'OSiOC(O)*C*$(CH_3)_3$], 35.6, 35.5, 26.9, 25.5 (6x) [C2'OSiOC(*C*$H_3)_2$], 25.4 (3x) [C2'OSiOC(O)C(*C*$H_3)_3$], 22.9, 21.1, 21.0, 14.7, and 10.4.

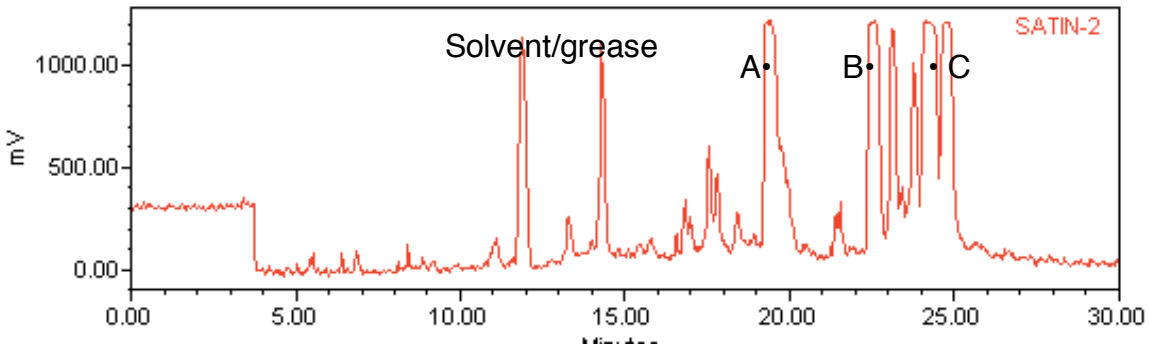

Figure S3.1 I Reverse-phase HPLC purification chromatogram at 230 nm of PTX-2'-Si(O^{t}Bu)$_2$(OPiv). Yielded PTX, PTX-2'-Si(O^{t}Bu)$_2$OH, and the title compound. **A** = **PTX**, **B** = PTX-2'-Si(O^{t}Bu)$_2$OH. **C** = PTX-2'-Si(O^{t}Bu)$_2$(OPiv)

2'-*O*-(Di-*t*-butoxypivaloxysilyl)paclitaxel (301p).

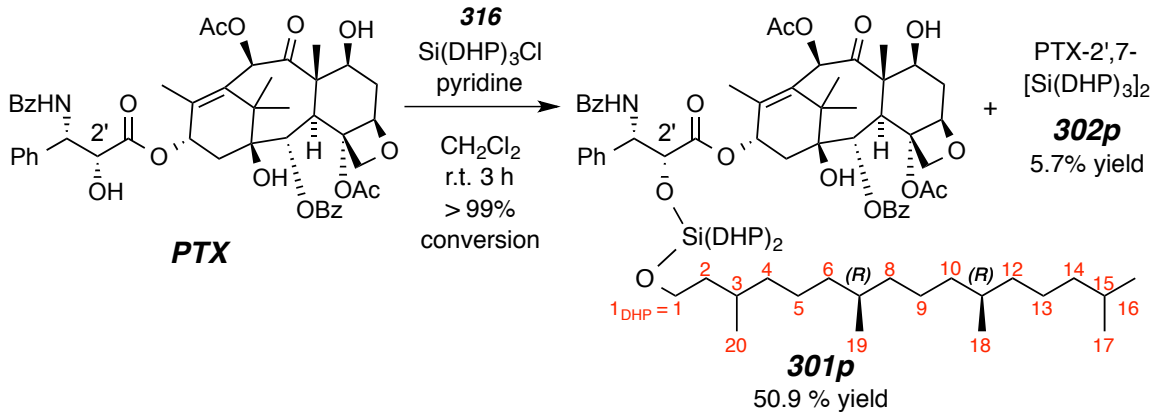

Paclitaxel (92.3 mg, 0.1081 mmol, 1.0 equiv) was dissolved in dry CH_2Cl_2 (3 mL) in an oven-dried culture tube fitted with a Teflon-lined cap and magnetic stir bar. Pyridine (100 μL, 1.24 mmol, 11.5 equiv) was added by Wiretrol®. A 1:1.7 mixture based on moles (^{1}H NMR) which corresponds to a 1:1.3 mixture based on mass (^{1}H NMR) of the DHP-silicates tri-*n*-dihydrophytolchlorosilane (**316**):tetra-*n*-dihydrophytolchlorosilane (**317**) (300 μL, ca. 0.257 mmol based on an ca. density of 1.5, 1.6 equiv of tri-*n*- dihydrophytolchlorosilane) was added. The culture tube was capped and the solution was allowed to stir for 3 h at room temperature. The reaction solvent was removed on a rotary evaporator replaced with a mixture of hexanes:EtOAc (5:1), the slurry filtered through a short plug of Celite® to remove the pyridinium salt, the filtrate concentrated under reduced pressure. The residue redissolved in 2 mL of hexanes:EtOAc (5:1). Chromatography (SiO_2, 5:1 hexanes:EtOAc) via MPLC yielded the title compound as a clear, glassy solid

(98.5 mg, 0.055 mmol, 50.9%) and the bis-functionalized product **302p** (16.6 mg, 0.006 mmol, 5.7%).

^{1}H NMR (500 MHz, $CDCl_3$): δ 8.13 (dd, *J* = 8.0, 1.5 Hz, 2H, C2O_2C-*o*-Ph), 7.77 (dd, *J* = 7.9, 1.4 Hz, 2H, C3'NHCO-*o*-Ph), 7.61 (tt, *J* = 8.3, 1.2 Hz, 1H, C2O_2C-*p*-Ph), 7.55-7.47 (m, 3H, C2O_2C-*m*-Ph and C3'NHCO-*p*-Ph), 7.42-7.35 (m, 6H, C3'-*o*-Ph, C3'-*m*-Ph and C3'NHCO-*m*-Ph), 7.28 (tt, *J* = 6.2, 1.6 Hz, 1H, C3'-*p*-Ph), 7.19 (d, *J* = 8.6 Hz, 1H, C3'NH), 6.28 (s, 1H, H10), 6.26 (br dd, *J* = 9, 9 Hz, 1H, H13), 5.73 (dd, *J* = 8.6, 3.1 Hz, 1H, H3'), 5.68 (d, *J* = 7.1 Hz, 1H, H2), 4.97 (dd, *J* = 9.6, 2.7 Hz, 1H, H5), 4.97 (overlapping d, *J* = 4.2 Hz, 1H, H2'), 4.44 (ddd, *J* = 10.9, 6.5, 4.1 Hz, 1H, H7), 4.31 (d, *J* = 8.6 Hz, 1H, H20α), 4.20 (d, *J* = 8.5 Hz, 1H, H20β), 3.80 (d, *J* = 7.1 Hz, 1H, H3), 3.71-3.60 {m, 6H, C2'OSi[OC1$_{DHP}$*H*$_2$]$_3$}, 2.55 (ddd, *J* = 15.4, 9.5, 6.7 Hz, 1H, H6α), 2.46 (d, *J* = 4.0 Hz, 1H, C7OH), 2.44 (s, 3H, C4OAc), 2.32 (dd, *J* = 15.4, 9.5 Hz, 1H, H14α), 2.24 (d, *J* = 1.0, 3H, C10OAc), 2.08 (dd, *J* = 15.3, 8.8 Hz, 1H, H14β), 1.92-1.86 (m, 1H, H6β), 1.90 (overlapping br s, 3H, C18H_3), 1.68 (s, 3H, C19H_3), 1.66 (s, 1H, C1OH), 1.56-1.49 [br td, *J* = 6.7, 6.7 Hz, 6H, C2'OSi[OC2$_{DHP}$*H*$_2$]$_3$], 1.48-1.31 {m, 12H, C2'OSi[OC3$_{DHP}$*H*$_1$]$_3$, C2'OSi[OC7$_{DHP}$*H*$_1$]$_3$, C2'OSi[OC11$_{DHP}$*H*$_1$]$_3$, C2'OSi[OC15$_{DHP}$*H*$_1$]$_3$}, 1.30-1.15 {m, 30H, C2'OSi[OC4$_{DHP}$*H*$_2$]$_3$, C2'OSi[OC5$_{DHP}$*H*$_2$]$_3$, C2'OSi[OC6$_{DHP}$*H*$_2$]$_3$, C2'OSi[OC8$_{DHP}$*H*$_2$]$_3$}, C2'OSi[OC9$_{DHP}$*H*$_2$]$_3$}, 1.24 (overlapping s, 3H, C17H_3), 1.14-0.99 {m, 30H, C2'OSi[OC10$_{DHP}$*H*$_2$]$_3$, C2'OSi[OC12$_{DHP}$*H*$_2$]$_3$, C2'OSi[OC13$_{DHP}$*H*$_2$]$_3$, C2'OSi[OC14$_{DHP}$*H*$_2$]$_3$}}, 1.13 (overlapping s, 3H, C16H_3), 0.86 {d, *J* = 6.6 Hz, 18H, C2'OSi[OC16$_{DHP}$*H*$_3$]$_3$, and C2'OSi[OC17$_{DHP}$*H*$_3$]$_3$}, and 0.84 {br d, *J* = 6.5 Hz, 27H, C2'OSi[OC18$_{DHP}$*H*$_3$]$_3$, C2'OSi[OC19$_{DHP}$*H*$_3$]$_3$, and C2'OSi[OC20$_{DHP}$*H*$_3$]$_3$}.

^{13}C NMR (125 MHz, $CDCl_3$): δ 203.7, 171.2, 170.3, 169.9, 166.8, 167.3, 142.6, 138.6, 133.9, 133.8, 132.8, 131.6, 130.5, 129.0, 128.8, 128.7, 128.4, 128.2, 127.5,

127.2, 84.3, 80.1, 78.8, 76.4, 75.5, 74.9, 74.4, 70.9, 72.0, {62.3, 62.3, 61.6, C_{dhp}1}, 58.4, 55.1, 45.3, 43.5, {40.3 (3x), C_{dhp}2}, {39.8 (2x), 39.7, C_{dhp}3}, {37.9 (3x), C_{dhp}4}, {37.8 (3x), C_{dhp}14}, {37.7 (6x), C_{dhp}8 and C_{dhp}10 }, {37.6 (3x), C_{dhp}12}, 35.7, 35.6, {33.2, 33.1 (2x), C_{dhp}6}, {29.8 (2x), 29.7, C_{dhp}7}, {28.3 (3x), C_{dhp}11}, 27.1, {25.1 (3x), C_{dhp}15}, {24.8 (3x), C_{dhp}5}, {24.7 (3x), C_{dhp}13}, {23.0 (3x), C_{dhp}9}, 23.0, {22.9 (3x), C_{dhp}16}, 22.9, 20.8, {20.1 (2x), 20.0, C_{dhp}17}, {20.0 (3x), C_{dhp}18}, {20.0, 19.9 (2x), C_{dhp}19}, {19.8 (2x), 19.7 C_{dhp}20},15.0, and 9.9.

HRMS (ESI) Calc'd for $C_{107}H_{173}NNaO_{17}Si$ $[M + Na]^+$ 1795.2365; found 1795.2383.

IR (thin film) 3904, 3857, 3751, 3677, 3569, 2954, 2926, 2867, 2368, 2343, 1722, 1657, 1641, 1480, 1463, 1375, 1271, 1241, 1093, 1024, 986, 907, 857, 805, and 771 cm^{-1}.

mp = 106–109 °C. **TLC** R_f (5:1 hexanes:EtOAc) = 0.41.

2',7-Di-*O*-(Triethoxysilyl)paclitaxel (302a).

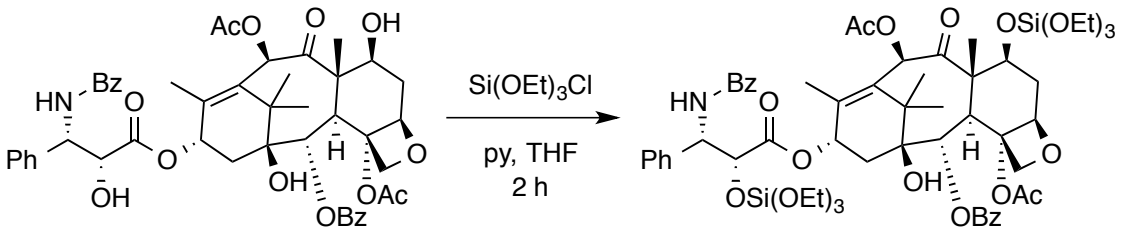

PTX ***302a***

Paclitaxel (58.0 mg, 0.0679 mmol, 1.0 equiv) was dissolved in dry THF (1.0 mL) in an oven-dried culture tube fitted with a Teflon-lined cap and a stir bar. Pyridine (25 μL, 0.309 mmol, 4.5 equiv) was added by Wiretrol®. Triethoxychlorosilane (**305a**) (50 μL, 0.255 mmol, 3.8 equiv) was added, and a white precipitate was immediately observed. The suspension was allowed to stir for 2 hours at room temperature and then diluted with hexanes:EtOAc (1:1). The slurry was filtered through a short plug of Celite® to remove the pyridinium salt, and the filtrate concentrated under reduced pressure. The residue was purified by MPLC (SiO_2, 2:1 hexanes:EtOAc) to yield **302a** as a white crystalline solid (68.0 mg, 0.058 mmol, 85%). If necessary, residual EtOAc was removed by storage under high vacuum for ≥ 24 h.

^{1}H NMR (500 MHz, $CDCl_3$): δ 8.12 (dd, *J* = 8.5, 1.5 Hz, 2H, C2O_2C-*o*-Ph), 7.78 (dd, *J* = 8.5, 1.5 Hz, 2H, C3'NHCO-*o*-Ph), 7.62 (tt, *J* = 7.5, 1.0 Hz, 1H, C2O_2C-*p*-Ph, 1H), 7.54-7.46 (m, 3H, C2O_2C-*m*-Ph and C3'NHCO-*p*-Ph), 7.44-7.36 (m, 6H, C3'-*o*-Ph, C3'-*m*-Ph and C3'NHCO-*m*-Ph), 7.29 (tt, *J* = 7.0, 1.5 Hz, 1H, C3'-*p*-Ph), 7.20 (d, *J* = 8.5 Hz, 1H, C3'NH), 6.58 (s, 1H, H10), 6.18 (br dd, *J* = 9, 9 Hz, 1H, H13), 5.72 (dd, *J* = 8.5, 3.0 Hz, 1H, H3'), 5.71 (d, *J* = 6.5 Hz, 1H,

H2), 4.98 (d, *J* = 3.0 Hz, 1H, 2'H), 4.96 (dd, *J* = 10.0, 2.0 Hz, 1H, H5), 4.62 (dd, *J* = 10.5, 6.7 Hz, 1H, H7), 4.31 (d, *J* = 8.5 Hz, 1H, H20α), 4.20 (d, *J* = 8.5 Hz, 1H, H20β), 3.85 (d, *J* = 7.0 Hz, 1H, H3), 3.76 [q, *J* = 7.0 Hz, 6H, C7OSi(OC*H*$_2$CH$_3$)$_3$], 3.71 [q, *J* = 7.0 Hz, 6H, C2'OSi(OC*H*$_2$CH$_3$)$_3$], 2.66 (ddd, *J* = 14.5, 9.5, 6.5 Hz, 1H, H6α), 2.45 (s, 3H, C4OAc), 2.33 (dd, *J* = 15.4, 9.4Hz, 1H, H14α), 2.15 (s, 3H, C10OAc), 2.08 (d, *J* = 1.5 Hz, 3H, C18H$_3$), 2.07 (dd, *J* = 15.1, 9.0 Hz, 1H, H14β), 1.96 (ddd, *J* = 14.5, 10.8, 2.2 Hz, 1H, H6β), 1.73 (s, 3H, C19H$_3$), 1.65 (br s, 1H, C1OH), 1.23 (s, 3H, C17H$_3$), 1.19 [t, *J* = 7.0 Hz, 9H, C7OSi(OCH$_2$C*H*$_3$)$_3$], 1.17 (s, 3H, C16H$_3$), and 1.15 [t, *J* = 7.0 Hz, 9H, C2'OSi(OCH$_2$C*H*$_3$)$_3$].

^{13}C NMR (75 MHz, $CDCl_3$): δ 202.6, 171.0, 169.8, 169.0, 167.3, 167.2, 141.0, 138.2, 134.3, 133.9, 133.3, 132.0, 130.4, 129.4, 128.9, 128.8, 128.7, 128.1, 127.3, 126.8, 84.5, 81.2, 78.9, 76.7, 75.9, 75.02, 74.99, 72.1, 71.6, 59.7, 59.5, 58.3, 55.5, 46.9, 43.4, 36.5, 35.5, 26.7, 23.0, 21.4, 21.0, 18.0 (x2), 14.2, and 10.4.

HRMS (ESI) Calc'd for $C_{59}H_{79}NNaO_{20}Si_2$ $[M + Na]^+$ 1200.4626, found 1200.4631.

IR (thin film) 3500 (br), 2976, 2928, 2896, 1744, 1725, 1644, 1603, 1580, 1541, 1486, 1451, 1370, 1314, 1268, 1238, 1169, 1098, 1080, 1027, 969, 891, 842, 795, and 708 cm^{-1}.

mp = 121-123 °C. **TLC** R_f (2:1 hexanes:EtOAc) = 0.4.

2',7-Di-*O*-(Tri-*n*-octyloxysilyl)paclitaxel (302b).

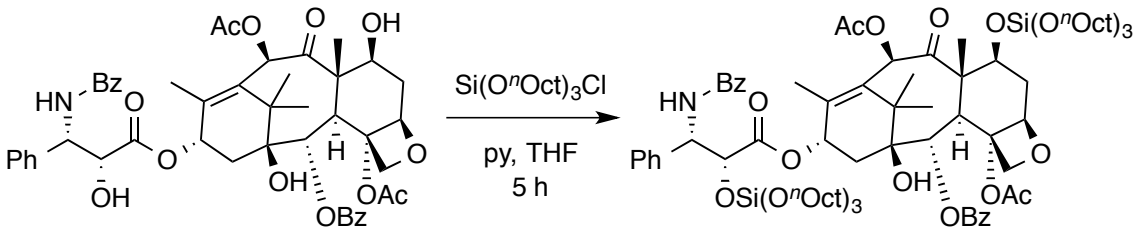

PTX ***302b***

Paclitaxel (57.8 mg, 0.0677 mmol, 1.0 equiv) was dissolved in dry THF (1.5 mL) in an oven-dried culture tube fitted with a Teflon-lined cap and magnetic stir bar. Pyridine (25 μL, 0.309 mmol, 4.6 equiv) was added by Wiretrol®. A 1.67:1 mixture of tri-*n*-octyloxychlorosilane (**305b**):tetra-*n*-octyloxysilane (0.155 mg, 0.199 mmol, 2.9 equiv of tri-*n*-octyloxychlorosilane) was added, and formation of a white precipitate was immediately observed. The culture tube was capped and the suspension was allowed to stir for 5 h at room temperature. The reaction mixture was diluted with a mixture of hexanes:EtOAc (1:1), and the slurry was filtered through a short plug of Celite® to remove the pyridinium salt. The filtrate was concentrated under reduced pressure, and the residue was purified by MPLC (SiO_2, 9:1 hexanes:EtOAc) to yield **302b** as a colorless viscous glass (88.1 mg, 0.0523 mmol, 77.3%). Additional elution with hexanes:EtOAc (2:1) yielded 1b (1.7 mg, 0.0013 mmol, 2.0 %).

^{1}H NMR (500 MHz, $CDCl_3$): δ 8.13 (dd, *J* = 8.6, 1.4 Hz, 2H, C2O_2C-*o*-Ph), 7.78 (dd, *J* = 8.6, 1.5 Hz, 2H, C3'NHCO-*o*-Ph), 7.60 (tt, *J* = 7.4, 1.2 Hz, 1H, C2O_2C-*p*-Ph, 1H), 7.54-7.46 (m, 3H, C2O_2C-*m*-Ph and C3'NHCO-*p*-Ph), 7.44-7.35 (m,

6H, C3'-*o*-Ph, C3'-*m*-Ph and C3'NHCO-*m*-Ph), 7.28 (tt, *J* = 7.2, 1.3 Hz, 1H, C3'-*p*-Ph), 7.22 (d, *J* = 8.7 Hz, 1H, C3'NH), 6.55 (s, 1H, H10), 6.23 (br dd, *J* = 10, 9 Hz, 1H, H13), 5.74 (dd, *J* = 8.6, 3.0 Hz, 1H, H3'), 5.70 (d, *J* = 7.1 Hz, 1H, H2), 4.99 (d, *J* = 3.0 Hz, 1H, 2'H), 4.94 (dd, *J* = 9.7, 1.9 Hz, 1H, H5), 4.61 (dd, *J* = 10.6, 6.8 Hz, 1H, H7), 4.31 (d, *J* = 8.4 Hz, 1H, H20α), 4.20 (d, *J* = 8.4 Hz, 1H, H20β), 3.86 (d, *J* = 7.0 Hz, 1H, H3), 3.67 {t, *J* = 6.7 Hz, 6H, C7OSi[OC*H*$_2$(CH$_2$)$_6$CH$_3$]$_3$}, 3.61 {t, *J* = 6.7 Hz, 6H, C2'OSi[OC*H*$_2$(CH$_2$)$_6$CH$_3$]$_3$}, 2.65 (ddd, *J* = 14.7, 9.7, 6.8 Hz, 1H, H6α), 2.45 (s, 3H, C4OAc), 2.33 (dd, *J* = 15.3, 9.4 Hz, 1H, H14α) 2.13 (s, 3H, C10OAc), 2.06 (d, *J* = 1.2 Hz, 3H, C18H$_3$), 2.09-2.02 (m, 1H, H14β), 1.96 (ddd, *J* = 14.5, 10.8, 2.2 Hz, 1H, H6β), 1.73 (s, 3H, C19H$_3$), 1.66 (br s, 1H, C1OH), 1.56-1.44 {m, 12H, C2'OSi[OCH$_2$C*H*$_2$(CH$_2$)$_5$CH$_3$]$_3$ and C7OSi[OCH$_2$C*H*$_2$(CH$_2$)$_5$CH$_3$]$_3$}, 1.34-1.21 {m, 63H, C17H$_3$, C2'OSi[OCH$_2$CH$_2$(C*H*$_2$)$_5$CH$_3$]$_3$, and C7OSi[OCH$_2$CH$_2$(C*H*$_2$)$_5$CH$_3$]$_3$}, 1.17 (s, 3H, C16H$_3$), and 0.88 {overlapping t's, *J* = 6.8 Hz, 18H, C2'OSi[OCH$_2$CH$_2$(CH$_2$)$_5$C*H*$_3$]$_3$ and C7OSi[OCH$_2$CH$_2$(CH$_2$)$_5$C*H*$_3$]$_3$}.

^{13}C NMR (75 MHz, CDCl$_3$): δ 202.4, 170.9, 169.8, 168.7, 167.3, 167.2, 140.9, 138.3, 134.3, 133.8, 133.3, 131.9, 130.4, 129.4, 128.91, 128.89, 128.8, 128.1, 127.3, 126.8, 84.6, 81.2, 79.0, 76.8, 75.8, 75.1, 74.9, 72.0, 71.5, 64.1, 63.9, 58.3, 55.5, 46.8, 43.5, 36.6, 35.6, 32.5, 32.4, 32.1, 32.0, 29.6, 29.63, 29.60, 29.57, 26.7, 25.92, 25.89, 23.0, 22.91, 22.90, 21.6, 21.1, 14.3 (x2), 14.1, and 10.4.

HRMS (ESI) Calc'd for C$_{95}$H$_{151}$NNaO$_{20}$Si$_2$ [M + Na]$^+$ 1705.0260; found 1705.0228.

IR (thin film) 3500 (br), 2927, 2856, 1741, 1728, 1634, 1580, 1545, 1456, 1371, 1315, 1270, 1239, 1174, 1095, 1028, 989, 968, 924, 893, 843, 779, and 709 cm^{-1}.

TLC R_f (3:1 hexanes:EtOAc) = 0.55.

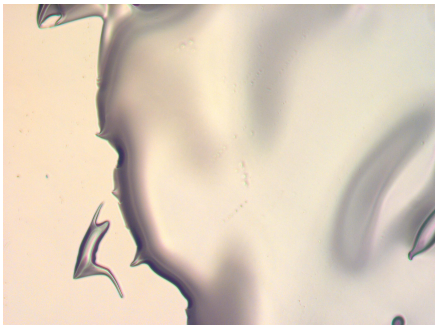

Figure S3.2 I Image of 2',7-Di-O-(Tri-n-octyloxysilyl)paclitaxel (**302b**) at 200 times magnification shows a glassy solid, no mp. could be obtained.

2',7-Di-*O*-(Tri-*i*-propoxysilyl)paclitaxel (302c).

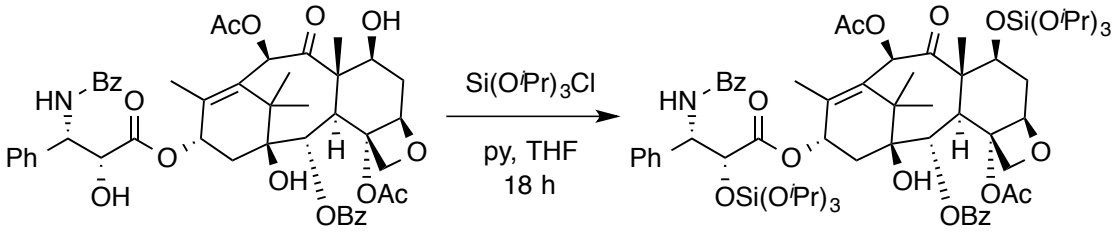

PTX ***302c***

Paclitaxel (30.1 mg, 0.0352 mmol, 1.0 equiv) was dissolved in dry THF (1.0 mL) in an oven-dried culture tube fitted with a Teflon-lined cap and magnetic stir bar. Pyridine (15 μL, 0.185 mmol, 5.3 equiv) was added by Wiretrol®. A 3.5:1 mixture of tri-*i*-propoxychlorosilane (**305c**) :tetra-*i*-propoxysilane (0.0424 mg, 0.134 mmol, 2.9 equiv of tri-*i*-propoxychlorosilane) was added. The culture tube was capped and a white precipitate was observed within minutes. The suspension was stirred at room temperature for 18 hours, and the mixture was filtered through a short plug of Celite® to remove the triethylammonium salt. The filtrate was concentrated under reduced pressure, and the residue was redissolved in a mixture of hexanes:EtOAc (2:1). Purification by MPLC (SiO_2, 2:1 hexanes:ethyl acetate) yielded the title compound as a white, crystalline solid (29.8 mg, 0.0236 mmol, 67.0%).

^{1}H NMR (500 MHz, $CDCl_3$): δ 8.12 (dd, *J* = 8.5, 1.5 Hz, 2H, C2O_2C-*o*-Ph), 7.80 (dd, *J* = 8.4, 1.5 Hz, 2H, C3'NHCO-*o*-Ph), 7.62 (tt, *J* = 7.4, 1.7 Hz, 1H, C2O_2C-*p*-Ph, 1H), 7.55-7.46 (m, 3H, C2O_2C-*m*-Ph and C3'NHCO-*p*-Ph), 7.43-7.34 (m, 6H, C3'-*o*-Ph, C3'-*m*-Ph and C3'NHCO-*m*-Ph), 7.29-7.24 (m, 1H, C3'-*p*-Ph), 7.17 (d, *J* = 8.4 Hz, 1H, C3'NH), 6.53 (s, 1H, H10), 6.14 (br dd, *J* = 9, 9 Hz,

1H, H13), 5.70 (d, *J* = 7.3 Hz, 1H, H2), 5.67 (dd, *J* = 8.4, 3.6 Hz, 1H, H3'), 5.00 (d, *J* = 3.6 Hz, 1H, H2'), 4.96 (dd, *J* = 9.4, 2.0 Hz, 1H, H5), 4.61 (dd, *J* = 10.7, 6.7, Hz, 1H, H7), 4.31 (d, *J* = 8.8 Hz, 1H, H20α), 4.19 (d, *J* = 8.6 Hz, 1H, H20β), 4.13 and 4.12 {overlapping septs, *J* = 6.2 Hz, 6H, C2'OSi[OC*H*$(CH_3)_2]_3$ and C7OSi[OC*H*$(CH_3)_2]_3$}, 3.85 (d, *J* = 7.4 Hz, 1H, H3), 2.68 (ddd, *J* = 14.7, 9.7, 6.8 Hz, 1H, H6α), 2.41 (s, 3H, C4OAc), 2.30 (dd, *J* = 15.1, 9.3 Hz, 1H, H14α), 2.14 (s, 3H, C10OAc), 2.10 (d, *J* = 1.2 Hz, 3H, $C18H_3$), 2.03 (dd, *J* = 15.7, 9.5 Hz, 1H, H14β), 1.95 (ddd, *J* = 14.6, 10.9, 2.2 Hz, 1H, H6β), 1.72 (s, 3H, $C19H_3$), 1.61 (br s, 1H, C1OH), 1.23 (m, 3H, $C17H_3$), and 1.18-1.10 {m, 39H, C2'OSi[OCH$(CH_3)_a$(C*H*$_3)_b]_3$}, C2'OSi[OCH(C*H*$_3)_a(CH_3)_b]_3$, C7OSi[OCH$(CH_3)_a$(C*H*$_3)_b]_3$}, C7OSi[OCH(C*H*$_3)_a(CH_3)_b]_3$, and $C16H_3$}.

^{13}C NMR (125 MHz, $CDCl_3$): δ 202.6, 171.1, 169.6, 168.9, 167.3, 167.2, 141.2, 138.4, 134.4, 133.8, 133.3, 131.9, 130.4, 129.5, 128.9 (x2), 128.8, 128.1, 127.3, 127.0, 84.6, 81.2, 80.0, 76.8, 75.9, 75.2, 74.9, 72.3, 71.7, 66.6, 66.2, 58.3, 55.9, 46.8, 43.5, 36.7, 35.5, 26.8, 25.5, 25.42, 25.41, 25.38, 23.0, 21.5, 21.1, 14.7, and 10.5.

HRMS (ESI) Calc'd for $C_{65}H_{91}NNaO_{20}Si_2$ $[M + Na]^+$ 1284.5565, found 1284.5563.

IR (thin film) 3500 (br), 2973, 2933, 1725, 1671, 1603, 1582, 1512, 1484, 1452, 1371, 1313, 1267, 1238, 1173, 1116, 1047, 989, 893, 839, 767, and 711.

mp = 108–113 °C. **TLC** R_f (2:1 hexanes:EtOAc) = 0.55.

2',7-Di-*O*-(Tri-menthyloxysilyl)paclitaxel (302d).

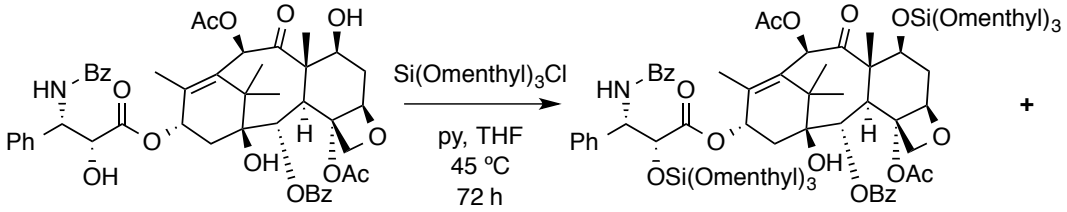

PTX ***302d***

Paclitaxel (85.0 mg, 0.100 mmol, 1.0 equiv) was dissolved in dry THF (8.0 mL) in an oven-dried culture tube fitted with a Teflon-lined cap and magnetic stir bar. Pyridine (100 μL, 1.24 mmol, 12.4 equiv) was added by Wiretrol®. Trimenthyloxychlorosilane (**305d**), judged to contain 90% of the chlorosilane (579.1 mg, 0.986 mmol, 9.9 equiv) by ^{1}H NMR analysis, was added by Wiretrol®. The culture tube was capped and the suspension was allowed to stir for 12 h at 45 ˚C. The THF was removed by evaporation under reduced pressure, the solid residue was triturated with a mixture of hexanes:EtOAc (3:1), and the resulting slurry was filtered through a short plug of Celite® to remove the pyridinium salt. The filtrate was concentrated under reduced pressure, and the residue was purified by MPLC (SiO_2, 3:1 hexanes:EtOAc) to yield the title compound (**302d**) as a white, crystalline solid (64.9 mg, 0.0353 mmol, 35.3 %) and the mono-silylated product **301d** (78.2 mg, 0.0581 mmol, 58.1 %).

^{1}H NMR (500 MHz, $CDCl_3$): δ 8.13 (dd, *J* = 8.5, 1.4 Hz 2H, O_2C-*o*-Ph), 7.78 (dd, *J* = 8.5, 1.4 Hz, 2H, C3'NHCO-*o*-Ph), 7.59 (tt, *J* = 7.4, 1.3 Hz, 1H, C2O_2C-*p*-Ph), 7.54-7.45 (m, 3H, C2O_2C-*m*-Ph and C3'NHCO-*p*-Ph), 7.43-7.35 (m, 6H, C3'-*o*-Ph, C3'-*m*-Ph and C3'NHCO-*m*-Ph), 7.30 (tt, *J* = 7.1, 2.1 Hz, 1H, C3'-*p*-

Ph), 7.14 (d, J = 8.5 Hz, 1H, C3'NH), 6.38 (s, 1H, H10), 6.23 (ddq, J = 10.2, 9.7, 1.5 Hz, 1H, H13), 5.73 (dd, J = 8.5, 3.4 Hz, 1H, H3'), 5.68 (d, J = 7.1 Hz, 1H, H2), 5.08 (d, J = 3.5 Hz, 1H, H2'), 4.90 (dd, J = 9.7, 2.3 Hz, 1H, H5), 4.64 (ddd, J = 10.0, 6.5 3.4 Hz, 1H, H7), 4.28 (bd, J = 8.2 Hz, 1H, H20α), 4.20 (d, J = 8.3, 0.9 Hz, 1H, H20β), 3.85 (d, J = 7.0 Hz, 1H, H3), 3.73-3.57 (m, 6H, $H1_{menth}$), 2.75 (ddd, J = 14.8, 9.8, 6.67 Hz, 1H, H6α), 2.38 (s, 3H, C4OAc), 2.30 (dd, J = 15.1, 9.7 Hz, 1H, H14α), 2.22 (s, 3H, C10OAc), 2.20-2.03 (m, 7H, H14β and $H7_{menth}$), 1.94 (bs, 3H, H18 $=CCH_3$), 1.92-1.87 (m, 4H, $H6eq_{menth}$ and H6β), 1.71 (s, 1H, C1OH), 1.70 (s, 3H, H19 $O=CCCH_3$), 1.66-1.53 (m, 18H, $H4eq_{menth}$, $H6eq_{menth}$, and $H10_{menthyl}$), 1.45-1.36 (m, 3H, $H5_{menth}$), 1.28-1.10 (m, 9H, $H3_{menth}$ and $H5_{menth}$), 1.23 (s, 3H, $C(Me)C16H_3$)), 1.18 [s, 3H, $C(Me)C17H_3$]), 1.08-0.94 (m, 6H, $H2_{menth}$), 0.93-0.90 [(d, J = 6.9, 9H, $H10_{menthyl}$) and (m, 6H, $H6ax_{menth}$)], 0.88-0.85 [(d, J = 6.9, 9H, $H8_{menthyl}$) and (m, 6H, $H3ax_{menth}$)], 0.84-0.81 [(d, J = 6.6, 9H, $H8_{menthyl}$) and (m, 3H, $H4ax_{menth}$)], and 0.80-0.73 [(m, 3H, $H4ax_{menth}$), (d, J = 6.9, 9H, $H9_{menthyl}$), and (d, J = 6.9, 9H, $H9_{menthyl}$].

^{13}C NMR (125 MHz, $CDCl_3$): δ 201.5, 170.3 (2x), 169.4, 166.8, 166.4, 140.8, 138.2, 133.9, 133.4, 133.0, 132.1, 130.2, 130.0, 129.1, 128.9, 128.5, 128.2, 127.8, 127.6, 84.0, 81.0, 78.8, 77.1, 75.3, 74.9, 73.6, 72.7, 71.8, 71.4 ($C1_{menth}$), 71.0 ($C1_{menth}$), 58.0, 53.6, 49.7 ($C2_{menth}$), 49.3 ($C2_{menth}$), 44.1 ($C7_{menth}$), 43.1($C7_{menth}$), 45.8, 43.2, 35.4, 34.1, 34.1 ($C5_{menth}$), 33.7 ($C5_{menth}$), 31.5 ($C6_{menth}$), 31.1 ($C6_{menth}$), 26.3, 25.4 ($C3_{menth}$), 25.0 ($C3_{menth}$), 23.4($C4_{menth}$), 22.7($C4_{menth}$), 22.4, 22.4 ($C8_{menth}$), 22.1 ($C8_{menth}$), 21.5, 21.4 ($C9_{menth}$), 21.1 ($C9_{menth}$), 20.7, 15.6 ($C10_{menth}$), 15.5 ($C10_{menth}$), 14.2, and 9.8.

HRMS (ESI) Calc'd for $C_{107}H_{163}NNaO_{20}Si_2^+$ $[M + Na]^+$ 1861.1199; found 1861.1578.

IR (thin film) 3256, 3163, 2953, 2924, 2868, 2345, 1737, 1722, 1673, 1509, 1456, 1373, 1246, 1180, 1155, 1084, 1072, 1055, 1001, 989, 950, 921, 894, 818, 803, and 788 cm^{-1}.

mp = 93–95 °C. **TLC** Rf (9:1 hexanes:EtOAc) = 0.30.

7-*O*-(Triethoxysilyl)paclitaxel (303a).

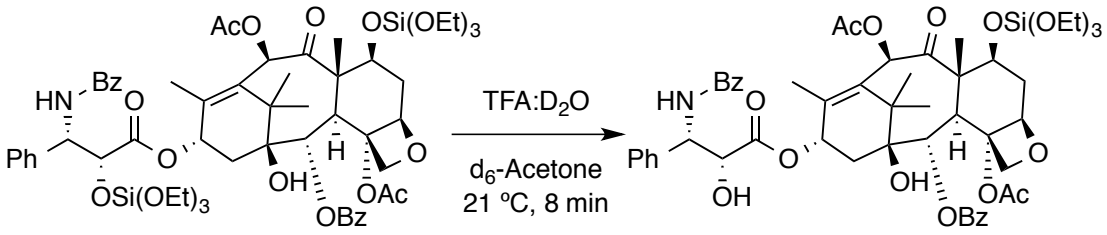

302a ***303a***

Bis(triethoxy)silicate ester **302a** (99.5 mg, 0.0845 mmol, 1.0 equiv) was dissolved in d_6-acetone (1.8 mL, dried over 3Å molecular sieves) in an NMR sample tube. A 9:1 mixture of D_2O:TFA was added (200 μL) and the reaction progress was monitored by ^{1}H NMR spectroscopy. After eight minutes at 21.4 °C, the mixture was transferred into saturated aqueous $NaHCO_3$ (2 mL). This mixture was extracted with CH_2Cl_2 (3 x 5 mL). The combined organic extracts were dried over $MgSO_4$, filtered, and concentrated under reduced pressure. The residue was purified by MPLC (SiO_2, 2:1 hexanes:EtOAc) to provide recovered starting material **302a** (27.3 mg, 0.0232 mmol, 27.4%). Additional elution in 1:1 hexanes:EtOAc gave the title compound as a white, crystalline solid [56.9 mg, 0.0560 mmol, 66.3% (91.4% brsm)].

^{1}H NMR (500 MHz, $CDCl_3$): δ 8.12 (dd, *J* = 8.5, 1.3 Hz, 2H, C2O_2C-*o*-Ph), 7.75 (dd, *J* = 8.5, 1.4 Hz, 2H, C3'NHCO-*o*-Ph), 7.61 (tt, *J* = 7.5, 1.2 Hz, 1H, C2O_2C-*p*-Ph, 1H), 7.53-7.46 (m, 5H, C2O_2C-*m*-Ph, C3'NHCO-*p*-Ph, and C3'-*o*-Ph,), 7.43-7.37 (m, 4H, C3'-*m*-Ph and C3'NHCO-*m*-Ph), 7.34 (tt, *J* = 7.3, 1.2 Hz, 1H, C3'-*p*-Ph), 7.09 (d, *J* = 9.0 Hz, 1H, C3'NH), 6.56 (s, 1H, H10), 6.18 (br dd, *J* = 9, 9 Hz, 1H, H13), 5.80 (dd, *J* = 6.9, 2.5 Hz, 1H, H3'), 5.69 (d, *J* = 6.9 Hz, 1H,

H2), 4.93 (dd, *J* = 9.6, 1.7 Hz, 1H, H5), 4.78 (dd, *J* = 4.9, 2.7 Hz, 1H, 2'H), 4.57 (dd, *J* = 10.5, 6.9 Hz, 1H, H7), 4.30 (d, *J* = 8.4 Hz, 1H, H20α), 4.19 (dd, *J* = 8.3, 0.9 Hz, 1H, H20β), 3.83 (d, *J* = 6.9 Hz, 1H, H3), 3.76 [q, *J* = 7.0 Hz, 6H, C7OSi(OC*H*$_2$CH$_3$)$_3$], 3.69 (br s, 1H, C2'OH), 2.65 (ddd, *J* = 14.7, 9.7, 6.9 Hz, 1H, H6α), 2.37 (s, 3H, C4OAc), 2.35-2.25 (m, 2H, H14α and H14β), 2.15 (s, 3H, C10OAc), 1.95 (ddd, *J* =14.6, 10.7, 2.1 Hz, 1H, H6β), 1.93 (d, *J* = 1.3 Hz, 3H, C18H$_3$), 1.76 (br s, 1H, C1OH), 1.73 (s, 3H, C19H$_3$), 1.23 (s, 3H, C17H$_3$), 1.19 [t, *J* = 7.0 Hz, 9H, C7OSi(OCH$_2$C*H*$_3$)$_3$], and 1.16 (s, 3H, C16H$_3$).

^{13}C NMR (125 MHz, $CDCl_3$): δ 202.4, 172.6, 170.4, 169.0, 167.2, 167.1, 140.1, 138.2, 133.9, 133.8, 132.1, 130.3, 129.4, 129.1, 128.89, 128.87, 128.5, 127.3, 127.24, 127.23, 84.4, 81.5, 78.8, 76.8, 76.1, 74.8, 73.4, 72.5, 72.1, 59.5, 58.6, 55.0, 47.0, 43.4, 36.7, 35.6, 26.8, 22.9, 21.1, 21.0, 18.2, 14.5, and 10.3.

HRMS (ESI) Calc'd for $C_{53}H_{65}NNaO_{17}Si$ $[M + Na]^+$ 1038.3914, found 1038.3914.

IR (thin film) 3500 (br), 2975, 2898, 1724, 1653, 1602, 1580, 1515, 1485, 1451, 1394, 1370, 1314, 1266, 1240, 1172, 1079, 1025, 969, 913, 888, 839, 797, and 712 cm^{-1}.

mp = 141-146 °C. **TLC** R_f (1:1 hexanes:EtOAc) = 0.5.

7-*O*-(Tri-*n*-octyloxysilyl)paclitaxel (303b).

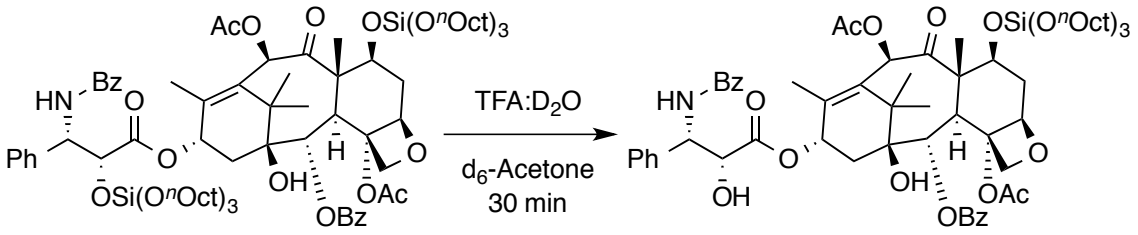

302b ***303b***

Bis(trioctyloxy)silicate ester **302b** (88.1 mg, 0.0523 mmol, 1.0 equiv) was dissolved in *d*$_6$-acetone (1.8 mL, dried over 3Å molecular sieves) in an NMR tube. A 9:1 mixture of D_2O:TFA was added (200 μL) and the solution became white and cloudy. Upon vigorous mixing for 30 seconds, the mixture became homogeneous and transparent. The hydrolysis progress was monitored by ^{1}H NMR spectroscopy. After 30 minutes at room temperature, the solution was transferred into saturated aqueous $NaHCO_3$ (2 mL). This mixture was extracted with CH_2Cl_2 (3 x 5 mL). The combined organic layers were dried over $MgSO_4$ and concentrated under reduced pressure. The residue was purified by MPLC (SiO_2, 3:1 hexanes:EtOAc) to provide recovered **302b** (12.9 mg, 0.0076 mmol, 27.4%). Additional elution in 2:1 hexanes:EtOAc gave the title compound as a crystalline solid [37.3 mg, 0.0294 mmol, 56.2% (65.7% brsm)].

^{1}H NMR (500 MHz, $CDCl_3$): δ 8.12 (dd, *J* = 8.5, 1.3 Hz, 2H, C2O_2C-*o*-Ph), 7.75 (dd, *J* = 8.5, 1.4 Hz, 2H, C3'NHCO-*o*-Ph), 7.61 (tt, *J* = 7.4, 1.3 Hz, 1H, C2O_2C-*p*-Ph, 1H), 7.53-7.47 (m, 5H, C2O_2C-*m*-Ph, C3'NHCO-*p*-Ph, and C3'-*o*-Ph,), 7.43-7.38 (m, 4H, C3'-*m*-Ph and C3'NHCO-*m*-Ph), 7.34 (tt, *J* = 7.2, 1.3 Hz, 1H, C3'-*p*-Ph), 7.06 (d, *J* = 9.0 Hz, 1H, C3'NH), 6.53 (s, 1H, H10), 6.17 (br dd, *J* =

9, 9 Hz, 1H, H13), 5.81 (dd, *J* = 6.8, 2.4 Hz, 1H, H3'), 5.68 (d, *J* = 6.9 Hz, 1H, H2), 4.92 (dd, *J* = 9.6, 1.8 Hz, 1H, H5), 4.78 (dd, *J* = 4.8, 2.6 Hz, 1H, 2'H), 4.56 (dd, *J* = 10.5, 6.7 Hz, 1H, H7), 4.29 (d, *J* = 8.3 Hz, 1H, H20α), 4.19 (d, *J* = 8.5 Hz, 1H, H20β), 3.83 (d, *J* = 7.0 Hz, 1H, H3), 3.66 {t, *J* = 6.7 Hz, 6H, C7OSi[OC*H*$_2$(CH$_2$)$_6$CH$_3$]$_3$}, 3.60 (d, *J* = 4.9 Hz, 1H, C2'OH), 2.64 (ddd, *J* = 14.7, 9.7, 6.9 Hz, 1H, H6α), 2.37 (s, 3H, C4OAc), 2.34-2.27 (m, 2H, H14α and H14β), 2.14 (s, 3H, C10OAc), 1.97-1.90 (m, 4H, H6β and C18H$_3$), 1.74-1.70 (m, 4H, C1OH and C19H$_3$), 1.52 {tt, *J* = 6.8, 6.8 Hz, 6H, C7OSi[OCH$_2$C*H*$_2$(CH$_2$)$_5$CH$_3$]$_3$}, 1.34-1.22 {m, 33H, C17H$_3$ and C7OSi[OCH$_2$CH$_2$(C*H*$_2$)$_5$CH$_3$]$_3$}, 1.16 (s, 3H, C16H$_3$), and 0.88 {t, *J* = 6.8 Hz, 9H, C7OSi[OCH$_2$CH$_2$(CH$_2$)$_5$C*H*$_3$]$_3$}.

^{13}C NMR (125 MHz, CDCl$_3$): δ 202.2, 172.7, 170.3, 168.8, 167.2, 167.0, 140.0, 138.3, 133.93, 133.89, 132.1, 130.4, 129.4, 129.1, 128.9 (x3), 128.5, 127.3, 127.2, 84.5, 81.5, 78.8, 76.8, 76.0, 74.9, 72.5, 72.3, 71.7, 63.9, 58.6, 54.9, 47.0, 43.4, 36.6, 35.6, 32.5, 32.1, 29.62, 29.57, 26.8, 25.9, 22.91, 22.88, 21.1, 21.0, 14.5, 14.3, and 10.3.

HRMS (ESI) Calc'd for C$_{71}$H$_{101}$NNaO$_{17}$Si [M + Na]$^+$ 1290.6731; found 1290.6738.

IR (thin film) 3500 (br), 2926, 2855, 1732, 1710, 1673, 1602, 1582, 1452, 1396, 1370, 1317, 1281, 1269, 1241, 1179, 1093, 1025, 988, 968, 890, 844, 809, and 712 cm^{-1}.

mp = 69-73 °C. **TLC** R_f (2:1 hexanes:EtOAc) = 0.4.

7-*O*-(Tri-*i*-propoxysilyl)paclitaxel (303c).

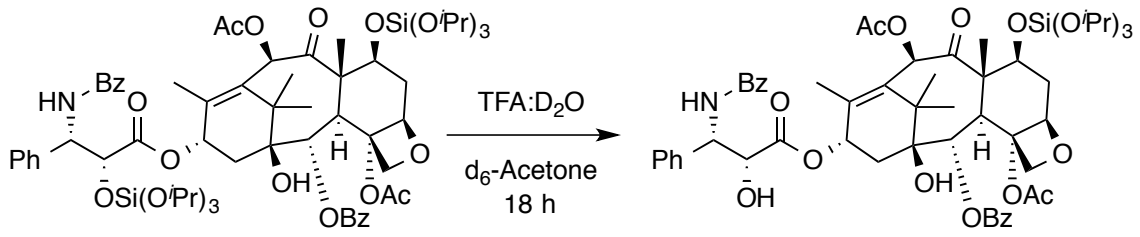

302c ***303c***

Bis-silicate ester **302c** (102.3 mg, 0.081 mmol, 1.0 equiv) was dissolved in d_6-acetone (1.35 mL, dried over 3Å molecular sieves). A 9:1 mixture of D_2O:TFA was added (150 μL) and the solution became white and cloudy. Upon being shaken for ca. 30 seconds, the mixture became homogeneous and transparent. The hydrolysis progress was monitored by ^{1}H NMR spectroscopy. After 18 hours at room temperature, the solution was transferred into saturated aqueous $NaHCO_3$ (3 mL). This mixture was extracted with CH_2Cl_2 (3 x 5 mL). The combined organic layers were dried over $MgSO_4$ and concentrated. The residue was purified by MPLC (SiO_2, 1:1 hexanes:EtOAc) to provide recovered **302c** (35.8 mg, 0.028 mmol, 35%) and the title compound as a crystalline solid [43.3 mg, 0.041 mmol, 50.5% (77% brsm)].

^{1}H NMR (500 MHz, $CDCl_3$): δ 8.13 (dd, *J* = 8.4, 1.3 Hz, 2H, C2O$_2$C-*o*-Ph), 7.75 (dd, *J* = 8.5, 1.3 Hz, 2H, C3'NHCO-*o*-Ph), 7.62 (tt, *J* = 7.0, 1.3 Hz, 1H, C2O$_2$C-*p*-Ph, 1H), 7.53-7.49 (m, 5H, C2O$_2$C-*m*-Ph, C3'NHCO-*p*-Ph, and C3'-*o*-Ph,), 7.43-7.39 (m, 4H, C3'-*m*-Ph and C3'NHCO-*m*-Ph), 7.34 (tt, *J* = 7.3, 1.2 Hz, 1H, C3'-*p*-Ph), 7.05 (d, *J* = 9.0 Hz, 1H, C3'NH), 6.50 (s, 1H, H10), 6.19 (ddq, *J* = 9.1, 9.1, 1.4 Hz, 1H, H13), 5.80 (dd, *J* = 9.0, 2.4 Hz, 1H, H3'), 5.68 (d, *J* = 7.0

Hz, 1H, H2), 4.94 (dd, *J* = 9.6, 1.9 Hz, 1H, H5), 4.81 (d, *J* = 2.6 Hz, 1H, H2'), 4.57 (dd, *J* = 6.8, 10.5 Hz, 1H, H7), 4.30 (d, *J* = 8.4 Hz, 1H, H20α), 4.19 (d, *J* = 8.5 Hz, 1H, H20β), 4.11 {sept, *J* = 6.1 Hz, 3H, C7OSi[OC*H*(CH_3)$_2$]$_3$}, 3.83 (d, *J* = 7.0 Hz, 1H, H3), 3.60 (br s, 1H, C2'OH), 2.67 (ddd, *J* = 14.8, 9.8, 6.9 Hz, 1H, H6α), 2.37 (s, 3H, C4OAc), 2.36–2.25 (m, 2H, H14α and H14β), 2.14 (s, 3H, C10OAc), 1.96 (d, *J* = 1.5 Hz, C18H_3), 1.95-1.91 (ddd, *J* 14.7, 10.6, 2.1 Hz, 1H, H6β), 1.73 (s, 3H, C19H_3), 1.65 (br s, 1H, C1OH), 1.24 (s, C17H_3), 1.160 (s, 3H, C16H_3), 1.160, {d, *J* = 6.1, 9H, C7OSi[OCH(C*H*$_3$)$_3$]}, and 1.15 {d, *J* = 6.1 Hz, 9H C7OSi[OCH(C'*H*$_3$)$_3$]}.

^{13}C NMR (125 MHz, $CDCl_3$): δ 202.5, 172.7, 170.3, 168.9, 167.2, 167.1, 140.3, 138.2, 133.92, 133.80, 132.1, 130.4, 129.4, 129.2 (2x), 128.9 (2x), 128.5, 127.3, 127.2, 84.5, 81.5, 78.8, 76.8, 76.0, 74.9, 73.3, 72.6, 72.4, 66.3 {SiO*C*H(CH_3)$_2$}, 58.5, 54.9, 47.0, 43.4, 36.8, 35.6, 26.9, 25.5 {SiOCH(*C*H_3)$_2$}, 25.4 {SiOCH(*C*'H_3)$_2$}, 22.9, 21.1, 21.0, 14.8, and 10.4.

HRMS (ESI) Calc'd for $C_{56}H_{71}NNaO_{17}Si$ $[M + Na]^+$ 1080.4383 ; found 1080.4393.

IR (thin film) (br) 3448, 3067, 3026, 2972, 2934, 2898, 1724, 1662, 1602, 1581, 1485, 1452, 1370, 1315, 1289, 1269, 1239, 1174, 1136, 1113, 1048, 987, 969, 949, 892, 838, 803, and 775 cm^{-1}.

mp = 134.5-136 °C. **TLC** R_f (1:1 hexanes:EtOAc) = 0.40.

7-*O*-(Tri-*i*-propoxysilyl)paclitaxel (303p).

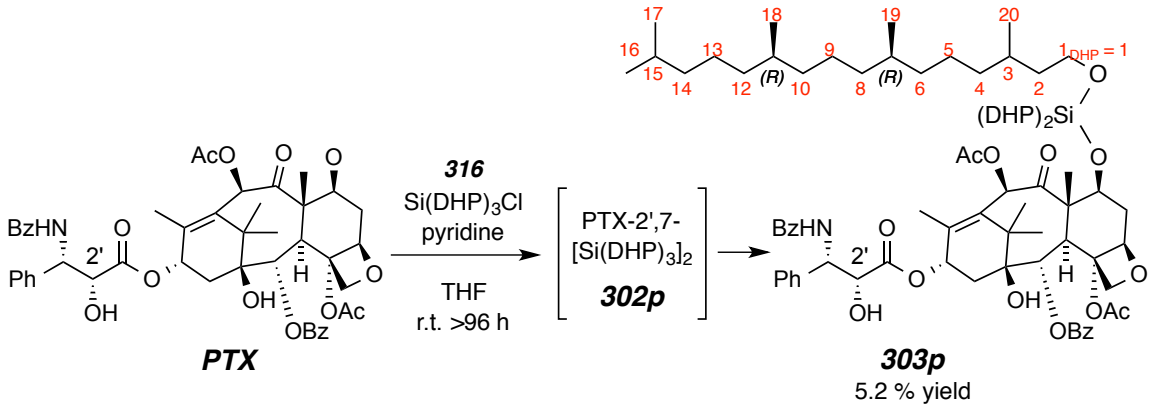

Paclitaxel (76.1 mg, 0.089 mmol, 1.0 equiv) was dissolved in dry THF (3 mL) in an oven-dried culture tube fitted with a Teflon-lined cap and magnetic stir bar. Pyridine (500 μL, 6.20 mmol, 69.7 equiv) was added by Wiretrol®. A 1:1.7 mixture based on moles (^{1}H NMR) which corresponds to a 1:1.3 mixture based on mass (^{1}H NMR) of the DHP-silicates tri-*n*-dihydrophytolchlorosilane (**316**):tetra-*n*-dihydrophytolchlorosilane (**317**) (500 μL, ca. 0.428 mmol based on an ca. density of 1.5, 1.6 equiv of tri-*n*- dihydrophytolchlorosilane) was added. The culture tube was capped and the suspension was allowed to stir for 27 h at room temperature. The reaction solvent was removed on a rotary evaporator replaced with a mixture of hexanes:EtOAc (2:1), the slurry filtered through a short plug of Celite® to remove the pyridinium salt, the filtrate concentrated under reduced pressure. The residue redissolved in 2 mL of hexanes:EtOAc (2:1). Three sequential purifications by MPLC chromatography (SiO_2, 2:1 hexanes:EtOAc), (SiO_2, 3:1

hexanes:EtOAc), (SiO_2, 5:1 hexanes:EtOAc), yielded the title compound as a clear, glassy solid (8.3 mg, 0.0046 mmol, 5.2%).

^{1}H NMR (500 MHz, $CDCl_3$): δ 8.12 (dd, *J* = 7.4, 1.5 Hz, 2H, C2O_2C-*o*-Ph), 7.75 (dd, *J* = 7.4, 1.4 Hz, 2H, C3'NHCO-*o*-Ph), 7.61 (tt, *J* = 7.6, 1.2 Hz, 1H, C2O_2C-*p*-Ph), 7.52-7.48 (m, 5H, C2O_2C-*m*-Ph, C3'-*o*-Ph, C3'NHCO-*p*-Ph), 7.43-7.39 (m, 4H, C3'-*m*-Ph and C3'NHCO-*m*-Ph), 7.34 (tt, *J* = 7.4, 2.3 Hz, 1H, C3'-*p*-Ph), 7.05 (overlapping s, 1H, H10), 7.04 (d, *J* = 8.7 Hz, 1H, C3'NH), 6.17 (br dd, *J* = 8.7, 8.7 Hz, 1H, H13), 5.80 (dd, *J* = 8.9, 2.2 Hz, 1H, H3'), 5.68 (d, *J* = 6.9 Hz, 1H, H2), 4.92 (dd, *J* = 9.0, 1.0 Hz, 1H, H5), 4.79 (dd, *J* = 4.4, 2.6 Hz, 1H, H2'), 4.55 (dd, *J* = 10.4, 7.0, Hz, 1H, H7), 4.29 (d, *J* = 8.4 Hz, 1H, H20α), 4.19 (d, *J* = 8.4 Hz, 1H, H20β), 3.83 (d, *J* = 6.9 Hz, 1H, H3), 3.74-3.65 {m, 6H, C7OSi[OC1$_{DHP}$*H*$_2$]$_3$}, 3.54 (d, 2.55, *J* = 4.4 Hz, 1H, C2'OH), 2.63 (ddd, *J* = 15.0, 9.4, 7.2 Hz, 1H, H6α), 2.36 (s, 3H, C4OAc), 2.32 (dd, *J* = 10.3, 9.3 Hz, 1H, H14α), 2.13 (s, 3H, C10OAc), 2.08 (dd, *J* = 14.8, 8.8 Hz, 1H, H14β), 1.98-1.92 (m, 1H, H6β), 1.93 (overlapping br s, 3H, C18H_3), 1.73 (s, 3H, C19H_3), 1.70 (s, 1H, C1OH),1.55-1.48 [br td, *J* = 6.6, 6.6 Hz, 6H, C7OSi[OC2$_{DHP}$*H*$_2$]$_3$], 1.42-1.30 {m, 12H, C7OSi[OC3$_{DHP}$*H*$_1$]$_3$, C7OSi[OC7$_{DHP}$*H*$_1$]$_3$, C7OSi[OC11$_{DHP}$*H*$_1$]$_3$, C7OSi[OC15$_{DHP}$*H*$_1$]$_3$}, 1.30-1.20 {m, 30H, C7OSi[OC4$_{DHP}$*H*$_2$]$_3$, C7OSi[OC5$_{DHP}$*H*$_2$]$_3$, C7OSi[OC6$_{DHP}$*H*$_2$]$_3$, C7OSi[OC8$_{DHP}$*H*$_2$]$_3$}, C7OSi[OC9$_{DHP}$*H*$_2$]$_3$}, 1.16 (overlapping s, 3H, C17H_3), 1.16-1.02 {m, 33H, C7OSi[OC10$_{DHP}$*H*$_2$]$_3$, C7OSi[OC12$_{DHP}$*H*$_2$]$_3$, C7OSi[OC13$_{DHP}$*H*$_2$]$_3$, C7OSi[OC14$_{DHP}$*H*$_2$]$_3$, and C16H_3), 0.86 {d, *J* = 6.5 Hz, 27H, C7OSi[OC16$_{DHP}$*H*$_3$]$_3$, and C7OSi[OC17$_{DHP}$*H*$_3$]$_3$ C7OSi[OC18$_{DHP}$*H*$_3$]$_3$, }, and 0.84 {br d, *J* = 6.5 Hz, 18H, C7OSi[OC19$_{DHP}$*H*$_3$]$_3$, and C7OSi[OC20$_{DHP}$*H*$_3$]$_3$}.

^{13}C NMR (125 MHz, $CDCl_3$): δ 201.5, 174.2, 169.9, 168.6, 167.7, 166.8, 139.5, 137.8, 133.5, 133.0, 131.8, 130.2, 128.7 (2x), 128.6, 128.4 (2x), 127.9, 127.1,

126.9, 84.3, 78.3, 75.8, 76.5, 75.6, 74.6, 73.0, 72.2, 71.8, 57.5, {61.9 (3x), C_{dhp}1}, 54.6, 46.7, 42.0, {39.3 (9x), C_{dhp}2, C_{dhp}3, and C_{dhp}4}, {37.5 (6x), C_{dhp}14, and C_{dhp}8}, {37.4 (6x), C_{dhp}10, andC_{dhp}12}, 36.6, 35.4, {32.9 (3x), C_{dhp}6}, {29.6, 29.3, 28.0 C_{dhp}7}, 28.0, {27.9 (3x), C_{dhp}11},{24.6 (3x), C_{dhp}15}, {24.5 (6x), C_{dhp}5, and C_{dhp}13}, {23.7 (2x), 23.4 C_{dhp}9}, 23.2, {23.0 (3x), 22.6 (3x), C_{dhp}16, and C_{dhp}17}, 22.7, {21.7 (3x), C_{dhp}18}, 20.8, {20.5 (2x), 20.3, C_{dhp}19}, {20.0 (2x), 19.7 C_{dhp}20}, 14.2, 10.0.

TLC R_f (5:1 hexanes:EtOAc) = 0.38.

2'-*O*-(Triethoxysilyl)docetaxel (304a).

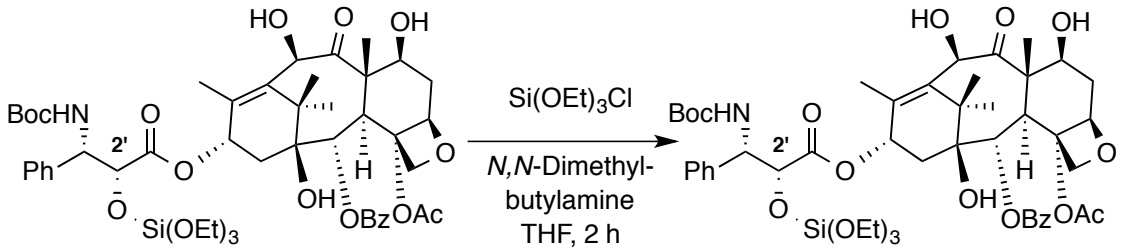

DTX ***304a***

Docetaxel (75.0 mg, 0.0930 mmol, 1.0 equiv) was dissolved in dry THF (2.0 mL) in an oven-dried culture tube fitted with a Teflon-lined cap and magnetic stir bar. *N,N*-Dimethylbutylamine (35 µL, 0.250 mmol, 2.7 equiv) was added by Wiretrol®. Triethoxychlorosilane (**305a**) (50 *µ*L, 50.6 mg, 0.255 mmol, 2.7 equiv.) was added. The culture tube was sealed and the suspension was allowed to stir for 2 h at room temperature. A white precipitate was observed immediately upon the addition of the chlorosilane to the reaction mixture. The THF was removed by evaporation under reduced pressure and the solid residue was triturated with a mixture of hexanes:EtOAc (1:1), and the resulting slurry was filtered through a short plug of Celite® to remove the ammonium salt. The filtrate was concentrated under reduced pressure, and the residue was purified by MPLC (SiO_2, 1:1 hexanes:EtOAc) to yield the title compound as a white, crystalline solid (58.1 mg, 0.060 mmol, 64.5%).

^{1}H NMR (500 MHz, $CDCl_3$, some resonances were broadened presumably due to the presence of NBoc rotamers): δ 8.10 (d, *J* = 7.9 Hz 2H, O_2C-*o*-Ph), 7.60 (t, *J* = 7.2 Hz, 1H, O_2C-*p*-Ph), 7.50 (t, *J* = 7.9 Hz, 2H, O_2C-*m*-Ph), 7.36 (t, 2H, *J* =

8.0 Hz, C3'-*m*-Ph), 7.33 (d, 2H, *J* = 7.2 Hz, C3'-*o*-Ph), 7.25 (t, *J* = 6.5 Hz 1H, C3'-*p*-Ph), 6.27 (br m, 1H, H13), 5.67 (d, *J* = 7.3 Hz, 1H, H2), 5.62 (d, *J* = 8.9 Hz, 1H, H3'), 5.28 (br s, 1H, NH), 5.21 (s, 1H, H10), 4.96 (dd, *J* = 9.9, 1.9 Hz, 1H, H5), 4.81 (br s, 1H, H2'), 4.31 (d, *J* = 8.6 Hz, 1H, H20α), 4.25 (br dd, *J* = 11.6, 7.2, Hz, 1H, H7), 4.22 (d, *J* = 1.5 Hz, 1H, C10O*H*), 4.19 (d, *J* = 8.6 Hz 1H, H20β), 3.92 (d, *J* = 6.9 Hz, 1H, H3), 3.66 {br q, *J* = 6.7, 5.8 Hz, 6H, C2'OSi[OCH_2CH$_3$]$_3$}, 2.58 (ddd, *J* = 14.0, 9.9, 6.4 Hz, 1H, H6α), 2.44 (s, 3H, C4OAc), 2.29 (br m, 1H, H14α), 2.11 (br m, 1H, H14β), 1.93 (s, 3H, =CCH$_3$), 1.85 (ddd, *J* = 14.6, 11.5, 2.8 Hz 1H, H6β), 1.74 (s, 3H, O=CCCH_3), 1.71 (s, 1H, C1O*H*), 1.32 (br s, 9H, *t*Boc), 1.25 {s, C(Me)C16H_3}, 1.12 [t, *J* = 7.0 Hz, 9H, C2'OSi(OCH$_2$CH_3)$_3$], and 1.11 (s, 3H, C(Me)C17H_3).

^{13}C NMR (125 MHz, CDCl$_3$): δ 211.6 (C9), 170.7 (C1'), 170.0 (C21), 167.1 (C2-O*C*OBz), 155.4 (C3'-NH*C*O), 139.3 (C3'-*ipso*-Ph), 138.6 (C12), 135.4 (C11), 133.7 (OBz-*p*), 130.2 (OBz-*i*), 129.2 (OBz-*o*), 128.7 (OBz-*m*), 128.5 (2x C3'-*o*-Ph), 127.6 (C3'-*m*-Ph), 126.5 (C3'-*p*-Ph), 84.2 (C5), 80.9 (O*C*Me$_3$), 79.9 (C1), 79.0 (C4), 76.6 (C20), 75.2 (C2), 75.0 (C10), 74.5 (C2'), 71.9 (C13), 71.2 (C7), 59.4 (3x C2'OSiO*C*H$_2$CH$_3$), 57.5 (C8), 56.3 (C3'), 46.4 (C3), 43.1 (C15), 36.9 (C6), 35.6 (C14), 28.2 [C3'-NHCOC(*C*H$_3$)], 26.4 (C16), 22.7 (C22), 21.0 (C17), 18.0 (SiOCH$_2$*C*H$_3$), 14.1 (C18), and 9.9 (C19).

HRMS (ESI) Calc'd for $C_{49}H_{67}NNaO_{17}Si$ $[M + Na]^+$ 992.4070; found 992.4083.

IR (thin film) 3443, 2977, 2930, 2897, 2368, 1756, 1712, 1495, 1453, 1392, 1367, 1314, 1271, 1244, 1166, 1105, 1081, 1025, 983, 915, 88, 798, 786, and 758 cm^{-1}.

mp = 117-119 °C.**TLC** R_f (1:1 hexanes:EtOAc) = 0.42.

2'-*O*-(Tri-*n*-octyloxysilyl)docetaxel (304b).

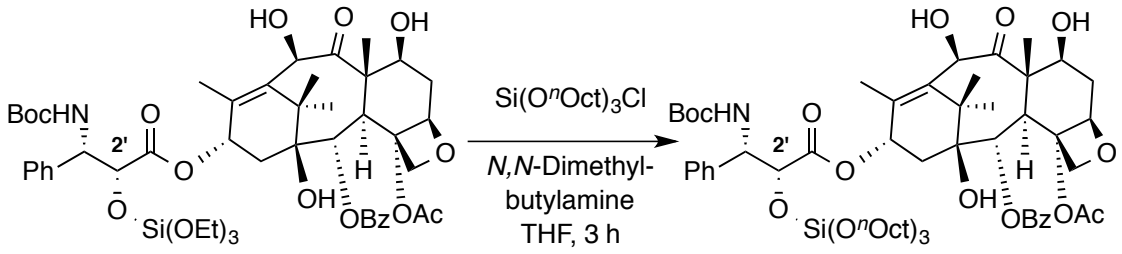

DTX ***304b***

Docetaxel (36.4 mg, 0.0450 mmol, 1.0 equiv) was dissolved in dry THF (2.0 mL) in an oven-dried culture tube fitted with a Teflon-lined cap and magnetic stir bar. *N,N*-Dimethylbutylamine (35 µL, 0.250 mmol, 5.5 equiv) was added by Wiretrol®. Tri-*n*-octyloxychlorosilane (**305b**) (containing ca. 20% of tetra-*n*-octyloxysilane; 50 *µ*L, estimated to contain 32.0 mg, 0.071 mmol, 1.6 equiv of the tri-*n*-octyloxychlorosilane) was added. The culture tube was sealed and the suspension was allowed to stir for 3 h at room temperature. A white precipitate was observed to grow over the first 30 min of the reaction period. The THF was removed by evaporation under reduced pressure and the solid residue was triturated with a mixture of hexanes:EtOAc (2:1), and the resulting slurry was filtered through a short plug of Celite® to remove the ammonium salt. The filtrate was concentrated under reduced pressure, and the residue was purified by MPLC (SiO_2, 2:1 hexanes:EtOAc) to yield the title compound as a white, crystalline solid (35.1 mg, 0.0287 mmol, 63.7%).

^{1}H NMR (500 MHz, $CDCl_3$, some resonances were broadened presumably due to the presence of NBoc rotamers): δ 8.12 (d, *J* = 7.9 Hz 2H, O_2C-*o*-Ph), 7.60 (t, *J* = 7.3 Hz, 1H, O_2C-*p*-Ph), 7.50 (t, *J* = 7.8 Hz, 2H, O_2C-*m*- Ph), 7.35 (t, 2H, *J* = 7.9 Hz, C3'-*m*-Ph), 7.32 (d, 2H, *J* = 6.9 Hz, C3'-*o*-Ph), 7.25 (t, *J* = 6.8 Hz 1H, C3'-*p*-Ph), 6.28 (br dd, *J* = 9, 9 Hz, 1H, H13), 5.69 (d, *J* = 7.1 Hz, 1H, H2), 5.62 (d, *J* = 9 Hz H3'), 5.28 (br s, 1H, NH), 5.20 (s, 1H, H10), 4.96 (dd, *J* = 9.6, 1.8 Hz, 1H, H5), 4.81 (br s, 1H, H2'), 4.32 (d, *J* = 8.5 Hz, 1H, H20a), 4.25 (br dd, *J* = 10.2, 7.0, Hz, 1H, H7), 4.20 (d, *J* = 8.1 Hz, 1H, H20b), 4.19 (br s, 1H, C10OH), 3.93 (d, *J* = 7.1 Hz, 1H, H3), 3.56 {t, *J* = 6.5 Hz, 6H, C2'OSi[OCH_2 $(CH_2)_6CH_3]_3$}, 2.59 (ddd, *J* = 15.8, 9.5, 6.5 Hz, 1H, H6a), 2.43 (s, 3H, C4OAc), 2.29 (br m, 1H, H14a), 2.12 (br m, 1H, H14b), 1.93 (s, 3H, =CCH_3), 1.85 (ddd, *J* = 13.9, 11.6, 2.2 Hz 1H, H6b), 1.75 (s, 3H, O=CCCH_3), 1.65 (d, 1H, *J* = 2.6, C1OH), 1.46 {br pent, *J* = 6.4 Hz, 6H, C2'OSi[OCH_2C*H*$_2(CH_2)_5CH_3]_3$}, 1.32 (br s, 9H, *t*Boc), 1.31-1.24 {m, 33H, C2'OSi[$OCH_2CH_2(C$*H*$_2)_5CH_3]_3$}, and C(Me)C16H_3}, 1.12 (s, 3H, C(Me)C17H_3), and 0.89 {t, *J* = 6.7 Hz, 9H, C2'OSi[$OCH_2CH_2(CH_2)_5C$*H*$_3]_3$}.

^{13}C NMR (125 MHz, $CDCl_3$): δ 211.9, 170.8, 170.1, 167.3, 155.3, 139.6, 138.9, 135.5, 133.8, 130.4, 129.4, 128.9 128.7, 127.8, 126.7, 84.4, 81.1, 80.0, 79.2, 77.6, 76.8, 75.2, 74.7, 72.1, 71.3, 64.0, 57.7, 56.3, 46.6, 43.3, 37.2, 35.9, 32.4, 32.1, 29.6, 29.5, 28.4, 26.5, 25.8, 22.93, 22.90, 21.2, 14.4, 14.3, and 10.2.

HRMS (ESI) Calc'd for $C_{67}H_{103}NNaO_{17}Si$ $[M + Na]^+$ 1244.6887; found 1244.6954.

IR (thin film) 3454, 3382, 2926, 2855, 1755, 1737, 1713, 1699, 1495, 1454, 1367, 1272, 1245, 1165, 1095, 1025, 987, 946, 943, 920, 888, 865, 824, 800, and 778 cm^{-1}.

mp = 54-58 °C. **TLC** Rf (3:1 hexanes:EtOAc) = 0.13.

2'-*O*-(Tri-*i*-propoxysilyl)docetaxel (304c).

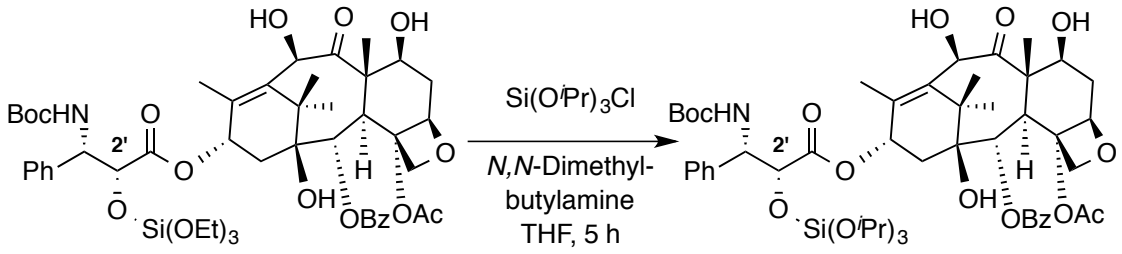

DTX ***304c***

Docetaxel (40.0 mg, 0.0490 mmol, 1.0 equiv) was dissolved in dry THF (2.0 mL) in an oven-dried culture tube fitted with a Teflon-lined cap and magnetic stir bar. *N,N*-Dimethylbutylamine (50 µL, 0.357 mmol, 7.3 equiv) was added by Wiretrol®. Tri-*i*-propoxychlorosilane (**305c**) (containing ca. 80% of tri-*i*-propoxychlorosilane; 50 *µ*L, estimated to contain 42.0 mg, 0.175 mmol, 3.8 equiv of the tri-*i*-propoxychlorosilane) was added. The culture tube was capped and the suspension was allowed to stir for 5 h at room temperature. A white precipitate was observed to grow over 3 hours of the reaction. The THF was removed by evaporation under reduced pressure and the solid residue was triturated with a mixture of hexanes:EtOAc (2.4:1). The resulting slurry was filtered through a short plug of Celite® to remove the ammonium salt. The filtrate was concentrated under reduced pressure, and the residue was purified by MPLC (SiO_2, 2.4:1 hexanes:EtOAc) to yield the title compound as a white, crystalline solid (31.2 mg, 0.0308 mmol, 62.8%).

^{1}H NMR (500 MHz, $CDCl_3$, some resonances were broadened presumably due to the presence of NBoc rotamers): δ 8.10 (d, *J* = 7.6 Hz 2H, O_2C-*o*-Ph), 7.62 (t, *J* = 7.4 Hz, 1H, O_2C-*p*-Ph), 7.51 (t, *J* = 7.8 Hz, 2H, O_2C-*m*-Ph), 7.35 (t, 2H, *J* = 8.0 Hz, C3'-*m*-Ph), 7.32 (d, 2H, *J* = 6.9 Hz, C3'-*o*-Ph), 7.23 (t, *J* = 6.6 Hz 1H, C3'-*p*-Ph), 6.21 (br m, 1H, H13), 5.69 (d, *J* = 9 Hz, 1H, H3'), 5.68 (d, *J* = 7.0 Hz, H2), 5.21 (br s, 1H, NH), 5.20 (s, 1H, H10), 4.96 (dd, *J* = 9.6, 2.1 Hz, 1H, H5), 4.81 (br s, 1H, H2'), 4.31 (d, *J* = 8.5 Hz, 1H, H20a), 4.25 (ddd, *J* = 11.3, 8.0, 7.0 Hz, 1H, H7), 4.19 (br s, 1H, C10OH), 4.18 (d, *J* = 8.6 Hz, 1H, H20b), 4.09 {br septet, *J* = 5.9 Hz, 3H, OSi[OC*H*$(CH_3)_2]_3$}, 3.91 (d, *J* = 7.1 Hz, 1H, H3), 2.60 (ddd, *J* = 14.4, 9.7, 6.5 Hz, 1H, H6a), 2.40 (s, 3H, C4OAc), 2.22 (br m, 1H, H14a), 2.05 (br m, 1H, H14b), 1.93 (s, 3H, =CCH_3), 1.84 (ddd, *J* = 14.1, 11.3, 2.5 Hz 1H, H6b), 1.75 (s, 3H, O=CCC19H_3), 1.60 (br s, 1H, C1OH), 1.46 (d, 1H, *J* = 8.0 Hz, C7OH), 1.33 (br s, 9H, *t*Boc), 1.24 [s, 3H, C(Me)C16H_3], and 1.14-1.10 {m, 21H, C(Me)C17H_3 and OSi[OCH(C$H_3)_2]_3$}

^{13}C NMR (125 MHz, $CDCl_3$): δ 211.7, 170.7, 169.9, 167.1, 155.4, 139.5, 138.7, 135.2, 133.7, 130.2, 129.2, 128.7, 128.5, 127.6, 126.6, 84.2, 80.9, 79.0, 76.6, 75.1, 75.0, 74.5, 73.2, 71.9, 71.1, 66.3, 57.5, 56.7, 46.4, 43.1, 36.9, 35.6, 28.2, 26.3, 25.2, 22.7, 21.0, 14.4, and 10.0.

HRMS (ESI) Calc'd for $C_{52}H_{73}NNaO_{17}Si$ $[M + Na]^+$ 1034.4540; found 1034.4545.

IR (thin film) 3683, 2973, 2917, 2849, 2349, 1757, 1733, 1717, 1701, 1649, 1631, 1547, 1494, 1461, 1452, 1369, 1271, 1244, 1167, 1114, 1051, 986, 892, 846, and 778 cm^{-1}.

mp = 118.5-121 °C. **TLC** R_f (2.4:1 hexanes:EtOAc) = 0.10.

2'-(Trimenthyloxysilyloxy)docetaxel (304d).

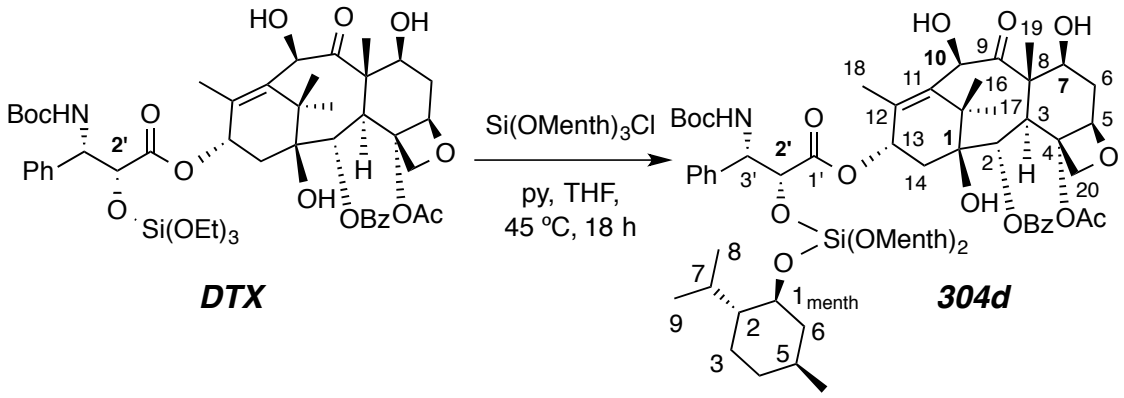

Docetaxel (50.5 mg, 0.063 mmol, 1.0 equiv) was dissolved in dry THF (1.0 mL) in an oven-dried culture tube fitted with a Teflon-lined cap and magnetic stir bar. Pyridine (35 µL, 0.45 mmol, 7.2 equiv) was added by Wiretrol®. Trimenthyloxychlorosilane (**305d**) (50 *µ*L, 44 mg, 0.083 mmol, 1.3 equiv) was added. The culture tube was sealed and the suspension was allowed to stir for 18 h at 45 ºC. The THF was removed by evaporation under reduced pressure, the solid residue was triturated with a mixture of hexanes:EtOAc (2:1), and the resulting slurry was filtered through a short plug of Celite® to remove the pyridinium salt. The filtrate was concentrated under reduced pressure, and the residue was purified by MPLC (SiO_2, 2.3:1 hexanes:EtOAc) to yield the title compound as a white, crystalline solid (36.0 mg, 0.028 mmol, 44%).

^{1}H NMR (500 MHz, $CDCl_3$, some resonances were broadened presumably due to the presence of NBoc rotamers): δ 8.11 (d, *J* = 7.5 Hz 2H, O_2C-*o*-Ph, 7.59 (t, *J* = 7.2 Hz, 1H, O_2C-*p*-Ph), 7.49 (t, *J* = 7.8 Hz, 2H, O_2C-*m*-Ph), 7.36 (t, 2H, *J* = 7.7 Hz, C3'-*m*-Ph), 7.33 (d, 2H, *J* = 7.2 Hz, C3'-*o*-Ph), 7.27 (t, *J* = 7.0 Hz 1H,

C3'-*p*-Ph), 6.23 (br dd, *J* = 8.3, 8.4 Hz, 1H, H13), 5.70 (d, *J* = 7.1 Hz, 1H, H2), 5.50 (d, *J* = 9.3 Hz, 1H H3'), 5.24 (br d, *J*= 8.8 Hz 1H, NH), 5.22 (s, 1H, H10), 4.95 (dd, *J* = 9.5, 1.5 Hz, 1H, H5), 4.90 (br s, 1H, H2'), 4.31 (d, *J* = 8.5 Hz, 1H, H20a), 4.26 (br dd, *J* = 11.0, 7.2, Hz, 1H, H7), 4.21 (d, *J* = 7.1 Hz, 1H, H20b), 4.19 (br s, 1H, C10OH), 3.94 (dd, *J* = 7.6, 5.2 Hz, 1H, H3), 3.60 (dt, *J* = 10.2, 3.8 Hz, 3H, $H1_{menth}$), 2.60 (ddd, *J* = 14.5, 9.7, 6.6 Hz, 1H, H6a), 2.39 (s, 3H, C4OAc), 2.28 (br m, 1H, H14a), 2.21 (br m, 1H, H14b), 2.20 (dsep, *J* = 7.0, 2.1 Hz, 3H, $H7_{menth}$), 1.96 (s, 3H, H18 $=CCH_3$), 1.85 (m, 1H, H6b), 1.84 (m, 3H, $H6_{menth}$), 1.75 (s, 3H, H19 $O=CCCH_3$), 1.67 (s, 1H, C1OH), 1.58 (m, 6H, $H3_{menth}$ and $H4_{menth}$), 1.33 (br s, 9H, *t*Boc), 1.26-1.24 [m, 6H, $H5_{menth}$ and $C(Me)C16H_3$], 1.30 [s, 3H, $C(Me)C17H_3$], 1.11 (m, 3H, $H2_{menth}$), 0.93-0.86 (m, 6H, $H4_{menth}$ and $H6_{menth}$), 0.88 (br d, 9H, $H8_{menth}$), 0.87 (br d, 9H, $H9_{menth}$), 0.79 (m, 3H, $H3_{menth}$), and 0.73 (d, *J* = 6.9 Hz, 9H, $H10_{menth}$).

^{13}C NMR (125 MHz, $CDCl_3$): δ 212.1, 170.8, 169.9, 167.3, 155.7, 139.9, 139.1, 135.3, 133.8, 130.4, 129.4, 128.9, 128.8, 127.7, 126.6, 84.4, 81.0, 79.9, 79.2, 76.8, 75.2, 74.8, 74.7, 73.9, 72.2, 71.4 ($C1_{menth}$),, 57.7, 56.5 (br), 49.7 ($C2_{menth}$), 46.5, 45.0 ($C7_{menth}$), 43.3, 37.2, 36.0, 34.6 ($C5_{menth}$), 31.7 ($C6_{menth}$), 28.4, 26.5, 25.3 ($C3_{menth}$), 22.82, 22.78 ($C4_{menth}$), 22.5 ($C8_{menth}$), 21.5 ($C9_{menth}$), 21.3, 15.8 ($C10_{menth}$), 14.7, and 10.2 ppm. (assignments of resonances of the menthyl moieties deduced from ^{13}C NMR spectrum assignments of $[(MenthO)_3SiOH]$.

HRMS (ESI) Calc'd for $C_{67}H_{103}NNaO_{17}Si$ $[M + Na]^+$ 1322.7357; found 1322.7351.

IR (thin film) 3445, 2953, 2927, 2872, 2360, 2340, 1762, 1717, 1496, 1454, 1368, 1274, 1245, 1163, 1108, 1083, 1070, 1052, 986, and 889 cm^{-1}.

mp = 119-121 °C. **TLC Rf** (1.5:1 hexanes:EtOAc) = 0.30.

2'-(Di-*t*-butoxyethoxysilyl)docetaxel (304e).

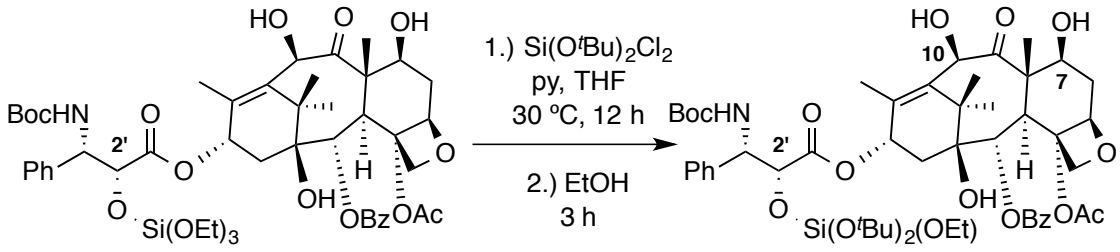

DTX ***304e***

Docetaxel (40.0 mg, 0.049 mmol, 1.0 equiv) was dissolved in dry THF (2.0 mL) in an oven-dried culture tube fitted with a Teflon-lined cap and magnetic stir bar. Pyridine (50 µL, 0.63 mmol, 12.8 equiv) was added by Wiretrol®. Dichlorodi-*t*-butoxysilane (**406**) solution consisting of ca. 90% of the dichlorosilane and ca. 10% of the monochlorosilane (100 µL, 93 mg, 0.38 mmol, 7.8 equiv) was added. The culture tube was sealed and the suspension was allowed to stir for 12 h at 30 ºC. Absolute ethanol dried over 4 Aº molecular sieves (50 µL, 0.85 mmol, 17.5 equiv) was added and the reaction mixture continued to stir for another 3 h. The THF was removed by evaporation under reduced pressure, the solid residue was triturated with a mixture of hexanes:EtOAc (2:1), and the resulting slurry was filtered through a short plug of Celite® to remove the pyridinium salt. The filtrate was concentrated under reduced pressure, and the residue was purified by MPLC (SiO_2, 2:1 hexanes:EtOAc) to yield the title compound as a white, crystalline solid (30.2 mg, 0.029 mmol, 60%).

^{1}H NMR (500 MHz, $CDCl_3$, some resonances were broadened presumably due to the presence of NBoc rotamers): δ 8.09 (d, *J* = 7.6 Hz 2H, O_2C-*o*-Ph, 7.63 (t, *J*

= 6.8 Hz, 1H, O_2C-*p*-Ph), 7.52 (t, *J* = 7.5 Hz, 2H, O_2C-*m*-Ph), 7.43 (t, 2H, *J* = 8.0 Hz, C3'-*m*-Ph), 7.33 (br d, 2H, C3'-*o*-Ph), 7.20 (br t, 1H, C3'-*p*-Ph), 6.15 (br m, 1H, H13), 5.81 (d, *J* = 7.2 Hz, 1H, H2), 5.66 (d, *J* = 6.9 Hz, 1H H3'), 5.18 (s, 1H, H10), 5.14 (br s, 1H, NH), 4.94 (br dd, *J* = 9.5, 2.3 Hz, 1H, H5), 4.76 (br s, 1H, H2'), 4.30 (d, *J* = 8.4 Hz, 1H, H20a), 4.24 (br dd, *J* = 10.7, 6.4, Hz, 1H, H7), 4.18 (d, 1H, *J* = 9.5 Hz, C7OH), 4.17 (d, *J* = 8.5 Hz, 1H, H20b), 3.89 (br d, *J* = 7 Hz, 1H, H3), 3.67 [br q, 2H, C2'OSi(OC$H_2$$CH_3$)], 2.58 (ddd, *J* = 14.7, 9.7, 6.5 Hz, 1H, H6a), 2.43 (br d, 1H, C7OH), 2.35 (s, 3H, O=CCH_3), 2.12 (br m, 1H, H14a), 1.94 (very br m, 1H, H14b, chemical shift deduced from the COSY spectrum), 1.91 (br s, 3H, H18 =CCH_3), 1.83 (ddd, *J* = 13.8, 11.3, 2.0 Hz, 1H, H6b), 1.73 (s, 3H, H19 O=CCCH_3), 1.60 (br s, 2H C7OH and C1OH), 1.35 (br s, 9H, *t*Boc), 1.29 (br s, 9H, C2'OSi[OC(CH_3)], 1.26 (br s, 9H, C2'OSi[OC(CH_3)'], 1.22 (s, 3H, C17H_3), 1.15 (br t, *J* = 6.8 Hz, 3H, C2'OSi[OCH_2CH_3]), and 1.10 (br s, 3H, C16H_3).

^{13}C NMR (125 MHz, $CDCl_3$): δ 211.9, 170.8, 170.1, 167.2, 155.7, 139.7, 139.0, 135.4, 133.9, 130.4, 129.9, 129.5, 128.9, 128.7, 127.0, 84.4, 81.0, 79.9, 79.1, 76.8, 75.2, 75.1, 74.7, 74.0, 72.1, 71.0, 57.7, 59.3, 57.4, 46.5, 43.2, 37.1, 35.7, 31.41, 31.40, 28.4, 26.5, 22.9, 21.2, 18.2, 14.6, and 10.2 ppm.

HRMS (ESI) Calc'd for $C_{53}H_{75}NNaO_{17}Si$ $[M + Na]^+$ 1048.4696; found 1048.4695.

IR (thin film) 3456, 2975, 2931, 1757, 1715, 1602, 1494, 1453, 1391, 1367, 1315, 1286, 1270, 1243, 1166, 1070, 1026, 986, 949, 915, 889, 870, 834, 782, 759, 730, and 650 cm^{-1}.

mp = 97-104 °C. **TLC** R_f (2:1 hexanes:EtOAc) = 0.50.

2-*O*-[(Di-*n*-octyloxy)(hydrogen)silyl]paclitaxel (313).

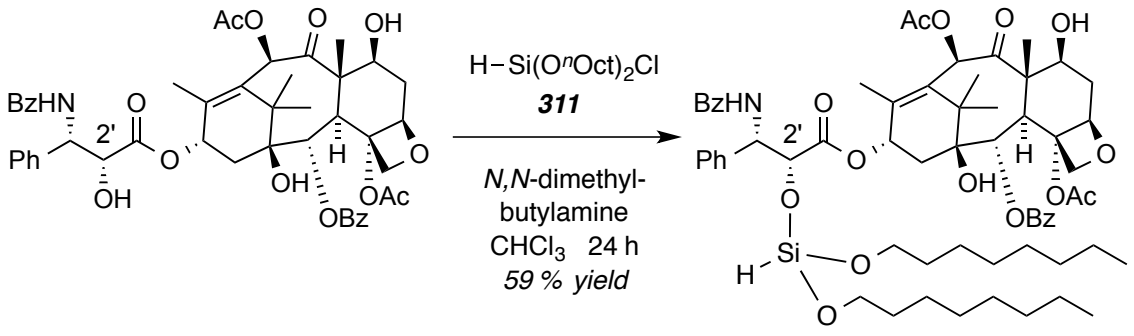

PTX ***313***

Paclitaxel (96.5 mg, 0.113 mmol, 1.0 equiv) was dissolved in dry THF (3 mL) in an oven-dried culture tube fitted with a Teflon-lined cap and magnetic stir bar. *N,N*-dimethylbutylamine (100 μL, 0.713 mmol, 6.3 equiv) was added by Wiretrol®. Since a slight excess of the alcohol was used, the corresponding trioctyloxysilane (**312**) was observed by GC-MS at longer retention time of 15.6 minutes compared to the monochlorosilane (13.2 minutes). An 80% mixture of di-*n*-octyloxyhydrogen-chlorosilane (**311**): tri-*n*-octyloxyhydrogensilane (200 μL, 0.613 mmol, 5.5 equiv of di-*n*-octyloxyhydrogen-chlorosilane) was added and a white precipitate was immediately observed. The culture tube was capped and the suspension was allowed to stir for 14 h at room temperature. An aliquot was taken out an analyzed by ^{1}H-NMR which showed little to no conversion. The THF was exchanged for $CDCl_3$, another portion of **311** was added (100 μL, 0.31 mmol, 2.7 equiv), and the reaction was allowed to stir at room temperature for 24 h. The reaction slurry was diluted with a mixture of hexanes:EtOAc (2:1), the slurry filtered through a plug of Celite® (2x) to remove the triethylammonium salt,

the filtrate concentrated under reduced pressure, and the residue redissolved in a mixture of hexanes:EtOAc (2:1). The resulting slurry was purified by flash Chromatography (SiO_2, 2:1 hexanes:EtOAc) give pure **313** (14.8 mg, 0.0130 mmol, 11.5%). The impure fractions were combined and subjected to MPLC purification to yielded the title compound as a white, crystalline solid (60.7 mg, 0.0532 mmol, 47.1%). The combined purified yield was (58.6%).

^{1}H NMR (500 MHz, $CDCl_3$): δ 8.13 (dd, *J* = 8.5, 1.4 Hz, 2H, C2O_2C-*o*-Ph), 7.77 (dd, *J* = 8.5, 1.4 Hz, 2H, C3'NHCO-*o*-Ph), 7.62 (tt, *J* = 7.4, 1.3 Hz, 1H, C2O_2C-*p*-Ph), 7.54-7.47 (m, 3H, C2O_2C-*m*-Ph and C3'NHCO-*p*-Ph), 7.43-7.36 (m, 6H, C3'-*o*-Ph, C3'-*m*-Ph and C3'NHCO-*m*-Ph), 7.28 (tt, *J* = 6.7, 1.8 Hz, 1H, C3'-*p*-Ph), 7.20 (d, *J* = 8.7 Hz, 1H, C3'NH), 6.28 (s, 1H, H10), 6.24 (br dd, *J* = 9.1, 9 Hz, 1H, H13), 5.72 (dd, *J* = 8.6, 3.1 Hz, 1H, H3'), 5.68 (d, *J* = 7.1 Hz, 1H, H2), 4.97 (dd, *J* = 8.7, 1.9 Hz, 1H, H5), 4.96 (d, *J* = 3.1 Hz, 1H, H2'), 4.44 (ddd, *J* = 10.8, 6.6, 4.1 Hz, 1H, H7), 4.32 (d, *J* = 8.4 Hz, 1H, H20α), 4.20 (d, *J* = 8.2 Hz, 1H, H20β), 3.80 (d, *J* = 7.0 Hz, 1H, H3), 3.61 {t, *J* = 6.8 Hz, 4H, C2'OSi(H)[OC*H*$_2$(CH_2)$_6$$CH_3$]$_2$}, 2.56 (ddd, *J* = 14.9, 9.6, 6.6 Hz, 1H, H6α), 2.48 (d, *J* = 4.0 Hz, 1H, C7OH), 2.44 (s, 3H, C4OAc), 2.32 (dd, *J* = 15.4, 9.4 Hz, 1H, H14α), 2.24 (s, 3H, C10OAc), 2.08 (dd, *J* = 15.4, 8.8 Hz, 1H, H14β), 1.89 (d, *J* = 1.3 Hz, 3H, C18H_3), 1.89 (m, 1H, H6β), 1.77 {s, 1H, C2'OSi(*H*)[$OCH_2CH_2(CH_2)_5CH_3$]$_2$}1.68 (s, 3H, C19H_3), 1.64 (br s, 1H, C1OH), 1.48 {tt, *J* = 6.7, 6.7 Hz, 4H, C2'OSi(H)[$OCH_2CH_2(CH_2)_5CH_3$]$_2$}, 1.32-1.22 {m, 23H, C2'OSi(H)[$OCH_2CH_2(CH_2)_5CH_3$]$_2$ and C17H_3}, 1.13 (s, 3H, C16H_3), and 0.88 {t, *J* = 6.8 Hz, 6H, C2'OSi(H)[$OCH_2CH_2(CH_2)_5CH_3$]$_2$}.

^{13}C NMR (125 MHz, $CDCl_3$): δ 204.0, 171.6, 170.9, 170.1, 167.3, 167.2, 143.0, 138.2, 134.2, 133.9, 132.9, 132.0, 130.4, 129.3, 129.0, 128.9, 128.8, 128.2, 127.3, 126.8, 84.7, 81.2, 79.3, 77.4, 75.8, 75.3, 74.9, 72.4, 71.5, 64.1 (C1$_{oct}$),

58.7 , 55.5, 45.7, 43.4, 35.8, 35.7, 32.4 ($C2_{oct}$), 32.1 ($C3_{oct}$), 29.6 ($C4_{oct}$), 29.5 ($C5_{oct}$), 27.0, 25.8 ($C6_{oct}$), 23.0, 22.9 ($C7_{oct}$), 22.4, 21.1, 14.9, 14.3 ($C8_{oct}$), and 9.8.

HRMS (ESI) Calc'd for $C_{63}H_{85}NKO_{16}Si$ $[M + K]^+$ 1178.5290; found 1178.7726.

IR (thin film) 2927, 2856, 2355 (Si-H), 2324,1731, 1717, 1698, 1669, 1648, 1555, 1538, 1519, 1506, 1489, 1241, 1170, 1096, 1025, and 839 cm^{-1}.

mp = 72–75 °C. **TLC R_f** (2:1 hexanes:EtOAc) = 0.27.

2',7-Di-*O*-(Triethoxysilyl)docetaxel (318a).

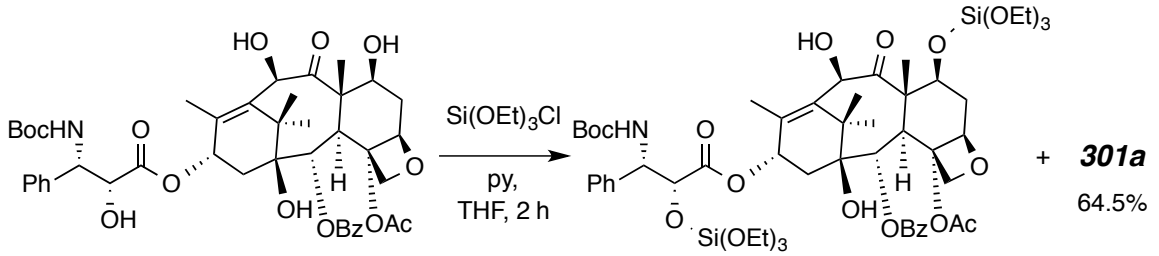

DTX ***318a*** 19.7%

Docetaxel (75.0 mg, 0.0930 mmol, 1.0 equiv) was dissolved in dry THF (2.0 mL) in an oven-dried culture tube fitted with a Teflon-lined cap and magnetic stir bar. Pyridine (35 µL, 0.250 mmol, 2.7 equiv) was added by Wiretrol®. Triethoxychlorosilane (**305a**) (50 *µ*L, 50.6 mg, 0.255 mmol, 2.7 equiv.) was added. The culture tube was sealed and the suspension was allowed to stir for 2 h at room temperature. A white precipitate was observed immediately upon the addition of the chlorosilane to the reaction mixture. The THF was removed by evaporation under reduced pressure and the solid residue was triturated with a mixture of hexanes:EtOAc (1:1), and the resulting slurry was filtered through a short plug of Celite® to remove the ammonium salt. The filtrate was concentrated under reduced pressure, and the residue was purified by MPLC (SiO_2, 1:1 hexanes:EtOAc) to yield **401a** (58.1 mg, 0.060 mmol, 64.5%) and the title compound as a white, crystalline solid (20.7 mg, 0.018 mmol, 19.7%).

^{1}H NMR (500 MHz, $CDCl_3$, some resonances were broadened presumably due to the presence of NBoc rotamers): δ 8.11 (d, *J* = 7.5 Hz 2H, O_2C-*o*-Ph), 7.61 (t, *J* = 7.2 Hz, 1H, O_2C-*p*-Ph), 7.50 (t, *J* = 7.8 Hz, 2H, O_2C-*m*-Ph), 7.35 (t, 2H, *J* =

7.4 Hz, C3'-*m*-Ph), 7.33 (d, 2H, *J* = 7.1 Hz, C3'-*o*-Ph), 7.26 (t, *J* = 6.6 Hz 1H, C3'-*p*-Ph), 6.27 (br m, 1H, H13), 5.67 (d, *J* = 7.0 Hz, 1H, H2), 5.61 (d, *J* = 8.8 Hz, 1H, H3'), 5.42 (s, 1H, H10), 5.28 (br s, 1H, NH), 4.95 (dd, *J* = 9.5, 1.8 Hz, 1H, H5), 4.82 (br s, 1H, H2'), 4.54 (br dd, *J* = 10.6, 6.7, Hz, 1H, H7), 4.31 (d, *J* = 8.4 Hz, 1H, H20α), 4.20 (d, *J* = 8.5 Hz 1H, H20β), 4.16 (d, *J* = 1.8 Hz, 1H, C10O*H*), 3.91 (d, *J* = 7.0 Hz, 1H, H3), 3.79 {q, *J* = 7.9, 7.0, Hz, 6H, C7OSi[OCH_2CH$_3$]$_3$}, 3.66 {br q, *J* = 5.9, 5.3 Hz, 6H, C2'OSi[OCH_2CH$_3$]$_3$}, 2.60 (ddd, *J* = 14.6, 9.7, 6.7 Hz, 1H, H6α), 2.44 (s, 3H, C4OAc), 2.30 (br m, 1H, H14α), 2.12 (br m, 1H, H14β), 1.97 (s, 3H, =CCH$_3$), 1.85 (ddd, *J* = 14.4, 10.9, 2.3 Hz 1H, H6β), 1.77 (s, 3H, O=CCCH_3), 1.63 (s, 1H, C1O*H*), 1.34 (br s, 9H, *t*Boc), 1.25 {s, C(Me)C16H_3}, 1.22 [t, *J* = 7.1 Hz, 9H, C7OSi(OCH$_2$CH_3)$_3$], 1.13 [t, *J* = 7.0 Hz, 9H, C2'OSi(OCH$_2$CH_3)$_3$], and 1.12 (s, 3H, C(Me)C17H_3).

^{13}C NMR (125 MHz, CDCl$_3$): δ 210.2 (C9), 169.9 (C1'), 169.4 (C21), 166.8 (C2-O*C*OBz), 154.3 (C3'-NH*C*O), 138.6 (C3'-*ipso*-Ph), 135.6 (C12), 135.2 (C11), 133.4 (OBz-*p*), 130.2 (OBz-*i*), 128.9 (OBz-*o*), 128.5 (OBz-*m*), 127.9 (2x C3'-*o*-Ph), 127.2 (C3'-*m*-Ph), 126.6 (C3'-*p*-Ph), 84.2 (C5), 80.5 (O*C*Me$_3$), 78.8 (C1), 77.1 (C4), 76.4 (C20), 74.8 (C2), 74.2 (C10), 73.5 (C2'), 72.6 (C13), 72.2 (C7), 59.3 (3x C2'OSiO*C*H$_2$CH$_3$), 56.4 (C8), 56.1 (C3'), 46.4 (C3), 43.2 (C15), 36.3 (C6), 35.4 (C14), 28.2 [C3'-NHCOC(*C*H$_3$)], 27.3 (C16), 22.7 (C22), 20.8 (C17), 17.9 (SiOCH$_2$*C*H$_3$), 14.0 (C18), and 9.8 (C19).

HRMS (ESI) Calc'd for $C_{55}H_{81}NKO_{20}Si_2$ $[M + K]^+$ 1170.4522; found 1170.4535.

IR (thin film) 3459, 2976, 2929, 2897, 2359, 1717, 1716, 1502, 1453, 1368, 1246, 167, 1082, 973, 889, and 796 cm^{-1}.

mp = 95.6-97.5 °C.**TLC** R$_f$ (1:1 hexanes:EtOAc) = 0.53.

Table S3.1 I Additional calculated values of physical properties for the silicate esters **301–304, 308a, 313, 318a.** Calculated octanol:water partition coefficient are shown as: Actelion LogP [AC logP], atom fragment contribution LogP [KOWWIN], molinspiration [miLogP],and atom additive LogP [XLOGP3].

Sub-strate	2' alkyl	7 alkyl	AC logP	KOWWIN	miLogP	XLOGP3
PTX	**-**	**-**	3.64	3.31	4.945	2.49
301a	**Et**	**-**	4.27	3.49	6.563	4.30
301b	**^{n}Oct**	**-**	12.62	12.33	10.176	13.45
301c	**^{i}Pr**	**-**	5.48	4.74	7.653	5.60
301d	**menthyl**	**-**	11.28	14.05	10.241	13.63
301f	**(^{t}Bu)$_2$/Et**	**-**	5.38	5.23	8.167	5.53
301g	**(^{t}Bu)$_2$/Ac**	**-**	4.98	–	–	5.20
301h	**(^{t}Bu)$_2$/Piv**	**-**	6.30	–	–	6.61
301p	**DHP**	**-**	27.84	–	–	30.03
308a	***PTX-SiEt$_3$***	**-**	4.95	7.26	6.687	6.03
313	**(^{n}Oct)$_2$/H**	**-**	–	–	–	9.65[a]
302a	**Et**	**Et**	4.89	3.26	8.167	6.11
302b	**^{n}Oct**	**^{n}Oct**	21.60	20.94	10.979	24.41
302c	**^{i}Pr**	**^{i}Pr**	7.31	5.76	9.212	8.70
302d	**menthyl**	**menthyl**	18.93	–	–	24.77
302p	**DHP**	**DHP**	52.03	–	–	57.57
303a	**-**	**Et**	4.27	3.49	6.563	4.30
303b	**-**	**^{n}Oct**	12.62	12.33	10.176	13.45
303c	**-**	**^{i}Pr**	5.48	4.74	7.653	5.60
303p	**-**	**DHP**	27.84	–	–	30.03

Table S3.1 l Continued

Sub-strate	2' alkyl	7 alkyl	AC logP	KOWWIN	miLogP	XLOGP3
DTX	**-**	**-**	2.92	2.83	4.243	1.65
304a	**Et**	**-**	3.55	3.01	5.861	3.45
304b	**^{n}Oct**	**-**	11.90	11.85	10.093	12.61
304c	**^{i}Pr**	**-**	4.76	4.26	6.950	4.75
304d	**menthyl**	**-**	10.57	13.23	10.163	12.79
304e	**(^{t}Bu)$_2$/Et**	**-**	4.66	4.75	7.480	4.69
318a	**Et**	**Et**	4.18	–	–	5.26

[a]XLOGP2 value provided when XLOGP3 value not found.

Table S3.2 l Additional calculated values of physical and chemical properties for the silicate esters **301–304, 308a, 313, 318a**. Calculated water solubility. (AC = Acetion pharma company).

Sub-strate	2' alkyl	7 alkyl	ALOGpS	mg/L	AC logS Solubility	AC Aqueous
PTX	**-**	**-**	-5.19	5.56	-6.29	0.44 mg/L
301a	**Et**	**-**	-5.58	2.66	-4.79	16.33 mg/L
301b	**^{n}Oct**	**-**	-6.72	0.24	-9.65	0.28 μg/L
301c	**^{i}Pr**	**-**	-5.83	1.57	-5.93	1.25 mg/L
301d	**menthyl**	**-**	-6.74	0.25	-10.86	18.38 ng/L
301f	**(^{t}Bu)$_2$/Et**	**-**	-6.06	0.94	-5.77	1.83 mg/L
301g	**(^{t}Bu)$_2$/Ac**	**-**	-6.04	0.98	-5.75	1.93 mg/L
301h	**(^{t}Bu)$_2$/Piv**	**-**	-6.24	0.66	-6.36	0.50 mg/L

Table S3.2 l Continued

Sub-strate	2' alkyl	7 alkyl	ALOGpS	mg/L	AC logS Solubility	AC Aqueous
301p	**DHP**	**-**	-7.79	0.03	-18.05	0 ng/L
308a	***PTX-SiEt$_3$***	**-**	-5.96	1.06	-13.40	0.04 ng/L
301f	**(^{n}Oct)$_2$/H**	**-**	-6.62	0.27	–	–
302a	**Et**	**Et**	-5.84	1.70	-3.30	0.59 g/L
302b	**^{n}Oct**	**^{n}Oct**	-7.12	0.13	-13.02	0.16 ng/L
302c	**^{i}Pr**	**^{i}Pr**	-6.16	0.87	-5.57	3.42 mg/L
302d	**menthyl**	**menthyl**	-7.31	0.09	-15.44	0 ng/L
302p	**DHP**	**DHP**	-8.13	0.02	-29.82	0 ng/L
303a	**-**	**Et**	-5.64	2.33	-4.79	16.37 mg/L
303b	**-**	**^{n}Oct**	-6.76	0.22	-9.65	0.28 μg/L
303c	**-**	**^{i}Pr**	-5.87	1.44	-5.93	1.25 mg/L
303p	**-**	**DHP**	-7.84	0.03	-18.05	0 ng/L
DTX	**-**	**-**	-4.80	12.72	-5.81	1.25 mg/L
304a	**Et**	**-**	-5.15	6.84	-4.32	46.87 mg/L
304b	**^{n}Oct**	**-**	-6.58	0.32	-9.18	0.82 μg/L
304c	**^{i}Pr**	**-**	-5.43	3.78	-5.45	3.59 mg/L
304d	**menthyl**	**-**	-6.65	0.29	-10.39	53.24 ng/L
304e	**(^{t}Bu)$_2$/Et**	**-**	-5.60	2.58	-5.29	5.26 mg/L
318a	**Et**	**Et**	-5.46	3.92	-2.82	1.71 g/L

Table S3.3 I Additional calculated values of chemical properties for the silicate esters **301–304**. Calculated volume, total number of non hydrogen atoms/number of oxygen and nitrogen atoms/number of O-H and N-H bonds [natoms/nON/nOHNH], number of rotable bonds [nrotbonds], and Molecular Polar Surface Area [TPSA].

Sub-strate	2' alkyl	7 alkyl	Volume	natoms/ nON/nOHNH	nrotbonds	TPSA
PTX	**-**	**-**	756.598	62/15/4	14	221.307
301a	**Et**	**-**	914.156	72/18/3	22	238.015
301b	**^{n}Oct**	**-**	1216.588	90/18/3	40	238.015
301c	**^{i}Pr**	**-**	963.917	75/18/3	22	238.015
301d	**menthyl**	**-**	1283.74	96/18/3	25	238.015
301f	**(^{t}Bu)$_2$/Et**	**-**	979.803	76/18/3	22	238.015
308a	***PTX-SiEt$_3$***	**-**	887.202	69/15/3	19	210.313
302a	**Et**	**Et**	1071.714	82/21/2	30	254.723
302b	**^{n}Oct**	**^{n}Oct**	1676.579	118/21/2	66	254.723
302c	**^{i}Pr**	**^{i}Pr**	1171.235	88/21/2	30	254.723
303a	**-**	**Et**	914.156	72/18/3	22	238.015
303b	**-**	**^{n}Oct**	1216.588	90/18/3	40	238.015
303c	**-**	**^{i}Pr**	963.917	75/18/3	22	238.015
DTX	**-**	**-**	723.849	58/15/5	13	224.464
304a	**Et**	**-**	881.407	68/18/4	21	241.172
304b	**^{n}Oct**	**-**	1183.84	86/18/4	39	241.172
304c	**^{i}Pr**	**-**	931.168	71/18/4	21	241.172
304d	**menthyl**	**-**	1250.991	92/18/4	24	241.172
304e	**(^{t}Bu)$_2$/Et**	**-**	947.055	72/18/4	21	241.172

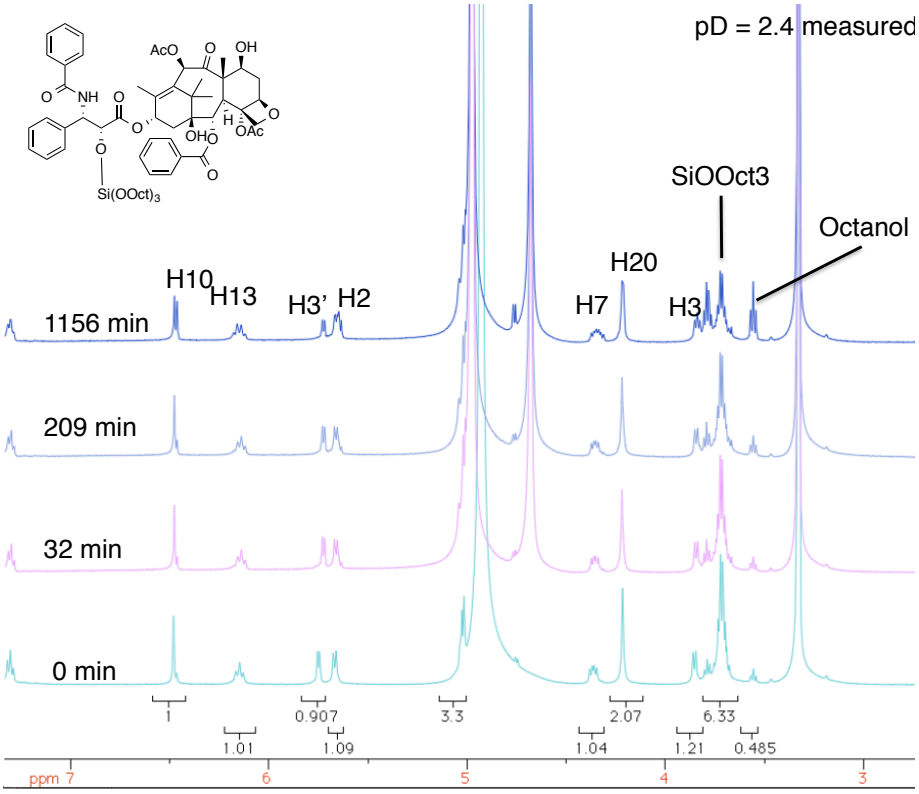

Figure S3.3 I ^{1}H-NMR hydrolysis acid buffer study containing **301b** in 300 μL MeOH, and 700 μL of D3PO4 in D2O plotted over time shows the cleavage of the silicate to return free PTX after > 1,156 mins.

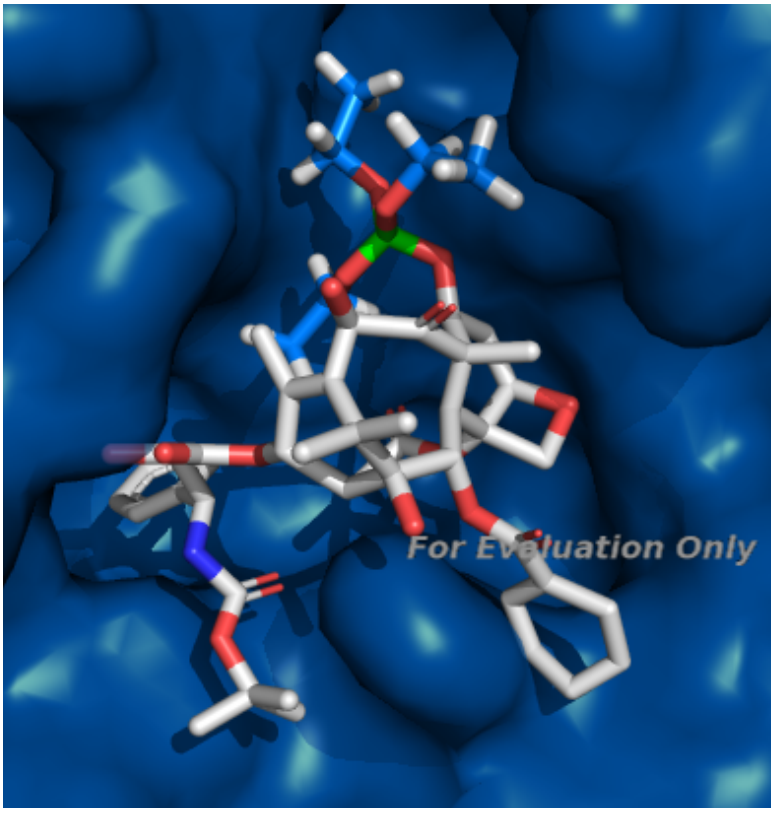

Figure S3.4 I 7-position modification of **DTX** to estimate the silicate **304c**, to provide a very crude idea of the possible binding of the silicate prodrugs to microtubules.[220]

[220] Meurer-Grob, P.; Kasparian, J.; Wade, R. H. Microtubule Structure at Improved Resolution. *Biochemistry* **2001**, *40*, 8000–8008.

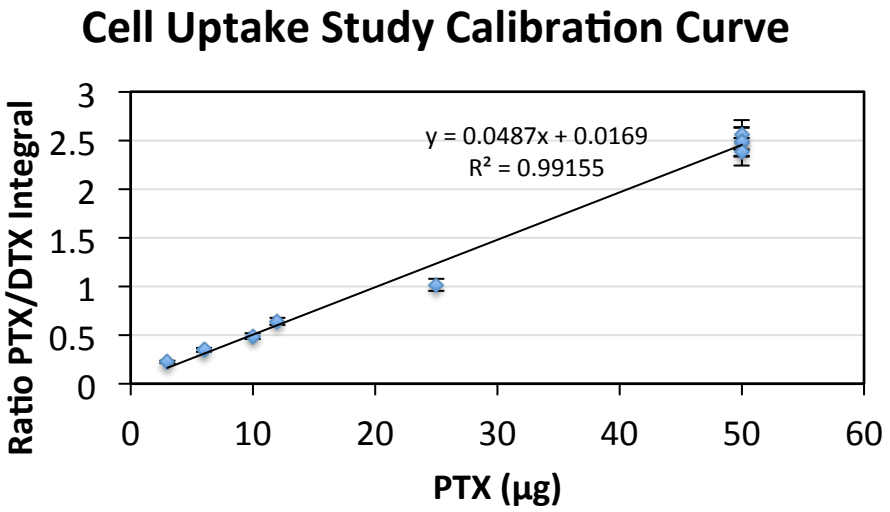

Figure S3.5 I Calibration curve of the ratio of **PTX/DTX** used to quantify the amount of PTX present in during the stability and uptake studies. (prodrug calibration curves not shown).

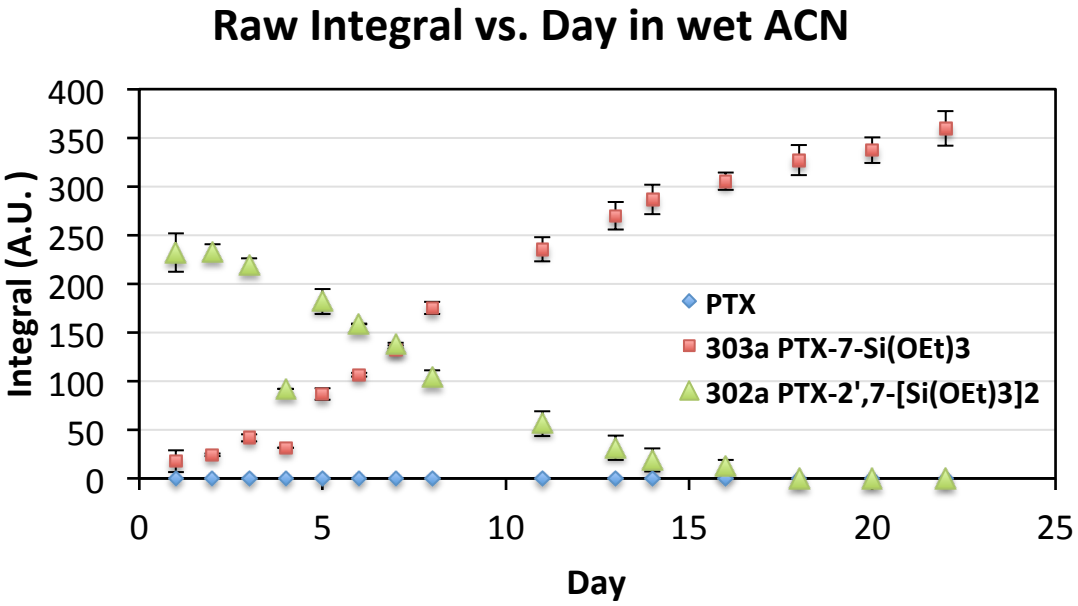

Figure S3.6 I Raw integral intensity at 227 nm of **302a**, **303a**, **PTX** vs. time in wet ACN.

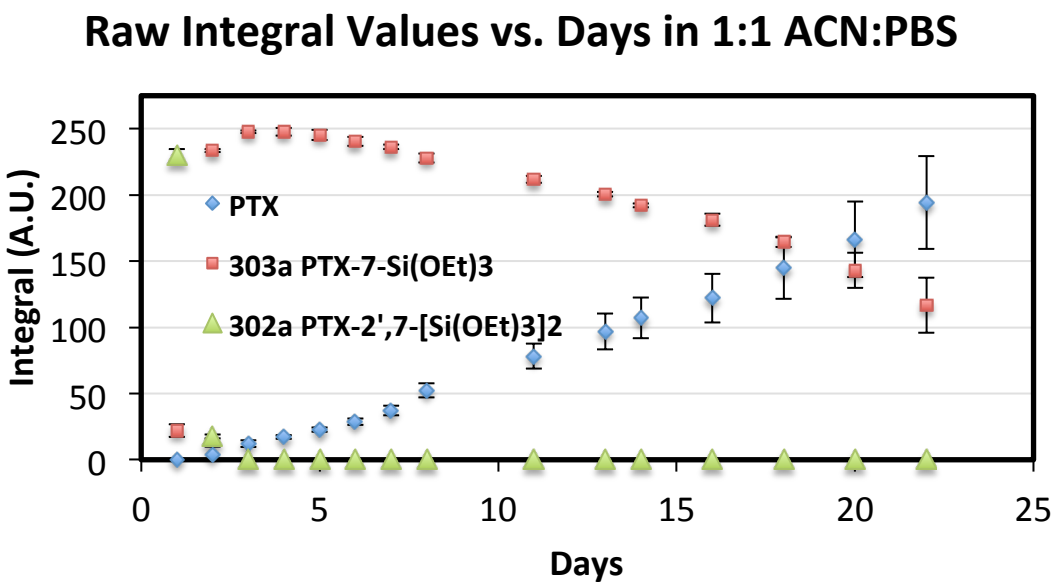

Figure S3.7 I Raw integral intensity at 227 nm of **302a**, **303a**, **PTX** vs. time in 1:1 ACN:PBS.

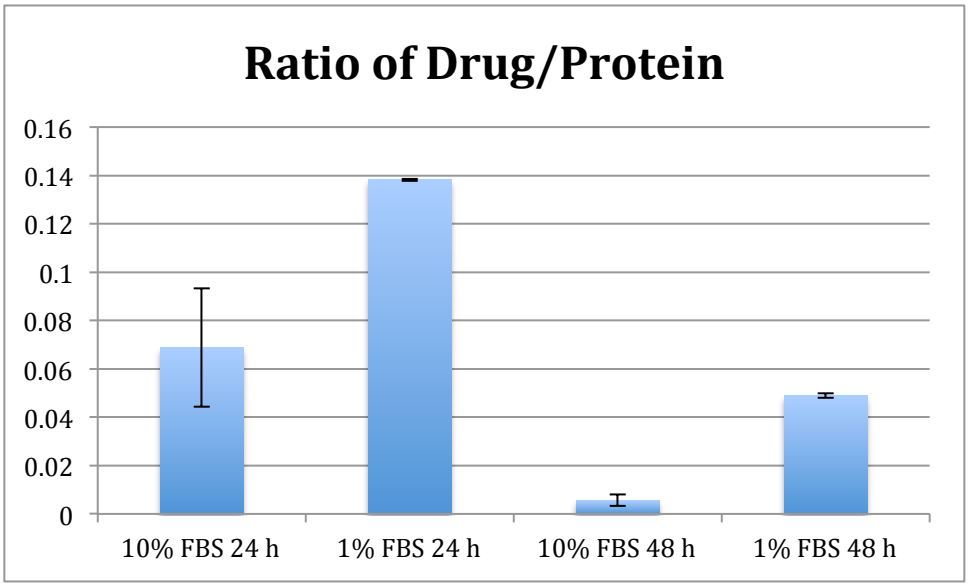

Figure S3.8 I Ratio of total taxane quantified to the total amount of protein present determined from a Bradford Assay.

Experimental Section for Chapter 4

Methoxy-capped poly(ethylene glycol)-block-poly[(lactic)-co-(glycolic) acid] (405)

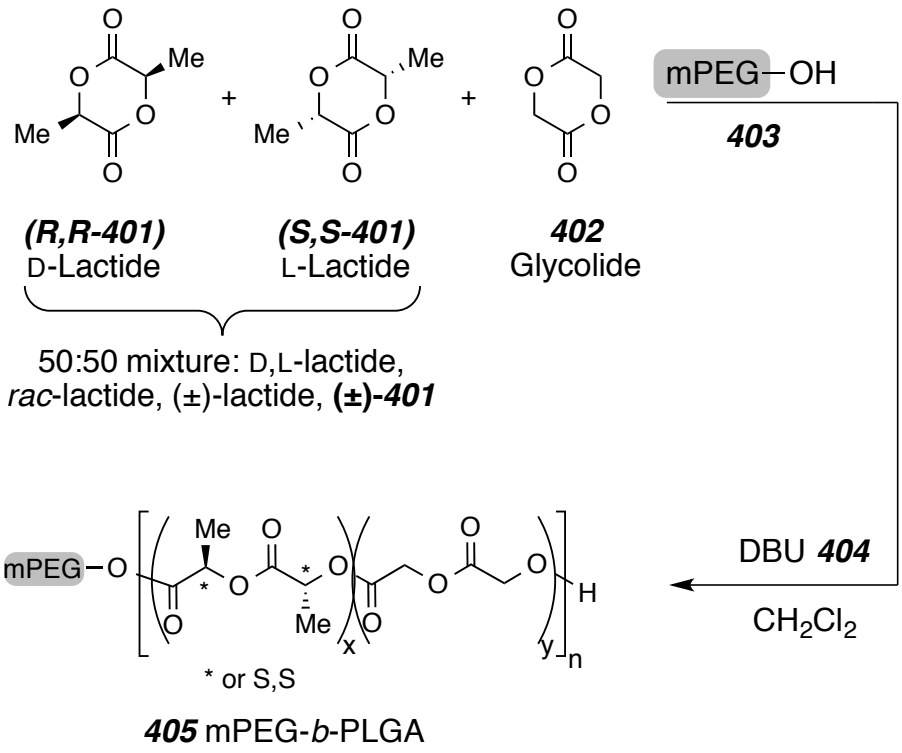

MeO-PEG-OH (**403**, 5K, 5.0 g) was dissolved in 10 mL of dry CH_2Cl_2 and stored over 3 Å molecular sieves. From this stock solution **403** (3.0 mL, 1.5 g, 0.3 mmol, 1.0 equiv.) was added to the *rac*-lactide **401** (3.56 g, 24.7 mmol, 82.4 equiv.) in an oven-dried round-bottom flask containing a magnetic stir bar and 70 mL of CH_2Cl_2. The glycolide (**402**) (1.82 g, 15.7 mmol, 52.3 equiv.) was vigorously stirred in 20.0 mL of THF. The glycolide solution was fed into the reaction with a syringe pump running at 1.82 mL/min and started simultaneously upon the

addition of the DBU catalyst **404** (100 μL, 0.67 mmol, 2.2 equiv.) was added to the reaction. After 11 min of reaction solid benzoic acid (ca. 500 mg) was added to arrest the polymerization. The mPEG-*b*-PLGA (**405**) was purified by removing all of the CH_2Cl_2 by rotary evaporation, dissolving the crude polymer in a minimal amount of $CHCl_3$, two sequential precipitations into 500 mL ice cold isopropanol, and drying at 50 °C under vacuum overnight yielding the desired product as a white solid (98% yield) with M_n [PLGA] = 13,860 g/mol, ca. 64:36 lactic:glycolic ratio by mass.

^{1}H NMR (500 MHz, $CDCl_3$): δ 5.29-5.11 [m, 124H, PLA(-C*H*CH_3)], 4.91-4.62 [m, 170H, PGA(-C*H_2*-)], 4.41-4.20 [m, 9H, mPEG-(-O*CH_2*-PGA/PLA) and mPEG-PLGA-*CH*(CH3)-OH})], 3.79-3.49 [m, 455H, MeO-PEG(-OC*H_2*C*H_2*O-)], 3.38 (s, 3H, *Me*O-PEG-), and 1.69-1.45 [m, 430H, PLA(-CHC*H_3*)].

SEC (Polystyrene standards) PDI = 1.02.

tetra-(-)-menthoxy silicate $(MenO)_4Si$ (411).

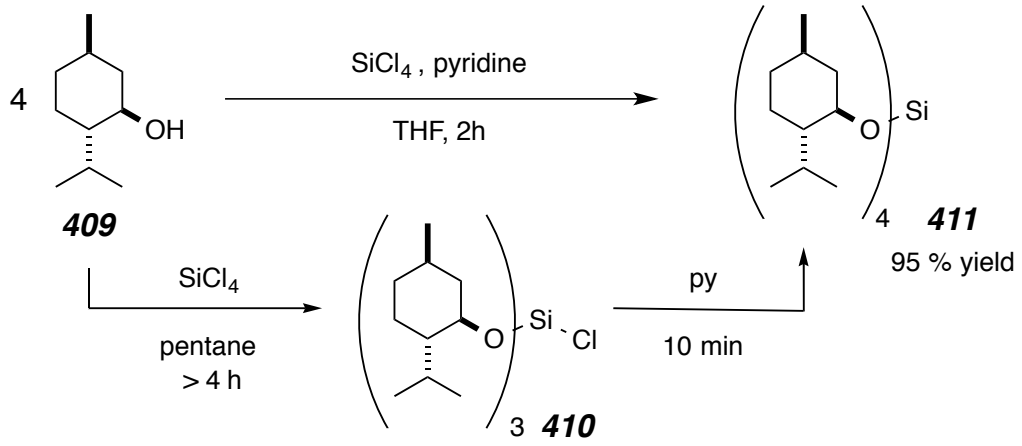

Silicaon tetrachloride ($SiCl_4$ 0.36 mL, 3.14 mmol, 1.0 equiv) was dissolved in dry pentane (5.0 mL) in an oven-dried three neck round bottom flask fitted with a magnetic stir bar. (-)-Menthol (2.05 g, 13.12 mmol, 4.2 equiv) was dissolved in pentane and added dropwise by a liquid addition funnel to the round bottom flask. ^{1}H-NMR determined that the monochlorosilane (**410**) and excess starting material **409** remained even after 4 hours. Pyridine (1 mL, 7.14 mmol, 2.3 equiv) was added by syringe to the reaction mixture. A white precipitate was observed immediately upon the addition of the pyridine and ^{1}H-NMR confirmed **411** as the dominant product. The pentane was removed by evaporation under reduced pressure and the solid residue was triturated with a mixture of hexanes:EtOAc (95:5), and the resulting slurry was filtered through a short plug of Celite® to remove the ammonium salt. The filtrate was concentrated under reduced pressure, and the residue was purified by flash chromatography (SiO_2, 95:5

hexanes:EtOAc) to yield the title compound **411** as a white, crystalline solid (1.94 g, 2.98 mmol, 95%).

^{1}H NMR (500 MHz, $CDCl_3$): δ 3.65 (dt, *J* = 10.5, 4.2 Hz, 4H, H1), 2.28 (dq, *J* = 7.0, 2.5 Hz, 4H, H7), 2.09 (m, 4H, H6), 1.66-1.56 (m, 8H, H3 and H4), 1.33 (m, 4H, H5), 1.18 (dt, *J* = 10.2, 5.9, 2.9 Hz, 4H, H2), 1.03 (dd, *J* = 12.1, 4H. H6), 0.94 (dd, *J* = 12.5, 2.9, 4H. H3), 0.90 (d, *J* = 6.6, 12H, H8), 0.88 (d, *J* = 7.1, 12H, H9), 0.82 (dd, *J* = 12.3, 2.9, 4H. H4), and 0.74 (d, *J* = 6.9, 12H, H10).

^{13}C NMR (125 MHz, $CDCl_3$)[127] δ 73.2 (C-1), 49.7 (C-2), 44.9 (C-6), 34.5 (C-4), 31.7 (C-5), 25.1 (C-7), 22.7 (C-3), 22.3 (C-8), 21.3 (C-9), 15.6 (C-10).

GC-MS t_r (5031022H) = 13.66 min; m/z: 649.

mp = 103-104 °C. **TLC** Rf (95:5 hexanes:EtOAc) = 0.66.

tris((1R,2S,5R)-2-isopropyl-5-methylcyclohexyl) (2,4,6-triiodophenyl) silicate (413)

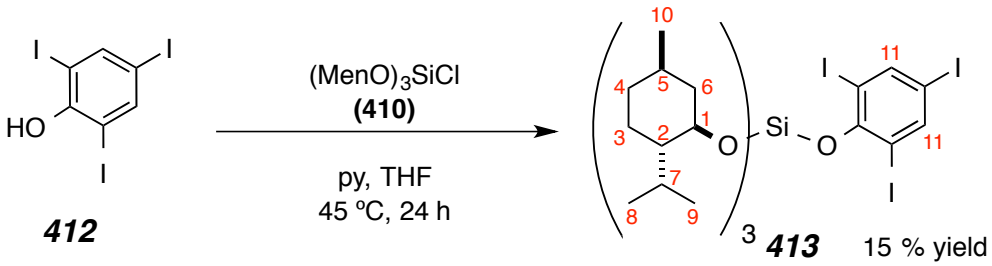

Triiodophenol (206 mg, 0.44 mmol, 1.0 equiv.) was dissolved in dry THF (3.0 mL) in an oven-dried culture tube fitted with a Teflon-lined cap and magnetic stir bar. Pyridine (104 µL, 1.30 mmol, 3.0 equiv.) was added by Wiretrol®. Trimenthoxychlorosilane (**305d**) (690 mg, 1.30 mmol, 3.0 equiv.) was added by a syringe. The culture tube was sealed and the suspension was allowed to stir for 24 h at 45 ºC. A white precipitate was observed to grow in upon the addition of the chlorosilane to the reaction mixture. The THF was removed by evaporation under reduced pressure and the solid residue was triturated with a mixture of hexanes:EtOAc (98:2), and the resulting slurry was filtered through a short plug of Celite® to remove the pyridinium salt. The filtrate was concentrated under reduced pressure, and the residue was purified by sequential MPLC (SiO_2, 98:2, 99:1, then 100:0 hexanes:EtOAc) to yield **413** the title compound as a white **413**, crystalline solid (62.7 mg, 0.065 mmol, 15%) as well as monochlorosilane **410** and **411**.

^{1}H NMR (500 MHz, $CDCl_3$): δ 8.03 (s, 2H, H11), 3.89 (dt, *J* = 10.5, 4.2 Hz, 3H, H1), 2.29 (dq, *J* = 7.0, 2.5 Hz, 3H, H7), 2.14 (m, 3H, H6), 1.65-1.56 (m, 6H, H3 and H4), 1.35 (m, 3H, H5), 1.18 (dt, *J* = 10.2, 5.7, 2.9 Hz, 3H, H2), 1.05 (dd, *J* = 11.2, 3H. H6), 0.89 (m, 3H. H3), 0.84 (d, *J* = 6.9, 9H, H8), 0.75 (d, *J* = 7.1, 9H, H9), 0.74 (m, 3H. H4), and 0.70 (d, *J* = 6.9, 9H, H10).

GC-MS t_r (5031022H) = 18.18 min; m/z: 964, 921, 879, 826, 688, 533, 471, 406, 280, 137, 81 and 55.

TLC Rf (100:0 hexanes:EtOAc) = 0.60

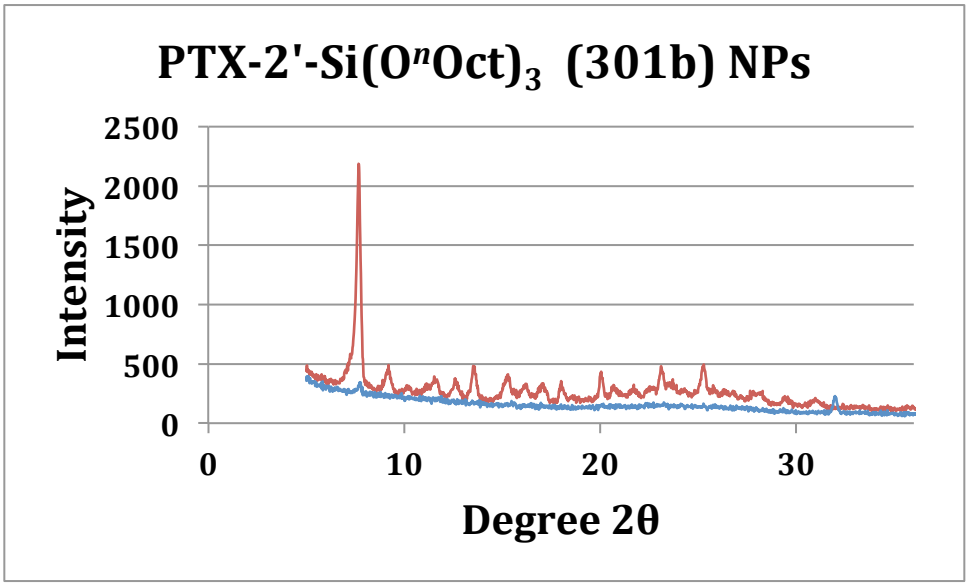

Figure S4.1 I X-ray powder diffraction (XRD) of PTX-2'-Si(O^{n}Oct)$_3$ **(301b)** as the pure compound (red) vs. nanoparticles (5k-10k mPEG-*b*-PLGA BCP) loaded with 65.0 wt% (blue).

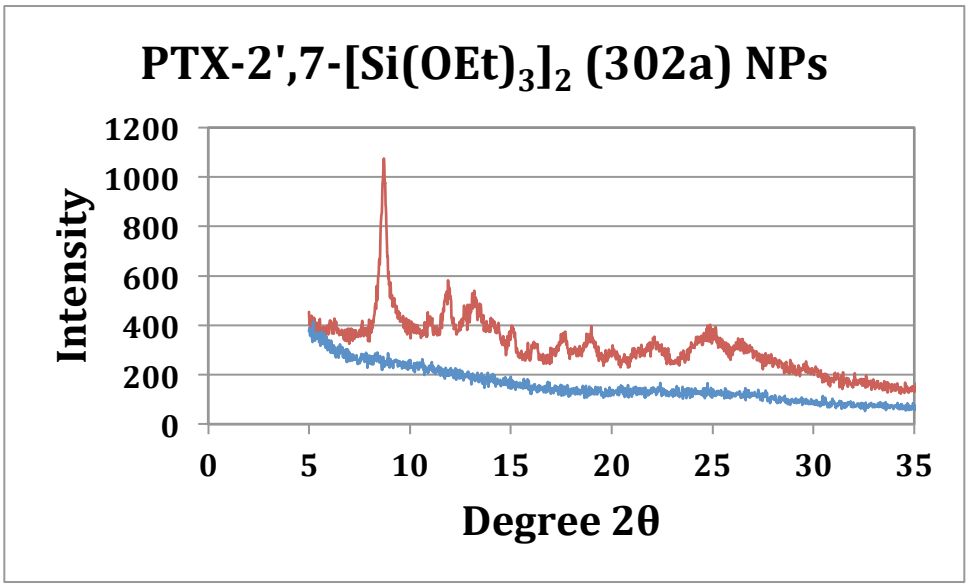

Figure S4.2 I X-ray powder diffraction (XRD) of PTX-2',7-[Si(OEt)$_3$]$_2$ **(302a)** as the pure compound (red) vs. nanoparticles (5k-10k mPEG-*b*-PLGA BCP) loaded with 60.4 wt% (blue).

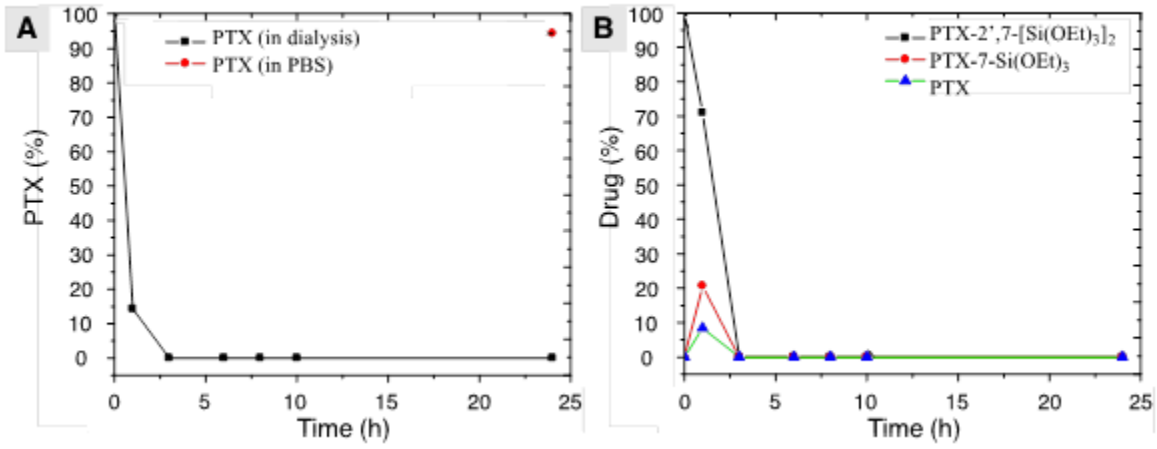

Figure S4.3 I Dialysis permeability control experiments. (**A**) Percentage of paclitaxel remaining inside dialysis capsules and diffusing out of the capsules into PBS over time. (**B**) Percentage of PTX-2',7-[Si(OEt)$_3$]$_2$ (**8**), intermediate PTX-7-Si(OEt)$_3$ (**6**), and **PTX** remaining inside dialysis capsules over time.

Release profiles at pH = 7.4.

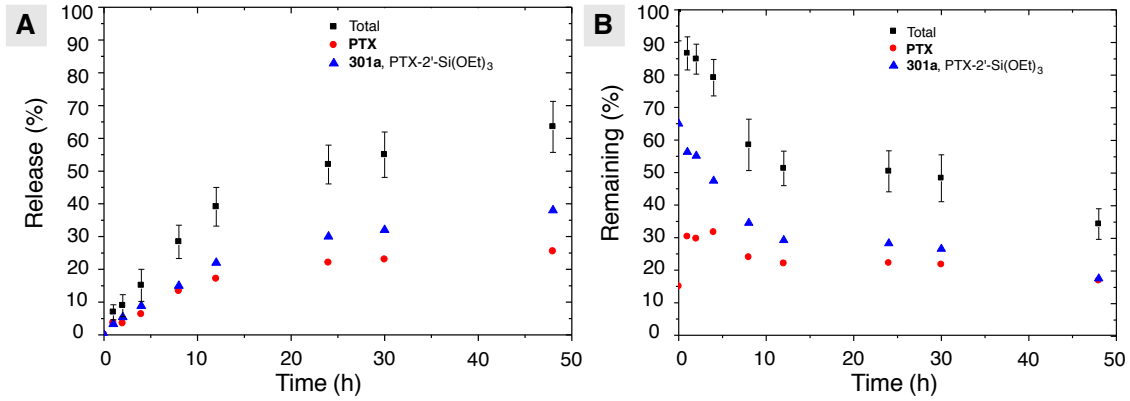

Figure S4.4 I Release profiles for nanoparticles loaded with PTX-2'-Si(OEt)$_3$ (**301a**) at pH 7.4. Amount of PTX-2'-Si(OEt)$_3$ (**301a**) (**A**) appearing outside or (**B**) remaining inside dialysis capsules vs. time.

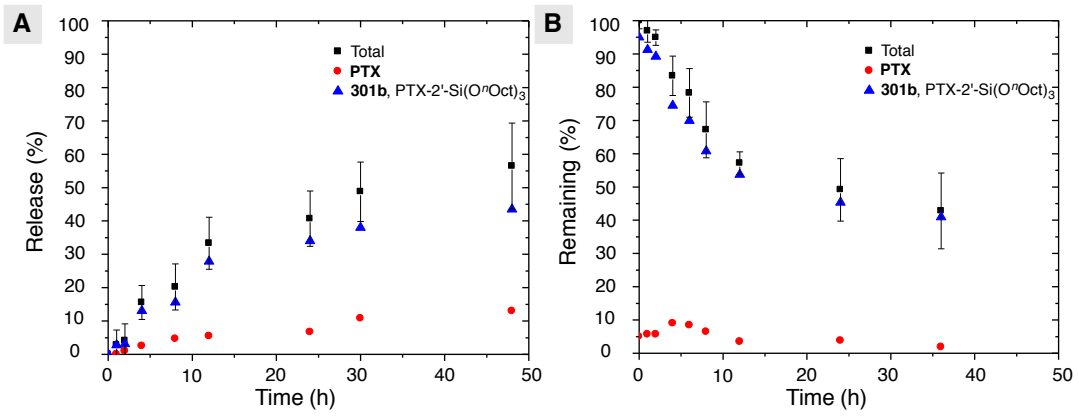

Figure S4.5 I Release profiles for nanoparticles loaded with PTX-2'-Si(O^{n}Oct)$_3$ (**301b**) at pH 7.4. Amount of PTX-2'-Si(O^{n}Oct)$_3$ (**301b**) (**A**) appearing outside or (**B**) remaining inside dialysis capsules vs. time.

Release profiles at pH=5.0

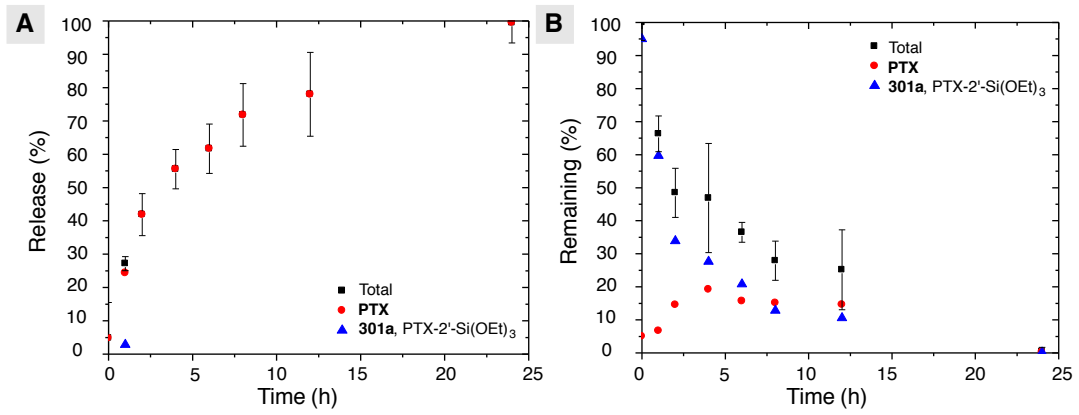

Figure S4.6 I Release profiles for nanoparticles loaded with PTX-2'-Si(OEt)$_3$ (**301a**) at pH 5.0. Amount of PTX-2'-Si(OEt)$_3$ (**301a**) (**A**) appearing outside or (**B**) remaining inside dialysis capsules vs. time.

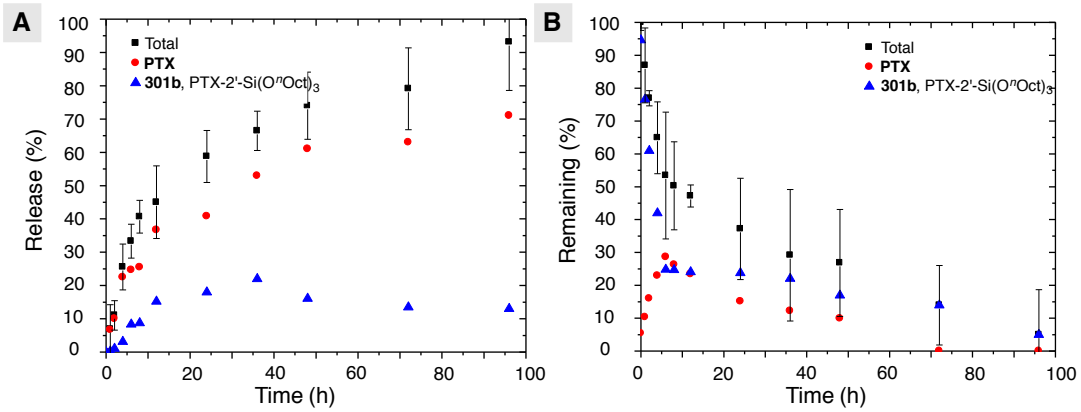

Figure S4.7 I Release profiles for nanoparticles loaded with PTX-2'-Si(O^{n}Oct)$_3$ (**301b**) at pH 5.0. Amount of PTX-2'-Si(O^{n}Oct)$_3$ (**301b**) (**A**) appearing outside or (**B**) remaining inside dialysis capsules vs. time.

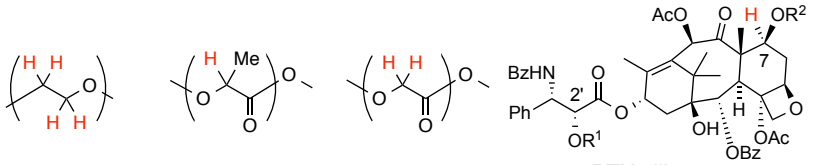

	oxyethyl	lactyl	glycolyl	PTX-silicate [R^1 or/and R^2 = $Si(Oalk)_3$]
MW per repeat unit	44 g/mol	72 g/mol	58 g/mol	$MW_{silicate}$ g/mol
MW normalized per ^1H	11g/mol•^1H	72 g/mol•^1H	29 g/mol•^1H	$MW_{silicate}$ g/mol•^1H
Integration range (ppm)	$\int_{oxyethyl}$ (3.65-3.60)	$\int_{lactyl}$ (5.31-5.15)	$\int_{glycolyl}$ (4.92-4.65)	$\int_{PTX\text{-}silicate}$ (4.47-4.40)

$$\textit{Loading Level}\ (\text{wt\% of PTX-silicate in the loaded NP}) = \frac{(MW_{silicate} \cdot \int_{PTX\text{-}silicate})}{(11 \cdot \int_{oxyethyl} + 72 \cdot \int_{lactyl} + 29 \cdot \int_{glycolyl} + MW_{silicate} \cdot \int_{PTX\text{-}silicate})} \times 100$$

$$\textit{Loading Level}\ (\text{equivalent wt\% of free PTX in the silicate-loaded NP}) = \textit{Loading Level}\ (\text{wt\% of PTX-silicate in the loaded NP}) \times \frac{MW_{PTX}\ (\text{i.e., } 853.9)\ \text{g/mol}}{MW_{silicate}\ \text{g/mol}}$$

$$\textit{Efficiency of prodrug incoporation}\ (\text{into final NP preparation}) = \frac{\text{wt \% PTX-silcate} \cdot \text{mass NP recovered after centrifugation}}{\text{initial mass of PTX-silcate used for the FNP}}$$

Figure S4.8 I Equations used to determine the wt% of PTX-silicate-loaded NP, the equivalent wt% of free **PTX** in the silicate-loaded NP, and the efficiency of prodrug incorporation by ^1H-NMR spectroscopy.

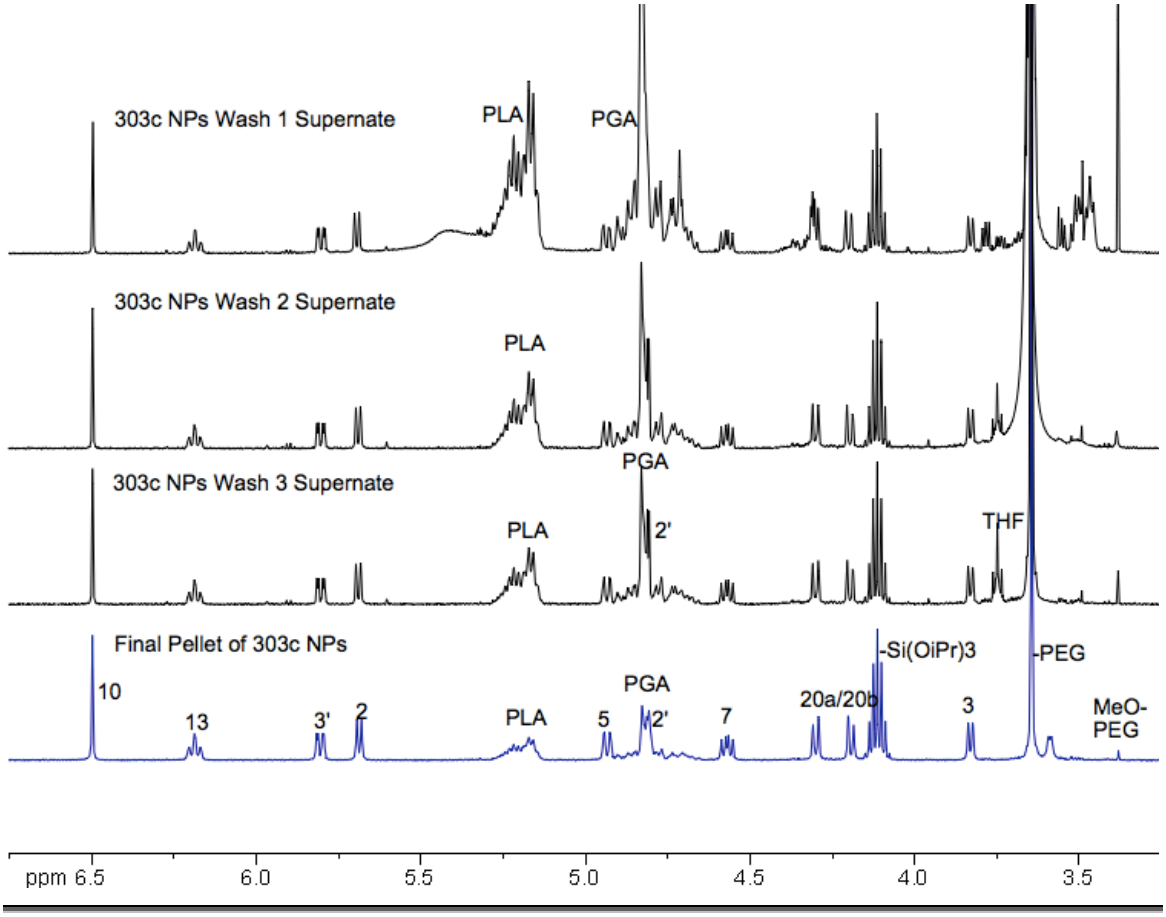

Figure S4.9 I ^{1}H-NMR of **303c** nanoparticles throughout the ultracentrifugation process. All ^{1}H-NMR intensity is normalized to H2. Each wash step removes more polymer than prodrug, resulting in a greater loading level of **303c** in the final nanoparticle dry pellet (blue).

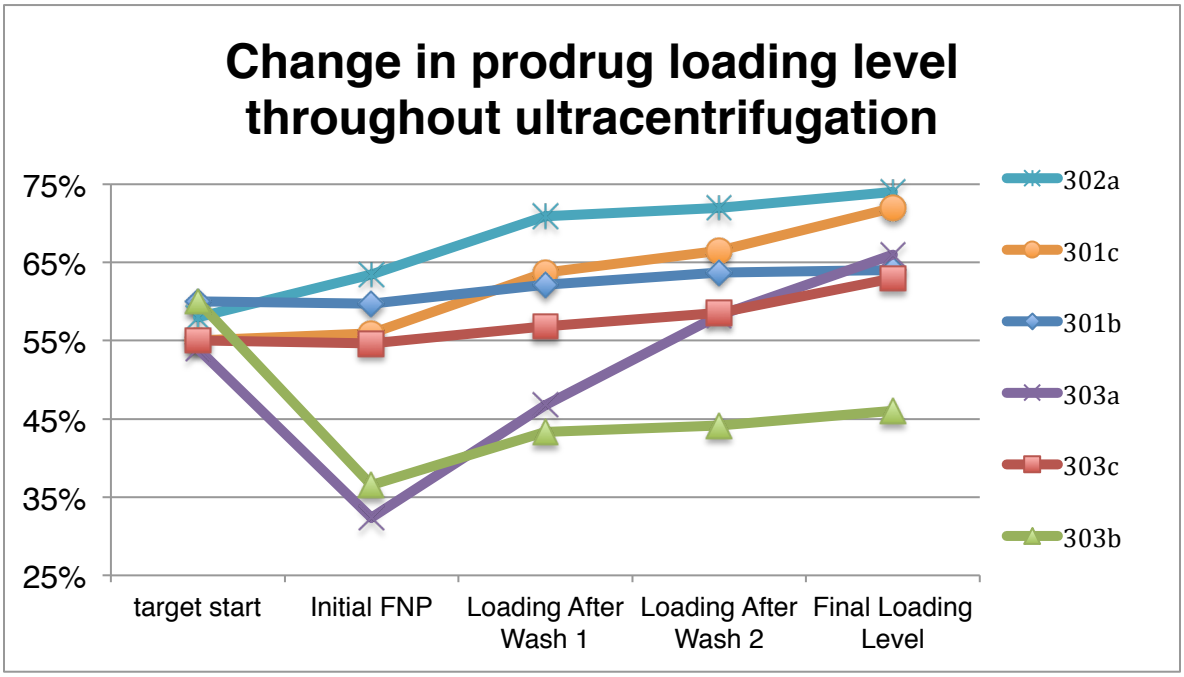

Figure S4.10 I The change in loading level (wt%) of prodrug nanoparticle formulations of **301b**, **301c**, **302a**, **303a**, **303b**, and **303c** after each ultracentrifugation step. The plot was generated by taking the final weight pellet at the end of the process and adding back in the masses of prodrug polymer lost in each wash step of the ultracentrifugation, back to the initial FNP experiment. The target loading is depicted on the left.

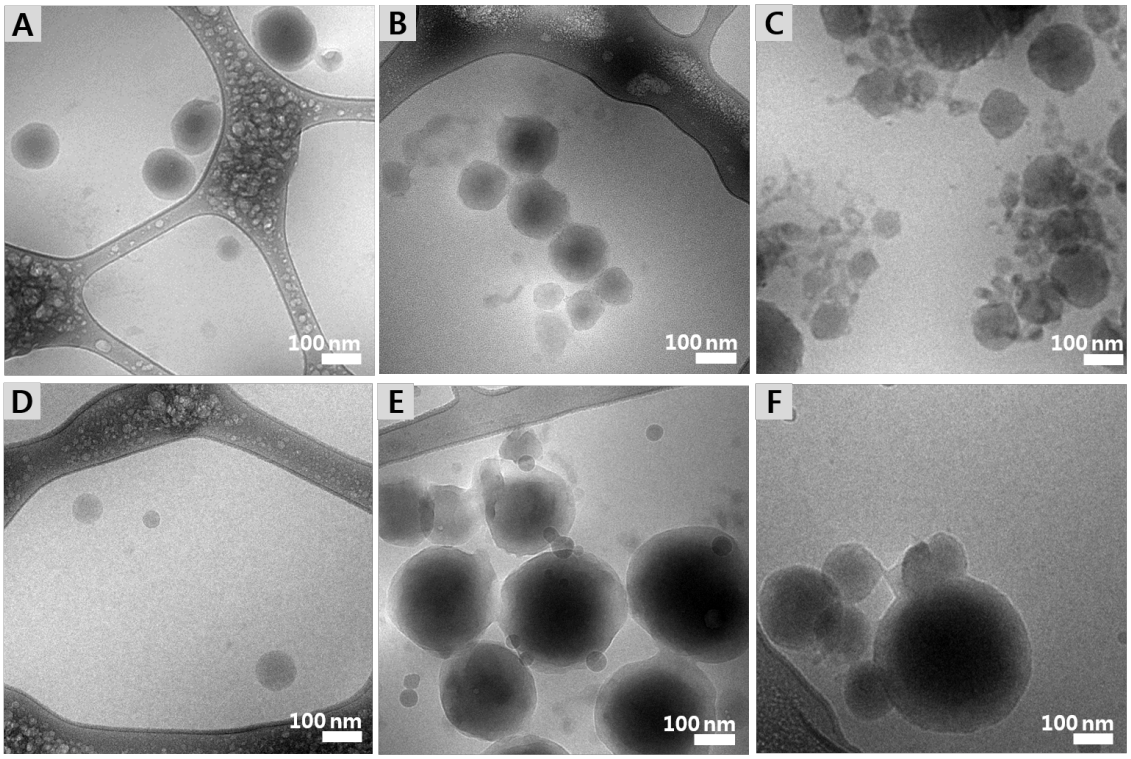

Figure S4.11 I Cryo-TEM images of nanoparticles loaded with **A-C)** PTX-2´7,-[Si(OEt)$_3$]$_2$ (**302a**), **D-F)** PTX-2'Si(O^{t}Bu)$_2$(OEt) (**301f**). **A** and **D)** freshly prepared (i.e., prior to centrifugation), **B** and **E)** lyophilized, immediately following redispersion into PBS, and **C** and **F)** lyophilized following redispersion into PBS and aging for 24 h in a dialysis cassette suspended in PBS (pH 7.4). Particles made from **302a,** which hydrolyzed rapidly, lost their cores and appear to shrink while **301d**, with very slow hydrolysis, did not change with 24 hr aging.

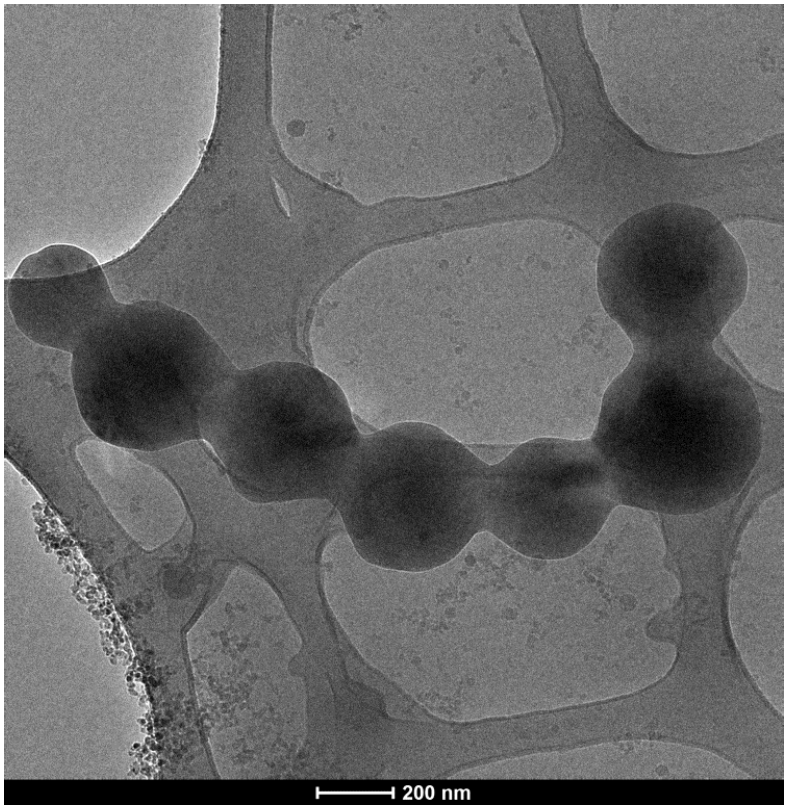

Figure S4.12 I Cryo-TEM images of PEG-*b*-PLGA (5k-10k) nanoparticles loaded with PTX-2'Si(O^tBu)$_2$(OEt) (**301f**) lyophilized, immediately following redispersion into PBS, in aqueous solution. The chain of fused particles clearly shows aggregation after freeze drying.

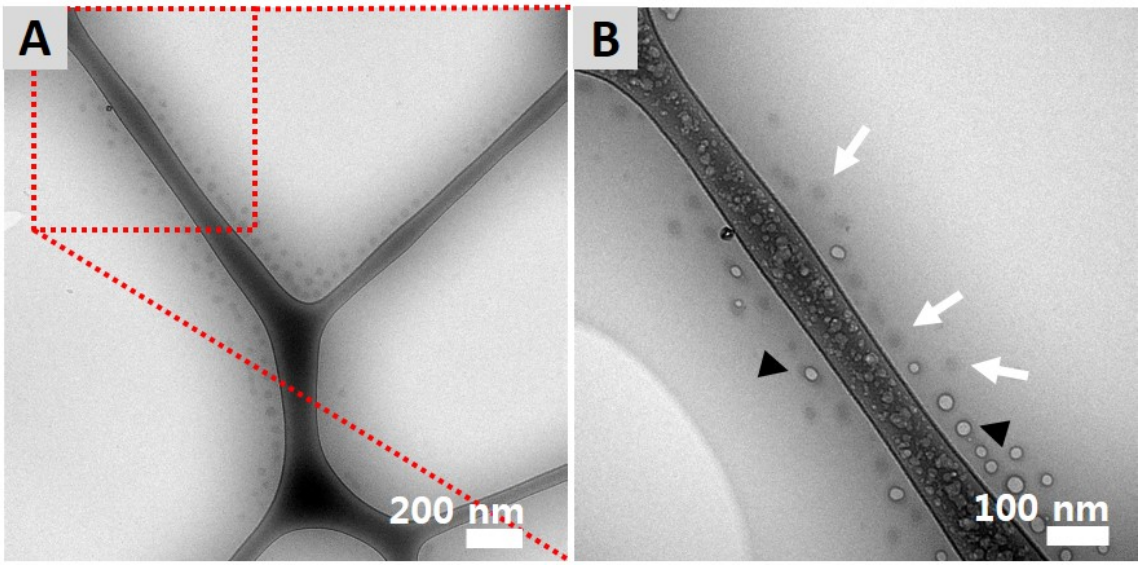

Figure S4.13 I Cryo-TEM images of PEG-*b*-PLGA block copolymer in aqueous solution. **A)** Low magnification of block copolymer particles **B)** high magnification of red box in **A)** white arrows may suggest PEO halos and black arrowheads are beam-damaged block copolymers. We observe such beam damage only for nanoparticles with no drug. The PEO halo may be observed in the very thin vitrified aqueous film in an underfocused mode (6 μm).

Methoxypolyethylene glycol tosylate (422b)

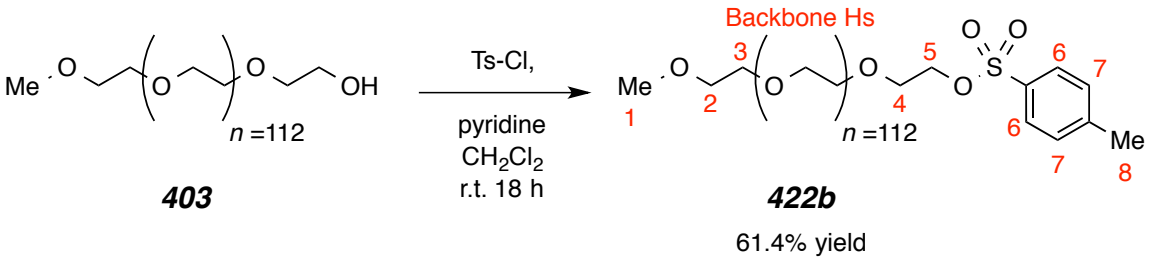

403 ***422b***

61.4% yield

In an oven dried culture tube, MeO-PEG-OH **403** (3.08 g, 0.60 mmol, 1.0 equiv.) was dissolved in 15 mL of CH_2Cl_2. p-Toluenesulfonyl chloride (Ts-Cl, 1.51 g, 6.0 mmol, 10 equiv.) was added and the reaction mixture was stirred at rt for 5 mins. Pyridine (485 μL, 6.0 mmol, 10 equiv.) was added and the reaction was allowed to run overnight ca. 18 hours. The crude product was concentrated and . added dropwise into 50 mL of ice cold (0 ^{o}C) ether, which precipitated the polymer. The ether was decanted and the polymer was dried over vacuum to yield the title polymer **422b** as a white solid (1.90 g, 0.368 mmol, 61.4%).

^{1}H NMR (500 MHz, $CDCl_3$): δ 7.80 (d, *J* = 8.4 Hz, 2H, H6), 7.34 (d, *J* = 7.9 Hz, 2H, H7), 4.16 (m, 2H, H5), 3.79 (m, 2H, H4), 3.75-3.57 (m, 447H, backbone Hs), 3.55 (m, 2H, H3), 3.50 (m, 2H, H2), 3.38 (s, 3H, H1), and 2.45 (s, 3H, H8).

Methoxypolyethylene glycol mesylate (422c)

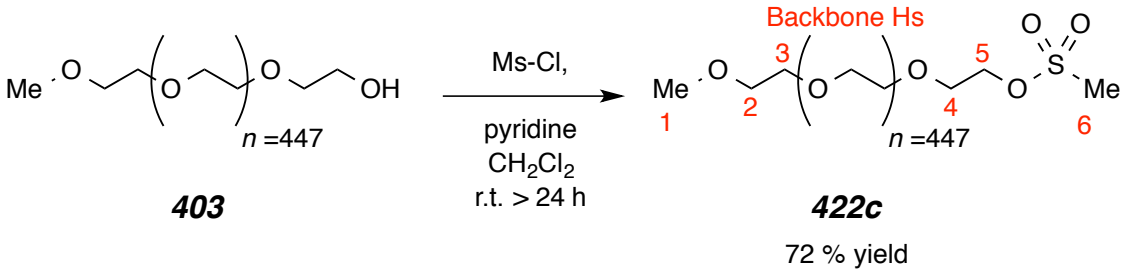

MeO-PEG-OH **403** (5.00 g, 1.0 mmol, 1.0 equiv.) was dissolved in 10 mL of CH_2Cl_2 and 3 Å molecular sieves over night. The reaction mixture was then transferred to an oven-dried culture tube with stir bar and pyridine (240 μL, 3.0 mmol, 3 equiv.) and methanesulfonyl chloride (230 μL, 3.0 mmol, 3 equiv.) were added. The culture tube was capped with a Teflon-lined cap and allowed to stir overnight. The crude product was concentrated and . added dropwise into 50 mL of ice cold (0 ºC) ether, which precipitated the polymer. The ether was decanted and the polymer was dried over vacuum to yield the title polymer **422b** as a white solid (3.66 g, 0.72 mmol, 72 %).

^{1}H NMR (500 MHz, $CDCl_3$): δ 4.39 (t, J = 4.4 Hz, 2H, H5), 3.75-3.57 (m, 453H, H2, H3, H4, and backbone Hs), 3.38 (s, 3H, H1), and 3.09 (s, 3H, H6).

Methoxypolyethylene glycol azide (420b)

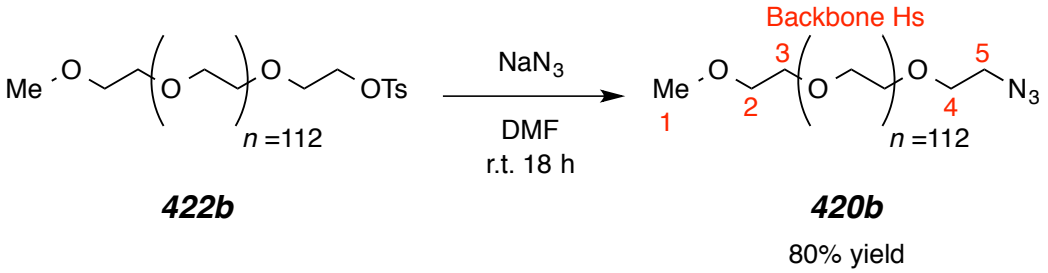

422b ***420b***

80% yield

In a 10 mL oven dried culture tube, MeO-PEG-OTs **422b** (393 mg, 0.08 mmol 1.0 equiv.) was dissolved in 5 mL of DMF dried over 3 Å molecular sieves. NaN_3 (51 mg, 0.8 mmol, 10 equiv.) was added and the reaction mixture was stirred at r.t. for 18 hours. The crude product was extracted 3 times with CH_2Cl_2 and washed with water, and brine. The organic extracts were concentrated and added dropwise into 50 mL of ice cold (0 °C) ether, which precipitated the polymer. The ether was decanted and the polymer was dried over vacuum to yield the title polymer **420b** as a white solid (320 mg, 80%).

^{1}H NMR (500 MHz, $CDCl_3$): δ 3.79 (m, 2H, H4), 3.70-3.63 (m, 447H, backbone Hs), 3.55 (m, 2H, H3), 3.50 (m, 2H, H2), 3.40 (m, 2H, H5), and 3.38 (s, 3H, H1).

Methoxypolyethylene glycol amine (421b)

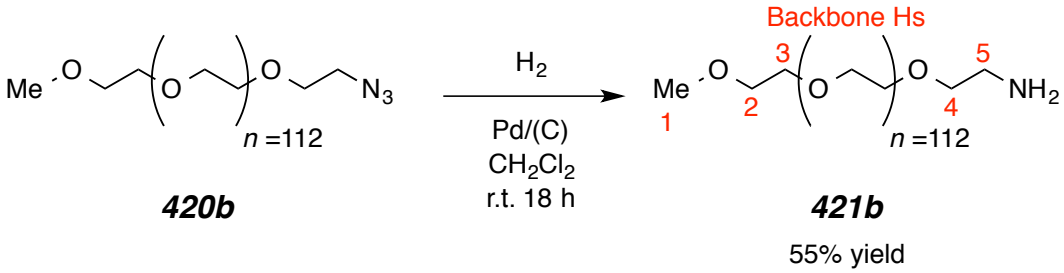

420b ***421b***

55% yield

In a 25 mL oven dried round bottom flask, MeO-PEG-N_3 **420b** (79.5 mg, 0.0159 mmol, 1.0 equiv.) was dissolved in 5 mL of CH_2Cl_2. Palladium on carbon [Pd/(C), 15.7 mg was added to the reaction. The headspace was flushed with N_2 followed by a H_2 purge. Lastly, a hydrogen (H_2) balloon was fixed to the septa of the flask and the reaction was allowed to stir at r.t. overnight. The solution was passed through a plug of cealite and washed 2x 5 mL with CH_2Cl_2. The crude product was concentrated added dropwise into 10 mL of ice cold (0 ºC) ether, which precipitated the polymer. The ether was decanted and the polymer was dried over vacuum to yield the title polymer **421b** as a white solid (43.7 mg, 0.009 mmol, 55%).

^{1}H NMR (500 MHz, $CDCl_3$): δ 3.75-3.63 (m, 453H, H2, H3, H4, and backbone Hs), 3.55 (m, 2H, H3), 3.50 (m, 2H, H2), 3.40 (m, 2H, H5), and 3.38 (s, 3H, H1), 2.89 (t, *J* = 5.2 Hz, 2H, H5), and 1.9 (br s, 2H, -NH_2).

Methoxypolyethylene glycol carbamate (421c)

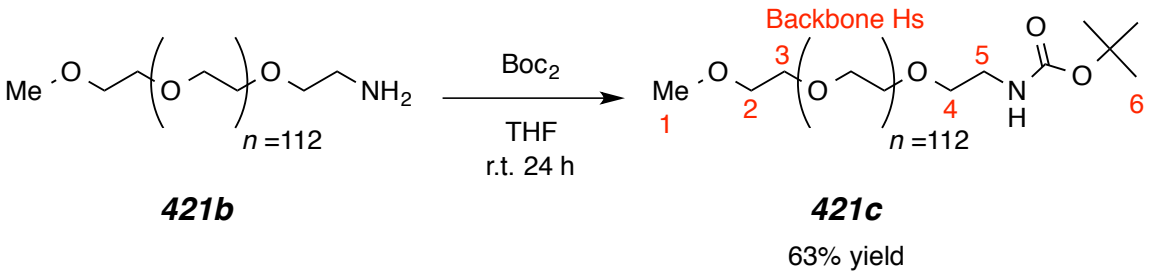

421b ***421c***

63% yield

In a 10 mL oven dried culture tube, MeO-PEG-NH_2 **421b** (48 mg, 0.0096 mmol, 1.0 equiv.) was dissolved in 6 mL of THF. Di-tert-butyl dicarbonate (BOC_2, 2.1 mg, 0.0096 mmol, 1.0 equiv.) was added and the reaction was allowed to stir at r.t. for 24 hours. The crude product was concentrated to ca. 1 mL THF and added dropwise into 12 mL of ice cold (0 ºC) ether, which precipitated the polymer. The ether was decanted and the polymer was dried over vacuum to yield the title polymer **421c** as a white solid (30.6 mg, 0.006 mmol, 63%).

^{1}H NMR (500 MHz, $CDCl_3$): δ 4.32 (br m, 1H, -N*H*BOC), 3.79-3.50 (m, 455H, H2, H3, H4, H5, and backbone Hs), 3.38 (s, 3H, H1), and 1.25 (s, 9H, H6)

Methoxypolyethylene glycol amine (421b)

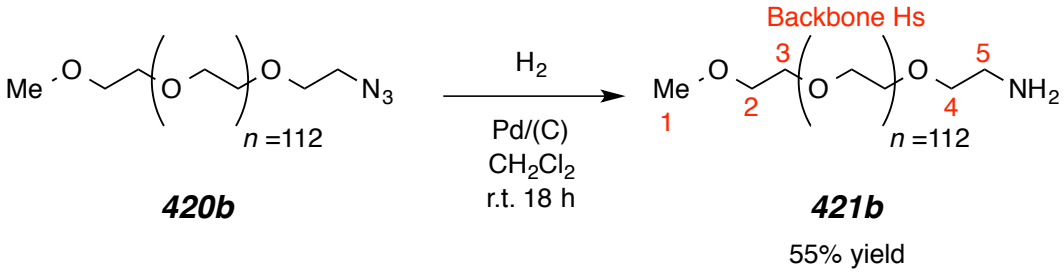

420b ***421b***

55% yield

In a 25 mL oven dried round bottom flask, MeO-PEG-N_3 **420b** (79.5 mg, 0.0159 mmol, 1.0 equiv.) was dissolved in 5 mL of CH_2Cl_2. Palladium on carbon [Pd/(C), 15.7 mg was added to the reaction. The headspace was flushed with N_2 followed by a H_2 purge. Lastly, a hydrogen (H_2) balloon was fixed to the septa of the flask and the reaction was allowed to stir at r.t. overnight. The solution was passed through a plug of cealite and washed 2x 5 mL with CH_2Cl_2. The crude product was concentrated added dropwise into 10 mL of ice cold (0 ºC) ether, which precipitated the polymer. The ether was decanted and the polymer was dried over vacuum to yield the title polymer **421b** as a white solid (43.7 mg, 0.009 mmol, 55%).

^{1}H NMR (500 MHz, $CDCl_3$): δ 3.75-3.63 (m, 453H, H2, H3, H4, and backbone Hs), 3.55 (m, 2H, H3), 3.50 (m, 2H, H2), 3.40 (m, 2H, H5), and 3.38 (s, 3H, H1), 2.89 (t, *J* = 5.2 Hz, 2H, H5), and 1.9 (br s, 2H, -NH_2).

2-(2-(2-azidoethoxy)ethoxy)ethan-1-ol (424)

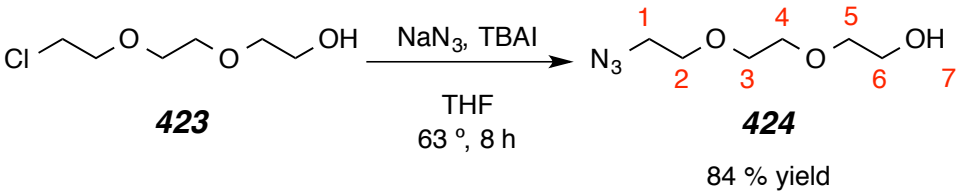

A 100 mL round bottom flask was charged with NaN_3 (1.75 g, 27.2 mmol, 3.1 equiv.) and tetrabutyl-ammonium iodide (TBAI, 331 mg, 0.90 mmol, 0.1 equiv.) and dissolved with 20 mL of THF. The reaction was allowed to stir for 20 mins at which point **423** (1.50 g, 8.90 mmol, 1 equiv.) was added dropwise over the course of 5 mins. The reaction proceeded for 8 hours. The THF was removed by rotary evaporation and replaced with 20 mL of EtOAc, washed with brine, dried over $MgSO_4$. The EtOAC was removed and the residue was purified via flash column chromotagraphy (hexane:EtOAc = 7:3; to yield the title compound **424** (1.31 g, 7.48 mmol, 84%) as a light orange oil.

^{1}H NMR (500 MHz, $CDCl_3$): δ 3.75 (br t, 1H, H7), 3.71-3.66 (m, 8H, H3–H6), 3.63 (m, 2H, H2), and 3.41 (t, J = 5.0 Hz, 2H, H1).

^{13}C NMR (125 MHz, $CDCl_3$): δ 72.5, 70.6, 70.3, 70.0, 61.6, and 50.6.

GC- MS: [30 m x 0.25 mm ID, HP-5, 50 °C/1.5 min/10 °C min-1/290 °C, (5029021)] t_R = 9.86 min [m/z] 175 (M^+), 158 ($M^{+\bullet}$ -OH), 100 ($M^{+\bullet}$ -$C_3H_7O_2$), and 56 ($M^{+\bullet}$ -$C_5H_{11}O_3$).

3-(2-(2-(2-Azidoethoxy)ethoxy)ethoxy)prop-1-yne (426)

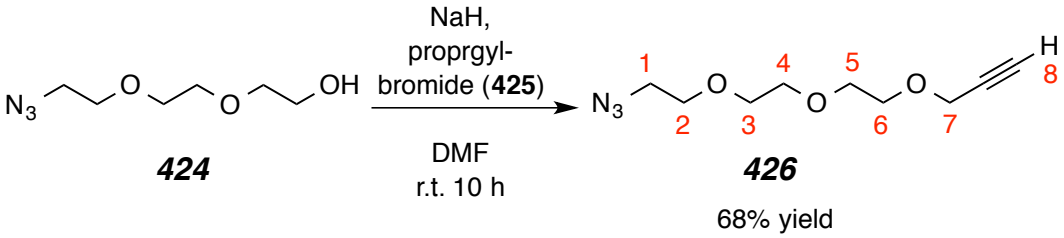

424 ***426***

68% yield

In a 100 mL round bottom flask, **424** (226 mg, 1.5 mmol, 1 equiv.) was dissolved in 10 mL of DMF. NaH (48 mg, 2.0 mmol, 1.3 equiv.) and propargyl bromide **425** (330 μL, 3.0 mmol, 2.0 equiv.) were added slowly to the solution, which was then stirred at r.t. for 10 hours. The DMF was removed and the residue was purified via flash column chromotagraphy (hexane:EtOAc = 7:3; to yield the title compound **426** (217 mg, 1.02 mmol, 68%) as an orange oil.

^{1}H NMR (500 MHz, $CDCl_3$): δ 4.15 (d, *J*= 2.5 Hz, 2H, H7), 3.60-3.68 (m, 10H, H2–H6), 3.34 (t, *J* = 5.0 Hz, 2H, H1), and 2.37 (t, *J* = 2.5 Hz, 1H, H8).

^{13}C NMR (125 MHz, $CDCl_3$): δ 78.24, 74.53, 70.71, 70.69, 70.52, 70.07, 69.12, 58.42, and 50.70.

GC- MS: [30 m x 0.25 mm ID, HP-5, 50 °C/1.5 min/10 °C min-1/290 °C, (5029021)] t_R = 9.3 min [m/z] 213 (80, M^+), 126 (100, $M^{+\bullet}$ -$C_2H_4N_3OH$), and 54 (99, $M^{+\bullet}$ -$C_6H_{12}N_3O_2H$).

TLC R_f (7:3 hexanes:EtOAc) = 0.4.

3-(2-(2-(2-Aminoethoxy)ethoxy)ethoxy)prop-1-yne (428)

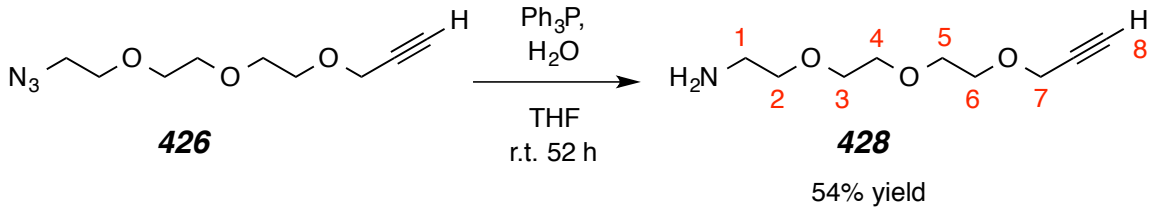

426 ***428***

54% yield

In a 25 mL culture tube, **426** (135 mg, 0.63 mmol, 1.0 equiv.) and triphenylphosphine (Ph_3P, 332 mg, 1.27 mmol, 2.0 equiv.) were dissolved in 10 mL of THF. The reaction mixture was stirred at r.t. for 4 hours, after which HPLC grade H_2O (1 mL) was added. The reaction mixture was stirred for an additional 48 hours, concentrated, and purified by flash column chromatography (CH_2Cl_2:MeOH:TEA = 80:20:1) to yield **428** as an oil (64 mg, 0.340 mmol, 54%).

^{1}H NMR (500 MHz, $CDCl_3$): δ 4.21 (d, *J* = 2.5 Hz, 2H, H7), 3.68-3.70 (m, 8H, H3-H6), 3.41 (t, *J* = 5.0 Hz, 2H, H2), 3.39 (t, *J* = 5.0 Hz, 2H, H1), 2.44 (t, *J* = 2.0 Hz, 1H, H8), and 1.47 (br s, 2H, -NH_2).

^{13}C NMR (125 MHz, $CDCl_3$): δ 79.75, 74.92, 73.12, 70.51, 69.70, 69.44, 69.11, 58.39, and 41.68.

GC- MS: [30 m x 0.25 mm ID, HP-5, 50 °C/1.5 min/10 °C min-1/290 °C, (5029021)] t_R = 6.5 min [m/z] 187 (4, M^+), 127 (5, $M^{+\bullet}$ -C_2H_6NO), 87 (100, $M^{+\bullet}$ -C_5H_7OH).

LC-MS: Waters Symmetry-C8 3.9 x 150 mm particle size 5 *μ*m; 1 mL/min Isocratic Method 100 % for 20 min (Solvent System of 98:2 MeOH:H_2O,15 mM NH_4OAc), MM-ES+APCI Positive Scan 2.4 min 188.2 (100, $M+H)^+$.

TLC Rf (CH_2Cl_2:MeOH:TEA = 80:20:1) = 0.38.

3-(2-(2-(2-chloroethoxy)ethoxy)ethoxy)prop-1-yne (427)

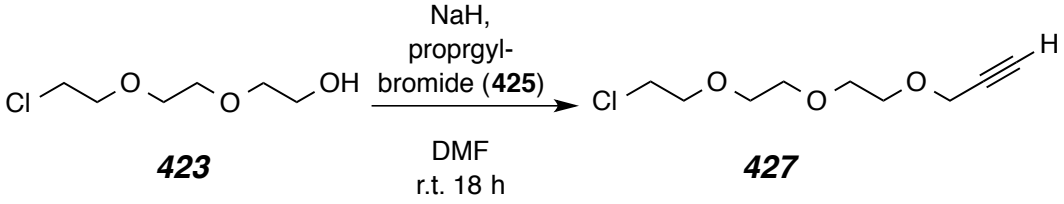

423 ***427***

In an oven-dried culture tube, **423** (554 mg, 3.28 mmol, 1.0 equiv.) was dissolved in 5 mL of DMF. NaH (77.7 mg, 3.29 mmol, 1.0 equiv.) and propargyl bromide **425** (584.5 μL, 6.56 mmol, 2.0 equiv.) were added slowly to the solution, which was then stirred at r.t. for 18 hours. GC-MS determined **427** was the major compound. The chloro-alkyne **427** was taken forward to the next step without purification.

GC- MS: [30 m x 0.25 mm ID, HP-5, 50 °C/1.5 min/10 °C min-1/290 °C, (5029021)] t_R = 10.097 min [m/z] 206 (M^+), 151 ($M^{+\bullet}$ -C_3H_3O), 133 ($M^{+\bullet}$ -C_3H_2Cl), 107 ($M^{+\bullet}$ -$C_5H_{17}O_2$), and 55 ($M^{+\bullet}$ -$C_6H_{12}ClO_2$).

3-(2-(2-(2-Aminoethoxy)ethoxy)ethoxy)prop-1-yne (428)

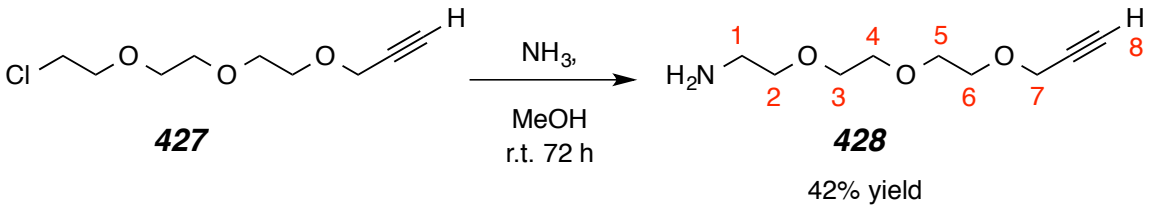

427 ***428***

42% yield

In a culture tube, **427** (546.3 mg, 3.24 mmol, 1.0 equiv.) and ammonia in methanol (454.2 mg, 12.96 mmol, 4.0 equiv.) were dissolved in 10 mL of MeOH. The reaction mixture was stirred at r.t. for 72 hours. The crude reaction mixture was concentrated, and purified by flash column chromatography (CH_2Cl_2:MeOH:TEA = 80:20:1) to yield **428** as an oil (254 mg, 1.36 mmol, 42%).

^{1}H NMR (500 MHz, $CDCl_3$): δ 4.21 (d, *J* = 2.5 Hz, 2H, H7), 3.68-3.70 (m, 8H, H3-H6), 3.41 (t, *J* = 5.0 Hz, 2H, H2), 3.39 (t, *J* = 5.0 Hz, 2H, H1), 2.44 (t, *J* = 2.0 Hz, 1H, H8), and 1.47 (br d, 2H, NH_2).

^{13}C NMR (125 MHz, $CDCl_3$): δ 79.75, 74.92, 73.12, 70.51, 69.70, 69.44, 69.11, 58.39, and 41.68.

GC- MS: [30 m x 0.25 mm ID, HP-5, 50 °C/1.5 min/10 °C min-1/290 °C, (5029021)] t_R = 6.5 min [m/z] 187 (4, M^+), 127 (5, $M^{+\bullet}$ -C_2H_6NO), 87 (100, $M^{+\bullet}$ -C_5H_7OH).

LC-MS: Waters Symmetry-C8 3.9 x 150 mm particle size 5 *μ*m; 1 mL/min, Isocratic Method 100 % for 20 min (Solvent System of 98:2 MeOH:H_2O,15 mM NH_4OAc) MM-ES+APCI Positive Scan 2.4 min 188.2 (100, M+H)$^+$.

TLC Rf (CH_2Cl_2:MeOH:TEA = 80:20:1) = 0.38.

(+)-Biotin N-hydroxysuccinimide ester (429a)

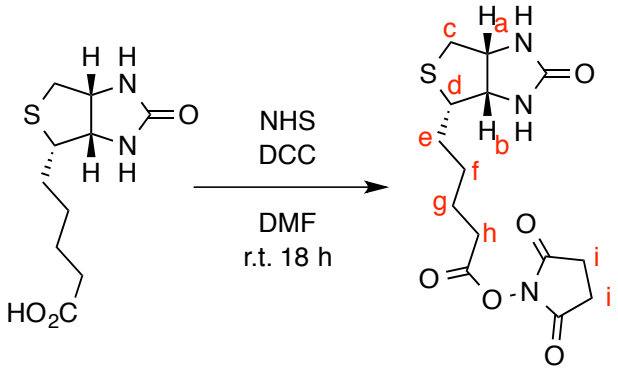

429 ***429a***
quant. yield

In an oven dried culture tube, biotin (**429)** (112 mg, 0.459 mmol, 1.0 equiv.), *N*-hydroxysuccinimide (NHS, 40.6 mg, 0.459 mmol, 1.0 equiv.), and *N,N'*-dicyclohexylcarodiimide (DCC, 141.9 mg, 0.69 mmol, 1.5 equiv.), were dissolved in 5 mL of DMF. The reaction mixture was stirred at r.t. for overnight. The reaction mixture was concentrated, and the solid product **429a** was placed on a Büchner funnel and washed with 10 mL ether 3x the resulting white solid **429a** (156.5 mg, 0.459 mmol, quant.) was used without further purification.

^{1}H NMR (500 MHz, $CDCl_3$): δ 5.65 (s, 1H, NHb), 5.58 (s, 1H, NHa), 4.49-4.47 (m, 1H, Hb), 4.29 (ddd, *J* = 7.4, 4.9, 2.2 Hz, 1H, Ha), 3.16 (ddd, *J* = 8.2, 6.5, 4.6 Hz, 1H, Hd), 2.90 (dt, *J* = 12.0, 5.7 Hz, 1H, Hc), 2.86 (s, 4H, Hi), 2.75 (d, *J* = 12.7 Hz, 1H, Hc), 2.64 (dd, *J* = 7.2, 5.6 Hz, 2H, Hh), 1.90-1.62 (m, 4H, He and Hg), 1.58-1.52 (m, 2H, Hf).

^{13}C NMR ($CDCl_3$)[221]: δ 170.2, 168.4, 165.3, 62.2, 60.1, 56.7, 42.4, 31.8, 28.4, 25.3, 24.1, 23.2.

LC-MS: Waters Symmetry-C8 3.9 x 150 mm particle size 5 μm; 1 mL/min, Gradient Method 50% B to 100% B over 15 min, hold at 100% B for 10 min (Solvent System A, 5:95 MeOH:H_2O,15 mM NH_4OAc) (Solvent System B, 98:2 MeOH:H_2O,15 mM NH_4OAc), MM-ES+APCI Positive Scan 10.3 min 359 $(M+NH_4)^+$, 364 $(M+Na)^+$; Negative Scan 10.3 min 400 $(M+OAc)^-$, and 376 $(M+Cl)^-$.

[221] Ma, M.; Bong, D. Protein Assembly Directed by Synthetic Molecular Recognition Motifs. *Org. Biomol. Chem.* **2011**, *9*, 7296.

5-((3a*S*,4*S*,6a*R*)-2-oxohexahydro-1*H*-thieno[3,4-*d*]imidazol-4-yl)-*N*-(2-(2-(2-(prop-2-yn-1-yloxy)ethoxy)ethoxy)ethyl)pentanamide (430)

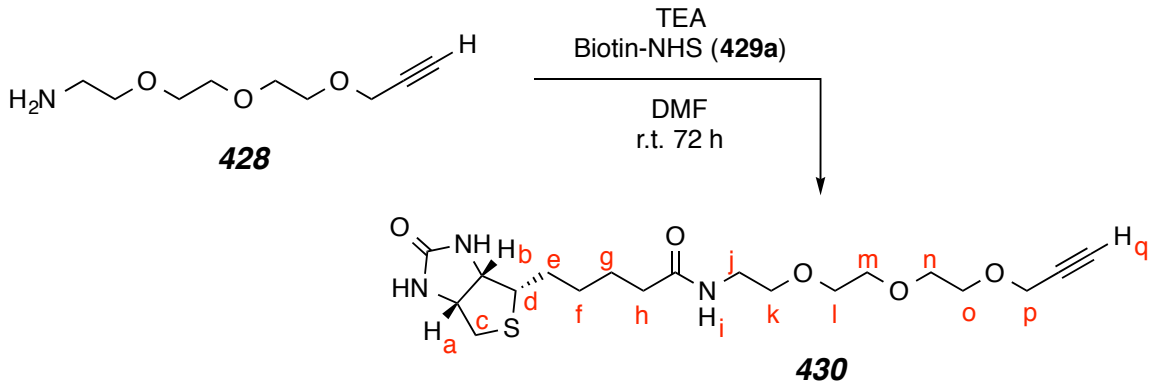

428

430

54 % yield

In an oven dried culture tube, biotin-NHS (**429a**) (23.97 mg, 0.072 mmol, 1.0 equiv.), 3-(2-(2-(2-Aminoethoxy)ethoxy)ethoxy)prop-1-yne (**428**) (20.3 mg, 0.108 mmol, 1.5 equiv.), and triethylamine (TEA, 20 μL, 0.144 mmol, 2.0 equiv.) were dissolved in 1.0 mL of dry DMF. After 72 h of reaction the DMF from removed and an LC-MS of the crude orange oil determined the completeion of the coupling along with the urea by-products from the formation of **429a**. The biotin linker **430** was purified by affinity chromatography. A 1 mL affinity column was made with Pierce™ NeutrAvidin™ Agarose resin. The oil was loaded onto the column with 0.5 mL of DMSO and vortexed for 5 min. The DMSO and byproducts were eluted off of the column, leaving the desired **430** product on the column. An additional 600 μL of DMSO was added and the affinity column was heated to 85 ºC for 1 min. The product was eluted off the column. The 1H-NMR and LC-MS determined the purity of the compound **430** (16.1 mg, 0.039 mmol, 54%).

^{1}H NMR (500 MHz, $CDCl_3$): δ 8.02 (s, 1H, NHi), 6.58 (t, *J* = 5.0 Hz, 1H, NHb), 6.28 (s, 1H, NHa), 4.53 (dd, *J* = 7.4, 5.0 Hz, 1H, Hb), 4.34 (dd, *J* = 7.4, 4.4, 1H, Ha), 4.20 (d, *J* = 2.3 Hz, 2H, Hp), 3.77-3.61 (m, 10H, Hk-Ho), 3.57 (t, *J* = 5.0 Hz, 2H, Hj), 3.16 (td, *J* = 7.2, 4.6 Hz, 1H, Hd), 2.92 (dd, *J* = 12.9, 4.9 Hz, 1H, Hc), 2.76 (d, *J* = 12.8 Hz, 1H, Hc), 2.47 (t, *J* = 2.3 Hz, 1H, Hq), 2.29-2.19 (m, 2H, Hh), 1.94-1.59 (m, 4H, He and Hg), 1.46 (dt, J = 14.5, 7.3 Hz, 2H, Hf).

LC-MS: Waters Symmetry-C8 3.9 x 150 mm particle size 5 *μ*m; 1 mL/min, Gradient Method 50% B to 100% B over 10 min, hold at 100% B for 15 min (Solvent System A, 5:95 MeOH:H_2O,15 mM NH_4OAc) (Solvent System B, 98:2 MeOH:H_2O,15 mM NH_4OAc), MM-ES+APCI Positive Scan 4.4 min 431 $(M+NH_4)^+$, 414 $(M+H)^+$; Negative Scan 4.4 min 472 $(M+OAc)^-$, 448 $(M+Cl)^-$, 458 $(M+O_2CH)^-$, 491 $(M+DMSO)^-$, and 412 $(M-H)^-$.

Methoxypolyethylene glycol 4-(trimethylsilyl)-1H-1,2,3-triazole (432b)

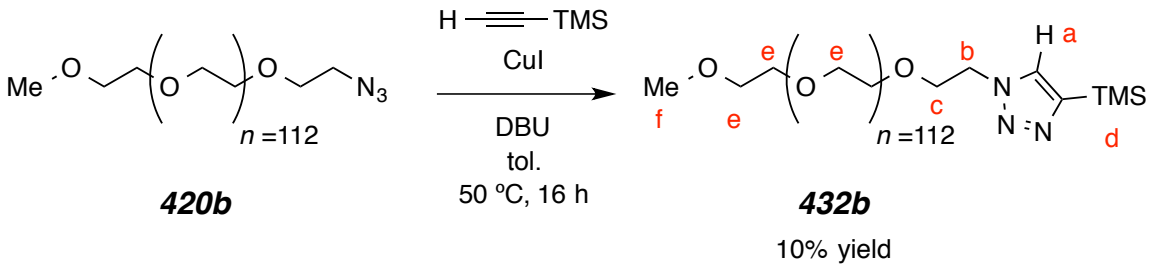

420b ***432b***

10% yield

In an oven dried culture tube, MeO-PEG-N_3 **420b** (195.6 mg, 0.0391 mmol, 1.0 equiv.) was dissolved in 10 mL of Toluene. A catalytic amount of copper(I) iodide (CuI, 3,72 mg, 0.0196 mmol, 0.5 equiv.) and an excess amount of DBU (112.8 mg, 0.782 mmol, 20.0 equiv.) was added. The reaction mixture was allowed to stir for 5 min at which point ethynyltrimethylsilane (38.4 mg, 0.391 mmol, 10.0 equiv.) was added. The culture tube was sealed with a Teflon lined cap and heated to 50 °C for 16 hours. The solution was passed through a plug of silica < 1 c.m and concentrated. The crude product with residual solvent was added dropwise into 10 mL of ice cold (0 °C) ether, which precipitated the polymer. The ether was decanted and the polymer was dried over vacuum to yield the title polymer **432b** as a dark solid (20.4 mg, 0.0040 mmol, 10.2%).

^{1}H NMR (500 MHz, $CDCl_3$): δ 7.68 (s, 1H, Ha), 4.56 (t, *J* = 5.1 Hz, 2H, Hb), 3.87 (t, *J* = 5.1 Hz, 2H, Hc), 3.79-3.57 (m, 451H, He), 3.38 (s, 3H, Hf), and 0.31 [s, 9H, TMS(Hd)].

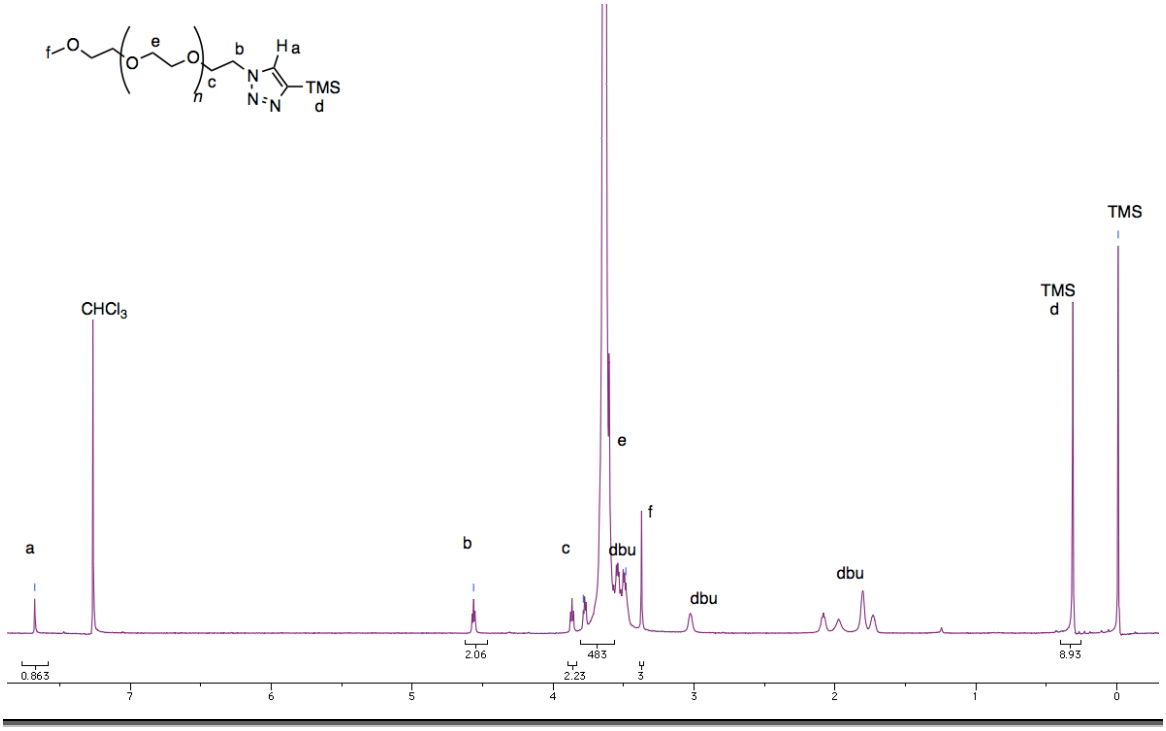

Figure S4.14 I ^{1}H-NMR of the polymer click reaction product after 1 precipitation into cold ether.

(S)-3-(benzyloxy)-2-hydroxypropanoic acid (436)

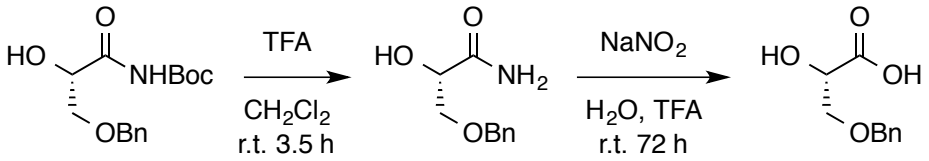

434 ***435*** ***436***

90% yield

In a 100 mL round bottom flask **434** (10.4 g, 35.2 mmol, 1.0 equiv.) and TFA (10.0 mL, 14.9 g, 130.6 mmol, 3.7 equiv.) were dissolved in 60 mL of CH_2Cl_2. The reaction mixture was stirred at r.t. for 3.5 hours. The crude reaction mixture was concentrated, and a crude ^{1}H-NMR showed full conversion to **435**, which matched literature. The waxy solid was taken forward to the next reaction without further purification. The amide **435** and $NaNO_2$ (3.42 g, 69.0 mmol, 1.4 equiv.) were dissolved in 25 mL of deionized H_2O. A second portion of TFA (4.0 mL, 52.2 mmol, 1.5 equiv.) was added and the headspace was purged 3 times with N_2. The reaction was allowed to stir at room temperature for overnight (~16 h). Solid NaCl was added to the reaction mixture. The aqueous solution was extracted with ethyl acetate. The combined organic layers were dried ($MgSO_4$) and concentrated to give the compound **436** as a yellow oil (6.2 g, 31.7 mmol, 90%). To remove residual amount of TFA, DCM was added to the mixture and evaporated under reduced pressure. This was repeated several times. The yellow oil obtained was used in the next reaction without further purification. The ^{1}H-NMR matched literature[175] so no other characterization was performed.

^{1}H NMR (500 MHz, $CDCl_3$): δ 7.35-7.186 (m, 5H, -OCH_2*Ph*), 4.49 (s, 2H, -OCH_2Ph), 4.31 (t, *J* = 4 Hz, 1H, -C*H*CH_2O-), 3.76 (dd, *J* = 4 Hz, 1H, -$CHCH_2OCH_2$Ph), and 3.69 (dd, *J* = 4 Hz, 1H, -$CHCH_2O$-).

(3S,6S)-3,6-bis((benzyloxy)methyl)-1,4-dioxane-2,5-dione (438)

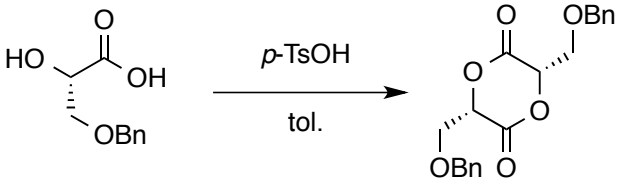

436 ***438***

In a round bottom flask, **436** (14.5 g, 73.9 mmol, 1.0 equiv.) and *p*-toluenesulfonic acid catalyst (*p*-TsOH, 800 mg, 4.7 mmol, 6 mol%) were dissolved in 1.5 L of toluene and brought to reflux. The reaction mixture was refluxed at 168 ºC for 7 days and the water removed through azeotropic distillation into a Dean-Stark trap. The toluene was removed and replaced with 20 mL of water, and extracted 3x 200 mL with diethyl ether. The organic layer was dried with $MgSO_4$ and the ether removed to yield the desired monomer **438** (8.95 g, 25.1 mmol, 34%). ^{1}H-NMR matched literature[175] so no other characterization was performed.

^{1}H NMR (500 MHz, $CDCl_3$): δ 7.36-7.26 (m, 10H, -OCH_2*Ph*), 5.13 (t, *J* = 4.0 Hz, 2H, -C*H*CH_2O-), 4.48 (d, *J* = 11.5 Hz, 2H, -$CHCH_2OCH_2$Ph), 4.44 (d, *J* = 11.5 Hz, 2H, -$CHCH_2OCH_2$Ph), and 3.89 (d, *J* = 4.0 Hz, 4H, -$CHCH_2O$-).

3-(2-(2-(2-Aminoethoxy)ethoxy)ethoxy)prop-1-yne (428)

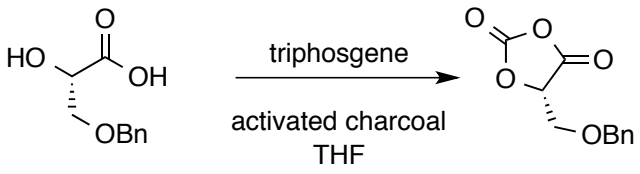

436 ***437***

In a 50 mL oven dried round-bottom flask charged with a magnetic stir bar **436** (2.50 g, 12.7 mmol, 1.0 equiv.), triphosgene (3.92 g, 13.2 mmol, 1.1 equiv.) were dissolved in 10 mL of dry THF. Activated charcoal (30 mg) was added added and the reaction mixture was stirred at r.t. for 8 hours. The crude reaction mixture was filtered through a plug of cealite, concentrated, and purified by three MPLC runs (SiO_2, 1:1, hexanes:EtOAc) to yield the title compound **437** as a white solid (1.52 g, 6.86 mmol, 54%).

^{1}H NMR (500 MHz, $CDCl_3$): δ 7.40-7.25 (m, 5H, -OCH_2*Ph*), 5.12 (t, *J* = 2.1 Hz, 1H, -C*H*CH_2O-), 4.61 (d, *J* = 12.6 Hz, 1H, -$CHCH_2OCH_2$Ph), 4.56 (d, *J* = 12.3 Hz, 1H, -$CHCH_2OCH_2$Ph), and 3.89 (m, 2H, -$CHCH_2O$-).

^{13}C NMR (125 MHz, $CDCl_3$): δ 165.5, 148.4, 136.2, 128.7 (2x), 128.3, 127.7 (2x), 79.6, 73.8, and 66.1.

GC- MS: [30 m x 0.25 mm ID, HP-5, 35 °C/1.5 min/10 °C min-1/250 °C, (3525018)] t_R = 7.20 min [m/z] 222 (M^+), 208 ($M^{+\bullet}$ -H_2O), 107 ($M^{+\bullet}$ -$C_4H_3O_4$), 91 ($M^{+\bullet}$ -$C_4H_3O_5$), and 91 ($M^{+\bullet}$ -$C_5H_5O_5$).

Methoxy-capped poly(ethylene glycol)-block-poly(benzyloxy lactic acid) (439)

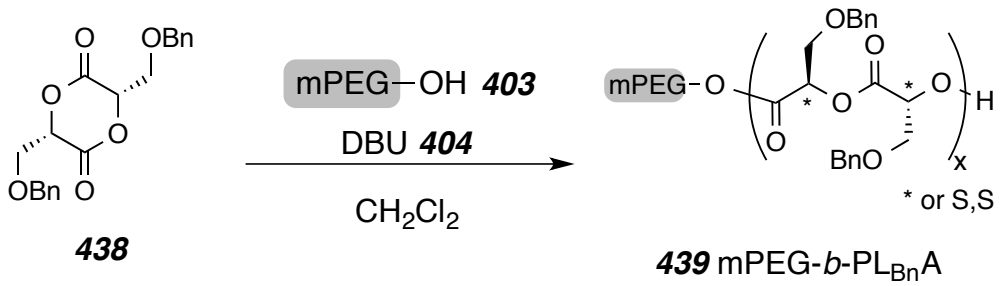

438 ***439*** mPEG-*b*-$PL_{Bn}A$

MeO-PEG-OH (**403**, 5K, 5.0 g) was dissolved in 10 mL of dry CH_2Cl_2 and stored over 3 Å molecular sieves. From this stock solution **403** (200 μL, 100 mg, 0.02 mmol, 1.0 equiv.) was added to the benzyl-protected lactide **4.38** (205.8 mg, 0.58 mmol, 28.9 equiv.) in an oven-dried round-bottom flask containing a magnetic stir bar and 2 mL of CH_2Cl_2. The DBU catalyst (25 μL, 0.17 mmol, 8.4 equiv.) was added to the reaction. After 1 hour of reaction solid benzoic acid (ca. 15 mg) was added to arrest the polymerization. The mPEG-*b*-$PL_{Bn}A$ (**439**) was purified by precipitation twice into ice cold isopropanol from CH_2Cl_2 and dried at 50 °C under vacuum overnight yielding the desired product as a white solid with M_n [PL(Bn)A] = 11,000 g/mol.

^{1}H NMR (500 MHz, $CDCl_3$): δ 7.34-7.24 [m, 567H, $PL_{Bn}A$(-OCH_2-*o*-*Ph*), $PL_{Bn}A$(-OCH_2-*m*-*Ph*), and $PL_{Bn}A$(-OCH_2-*p*-*Ph*)], 5.53-5.35 [m, 35H, $PL_{Bn}A$(-C*H*CH_2O-)], 4.64-4.46 [m, 173H, $PL_{Bn}A$(-CHC*H_2*O-)], 4.03-3.81 [m, 133H, $PL_{Bn}A$(-O*CH_2*Ph)], 3.79-3.49 [m, 455H, MeO-PEG(-OC*H_2CH_2*O-)], and 3.38 (s, 3H, *Me*O-PEG-).

Methoxy-capped poly(ethylene glycol)-block-poly[(benzyloxy lactic)-co-(lactic) acid] (440)

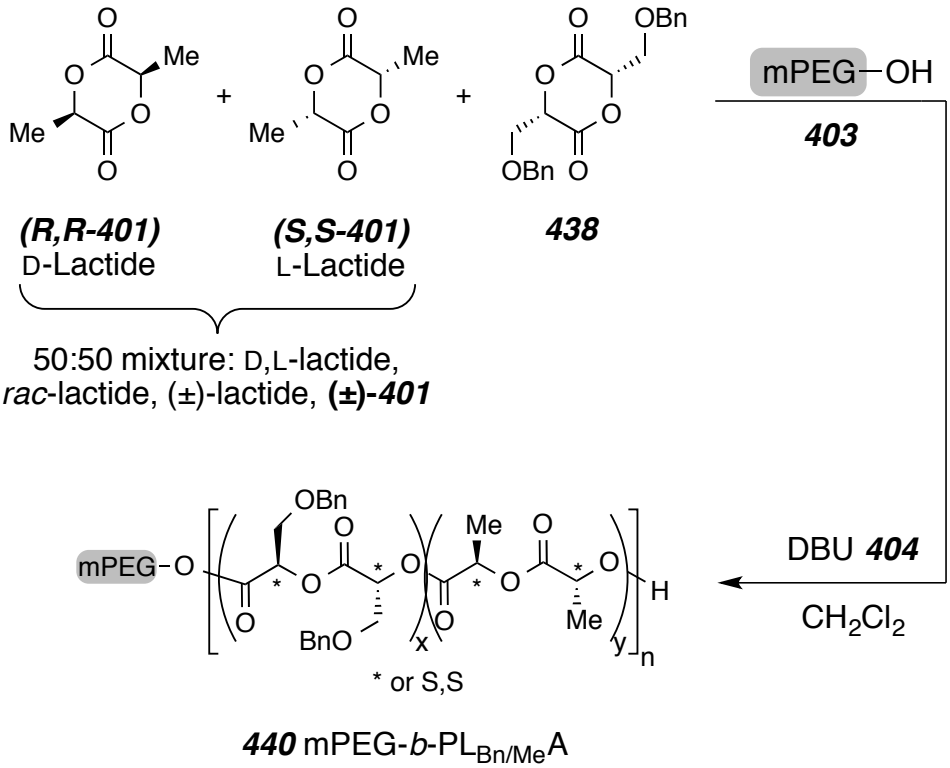

MeO-PEG-OH (**403**, 5K, 5.0 g) was dissolved in 10 mL of dry CH_2Cl_2 and stored over 3 Å molecular sieves. From this stock solution **403** (200 μL, 100 mg, 0.02 mmol, 1.0 equiv.) was added to the benzyl-protected lactide **4.38** (122.5 mg, 0.34 mmol, 17.2 equiv.) and *rac*-lactide **401** (122.8 mg, 0.85 mmol, 42.6 equiv.) in an oven-dried round-bottom flask containing a magnetic stir bar and 10 mL of CH_2Cl_2. The DBU catalyst (30 μL, 0.20 mmol, 10.2 equiv.) was added to the reaction. After 1 hour of reaction solid benzoic acid (ca. 50 mg in 5 mL CH_2Cl_2) was added to arrest the polymerization. The mPEG-*b*-PL(Bn/Me)A (**440**) was purified by precipitation 50 mL into ice cold isopropanol from CH_2Cl_2, centrifuged

at 5,000 rpm, and dried at 50 °C under vacuum overnight yielding the desired product as a white solid (53% yield) with M_n [PL(Bn/Me)A] = 16,600 g/mol, ca. 53:47 lactic(Bn):lactic(Me) ratio by mass.

^{1}H NMR (500 MHz, $CDCl_3$): δ 7.37-7.21 [m, 261H, $PL_{Bn}A$(-OCH_2-*o*-*Ph*), $PL_{Bn}A$(-OCH_2-*m*-*Ph*), and $PL_{Bn}A$(-OCH_2-*p*-*Ph*)], 5.53-5.33 [m, 42H, $PL_{Bn}A$(-C*H*CH_2O-)], 5.27-5.10 [m, 109H, $PL_{Me}A$(-C*H*CH_3)], 4.65-4.35 [m, 119H, $PL_{Bn}A$(-CHC*H_2*O-)], 4.11-3.77 [m, 93H, $PL_{Bn}A$(-O*CH_2*Ph)], 3.73-3.49 [m, 455H, MeO-PEG(-OC*$H_2C H_2$*O-)], 3.39 (s, 3H, *Me*O-PEG-), and 1.64-1.43 [m, 430H, $PL_{Me}A$(-CHC*H_3*)].

SEC (Polystyrene standards) PDI = 1.08.

Experimental Section for Chapter 5

Table S5.1 I Characterization data for loaded nanoparticles used for intra-tumoral studies.

Pro-drug #	Pro-drug (mg)	Poly-mer (mg)	Total Mass Recovered (mg)	wt% Recovered following centrifugation and lyophilization	d_I (nm) of the initially prepared FNP NPs	PDI of the initially prepared FNP NPs	PTX equivalent Loading
2	88.4	59.5	114.2	77%	130	0.15	43%
3	70.2	56.6	85.5	67%	93	0.15	58%
6	33.7	28.3	21.1	34%	110	0.22	56%
7	12.1	8.1	15.8	78%	110	0.18	31%
8	72.2	52.3	76.0	61%	120	0.16	53%

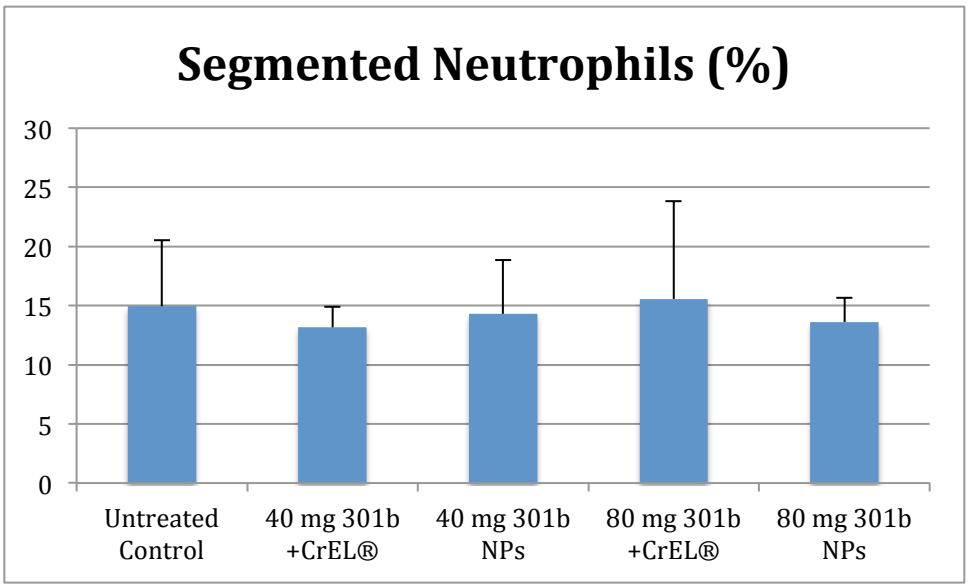

Figure S5.1 I Differential percentage of segmented neutrophils from the total white blood cell count (WBC). [normal range 10-40 %]

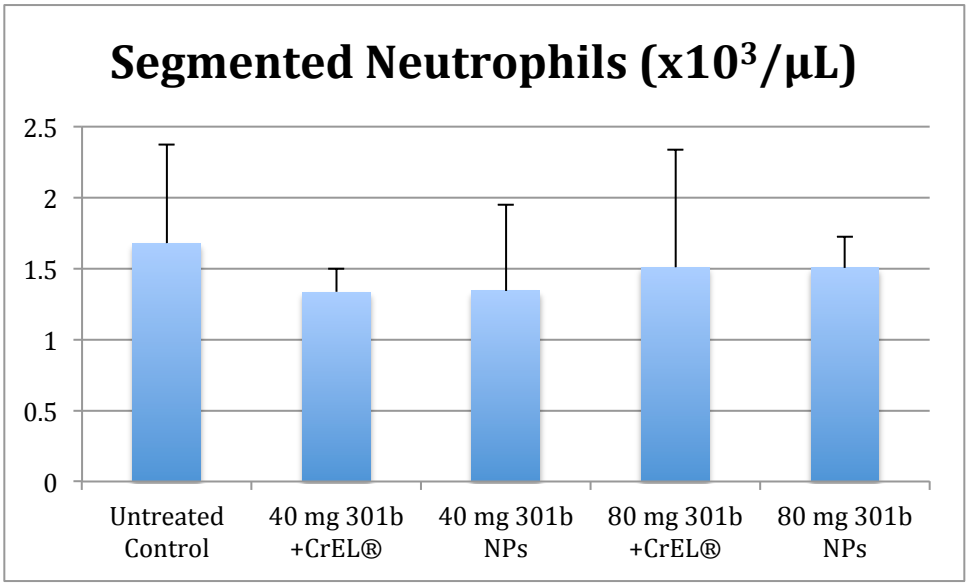

Figure S5.2 I Absolute number of segmented neutrophils calculated from the differential % of the whole mouse plasma. [normal range 0.1-2.4 x10^3/μL]

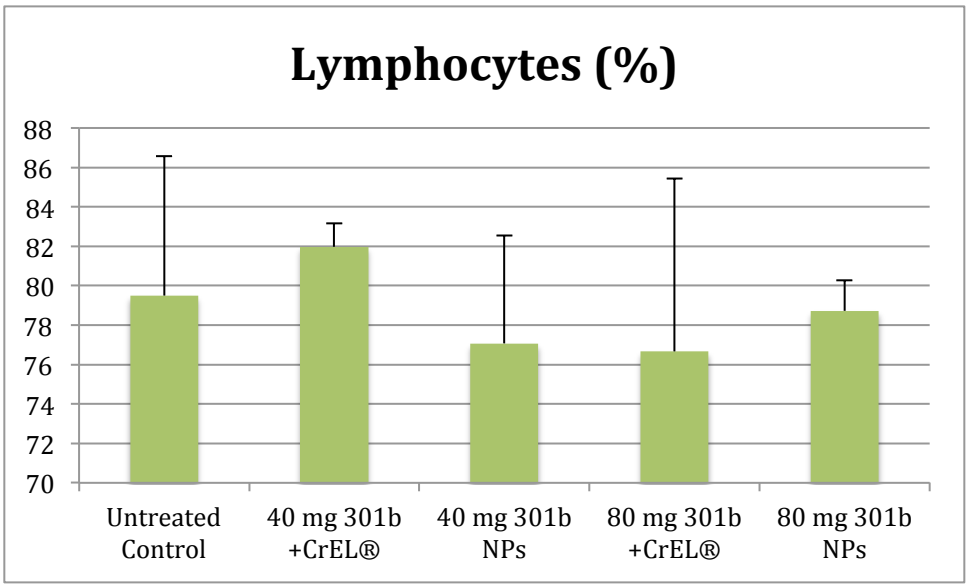

Figure S5.3 I Differential percentage of lymphocytes from the total white blood cell count (WBC). [normal range 55-95 %]

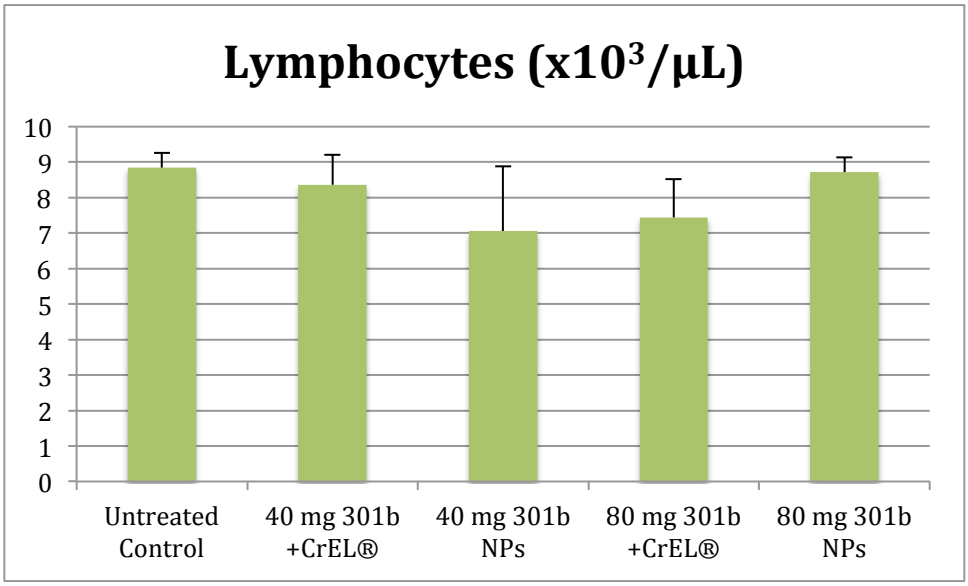

Figure S5.4 I Absolute number of lymphocytes calculated from the differential percentage of the whole mouse plasma. [normal range 0.9-9.3 x10^3/µL]

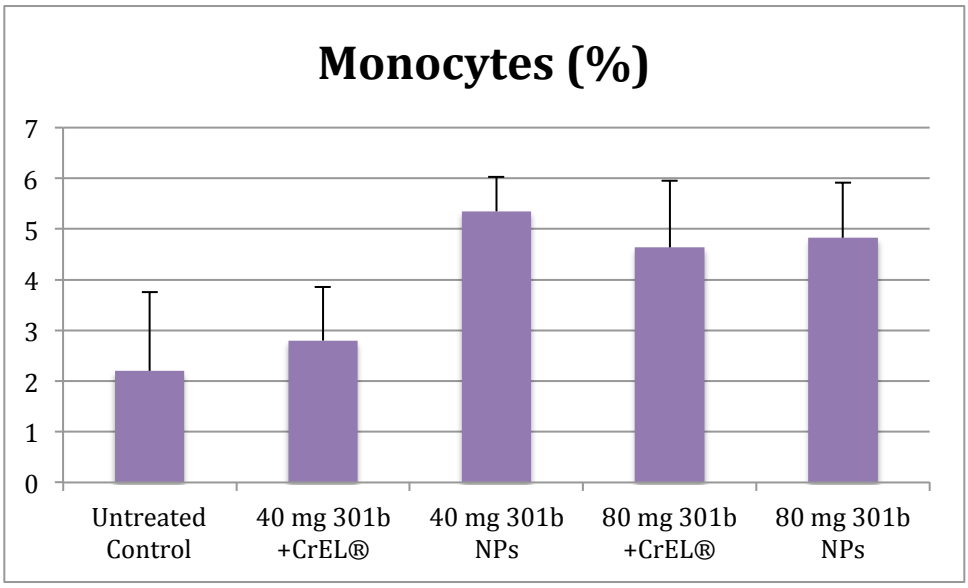

Figure S5.5 I Differential percentage of monocytes from the total white blood cell count (WBC). [normal range 0.1-3.5 %]

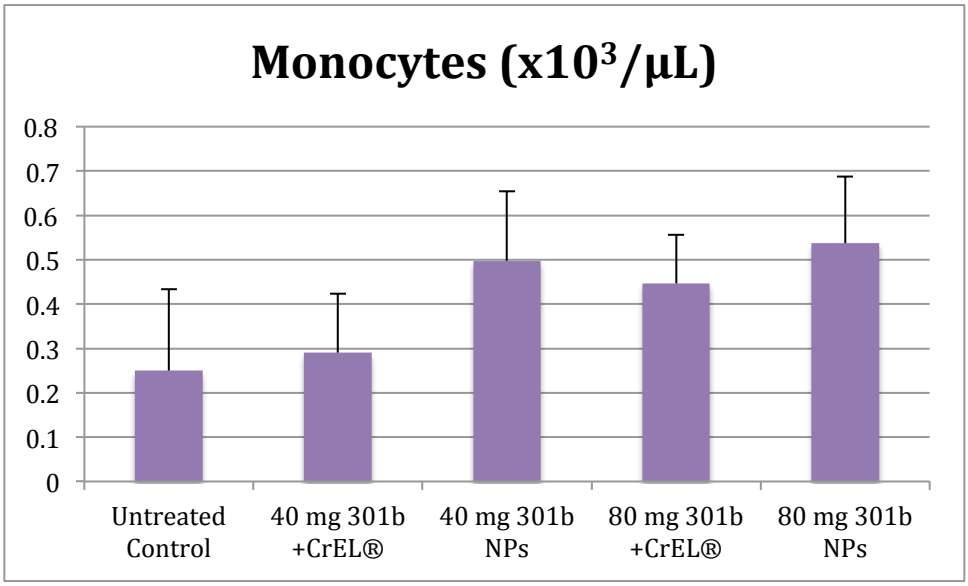

Figure S5.6 I Absolute number of monocytes calculated from the differential percentage of the whole mouse plasma. [normal range 0-0.4 x10^3/μL]

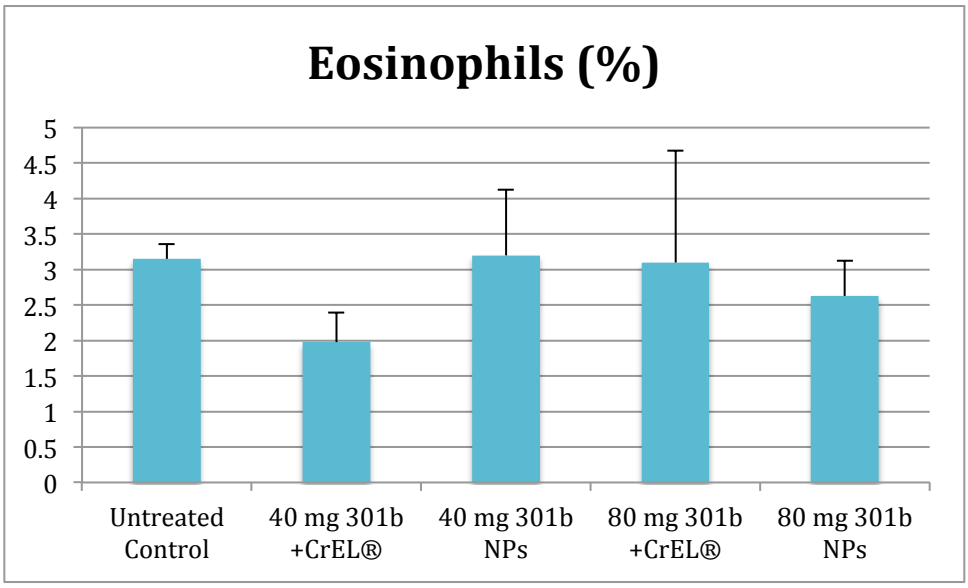

Figure S5.7 I Differential percentage of eosinophils from the total white blood cell count (WBC). [normal range 0-4 %]

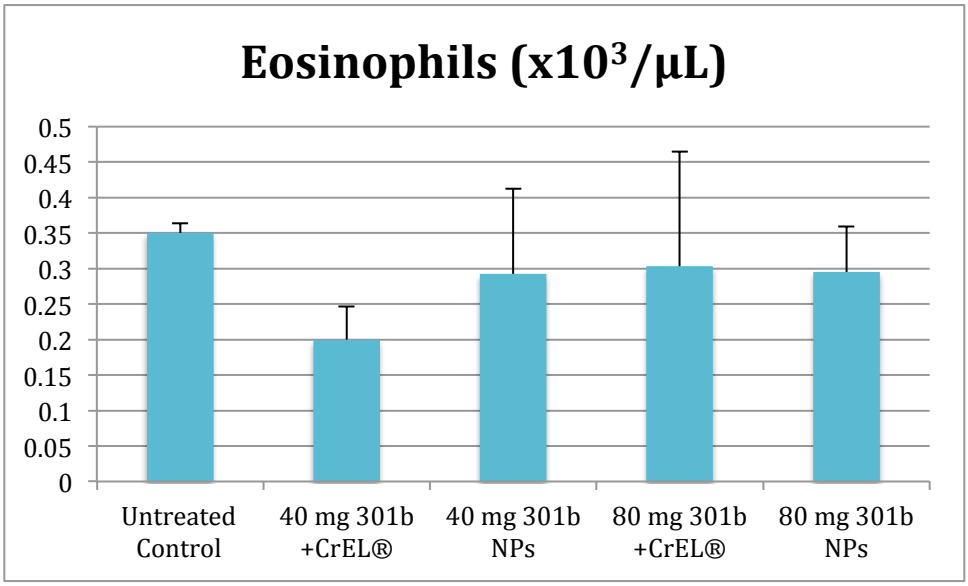

Figure S5.8 I Absolute number of eosinophils calculated from the differential percentage of the whole mouse plasma. [normal range 0-0.2 x10^3/µL]

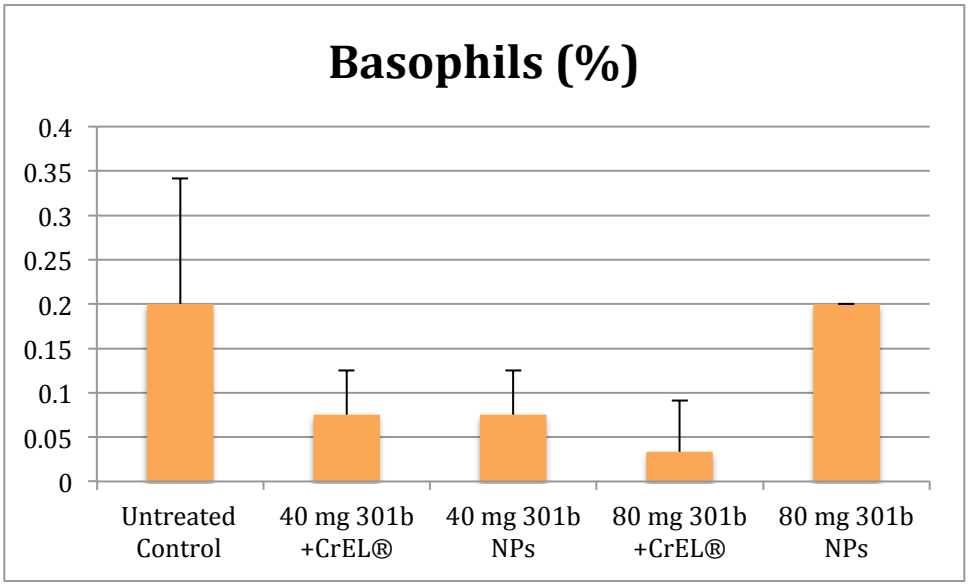

Figure S5.9 I Differential percentage of basophils from the total white blood cell count (WBC). [normal range 0-2 %]

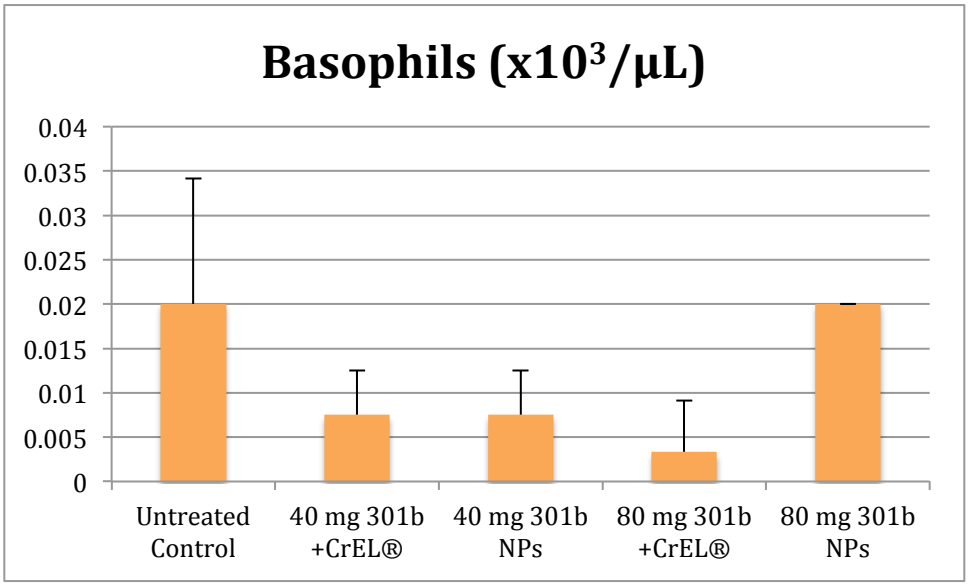

Figure S5.10 I Absolute number of basophils calculated from the differential percentage of the whole mouse plasma. [normal range 0-0.2 x10^3/μL]

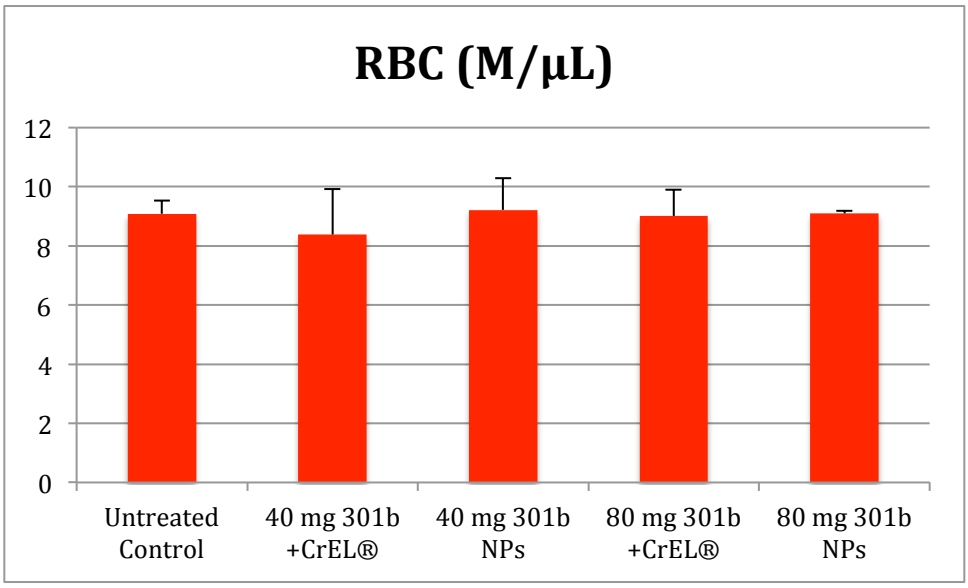

Figure S5.11 I Absolute number of red blood cells (RBC) counted at millions per micro-liter (M/μL). [normal range 6.36-9.42 M/μL]

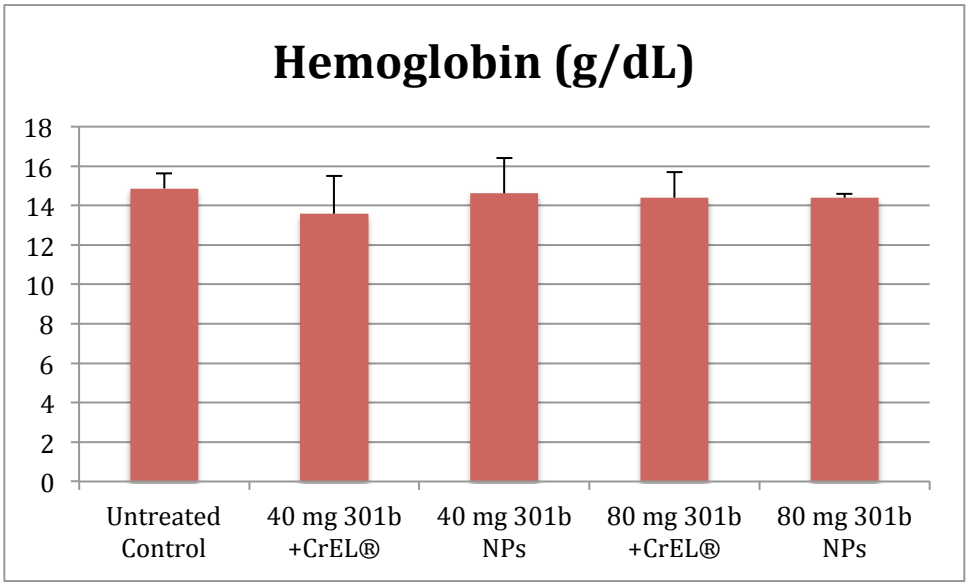

Figure S5.12 I Amount of hemoglobin protein present in the red blood cells measured as grams per deciliter (g/dL). [normal range 11.0-15.1 g/dL]

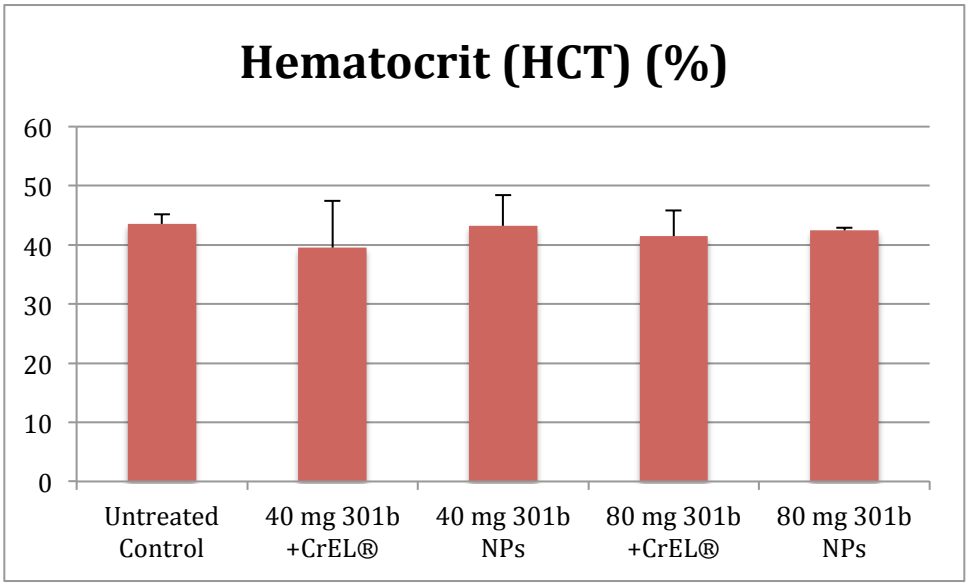

Figure S5.13 I The percentage of red blood cells present (HCT) in the mouse whole blood sample. [normal range 35.1-45.4 %]

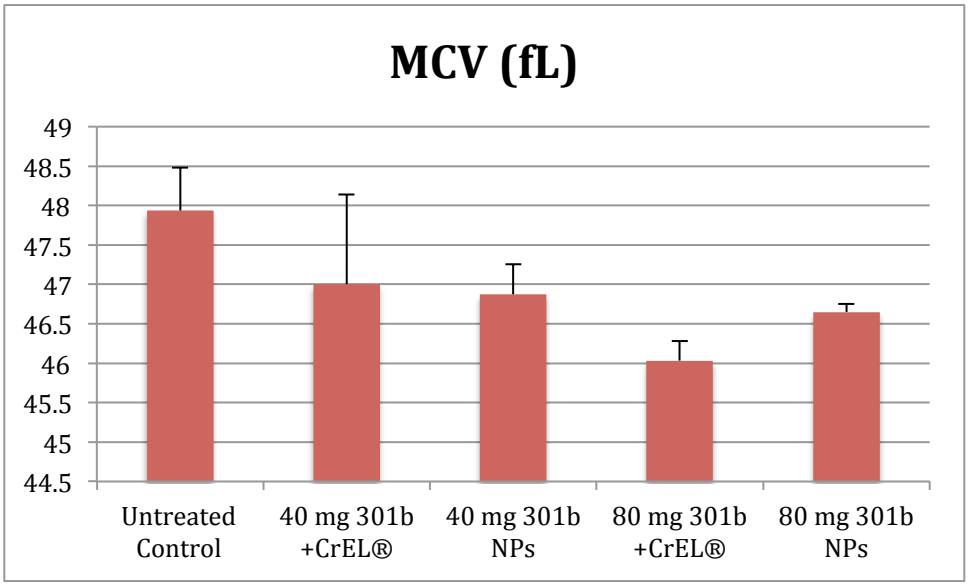

Figure S5.14 I The volume of red blood cells in the sample presented as the mean cell volume (MCV) measured in femtoliters (fL). [normal range 45.4-60.3 fL]

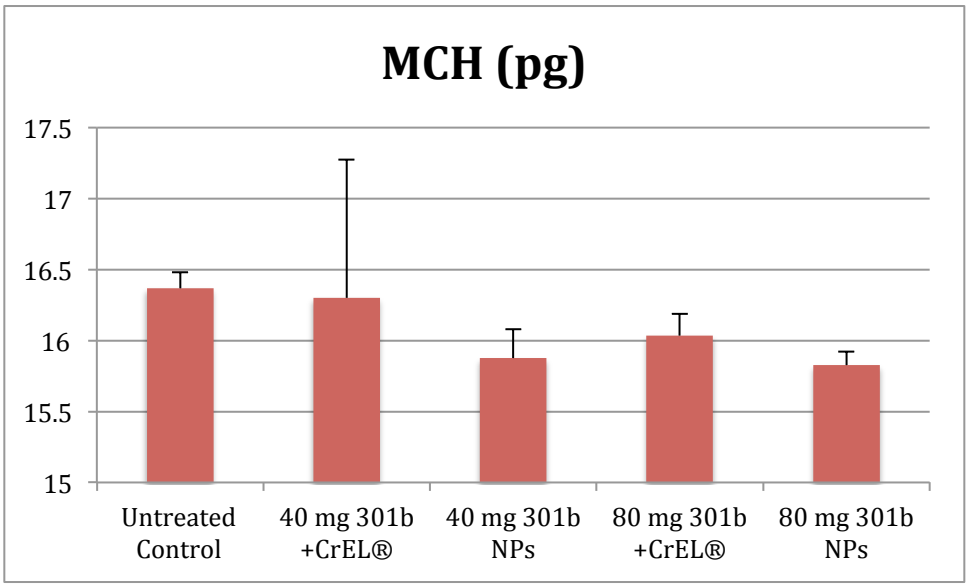

Figure S5.15 I The amount of hemoglobin contained by each red blood cell presented as mean cell hemoglobin (MCH) measured in picograms (pg). [normal range 14.1-19.3 pg]

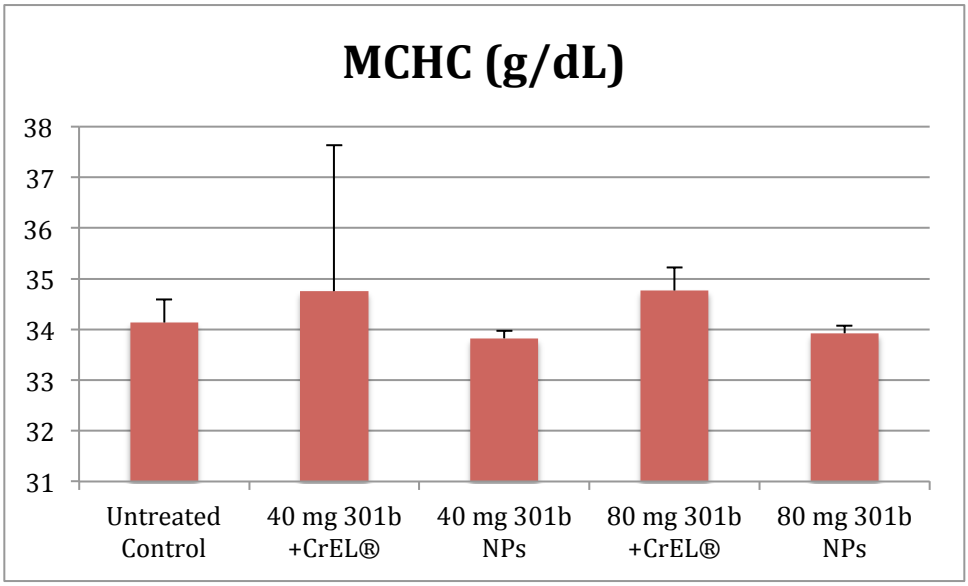

Figure S5.16 I The mean corpuscular hemoglobin concentration (MCHC) shown in grams per deciliter (g/dL). [normal range 30.2-34.2 g/dL]

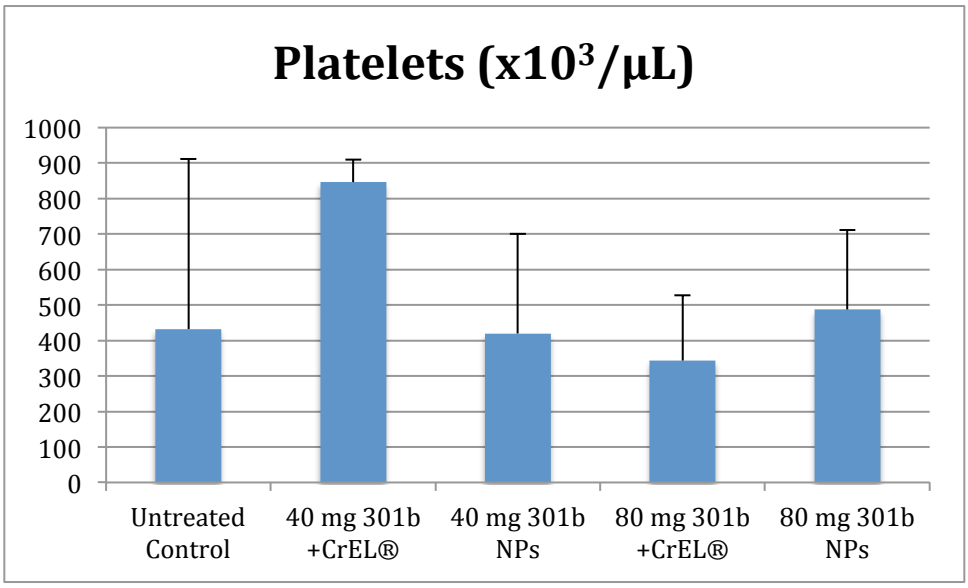

Figure S5.17 I Absolute number of platelets found in the whole mouse plasma. [normal range 592-2972 x10^3/μL]

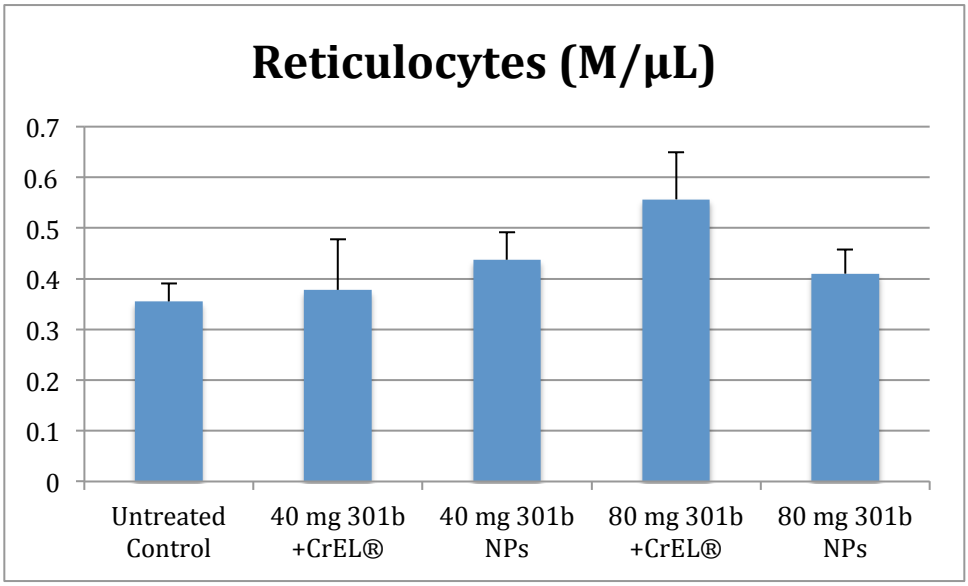

Figure S5.18 I Absolute number of reticulocytes counted at millions per microliter (M/μL).

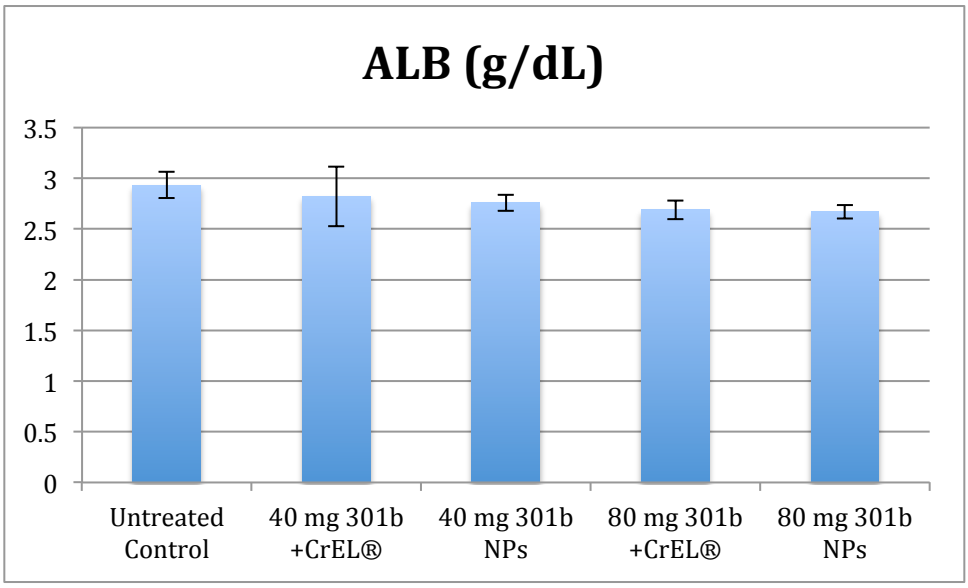

Figure S5.19 I The concentration of albumin (ALB) found in the mouse plasma measured in grams per deciliters (g/dL).

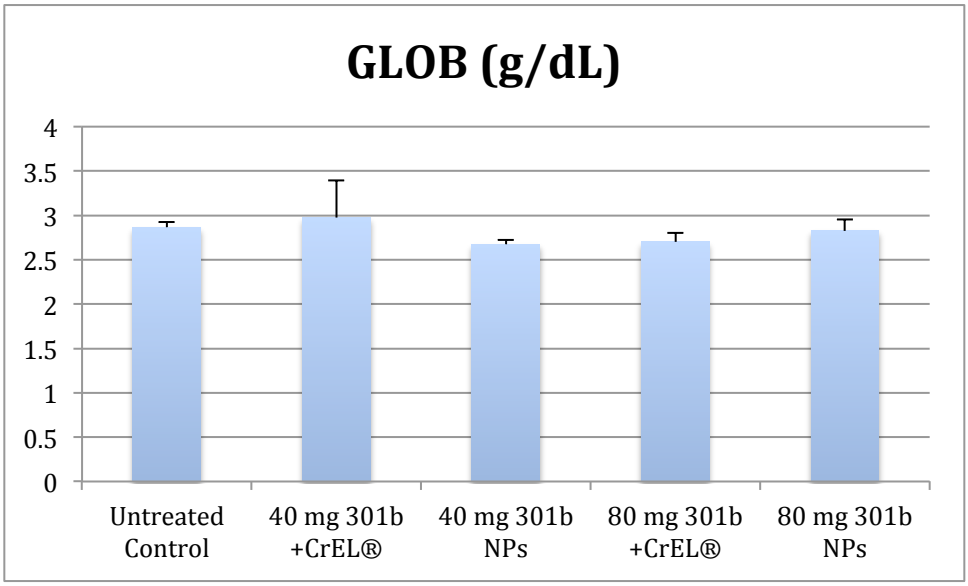

Figure S5.20 I The concentration of globulins (GLOB) found in the mouse plasma measured in grams per deciliters (g/dL).

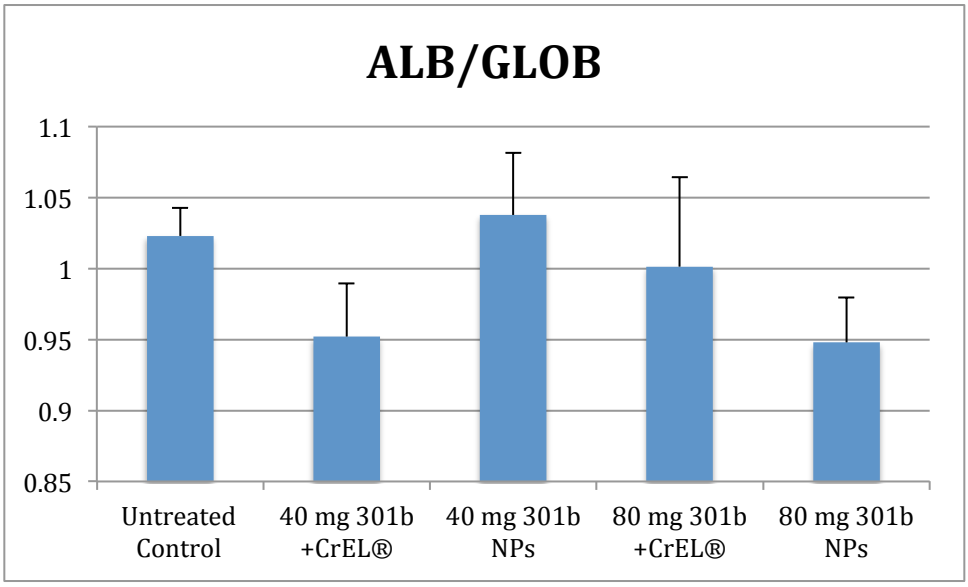

Figure S5.21 I The ratio of albumin (ALB) to globulins (GLOB) found in the mouse plasma from the MTD study.

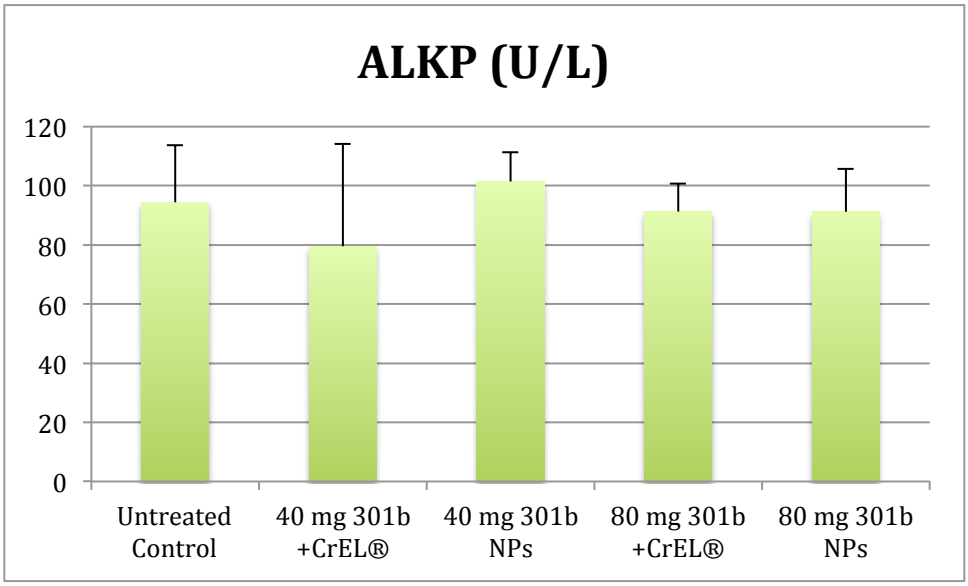

Figure S5.22 I The amount of alkaline phosphatase (ALKP) presented as units of activity per liter (U/L).

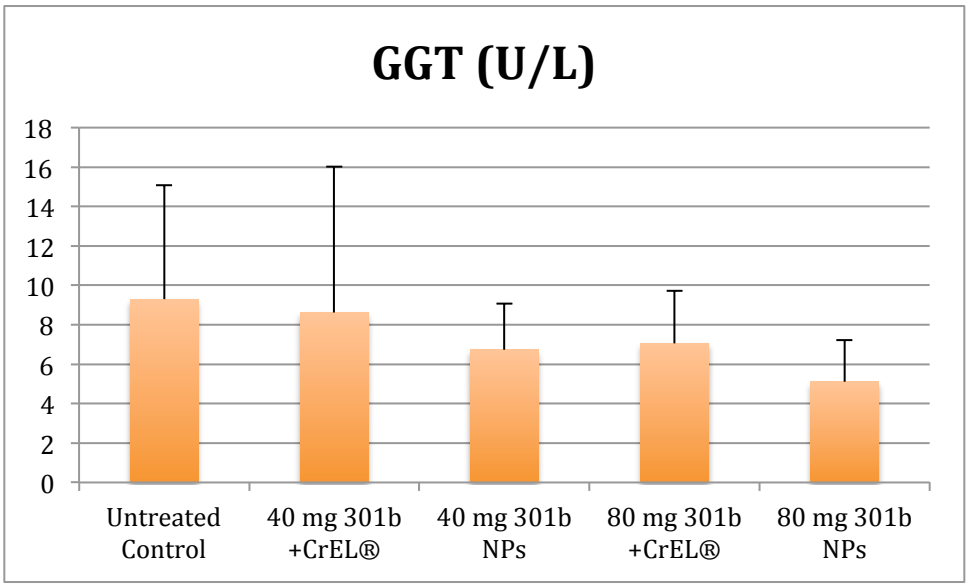

Figure S5.23 I The amount of gamma glutamyl transpeptidase (GGT) presented as units of activity per liter (U/L).

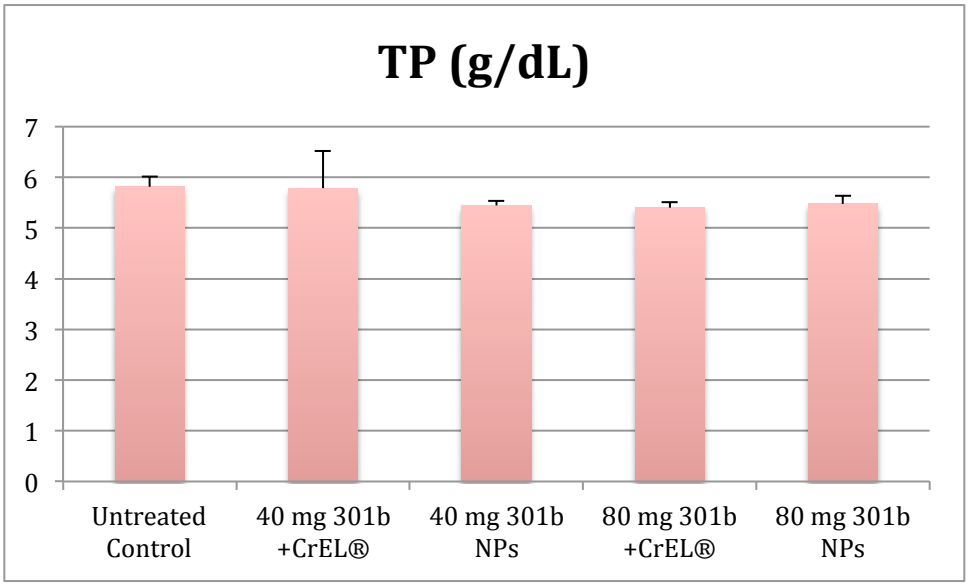

Figure S5.24 I The concentration of total protein measured in the mouse plasma measured as grams per deciliter (g/dL).

Experimental Section for Chapter 6

(*E*)-cinnamic (triethyl silicic) anhydride (602k)

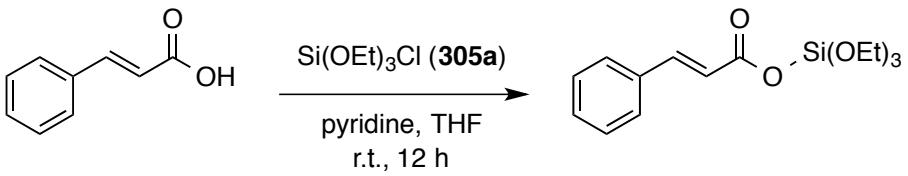

604 ***602k***

30% yield

In an oven dried culture tube fitted with a magnetic stir bar and Teflon lined cap, cinnamic acid **604** (133.5 mg, 0.90 mmol, 1.0 equiv.) and pyridine (py, 72 μL, 0.90 mmol 1.0 equiv.) were dissolved in 3 mL of THF. The reaction was stirred for 5 mins and triethoxychlorosilane (**305a**) (176 μL, 0.90 mmol, 1.0 equiv.) was added by Wiretrol®. The mixture turned cloudy instantly upon the addition of the chlorosilane. The reaction was allowed to stir overnight ca. 12 hours, and the mixture was filtered through a short plug of Celite® to remove the pyridinium salt. The filtrate was concentrated under reduced pressure, and the residue was redissolved in a mixture of hexanes:EtOAc (5:1). Purification by MPLC (SiO_2, 5:1 hexanes:ethyl acetate) yielded the title compound as a colorless oil (81.9 mg, 0.26 mmol, 30% yield). ^{1}H-NMR revealed a 1:2 mixture of the product to the starting materials. The TLC also showed considerable streaking on the plate, which suggests some column degradation of the compound, so no further purification was performed.

^{1}H NMR (500 MHz, $CDCl_3$): δ 7.72 (d, *J* = 15.9 Hz, 1H, PhC*H*=CHCO$_2$-), 7.55-7.51 (m, 2H, *o-Ph*CH=CH-), 7.40-7.39 (m, 3H, *m-Ph*CH=CH- and *p-Ph*CH=CH-), 6.45 (d, *J* = 15.9 Hz, 1H, PhCH=C*H*CO$_2$-), 3.99 (q, *J* = 7.0 Hz, 6H, -Si(OC*H*$_2$CH$_3$)$_3$, and 1.29 (t, *J* = 7.0 Hz, 9H, -Si(OCH$_2$C*H*$_3$)$_3$.

GC- MS: [30 m x 0.25 mm ID, HP-5, 50 °C/1.5 min/10 °C min-1/310 °C, (5031022H)] t_R = 9.05 min [m/z] 310 (M^+), 265 ($M^{+\bullet}$ -C_2H_5O), 237 ($M^{+\bullet}$ -C_4H_9O), 219 ($M^{+\bullet}$ -$C_4H_{11}O_2$), 163 ($M^{+\bullet}$ -$C_9H_7O_2$), 147 ($M^{+\bullet}$ -$C_6H_{15}O_3Si$), 131 ($M^{+\bullet}$ -$C_6H_{15}O_4Si$), and 103 ($M^{+\bullet}$ -$C_7H_{15}O_5Si$).

TLC Rf (5:1 hexanes:EtOAc) = 0.71.

(*E*)-cinnamic (triisopropyl silicic) anhydride (602l)

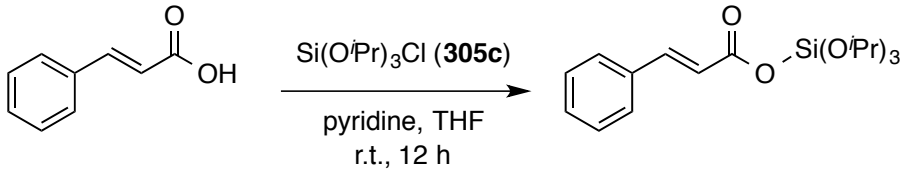

604 ***602l***

73% yield

In an oven dried culture tube fitted with a magnetic stir bar and Teflon lined cap, cinnamic acid **604** (139 mg, 0.94 mmol, 1.0 equiv.) and pyridine (py, 75 μL, 0.93 mmol 1.0 equiv.) were dissolved in 3 mL of THF. The reaction was stirred for 5 mins and triisopropoxychlorosilane (**305c**) (250 μL, 1.0 mmol, 1.1 equiv.) was added by Wiretrol®. The mixture turned cloudy instantly upon the addition of the chlorosilane. The reaction was allowed to stir overnight ca. 12 hours, and the mixture was filtered through a short plug of Celite® to remove the pyridinium salt.

The filtrate was concentrated under reduced pressure, and the residue was redissolved in a mixture of hexanes:EtOAc (8:1). Purification by MPLC (SiO_2, 8:1 hexanes:ethyl acetate) yielded the title compound (**602l**) as a white waxy solid (242.5 mg, 0.69 mmol, 73% yield).

^{1}H NMR (500 MHz, $CDCl_3$): δ 7.70 (d, *J* = 15.9 Hz, 1H, PhC*H*=CHCO$_2$-), 7.53-7.49 (m, 2H, *o-Ph*CH=CH-), 7.38-7.37 (m, 3H, *m-Ph*CH=CH- and *p-Ph*CH=CH-), 6.45 (d, *J* = 15.9 Hz, 1H, PhCH=C*H*CO$_2$-), 4.42 (sept, *J* = 6.1 Hz, 3H, -Si[OC*H*(CH$_3$)$_2$]$_3$), and 1.27 (d, *J* = 6.2 Hz, 18H, -Si[OCH(C*H*$_3$)$_2$]$_3$).

^{13}C NMR (125 MHz, $CDCl_3$): δ 164.9, 146.2, 134.4, 130.5, 129.0 (2x), 128.3 (2x), 119.2, 66.9 (3x), and 25.3 (6x).

HRMS (ESI) Calc'd for $C_{18}H_{28}NaO_5Si^+$ $[M + Na]^+$ 375.1598; found 375.1585.

IR (thin film) 2974, 1706, 1633, 1466, 1451, 1382, 1371, 1315, 1282, 1173, 1118, 1053, 984, 879, and 766 cm^{-1}.

GC- MS: [30 m x 0.25 mm ID, HP-5, 50 °C/1.5 min/10 °C min-1/290 °C, (5029021)] t_R = 9.22 min [m/z] 352 (M^+), 293 ($M^{+\bullet}$ -C_3H_7O), 251 ($M^{+\bullet}$ -$C_6H_{13}O$), 209 ($M^{+\bullet}$ -$C_9H_{19}O$), 147 ($M^{+\bullet}$ -$C_9H_{21}O_3Si$), 131 ($M^{+\bullet}$ -$C_9H_{21}O_4Si$), and 103 ($M^{+\bullet}$ -$C_{10}H_{21}O_5Si$).

(*E*)-(tri-*tert*-butyl silicic) cinnamic anhydride (602i)

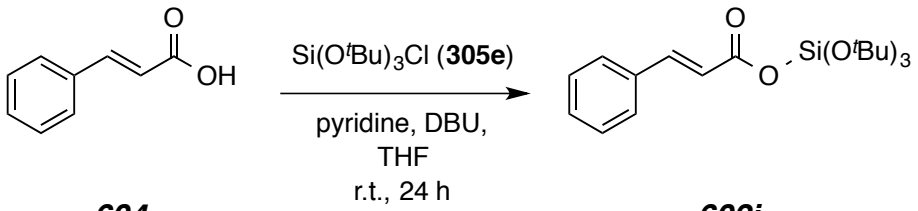

604 ***602i***

38% yield

In an oven dried culture tube fitted with a magnetic stir bar and Teflon lined cap, cinnamic acid **604** (744.9 mg, 5.03 mmol, 1.0 equiv.) and pyridine (py, 600 μL, 7.45 mmol 1.5 equiv.) were dissolved in 5 mL of THF. The reaction was stirred for 5 mins and tritertbutoxychlorosilane (**305e**) (1.68 mL, 7.54 mmol, 1.5 equiv.) was added by syringe, however the mixture remained clear upon addition of the chlorosilane. After 12 h of no reaction, DBU (1.0 mL, 6.69 mmol, 1.0 equiv.) was added and the reaction immediately turned cloudy. Several previous attempts at heating this reaction, suggested that the stronger base was required. The reaction was allowed to stir for an additional 12 hours, and the mixture was filtered through a short plug of Celite® to remove the salts. The filtrate was concentrated under reduced pressure, and the residue was redissolved in a mixture of hexanes:EtOAc (8:1). Purification by flash chromatography (SiO_2, 8:1 hexanes:ethyl acetate) yielded the title compound (**602i**) as a white solid (750.8 mg, 1.90 mmol, 38% yield).

^{1}H NMR (500 MHz, $CDCl_3$): δ 7.66 (d, *J* = 15.9 Hz, 1H, PhC*H*=CHCO$_2$-), 7.54-7.50 (m, 2H, *o*-*Ph*CH=CH-), 7.40-7.35 (m, 3H, *m*-*Ph*CH=CH- and *p*-

*Ph*CH=CH-), 6.44 (d, *J* = 15.9 Hz, 1H, PhCH=C*H*CO_2-), and 1.37 (s, 27H, -Si[OC(CH_3)$_3$]$_3$).

^{13}C NMR (125 MHz, $CDCl_3$): δ 164.4, 145.3, 134.7, 130.3, 129.0 (2x), 128.3 (2x), 120.6, 74.2 (3x), and 31.5 (9x).

HRMS (ESI) Calc'd for $C_{21}H_{34}NaO_5Si^+$ $[M + Na]^+$ 417.2068; found 417.2073.

IR (thin film) 2974, 1701, 1366, 1189, 1086, 977, and 769 cm^{-1}.

GC- MS: [30 m x 0.25 mm ID, HP-5, 50 °C/1.5 min/10 °C min-1/290 °C, (5029021)] t_R = 9.77 min [m/z] 394 (M^+), 321 ($M^{+\bullet}$ -C_4H_9O), 265 ($M^{+\bullet}$ -$C_8H_{17}O$), 209 ($M^{+\bullet}$ -$C_{12}H_{25}O$), 147 ($M^{+\bullet}$ -$C_{12}H_{27}O_4Si$), and 103 ($M^{+\bullet}$ -$C_{13}H_{27}O_5Si$).

TLC R_f (8:1 hexanes:EtOAc) = 0.67.

***tert*-butyldimethylsilyl cinnamate (602j)**

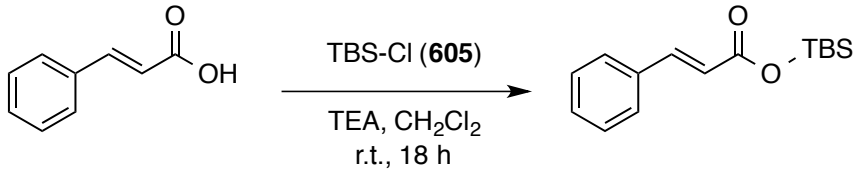

604 ***602j***

56% yield

In an oven dried culture tube fitted with a magnetic stir bar and Teflon lined cap, cinnamic acid **604** (604 mg, 4.07 mmol, 1.0 equiv.) and triethylamine (TEA, 378 *μ*L, 2.69 mmol 0.7 equiv.) were dissolved in 10 mL of CH_2Cl_2. The reaction was stirred for 5 mins and tert-butyldimethylsiyl chloride (**605**) (TBS-Cl, 787 mg, 5.22 mmol, 1.3 equiv.) was added to the reaction mixture. The reaction was allowed to

stir for overnight ca. 18 hours. The reaction mixture was concentrated under reduced pressure, and the residue was redissolved in a mixture of hexanes:EtOAc (8:1) and filtered through a short plug of Celite® to remove the salts. Purification by flash chromatography (SiO_2, 8:1 hexanes:ethyl acetate) yielded the title compound (**602j**) as a white crystalline solid (595.5 mg, 2.27 mmol, 56% yield).

^{1}H NMR (500 MHz, $CDCl_3$): δ 7.62 (d, *J* = 15.9 Hz, 1H, PhC*H*=CHCO$_2$-), 7.54-7.51 (m, 2H, *o-Ph*CH=CH-), 7.40-7.35 (m, 3H, *m-Ph*CH=CH- and *p-Ph*CH=CH-), 6.41 (d, *J* = 15.9 Hz, 1H, PhCH=C*H*CO$_2$-), 1.00 [s, 9H, -Si(CH$_3$)$_2$C(C*H$_3$*)$_3$], and 0.34 [s, 6H, -Si(C*H$_3$*)$_2$C(CH$_3$)$_3$].

^{13}C NMR (125 MHz, $CDCl_3$): δ 167.0, 145.2, 134.6, 130.4, 129.0 (2x), 128.3 (2x), 120.2, 25.9 (3x), 18.0, and -4.5 (2x).

HRMS (ESI) Calc'd for $C_{15}H_{22}NaO_2Si^+$ $[M + Na]^+$ 285.1281; found 285.1290.

GC- MS: [30 m x 0.25 mm ID, HP-5, 50 °C/1.5 min/10 °C min-1/290 °C, (5029021)] t_R = 8.52 min [m/z] 262 (M^+), 247 ($M^{+\bullet}$ -CH_3), 205 ($M^{+\bullet}$ -C_4H_9), 190 ($M^{+\bullet}$ -C_5H_{12}), 131 ($M^{+\bullet}$ -C_9H_7O), 131 ($M^{+\bullet}$ -$C_6H_{15}OSi$), 115 ($M^{+\bullet}$ -$C_9H_7O_2$), and 103 ($M^{+\bullet}$ -$C_7H_{15}O_2Si$).

TLC R$_f$ (8:1 hexanes:EtOAc) = 0.38.

***N*-(tri-*tert*-butoxysilyl)benzamide (603c)**

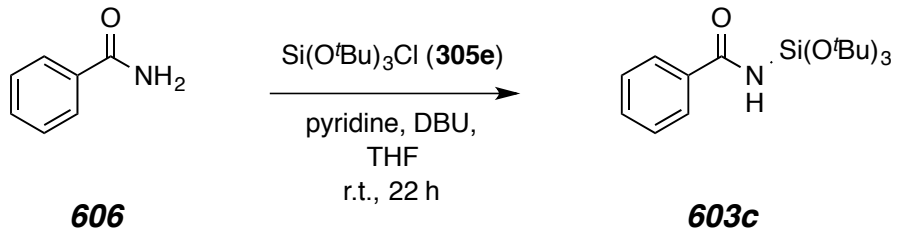

606 ***603c***

60% yield

In an oven dried culture tube fitted with a magnetic stir bar and Teflon lined cap, benzamide **606** (670 mg, 5.53 mmol, 1.0 equiv.) and pyridine (py, 445 μL, 5.53 mmol 1.0 equiv.) were dissolved in 5 mL of THF. The reaction was stirred for 5 mins and tritertbutoxychlorosilane (**305e**) (1.20 mL, 5.53 mmol, 1.0 equiv.) was added by syringe, the mixture remained clear upon addition of the chlorosilane. After 12 h of no reaction, DBU (400 μL, 3.02 mmol, 0.5 equiv.) was added and the reaction immediately turned cloudy. The reaction was allowed to stir for overnight ca. 10 hours. The suspension was concentrated under reduced pressure, and the residue was redissolved in a mixture of hexanes:EtOAc (2:1) and filtered through a short plug of Celite® to remove the salts. Purification by flash chromatography (SiO_2, 2:1 hexanes:ethyl acetate) yielded the title compound (**603c**) as a white crystalline solid (1.23 g, 3.35 mmol, 60.5% yield).

^{1}H NMR (500 MHz, $CDCl_3$): δ 7.84-7.77 (m, 2H, *o-Ph*C=ONH-), 7.49 (tt, *J* = 7.3, 6.2, 2.4, 1.2 Hz, 1H, *p-Ph*C=ONH-), 7.44-7.40 (m, 2H, *m-Ph*C=ONH-), 5.78 (s, 1H, PhC=ON*H*-), and 1.38 (s, 27H, -Si[OC(CH_3)$_3$]$_3$).

^{13}C NMR (125 MHz, $CDCl_3$): δ 171.3, 136.1, 131.5, 128.6 (2x), 127.4 (2x), 74.3 (3x), and 31.7 (9x).

HRMS (ESI) Calc'd for $C_{19}H_{33}NNaO_4Si^+$ $[M + Na]^+$ 390.2071; found 390.2078.

GC- MS: [30 m x 0.25 mm ID, HP-5, 50 °C/1.5 min/10 °C min-1/290 °C, (5029021)] t_R = 8.95 min [m/z] 367 (M^+), 352 ($M^{+\bullet}$ -CH_3), 311 ($M^{+\bullet}$ -C_4H_8), and 294 ($M^{+\bullet}$ -C_4H_9O).

mp = 45-52 °C. **TLC** R_f (2:1 hexanes:EtOAc) = 0.50.

***N*-(*tert*-butyldimethylsilyl)benzamide (603a)**

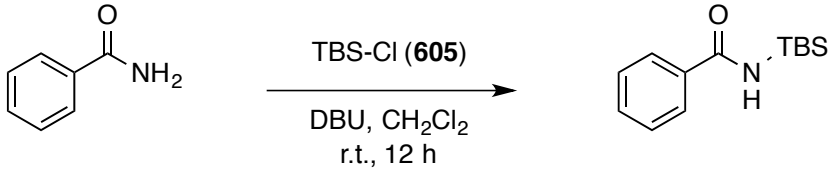

606 ***603a***

31% yield

In an oven dried round bottom flask fitted with a magnetic stir bar and septum, benzamide **606** (1.14 g, 4.07 mmol, 1.0 equiv.) and DBU (1.5 mL, 11.33 mmol 1.2 equiv.) were dissolved in 20 mL of CH_2Cl_2. The reaction was stirred for 5 mins and tert-butyldimethylsiyl chloride (**605**) (TBS-Cl, 2.76 g, 18.31 mmol, 1.9 equiv.) was added to the reaction mixture. The reaction was allowed to stir for overnight 12 hours. The reaction mixture was concentrated under reduced pressure, and the residue was redissolved in a mixture of hexanes:EtOAc (3:1) and filtered through a short plug of Celite® to remove the salts. Purification by

flash chromatography (SiO_2, 3:1 hexanes:ethyl acetate) followed by a silica plug (SiO_2, 95:5 hexanes:ethyl acetate) yielded the title compound (**603a**) as a white crystalline solid (294.4 mg, 1.25 mmol, 31% yield).

^{1}H NMR (500 MHz, $CDCl_3$): δ 7.79 (d, *J* = 7.7 Hz, 2H, *o-Ph*C=ONH-), 7.48 (tt, *J* = 7.3, 2.2 Hz, 1H, *p-Ph*C=ONH-), 7.41 (dt, *J* = 7.7, 2.7 Hz, 2H, *m-Ph*C=ONH-), 5.72 (s, 1H, PhC=ON*H*-), 1.00 [s, 9H, -Si(CH_3)$_2$C(C*H*$_3$)$_3$], and 0.33 [s, 6H, -Si(C*H*$_3$)$_2$C(CH_3)$_3$].

^{13}C NMR (125 MHz, $CDCl_3$): δ 172.5, 169.8, 135.5, 133.5, 132.2, 128.8, 127.5, 25.9 (3x), 18.2, and -3.4 (2x).

HRMS (ESI) Calc'd for $C_{13}H_{21}NNaOSi^+$ [M + Na]$^+$ 258.1285; found 258.1305.

GC- MS: [30 m x 0.25 mm ID, HP-5, 50 °C/1.5 min/10 °C min-1/290 °C, (5029021)] t_R = 7.80 min [m/z] 235 (M^+), 220 ($M^{+\bullet}$ -CH_3), 178 ($M^{+\bullet}$ -C_4H_9), 121 ($M^{+\bullet}$ -$C_6H_{14}Si$), and 104 ($M^{+\bullet}$ -$C_6H_{17}NSi$).

***N*-(triisopropylsilyl)benzamide (603b)**

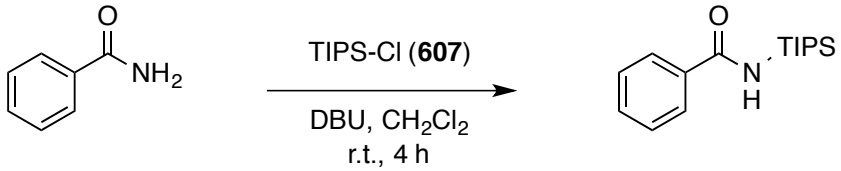

606 ***603b***

97% yield

In an oven dried culture tube fitted with a magnetic stir bar and Teflon lined cap, benzamide **606** (273.4 g, 2.26 mmol, 1.0 equiv.) and DBU (438 μL, 2.93 mmol 1.3 equiv.) were dissolved in 5.0 mL of CH_2Cl_2. The reaction was stirred for 5

mins and triisopropylsiyl chloride (**607**) (TIPS-Cl, 628 μL, 2.93 mmol, 1.3 equiv.) was added to the reaction mixture. The slight yellow in color reaction was allowed to stir for 4 hours. An aliquot was analyzed by GC-MS and showed the desired product as the major component > 90%. The reaction mixture was concentrated under reduced pressure, and the residue was redissolved in a mixture of hexanes:EtOAc (2:1) and filtered through a short plug of Celite® to remove the salts. Purification by flash chromatography (SiO_2, 2:1 hexanes:ethyl acetate) yielded the title compound (**603b**) as a white crystalline solid (714.8 mg, 2.26 mmol, 97% yield).

^{1}H NMR (500 MHz, $CDCl_3$): δ 7.80 (dd, *J* = 7.6, 1.5 Hz, 2H, *o-Ph*C=ONH-), 7.51 (tt, *J* = 7.3, 1.7 Hz, 1H, *p-Ph*C=ONH-), 7.46-7.43 (m, 2H, *m-Ph*C=ONH-), 5.59 (s, 1H, PhC=ON*H*-), 1.43 [sept, *J* = 7.5 Hz, 3H, -Si{C*H*$(CH_3)_2$}$_3$], and 1.14 [d, *J* = 7.5 Hz, 18H, -Si{CH(C*H*$_3$)$_2$}$_3$].

GC- MS: [30 m x 0.25 mm ID, HP-5, 50 °C/1.5 min/10 °C min-1/290 °C, (5029021)] t_R = 9.31 min [m/z] 325 (M^+), 262 ($M^{+\bullet}$ -CH_3), 234 ($M^{+\bullet}$ -C_3H_7), 192 ($M^{+\bullet}$ -C_6H_{13}), 191 ($M^{+\bullet}$ -C_6H_{14}), 148 ($M^{+\bullet}$ -C_9H_{21}), and 104 ($M^{+\bullet}$ -$C_9H_{23}NSi$).

TLC Rf (2:1 hexanes:EtOAc) = 0.75.

4-(tri-*tert*-butoxysilyl)morpholine (603e)

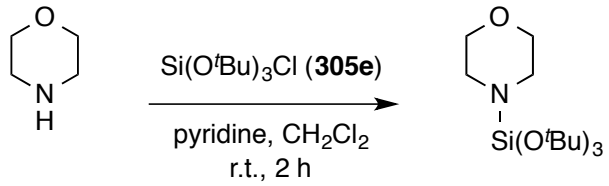

608 ***603e***

29% yield

In an oven dried culture tube fitted with a magnetic stir bar and Teflon lined cap, morpholine **608** (600 μL, 6.93 mmol, 1.0 equiv.) and pyridine (558 μL, 6.93 mmol 1.0 equiv.) were dissolved in 7 mL of dry CH_2Cl_2. The reaction was stirred for 5 mins and tritertbutoxychlorosilane (**305e**) (1.54 mL, 6.93 mmol, 1.0 equiv.) was added by syringe, the mixture turned cloudy within 5 mins. After 2 h of reaction, an aliquot was analyzed by GC-MS and showed the desired product as the major component > 90%. The reaction mixture was concentrated under reduced pressure, and the residue was redissolved in a mixture of hexanes:EtOAc (20:1) and filtered through a short plug of Celite® to remove the salts. Purification by two sequential MPLC runs (SiO_2, 20:1, and 30:1 hexanes:ethyl acetate) yielded the title compound (**603e**) as a clear viscous oil (680.7 mg, 2.04 mmol, 29% yield).

^{1}H NMR (500 MHz, $CDCl_3$): δ 3.57 (t, J = 4.6 Hz, 4H, -$CH_2CH_2OCH_2CH_2$-), 2.93 (t, J = 4.7 Hz, 4H, -$CH_2N(Si[OC(CH_3)_3]_3CH_2$-), and 1.30(s, 27H, -$CH_2N(Si[OC(CH_3)_3]_3CH_2$-).

^{13}C NMR (125 MHz, $CDCl_3$): δ 72.6 (3x), 68.5 (2x), 45.5 (2x), and 31.8 (9x).

HRMS (ESI) Calc'd for $C_{16}H_{36}NO_4Si^+$ $[M + H]^+$ 334.2408; found 334.2402.

GC- MS: [30 m x 0.25 mm ID, HP-5, 50 °C/1.5 min/10 °C min-1/290 °C, (5029021)] t_R = 7.08 min [m/z] 333 (M^+), 318 ($M^{+\bullet}$ -CH_3), 302 ($M^{+\bullet}$ -C_2H_7), 288 ($M^{+\bullet}$ -C_2H_5O), 276 ($M^{+\bullet}$ -C_4H_9), 260 ($M^{+\bullet}$ -C_4H_9O), 220 ($M^{+\bullet}$ -C_8H_{17}), and 164 ($M^{+\bullet}$ -$C_{12}H_{25}$).

TLC R_f (20:1 hexanes:EtOAc) = 0.47.

4-(*tert*-butyldimethylsilyl)morpholine (603d)

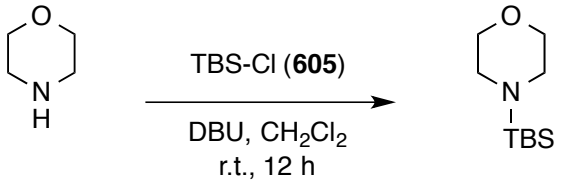

608 ***603d***

67% yield

In an oven dried culture tube fitted with a magnetic stir bar and Teflon lined cap, morpholine **608** (863 μL, 10.0 mmol, 1.0 equiv.) and DBU (1.73 mL, 11.64 mmol 1.1 equiv.) were dissolved in 8 mL of dry CH_2Cl_2. The reaction was stirred for 5 mins and tert-butyldimethylsiyl chloride (**605**) (TBS-Cl, 174.6 mg, 11.64 mmol, 1.1 equiv.) was added and allowed to stir overnight ca. 12 h. The reaction mixture was concentrated under reduced pressure, and the residue was redissolved in a mixture of hexanes:EtOAc (2:1) and filtered through a short plug of Celite® to remove the salts followed by a plug of silica (SiO_2, 2:1, hexanes:ethyl acetate). An aliquot was analyzed by GC-MS and showed the desired product as the major component > 98% so no further purification was performed. The title compound

(**603d**) was obtained as clear viscous oil (1.35 g, 6.69 mmol, 67% yield). Further characterization has been presented before. [222]

GC- MS: [30 m x 0.25 mm ID, HP-5, 50 °C/1.5 min/10 °C min-1/290 °C, (5029021)] t_R = 5.07 min [m/z] 201 (M^+), 186 ($M^{+\bullet}$ -CH_3), 144 ($M^{+\bullet}$ -C_4H_9), 114 ($M^{+\bullet}$ -C_6H_{15}), 100 ($M^{+\bullet}$ -$C_5H_{11}NO$), and 86 ($M^{+\bullet}$ -$C_6H_{15}Si$).

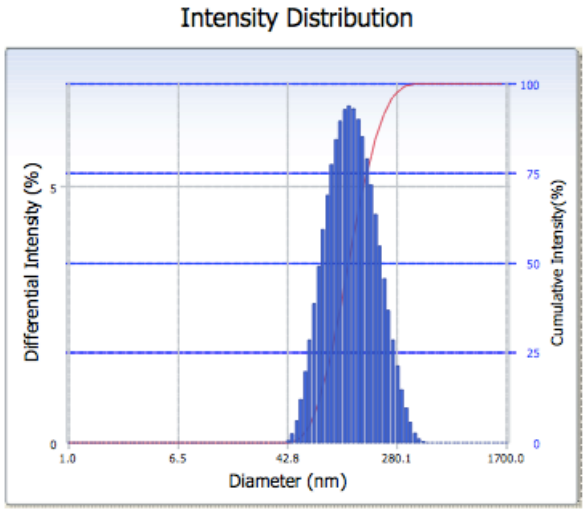

Figure S6.1 I Intensity distribution of freshly prepared Cinnamic-silicate **602i** loaded mPEG-*b*-PLGA (5k-10k) based nanoparticles ca. 50 wt%.

[222] Millar, R. W.; Philbin, S. P. Clean Nitrations: Novel Syntheses of Nitramines and Nitrate Esters by Nitrodesilylation Reactions Using Dinitrogen Pentoxide (N2O5). *Tetrahedron* **1997**, *53*, 4371–4386.

Experimental Section for Chapter 7

2-((9*R*,10*S*,11*S*,13*S*,14*S*,16*R*,17*R*)-9-fluoro-11,17-dihydroxy-10,13,16-trimethyl-3-oxo-6,7,8,9,10,11,12,13,14,15,16,17-dodecahydro-3*H*-cyclopenta[*a*]phenanthren-17-yl)-2-oxoethyl trioctyl silicate (702b)

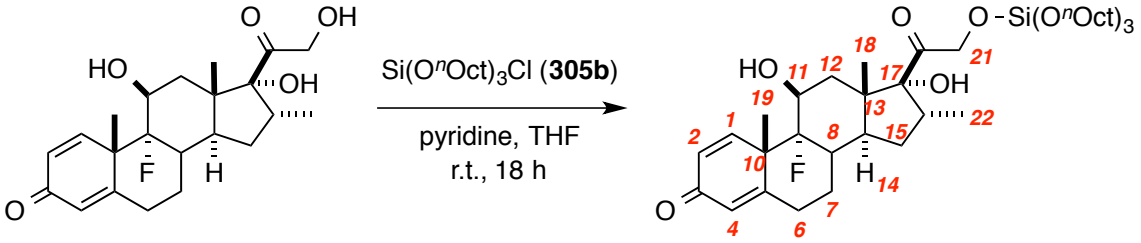

Dexamethasone

701

702b

32% yield

In an oven dried culture tube fitted with a magnetic stir bar and Teflon lined cap, dexamethasone **701** (133.1 mg, 0.33 mmol, 1.0 equiv.) and pyridine (50 μL, 0.41 mmol 1.2 equiv.) were dissolved in 2 mL of THF. The reaction was stirred for 5 mins and Tri-*n*-octyloxychlorosilane (**305b** (200 mg, 0.41 mmol, 1.2 equiv.) was added by syringe the mixture turned cloudy instantaneously upon the addition of the chlorosilane. The reaction stirred overnight (18 h). The THF was removed by evaporation under reduced pressure, the solid residue was triturated with a mixture of hexanes:EtOAc (2:1), and the resulting slurry was filtered through a short plug of Celite® to remove the pyridinium salt. The filtrate was concentrated under reduced pressure, and the residue was purified by flash chromatography

(SiO_2, 20:1 hexanes:EtOAc), followed by MPLC (SiO_2, 2:1 hexanes:EtOAc) to yield the title compound as a white, crystalline solid (84.2 mg, 0.104 mmol, 32%).

^{1}H NMR (500 MHz, $CDCl_3$): δ 7.21 (d, *J* = 10.1 Hz, 1H, H1), 6.32 (dd, *J* = 10.1, 1.8 Hz, 1H, H2), 6.11 (s, 1H, H4), 4.79 (d, *J* = 18.4 Hz, 1H, H21α), 4.52 (d, *J* = 18.4 Hz, 1H, H21β), 4.35 (br d, *J* = 9.8 Hz, 1H, H11), 3.79 (t, *J* = 6.7 Hz, 6H, -Si[OC*H*$_2$$(CH_2)_6CH_3]_3$), 3.07 (dqd, *J* = 10.9, 7.2, 3.8 Hz, 1H, H16), 2.67 (s, 1H, -O*H*), 2.64-2.58 (m, 1H, H6β), 2.40-2.31 (m, 3H, H6α, H8, H12β), 2.18 (td, *J* = 11.8, 8.3 Hz, 1H, H14), 2.03 (s, 1H -O*H*), 1.82 (dt, *J* = 12.1, 5.7 Hz, 1H, H7α), 1.74 (q, *J* = 11.9 Hz, 1H, H15β), 1.61-1.52 (m, 6H, -Si[OCH_2C*H*$_2$$(CH_2)_5CH_3]_3$, 1.54 (s, 3H, H19), 1.44 (dd, *J* = 14.3, 1.2 Hz, 1H, H12α), 1.36-1.22 (m, 32H, H7β, H15α, and -Si[$OCH_2CH_2(C$*H*$_2$$)_5CH_3]_3$), 1.06 (s, 3H, H18), 0.91 (d, *J* = 7.26 Hz, 3H, H22), and 0.88 (t, *J* = 6.9 Hz, 9H, -Si[$OCH_2CH_2(CH_2)_5C$*H*$_3$$]_3$).

^{13}C NMR (125 MHz, $CDCl_3$): δ 208.4, 186.8, 166.4, 152.3, 130.0, 125.2, 101.1, 90.7, 72.5, 72.1, 68.7, 64.1 (3x), 48.6, 43.9, 37.1, 35.9, 34.5, 34.3, 32.5 (3x), 32.0 (3x), 31.2, 29.6 (3x), 29.5 (3x), 27.5, 25.9 (3x), 23.2, 22.9 (3x), 17.3, 14.3 (3x), and 14.2.

HRMS (ESI) Calc'd for $C_{46}H_{79}FNaO_8Si^+$ $[M + Na]^+$ 829.5420; found 829.5546.

TLC R$_f$ (2:1 hexanes:EtOAc) = 0.20.

(tri-*tert*-butyl silicic) 2-(4-isobutylphenyl)propanoic anhydride (704)

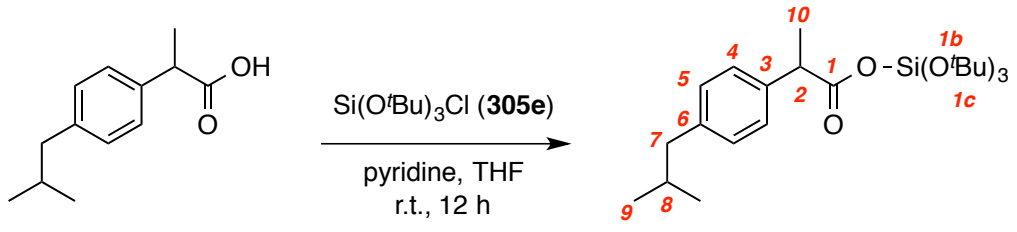

Ibuprofen

703

704

2% yield

Ibuprofen pills (609.4 mg) were ground in a motor and pestle and suspended into 10 mL of ethyl acetate in a round bottom flask. The mixture was stirred overnight ca. 12 hours, and filtered through a plug of Celite® to remove the filler from the ibuprofen tablet. ^{1}H-NMR showed the ibuprofen (**703**) extracted (465.1 mg, 2.25 mmol, 1.0 equiv.) was > 95% pure, and was used as the starting material for the subsequent reaction. In an oven dried culture tube fitted with a magnetic stir bar and Teflon lined cap, ibuprofen **703** and pyridine (1.0 mL, 12.42 mmol 5.5 equiv.) were dissolved in 10 mL of THF. The reaction was stirred for 5 mins and tritertbutoxychlorosilane (**305e**) (1.0 mL, 4.48 mmol, 2.0 equiv.) was added by syringe the mixture slowly turned cloudy upon addition of the chlorosilane. The reaction was allowed to stir for an additional 12 hours, the THF was removed under reduced pressure and then resuspended in a mixture of hexanes:EtOAc (2:1). The suspension was filtered through a short plug of Celite® to remove the salts. The filtrate was concentrated under reduced pressure, and the residue was redissolved in a mixture of hexanes:EtOAc (30:1). Purification by MPLC (SiO_2,

30:1 hexanes:ethyl acetate) followed by a small silica plug eluting with 100% hexanes first followed by a mixture of hexanes:EtOAc (1:1) yielded the title compound (**704**) as a white solid (18.1 mg, 0.018 mmol, 1.8% yield).

^{1}H NMR (500 MHz, $CDCl_3$): δ 7.19 (d, *J* = 8.0 Hz, 2H, H4), 7.06 (d, *J* = 8.0 Hz, 2H, H5), 3.64 (q, *J* = 7.1 Hz, 1H, H2), 2.43 (d, *J* = 7.2 Hz, 2H, H7), 1.82 (dq, *J* = 7.2, 6.7 Hz, 1H, H8), 1.48 (d, *J* = 7.1 Hz, 3H, H10), 1.22 (s, 27H, -Si[OC(CH_3)$_3$]$_3$ H1c), and 0.86 (d, *J* = 6.6 Hz, 6H, H9).

^{13}C NMR (125 MHz, $CDCl_3$): δ 185.9, 129.3, 127.7, 73.9, 31.5, and 31.3.

GC-MS: [30 m x 0.25 mm ID, HP-5, 50 °C/1.5 min/10 °C min-1/290 °C, (5029021)] t_R = 10.13 min [m/z] 452 ($M^{+\bullet}$), 437 ($M^{+\bullet}$ -CH_3), 379 ($M^{+\bullet}$ -C_4H_9O), 323 ($M^{+\bullet}$ -$C_8H_{17}O$), 267 ($M^{+\bullet}$ -$C_{12}H_{25}O$), 247 ($M^{+\bullet}$ -$C_{13}H_{17}O_2$), 161 ($M^{+\bullet}$ -$C_{13}H_{27}O_5Si$), and 135 ($M^{+\bullet}$ -$C_{15}H_{29}O_5Si$).

LC-MS: Waters Symmetry-C8 3.9 x 150 mm particle size 5 *μ*m; 0.5 mL/min, Gradient Method 50% B to 100% B over 10 min, hold at 100% B for 10 min (Solvent System A, 5:95 MeOH:H_2O,15 mM NH_4OAc) (Solvent System B, 98:2 MeOH:H_2O,15 mM NH_4OAc), MM-ES+APCI Positive Scan 18.48 min 475.3 $(M+Na)^+$.

TLC R_f (30:1 hexanes:EtOAc) = 0.72.

(*S*)-2-((2*R*,5*R*,6*R*)-6-((2*R*,3*S*,4*S*,6*R*)-6-((2*S*,5*S*,7*R*,9*S*,10*S*,12*R*,15*R*)-2-((2*R*,5*R*,6*R*)-5-ethyl-5-hydroxy-6-methyltetrahydro-2*H*-pyran-2-yl)-15-hydroxy-2,10,12-trimethyl-1,6,8-trioxadispiro[4.1.5^{7}.3^{5}]pentadec-13-en-9-yl)-3-hydroxy-4-methyl-5-oxooctan-2-yl)-5-methyltetrahydro-2*H*-pyran-2-yl)butanoic (triisopropyl silicic) anhydride (706b)

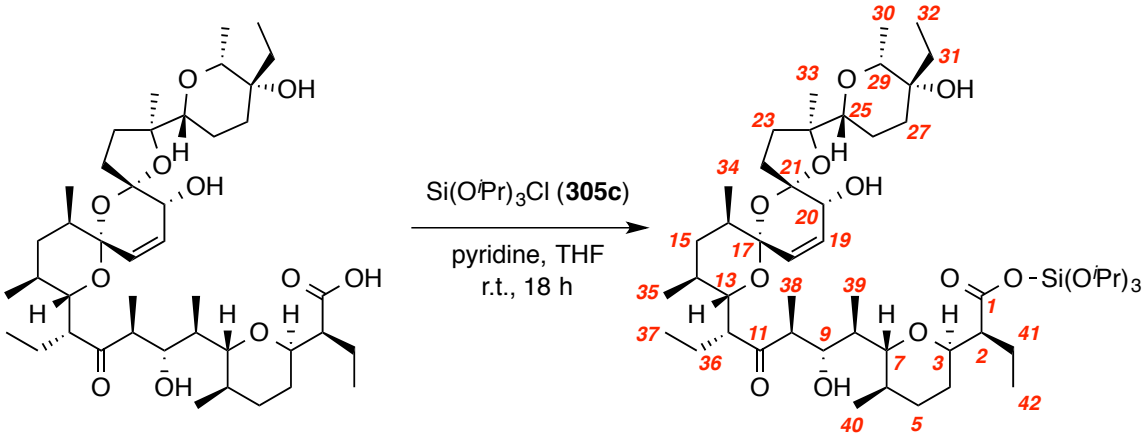

Salinomycin

705

706b

23% yield

In an oven dried culture tube fitted with a magnetic stir bar and Teflon lined cap, salinomycin **705** (173.2 mg, 0.23 mmol, 1.0 equiv.) and pyridine (6.0 mL, 2.24 mmol 9.7 equiv.) were dissolved in 3 mL of THF and allowed to stir at r.t. for 5 mins. Tri-*i*-propoxychlorosilane (**305c**) (containing ca. 80% of tri-*i*-propoxychlorosilane; 500 μL, estimated to contain 420.0 mg, 1.75 mmol, 7.7 equiv.) was added by syringe and the reaction instantly turned cloudy. The reaction stirred overnight (18 h). The THF was removed by evaporation under reduced pressure, the solid residue was triturated with a mixture of hexanes:EtOAc (2:1), and the resulting slurry was filtered through a short plug of

Celite® to remove the pyridinium salt. The filtrate was concentrated under reduced pressure, and the residue was purified by MPLC (SiO_2, 2:1 hexanes:EtOAc) to yield the title compound as a white, crystalline solid (50.6 mg, 0.053 mmol, 23%).

^{1}H NMR (500 MHz, $CDCl_3$): δ 6.04 (dd, *J* = 10.8, 2.5 Hz, 1H, H18), 5.95 (d, *J* = 11.0 Hz, 1H, H19), 4.34 (br s, 1H, H20), 4.22 (q, *J* = 6.1 Hz, 3H, -Si[OC*H*$(CH_3)_2]_3$), 4.14 (s, 1H, -O*H*), 4.12 (q, *J* = 7.1 Hz, 1H, H29), 3.98 (dd, *J* = 10.9, 5.7 Hz, 1H, H9), 3.88-3.84 (m, 1H, H3), 3.82 (d, *J* = 10.3 Hz, 1H, H13), 3.65 (d, *J* = 9.6 Hz, 1H, H7), 3.47 (dd, *J* = 10.0, 2.8 Hz, 1H, H25), 2.89 (td, *J* = 10.9, 3.5 Hz, 1H, H2), 2.79-2.7 (m, 1H, H10), 2.64 (dd, *J* = 10.7, 1.9 Hz, 1H, H12), 2.35-2.27 (m, 2H, H22α and H23α), 2.05 (s, 1H, -O*H*), 2.04-1.85 (m, 6H, H4α, H5α, H6, H22β, H23β, and H36α), 1.83-1.78 (m, 2H, H15α and H16), 1.76-1.66 (m, 3H, H27α H27β, and H14), 1.66-1.53 (m, 5H, H4β, H5β, H8, H26α, and H26β), 1.50 (s, 3H, H33), 1.47-1.29 (m, 5H, H31α, H31β, H36β, H41α, and H41β), 1.26 (dd, *J* = 7.1, 0.7 Hz, 3H, H30), 1.21 (ddd, *J* = 6.1, 1.1 Hz, 1H, H15β), 1.19 (s, 1H, -O*H*), 1.17 (d, *J* = 6.2 Hz, 18H -Si[OCH(C$H_3)_2]_3$), 0.95 (t, *J* = 7.1 Hz, 3H, H42), 0.93 (t, *J* = 6.0 Hz, 3H, H32), 0.90 (overlapping d, *J* = 7.7 Hz, 6H, H35 and H40), 0.81 (d, *J* = 7.4 Hz, 3H, H38), 0.78 (t, *J* = 7.4 Hz, 3H, H37), 0.72 (d, *J* = 7.2 Hz, 3H, H39), and 0.71 (d, *J* = 7.0 Hz, 3H, H34),

^{13}C NMR (125 MHz, $CDCl_3$): δ 215.4, 178.1, 131.7, 122.3, 106.4, 99.8, 87.9, 76.6, 75.5, 75.0, 72.8, 71.8, 71.6, 68.6, 68.4, 66.2 (3x), 56.1, 50.2, 49.4, 41.4,

39.3, 36.6, 34.5, 34.0, 33.2, 29.7, 29.2, 28.2, 26.5, 25.5 (6x), 23.0, 22.9, 21.0, 20.1, 18.1, 17.3, 15.8, 14.4, 13.5, 13.0, 12.3, 11.2, 6.9, and 6.7.

HRMS (ESI) Calc'd for $C_{51}H_{90}NaO_{14}Si^{+}$ $[M + Na]^{+}$ 977.5992; found 977.6020.

LC-MS: ACE ODS-C18 4.6 x 150 mm particle size 5 μm; 0.5 mL/min, Gradient Method 55% B to 100% B over 15 min, hold at 100% B for 15 min (Solvent System A, 5:95 MeOH:H_2O,15 mM NH_4OAc) (Solvent System B, 98:2 MeOH:H_2O,15 mM NH_4OAc), MM-ES+APCI Positive Scan 19.70 min 955.2 $(M+H)^{+}$, 972.4 $(M+NH_4)^{+}$, and 977.2 $(M+Na)^{+}$, Negative Scan 19.70 min 953.2 $(M-H)^{-}$.

TLC R_f (2:1 hexanes:EtOAc) = 0.61.

5-fluoro-1,3-bis(tri-*tert*-butoxysilyl)pyrimidine-2,4(1*H*,3*H*)-dione (708c)

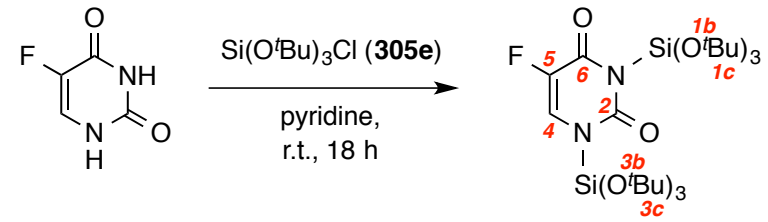

5-Fluorouracil

707

708c

20% yield

In an oven dried culture tube fitted with a magnetic stir bar and Teflon lined cap, 5-fluorouracil **707** (474.5 mg, 3.67 mmol, 1.0 equiv.) and pyridine (6.0 mL, 74.52 mmol 20.3 equiv.) were allowed to stir at r.t. for 5 mins. The tritertbutoxychlorosilane (**305e**) (2.45 mL, 11.03 mmol, 3.0 equiv.) was added by syringe and the reaction turned cloudy after 10 mins. The reaction stirred overnight (18 h). The pyridine was removed by a high vacuum rotary evaporator and the oil residue was filtered through a short plug of Celite® and the plug was washed with CH_2Cl_2. TheCH2Cl2 was removed and the crude reaction was redissolved in a mixture of hexanes:EtOAc (5:1), and purified by two sequential MPLC runs (SiO_2, 3:1 and 20:1 hexanes:ethyl acetate), which yielded the title compound (**708c**) as a white crystalline solid (453.9 mg, 0.73 mmol, 19.8% yield).

^{1}H NMR (500 MHz, $CDCl_3$): δ 8.12 (d, $^3J(H4\text{-}F5)$ = 2.3 Hz, 1H, H4), 1.33 (s, 27H, -Si[OC(C*H*$_3$)$_3$]$_3$ H1c), and 1.32 (s, 27H, -Si[OC(C*H*$_3$)$_3$]$_3$ H3c).

^{13}C NMR (125 MHz, $CDCl_3$): δ 157.3 (d, *^{4}J(C2-F5)* = 3.5 Hz, C2), 157.0 (d, *^{2}J(C6-F5)* = 11.9 Hz, C6), 144.9 (d, *^{2}J(C4-F5)* = 21.1 Hz, C4), 144.8 (d, *^{1}J(C5-F5)* = 253.4 Hz, C5), 74.3 (C1b, 3x), 73.9 (C3b, 3x), 31.5 (C1c, 9x), and 31.4 (C3c, 9x).

HRMS (ESI) Calc'd for $C_{28}H_{55}FN_2NaO_8Si_2^+$ $[M + Na]^+$ 645.3373; found 645.3548.

GC-MS: [30 m x 0.25 mm ID, HP-5, 50 °C/1.5 min/10 °C min-1/290 °C, (5029021)] t_R = 10.13 min [m/z] 549 ($M^{+\bullet}$ -C_4H_9O), 493 ($M^{+\bullet}$ -$C_8H_{17}O$), 437 ($M^{+\bullet}$ -$C_{12}H_{25}O$), 381 ($M^{+\bullet}$ -$C_{16}H_{33}O$), 325, 287, 269, 251, 155, and 57.

LC-MS: Waters Symmetry-C8 3.9 x 150 mm particle size 5 μm; 1 mL/min, Gradient Method 50% B to 100% B over 10 min, hold at 100% B for 15 min (Solvent System A, 5:95 MeOH:H_2O,15 mM NH_4OAc) (Solvent System B, 98:2 MeOH:H_2O,15 mM NH_4OAc), MM-ES+APCI Positive Scan 20.28 min 623.2 $(M+H)^+$.

TLC Rf (5:1 hexanes:EtOAc) = 0.71.

(*E*)-5-(3,3-dimethyltriaz-1-en-1-yl)-*N*,1-bis(tri-*tert*-butoxysilyl)-1*H*-imidazole-4-carboxamide (710a)

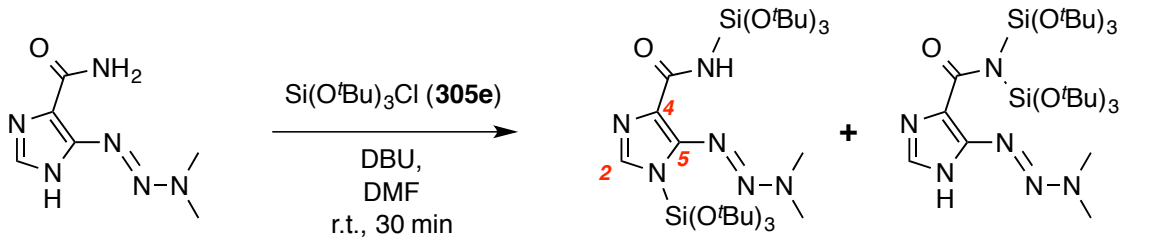

Dacarbazine

709

Dacarbazine-silicate

710a

21.3% yield

Dacarbazine-silicate

710b

In an oven dried culture tube fitted with a magnetic stir bar and Teflon lined cap, dacarbazine **709** (133.3 mg, 0.73 mmol, 1.0 equiv.) and DBU (339 μL, 2.27 mmol 3.1 equiv.) were dissolved in 2 mL of DMF. The yellow reaction was stirred for 5 mins and tritertbutoxychlorosilane (**305e**) (505 μL, 2.27 mmol, 3.1 equiv.) was added by syringe and the reaction turned completely clear after 30 mins. The DMF was removed by a high vacuum rotary evaporator and the residue was resuspended in a mixture of hexanes:EtOAc (2:1), filtered through a short plug of silica (SiO_2, 2:1 hexanes:ethyl acetate) and purification by flash chromatography (SiO_2, 98:2 hexanes:ethyl acetate) followed by MPLC (SiO_2, 5:1 hexanes:ethyl acetate) yielded the title compound (**710a**) as a white crystalline solid (105.1 mg, 0.16 mmol, 21.3% yield).

^{1}H NMR (500 MHz, $CDCl_3$): δ 7.58 (s, 1H, H2), 7.03 (s, 1H, -N*H*(Si[OC(CH_3)$_3$]$_3$) 3.52 (br s, 3H, -N=N-N*C**H**$_3$*CH_3), 3.21 (br s, 3H, -N=N-N*C*H$_3$C*H$_3$*), 1.36 (s, 27H, -NH(Si[OC(C*H*$_3$)$_3$]$_3$), and 1.32 (s, 27H, N1-(Si[OC(C*H*$_3$)$_3$]$_3$).

^{13}C NMR (125 MHz, $CDCl_3$): δ 166.3, 150.1, 139.0, 135.5, 116.8 75.5 (3x), 74.2 (3x), 73.0, 31.8 (9x), and 31.6 (9x).

HRMS (ESI) Calc'd for $C_{30}H_{62}N_6NaO_7Si_2^+$ $[M + Na]^+$ 697.4111; found 697.4119.

TLC R$_f$ (5:1 hexanes:EtOAc) = 0.37.

(E)-5-(3,3-dimethyltriaz-1-en-1-yl)-N,N-bis(tri-tert-butoxysilyl)-1H-imidazole-4-carboxamide (710b)

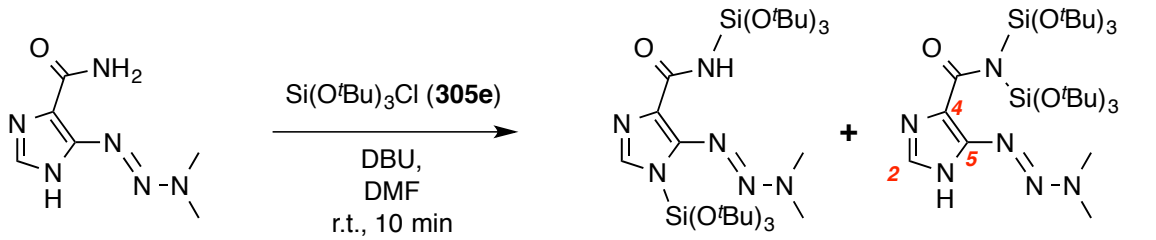

Dacarbazine

709

Dacarbazine-silicate

710a

Dacarbazine-silicate

710b

12.4% yield

In an oven dried culture tube fitted with a magnetic stir bar and Teflon lined cap, dacarbazine **709** (114.1 mg, 0.62 mmol, 1.0 equiv.) and DBU (280 μL, 1.87 mmol 3.0 equiv.) were dissolved in 5 mL of DMF. The yellow reaction was stirred for 5 mins and tritertbutoxychlorosilane (**305e**) (415 μL, 1.87 mmol, 3.0 equiv.) was added by syringe and the mixture turned clear after 10 mins. The DMF was removed by a high vacuum rotary evaporator and the residue was resuspended in a mixture of hexanes:EtOAc (1:1), filtered through a short plug of Celite® to remove the salts, and purification by MPLC (SiO_2, 1:1 hexanes:ethyl acetate) yielded the title compound (**710b**) as a white-yellow crystalline solid (52 mg, 0.077 mmol, 12.4% yield).

^{1}H NMR (500 MHz, $CDCl_3$): δ 7.91 (s, 1H, H2), 7.80 (s, 1H, H1), 3.61 (br s, 3H, -N=N-N*C*H$_3$CH$_3$), 3.24 (br s, 3H, -N=N-NCH$_3$C*H*$_3$), 1.35 (s, 54H, -N{(Si[OC(CH$_3$)$_3$]$_3$}$_2$).

^{13}C NMR (125 MHz, $CDCl_3$): δ 162.5, 151.7, 145.2, 121.3, 75.2 (3x), 73.9 (3x), 43.7, 37.0, 31.8 (9x), and 31.6 (9x).

HRMS (ESI) Calc'd for $C_{30}H_{63}N_6O_7Si_2^+$ $[M + H]^+$ 675.4291; found 675.6186.

mp = 179-180.5 °C.**TLC** Rf (1:1 hexanes:EtOAc) = 0.33.

1-isobutyl-*N*-(tri-*tert*-butoxysilyl)-1*H*-imidazo[4,5-*c*]quinolin-4-amine) (712)

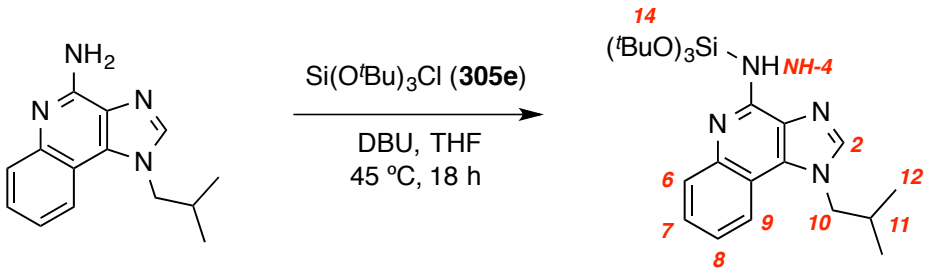

Imiquimod

711

Imiquimod-silicate

712

58% yield

In an oven dried culture tube fitted with a magnetic stir bar and Teflon lined cap, imiquimod **711** (94.9 mg, 0.39 mmol, 1.0 equiv.) and DBU (176 μL, 1.18 mmol 3.0 equiv.) were dissolved in 3 mL of THF. The reaction was stirred for 5 mins and tritertbutoxychlorosilane (**305e**) (263 μL, 1.18 mmol, 3.0 equiv.) was added by syringe and the mixture turned slightly cloudy. The reaction was heated to 45 ºC for 18 h and more precipitate formed as the reaction progressed. The THF was removed and the reaction was resuspended in a mixture of hexanes:EtOAc (1:1), filtered through a short plug of Celite® to remove the salts, and purified by MPLC (SiO_2, 1:1 hexanes:ethyl acetate) which yielded the title compound (**712**) as a white crystalline solid (110.0 mg, 0.23 mmol, 58% yield).

^{1}H NMR (500 MHz, $CDCl_3$): δ 7.89 (dd, J = 8.3, 0.8 Hz, 2H, H6 and H9), 7.72 (s, 1H, H2), 7.48 (t, J = 7.8 Hz, 1H, H7), 7.29 (t, J = 7.5 Hz, 1H, H8), 5.61 (s, 1H, H4), 4.27 (d, J = 7.4 Hz, 2H, H10), 2.36 (dq, J = 13.7, 6.9 Hz, H11), 1.41 (s, 27H, H14), and 1.02 (d, J = 6.6 Hz, 6H, H12).

HRMS (ESI) Calc'd for $C_{26}H_{43}N_4O_3Si^+$ $[M + H]^+$ 487.3099; found 487.3104.

TLC Rf (2:1 hexanes:EtOAc) = 0.32.

(tri-*tert*-butyl silicic) 1-cyclopropyl-6-fluoro-4-oxo-7-(4-(tri-*tert*-butoxysilyl)piperazin-1-yl)-1,4-dihydroquinoline-3-carboxylic anhydride (714)

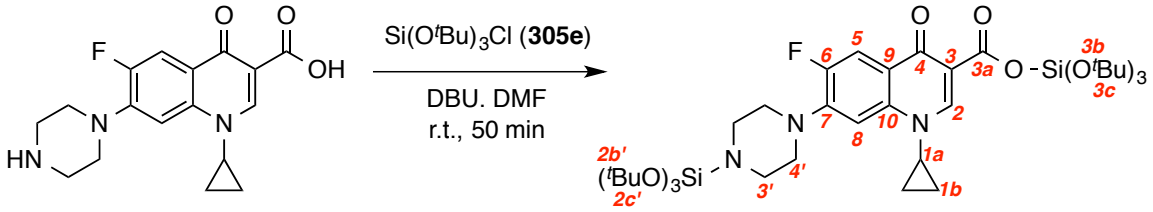

Ciprofloxacin

713

Ciprofloxacin-silicate

714

30.6% yield

In an oven dried culture tube fitted with a magnetic stir bar and Teflon lined cap, ciprofloxacin **713** (133.8 mg, 0.40 mmol, 1.0 equiv.) and DBU (181 μL, 1.21 mmol 3.0 equiv.) were dissolved in 4 mL of DMF. The green-yellow reaction was stirred for 5 mins and tritertbutoxychlorosilane (**305e**) (270 μL, 1.21 mmol, 3.0 equiv.) was added by syringe and the reaction turned clear after 50 mins. The DMF was removed by a high vacuum rotary evaporator and the yellow oil residue was resuspended in a mixture of hexanes:EtOAc (3:1), filtered through a short plug of Celite® to remove the salts, and purified by MPLC (SiO_2, 3:1 hexanes:ethyl acetate), which yielded the title compound (**714**) as a white crystalline solid (112 mg, 0.12 mmol, 30.6% yield).

^{1}H NMR (500 MHz, $CDCl_3$): δ 8.58 (s, 1H, H2), 8.06 (d, $^3J(H5\text{-}F6)$ = 13.5 Hz, 1H, H5), 7.22 (d, $^4J(H8\text{-}F6)$ = 7.1 Hz, 1H, H8), 3.41 (tt, J = 7.1, 3.6, 1H, H1a), 3.17-3.07 (m, 8H, H3' and H4'), 1.38 (s, 27H, -Si[OC(CH_3)$_3$]$_3$ H3c), 1.33 (s, 27H, -

$Si[OC(CH_3)_3]_3$ H2c'), 1.29 (dd, *J* = 12.7, 6.3 Hz, 2H, H1b$_\alpha$), and 1.11 (dd, *J* = 9.9, 6.3 Hz, 2H H1b$_\beta$).

^{13}C NMR (125 MHz, $CDCl_3$): δ 173.4 (C4) 161.2 (C3a), 154.3 (C6), 148.6 (C2), 145.2 (C7), 137.8 (C9), 137.3 (C3), 122.6 (C10), 113.3 (C5), 104.3 (C8), 73.6 (C3b, 3x), 72.3 (C2b', 3x), 51.5 (C3'), 51.2 (C3'), 44.7 (C4'), 44.5 (C4'), 34.1 (C1a), 31.5 (C2c', 9x), 31.1 (C3c, 9x), 7.9 (C1b), and 7.6 (C1b).

^{19}F NMR (470 MHz, $CDCl_3$): δ -123.9 (dd, $^3J(H5\text{-}F6)$ = 13.4 and $^4J(H8\text{-}F6)$ = 6.9 Hz)

HRMS (ESI) Calc'd for $C_{41}H_{70}FN_3NaO_9Si_2^+$ $[M + Na]^+$ 846.4527; found 846.4557.

TLC Rf (3:1 hexanes:EtOAc) = 0.61.

triisopropylsilyl (*S*)-2-((2*R*,5*R*,6*R*)-6-((2*R*,3*S*,4*S*,6*R*)-6-((2*S*,5*S*,7*R*,9*S*,10*S*,12*R*,15*R*)-2-((2*R*,5*R*,6*R*)-5-ethyl-5-hydroxy-6-methyltetrahydro-2*H*-pyran-2-yl)-15-hydroxy-2,10,12-trimethyl-1,6,8-trioxadispiro[4.1.5^{7}.3^{5}]pentadec-13-en-9-yl)-3-hydroxy-4-methyl-5-oxooctan-2-yl)-5-methyltetrahydro-2*H*-pyran-2-yl)butanoate (715)

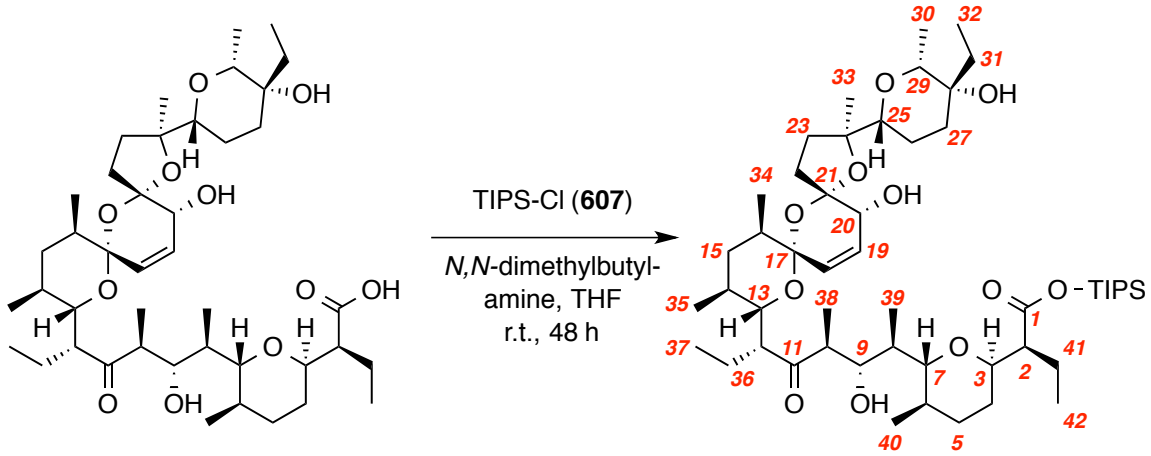

Salinomycin

705

715

63% yield

In an oven dried culture tube fitted with a magnetic stir bar and Teflon lined cap, salinomycin **705** (107.6 mg, 0.14 mmol, 1.0 equiv.) and *N,N*-dimethylbutylamine (98 μL, 0.70 mmol 5.0 equiv.) were dissolved in 2 mL of THF and allowed to stir at r.t. for 5 mins. Triisopropylsiyl chloride (**607**) (TIPS-Cl, 149 μL, 0.70 mmol, 5.0 equiv.) was added by Wiretrol® and the reaction instantly turned cloudy. The reaction stirred for 48 h. The THF was removed by evaporation under reduced pressure, the solid residue was triturated with a mixture of hexanes:EtOAc (1:1), and the resulting slurry was filtered through a short plug of Celite® to remove the pyridinium salt. The filtrate was concentrated under reduced pressure, and the

residue was purified by MPLC (SiO_2, 1:1 hexanes:EtOAc) to yield the title compound as a white, crystalline solid (80.3 mg, 0.089 mmol, 63%).

^{1}H NMR (500 MHz, $CDCl_3$): δ 6.11 (dd, *J* = 10.8, 2.1 Hz, 1H, H18), 5.96 (d, *J* = 11.0 Hz, 1H, H19), 4.01 (dd, *J* = 9.3, 5.3 Hz, 1H, H3), 4.04-3.98 (m, 2H, H9 and -O*H*), 3.92 (d, *J* = 9.4 Hz, 1H, -O*H*), 3.83 (q, *J* = 6.9 Hz, 1H, H29), 3.76 (dd, *J* = 9.7, 2.2 Hz, 1H, -O*H*), 3.66 (dd, *J* = 11.3, 2.9 Hz, 1H, H7), 3.60 (dd, *J* = 10.3, 3.5 Hz, 1H, H13), 3.50 (d, *J* = 5.5 Hz, 1H, H25), 3.14 (dq, *J* = 10.0, 7.1 Hz, 1H, H10), 3.02 (td, *J* = 10.8, 3.9 Hz, 1H, H2), 2.74 (dt, *J* = 9.0, 3.1 Hz, 1H, H12), 2.38 (dt, *J* = 12.5, 9.1 Hz, 1H, H22α) 2.21 (td, *J* = 10.8, 4.7 Hz, 1H, H23α), 2.08-2.02 (m, 2H, H22β,), 1.95-1.69 (m, 8H, H4α, H5α, H6, H14, H15α, H16, H23β, and H36α), 1.69-1.63 (m, 2H, H27α, and H27β), 1.57-1.45 (m, 8H, H4β, H5β, H8, H26α, H26β, and H33), 1.44-1.44-1.29 (m, 9H, H31α, H31β, H36β, H41α, H41β, H15β, and -Si[C*H*$(CH_3)_2]_3$), 1.22 (d, *J* = 7.0 Hz, 3H, H30), 1.12 (dd, *J* = 7.5, 5.5 Hz, 18H -Si[CH(C*H*$_3)_2]_3$), 0.97 (br t, 3H, H42), 0.89 (br t, 3H, H32), 0.92-0-86 (m, 6H, H35 and H40), 0.79 (br t, *J* = 7.5 Hz, 9H, H37, H38, and H39), and 0.69 (d, *J* = 6.8 Hz, 3H, H34).

^{13}C NMR (125 MHz, $CDCl_3$): δ 214.0, 171.4, 132.9, 121.4, 106.4, 99.3, 87.7, 79.7, 77.1, 75.3, 74.2, 71.6, 71.1, 69.7, 68.1, 57.8, 49.4, 47.5, 40.5, 39.5, 36.7, 36.5, 34.1, 30.7, 30.5, 29.3, 28.5, 26.4, 25.8 (3x), 22.4, 22.2, 20.9, 20.4, 18.2, 18.1 (6x), 17.7, 15.8, 14.7, 13.9, 12.6, 12.5, 12.0, 7.7, 6.5

HRMS (ESI) Calc'd for $C_{51}H_{90}NaO_{11}Si^+$ $[M + Na]^+$ 929.6145; found 929.6158

LC-MS: ACE ODS-C18 4.6 x 150 mm particle size 5 μm; 0.5 mL/min, Gradient Method 55% B to 100% B over 15 min, hold at 100% B for 15 min (Solvent System A, 5:95 MeOH:H_2O,15 mM NH_4OAc) (Solvent System B, 98:2 MeOH:H_2O,15 mM NH_4OAc), MM-ES+APCI Positive Scan 27.00 min 924.7 $(M+NH_4)^+$, and 977.2 $(M+Na)^+$.

TLC R_f (1:1 hexanes:EtOAc) = 0.35.

_N_-(3-ethynylphenyl)-6,7-bis(2-methoxyethoxy)-_N_-(triisopropylsilyl)quinazolin-4-amine (718)

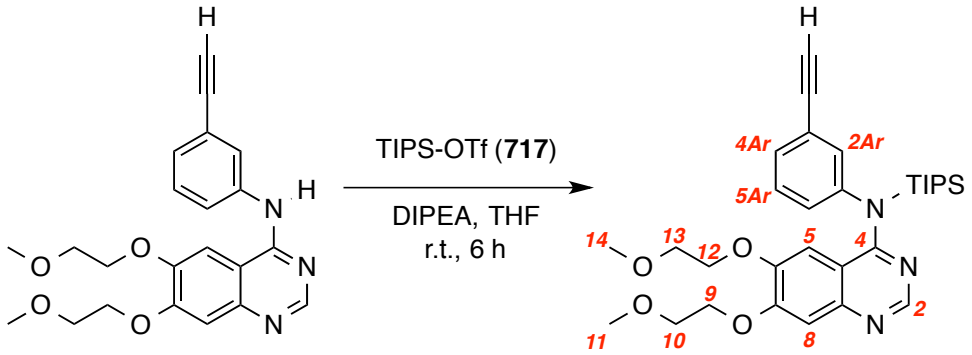

Erlotinib

716

718

97.8% yield

In an oven dried culture tube fitted with a magnetic stir bar and Teflon lined cap, erlotinib **716** (93.8 mg, 0.239 mmol, 1.0 equiv.) and diisopropylethylamine (DIPEA, 300 μL, 200 mg, 1.73 mmol 7.2 equiv.) were dissolved in 10 mL of THF. The reaction was stirred for 5 mins and triisopropylsilyl trifluoromethanesulfonate (**717**) (400 μL, 456 mg, 1.48 mmol, 6.2 equiv.) was added by syringe and the mixture turned yellow. The reaction was stirred for 6 h and a white precipitate formed as the reaction progressed. The THF was removed and the reaction was resuspended in a mixture of hexanes:EtOAc (1:1), filtered through a short plug of Celite® to remove the salts, and purified by MPLC (SiO_2, 1:1 hexanes:ethyl acetate) which yielded the title compound (**718**) as a white crystalline solid (128.6 mg, 0.23 mmol, 97.8% yield).

^{1}H NMR (500 MHz, $CDCl_3$): δ 8.52 (s, 1H, H2), 7.57-7.30 (m, 4H, H8, H4Ar, H5Ar, and H6Ar), 7.12 (s, 1H, H5), 6.17 (s, 1H, H2Ar), 4.21 (t, *J* = 4.8 Hz, 2H, H12), 3.80 (t, *J* = 4.8 Hz, 2H, H9), 3.60 (t, *J* = 4.6 Hz, 2H, H13), 3.50 (t, *J* = 4.7 Hz, 2H, H10), 3.43 (s, 3H, H14), 3.41 (s, 3H, H11), 3.12 (s, 1H, -3Ar-CC-*H*), 1.51 (sept., *J* = 7.4 Hz, 3H, -Si[C*H*$(CH_3)_2]_3$), and 1.05 (d, *J* = 7.3 Hz, 18H, -Si[CH(C*H*$_3)_2]_3$).

^{13}C NMR (125 MHz, $CDCl_3$): δ 171.3, 153.3, 146.8, 129.8, 123.7, 110.7, 108.7, 82.7, 78.7, 70.6 (2x), 68.3, 67.8, 60.6, 59.5, 59.4, 21.3, 19.1 (6x), 18.2, 17.9, 14.4, 13.9 (3x), 12.5, and 12.0.

HRMS (ESI) Calc'd for $C_{31}H_{43}N_3NaO_4Si^+$ $[M + Na]^+$ 572.2915; found 572.2938

LC-MS: Waters Symmetry-C8 3.9 x 150 mm particle size 5 μm; 0.5 mL/min, Gradient Method 50% B to 100% B over 10 min, hold at 100% B for 10 min (Solvent System A, 5:95 MeOH:H_2O,15 mM NH_4OAc) (Solvent System B, 98:2 MeOH:H_2O,15 mM NH_4OAc), MM-ES+APCI Positive Scan 17.51 min 550.4 $(M+H)^+$. Negative Scan 17.51 min 392 $(M+2OAc+HOAc)^{-2}$.

TLC Rf (1:1 hexanes:EtOAc) = 0.26.

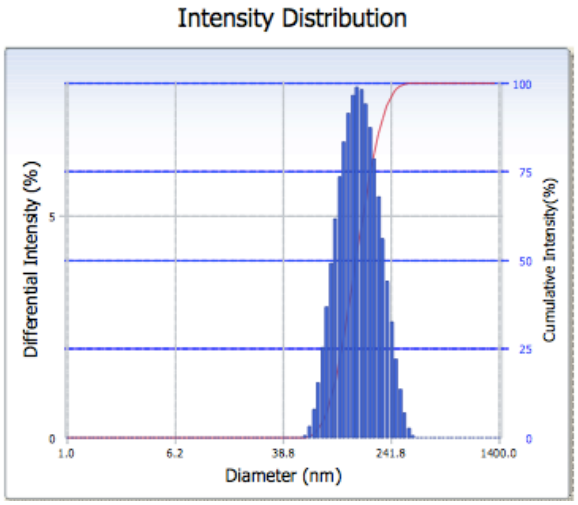

Figure S7.1 I Intensity distribution of freshly prepared Salinomycin-silicate **706b** loaded mPEG-*b*-PLGA (5k-10k) based nanoparticles ca. 50 wt%.

Bibliography

For Chapters 2–7

[1] Siegel, R.; Naishadham, D. Cancer Statistics, 2014. *CA Cancer J. Clin.* **2014,** *64,* 9-29.

[2] Siegel, R.; Naishadham, D. Cancer Statistics, 2012. *CA Cancer J. Clin.* **2012,** *62,* 10-29. [National Cancer Database, American College of Surgeons Commission on Cancer, **2008** Data Submission.]

[3] Kingston, D. G. I. Taxol, a Molecule for All Seasons. *Chem. Commun.* **2001**, *10*, 867–880.

[4] Kingston, D. G. I. The Shape of Things to Come: Structural and Synthetic Studies of Taxol and Related Compounds. *Phytochemistry* **2007**, *68*, 1844–1854.

[5] Rao, S.; Orr, G. A.; Chaudhary, A. G.; Kingston, D. G.; Horwitz, S. B. Characterization of the Taxol Binding Site on the Microtubule. 2-(M-Azidobenzoyl)Taxol Photolabels a Peptide (Amino Acids 217-231) of Beta-Tubulin. *J. Biol. Chem.* **1995**, *270*, 20235–20238.

[6] Schiff, P. B.; Fant, J.; Horwitz, S. B. Promotion of Microtubule Assembly *in vitro* by Taxol. *Nature* **1979**, *277*, 1–3.

[7] Holton, R. Semi-synthesis of Taxane Derivatives using Metal Alkoxides and Oxazinones. U.S. Patent 5, 254, 703, October 19, **1993.**

[8] Patel, R. Tour De Paclitaxel: Biocatalysis for Semisynthesis. *Annu. Rev. Microbiol.* **1998**, *98*, 361-395.

[9] Holton, R. A.; Kim, H. B.; Somoza, C.; Liang, F.; Biediger, R. J.; Boatman, P. D.; Shindo, M.; Smith, C. C.; Kim, S. First Total Synthesis of Taxol. 2. Completion of the C and D Rings. *J. Am. Chem. Soc.* **1994**, *116*, 1599–1600.

[10] Nicolaou, K. C.; Yang, Z.; Liu, J. J.; Ueno, H.; Nantermet, P. G.; Guy, R. K.; Claiborne, C. F.; Renaud, J.; Couladouros, E. A.; Paulvannan, K. Total Synthesis of Taxol. *Nature* **1994**, *367*, 630–634.

[11] Venkat, K. In *Pure Appl. Chem.,* Proceedings of the International Conference on Biodiversity and Bioresources, (Phuket), Thialand, November 23-27, **1997**.

[12] Magri, N. F.; Kingston, D. G. I. Modified Taxols. 2. Oxidation Products of Taxol. *J. Org. Chem.* **1986**, *51*, 797–802.

[13] Magri, N. F.; Kingston, D. G. Modified Taxols, 4. Synthesis and Biological Activity of Taxols Modified in the Side Chain. *J. Nat. Prod.* **1988**, *51*, 298–306.

[14] Magri, N. F.; Kingston, D. G. I.; Jitrangsri, C.; Piccariello, T. Modified Taxols. 3. Preparation and Acylation of Baccatin III. *J. Org. Chem.* **1986**, *51*, 3239–3242.

[15] Samaranayake, G.; Magri, N. F.; Jitrangsri, C.; Kingston, D. G. I. Modified Taxols. 5. Reaction of Taxol with Electrophilic Reagents and Preparation of a Rearranged Taxol Derivative with Tubulin Assembly Activity. *J. Org. Chem.* **1991**, *56*, 5114–5119.

[16] Chaudhary, A. G.; Rimoldi, J. M.; Kingston, D. G. I. Modified Taxols. 10. Preparation of 7-Deoxytaxol, a Highly Bioactive Taxol Derivative, and Interconversion of Taxol and 7-Epi-Taxol. *J. Org. Chem.* **1993**, *58*, 3798–3799.

[17] Zhao, Z.; Kingston, D. G. I.; Crosswell, A. R. Modified Taxols, 6. Preparation of Water-Soluble Prodrugs of Taxol. *J. Nat. Prod.* **1991**, *54*, 1607–1611.

[18] Kingston, D. G.; Gunatilaka, A. A.; Ivey, C. A. Modified Taxols, 7. a Method for the Separation of Taxol and Cephalomannine. *J. Nat. Prod.* **1992**, *55*, 259–261.

[19] Samaranayake, G.; Neidigh, K. A.; Kingston, D. G. Modified Taxols, 8. Deacylation and Reacylation of Baccatin III. *J. Nat. Prod.* **1993**, *56*, 884–898.

[20] Rimoldi, J. M.; Kingston, D. G.; Chaudhary, A. G.; Samaranayake, G.; Grover, S.; Hamel, E. Modified Taxols, 9. Synthesis and Biological Evaluation of 7-Substituted Photoaffinity Analogues of Taxol. *J. Nat. Prod.* **1993**, *56*, 1313–1330.

[21] Kingston, D. G. I.; Jagtap, P. G.; Yuan, H.; Samala, L. The Chemistry of Taxol and Related Taxoids. Progress in the Chemistry of Organic Natural Products; Springer Vienna: Vienna, **2002**, *84*, 53–225.

[22] Snyder, J. P.; Nettles, J. H.; Cornett, B.; Downing, K. H.; Nogales, E. The Binding Conformation of Taxol in Beta-Tubulin: a Model Based on Electron Crystallographic Density. *Proc. Natl. Acad. Sci. U.S.A.* **2001**, *98*, 5312–5316.

[23] Sisti, N. Method for Docetaxel Synthesis. U.S. Patent 5,688,977, November 18, **1997**.

[24] Sparreboom, A.; van Tellingen, O.; Nooijen, W. J.; Beijnen, J. H. Preclinical Pharmacokinetics of Paclitaxel and Docetaxel. *Anti-cancer Drugs* **1998**, *9*, 1-17.

[25] Rose, W.; Fairchild, C.; Lee, F. Y. F. Preclinical Antitumor Activity of Two Novel Taxanes. *Cancer Chemoth. and Pharm.* **2001**, *47*, 97-105.

[26] Altstadt, T. J.; Fairchild, C. R.; Golik, J.; Johnston, K. A.; Kadow, J. F.; Lee, F. Y.; Long, B. H.; Rose, W. C.; Vyas, D. M.; Wong, H.; Wu, M.-J.; Wittman, M. D. Synthesis and Antitumor Activity of Novel C-7 Paclitaxel Ethers: Discovery of BMS-184476. *J. Med. Chem.* **2001**, *44*, 4577–4583.

[27] Kingston, D. G. I. A Natural Love of Natural Products. *J. Org. Chem.* **2008**, *73*, 3975–3984.

[28] Ojima, I.; Das, M. Recent Advances in the Chemistry and Biology of New Generation Taxoids *J. Nat. Prod.* **2009**, *72*, 554–565.

[29] Rice, A.; Liu, Y.; Michaelis, M. L.; Himes, R. H.; Georg, G. I.; Audus, K. L. Chemical Modification of Paclitaxel (Taxol) Reduces P-Glycoprotein Interactions and Increases Permeation Across the Blood-Brain Barrier in Vitro and in Situ. *J. Med. Chem* **2005**, *48*, 832–838.

[30] Sinkula, A. A.; Yalkowsky, S. H. Rationale for Design of Biologically Reversible Drug Derivatives: Prodrugs. *J. Pharm. Sci.* **1975**, *64*, 181–210.

[31] Majumdar, S.; Duvvuri, S.; Mitra, A. K. Membrane transporter/ receptor-targeted prodrug design: strategies for human and veterinary drug development. *Adv. Drug Delivery Rev.* **2004**, *56*, 1437-1452.

[32] Schmidt, F.; Ungureanu, I.; Duval, R.; Pompon, A.; Monneret, C. Cancer Chemotherapy: a Paclitaxel Prodrug for ADEPT (Antibody-Directed Enzyme Prodrug Therapy). *Eur. J. Org. Chem.* **2001**, *2001*, 2129–2134.

[33] Skwarczynski, M.; Hayashi, Y.; Kiso, Y. Paclitaxel Prodrugs: Toward Smarter Delivery of Anticancer Agents. *J. Med. Chem.* **2006**, *49*, 7253–7269.

[34] Yewale, C.; Baradia, D.; Vhora, I.; Misra, A. Proteins: Emerging Carrier for Delivery of Cancer Therapeutics. *Expert. Opin. Drug Deliv.* **2013**, *10*, 1429–1448.

[35] Xiao, H.; Verdier-Pinard, P.; Fernandez-Fuentes, N.; Burd, B.; Angeletti, R.; Fiser, A.; Horwitz, S. B.; Orr, G. A. Insights Into the Mechanism of Microtubule Stabilization by Taxol. *Proc. Natl. Acad. Sci. U.S.A.* **2006**, *103*, 10166–10173.

[36] Vyas, D. M.; Wong, H.; Crosswell, A. R.; Casazza, A. M.; Knipe, J. O.; Mamber, S. W.; Doyle, T. W. Synthesis and Antitumor Evaluation of Water Soluble Taxol Phosphates. *Bioorg. Med. Chem. Lett.* **1993**, *3*, 1357–1360.

[37] Paradis, R.; Pagé, M. New Active Paclitaxel Amino Acids Derivatives with Improved Water Solubility. *Anticancer Res.* **1998**, *18*, 2711–2716.

[38] de Bont, D. B. A.; Leenders, R. G. G.; Haisma, H. J.; van der Meulen-Muileman, I.; Scheeren, H. W. Synthesis and Biological Activity of β-glucuronyl Carbamate-based Prodrugs of Paclitaxel as Potential Candidates for ADEPT. *Bioorg. Med. Chem. Lett.* **1997**, *5*, 405–414.

[39] Hayashi, Y.; Skwarczynski, M.; Hamada, Y.; Sohma, Y.; Kimura, T.; Kiso, Y. A Novel Approach of Water-soluble Paclitaxel Prodrug with No Auxiliary and No Byproduct: Design and Synthesis of Isotaxel. *J. Med. Chem.* **2003**, *46*, 3782–3784.

[40] Hemamalini, S.; Chander, M.; Baker, S.; He, L. Tumor Targeting by Covalent Conjugation of a Natural Fatty Acid to Paclitaxel. *Clin. Cancer Res.* **2001**, *7,* 3229–3238.

[41] Bradley, M.; Swindell, C.; Anthony, F. Tumor targeting by Conjugation of DHA to Paclitaxel. *J. Control. Release* **2001**, *74*, 233-236.

[42] Dubowchik, G.; Mosure, K.; Knipe, J. Cathepsin B-sensitive Dipeptide Prodrugs. 2. Models of Anticancer Drugs Paclitaxel (Taxol®), Mitomycin C and Doxorubicin. *Bioorg. Med. Chem. Lett.* **1998**, *8*, 3347-3352.

[43] Greenwald, R.; Choe, Y.; McGuire, J. Effective Drug Delivery by PEGylated Drug Conjugates. *Adv. Drug Deliver. Rev.* **2003**, *55*, 217-250.

[44] Vyas, D. M.; Ueda, Y.; Wong, H.; Matiskella, J. D.; Hauck, S.; Mikkilineni, A. B.; Farina, V.; Rose, W. C.; Casazza, A. M. *ACS Symposium Series*; Georg, G. I.; Chen, T. T.; Ojima, I.; Vyas, D. M., Eds. ACS Symposium Series, 1947 American Chemical Society: Washington, DC, 2009; Vol. 583, pp. 124–137.

[45] Skwarczynski, M.; Sohma, Y.; Kimura, M.; Hayashi, Y.; Kimura, T.; Kiso, Y. O–N Intramolecular Acyl Migration Strategy in Water-soluble Prodrugs of Taxoids. *Bioorg. Med. Chem. Lett.* **2003**, *13*, 4441–4444.

[46] Yashveer Singh, M. P. P. J. S. Recent Trends in Targeted Anticancer Prodrug and Conjugate Design. *Curr. Med. Chem.* **2008**, *15*, 1802.

[47] Carvalho, I.; Milanezi, F.; Martins, A.; Reis, R. M.; Schmitt, F. Overexpression of Platelet-Derived Growth Factor Receptor Alpha in Breast Cancer Is Associated with Tumour Progression. *Breast Cancer Res.* **2005**, *7*, R788–R795.

[48] Jin, S.; Wan, J.; Meng, L.; Huang, X.; Guo, J.; Liu, L.; Wang, C. Biodegradation and Toxicity of Protease/Redox/pH Stimuli-Responsive PEGlated PMAA Nanohydrogels for Targeting Drug Delivery. *ACS Appl. Mater. Interfaces* **2015**, ASAP.

[49] Xiong, M.-H.; Bao, Y.; Du, X.-J.; Tan, Z.-B.; Jiang, Q.; Wang, H.-X.; Zhu, Y.-H.; Wang, J. Differential Anticancer Drug Delivery with a Nanogel Sensitive to Bacteria-Accumulated Tumor Artificial Environment. *ACS Nano* **2013**, *7*, 10636–10645.

[50] Garber, K. Energy Deregulation: Licensing Tumors to Grow. *Science* **2006**, *312*, 1158–1159.

[51] Damen, E. W. P.; Wigerinck, P. H. G.; Braamer, L.; Sperling, D.; de Vos, D.; Scheeren, H. W. Paclitaxel Esters of Malic Acid as Prodrugs with Improved Water Solubility. *Bioorg. Med. Chem. Lett.* **2000**, *8*, 427–432.

[52] Greenwald, R. B.; Pendri, A.; Bolikal, D. Highly Water Soluble Taxol Derivatives: 2′-Polyethyleneglycol Esters as Potential Prodrugs. *Bioorg. Med. Chem. Lett.* **1994**, *4,* 2465–2470.

[53] Smith, T. A. D.; Cheyne, R. W. Predicting Tumour Response to Anti-HER1 Therapy using Medical Imaging: a Literature Review and in vitro Study of [18F]-FDG Incorporation by Breast Cancer Cells Responding to Cetuximab. *J. Biomed. Sci.* **2011**, *68*, 158–166.

[54] Hennenfent, K. L. Novel Formulations of Taxanes: a Review. Old Wine in a New Bottle? *Ann. Oncol.* **2006**, *17*, 735–749.

[55] Sparreboom, A.; Van Asperen, J.; Mayer, U.; Schinkel, A. H.; Smit, J. W.; Meijer, D. K. F.; Borst, P.; Nooijen, W. J.; Beijnen, J. H.; Van Tellingen, O. Limited Oral Bioavailability and Active Epithelial Excretion of Paclitaxel (Taxol) caused by P-glycoprotein in the Intestine *P. Natl. Acad. Sci. USA* **1997**, *94*, 2031-2035.

[56] Gelderblom, H.; Verweij, J.; Nooter, K.; Sparreboom, A. Cremophor EL: the Drawbacks and Advantages of Vehicle Selection for Drug Formulation. *Eur. J. Cancer.* **2001**, *37*, 1590–1598.

[57] Weiss, R.; Donehower, R.; Wiernik, P. Hypersensitivity Reactions from Taxol. *J. Clin. Oncol.* **1990**, *8*, 1263-1268.

[58] Friedland, D.; Gorman, G.; Treat, J. Hypersensitivity Reactions From Taxol and Etoposide. *J. Natl. Cancer I.* **1993**, *85*, 2036.i

[59] van Tellingen, O.; Huizing, M. Cremophor EL Causes (Pseudo-) Non-linear Pharmacokinetics of Paclitaxel in Patients. *Brit. J. Cancer* **1999**, *81*, 330-335.

[60] Schwartz, E.; Einzig, A.; Strauman, J. Phase I trial of taxol Given as a 24-hour Infusion every 21 Days: Responses Observed in Metastatic Melanoma. *J. Clin. Oncol.* **1987**, *5*, 1232-1239.

[61] Crown, J. Docetaxel and Paclitaxel in the Treatment of Breast Cancer: A Review of Clinical Experience. *Oncologist* **2004**, *9*, 24–32.

[62] Bernstein, B. Docetaxel as an Alternative to Paclitaxel After Acute Hypersensitivity Reactions. *Ann. Pharmacother.* **2000***, 34*, 1332-1335.

[63] Norris, L. B.; Qureshi, Z. P.; Bookstaver, P. B.; Raisch, D. W.; Sartor, O.; Chen, H.; Bennet C.L. Polysorbate 80 Hypersensitivity Reactions: a Renewed Call to Action. *J. Community Support. Oncol.* **2010**, *7*, 425–428.

[64] Eckhoff, L.; Nielsen, M.; Moeller, S.; Knoop, A. TAXTOX - a Retrospective Study Regarding the Side Effects of Docetaxel Given as Part of the Adjuvant Treatment to Patients with Primary Breast Cancer in Denmark from 2007 to 2009. *Acta Oncologica.* **2011**, *50*, 1075–1082.

[65] Sparreboom, A.; van Tellingen, O.; Nooijen, W. J.; Beijnen, J. H. Tissue Distribution, Metabolism and Excretion of Paclitaxel in Mice. *Anti-cancer Drugs* **1996**, *7*, 78–86.

[66] Harries, M.; O'Donnell, A.; Scurr, M.; Reade, S. Phase I/II Study of DHA–paclitaxel in Combination with Carboplatin in Patients with Advanced Malignant Solid Tumours. *Brit. J. Cancer* **2004**, *91*, 1651-1655.

[67] Desai, N. Methods for *in vivo* delivery of Substantially Water Insoluble Pharmacologically Active Agents and Compositions Useful Therefor. U.S. Patent 5,439,686, August 8, **1995**.

[68] U.S. FDA approved leaflet Abraxane Package Insert Version 12. **2005**, 1–26.

[69] Dosio, F.; Arpicco, S.; Brusa, P.; Stella, B.; Cattel, L. Poly(ethylene glycol)–human serum albumin–paclitaxel Conjugates: Preparation, Characterization and Pharmacokinetics. *J. Control. Release* **2001**, 1–11.

[70] Nyman, D. W. Phase I and Pharmacokinetics Trial of ABI-007, a Novel Nanoparticle Formulation of Paclitaxel in Patients With Advanced Nonhematologic Malignancies. *J. Clin. Oncol.* **2005**, *23*, 7785–7793.

[71] Herper, M. Cancer Man. *Forbes* **2009**, 1–2.

[72] Sparreboom, A. Comparative Preclinical and Clinical Pharmacokinetics of a Cremophor-Free, Nanoparticle Albumin-Bound Paclitaxel (ABI-007) and Paclitaxel Formulated in Cremophor (Taxol). *Clin. Cancer Res.* **2005**, *11*, 4136–4143.

[73] Joshi-Hangal, R. Paclitaxel Formulation. U.S. Patent, 6,538,020, March 25, **2011**.

[74] Kim, T. Y. Phase I and Pharmacokinetic Study of Genexol-PM, a Cremophor-Free, Polymeric Micelle-Formulated Paclitaxel, in Patients with Advanced Malignancies. *Clin. Cancer Res.* **2004**, *10*, 3708–3716.

[75] Lee, K. S.; Chung, H. C.; Im, S. A.; Park, Y. H.; Kim, C. S.; Kim, S.-B.; Rha, S. Y.; Lee, M. Y.; Ro, J. Multicenter Phase II trial of Genexol-PM, a Cremophor-free, Polymeric Micelle Formulation of Paclitaxel, in Patients with Metastatic Breast Cancer. *Breast Cancer Res. Tr.* **2007**, *108*, 241–250.

[76] Prud'homme, R.; Saad, W. Paclitaxel Conjugate Block Copolymer Nanoparticle Formation by Flash Nanoprecipitation. *Nanotech.* **2006**, *2*, 824-826.

[77] Kataoka, K.; Matsumoto, T.; Yokoyama, M.; Okano, T. Doxorubicin-Loaded Poly (Ethylene Glycol)–Poly (B-Benzyl-L-Aspartate) Copolymer Micelles: Their Pharmaceutical Characteristics and Biological Significance. *J. Control. Release* **2000**, *64*, 143–153.

[78] Ansell, S. M.; Johnstone, S. A.; Tardi, P. G.; Lo, L.; Xie, S.; Shu, Y.; Harasym, T. O.; Harasym, N. L.; Williams, L.; Bermudes, D.; Liboiron, B. D.; Saad, W.; Prud'homme, R. K.; Mayer, L. D. Modulating the Therapeutic Activity of Nanoparticle Delivered Paclitaxel by Manipulating the Hydrophobicity of Prodrug Conjugates. *J. Med. Chem.* **2008**, *51*, 3288–3296.

[79] Zhu, Z.; Anacker, J. L.; Ji, S.; Hoye, T. R.; Macosko, C. W.; Prud'homme, R. K. Formation of Block Copolymer-Protected Nanoparticles via Reactive Impingement Mixing. *Langmuir* **2007**, *23*, 10499–10504.

[80] Zhu, Z. Polymer Stabilized Nanosuspensions Formed via Flash Nanoprecipitation: Nanoparticle Formulation, Formulation, and Stability. Ph.D. Dissertation, University of MN, Minneapolis, MN, **2010**. 1-240.

[81] Johnson, B. K. Flash NanoPrecipitation of Organic Actives via Confined Micromixing and Block Copolymer Stabilization. Ph.D. Dissertation, Princeton University, Princeton, NJ, **2003**. 1-337.

[82] Saad, W. S. Drug Nanoparticle Formation via Flash Nanoprecipitation: Conjugation to Encapsulate and Control the Release of Paclitaxel. Ph.D. Dissertation, Princeton University, Princeton, NJ, **2007**. 1-198.

[83] Shen, H.; Hong, S.; Prud'homme, R. K.; Liu, Y. Self-assembling Process of Flash Nanoprecipitation in a Multi-inlet Vortex mixer to Produce Drug-loaded Polymeric Nanoparticles. *J. Nanopart. Res.* **2011**, *13*, 4109–4120.

[84] Liu, Y.; Prudhomme, R. Optimized Descriptive Model for Micromixing in a Vortex Mixer. *Chem. Eng. Commun.* **2010**, *197*, 1068-1075.

[85] Han, J.; Zhu, Z.; Qian, H.; Wohl, A. R.; Beaman, C. J.; Hoye, T. R.; Macosko, C. W. A Simple confined impingement jets mixer for flash nanoprecipitation. *J. Pharm. Sci.* **2012**, *101*, 4018–4023.

[86] Pustulka, K. M.; Wohl, A. R.; Lee, H. S.; Michel, A. R.; Han, J.; Hoye, T. R.; McCormick, A. V.; Panyam, J.; Macosko, C. W. Flash nanoprecipitation: Particle structure and stability. *Mol. Pharmaceut.* **2013**, *10*, 4367–4377.

[87] Voorhees, P. W. The Theory of Ostwald Ripening. *J. Stat. Phys.* **1985**, *38*, 231–252.

[88] Zhu, Z. Effects of amphiphilic diblock copolymer on drug nanoparticle formulation and stability. *Biomaterials* **2013**, *34*, 10238–10248.

[89] Zhu, Z. Flash Nanoprecipitation: Prediction and Enhancement of Particle Stability via Drug Structure. *Mol. Pharm.* **2014**, *11*, 776–786.

[90] Mura, S.; Zouhiri, F.; Lerondel, S.; Maksimenko, A.; Mougin, J.; Gueutin, C.; Brambilla, D.; Caron, J.; Sliwinski, E.; LePape, A.; *et al.* Novel Isoprenoyl Nanoassembled Prodrug for Paclitaxel Delivery. *Bioconjugate Chem.* **2013**, *24*, 1840–1849.

[91] Ali, S.; Ahmad, I.; Peters, A.; Masters, G.; Minchey, S.; Janoff, A.; Mayhew, E. Hydrolyzable Hydrophobic Taxanes: Synthesis and Anti-Cancer Activities. *Anti-cancer Drugs* **2001**, *12*, 117–128.

[92] Ma, P.; Rahima Benhabbour, S.; Feng, L.; Mumper, R. J. 2′-Behenoyl-Paclitaxel Conjugate Containing Lipid Nanoparticles for the Treatment of Metastatic Breast Cancer. *Cancer Lett.* **2013**, *334*, 253–262.

[93] Forrest, M. L.; Yáñez, J. A.; Remsberg, C. M.; Ohgami, Y.; Kwon, G. S.; Davies, N. M. Paclitaxel Prodrugs with Sustained Release and High Solubility in Poly(Ethylene Glycol)-B-Poly(E-Caprolactone) Micelle Nanocarriers: Pharmacokinetic Disposition, Tolerability, and Cytotoxicity. *Pharm. Res.* **2007**, *25*, 194–206.

[94] Desmaële, D.; Gref, R.; Couvreur, P. Squalenoylation: a Generic Platform for Nanoparticular Drug Delivery. *J. Control. Release* **2012**, *161*, 609–618.

[95] Reddy, L. H.; Marque, P. E.; Dubernet, C.; Mouelhi, S. L.; Desmaele, D.; Couvreur, P. Preclinical Toxicology (Subacute and Acute) and Efficacy of a New Squalenoyl Gemcitabine Anticancer Nanomedicine. *J. Pharmacol. Exp. Ther.* **2008**, *325*, 484–490.

[96] Swindell, C. S.; Krauss, N. E.; Horwitz, S. B.; Ringel, I. Biologically active taxol analogs with deleted A-ring side chain substituents and variable C-2' configurations. *J. Med. Chem.* **1991**, 34, 1176–1184.

[97] Haag, R.; Kratz, F. Polymer Therapeutics: Concepts and Applications. *Angew. Chem. Int. Ed.* **2006**, *45*, 1198–1215.

[98] Fang, J.; Nakamura, H.; Maeda, H. The EPR Effect: Unique Features of Tumor Blood Vessels for Drug Delivery, Factors Involved, and Limitations and Augmentation of the Effect. *Adv. Drug Deliv. Rev.* **2011**, *63*, 136–151.

[99] Tang, L.; Yang, X.; Yin, Q.; Cai, K.; Wang, H.; Chaudhury, I.; Yao, C.; Zhou, Q.; Kwon, M.; Hartman, J. A.; *et al.* Investigating the Optimal Size of Anticancer Nanomedicine. *Proc. Natl. Acad. Sci. U.S.A.* **2014**, *111*, 15344–15349.

[100] P. Caliceti, F. M. Veronese, Pharmacokinetic and biodistribution properties of poly(ethylene glycol)-protein conjugates *Drug Deliv. Rev.* **2003**, *55*, 1261–1277.

[101] Erickson, H. P. Size and Shape of Protein Molecules at the Nanometer Level Determined by Sedimentation, Gel Filtration, and Electron Microscopy. *Biol. Proced. Online* **2009**, *11*, 32–51.

[102] Harris, A. L. Hypoxia—a Key Regulatory Factor in Tumour Growth. *Nat. Rev. Cancer.* **2002**, *2*, 38–47.

[103] Ebelmen, M. *Ann. Chim. Phys.* **1845** *15,* 319.

[104] Arkles, B. Silicon Esters. In *Kirk-Othmer Encyclopedia of Chemical Technology, Fourth Edition, Volume 22*; Kroschwitz, J. I.; Howe-Grant, M., ed. John Wiley & Sons, Inc: New York, 1997, 69–81.

[105] Wright, J. R. Bolt, R. O.; Goldschmidt, A.; Abbott, A. D. Silicate Esters and Related Compounds. I. Synthesis of Certain Tetraalkoxysilanes, Polyalkoxysilanes, Bis-(trialkoxysilyl)-alkanes, and Related Intermediates. *J. Am. Chem. Soc.* **1957**, *80*, 1733–1737.

[106] Tang, L.; Yang, X.; Dobrucki, L. W.; Chaudhury, I.; Yin, Q.; Yao, C.; Lezmi, S.; Helferich, W. G.; Fan, T. M.; Cheng, J. Aptamer-Functionalized, Ultra-Small, Monodisperse Silica Nanoconjugates for Targeted Dual-Modal Imaging of Lymph Nodes with Metastatic Tumors. *Angew. Chem. Int. Ed.* **2012**, *51*, 12721–12726.

[107] Tang, L.; Fan, T. M.; Borst, L. B.; Cheng, J. Synthesis and Biological Response of Size-Specific, Monodisperse Drug–Silica Nanoconjugates. *ACS Nano* **2012**, *6*, 3954–3966.

[108] Tang, L.; Gabrielson, N. P.; Uckun, F. M.; Fan, T. M.; Cheng, J. Size-Dependent Tumor Penetration and in VivoEfficacy of Monodisperse Drug–Silica Nanoconjugates. *Mol. Pharm.* **2013**, *10*, 883–892.

[109] Tang, L.; Cheng, J. Nonporous Silica Nanoparticles for Nanomedicine Application. *Nano Today* **2013**, *8*, 290–312.

[110] Xu, Z.; Liu, S.; Kang, Y.; Wang, M. Glutathione- and pH-Responsive Nonporous Silica Prodrug Nanoparticles for Controlled Release and Cancer Therapy. *Nanoscale* **2015**, *7*, 5859–5868.

[111] Parrott, M. C.; Luft, J. C.; Byrne, J. D.; Fain, J. H.; Napier, M. E.; DeSimone, J. M. Tunable Bifunctional Silyl Ether Cross-Linkers for the Design of Acid-Sensitive Biomaterials. *J. Am. Chem. Soc.* **2010**, *132*, 17928–17932.

[112] Parrott, M. C.; Finniss, M.; Luft, J. C.; Pandya, A.; Gullapalli, A.; Napier, M. E.; DeSimone, J. M. Incorporation and Controlled Release of Silyl Ether Prodrugs From PRINT Nanoparticles. *J. Am. Chem. Soc.* **2012**, *134*, 7978–7982.

[113] Hoye, T. R.; Wohl, A. W.; Macosko, C. W.; Panyam, J. Silicate prodrugs and nanoparticles. U.S. Patent Application PCT/US2012/040247, May 31, 2012.

[114] Reaxys, version 2.19790.2; Elsevier; 2015; RRN 969209 (accessed July 13, 2015).

[115] Ismael, G. F. V.; Rosa, D. D.; Mano; M. S., Awada, A. Novel cytotoxic drugs: Old challenges, new solutions. *Cancer Treat. Rev.* **2008**, *34*, 81–91.

[116] Johnson, B. K.; Prud'homme, R. K. Chemical processing and micromixing in confined impinging jets. *AIChE.* **2003**, *49*, 2264–2282.

[117] Johnson, B. K.; Prud'homme, R. K. Flash nanoprecipitation of organic actives and block copolymers using a confined impinging jets mixer. *Aust. J. Chem.* **2003**, *56*, 1021–1024.

[118] Wohl, A. R.; Michel, A. R.; Kalscheuer, S.; Macosko, C. W.; Panyam, J.; Hoye, T. R. Silicate esters of paclitaxel and docetaxel: synthesis, hydrophobicity, hydrolytic stability, cytotoxicity, and prodrug potential. *J. Med. Chem.* **2014**, *57*, 2368–2379.

[119] Corriu, R. J. P.; Granier, M.; Lanneau, G. F. Synthesis and reactivity of bis(triethoxysilyl)methane, tris(triethoxysilyl)methane and some derivatives. *J. Organomet. Chem.* **1998**, *562*, 79–88.

[120] Wohl, A. R. Synthesis and characterization of silicate esters prodrugs and poly(ethylene glycol)-b-poly(lactic-co-glycolic acid) block copolymers for formulation into prodrug-loaded nanoparticles. Ph.D. Dissertation, University of Minnesota, Minneapolis, 2012.

[121] Gitelman, H. J.; Alderman, F.; Perry, S. J. Renal handling of silicon in normals and patients with renal insufficiency. *Kidney Int.* **1992**, *42*, 957–959.

[122] Marco-Franco, J. E.; Torres, V. E.; Nixon, D. E.; Wilson, D. M.; James, E. M.; Bergstrahl, E. J.; McCarthy, J. T. Oxalate, silicon, and vanadium in acquired cystic kidney disease. *Clin. Nephrol.* **1991**, *35*, 52–58.

[123] Anglin, E. J.; Cheng, L.; Freeman, W. R.; Sailor, M. J. Porous silicon in drug delivery devices and materials. *Adv. Drug Deliv. Rev.* **2008**, *60*, 1266–1277.

[124] Skwarczynski, M.; Hayashi, Y.; Kiso, Y. Paclitaxel prodrugs: Toward smarter delivery of anticancer agents. *J. Med. Chem.* **2006**, *49*, 7253–7269.

[125] Gerrard, W.; Howe, B. K. The behaviour of 1,1,1,3,3,3-hexachloropropan-2-ol with inorganic non-metal halides. *J. Chem. Soc.* **1955**, 505–510.

[126] Chappelow, C. C.; Elliot, R. L.; Goodwin, J. T. The phenylation and methylation of alkoxychlorosilanes. *J. Org. Chem.* **1960***, 25*, 435–439.

[127] Beckman, J.; Daketernieks, D.; Tiekink, E. R. T. Chiral trialkoxysilanols derived from terpene alcohols. Molecular structures of tris([(1S)-endo]-(–)-bornoxy)silanol and tetrakis((–)-menthoxy)silane. *J. Organomet. Chem.* **2002,** *648*, 188-192.

[128] Gerrard, W.; Woodhead, A. H. Interaction of alcohols with silicon tetrachloride. *J. Chem. Soc.* **1951**, 519–522.

[129] Miner, C. S., Jr.; Bryan, L. A.; Holysz, R. P., Jr.; Pedlow, G. W., Jr. *tert*-Alkoxyaminosilanes. *Indust. Engin. Chem.* **1947**, *39*, 1368–1371

[130] Showell, G. A.; Mills, J. S. Chemistry Challenges in Lead Optimization: Silicon Isosteres in Drug Discovery. *Drug Discov. Today* **2003**, *8*, 551–556.

[131] Burns, C. J.; Field, L. D.; Hashimoto, K.; Petteys, B. J.; Ridley, D. D.; Rose, M. Synthesis of Stereoisomerically Pure Monoether Lipids. *Aust. J. Chem.* **1999**, *52*, 387–394.

[132] Tetko, I. V.; Gasteiger, J.; Todeschini, R.; Mauri, A.; Livingstone, D.; Ertl, P.; Palyulin, V. A.; Radchenko, E. V.; Zefirov, N. S.; Makarenko, A. S.; Tanchuk, V. Y.; Prokopenko, V. V. Virtual computational chemistry laboratory—design and description. *J. Comput. Aid. Mol. Des.* **2005**, *19*, 453–463.

[133] Tetko, I. V.; Tanchuk, V. Y.; Kasheva, T. N.; Villa, A. E. Estimation of aqueous solubility of chemical compounds using E-state indices. *J. Chem. Inf. Comput. Sci.* **2001**, 41, 1488–1493.

[134] Eros, D.; Kovesdi, I.; Orfi, L.; Takacs-Novak, K.; Acsady, G.; Keri, G. Reliability of logP predictions based on calculated molecular descriptors: a critical review. *Curr. Med. Chem.* **2002**, *9*, 1819–1829.

[135] Turner, C. W.; Franklin, K. J. Studies of the hydrolysis and condensation of tetraethylorthosilicate by multinuclear (^{1}H ^{17}O ^{29}Si) NMR spectroscopy. *J. Non-Cryst. Solids* **1986**, *91*, 402–415.

[136] Glasoe, P. K.; Long, F. A.; Use of glass electrodes to measure acidities in deuterium oxide. *J. Phys. Chem.* **1960,** *64,* 188—189.

[137] Gary, R.; Bates, R. B.; Robinson, R. A. Second dissociation" constant of deuteriophosphoric acidin deuterium oxide from 5-50°. Standardization of a pD scale. *J. Phys. Chem*. **1964**, *68*, 6–9.

[138] Long, F. A.; Dahlgren, G. Relative hydrogen bonding of deuterium. I. Ionization constants of maleic and fumaric acids of their nonethyl esters in H_2O and D_2O. *J. Am. Chem. Soc.* **1960,** *82,* 1303—1308.

[139] Han, J. Diblock copolymer stabilized nanoparticles for drug delivery via flash nanoprecipitation. Ph.D. Dissertation, University of Minnesota, Minneapolis, 2014.

[140] Li, H.; DeRosier, D. J.; Nicholson, W. V.; Nogales, E.; Downing, K. H. Microtubule Structure at 8 Å Resolution. *Structure* **2002**, *10*, 1317–1328.

[141] Amos, L. A.; Löwe, J. How Taxol Stabilises Microtubule Structure. *Chem. Biol.* **1999**, *6*, R65–R69.

[142] Kim, S.; Cho, S.; Chu, L. Biotin-Conjugated Block Copolymeric Nanoparticles as Tumor-Targeted Drug Delivery Systems. *Macromol. Res.* **2007**, *15*, 646-655.

[143] Dechy-Cabaret, O.; Martin-Vaca, B. Controlled Ring-opening Polymerization of Lactide and Glycolide. *Chem. Rev.* **2004**, *104*, 6147-76.

[144] Liggins, R. Polyether-polyester Diblock Copolymers for the Preparation of Paclitaxel Loaded Polymeric Micelle Formulations. *Adv. Drug Deliver. Rev.* **2002**, *54*, 191-202.

[145] Kowalski, A.; Duda, A.; Penczek, S. Kinetics and Mechanism of Cyclic Esters Polymerization Initiated with Tin(II) Octoate. 3. †Polymerization of l, l-Dilactide. *Macromolecules* **2000**, *33*, 7359–7370.

[146] Qian, H.; Wohl, A. R.; Crow, J. T.; Macosko, C. W.; Hoye, T. R. A Strategy for Control of "Random" Copolymerization of Lactide and Glycolide: Application to Synthesis of PEG- b-PLGA Block Polymers Having Narrow Dispersity. *Macromolecules* **2011**, *44*, 7132—7140.

[147] Kamber, N. E.; Jeong, W.; Waymouth, R. M.; Pratt, R. C.; Lohmeijer, B. G. G.; Hedrick, J. L. Organocatalytic Ring-Opening Polymerization. *Chem. Rev.* **2007**, *107*, 5813–5840.

[148] Lohmeijer, B. G. G.; Pratt, R. C.; Leibfarth, F.; Logan, J. W.; Long, D. A.; Dove, A. P.; Nederberg, F.; Choi, J.; Wade, C.; Waymouth, R. M.; Hedrick, J. L. Guanidine and amidine organocatalysts for ring-opening polymerization of cyclic esters. *Macromolecules* **2006**, *39*, 8574–8583.

[149] Mojaat, M.; Foucault, A.; Pruvost, J.; Legrand, J. Optimal Selection of Organic Solvents for Biocompatible Extraction of Beta-Carotene From Dunaliella Salina. *J. Biotechnol.* **2008**, *133*, 433–441.

[150] Abdelwahed, W.; Degobert, G.; Stainmesse, S.; Fessi, H. Freeze-Drying of Nanoparticles: Formulation, Process and Storage Considerations. *Adv. Drug Deliv. Rev.* **2006**, *58*, 1688–1713.

[151] Greenwood, R. Review of the Measurement of Zeta Potentials in Concentrated Aqueous Suspensions Using Electroacoustics. *Adv. Colloid Interfac.* **2003**, *106*, 55–81.

[152] Tarr, B. D.; Yalkowsky, S. H. A new parenteral vehicle for the administration of some poorly water soluble anti-cancer drugs. *J. Parenter. Sci. Technol.* **1987**, *41*, 31–3.

[153] ABRAXANE™ for Injectable Suspension (paclitaxel protein-bound particles for injectable suspension) (albumin-bound). http://www.accessdata.fda.gov/drugsatfda_docs/label/2005/021660lbl.pdf (accessed April 26, 2015).

[154] Gradishar, W. J.; Tjulandin, S.; Davidson, N.; Shaw, H.; Desai, N.; Bhar, P.; Hawkins, M.; O'Shaughnessy, J. Phase III trial of nanoparticle albumin-bound paclitaxel compared with polyethylated castor oil-based paclitaxel in women with breast cancer. *J. Clin. Oncol.* **2005**, *23*, 7794–803.

[155] Smith, J. Overview of breast cancer drug therapy. *US PHARMACIST.* **2005**, *30*, 9.

[156] Pustulka, K. M. Polymer stabilized nanosuspension via flash nanoprecipitation: particle formulation, structure and freeze drying. M.S. Dissertation, University of Minnesota, Minneapolis, 2012.

[157] Huang, X.; Brazel, C.S. On the importance and mechanisms of burst release in matrix-controlled drug delivery systems. *J. Control. Release*. **2001**, *73*, 121–136.

[158] Lee, M. K.; Kim, M. Y.; Kim, S.; Lee, J. Cryoprotectants for freeze drying of drug nano-suspensions: effect of freezing rate. *J. Pharm. Sci.* **2009**, *98*, 4808–4817.

[159] Schuch, H.; Klingler, J.; Rossmanith, P.; Frechen, T.; Gerst, M.; Feldthusen, J.; Müller, A. H. E. Characterization of Micelles of Polyisobutylene- Block-Poly(Methacrylic Acid) in Aqueous Medium. *Macromolecules* **2000**, *33*, 1734–1740.

[160] Kulinski, Z.; Piorkowska, E.; Gadzinowska, K.; Stasiak, M. Plasticization of poly(L-lactide) with Poly(propylene Glycol). *Biomacromolecules* **2006**, *7*, 2128–35.

[161] Larive, R. M.; Moriggi, G.; Menacho-Márquez, M.; Cañamero, M.; de Álava, E.; Alarcón, B.; Dosil, M.; Bustelo, X. R. Contribution of the R-Ras2 GTP-Binding Protein to Primary Breast Tumorigenesis and Late-Stage Metastatic Disease. *Nat. Commun.* **2014**, *5*, 3881.

[162] Reed, N. N.; Janda, K. D. A One-step Synthesis of Monoprotected Polyethylene glycol Ethers. *J. Org. Chem.* **2000**, *65*, 5843–5845.

[163] Wirth, P. Chemical Modification of Horseradish Peroxidase with Ethanal-methoxypolyethylene glycol: Solubility in Organic Solvents, Activity, and Properties. *Bioorg. Chem.* **1991**, *19*, 133–142.

[164] Kulkarni, M. Single Step Room Temperature Oxidation of Poly(ethylene glycol) to Poly(oxyethylene)-dicarboxylic acid. *J. Appl. Polym. Sci.* **1998**, *70*, 883-890.

[165] Gill, H. S.; Tinianow, J. N.; Ogasawara, A.; Flores, J. E.; Vanderbilt, A. N.; Raab, H.; Scheer, J. M.; Vandlen, R.; Williams, S.-P.; Marik, J. A Modular Platform for the Rapid Site-specific Radiolabeling of Proteins with 18F Exemplified by Quantitative Positron Emission Tomography of Human Epidermal Growth Factor Receptor 2. *J. Med. Chem.* **2009**, *52*, 5816–5825.

[166] Ji, S.; Zhu, Z.; Hoye, T. R.; Macosko, C. W. Maleimide Functionalized Poly(ε-caprolactone)-b-poly(ethylene glycol) (PCL-PEG-MAL): Synthesis, Nanoparticle Formation, and Thiol Conjugation. *Macromol. Chem. Phys.* **2009**, *210*, 823.

[167] Chae, S. Y.; Kim, T. H.; Park, K.; Jin, C.-H.; Son, S.; Lee, S.; Youn, Y. S.; Kim, K.; Jo, D.-G.; Kwon, I. C.; Chen, X.; Lee, K. C. Improved Antitumor Activity and Tumor Targeting of NH(2)-terminal-specific PEGylated Tumor Necrosis Factor-Related Apoptosis-inducing Ligand. *Mol. Cancer Ther.* **2010**, *9*, 1719–1729.

[168] Song, S.; Liu, D.; Peng, J.; Sun, Y.; Li, Z.; Gu, J. Peptide Ligand-mediated Liposome Distribution and Targeting to EGFR Expressing Tumor in vivo. *Int. J. Pharm.* **2008**, *363*, 155-161.

[169] Wang, M.; Thanou, M. Targeting Nanoparticles to Cancer. *Pharmacol. Res.* **2010**, *62*, 90–99.

[170] Tong, R.; Tang, L.; Ma, L.; Tu, C.; Baumgartner, R.; Cheng, *J. Chem. Soc. Rev.* **2014**, *43*, 6982–7012.

[171] Zhang, S.; Chan, K. H.; Prud'homme, R. K.; Link, A. J. Synthesis and Evaluation of Clickable Block Copolymers for Targeted Nanoparticle Drug Delivery. *Mol. Pharm.* **2012**, *9*, 2228–2236.

[172] Polito, L.; Monti, D.; Caneva, E.; Delnevo, E.; Russo, G.; Prosperi, D. One-step Bioengineering of Magnetic Nanoparticles via a Surface Diazo Transfer/Azide-Alkyne Click Reaction Sequence. *Chem. Comm.* **2008**, *5,* 621–623.

[173] Natarajan, A.; Du, W.; Xiong, C.; DeNardo, G. Construction of Di-scFv through a Trivalent Alkyne–azide 1, 3-dipolar Cycloaddition. *Chem. Comm.* **2007**, *7*, 695-697.

[174] Tang, L.; Deng, L. Dynamic Kinetic Resolution via Dual-Function Catalysis of Modified Cinchona Alkaloids: Asymmetric Synthesis of Alpha-Hydroxy Carboxylic Acids. *J. Am. Chem. Soc.* **2002**, *124*, 2870–2871.

[175] Leemhuis, M.; van Nostrum, C. F.; Kruijtzer, J. A. W.; Zhong, Z. Y.; Breteler, ten, M. R.; Dijkstra, P. J.; Feijen, J.; Hennink, W. E. Functionalized Poly(A-Hydroxy Acid)S via Ring-Opening Polymerization: Toward Hydrophilic Polyesters with Pendant Hydroxyl Groups. *Macromolecules* **2006**, *39*, 3500–3508.

[176] Pounder, R. J.; Dove, A. P. Synthesis and Organocatalytic Ring-Opening Polymerization of Cyclic Esters Derived From L-Malic Acid. *Biomacromolecules* **2010**, *11*, 1930–1939.

[177] Kim, S. C.; Kim, D. W.; Shim, Y. H.; Bang, J. S.; Oh, H. S.; Wan Kim, S.; Seo, M. H. In Vivo Evaluation of Polymeric Micellar Paclitaxel Formulation: Toxicity and Efficacy. *J. Control. Release* **2001**, *72*, 191–202.

[178] Huizing, M. T.; Sparreboom, A.; Rosing, H.; van Tellingen, O.; Pinedo, H. M.; Beijnen, J. H. Quantification of Paclitaxel Metabolites in Human Plasma by High-Performance Liquid Chromatography. *J. Chromatogr. B* **1995**, *674*, 261–268.

[179] McChesney, J.; Zygmunt, J.; Bannister, S. Measurement of paclitaxel in biological matrices: high-throughput liquid chromatographic-tandem mass spectrometric quantification of paclitaxel and metabolites in human and dog plasma *J. Chromatogr. B* **2003**, *785*, 253-261.

[180] Rosing, H.; Beijnen, J. A Simple and Sensitive Assay for the Quantitative Analysis of Paclitaxel in Human and Mouse Plasma and Brain Tumor Tissue using Coupled Liquid Chromatography and Tandem Mass Spetrometry. *J. Mass Spectrom.* **2004**, *39*, 1506-1512.

[181] Kim, S. C.; Yu, J.; Lee, J. W.; Park, E.-S.; Chi, S.-C. Sensitive HPLC Method for Quantitation of Paclitaxel (Genexol in Biological Samples with Application to Preclinical Pharmacokinetics and Biodistribution. *J. Pharmaceut. Biomed.* **2005**, *39*, 170–176.

[182] Gréen, H.; Vretenbrant, K.; Norlander, B.; Peterson, C. Measurement of Paclitaxel and its Metabolites in Human Plasma using Liquid Chromatography/Ion Trap Mass Spectrometry with a Sonic Spray Ionization Interface. *Rapid Commun. Mass Sp.* **2006**, *20*, 2183–2189.

[183] Suno, M.; Ono, T.; Iida, S.; Umetsu, N.; Ohtaki, K.-I.; Yamada, T.; Awaya, T.; Satomi, M.; Tasaki, Y.; Shimizu, K.; Matsubara, K. Improved High-performance Liquid Chromatographic Detection of Paclitaxel in Patient's Plasma using Solid-Phase Extraction, and Semi-micro-bore C18 Separation and UV detection. *J. Chromatogr. B* **2007**, *860*, 141–144.

[184] Martinez, M. A Mechanistic Approach to Understanding the Factors Affecting Drug Absorption: a Review of Fundamentals. *J. Clin. Pharmacol.* **2002**, *42*, 620-643.

[185] Varma, M.; Sateesh, K. Functional Role of P-glycoprotein in Limiting Intestinal Absorption of Drugs: Contribution of Passive Permeability to P-glycoprotein Mediated Efflux Transport. *Mol. Pharm.* **2005**, *2*, 12-21.

[186] Most generally, names for compounds containing silicon are named from the simplest silane, SiH_4. However, compounds that consist of four Si-O bonds are commonly named as a derivative of orthosilicic acid rather than as a silane derivative.

[187] Bassindale, A. R.; Taylor, P. G. Reaction Mechanisms of Nucleophilic Attack at Silicon. In *The Chemistry of Organic Silicon Comounds*. Patai, S.; Rappoport, Z., eds. John Wiley & Sons, Inc: New York, 1989, 839-892 and references therein.

[188] Holmes, R. R. The Stereochemistry of Nucleophilic Substitution at Tetracoordinated Silicon. *Chem. Rev.* **1990**, *90*, 17-31 and references therein.

[189] Aelion, R.; Loebel, A.; Eirich, F. Hydrolysis of Ethyl Silicate. *J. Am. Chem. Soc.* **1950**. *69*, 61-75.

[190] Ro, J. C.; Chung, I. J. Sol-Gel Kinetics of Tetraethylorthosilicate (TEOS) in Acid Catalyst. *J. Non-Cryst. Solids* **1989**, *110*, 26-32.

[191] Zerda, T. W.; Hoang, G. Effects of Solvents on the Hydrolysis Reaction of Tetramethyl Orthosilicate. *Chem. Mater.* **1990**, *2*, 372-376.

[192] Assink, R. A.; Kay, B. D.; Study of Sol-Gel Chemical Reaction Kinetics by NMR *Annu. Rev. Mater. Sci.* **1991**, *21*, 491-513.

[193] Zerda, T. W.; Hoang, G. Effects of Solvents on the Hydrolysis Reaction of Tetramethyl Orthosilicate. *Chem. Mater.* **1990**, *2*, 372-376.

[194] Arkles, B. Silicon Esters. In *Kirk-Othmer Encyclopedia of Chemical Technology, Fourth Edition, Volume 22*; Kroschwitz, J. I.; Howe-Grant, M., ed. John Wiley & Sons, Inc: New York, 1997, 69-81.

[195] Clausen, R. P.; Bols, M. The First Tri- and Tetraalkoxysilanes with Four Different Substituents. *J. Org. Chem.* **1997**, *62*, 4457-4464.

[196] Brinker, C. J. Hydrolysis and Condensation of Silicates: Effects on Structure. *J .Non-Cryst. Solids* **1988**, *100*, 31-50.

[197] Brinker, C. J.; Scherer, G. W. Hydrolysis and Condensation II: Silicates. In *Sol-Gel Science: The Physics and Chemistry of Sol-Gel Processing*. Academic Press, Inc: San Diego, CA, **1990**, 97-233.

[198] Belton, D. J.; Deschaume, O.; Perry, C. C. An overview of the fundamentals of the chemistry of silica with relevance to biosilicification and technological advances. *FEBS J.* **2012**, *279* 1710–1720.

[199] Sauvage, A.; Levy, M. *Dexamethasone: Therapeutic Uses, Mechanism of Action and Potential Side Effects*; Nova Science Pub Incorporated; 2013.

[200] Paulus, E. F.; Kurz, M.; Matter, H. Solid-State and Solution Structure of the Salinomycin-Sodium Complex: Stabilization of Different Conformers for an Ionophore in Different Environments. *J. Am. Chem. Soc.* **1998**, *120*, 8209-8221.

[201] Borgström, B.; Huang, X.; Pošta, M.; Hegardt, C.; Oredsson, S.; Strand, D. Synthetic Modification of Salinomycin: Selective O-Acylation and Biological Evaluation. *Chem. Comm.* **2013**, *49*, 9944–9946.

[202] Huczyński, A.; Janczak, J.; Stefańska, J.; Antoszczak, M.; Brzezinski, B. Synthesis and Antimicrobial Activity of Amide Derivatives of Polyether Antibiotic-Salinomycin. *Bioorg. Med. Chem. Lett.* **2012**, *22*, 4697–4702.

[203] Davis, A. L.; Harris, J. A.; Russell, C.; Wilkins, J. Investigations by HPLC-Electrospray Mass Spectrometry and NMR Spectroscopy Into the Isomerisation of Salinomycin. *Analyst* **1999**, *124*, 251-256.

[204] Chi, G.; Wang, X.; Chen, R. Synthesis of Novel N1-(2-Furanidyl)-5-Fluorouracil Derivatives of A-Hydroxy (Thio) Phosphonates. *Heteroatom Chem.* **2002**, *13,* 211—215.

[205] Pizzirani, D.; Pagliuca, C.; Realini, N.; Branduardi, D.; Bottegoni, G.; Mor, M.; Bertozzi, F.; Scarpelli, R.; Piomelli, D.; Bandiera, T. Discovery of a New Class of Highly Potent Inhibitors of Acid Ceramidase: Synthesis and Structure-Activity Relationship (SAR). *J. Med. Chem.* **2013**, *56*, 3518–3530.

[206] Benci, K.; Wittine, K.; Radan, M.; Cetina, M.; Sedić, M.; Kraljević Pavelić, S.; Pavelić, K.; Clercq, E. D.; Mintas, M. The Unsaturated Acyclic Nucleoside Analogues Bearing a Sterically Constrained (Z)-4"-Benzamido-2-"Butenyl Moiety: Synthesis, X-Ray Crystal Structure Study, Cytostatic and Antiviral Activity Evaluations. *Bioorg. Med. Chem.* **2010**, *18*, 6249–6257.

[207] Amirmostofian, M.; Pourahmad Jaktaji, J.; Soleimani, Z.; Tabib, K.; Tanbakosazan, F.; Omrani, M.; Kobarfard, F. Synthesis and Molecular-Cellular Mechanistic Study of Pyridine Derivative of Dacarbazine. *Iran J. Pharm. Res.* **2013**, *12*, 255–265.

[208] Horton, J. K.; Stevens, M. F. A New Light on the Photo-Decomposition of the Antitumour Drug DTIC. *J. Pharm. Pharmacol.* **1981**, *33*, 808–811.

[209] Shealy, Y. F.; Krauth, C. A. Imidazoles. I. Coupling Reactions of 5-Diazoimidazole-4-Carboxamide. *J. Org. Chem.* **1962**, *27* (6), 2150-2154.

[210] Gerster, J. F.; Lindstrom, K. J.; Miller, R. L.; Tomai, M. A.; Birmachu, W.; Bomersine, S. N.; Gibson, S. J.; Imbertson, L. M.; Jacobson, J. R.; Knafla, R. T.; *et al.* Synthesis and Structure-Activity-Relationships of 1H-Imidazo[4,5-C]Quinolines That Induce Interferon Production. *J. Med. Chem.* **2005**, *48*, 3481–3491.

[211] Ward, T. R.; Turunen, B. J.; Haack, T.; Neuenswander, B.; Shadrick, W.; Georg, G. I. Synthesis of a Quinolone Library From Ynones. *Tetrahedron Lett.* **2009**, *50*, 6494–9497.

[212] Varanda, F.; de Melo, M. P.; Caco, A. I. Solubility of Antibiotics in Different Solvents. 1. Hydrochloride Forms of Tetracycline, Moxifloxacin, and Ciprofloxacin. *Ind. Eng. Chem. Res.* **2006**, *45,* 6368—6374.

[213] Zieba, A.; Maślankiewicz, A.; Sitkowski, J. 1H, 13C and 15N NMR Spectra of Ciprofloxacin. *Magn. Reson. Chem.* **2004**, *42*, 903–904.

[214] Rocha-Lima, C. M.; Soares, H.P.; Raez, L. E.; Singal, R. EGFR Targeting of Solid Tumors. *Cancer Control.* **2007**, *14,* 295-304.

[215] Marzaro, G.; Guiotto, A.; Pastorini, G.; Chilin, A. A Novel Approach to Quinazolin-4(3H)-One via Quinazoline Oxidation: an Improved Synthesis of 4-Anilinoquinazolines. *Tetrahedron* **2010**, *66*, 962–968.

[216] Hoye, T. R.; Hanson, P. R.; Vyvyan, J. R. A practical guide to first-order multiplet analysis in ^{1}H NMR spectroscopy. *J. Org. Chem.* **1994**, *59*, 4096–4103.

[217] Hoye, T. R.; Zhao, H. A method for easily determining coupling constant values: An addendum to "A practical guide to first-order multiplet analysis in ^{1}H NMR spectroscopy." *J. Org. Chem.* **2002**, *67*, 4014–4016.

[218] Shahani, K.; Swaminathan, S. K.; Freeman, D.; Blum, A.; Ma, L.; Panyam, J. Injectable sustained release microparticles of curcumin: A new concept for cancer chemoprevention. *Cancer Res*. **2010** *70*, 4443–4452.

[219] Meurer-Grob, P.; Kasparian, J.; Wade, R. H. Microtubule Structure at Improved Resolution. *Biochemistry* **2001**, *40*, 8000–8008.

[220] Lee, H. S.; Morrison, E. D.; Frethem, C. D.; Zasadzinski, J. A.; McCormick, A. V.; Cryogenic electron microscopy study of nanoemulsion formation from microemulsions. *Langmuir* **2014,** *30,* 10826-10833.

[221] Ma, M.; Bong, D. Protein Assembly Directed by Synthetic Molecular Recognition Motifs. *Org. Biomol. Chem.* **2011**, *9*, 7296.

[222] Millar, R. W.; Philbin, S. P. Clean Nitrations: Novel Syntheses of Nitramines and Nitrate Esters by Nitrodesilylation Reactions Using Dinitrogen Pentoxide (N2O5). *Tetrahedron* **1997**, *53*, 4371–4386.